
Final Research Report

**Characterization of Voids and Other Subsurface Deficiencies by Geophysical
Methods**

By:

Horst G. Brandes

Department of Civil & Environmental Engineering
University of Hawaii

Prepared in cooperation with:

State of Hawaii Department of Transportation
Highways Division

&

U. S. Department of Transportation
Federal Highway Administration

August 2013

The contents of this report reflect the view of the author, who is responsible for the facts and accuracy of the data presented herein. The contents do not necessarily reflect the official views or policies of the State of Hawaii, Department of Transportation or the Federal Highway Administration. This report does not constitute a standard, specification or regulation.

Technical Report Documentation Page

1. Report No. FHWA/HI-15-55161	2. Government Accession No.	3. Recipient's Catalog No.	
4. Title and Subtitle <i>Characterization of Voids and Other Subsurface Deficiencies by Geophysical Methods</i>		5. Report Date August 2013	
		6. Performing Organization Code	
7. Author(s) Brandes, Horst G.		8. Performing Organization Report No. 55161	
9. Performing Organization Name and Address Department of Civil and Environmental Engineering University of Hawaii at Manoa 2540 Dole Street, Holmes Hall 383 Honolulu, HI 96822		10. Work Unit No. (TRAVIS)	
		11. Contract or Grant No. 55161	
12. Sponsoring Agency Name and Address Hawaii Department of Transportation Harbors Division 79 S Nimitz Highway Honolulu, HI 96813		13. Type of Report and Period Covered Research report, 2006-2013	
		14. Sponsoring Agency Code	
15. Supplementary Notes Project performed in cooperation with the Hawaii Department of Transportation and the Federal Highways Administration.			
16. Abstract <p>The objective of this study was to evaluate and test a range of geophysical imaging systems for use in Hawaii's unique geological environment and range of soils. Of particular interest was the ability of these systems to identify and characterize subsurface deficiencies including cavities, loose soils, and other buried targets. The project employed ground penetrating radar (GPR), electro-magnetic (EM) surveying, and seismic refraction (SR) and reflection imaging. These techniques were used to make blind predictions of buried objects placed at various depths and locations in a long trench at each of three locations in Hawaii: Poamoho Research Station, Waimanalo Research Station and Kawaihae Harbor. Objects consisted mostly of Styrofoam shapes, but also some steel and PVC pipes.</p> <p>Of the three techniques, GPR was the most successful, resulting in an average of close to 50% of objects identified correctly and on the order of 20% of false predictions. The second technique in terms of success was seismic refraction, followed in a distant third place by EM. These rates should be viewed with caution since they included objects as small as 3 inches placed at depths of as much as 6 feet.</p>			
17. Key Words Void detection, soil, ground penetration radar, seismic surveying, electromagnetic surveying		18. Distribution Statement No restriction. This document is available to the public from the sponsoring agency at the website http://hidot.hawaii.gov .	
19. Security Classif. (of this report) Unclassified	20. Security Classif. (of this page) Unclassified	21. No. of Pages 335	22. Price

Table of Contents

Introduction.....	2
Field Studies at Poamoho, Waimanalo and Kawaihae Test Sites	2
Surveying of Hilo Harbor.....	5
Laboratory Testing of Soil Velocities.....	7
Recommendations for Future Work.....	8
Acknowledgements	8
Students and Theses.....	8
Research Publications.....	9
International Conference Presentation.....	10
Research Article: Brandes, H.G. (2013)	32
Research Article: Nicholson, P.G. and Brandes, H.G. (2011).....	41
Consultant Report, Dawood (2008): Geophysical Void Investigation	51
Consultant Report, Dawood (2008): Port of Hilo Geophysical Investigation	308

Introduction

The objective of this study was to evaluate and test a range of geophysical imaging systems for use in Hawaii's unique geological environment and range of soils. Of particular interest was the ability of these systems to identify and characterize subsurface deficiencies including cavities, loose soils, and other buried targets. After a review of available systems, it was decided that the most promising techniques were ground penetrating radar (GPR), electro-magnetic (EM) surveying, and seismic refraction (SR) and reflection imaging. Given the crucial role that signal frequency plays in GPR and SR surveying, each of these were tested at a number of frequencies in order to identify the optimum value for purposes of shallow imaging.

Field Studies at Poamoho, Waimanalo and Kawaihae Test Sites

Field comparisons were carried out at three field test sites (Figure 1): Poamoho Research Station, Waimanalo Research Station and Kawaihae Harbor. Similar procedures were used at each of the three locations. These sites were selected because the predominant soils were different from each other and yet common throughout Hawaii. The index properties for each one are shown in Table 1 and in Figure 2. At the Poamoho station, the soil consists of highly leached lateritic residual (red) soil, which is the most common agricultural soil in the State of Hawaii. In contrast, the soil at the Waimanalo station consists of dark, highly plastic silt (borderline clay) with a high affinity for water. At Kawaihae Harbor the soil consists of dredged calcareous sand and gravel. This field site is located adjacent to and just above sea level (Figure 3).

Field work at each of the three locations consisted of burying a series of Styrofoam blocks and other objects within a shallow trench and then attempting to identify them through GPR, EM and SR surveying. The trench measured 45 meters in length, 2.5 meters in width and up to 3 meters in depth. Styrofoam was selected because of its high

density contrast with the surrounding soil, in hopes that it would provide a strong target for detection with the selected geophysical techniques. A total of 39 to 41 objects were buried in each of the trenches using similar excavation and backfilling procedures (Figure 4a). Following their careful placement, each trench was backfilled to the original grade. The backfill was compacted a modest amount at the in situ moisture content in an attempt to attain a final density similar to the initial one.

Surveying was carried out by an outside geophysical contractor who was asked to provide blind predictions based solely on geophysical measurements and data interpretation and modeling. He was not present during burial operations and was only provided with minimum and maximum object sizes and types, as well as the dimensions and alignment of the trench. He was further instructed to consider the results of each technique independently from the others.

GPR, EM and SR surveying were conducted along three parallel survey lines, separated 2 feet from each other and extending the length of each of the trenches (Figure 4). They are referred to as L0(left), L2(middle) and L4(right) survey lines. Technical details on each of the techniques are provided in the attached journal publication and in the two attached reports by the geophysical contractor. GPR surveys were conducted at frequencies of 270MHz, 400MHz, 900MHz, and 1500MHz. Antenna frequency has a large impact on the resolution of objects in GPR images (Figure 5). Two EM tools were used, operating at frequencies of 31MHz and 38MHz, respectively. Seismic data collection employed a U-shaped land streamer with two lines of twelve 100-Hz geophones spaced 1 foot apart (Figure 4b). Energy was imparted into the ground by lowering a sledgehammer on a steel plate.

The surveyor provided lists of “picks”, i.e. the location along the traverse where he identified objects, using each of the three geophysical techniques in turn (see examples in Figures 6 through 8, and Table 2). Although he also provided depths in some cases, these interpretations were quite off the mark due to the lack of effective ground truth targets in or near the trench. Thus here we focus on the success rate of these picks while

disregarding depth of burial. The picks provided by the surveyor were compared to our inventory list. It should be pointed out that the surveyor was highly experienced in this type of work and therefore the findings below assume a significant level of expertise with geophysical surveying work.

A summary of the findings for each of the three techniques is presented in Tables 3 through 5. As expected, some of the objects were identified correctly and some were missed. In addition, some picks did not correspond to any specific object and are listed as “over-picks”. GPR with antenna in the 400MHz to 900MHz range yielded the best overall performance (Table 3). That is, the best combination of maximum number of correct picks and minimum number of over-picks. More objects were identified with the 1500MHz antenna, but many of these were incorrect ones. It appears that approximately 40 to 60% of all objects could be identified. Although this may not seem very high, it should be remembered that objects were as small as 3 inches, buried up to 6 feet, and sometimes offset laterally by as much as 2 feet from the center survey line (L2).

SR was the second most successful technique, with 18 to 58% of objects identified correctly (Table 4). Seismic refraction is usually conducted with geophones spaced further apart and employing larger energy sources in order to attain deeper penetration. Our testing indicates that this technique has some appeal for applications involving the identification of small objects at shallow depths. On the other hand, seismic refraction is more time consuming to carry out in the field, at least in comparison with GPR surveying.

EM surveying was the least successful method (Table 5). Inspection of the raw data led to the identification of only 2 to 8% of objects. An attempt was made to model the EM data using the program EMIGMA, but this proved successful only for the Waimanalo site (details on the modeling procedure are included in the report by the geophysical contractor). Why this only worked in one case but not the others is not clear.

When comparing among the three soil environments, it was found that GPR worked best for the two fine-grained soil sites (Waimanalo and Poamoho), but not too much worse for the coarse-grained Kawaihae Harbor site. Seismic refraction was most successful at Waimanalo, followed by Poamoho and then Kawaihae Harbor. EM surveying was only modestly successful in the highly plastic Waimanaolo soil (and only after modeling of the raw data). It showed very poor performance for the other two sites.

Surveying of Hilo Harbor

Construction of the port of Hilo began in 1914. This involved offshore dredging and construction of docking piers (Piers 1, 2 and 3) and a 3,000-meter long breakwater (Figure 9). The three piers consist of reinforced concrete decking supported on concrete piles located beyond the original shoreline in deeper water. Sheet piling was driven into the seabed adjacent to the piers and the area behind the piling was backfilled with loose dredge spoils from deepening of the navigation channel. A succession of pavements and other structural supports were added in the backfill area in order to accommodate port operations and transportation facilities.

Settlement in the filled areas has been a persistent problem almost since initial construction of the port (Figure 10). The reason for this is clear from boring logs that indicate very loose calcareous fill with SPT values as low as 1 and 2. These dredged spoils are underlain by soft mud deposits and loose finger and tree corals, extending to depths of about 11 to 18 m below ground surface. Beneath these materials are relatively hard basalt lava flows and boulders, similar to what is observed just inland of the harbor. Settlements have been addressed with constant re-filling, re-paving and limited attempts at densifying the loose fill. As a result, the subsurface, as revealed by our surveying, consists of a complex mix of materials and conditions. A major impetus of this study was to make sense of the subsurface conditions in order to plan for improvements and expansion of the port.

Due to abundant metal structures both above and below ground surface, it was decided to stick with GPR and SR surveying. The methods were similar to those described previously. GPR was conducted with a 400 MHz antenna. The location of the survey lines was selected to address problem settlement areas, while staying clear of obstacles and port operations. Three areas of interest were addressed with 7 traverses. GPR was conducted on all the lines shown in Figure 11, while SR was carried out along the “Crossing Line” and line 38.

Area 1 is located adjacent to the inter-island barge loading area and is therefore subjected to heavy loading. Subsidence has been a recurring problem and multiple repairs have been undertaken over the years. However, subsidence continues to take place. Area 2 in front of the warehouse for Pier 2 has not been affected by settlement as badly as Area 2, but some surface deflections were observed to the south. Area 3 is also problematic and has undergone repeated and continuing settlement problems.

An example of GPR surveying is shown in Figure 12 for line 120. A number of features are clearly visible, including engineered (compacted) fill, chaotic zones that suggest a mix of materials and lack of densification, buried reinforced concrete, and utilities. From these records it is also possible to identify the location of the water table and the bedrock. The latter shows up as large concave reflectors at the bottom of the survey and is labeled as “buried structures”. Note that GPR is even able to identify the reinforcement in the buried concrete close to the ground surface at the left end of the top image in Figure 12.

Figure 13 shows a comparison between GPR and SR records for the traverse labeled as “Crossing Line” in Figure 11. This line passes through Areas 1, 2 and 3 (Figure 11) and the results show a comparison between the two modes of surveying along the same alignment. Based in part on these results, a number of problematic areas were identified as A, B and C in Figure 14. They are interpreted to be pockets of loose ground and show up as hummocky, discontinuous reflectors in the GPR record, and as low-velocity zones in the SR profile. Areas D and E were identified in a similar manner from the other GPR and SR profiles.

In summary, experience with surveying at Hilo Harbor leads to the same findings as for Kawaihae Harbor, i.e. geophysical surveying in sandy and gravelly loose calcareous fills is accomplished most effectively with GPR, especially when using a mid-range frequency antenna on the order of 400MHz. This provides an optimum combination of resolution and penetration for near-surface investigations. SR surveying is also relatively effective, but more time consuming and therefore more intrusive from a port operations point of view

This approach, combining two geophysical techniques, turned out to be an effective method to identify problematic areas where unfavorable subsurface conditions lead to subsidence problems. These areas are in agreement with locations that port personnel had indeed identified as a concern.

Laboratory Testing of Soil Velocities

Identification of objects in the trenches focused on identifying the station of each one. The lack of effective ground truths and soil velocities made determining the depths of objects virtually impossible. It was decided to focus further efforts on determining shear wave velocities in soil by means of laboratory bender element tests with the objective to provide the necessary data to make better depth predictions in the future. Testing consisted of preparing specimens of representative soil in confining rings and subjecting them to increasing vertical loads and measuring shear wave velocity with bender elements installed in the top and bottom caps. Typical results are shown in Figure 15. As expected, shear velocity increases with normal stress (or depth of burial). Also, velocities for the sand are higher than those for the silt. Given the velocity values, travel times measured in the field can thus be converted into more accurate depths.

Recommendations for Future Work

GPR testing at Hilo Harbor proved to be very useful in diagnosing subsurface conditions and clarifying the reasons for the continuing subsidence problems there. We were able to identify not only low-density areas, but also buried concrete structures, areas of engineered (compacted) versus non-engineered fill, and the location of the bedrock and even the water table. With additional surveying, it would be possible to construct a clearer three-dimensional view of the entire harbor that would be very useful to those planning the future of the facility. The same could be done for other harbors in Hawaii. We therefore recommend that GPR surveying, and possibly SR surveying as well, be expanded in order to map what are often poorly understood subsurface conditions at other critical harbor and port facilities in Hawaii.

Acknowledgements

This study was made possible by a grant from the Hawaii Department of Transportation and the Federal Highway Administration. Their support is gratefully acknowledged. The author also wishes to thank Arnold Liu for his guidance and advice during the project.

Students and Theses

A number of students contributed to the project at various times and were supported partially with funds from the research grant. Their work included field and laboratory testing, analysis, and preparation of the findings. The following students made significant contributions:

Frank Cioffi: Mr. Cioffi participated in planning for the experiments and assisted with the field work at the three sites. The work conducted under this study comprised the bulk of his M.S. thesis project. His M.S. Plan B report is as follows:

Cioffi, F. (2009). Characterization of subsurface conditions at Hilo Harbor using geophysical methods. *M.S. Plan B Report*, Department of Civil & Environmental Engineering, University of Hawaii at Manoa, December 2009.

Alexander Hutchinson: Mr. Cioffi participated in planning for the experiments and assisted with the field work at the three sites. The work conducted under this study comprised the bulk of his M.S. thesis project. His M.S. Plan B report is as follows:

Hutchinson, A. (2008). Characterization of voids by geophysical methods in Hawaiian soils. *M.S. Plan B Report*, Department of Civil & Environmental Engineering, University of Hawaii at Manoa, December 2008.

Atrayee Singha: Mrs. Singha assisted with index property testing and carried out the laboratory shear wave velocity work.

Research Publications

Brandes, H.G. (2013). Effectiveness of geophysical methods in calcareous harbor fills. *32nd International Conference on Ocean, Offshore and Arctic Engineering*, **OMAE2013-10400**, pp. 1-8.

Nicholson, P.G. and Brandes, H.G. (2011). Investigation and identification of subsidence problems in Hilo Harbor, Hawaii, using geophysical methods. *Geo-Frontiers 2011: Advances in Geotechnical Engineering*, ASCE **GTP 211**:2803-2811.

Brandes, H.G. and Nicholson, P.G. (2010). Comparison of geophysical methods for detection of voids and other buried features. *Hawaiian Connections, The Hawaii Local Technical Assistance Program*, **12(1)**:3, 6.

Hoover, R.A. (2008). Geophysical void investigation report. *Dawood Project No. 208044-01*, 255p.

Hoover, R.A. (2008). Port of Hilo geophysical investigation report. *Dawood Project No. 208044-01*, 27p.

In addition, quarterly reports were submitted throughout the duration of the project.

International Conference Presentation

2013 – *Effectiveness of geophysical methods in calcareous fills and other soils*. 32nd
International Conference on Ocean, Offshore and Arctic Engineering, Nantes, France,
June 13.

Table 1. Soil Properties

	Waimanalo	Poamoho	Kawaihae
Index Properties:			
Water Content (%)	36	28	*
Liquid Limit (%)	65	47	NP
Plastic Limit (%)	36	36	NP
Sand (%)			
Fines (%)			
USCS	MH	ML	
Specific Gravity	2.87	2.89	2.90
Mineralogy:			
Quartz (%) <i>SiO₂</i>	2		
Tremolite (%) <i>(Ca,Na)₂₃Mg₅Si₈O₂₂(OH)₂</i>	3		
Anatase (%) <i>TiO₂</i>		7	
Ilmenite (%) <i>FeTiO₃</i>	3		
Pseudobrookite (%) <i>Fe₂TiO₅</i>	3		
Magnetite (%) <i>alpha-Fe₃O₄</i>	20	21	
Hematite (%) <i>alpha-Fe₂O₃</i>	8	14	
Goethite (%) <i>alpha-FeOOH</i>	8	3	
Halloysite (%) <i>Al₂Si₂O₅(OH)₄</i>	47	55	
Kaolinite (%) <i>Al₂Si₂O₅(OH)₄</i>	5		
Montmorillonite (%) <i>Na_{0.3}(Al,Mg)₂Si₄O₁₀(OH)₂·xH₂O</i>	1		
Calcite (%) <i>CaCO₃</i>			10
Aragonite (%) <i>CaCO₃</i>			66
Hi-Mg Calcite (%) <i>(Ca,Mg)CO₃</i>			22
Halite (%) <i>NaCl</i>			2

*Although water content was not measured, sand was damp and water content is estimated to have been about 10 to 20%; NP: Non-plastic

Table 2. Object Identification from GPR records by geophysical survey expert; Kawaihae Harbor field site, line L2, first 30 m of trench.

Object Number	Station (m)	Depth (cm)	Object Type ¹	Object Size ² (cm)	Offset from L2 ³ (cm)	GPR 270 MHz	GPR 400 MHz	GPR 900 MHz	GPR 1500 MHz
1	1.3	163	Block	61x61x61		✓	✓	✓	✓
2	3.3	163	Block	8x30x91	10(R)	✓	✓	✓	✓
3	5.3	150	Block	15x15x61			✓	✓	✓
4	6.8	160	Block	15x15x15	5(R)				✓
5	7.7	150	HDPE pipe	10	15(R)		✓	✓	✓
6	8.7	102	Block	15x15x61	25(L)		✓		✓
7	9.9	122	Block	15x30x91	5(R)	✓	✓		✓
8	11.8	135	PVC pipe	5	23(R)		✓	✓	✓
9	13.0	122	Block	30x30x30	18(L)			✓	✓
10	14.3	122	Steel pipe	5	23(L)				
11	15.2	97	Plastic pipe	10	25(L)		✓	✓	✓
12	16.5	97	HDPE pipe	10	13(L)			✓	✓
13	17.6	89	Block	15x30x61	25(L)		✓	✓	✓
14	19.0	112	Block	8x30x91	23(L)			✓	✓
15	20.8	69	PVC pipe	5	15(L)		✓		✓
16	21.8	97	Block	15x30x91	20(L)		✓	✓	✓
17	23.1	66	Block	30x30x30					
18	23.9	61	Block	15x30x61	8(L)				✓
19	23.9	10	Block	8x15x15					
20	25.4	58	Block	8x30x91	23(R)		✓	✓	✓
21	26.7	38	Block	15x15x30	66(R)		✓		✓
22	27.4	38	PVC pipe	5	61(R)				✓
23	27.5	38	Block	8x15x30	71(L)		✓	✓	✓
24	28.8	38	Block	15x15x15	58(L)				✓
25	28.8	38	Block	8x8x8	38(R)				✓
26	29.8	48	Steel pipe	5					✓

¹Block: Styrofoam; HDPE: High-density polyethylene; Plastic: corrugated drainage pipe; PVC: Polyvinyl chloride

²Block sizes are given as heightxwidthxlength, with width in the direction of the trench; pipe dimensions refer to diameter; all pipes were 61 cm long and were placed perpendicular to direction of trench (see Figure XX).

³Where indicated, refers to position offset relative to center line L2: L-left and R-right

Table 3. Object identification from GPR records

	Number of Buried Objects	Total Objects Identified (%)	Over-Picks (%)	Smallest Block Identified (in)
Kawaihae				
L0-270*	41	17	5	6x6x12
L0-900	41	68	27	3x3x3
L2-270	41	7	2	3x12x36
L2-900	41	51	27	3x3x3
L4-900	41	54	7	3x6x6
Averages		40	14	
Waimanalo				
L0-270	40	25	3	6x6x6
L0-400	40	38	5	6x6x12
L0-900	40	65	10	3x6x6
L0-1500	40	70	65	3x6x6
L2-270	40	20	18	6x6x12
L2-400	40	63	23	3x3x3
L2-900	40	65	8	3x3x3
L2-1500	40	70	70	3x3x3
L4-270	40	18	8	6x6x24
L4-400	40	48	10	3x6x6
L4-900	40	53	25	6x6x6
L4-1500	40	55	48	3x6x6
Averages		49	24	

Table 3 (continued). Object identification from GPR records

	Number of Buried Objects	Total Objects Identified (%)	Over- Picks (%)	Smallest Block Identified (in)
Poamoho				
L0-270	39	26	3	6x6x6
L0-400	39	44	5	6x6x6
L0-900	39	59	26	3x3x3
L2-270	39	26	21	2x12x12
L2-400	39	67	15	3x3x3
L2-900	39	67	33	3x3x3
L4-270	39	36	15	3x6x12
L4-400	39	54	18	3x3x3
L4-900	39	59	21	3x3x3
Averages		48	17	

Table 4. Object identification from EM surveys

		Number of Buried Objects	Total Objects Identified (%)	Over- Picks (%)	Smallest Block Identified (in)
Kawaihae					
	EM38:Raw				
	L0	41	7	0	6x6x12
	L2	41	5	2	6x6x24
	L4	41	2	0	24x24x24
	Averages		5	1	
Waimanalo					
	EM38:Raw				
	L2	40	3	0	*
	L4	40	3	0	*
	Averages		3	0	
	EM Model				
	L0	40	18	8	6x6x24
	L2	40	38	28	6x6x6
	L4	40	23	5	6x6x24
	Averages		26	13	
Poamoho					
	EM38:Raw				
	L2	39	5	0	6x6x24
	L4	39	8	0	6x12x36
	Averages		6	0	

*Only pipe-type objects were identified; EM modeling for Kawaihae and Poamoho did not reveal any features associated with buried objects

Table 5. Object identification from seismic refraction surveys

		Number of Buried Objects	Total Objects Identified (%)	Over- Picks (%)	Smallest Block Identified (in)
Kawaihae					
	L0	41	29	7	6x6x12
	L2	41	20	0	6x6x6
	Averages		24	4	
Waimanalo					
	L2	40	35	0	3x6x12
	L4	40	58	3	6x6x12
	Averages		46	1	
Poamoho					
	L2	39	18	3	6x6x24
	Averages		18	3	

Research Article: Brandes, H.G. (2013)

EFFECTIVENESS OF GEOPHYSICAL METHODS IN CALCAREOUS HARBOR FILLS

Horst G. Brandes
University of Hawaii
Department of Civil & Environmental Engineering
Honolulu, HI 96822, USA
E:mail: horst@hawaii.edu

ABSTRACT

The effectiveness of electromagnetic (EM), ground penetrating radar (GPR) and seismic refraction (SR) were evaluated by surveying a shallow trench in which a number of objects of varying composition and size were buried. The trench was excavated in granular calcareous fill material. An experienced geophysical contractor was asked to provide blind predictions of object locations using each of the techniques in turn. GPR with a 400 MHz antenna was the most successful, followed by SR and EM surveying. GPR and SR were also carried out at the port of Hilo to investigate complex subsurface conditions.

BACKGROUND

The Island of Hawaii has two major port facilities. Hilo Harbor serves the eastern half of the island, while Kawaihae Harbor, located on the Kohala coast, serves the western half (Figure 1). Both facilities were constructed in the early 1900s using similar hydraulic techniques. In other words, nearby calcareous marine sediments were dredged and deposited behind retaining structures that were placed beyond the shoreline in order to gain land for port operations. Construction techniques in those days were rather rudimentary and consisted of little more than scooping up the wet offshore sediments and dumping them as a loose fill until the grade in the reclaimed land would reach above sea level. Little effort was expended on densifying the fill materials after placement.

It is then no surprise that serious problems have occurred over the years due to significant settlements from ever heavier cargo-handling equipment, and as a result of densification from machinery vibrations, earthquakes, and vessel loads. In 2006, a 6.7-magnitude earthquake located only a few kilometers from Kawaihae Harbor caused extensive damage to the port facilities

there, including substantial liquefaction and settlement in the calcareous fill materials, lateral shifting and structural damage to one of the pile-supported piers, extensive damage to fuel unloading systems, and much more (Brandes et al., 2007). As a result, the harbor was closed for a period of several months, severely disrupting the flow of goods and services. The port had to undergo repairs worth tens of millions of US Dollars (Robertson et al., 2006).

Numerous improvements took place at both facilities over the years to accommodate port expansion and heavier traffic. Various foundation and retaining structures were constructed and sometimes abandoned and buried over the years. A complex network of underground utilities makes assessment of conditions very difficult.

There is also an unfortunate lack of documentation to assess the subsurface conditions at either harbor now that there is a new commitment on the part of the State of Hawaii to upgrade the two ports for improved and expanded use. Conventional investigation methods that rely on subsurface borings or other invasive techniques are not suitable due to heavy use of the facilities and the danger of causing damage to buried structures and utilities. As a result, non-invasive geophysical probing has been undertaken, or is being considered. The objective of this study was to assess which geophysical technique would be most suitable in this case, given that little is known about how well these techniques work for calcareous materials in the presence of a shallow marine water table.

Here we discuss the results of a research project that compared the effectiveness of Ground Penetrating Radar (GPR) surveying operating at various frequencies, Electro-Magnetic (EM) surveying, and Seismic Refraction (SR) surveying. Field comparisons were carried out at a test site at Kawaihae Harbor, and the findings were extended to a survey of Hawaii Harbor

aimed at identifying subsurface conditions there that may be responsible for the extensive subsidence that has taken place in the calcareous fill.

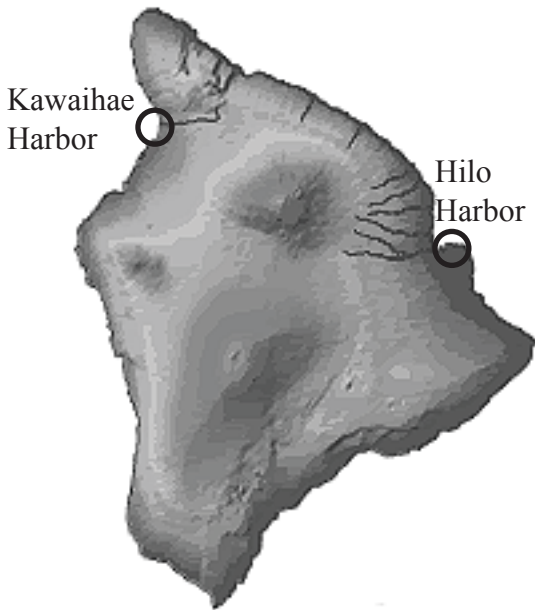


Figure 1. Location of two principal ports on Hawaii Island

KAWAIHAE HARBOR

Figure 2 shows the harbor from above. The light-colored calcareous fill areas are clearly visible, especially in contrast to the adjacent volcanic rock and soil deposits that are much darker in color. The dredged sand and gravel fill consists of the remains of coral reef, calcareous algae, mollusks, and other organisms with calcareous skeletons or shells. Index properties are summarized in Table 1 and the gradation of the material is indicated in Figure 3.

Field work consisted of burying a series of Styrofoam blocks and other objects within a shallow trench and then attempting to identify them through GPR, EM and SR surveying. The trench was excavated close to the shoreline (Figures 2 and 4). It measured 45 meters in length, 2.5 meters in width and up to 3 meters in depth. The water table was encountered at the bottom of the trench, i.e. about 3 meters below ground. The sand above the water table was slightly moist (water contents in the range of 5 to 12%). Styrofoam was selected because of its high density contrast with the surrounding soil, in hopes that it would provide a strong target for detection with the selected geophysical techniques.

A total of 41 objects were placed at various locations and depths along the length of the trench. Following their careful placement, the trench was backfilled to the original grade. The

backfill was compacted a modest amount at the in situ moisture content with jack hammers and the shovel on the excavator machine. The objective was to attain a final density similar to the initial one.



Figure 2. Kawaihae Harbor and location of trench test site

Surveying was carried out by an outside geophysical contractor, who was asked to provide blind predictions based solely on geophysical measurements and data interpretation and modeling. He was not present during burial operations and was only provided with minimum and maximum object sizes and types, as well as the dimensions and alignment of the trench. He was further instructed to consider the results of each technique independently from the others.

Table 1. Properties of Kawaihae Harbor Calcareous Fill

Index Properties	
Liquid limit, %	Non-Plastic
Plastic limit, %	Non-Plastic
Gravel	48%
Sand	45%
Fines	7%
USCS	GW-GM
Specific Gravity	2.90
Mineralogy	
Calcite	10%
Aragonite	66%
Hi-Mg Calcite	22%
Halite	2%

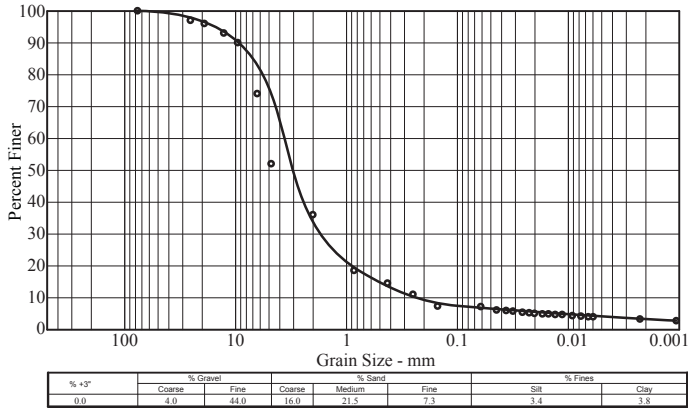


Figure 3. Gradation of Kawaihae Harbor calcareous fill



Figure 4. Burial of objects in Kawaihae Harbor trench

GPR uses electromagnetic (radar) energy that is transmitted into the ground from the surface in discrete pulses. Transmission and reflection through the subsurface are sensitive to the electrical properties of the medium. Echoes or reflections from interfaces between materials with differing dielectric properties, such as buried objects or layers with a sharp contrast, can be detected by antenna tuned to various frequencies. As surveying proceeds along a given traverse, cross-sectional images can be assembled and displayed in real time. An experienced surveyor can pick out specific anomalies from the raw or the processed data and infer the nature and size of the anomalies. GPR is most effective in identifying concrete, fiberglass and plastic structures. Depending on the dielectric properties and contrast offered with the overlying soil, GPR may also be effective in identifying soil-bedrock, soil-air, bedrock-air, and dry-saturated soil interfaces. Styrofoam blocks, plastic pipes and steel pipes were selected as targets because they were expected to provide a good contrast with the surrounding soil.

The dielectric permittivity and electrical conductivity of the soils and the frequency of the radar energy control the depth of signal penetration. In highly conductive materials, such as moist clays, the pulse is dissipated at very shallow depths (sometimes on the order of centimeters). Using a transmission antenna with a low frequency can improve penetration, but at a loss in resolution. Frequencies commonly employed are in the range of 80 to 1500 MHz. In this study we used interchangeable antenna with frequencies of 270, 400, 900 and 1500 MHz. In general, the use of GPR is limited to depths of 5 meters or less.

GPR data was collected along the length of the trench by surveying with each of the antenna (Figure 5). Positioning was maintained by using a string line stretched along the axis of the trench. A dielectric constant of 6.0 was used to estimated depths to features identified in the GPR records. This constant was developed based on general soil conditions and could not be corroborated in the field due to the lack of a reliable ground truth target at the site. The data was recorded digitally and processed using the software RADAN. This involved applying time shift corrections, a high-pass filter to remove background noise, and gain controls to yield a clear view of the return pulses. The software was also used to aid in the interpretation of potential buried features

The geophysical surveyor prepared tables of individual targets that he could discern, along with depths and locations along the traverse. It should be pointed out that the surveyor was highly experienced in this type of work and therefore the findings below assume a significant level of expertise in GPR surveying.



Figure 5. GPR surveying; antenna is visible at bottom of stroller

EM surveying was carried out along the same trench using a hand-held device (Figure 6). This method involves measurement of the electric and magnetic properties of the subsurface. These are dependent upon the density, porosity, moisture content, and the presence of electrolytes or colloids in the soil or rock materials. Typically, soils have a high conductivity and bedrock has low conductivity.

EM terrain conductivity instruments use a small transmitter coil through which an alternating current is passed to induce a time-varying magnetic field. The instrument is held on or close to the ground so that this magnetic field produces a current in the ground. In turn, this current generates a secondary magnetic field, also in the ground. Both magnetic fields are sensed by a receiver coil. The ratio of the secondary magnetic field, relative to the primary one, is the conductivity of the subsurface soil or rock. Similarly, the phase ratio between the primary and secondary magnetic fields is related to magnetic susceptibility and is typically referred to as the in-phase measurement. The actual magnitude of conductivity values is not always indicative of a specific soil or rock type. Trends as well as irregularities in the measurements are usually relied on to produce a qualitative interpretation of the data. Thus a high degree of experience is necessary for successful interpretation and evaluation of electromagnetic data.



Figure 6. EM38 conductivity meter with dipole in vertical orientation

EM data was collected with a Geonics EM38-RT conductivity meter (Figure 6). Data was collected at each measurement station with horizontal and vertical dipole orientations. These measurements were repeated every 15 cm along the traverse. A vertical dipole time test was also conducted at the field site to evaluate electromagnetic variability. The results indicated very little fluctuation, with confidence of 98.6% and 99.0% in in-phase and quadrature phase measurements, respectively.

Seismic data was collected using a U-shaped land streamer (Figure 7). This streamer included two parallel lines of twelve 100-Hz geophones mounted on two strips of fabric to maintain a constant 0.3 meter (1 foot) in-line distance between adjacent geophones. Energy was imparted into the ground by lowering a 1.5-kg (3-pound) hammer on a steel plate. The energy imparted traveled into the subsurface and reflected and refracted wherever a seismic velocity contrast was encountered, such as soil and rock interfaces, cavities, utilities, or other velocity anomalies. A seismograph measured the time, from energy transmission to energy reception at the geophone, which is a known distance from the source. From travel time and distance, the velocity of the subsurface could be determined. With the streamer at a given location, energy sources were imparted at various stations along the length of the geophone spread, in between the strips on which the geophones were mounted (Figure 7). Thereafter, the streamer was advanced one full spread and measurements were repeated in a similar manner. Multiple hammer blows were used to enhance the data.



Figure 7. SR surveying with closely spaced geophone streamer

The program Rayfract was used to analyze the refraction data. It allows the interpreter to pick first-energy breaks in the data, and to map these to refractors either manually or semi-automatically, based upon common mid-point velocities. Seismic energy travel time was processed on a per-refractor basis using a Delta-t-V pseudo 2D turning ray inversion technique (Dawood, 2008). The outcome is a continuous one-dimensional depth versus velocity profile for all profile stations. This allows identification of systematic velocity increases and strong velocity anomalies, such as those expected in connection with the Styrofoam and other buried objects. Prior to processing with Rayfract, the data from each of the 24 geophones was evaluated for noise content and was filtered

and/or gained, as necessary, to highlight energy associated with the seismic source.

As previously mentioned, 41 objects were buried in the trench at depths ranging from a few centimeters to as much as 1.6 meters. These objects consisted of 30 Styrofoam blocks ranging in size from 7.6x7.6x7.6 cm (3x3x3 in) to 61x61x61 cm (24x24x24 in), as well as 4 HDPE pipe sections 10.2 cm (4 in) in diameter, 4 PVC pipe sections 5.1 cm (2 in) in diameter, 2 steel pipes 5.1 cm (2 inches) in diameter, and 1 corrugated plastic pipe 10.2 cm (4 inches) in diameter. The pipes were 61 cm long and they were placed perpendicular to the axis of the trench.

The surveyor provided lists of “picks”, i.e. the location along the traverse where he identified objects, using each of the three geophysical techniques in turn. Although he also provided depths in some cases, these interpretations were quite off the mark due to the lack of effective ground truth targets in or near the trench. Thus here we focus on the success rate of these picks while disregarding depth of burial. The picks provided by the surveyor were compared to our inventory list.

A summary of the findings is shown in Table 2. As expected, some of the objects were identified correctly and some were missed. In addition, some picks did not correspond to any specific object and are listed as “over-picks”.

Table 2. Blind object identification rate of success

	Number of Objects	Total Objects Identified (%)	Over-Picks (%)	Smallest Block Identified (in x in x in)
GPR-270 ¹	41	7	2	3x12x36
GPR-900	41	51	27	3x3x3
EM38 Raw	41	5	2	6x6x24
SR	41	20	0	6x6x6

¹Numeric value refers to antenna frequency in MHz

Clearly, GPR with the 900 MHz antenna was the most successful technique. It was able to identify Styrofoam cubes as small as 7.6 cm in size at a depth of 38 cm. About half of all the objects in the trench were identified correctly. On the other hand, this method also produced 27% of over-picks. GPR with the 270 MHz antenna was significantly less successful. This is a reminder that selection of an appropriate frequency is crucial. Of course, the optimum frequency will depend on the specific project conditions.

SR was the second most successful technique, with 20% of objects correctly identified and no over-picks. It should be noted that seismic refraction is usually conducted with geophones spaced further apart and larger energy sources in order to attain deeper penetration. While the success rate is not very high, this technique does have limited appeal for applications involving the identification of small objects at shallow depths. It should be mentioned though that seismic refraction is more time consuming to carry out in the field, at least in comparison to GPR surveying.

EM surveying was the least successful method. Inspection of the raw data led to the identification of only rather large objects, and not that many. An attempt was made to model the EM data using the program EMIGMA, but this proved to be unsuccessful. Modeling worked better for similar survey results obtained from similar field testing at another test site on the Island of Oahu. It is not clear why that is the case.

HILO HARBOR

Hilo Harbor is the larger of the two port facilities on the island of Hawaii. It provides a range of maritime facilities and services and is the major distribution center for the island. Both overseas and inter-island ships and barges make regular calls, as well as large passenger cruise ships. Construction of the port began in 1914. This involved offshore dredging and construction of docking piers (Piers 1, 2 and 3) and a 3,000-meter long breakwater (Figure 8). The three piers consist of reinforced concrete decking supported on concrete piles located beyond the original shoreline in deeper water. Sheet piling was driven into the seabed adjacent to the piers and the area behind the piling was backfilled with loose dredge spoils from deepening of the navigation channel. A succession of pavements and other structural supports were added in the backfill area in order to accommodate port operations and transportation facilities. The fill materials are broadly similar to those at the Kawaihae Harbor and consist of coralline sands and gravels.



Figure 8. Aerial view of Hilo Harbor

Settlement in the filled areas has been a persistent problem almost since initial construction of the port (Figure 9). The reason for this is clear from boring logs that indicate very loose calcareous fill with SPT values as low as 1 and 2. These dredged spoils are underlain by soft mud deposits and loose finger and tree corals extending to depths of about 11 to 18 m below the existing surface (Geolabs, 1999, 2002, 2006). Beneath these materials are relatively hard basalt lava flows and boulders similar to what is observed at ground surface further inland from the harbor. Settlements have been addressed with constant re-filling, re-paving and limited attempts at densifying the loose fill. As a result, the subsurface, as revealed by our surveying, consists of a complex mix of materials and conditions. A major impetus of this study was to make sense of the subsurface conditions in order to plan for improvements and expansion of the port (Nicholson and Brandes, 2011; Cioffi, 2009).



Figure 9. SR surveying at Hilo Harbor (note settlement depressions in asphalt pavement)

Due to abundant metal structures both above and below ground surface, it was decided to stick with GPR and SR surveying. The methods were similar to those described previously. GPR was conducted with a 400 MHz antenna. The location of the survey lines was selected to address problem settlement areas, while staying clear of obstacles and port operations. Three areas of interest were addressed with 7 traverses. GPR was conducted on all the lines shown in Figure 10, while SR was carried out along the “Crossing Line” and line 38.

Area 1 is located adjacent to the inter-island barge loading area and is therefore subjected to heavy loading. Subsidence has been a recurring problem and multiple repairs have been undertaken over the years. However, subsidence continues to take place. Area 2 in front of the warehouse for Pier 2 has not been affected by settlement as badly as Area 2, but some surface deflections were observed to the south. Area 3 is also

problematic and has undergone repeated and continuing settlement problems.

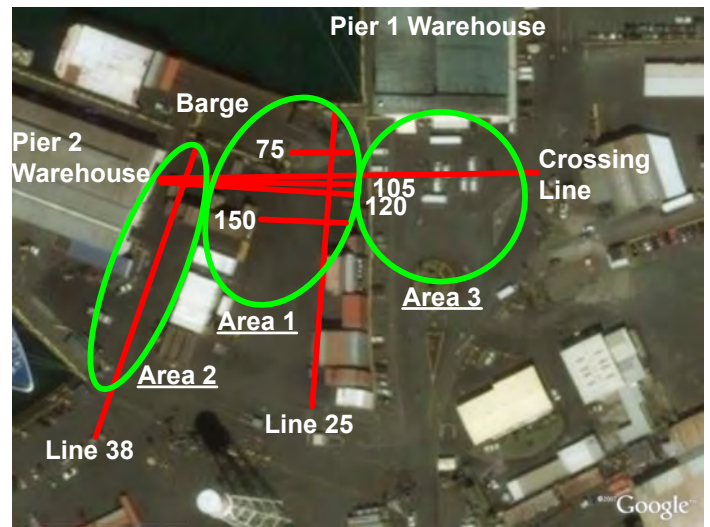


Figure 10. Survey traverses at Hilo Harbor.

An example of GPR surveying is shown in Figure 11 for line 120. A number of features are clearly visible, including engineered (compacted) fill, chaotic zones that suggest a mix of materials and lack of densification, buried reinforced concrete, and utilities. From these records it is also possible to identify the location of the water table and the bedrock. The latter shows up as large concave reflectors at the bottom of the survey and is labeled as “buried structures”. Note that GPR is even able to identify the reinforcement in the buried concrete close to the ground surface at the left end of the top image in Figure 11.

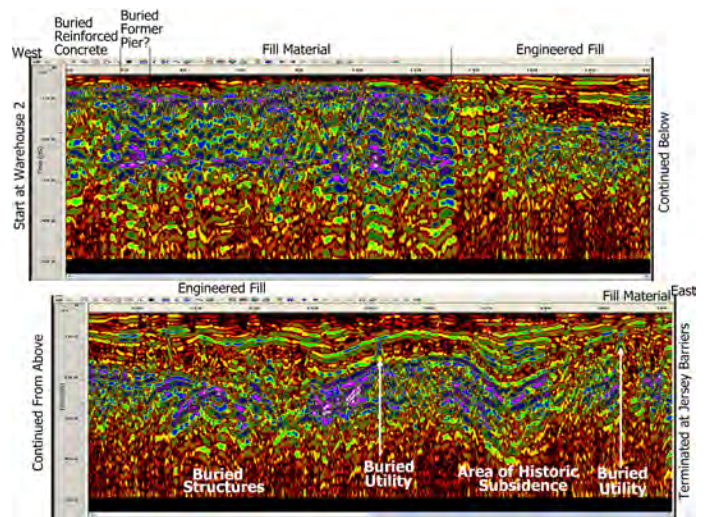


Figure 11. GPR data profile along line 120 and subsurface interpretations

Figure 12 shows a comparison between GPR and SR records for the traverse labeled as “Crossing Line” in Figure 10. This line passes through Areas 1, 2 and 3 (Figure 10) and the results show a comparison between the two modes of surveying along the same alignment. Based in part on these results, a number of problematic areas were identified as A, B and C in Figure 13. They are interpreted to be pockets of loose ground and show up as hummocky, discontinuous reflectors in the GPR record, and as low-velocity zones in the SR profile. Areas D and E were identified in a similar manner from the other GPR and SR profiles.

In summary, experience with surveying at Hilo Harbor leads to the same findings as for Kawaihae Harbor, i.e. geophysical surveying in sandy and gravelly loose calcareous fills is accomplished most effectively with GPR, especially when using a mid-range frequency on the order of 400MHz. This provides optimum combination of resolution and penetration for near-surface investigations. SR surveying is also relatively effective, but more time consuming and therefore intrusive from a port operations point of view.

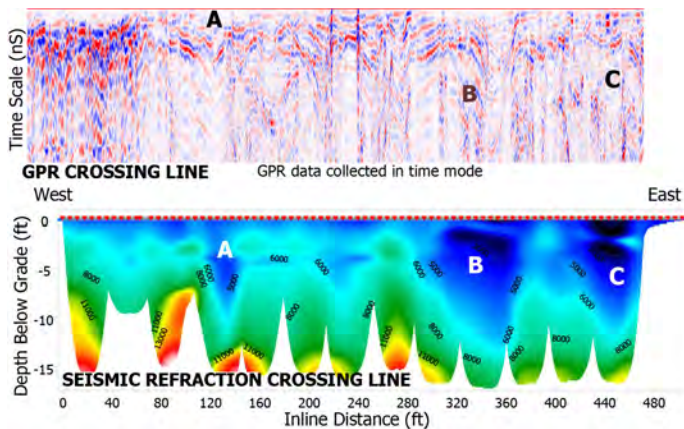


Figure 12. Comparison of GPR (top) and SR (bottom) surveys along Crossing Line

This approach, combining two geophysical techniques, turned out to be an effective method to identify problematic areas where unfavorable subsurface conditions lead to subsidence problems. These areas are in agreement with locations that port personnel had indeed identified as a concern.

CONCLUSIONS

EM, GPR and SR methods of surveying were carried out on similar loose sandy and gravelly calcareous fills. These materials have not been the subject of extensive geophysical surveying in the past. Their success rate has not been

compared in a systematic manner for these types of materials, as was carried in this study out at the Kawaihae Harbor test site. To accomplish this, a trench was excavated in fill material and a number of objects were buried for blind detection with EM, GPR and SR surveying. An expert in geophysical field methods was asked to survey the trench and identify the location of the buried objects without knowing their precise location or depth. These predictions were compared to actual burial locations in order to determine success rates for each technique. Such information is of importance when contemplating to use these methods under similar conditions where the subsurface conditions are unknown, as was the case at Hilo Harbor.

The results indicate that GPR with a medium frequency antenna on the order of 400 MHz is the most successful technique for finding discrete objects as small as 8 cm buried in less than 1 m of calcareous soil. About 50% of the buried objects were detected. Although this may not sound very impressive, it should be noted that the experiment did include objects this small located at greater depths that were purposely made more difficult to detect. In comparison to GPR, SR was less successful in identifying objects (20% of objects were detected), but it was able to delineate areas of low velocity and this may be useful in detecting the presence of loose soils. This was clearly the case for Hilo Harbor. EM appears to be the least useful technique for these types of applications, especially in crowded port areas where there may be significant numbers of metal structures that affect data collection. Even where such structures are absent, such as at the Kawaihae test site, EM was rather unsuccessful in identifying discrete buried objects. It was able to detect only 5% of the objects buried in the trench, and only the largest of these at best.

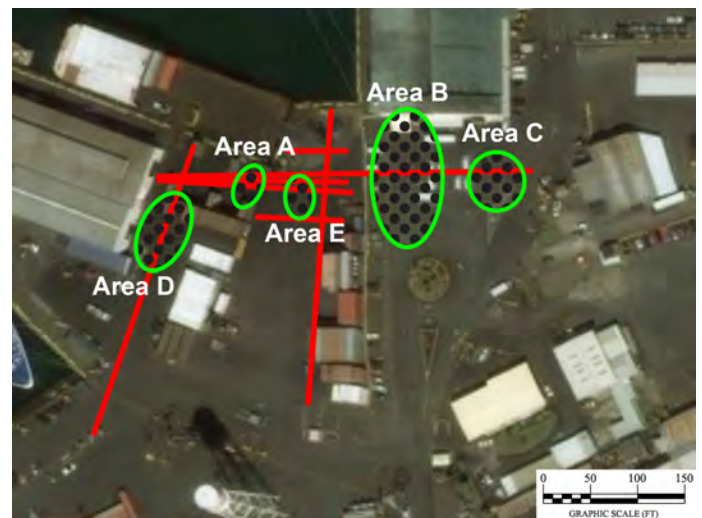


Figure 13. Locations of problematic subsurface conditions as determined from geophysical surveys

ACKNOWLEDGEMENTS

The author wishes to thank Rick Hoover of Dawood for carrying out the geophysical surveys. Many thanks also to graduate students Frank Cioffi and Alexander Hutchinson for assistance during the field work. This study was supported in part by a grant from the U.S. Federal Highway Administration and the Hawaii Department of Transportation. Their support is gratefully acknowledged.

REFERENCES

- Brandes, H.G., Nicholson, P.G. and Robertson, I. (2007). Liquefaction of Kawaihae Harbor and other effects of 2006 Hawaii earthquakes. *17th International Offshore and Polar Engineering Conference*, 2:1169-1176
- Cioffi, F. (2009). Characterization of subsurface conditions at Hilo Harbor using geophysical methods. *M.S. Plan B Report*, Department of Civil & Environmental Engineering, University of Hawaii at Manoa, December 2009.
- Dawood (2008). University of Hawaii at Manoa geophysical void investigation report. *Technical Report* prepared for Department of Civil & Environmental Engineering, University of Hawaii, Honolulu, HI, 61 pages.
- Geolabs (1999). Geotechnical Engineering Exploration Pier 1 Shed Office, Hilo Harbor, Island of Hawaii. *Technical Report*, August 10, 1999.
- Geolabs (2002). Geotechnical Engineering Exploration Pier 3, Breasting Dolphins and Catwalks Hilo Harbor, Island of Hawaii. *Technical Report*, April 19, 2002.
- Geolabs (2006). Geotechnical Engineering Exploration Inter-Island Cargo Terminal Facility, Phase 1 Dredging, Hilo Harbor, Island of Hawaii. *Technical Report*, August 25, 2006.
- Nicholson, P.G. and Brandes, H.G. (2011). Investigation and identification of subsidence problems in Hilo Harbor, Hawaii, using geophysical methods. *Geo-Frontiers 2011: Advances in Geotechnical Engineering*, ASCE **GTP 211**:2803-2811.
- Robertson, I.N., Nicholson, P.G. and Brandes, H.G. (2006). Reconnaissance following the October 15th, 2006 earthquakes on the Island of Hawaii. *Research Report UHM/CEE/06-07*, October 26, 2006.

Research Article: Nicholson, P.G. and Brandes, H.G. (2011)

Investigation and Identification of Subsidence Problems at Hilo Harbor, Hawaii Using Geophysical Methods

Peter G. Nicholson¹, Ph.D., P.E., D.GE, F.ASCE
Horst G Brandes², Ph.D., P.E., M.ASCE

¹University of Hawaii at Manoa, Department of Civil and Environmental Engineering, 2540 Dole Street, Honolulu, HI 96822; PH (808) 956-2378; FAX (808) 956-5014; email: pnichols@hawaii.edu

²University of Hawaii at Manoa, Department of Civil and Environmental Engineering, 2540 Dole Street, Honolulu, HI 96822; PH (808) 956-8969; FAX (808) 956-5014; email: horst@hawaii.edu

ABSTRACT

A geophysical survey was conducted of Hilo Harbor where persistent subsidence problems have been reported. The purpose was to identify subsurface conditions that may be causing the problems. Ground penetrating radar and seismic refraction/reflection with closely spaced geophones were conducted above fill areas that have been settling for nearly 100 years. The results confirm a very non-uniform subsurface with buried concrete structures, loose fill, and areas that have been remedied in the past. Major areas of subsidence are seen to correspond with concave reflectors in GPR profiles and low-velocity zones in refraction profiles. Previous borings suggest that these are zones of very low density with the granular fill settling as a result of ever-heavier cargo machinery and associated vibration from traffic and ships.

BACKGROUND AND PURPOSE OF STUDY

The port facility at Hilo Harbor on the Island of Hawaii (Figure 1) is the larger of the two main commercial ports that service the island. Hilo Harbor provides a wide range of maritime facilities and services and is the major distribution center for the Big Island. Both overseas and inter-island ships and barges make regular calls at Hilo Harbor, in addition to passenger cruise ships. The paved shipping offloading yards and adjacent heavily used traffic access to the cruise ship terminal have a long history of problematic subsidence and differential settlement that has hindered the operations of the facility over a substantial areal extent. The ensuing damage has cost more than 1 million dollars over the past ten years. Earlier hypotheses as to the origins of these problems have included sinkholes, lava tubes or other subsurface voids, and internal erosion. Previous studies typically included limited invasive and costly soil borings followed by recommended remedial work. These have proved to be only partially successful in remediating the problems.

Concerned with the continued subsidence and pavement distress at the facility, the Hawaii Department of Transportation commissioned a study to identify possible subsurface voids or other features that could explain the on-going problems at the harbor. A study was undertaken utilizing a variety of non-destructive

geophysical methods to investigate the subsurface at Hilo Harbor in an attempt to identify and understand the underlying problems causing the ongoing settlement.

HISTORY OF HILO HARBOR

Prior to 1914, large cargo and passenger ships had to be moored in the bay, with freight and passengers ferried to land in smaller vessels. Thus a need for a deepwater facility was envisioned by which ships could unload directly to shore. This required construction of docking piers and dredging of the channel. A 3,000 m (approximately 10,000 foot) long breakwater was also constructed for protection of the port facilities and to create a ‘calm’ harbor for docking. The primary piers (Piers 1, 2 & 3) are structural in nature, in that they are generally reinforced concrete decking supported on concrete piles. By examination of historic and present maps, it was determined that most of the study area (landward of the piers) was constructed of “reclaimed” land adjacent to the pre-existing shoreline from spoils generated from the dredging operations placed over lagoonal deposits and/or coralline detritus (Figure 2). Unfortunately, there appears to be no documentation or records of the fill efforts. A current master plan for the Harbor envisioned for 2020 includes new piers (with increased load capacity), additional roadways, new/additional terminals and more dredging (State of Hawaii, 1998, 2009). It is hoped that persistent settlement problems will be remedied prior to new construction.

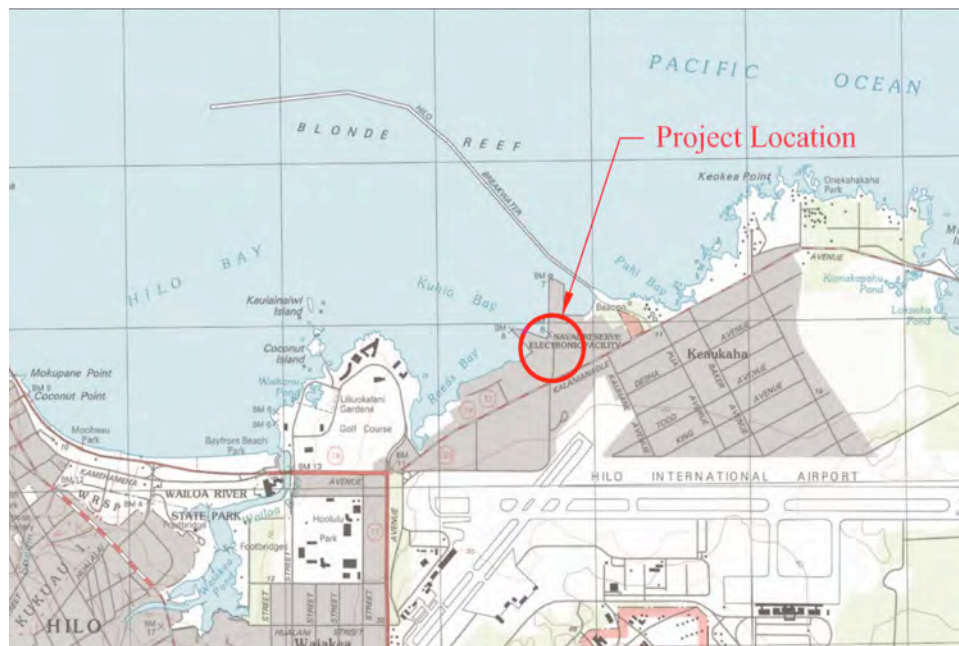


Figure 1 – Hilo Harbor site location



Figure 2 – Project study area and approximate historical shoreline

PREVIOUS INVESTIGATIONS AND REMEDIAL WORK

Differential settlement was addressed in 1990 by pressure grouting of problem areas but this failed to alleviate the settlement. Additional settlement between 1990 and 1998 was reported to range from 2.5 to 8.3 cm (1 to 3.25 inches). Borings drilled in 1999 to investigate the source of the settlement clearly showed pockets of loose to very loose sands with SPT penetration resistance values as low as 1 and 2 blows/30 cm (blows/ft) in sandy, coral gravel from near surface to below the water level in the distressed area (referred to later as Area 3) (Geolabs, 1999). In borings taken from a Board of Harbor Commissioners Drawing dated January 1924, the fill materials described above are underlain by soft mud deposits and loose finger and tree corals extending to depths of about 11 to 18 m (35 to 60 feet) below the existing ground surface. A 2002 investigation also noted very soft and/or loose natural deposits below the fill material towards the western side of the port facility (Geolabs, 2002). Previous investigations indicated that the depth to competent materials is highly variable over the study area (Geolabs, 1999, 2002, 2006).

TESTING PROGRAM

A number of non-invasive geophysical methods were considered for this study (FHWA, 2003), considering that it was desired to investigate a relatively large area relatively quickly without interfering with port operations. Ground-penetrating radar (GPR) and seismic reflection/refraction methods were chosen to define a number of subsurface profiles across the site in an attempt to identify the structure of the subsurface and potential related problems. Electromagnetic surveys were also considered but not utilized at this site because of an abundance of metal structures both above and below ground surface

GPR was performed using a Model SIR-3000 unit manufactured by Geophysical Survey Systems, Inc., with a 400 MHz antenna mounted in a stroller with a laptop computer for data acquisition (Figure 3). This method was very rapid,

advancing at a moderate walking pace. Significant profiles were recorded in two directions so offsets from the start and end of the line could be better estimated. A dielectric constant of 6.0 was used for all sites to estimate depths to features identified in the GPR record during field activities. This constant was developed based on general soil information, and may not be very accurate. As a result, depth estimates could not be estimated with great confidence. No subsurface utilities of known depth could be located that might have been used for calibration purposes.

The seismic refraction survey data was collected with 24 geophones mounted on a land streamer with 0.46-meter (1.5-foot) geophone spacing. This is an unusually close spacing, but necessary due to the relative shallow depth of interest. A 9-kg (20-lb) sledgehammer was used for the compressional seismic survey. Nine equally-spaced source locations were used along each spread, ranging from 1.8m (6ft) in front of the first geophone to 1.8m (6ft) off the last geophone in the receiver stream. The data was digitally recorded for analysis and reduction. The data quality was monitored as it was recorded to ensure adequate information and resolution was available for interpretation. The seismograph used was a Geode seismograph manufactured by Geometrics of San Jose CA. This 24-bit resolution instrument works well in noisy areas permitting deeper investigation with better resolution. The instrument's 14 kHz bandwidth yields a high resolution, which is necessary for detailed surveys such as this one (Dawood, 2008).

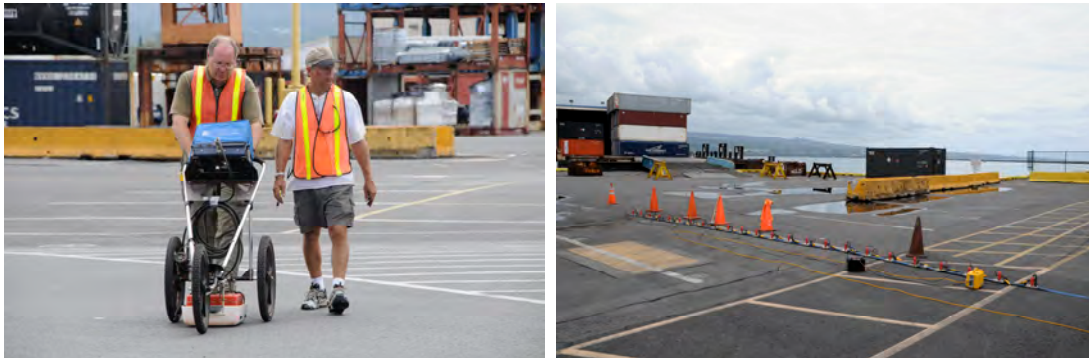


Figure 3 – GPR (left) and seismic refraction/reflection surveying (right) at Hilo Harbor. Subsidence areas are visible where rainwater has ponded.

The location of the surveys and traverses were chosen as a result of a variety of factors, including the harbormaster's indication of problem areas during the investigation, location of obstacles, and non-interference with port operations. Three general areas of interest were identified for examination using the geophysical methods chosen. These areas, labeled Areas 1, 2, and 3 depicted in Figure 4, were the three most prominent areas of historical distress:

Area 1: Barge off-load area – an area subject to heavy loading by equipment, where repairs have been made, but subsidence persists. This zone is located seaward of the original shoreline and therefore is underlain by thick dredge fill deposits.

Area 2: Pier 2 Warehouse – no settlement was identified in front of the warehouse, but settlement was visible to the south.

Area 3: In front of the Pier 1 Warehouse – this area has undergone repeated and continuing settlement problems

Within these areas, a number of survey passes were made with both GPR and seismic refraction/reflection equipment. Individual tracks are shown in red in Figure 4.

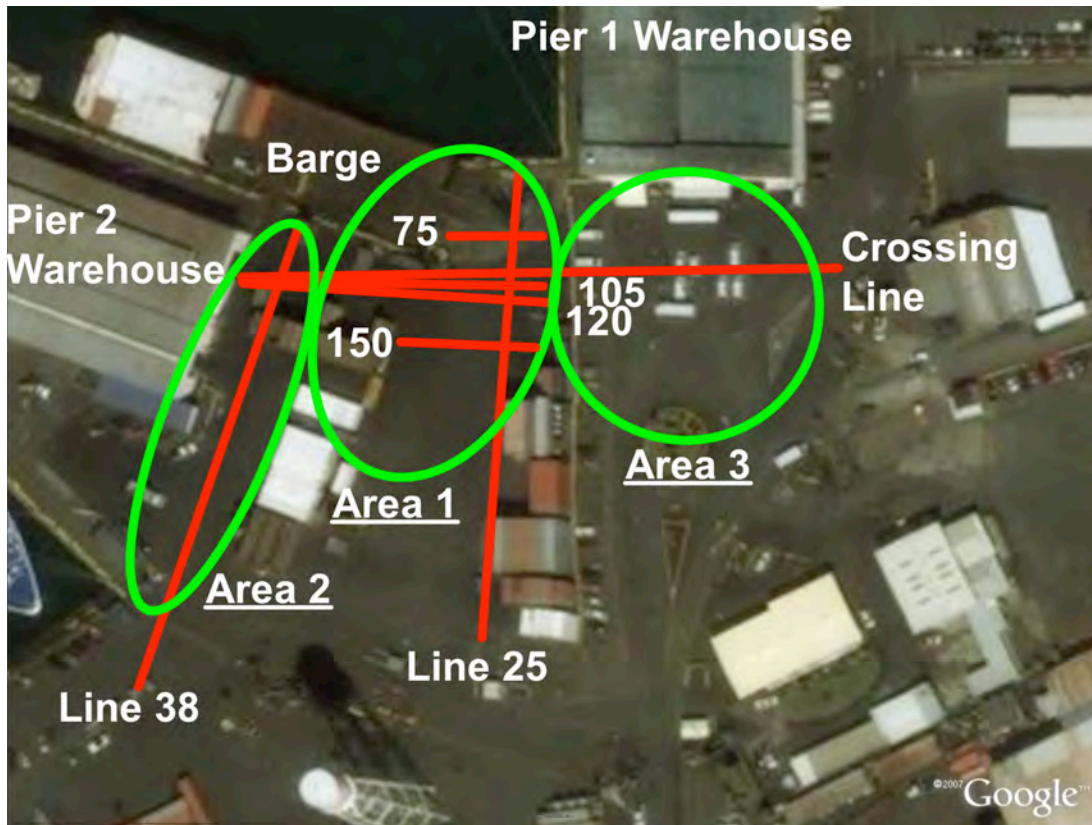


Figure 4 – Study areas of interest and survey traverse locations

RESULTS

An example of the results of GPR testing is depicted in Figure 5. Interpretations of subsurface features are labeled on the figure. A number of the features are clearly evident by distinctive shapes and/or changes in reflector amplitudes (shown by color changes). The results show that the subsurface is anything but uniform in the horizontal or vertical directions. GPR detected areas of engineered fill, chaotic zones that suggest a lack of proper compaction, buried reinforced concrete, utilities, location of the water table, and the elevation of the bedrock. The latter consists of basalt rock that shows up as large purple concave reflectors, labeled 'buried structures'. Also, an area of historic subsidence is evident

between two sets of utilities. Thus GPR surveying provides much relevant detail for evaluating subsurface conditions relating to subsidence.

On the other hand, there is no evidence from any of the GPR records (or the seismic records for that matter) that there are large voids present that may be causing the reported settlement issues. Instead, the problem appears to be one of densification of loose granular fill under ever-heavier cargo operating machinery. Thus both heavy loads and vibration may be causing progressive densification of the loose fill material. This is problematic in the sense that the granular soils may be susceptible to liquefaction and lateral spreading as a result of seismic loading. Hilo is located in a very active seismic region and the port could be damaged considerably if a very large earthquake were to strike. Indeed, the Big Island's other major port facility, Kawaihae Harbor, suffered extensive liquefaction and lateral spreading as a result of the 2006 M6.7 Kiholo Bay earthquake. It is suspected that both harbor have been filled with similar loose dredged sand and gravel.

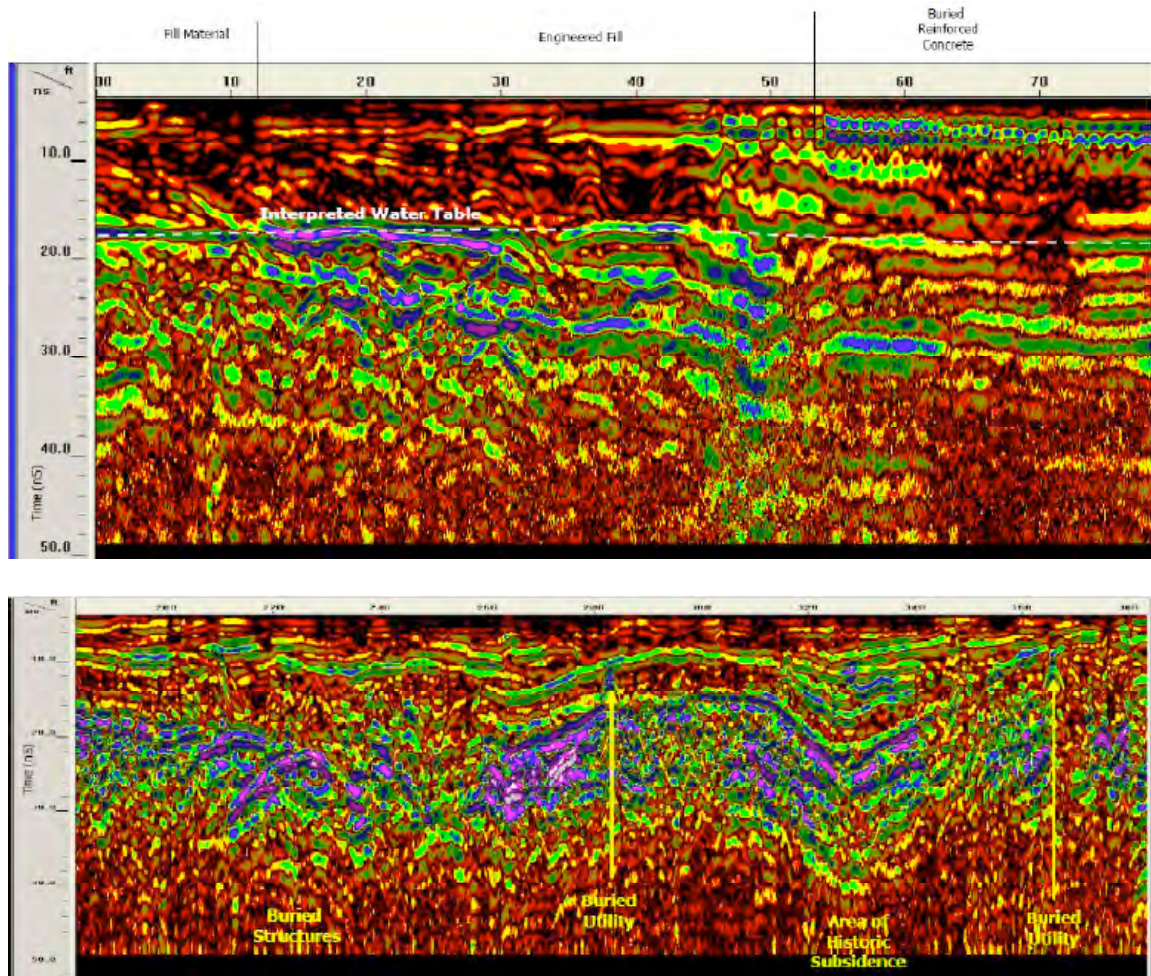


Figure 5 – Example of GPR data profile and subsurface interpretations (Top figure - line 75; bottom figure – line 120)

Figure 6 shows a comparison between GPR and seismic refraction records for the traverse labeled as “crossing line” in Figure 4. The crossing line passes through Areas 1, 2, and 3 and is presented to show a comparison between the two modes of surveying along the same alignment. By comparing the results of the surveys, a number of localized pockets in the subsurface were identified as A, B and C, (Figure 7) and interpreted to be soft/loose ground shown by the GPR as hummocky, discontinuous reflectors and by the seismic data as regions of low velocity (“cooler” blue tones). Other locations of subsurface irregularities (also manifested by surface settlements) were identified by additional survey traverses (e.g., areas D and E).

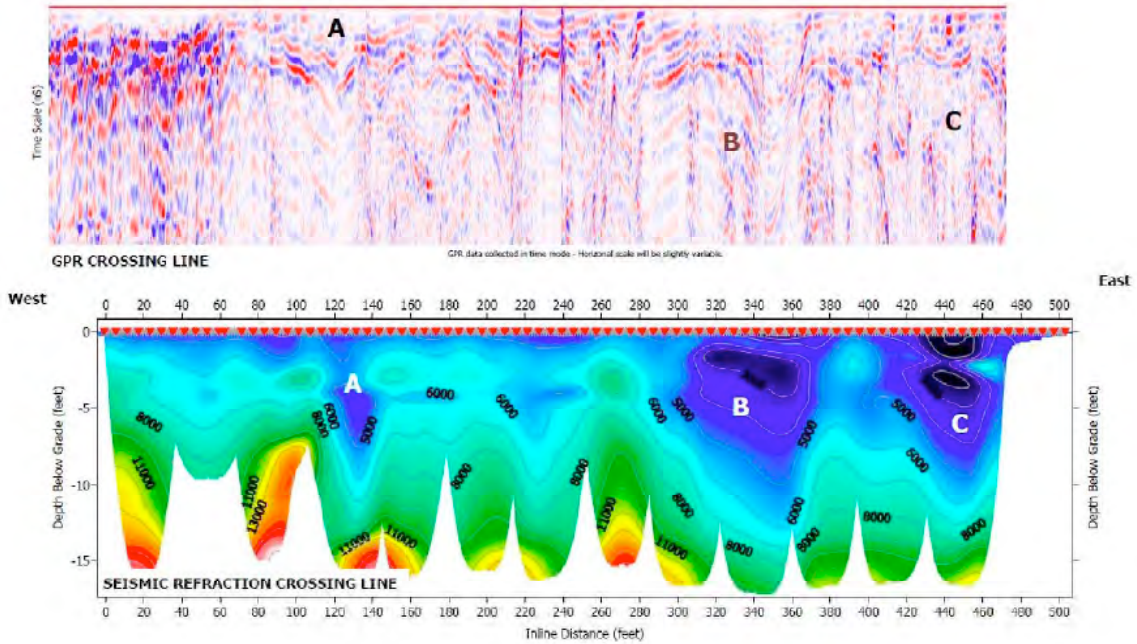


Figure 6 – Comparison of GPR (top) and seismic refraction data (bottom) for crossing line in figure 4

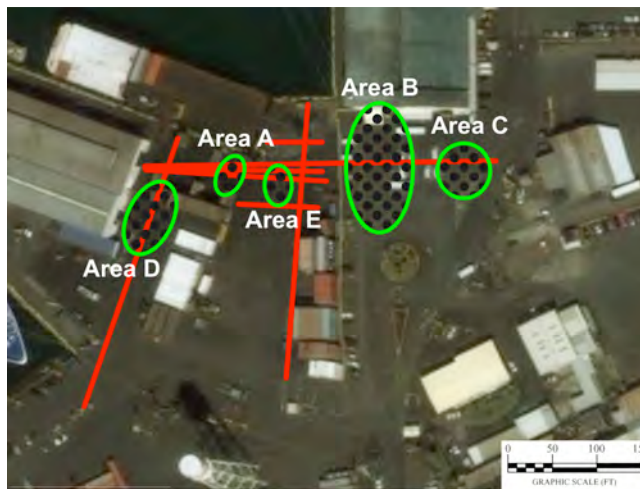


Figure 7 – Locations of soft/weak/irregular subsurface soils identified by the surveys

CONCLUSIONS

Results of the fieldwork completed over a two-day period did not detect any subsurface voids, but clearly identified areas of soft/loose material (identified by low shear wave velocity from seismic tests) and regions interpreted to be irregular, non-engineered fill (shown by GPR as hummocky, discontinuous reflectors) prevalent in all areas described as having settlement issues. Conversely, denser material with parallel layering (suggesting engineered fill) was identified at all locations described by onsite personnel as having been previously reconstructed.

Both GPR and seismic refraction methods provided useful information about the site features related to settlement issues. The methods provided complementary geophysical methods to assess the subsurface at this site. Site conditions, which include the movement of cargo and the presence of a shallow saltwater-table, did not significantly limit the geophysical data for the site, although not all areas could be surveyed due to physical restrictions. Top of the bedrock was visible in the GPR records in at several locations due to its sharp contrast with the overlying granular fill materials. Highly variable conditions were found in the fill soils. GPR data was effectively processed to enhance the apparent depth of penetration. The presence of saltwater and the salt vadose zone above the water table did not significantly limit the depth of penetration of the GPR. The GPR provided a rapid data collection method that was able to discriminate between those areas where reconstruction has occurred as indicated by numerous flat reflectors, and areas subject to settlement issues, where discontinuous hummocky and concave reflector patterns occurred.

Seismic refraction data identified unconsolidated material, weathered bedrock, and intermittently competent bedrock. These subsurface layers are variable across the site. It also identified a number of low velocity areas of limited areal extent. These low velocity areas were generally present where site personnel indicated settlement concerns.

It was concluded that these geophysical methods were very effective in rapidly identifying regions of the subsurface that may need rehabilitation or ground improvement over a significant areal extent. These methods provide much greater continuous coverage than possible with conventional discrete borings that require invasive/destructive testing. Furthermore, these methods are possible with light equipment and can be conducted quite fast. Some of the greatest drawbacks are that: 1) interpretations must be made requiring judgment and expertise, and 2) no physical samples are obtained by which to “ground truth” the conclusions. It is suggested that prior to moving forward with any remedial schemes some invasive testing may be warranted for verification of findings, but can be minimized and concentrated at locations shown to be most critical from the geophysical surveys. Also, future data collection should be organized in a systematic fashion with parallel traverses collected in a fashion that permits mapping of important site features. Given site activities observed, future surveys should be closely coordinated with port activities to minimize the impact on port work

ACKNOWLEDGEMENTS

We wish to thank Rick Hoover of Dawood for carrying out the geophysical surveys, Frank Cioffi for assistance during the field work, and the Hawaii Department of Transportation and the Federal Highway Administration for their funding in support of this project. Their assistance is gratefully acknowledged.

REFERENCES

- Cioffi, F. (2009), "Characterization of Subsurface Conditions at Hilo Harbor Using Geophysical Methods." Plan B Report, University of Hawaii at Manoa, December.
- Dawood (2008). "Port of Hilo Geophysical Investigation Report." August 1, 2008.
- Geolabs (1999). "Geotechnical Engineering Exploration Pier 1 Shed Office Hilo Harbor, Island of Hawaii." August 10, 1999.
- Geolabs (2002). "Geotechnical Engineering Exploration Pier 3 Breasting Dolphins and Catwalks Hilo Harbor, Island of Hawaii." April 19, 2002.
- Geolabs (2006). "Geotechnical Engineering Exploration Inter-Island Cargo Terminal Facility Phase 1 Dredging, Hilo Harbor, Island of Hawaii." August 25, 2006.
- Federal Highway Administration (FHWA) (2003). "Application of Geophysical Methods to Highway Related Problems." September, 2003.
- State of Hawaii, Department of Transportation, Harbors Division (HDOT) (1998). "Hawaii District Commercial Harbors 2020 Master Plan."
- State of Hawaii, Department of Transportation, Harbors Division (HDOT) (2009). "Port Hawaii Handbook." <http://hawaii.gov/dot/harbors/library/port-hawaii-handbook/>, accessed Sept., 2009.

Consultant Report, Dawood (2008): Geophysical Void Investigation

UNIVERSITY OF HAWAII
at Manoa

GEOPHYSICAL
VOID INVESTIGATION REPORT

AUGUST 27, 2008



DAWOOD

PEOPLE ENGINEERING INNOVATION



10105 Allentown Boulevard, Grantville, Pennsylvania 17028
Phone: (717) 469-0937 Fax: (717) 469-0938
Dawood Project No. **208044.01**

UNIVERSITY OF HAWAII
at Manoa

GEOPHYSICAL VOID
INVESTIGATION REPORT

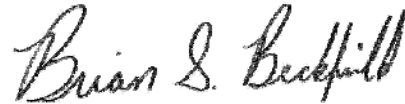
AUGUST 27, 2008

Report Prepared by:



Rick A. Hoover, PG
Director, Geophysical Services

Report Reviewed by:



Brian Beckfield, PG
Geophysical Manager

Approved for Distribution



Thomas J. Imholte, PE
Manager Geotechnical Services



DAWOOD
PEOPLE ENGINEERING INNOVATION



10105 Allentown Boulevard, Grantville, Pennsylvania 17028
Phone: (717) 469-0937 Fax: (717) 469-0938
Dawood Project No. 208044.01

Table of Contents

1. Introduction.....	1
2. Site Descriptions.....	1
2.1. Poamoho Research Station, Island of Oahu	1
2.2. Waimanalo Research Station, Island of Oahu.....	1
2.3. Port of Kawaihae, Island of Hawaii.....	1
3. Introduction to the Nondestructive geophysical Methods Employed.....	2
3.1. Electromagnetic Terrain Conductivity Method.....	2
3.1.1. EM Principles.....	2
3.1.2. EM Limitations.....	2
3.2. Ground Penetrating Radar	3
3.2.1. GPR Principles.....	3
3.2.2. GPR Limitations.....	4
3.3. Seismic Refraction.....	5
3.3.1. Seismic Refraction Principles.....	5
3.3.2. Seismic Refraction Limitations	6
3.4. Seismic Reflection Method	6
3.4.1. Seismic Reflection Principles.....	6
3.4.2. Seismic Reflection Limitations.....	6
4. Geophysical Data Collection	6
4.1. EM38 Data Collection	7
4.2. EM31 Data Collection	7
4.3. GPR Site Specific Data Collection Parameters.....	8
4.4. Seismic Reflection Data Collection.....	9
4.5. Seismic Refraction Data Collection Method	9
5. Geophysical Data Processing.....	10
5.1. EM DATA Processing	10
5.1.1. EM Data Modeling	10
5.2. GPR Processing.....	11
5.3. Seismic Refraction Data Processing	12
5.4. Seismic Reflection Data Processing	12
6. Geophysical Data Interpretation and Presentation	14
6.1. Interpretation Criteria and Assumptions.....	14
6.2. Poamoho Research Station, Island of Oahu	15
6.2.1. Poamoho EM.....	15
6.2.2. Poamoho GPR	16
6.2.3. Poamoho Seismic Refraction.....	18
6.2.4. Poamoho Seismic Reflection	19
6.3. Waimanalo Research Station, Island of Oahu.....	20
6.3.1. Waimanalo EM	20
6.3.2. Waimanalo GPR	21
6.3.3. Waimanalo Seismic Refraction	23
6.3.4. Waimanalo Seismic Reflection.....	24
6.4. Port of Kawaihae, Island of Hawaii.....	24
6.4.1. Kawaihae EM	24
6.4.2. Kawaihae GPR.....	25
6.4.3. Kawaihae Seismic Refraction	26
6.4.4. Kawaihae Seismic Reflection.....	27
7. Geophysical Data Summary and Conclusions.....	27

7.1.	Poamoho Research Station, Island of Oahu	28
7.2.	Waimanalo Research Station, Island of Oahu.....	28
7.3.	Port of Kawaihae, Island of Hawaii.....	28
7.4.	Electromagnetic Methods.....	29
7.5.	Ground Penetrating Radar Method	29
7.6.	Seismic Refraction Method.....	30
7.7.	Seismic Reflection Method	30
7.8.	Caveats	31
8.	References	32

FIGURES

Figure 1 – Poamoho Site Location Map	Following Text
Figure 2 – Waimanalo Site Location Map	Following Text
Figure 3 – Kawaihae Site Location Map	Following Text
Figure 4 – Poamoho Traverse Location Photograph	Following Text
Figure 5 – Waimanalo Traverse Location Photograph	Following Text
Figure 6 – Kawaihae Traverse Location Photograph	Following Text
Figure 7 – Target Hyperbolas Example.....	Following Text
Figure 8 – Poamoho GPR Velocity Profile	Following Text
Figure 9 - Poamoho EM38 EM Data.....	Following Text
Figure 10 – Poamoho EM31 EM Data	Following Text
Figure 11 – Poamoho Modeled Resistivities	Following Text
Figure 12 – Poamoho Antenna Comparison	Following Text
Figure 13 – Poamoho Void Examples	Following Text
Figure 14 – GPR Automatic Picking Comparison.....	Following Text
Figure 15 – Poamoho GPR Interpretation	Following Text
Figure 16 – Poamoho GPR Target Comparison	Following Text
Figure 17 – Poamoho Line 2 Refraction	Following Text
Figure 18 – Poamoho Line 2 Reflection CDP Stack	Following Text
Figure 19 - Waimanalo EM38 EM Data	Following Text
Figure 20 – Waimanalo EM31 EM Data.....	Following Text
Figure 21 – Waimanalo Modeled Resistivities.....	Following Text
Figure 22 – Waimanalo Resistivity Interpretation	Following Text
Figure 23 – Waimanalo Line 2 Refraction	Following Text
Figure 24 – Waimanalo Line 2 Reflection CDP Stack.....	Following Text
Figure 25 - Kawaihae EM38 EM Data	Following Text
Figure 26 – Kawaihae EM31 EM Data.....	Following Text
Figure 27 – Kawaihae Modeled Resistivities	Following Text
Figure 28 – Kawaihae GPR Line Lengths	Following Text
Figure 29 – Kawaihae Line 2 Refraction	Following Text
Figure 30 – Kawaihae Line 2 Reflection CDP Stack.....	Following Text

TABLES

Table 1 Compressional Velocities of Common Material.....	5
Table 2 Poamoho GPR Line 2 Interpreted Voids	17
Table 3 Poamoho Seismic Refraction Line 2 Interpreted Voids.....	19

Table 4 Waimanalo Line 2 Interpreted Resistivity Void Features	21
Table 5 Waimanalo GPR Line 2 Interpreted Voids.....	22
Table 6 Waimanalo Seismic Refraction Line 2 Interpreted Voids	23
Table 7 Kawaihae GPR Line 2 Interpreted Voids.....	25
Table 8 Kawaihae Refraction Line 2 Interpreted Voids	27
Table 9 Anticipated Seismic Travel Times	31

APPENDICES

Appendix A – Spectral Analysis for Seismic Reflection Data	Following Text
Appendix B – Normal Move Out (NMO) Panels for Seismic Reflection Data	Following Text
Appendix C – Poamoho GPR Traverse Data	Following Text
Appendix D – Poamoho Common Offset Data	Following Text
Appendix E – Waimanalo GPR Traverse Data	Following Text
Appendix F – Kawaihae GPR Traverse Data.....	Following Text

1. INTRODUCTION

The University of Hawaii has been awarded a contract to conduct field research utilizing a variety of geophysical techniques to identify subsurface voids of various shapes and sizes at relatively shallow depths in a variety of local soils. Three methods consisting of four non-destructive geophysical techniques were conducted at four field sites. At two of the test sites located on the Island of Oahu, a series of objects representing voids ranging in size from 2- to 24-inches in size were buried at depths less than 5 feet in trenches approximately 150 feet long and 3 to 5 feet wide. Buried material was composed of styrofoam fabricated with a high air void content in order to best represent subsurface voids.

Two test sites were located on the Island of Hawaii. The third test site represents a void test site similar to the test sites on Oahu. The fourth site is a natural site with suspected void issues, and is covered by a separate report. The field surveys were completed between June 17 and June 25, 2008.

Three different geophysical methods were identified for demonstration including electromagnetic (EM), seismic and ground penetrating radar (GPR). Two kinds of seismic data were collected including refraction and reflection. The selection of geophysical methods follows the ASTM standard guide for the selection of surface geophysical methods, adjusted for site conditions and target resolution. The design approach utilized included reasonably common geophysical tools, with acquisition parameters adjusted to meet the survey objective and voids that were put into place.

2. SITE DESCRIPTIONS

Three separate soil types were selected by University personnel to be included in this focused assessment of geophysical applications. The location of each site and soil type present as described by University personnel is discussed in the sections below.

2.1. Poamoho Research Station, Island of Oahu

Poamoho Research Station is located ([Figure 1](#)) on the northwest portion of the island of Oahu, north of Puu Kamananui, and west of Waimanalo Beach. Soils at this site are lateritic. This red residual soil commonly develops in humid tropical and subtropical regions of good drainage. These soils are leached of silica and contain concentrations of iron and aluminum hydroxides and tend to be very conductive.

2.2. Waimanalo Research Station, Island of Oahu

Waimanalo Research Station is located ([Figure 2](#)) on the northeastern portion of the Island of Oahu, just east of Puu o Kona. Soils at this site are montmorillonite. These clay mineral soils are characterized by swelling with water. These aluminum siliclastic soils have deficiencies in charge in the tetrahedral and octahedral positions balanced by the presence of calcium and sodium cations. These soils are commonly very conductive.

2.3. Port of Kawaihae, Island of Hawaii

Port of Kawaihae is located ([Figure 3](#)) on the western side of the Island of Hawaii. Soils at this site represent carbonate sand and gravel with a relatively shallow water table. Soils in the test

area were originally dredged from the Port of Kawaihae. Water table at this location is approximately 10-foot below ground surface.

3. INTRODUCTION TO THE NONDESTRUCTIVE GEOPHYSICAL METHODS EMPLOYED

3.1. Electromagnetic Terrain Conductivity Method

3.1.1. EM Principles

Electromagnetic (EM) terrain conductivity surveying is a reconnaissance method of determining the electric and magnetic properties of subsurface materials. The conductivity measurement is dependent upon the density, porosity, moisture content, and the presence or absence of electrolytes or colloids of the subsurface materials. Typically, soils have a high conductivity, and bedrock typically has a low conductivity. The difference is generally due to the presence of moisture in the soil and the generally low porosity of the rock. Because of the variety of factors that affect terrain conductivity measurements, the actual magnitude of the terrain conductivity values measured is less important than the trends and anomalies in the measurements. The presence of metallic debris or interferences, serve to raise the measured conductivity values significantly from natural levels.

EM terrain conductivity instruments utilize a small transmitter coil placed on or near the ground surface. An alternating current is passed through the coil, which creates a time-varying magnetic field around the coil. The magnetic field induces an electrical current within the earth called an eddy current. The induced electrical current in the subsurface material generates a secondary magnetic field. The secondary magnetic field (from the subsurface) and the primary magnetic field (from the transmitting coil) are both sensed by a receiver coil. For low induction values, the ratio of the secondary magnetic field, relative to the primary magnetic field, is the conductivity of the subsurface materials. This ratio is evaluated in conductivity units of milliMhos per meter (mM/m) or milliSiemen per meter (mS/m).

Similarly, the phase relationship between the primary and secondary magnetic fields can be related to the magnetic susceptibility and is evaluated as parts per thousand (ppt) of the total field strength. This additional parameter of the electromagnetic field is typically referred to as the inphase (inphase) measurement. The magnetic susceptibility measurement is typically more responsive to ferrous metals than the conductivity phase, and can therefore be used as a conductivity source-screening tool.

3.1.2. EM Limitations

The terrain conductivity is dependent upon the nature of the soil; subsurface porosity; permeability; moisture content; concentration or lack of concentration of dissolved electrolytes and colloids; and the presence of interferences such as electric lines, pipes, buildings, buried metal, and foundations. Thus, the actual magnitude of conductivity values measured does not always indicate a specific geologic condition. The trends as well as the irregularities in the measurements lead to a qualitative interpretation of the data. Toward this end, Dawood personnel are highly experienced in the interpretation and evaluation of electromagnetic data.

If a quantitative interpretation is necessary, the survey results must be correlated with the results from confirmatory test borings, test pits, or other secondary evaluation techniques.

3.2. Ground Penetrating Radar

3.2.1. GPR Principles

Ground-penetrating radar (GPR) is useful in locating and identifying features buried below grade level with a high degree of resolution. Common applications include the use of GPR to determine or verify the location and sizes of underground storage tanks (USTs), map utilities, delineate buried wastes, evaluate sinkhole/collapse features, detect archaeological features, and perform structural assessments.

GPR systems produce cross-sectional images of subsurface features by transmitting discrete radar pulses into the subsurface and recording the echoes or reflections from interfaces between materials with differing dielectric properties. In principle, GPR is entirely analogous to a medical sonogram or ultrasound, except that GPR uses electromagnetic (radar) energy rather than acoustic (sound) energy and is therefore sensitive to electrical properties (as opposed to ultrasound which is sensitive to densities).

Cross-sectional images of subsurface objects and layers are generated by rapidly and repeatedly transmitting radar pulses into the subsurface as the GPR transmitter and receiver are moved along a survey traverse. For each pulse, the antenna receiver records the reflections from subsurface dielectric contrasts. Data is a measurement of reflected energy amplitude vs. travel time. Successive reflections are plotted side-by-side on the record, and produce a cross-sectional image of the dielectric variations in the subsurface.

Reflection amplitudes are dependent on the magnitude of the dielectric contrast at depth. Since the electrical properties of most soils and metal tanks or pipes are dramatically different, these targets produce dramatic and characteristic reflections, which can be easily recognized on a radar record. Concrete, fiberglass, and plastic pipes, as well as tanks and other structures also produce recognizable, but more subtle reflections since they have electrical properties that more closely match many soils. Terra cotta pipes are often difficult to recognize since the electrical properties of terra cotta (clay) are very close to many clay-rich soils. Reflections are also obtained from naturally occurring electrical interfaces such as soil/bedrock, soil/air, bedrock/air, dry soil/saturated soils (i.e. the groundwater table), and other subsurface contacts.

The dielectric permeativity and electrical conductivity (frequently dictated by moisture content) of the soils and the frequency of the radar energy effectively control the depth of penetration by the radar systems. For a given radar frequency, a coherent pulse will travel more deeply into less conductive materials. In highly conductive materials (such as damp clays), the pulse is dissipated at very shallow depths (sometimes measured in inches). Using a transmission antenna with a lower frequency can increase penetration, but this causes a loss of resolution. Frequencies commonly employed fall within the 80 to 900 MHz range. In general, the use of GPR is limited to depths of 15 feet or less (although in very dry sand or bedrock, penetration depths up to 100 feet have been obtained).

Resolution of GPR systems is dependent on the frequency of the antenna employed. Very high frequency antennas (900 MHz or greater) can resolve features one-quarter inch or less in diameter (i.e. reinforcing rods), but penetrate to depths of only one or two feet. The most commonly used antennae (designed for optimum transmission at frequencies of 120 to 500 MHz) can resolve linear features with dimensions as small as one or two feet, at penetration depths up to 10 feet (i.e. utility lines, etc.).

Since they produce cross-sectional images GPR records are usually interpreted visually, often in real time. In the absence of a feature with known depth on the record, an absolute depth scale is unavailable, and only relative depth information can be obtained. However, if a feature with a known depth can be scanned, its position on the record establishes an empirical absolute depth scale.

Since the GPR antenna is towed at a sometimes-uneven speed, placing fiducial marks on the record at known locations or spacing along the profile achieves positioning along the record.

Unlike other electrical, EM, and magnetic techniques, GPR can provide relative (and sometimes absolute) data on the depth to various features. Most other techniques can delineate anomalies through contouring of measurements collected on a grid, or recognition of audible alarms or needle deflections, but cannot readily provide target depths. Because of the rapid pulse rate, GPR is probably the most continuous profiling technique. It is also one of the quickest (although not easiest) to perform. The antenna may be towed by hand at walking speed, or towed behind a vehicle at greater speeds for more extensive surveys. These capabilities make GPR particularly suited to reconnaissance-level stratigraphic or water table profiling, and scanning for unknown or suspected underground structures.

3.2.2. GPR Limitations

The greatest limitation of GPR is the loss of penetration in electrically conductive materials such as damp clays. This can be insidious, since an absolute depth scale is rarely available. In any GPR survey, an attempt should be made to locate and profile a nearby object or feature within known depth to ensure that sufficient penetration is being achieved. A single known utility or an auger-hole may be sufficient to calibrate the GPR penetration in many cases.

Since there is a trade-off between penetration depth and resolution, it may be difficult (or impossible) to choose an antenna with the correct frequency to attain the necessary penetration while maintaining the necessary resolution. An incorrect frequency selection will result in missing the desired feature.

Ringings, or antenna multiples from a single reflector are usually seen on the commonly raw, unprocessed GPR profiles. Although an experienced interpreter can usually recognize them, they can be misleading to the uninitiated.

The GPR antennae commonly used for shallow scanning are shielded to look only downward. However, unshielded antennae are occasionally used. Unshielded antennae are susceptible to spurious reflections from overhead or nearby structures, such as power lines, buildings, cars, etc.

3.3. Seismic Refraction

3.3.1. Seismic Refraction Principles

The seismic refraction method uses a linear spread of 24 energy sensors (geophones) with one energy source location off each end of this spread. Energy imparted into the subsurface reflects and refracts at soil and bedrock interfaces in the subsurface. As reflected and refracted energy is returned to the surface, geophones (receivers) change the energy (ground motion) into electrical signals for the seismograph. The seismograph measures the time, from energy transmission to energy reception at the geophone, which is a known distance from the source. Given the travel time and the distance, a velocity of the subsurface materials can be computed. Information on the lithology and density of subsurface materials can be gained by measuring the subsurface velocities. A series of sequential spreads and energy locations can be used to create a profile of the subsurface velocities across the investigation area.

Most igneous and metamorphic rocks have little or no porosity, and velocities depend mainly on the elastic properties of the minerals making up the rock material itself. This is also the case with massive limestone, dolomites and evaporates. Sandstone, shale and certain kinds of soft limestone has more complex microstructures with pore spaces between grains which may contain fluids or softer types of material such as clay. For such rock or soil, velocity is very dependant on porosity and the material filling the pores.

Table 1 Compressional Velocities of Common Material

Material	Typical Minimum (feet/second)	Typical Maximum (feet/second)
Unconsolidated Soils	500	2,500
Consolidated, Clayey Soils	2,000	4,500
Saturated Soil	4,800	5,200
Shale Bedrock	6,000	12,000
Sandstone Bedrock	9,000	14,000
Limestone Bedrock	12,000	18,000
Crystalline Bedrock	15,000	19,000
Basalts	16,500	20,000
Gneiss	12,000	24,000
Marble	13,000	23,000

In general, igneous rocks have seismic velocities which show a narrower range of variation than sedimentary or metamorphic rocks. Sedimentary rock velocities will also be dependent upon their age and depths of burial. Metamorphic rock velocities depend upon the composition of their host rock and the degree of metamorphic activity at the location of the survey.

3.3.2. Seismic Refraction Limitations

The presence of vibration sources near the seismic survey can provide unwanted noise, which can degrade the quality of the data and at times obscure the intended seismic source energy. Seismic refraction method has difficulty identifying the presence of a subsurface velocity inversion, where subsurface conditions change from a fast velocity material to a slow velocity material. When the low velocity material can be identified, depths to refractors below the low velocity material are suspect. Seismic refraction tomography represents the best method to address this issue, but seismic data in these settings are subject to cautious interpretation.

3.4. Seismic Reflection Method

3.4.1. Seismic Reflection Principles

Seismic reflection surveys are most useful in determining the depth to significant subsurface layers by measuring the velocities of subsurface material. Seismic reflection depends on contrasts in velocity and density to reflect seismic energy back to the surface. Changes in velocity and density can be the result of a material change (change in rock type), natural discontinuities (such as a faulting or fracturing), or man made discontinuities (such as mining). The accuracy experienced on your site will be dependent on the homogeneity of the subsurface soils and bedrock, and the amount of irregularity present on the reflector surface.

The seismic method uses a linear spread of 12 to 48 energy active sensors (geophones) with a series of energy source locations. Energy imparted into the subsurface reflects and refracts at soil and bedrock interfaces in the subsurface. As reflected and refracted energy is returned to the surface, geophones (receivers) change the energy (ground motion) into electrical signals for the seismograph. The seismograph measures the time, from energy transmission to energy reception at the geophone, which is a known distance from the source. Given the travel time and the distance, a velocity of the subsurface materials can be computed. Information on the lithology and density of subsurface materials can be gained by measuring the subsurface velocities. A series of sequential spreads and energy locations can be used to create a profile of the subsurface velocities across the investigation area.

3.4.2. Seismic Reflection Limitations

As in refraction, the presence of vibration sources near the seismic survey can provide unwanted noise, which can degrade the quality of the data and at times obscure the intended seismic source energy. The resolution of seismic reflection data is very dependent upon the frequency response of the data recorded. The earth can act like a frequency filter, attenuating the higher frequency energy necessary for high resolution seismic surveys. Therefore the resolution of a survey can be difficult to predict without prior information regarding the seismic characteristics of a site.

4. GEOPHYSICAL DATA COLLECTION

Data collection for all sites was reasonably consistent as described below. Previously buried objects were identified relative to site reference markers. The center-line (L2) was identified as well as two parallel lines offset two-feet to each side (L0 and L4). A peg was placed into the ground at each end of the three traverse locations and a string was pulled between them. A measuring tape was pulled along the string and used to maintain inline distances with the EM

and seismic data collection. GPR data was collected using the string for guidance and survey wheels. The approximate location of traverses for Poamoho (Figure 4), Kawaihae (Figure 5) and Waimanalo (Figure 6) are shown on air photographs to provide a relative location for each traverse.

4.1. EM38 Data Collection

Dawood utilized a Geonics Model EM38-RT conductivity meter with multi-phase digital recording capabilities. Data was collected with horizontal and vertical dipole orientations. With vertical dipole orientation, the majority of the subsurface response comes from the first 4.9 feet of the subsurface, with the maximum sensitivity in vertical dipole orientation at 1.3 feet below-grade while, near-surface effects are minimal. In horizontal dipole orientation, the majority of the response comes from the first 2.4-feet of subsurface, and near surface effects dominates the decaying penetration of the EM signal.

Survey parameters included measurements every 0.5 feet inline along the center-line and 1.0 feet inline along the outer lines, offset by two feet. Inline positioning was maintained through the use of a tape measure laid along the traverse being measured.

A vertical dipole time-test was conducted at the Port of Kawaihae. A time-test simply measures the variability of recorded data while the EM38 remains stationary for a period of time. This test measures instrument and site electromagnetic variability over the period tested. At Kawaihae, inphase data was found to vary +/- 0.25 parts per thousand (ppt) total field strength. Quadrature phase data (conductivity) was found to vary up to 4 milliSiemen/meter (mS/M). These variations represent a confidence of 98.6% and 99.0% in the inphase and quadrature phase measurements, respectively. Time-test data collected at Waimanalo indicated confidence intervals of 99.3% for both data sets.

Data was downloaded to a field computer daily for verification of the data quality. Although the presence of some highly metallic features in the subsurface may be apparent during data collection, all data was transferred from the data recorder to a PC for viewing. On the PC, the operator reviews the conductivity and magnetic susceptibility values recorded in the field. The survey limits are verified to determine that line lengths are adequate to meet the survey objectives and that adequate data quality was being gathered.

4.2. EM31 Data Collection

Since features of interest were buried to depths up to six-feet, the EM38 would not be expected to be able to identify the "deeper" features. In order to measure the effects of these deeper features, a Geonics Model EM31-DL conductivity meter with multi-phase digital recording capabilities was used. Data was collected with horizontal and vertical dipole orientations. With vertical dipole orientation, the majority of the subsurface response (70 percent of the total field strength) comes from the first 20 feet of the subsurface, which is the 'rule-of-thumb' depth if investigation. In the normal operating mode, the maximum sensitivity of this unit in vertical dipole orientation is 5.3 feet below-grade while, near-surface effects are minimal. In horizontal dipole orientation, the majority of the response comes from the first 9-feet of subsurface, and near surface effects dominate the decaying penetration of the EM signal.

Survey parameters included measurements every 1 feet inline with the lines spaced every two feet. Inline positioning was maintained through the use of a tape measure laid along the traverse being measured.

A vertical dipole time-test was conducted at the Port of Kawaihae. A time-test simply measures the variability of recorded data while the EM31 remains stationary for a period of time. This test measures instrument and site electromagnetic variability over the period tested. At Kawaihae, no variation was found in the inphase data. Quadrature phase data (conductivity) was found to vary +/- less than 1 milliSiemen/meter (mS/M), representing a confidence of 99.86% in the measurements.

Data was downloaded to a field computer daily for verification of the data quality. Although the presence of some highly metallic features in the subsurface may be apparent during data collection, all data was transferred from the data recorder to a PC for viewing. On the PC, the operator reviews the conductivity and magnetic susceptibility values recorded in the field. The survey limits are verified to determine that line lengths are adequate to meet the survey objectives, and adequate data quality was being gathered.

At the Kawaihae site, magnetic susceptibility data was not present in the downloaded EM31 data set. This was not identified until after people and equipment were demobilized from the area. Absence of this information limits interpretation of metallic features, which are more easily identifiable with this data component.

4.3. GPR Site Specific Data Collection Parameters

Dawood used a Model SIR-3000 GPR unit manufactured by Geophysical Survey Systems, Inc., of New Hampshire. Multiple antennas were used for this survey, including those with central frequencies of 270 megahertz (MHz), 400 MHz, 900 MHz and 1,500 MHz.

Data was collected along traverses spaced two feet apart. Positioning was maintained using the line reference string and the survey wheel for inline distance.

A dielectric constant of 6.0 was used for all sites to estimate depths to features identified in the GPR record during field activities. This constant was developed based on general soil information and may be incorrect for site-specific applications. No subsurface utilities with known depth were used to calibrate the measurements.

All data was digitally recorded, with each traverse represented by a separate data file. Data file numbers, line locations and survey traverse direction were recorded in a field log-book as the data was collected. Data acquisition parameters such as filename, antenna, samples/trace, scans/second, range-gain, vertical infinite impulse response (IIR) filters and horizontal trace stacking are stored in the header of each traverse. Each traverse was reviewed at the conclusion of data collection for preliminary evaluation and data quality assurance. Data acquisition parameters were adjusted as necessary based upon this review. Data was downloaded to a personal computer daily for back-up.

4.4. Seismic Reflection Data Collection

Seismic data was collected using a 24-channel Geode, manufactured by Geometrics of San Jose, California. The Geode was controlled with a personal computer, which also displayed and recorded the seismic data. A one-pound hammer with a steel plate was used for the survey. 100-hertz vertical geophones were placed on land-streamer plates every one-foot along the seismic line. Each reflection record was recorded after advancing the entire streamer spread one foot.

Seismic data at the test sites was collected using a "U" shaped land streamer configuration. With this configuration, two parallel lines of geophones, one foot apart were collected, with the source located along the centerline. Geophone 1 was opposite geophone 24, geophone 2 opposite 23, etcetera....

A brief seismic noise test was conducted at each site determined the sites to be adequately quiet for a seismic survey with no unusual background interferences to impede data collection. Due to the broad dynamic range of the seismograph utilized, the number of data bits recorded, and initial field observations of data quality, filters were not utilized during data collection.

At the Poamoho site, a common offset (source to receiver) separation evaluation was performed. Offsets of 1, 7, and 14 foot from the first geophones were assessed. Due to the shallow nature of the targets placed into the subsurface, a one foot offset was selected for all data collection. Refractor velocities indicated moderate speed velocities. Therefore, a 125 millisecond record length was selected for the surveys. A sample interval of 0.125 milliseconds was chosen for data acquisition.

During data collection, data was monitored on a computer screen to assess data quality and the level of noise within the data. Typically, one or two hammer blows provided adequate energy to gather the required data quality. If adequate energy was not recorded and noise was present, then the record was discarded and a replacement record was collected. The aversion to a large number of hammer blows and the light weight hammer were intended to optimize high frequencies in the recorded data. At the Port of Kaiwaihae, a 3-pound hand sledge was used as a source due to the attenuation of hammer energy by the fine grained sand present at the ground surface.

No distinct reflectors were observed in the field records. However, waveform variations were present in successive records at consistent station locations to indicate to field personnel the identification of buried features would be able to occur.

4.5. Seismic Refraction Data Collection Method

The seismic refraction survey conducted was integrated into the seismic reflection data collection. At the start of the survey, and each time the streamer had advanced one full spread length, a series of refraction sources were collected through the center of the geophone spread. Refractor source locations were one-foot from the first geophone station (between geophones 1 and 24 with the "U" shaped reflection configuration), and at stations coincident with geophones 3 (and 22), 6 (and 19), 9 (and 16) and 12 (and 13).

Data was recorded with the same equipment using the same acquisition parameters as the reflection data. However, for refraction data, multiple hammer blows were permitted to enhance the first breaks on the far-offset geophones.

At the Port of Kaiwaihae, a 3-pound hand sledge was used as a source due to the attenuation of hammer energy by the fine grained sand present at the ground surface.

5. GEOPHYSICAL DATA PROCESSING

5.1. EM DATA Processing

EM31 data was reformatted and initially managed using Geonics DAT31W™ software. Data was exported to comma delimited "X,Y,Z" files along with a time-stamp for quality assurance review and preliminary mapping. Data is automatically recorded with a flag establishing dipole orientation (horizontal or vertical), however exported files either contain horizontal or vertical dipole data only. Magnetic susceptibility (inphase data) and conductivity (quadrature phase data) for a given dipole orientation are exported into the same file. EM38 data was reformatted using Geonics DAT38W™ software and exported in the same fashion.

Comma delimited "X,Y,Z" files were imported into Microsoft Excel spreadsheets and compiled into comprehensive data files organized by line number, station number (inline distance) with, vertical dipole conductivity (VQ), horizontal dipole conductivity (HQ), vertical dipole magnetic susceptibility (VI), and horizontal dipole magnetic susceptibility (HI). This data was plotted with measurement value against station number and reviewed for quality assurance. If a station was not recorded in the field, a blank line was placed into the excel spreadsheet file. With the line number and station number organization, the spreadsheet files can be considered georeferenced, quality assured data.

Georeferenced EM data were processed for additional quality review using Golden Software's Surfer® mapping and processing system. An appropriate response scale was chosen for the data set that best illustrated variations in the subsurface materials. Data were also exported to comma delimited format for use in modeling. In order to ensure accurate models, the inphase data was adjusted so all measured values are positive. Field adjustment of the inphase scale is through knobs and should be near zero. However, due to mechanical method limitations, the measured and stored value is not always zero, but occasionally negative. Therefore, there is a need for value adjustment when quantitative manipulation of the data is to be performed.

5.1.1. EM Data Modeling

EMIGMA® is an electromagnetic simulation platform written by PetRos Eikon, Inc, of Brampton, Ontario. The program is designed to simulate the response of a variety of geophysical systems to geological structure. Modeling depends on the definition of physical parameters; however geological classifications are not typically based on the physical parameters that characterize a body. Therefore, geophysics often refers to typical values and ranges which are guides to the geologic material that is being measured. Electric current propagates through soil and rock in three ways including dielectric, electronic and electrolytic. Poor conductors and insulators conduct current by dielectric conductivity. Dielectric conduction occurs when electrons are slightly displaced from their nuclei in the presence of a varying electric field. Polarization may

occur with ions or molecules and is the means for the dielectric conduction. With electronic conductivity, electrons are the charge carriers. This is especially true in metals, and is a relatively rare phenomenon in the earth. Electronic conductivity is normally confined to metals and certain massive sulphide ores. Electrolytic conductivity is common in the ground and is associated with the presence of water, where ions are the charge carriers. Much of the conductivity encountered in geophysics is electrolytic and because of this, is difficult to characterize conductivities which are associated with particular lithologies since water content is such a dominating and variable factor when determining conductivity. Electrical resistivity can thus be quite variable depending on mobility, concentration, and the degree of dissociation of the ions. Electrolytic conduction is a slow process because the movement is actually a transfer of material and at times even a chemical change, so polarization phenomena often occurs at low frequencies.

Apparent resistivity and depth was calculated for each data set based upon measured dipole-dipole frequency electromagnetic data. This information forms an initial model for the one dimensional (1D) modeling. The 1D modeling is extended to two dimensions along the line or profile when EMIGMA[®] performs a data inversion computing resistivity and susceptibility for each layer at each point based on Maxwell's equations. Due to the void targets present, the magnetic susceptibility response was not modeled.

For each of the sites a database of EM data was assembled. The database contained quadrature and inphase data, dipole orientation, transmitter/receiver positional information, and transmission frequencies. Separate one dimensional (1D) models were constructed for each of the EM31 and EM38 data sets. With the extension to 2D, bounds of 1 and 10,000 ohm-meters conditioned the inversion. Real and imaginary components of the EM field calculated and the data inverted to provide the 2D model. Typically, 20 model blocks were constructed for each model. Models containing the EM31 data had a 7.532 meter (24.12 feet) model constructed, while the EM38 data alone were limited to 2.0 meters (6.5 feet). Models are limited to 20 vertical layers. Therefore, the EM31 model vertical layer resolution is 0.3766 meters (1.2 feet), while the EM38 model vertical resolution is 0.1 meter (0.33 feet). These model constraints limit the resolution of smaller void targets, but should be adequate resolution to identify larger features.

5.2. GPR Processing

A copy was made of each radar record and renamed to reflect the line and antenna being used. RADAN[™] software written by Geophysical Survey Systems was used to process and interpret the renamed GPR data. Position adjustment was made to the data. This time shift of the data places the first positive peak of the direct wave from a ground coupled, bistatic antenna to time zero. This permits the data to be examined so that the ground surface can be considered to be at time zero. Next, a finite impulse response (FIR) filter horizontal high pass filter was applied to the data to remove background noise. Background noise shows up as horizontal, low frequency bands in the data (caused most commonly by antenna ringing) to be removed from the data. For data at the Port of Kawaihae, this can remove indications of flay-lying water table reflections. A filter length of 1023 scans was used. As necessary, gain controls were applied to balance the GPR data across individual traverses, both along the traverse, and vertically.

The Poamoho site had a number of clearly identifiable hyperbolas associated with high contrast targets. Since a radar antenna radiates energy with a wide beam-width pattern, objects several feet away may be detected. As a consequence, objects of finite dimensions appear as hyperbolic reflectors on the radar record as the antenna detects the object from far off and is moved over and past it. An example of hyperbolic reflectors is presented on [Figure 7](#), which is discussed further in the data presentation of the report [[Section 6.2.2](#)]. The hyperbolic shapes are commonly migrated to collapse the hyperbolas to points in the subsurface. However, velocities can be variable with depth due to changes in soil chemistry, porosity, and moisture content. Therefore, RADAN provides for variable depth migration. However, in this instance, the analytical velocities measured in the migration routine can be used to establish an estimate of velocity variability in the subsurface. At Poamoho, the vertical velocity profile was found to be variable ([Figure 8](#)) The implication is that any depth estimates from the GPR data under the test conditions used, will be variable at best.

Some data interpretation was performed using RADAN. During velocity analysis ASCII “.vel” files are output. During interpretation, ASCII “.lay” files are output. These files were occasionally imported into Excel for manipulation and presentation, including some of the tables presented later in the report. Pick confidence information has been included in the tables. Pick confidence is an assessment by RADAN ranging from 0 (poor) to 1 (good), of the interpreted location or “pick” being located at the peak of an hyperbola.

5.3. Seismic Refraction Data Processing

Rayfract[®] written by Intelligent Resources Incorporated of Vancouver B.C was used to analyze the refraction data. Rayfract[®] permits the interpreter to pick first-energy breaks in the seismic data and be mapped to refractors manually or semi-automatically, based upon apparent (instantaneous) common mid point velocities. Seismic energy travel time is processed on a per-refractor basis according to three different interpretation methods, Common-Midpoint time refraction (Gegrande and Miller, 1985, Ruehl, 1995), Plus-Minus (Hagerdoon, 1959), and Wavefront (Brueckl, 1987, Jones and Jovanovich, 1985). Additionally, a Delta-t-V method (Gegrande and Miller, 1985) is available permitting pseudo-2D tuning ray inversion which delivers a continuous one-dimensional depth verses velocity profile for all profile stations. Using the Delta-t-v method permits the identification of systematic velocity increases (such as top-of-rock or basement) and strong velocity anomalies such as low velocity fault zones faults, or high velocity dykes. As a final processing step, the Delta-t-V results are subjected to Wavepath Eikonal Traveltime (WET) tomographic processing (Schuster, 1993, Watanabe, 1999).

During data analysis, Dawood examined data recorded by each of the 24-geophones for each source recorded. Dawood identified the onset of seismic energy and evaluated noise content. As necessary, data was gained or filtered to highlight energy associated with the seismic source, and de-emphasize site noise. During data modeling, the 1D and 2D velocities were examined in detail. Dawood also examined the relationship between modeled first break energy and interpreted first break energy picks.

5.4. Seismic Reflection Data Processing

Seismic reflection data was processed using WinSeis[®] Turbo, and SurfSeis[®], both written by personnel from the University of Kansas, and sold through the Kansas Geologic Survey. SurfSeis[®] was used for file conversion and initial steps of editing. WinSeis[®] Turbo was used for

all other data processing and analysis functions. Processing seismic reflection data occurred using a number of steps described as follows:

File Conversion: Individual data files were compiled into a “master” file for processing. During conversion all data are stored in a 32-bit floating-point format with individual traces containing a 120-word header followed by variable length data series.

Record and Trace Edits: Includes the removal of dead or noisy traces as required.

Header Geometry Verification and Editing: The location of each source and receiver that is recorded in the data header for each geophone is verified and edited as necessary.

Spectral Analysis: Performed to assess data frequency content. Spectral analyses seismic data are presented in [Appendix A](#).

Geometry Sort: Data are reorganized from gatherings of data by shot, to common mid-point (CMP sometimes referred to as common depth point [CDP]) and common offset locations. Common offset data are often displayed to present a preliminary seismic section of the area of interest. Additionally, the spread was split into right and left halves and processed as two dimensional data.

Brute Stack: The data was stacked without velocity compensation to assess the presence of reflectors in the subsurface.

Frequency Filter Application: Data was band pass filtered. A filter was applied to the compressional wave data. Based on review of the spectral analysis described above, all data was filtered with the following four point filter 75/100-150/175.

Velocity Analysis: Refraction analysis or hyperbolic velocity analysis is performed to estimate the vertical and lateral velocity changes in the subsurface. Minimal hyperbolic velocity was observed in the data with the limited distance offsets available, therefore as an alternative whole line velocity stacks were prepared to identify data stretch and distortion. Optimal (high frequency, low stretch) velocities were selected for application. The following normal move out (NMO) velocities were applied to the whole lines: Poamoho Line 2, Poamoho Line 2 500-feet per second (fps), Kawaihae Line 0 and Line 2 600-fps, and Waimanalo Line 2 and Line 500-fps. These velocities are consistent with the refraction velocities.

Normal move out velocity panels for reflection data used for assessment and analysis are presented in [Appendix B](#). It should be noted that stacking velocities can be significantly different than bedrock velocities measured by refraction surveys, or interval velocities associated with a particular subsurface layer. Stacking velocities apply only to the correction of normal moveout in seismic reflection data.

Normal Moveout: Correction to compensate for velocity differences associated with energy travel distances. This step applies the stacking velocities identified in the previous step.

CDP Stacking: Multiple data traces were added together to enhance the signal-to-noise ratio of the final data set. The number of traces stacked together is used to indicate the fold of the data. Initial stacking indicated lower than expected frequencies.

Frequency Filter Application: Data was band pass filtered a second time to mitigate lowered frequency content related to the stacking process.

Display: Velocity corrected, stacked, and filtered data are presented in cross-section view. The vertical scale is time; however, the horizontal scale is distance, with each CDP value equal to the 1-foot station numbers used in the field. Data scales are adjusted to present the data for interpretation.

Common Offset Panel Displays: Common source to receiver offset distances were displayed as single fold seismic data to assess resolution and noise within the data at various stations.

6. GEOPHYSICAL DATA INTERPRETATION AND PRESENTATION

6.1. Interpretation Criteria and Assumptions

Geophysical data presented in the following sections contains interpretations of void features. The interpretation focuses on Line 2, which is centered over the buried features. Parallel lines (L0 and L4 are available in the digital project records.) The interpretation is based upon the geophysical response as the geophysical method source energy passes from soil to a void and back to soil. However, the formation of a subsurface void would have other subsurface information that can be integrated into the interpretation of the void, such as the piping feature which is permitting the soil to be removed, or the compressional feature resulting from subsurface compaction creating a void with layers closer to the surface. With a real application, these components associated with a void problem would be integrated into the interpretation of void features.

The number, depth, sizes and orientations of the void features is not known at the time of the initial interpretation.

In performing interpretation of the geophysical data, several assumptions were made regarding the placement of the void features under consideration. Fundamental assumptions include:

1. Voids were of reasonable and predictable sizes, including 2, 3, 4, 6, 9, 12, 18, 24 and 36 inches on a side. Therefore, when sizes are presented, they are at times rounded to a reasonable size.
2. Most voids are spaced laterally in a fashion that a 45 degree angle will be present from the void feature to the ground surface, and that adjacent void features are spaced adequate distance apart to minimize overlap and interference.
3. Void features are buried at depths less than 6-feet below ground surface.

In performing the interpretation, based on the data, several violations of these assumptions may be presented based upon the data. The interpreted features are based on geophysical data response. When a clear target was interpreted present, and an uncertain target was present, the uncertain target was considered noise. However, when two uncertain targets or two relatively clear targets were present, violating the assumptions, both were included. Given the data response alone, there is inadequate information to suggest which interpreted feature is correct, or which assumption has been violated.

Finally, each geophysical method has been individually interpreted as a means to establish the viability of the geophysical method to detect void features. Outside of a research application, different geophysical methods would be integrated into a comprehensive interpretation of the subsurface to formulate a subsurface model. In formulating the comprehensive interpretation, inconsistent and anomalous responses due to subsurface variations would be overlooked or ranked as possible void features instead of probable void features in order to de-emphasize the importance of some responses. The interpretation presented in the following sections recognizes the natural variations associated with the subsurface and has focused on the responses which could be attributed to subsurface voids.

6.2. Poamoho Research Station, Island of Oahu

6.2.1. Poamoho EM

EM31 conductivities ranged from 40 to 200 milliSiemen/meter (mS/m) and 1 to 12 mS/m for the EM38 data. This initial observation indicates a lower conductivity near surface conditions is present. Exclusive of metallic features discussed in the next paragraph, conductivity for the EM38 in both horizontal and vertical dipole modes is approximately 9 mS/m, which is approximately 111 ohm-meters. This can be interpreted to indicate a relatively dry, homogeneous resistive near surface soil material. Generally, the vertical dipole orientation EM31 data (the deepest sensing) increases in conductivity with station number, suggesting shallower bedrock is likely present near the survey origin.

Inphase response ranges from -10 to 20 parts per thousand (ppt) of the total field strength for both data sets. Abrupt changes in inphase response are present at inline distances of 3 and 127 feet on the EM38 data ([Figure 9](#)), which are absent on the EM31 data ([Figure 10](#)). This response suggests small, shallow metallic targets or interference sources are present at these two locations.

EMIGMA[®] modeling of EM data for this site is available digitally for review in detail, and summarized on [Figure 11](#). Modeling suggests a high resistivity (above 10,000 ohm—meters) near surface (0 to 0.5 meters or 1.6 foot) layer was present at the time of the survey. High resistivity soils were not initially expected given the soil type present. However, examination of the data and model suggest this is a correct assessment of site conditions, and likely reflect the well drained nature of these soils. The resistive surface layer is underlain by a conductive (500 ohm meter) zone to the depth of investigation of the EM38. The deeper model from the EM31 supports the conductive layer in the subsurface. The EMIGMA[®] model does not identify the features that are observed in the raw EM data. The absence of these features is believed to be related to the highly resistive near surface layer identified by the model.

6.2.2. Poamoho GPR

The 270 mega-hertz (MHz) antenna has the lowest frequency, and hence the least resolution. The 400 MHz and 900 MHz antennas have increasingly higher resolution. Examination of [Figure 12](#) shows a number of common features on different antenna records. Feature "A", less apparent in the 900 MHz antenna data is within a "shadow" area suggesting poor antenna contact with the ground surface and a resulting decrease in overall energy being transferred into the ground from the antenna, and hence reflecting to the surface for recording. Close examination of the record however indicates the presence of the feature consistent with the other records. Feature "B" is a good example of increasing resolution with increasing antenna frequencies. Feature "C" is a shallow feature, broader in extent, and present on records from all frequencies.

The 270 MHz antenna data was collected and processed to produce a 125 nano-second (nS) record length. Examination of the data across a number of traverses suggests in the lateritic soils of this site a 75 nS penetration is attainable, with the soil moisture levels at the time of the survey. This suggests a longer record window may be recorded in the future with the lower frequency antennas. Examination of data from other antennas suggests penetration to near the total record length.

Interpreting the GPR Data, an electromagnetic pulse traveling from soil into an air filled void will have negative and then positive reflection coefficients. Examples of interpreted voids in the GPR data are presented on [Figure 13](#). This figure shows color-scale data, and "wiggle-trace" data, a presentation much like seismic data. The color scale data makes it relatively easy to identify anomalous areas, the wiggle-trace data, along with the trace spacing permits identification of interpreted void feature width. Subsequent presentations will only contain color-scale data.

In order to assess a simplistic approach to interpretation of void locations, an automatic target identification routine from RADAN was run on the data and compared with manual target identification ([Figure 14](#)). The auto-target functions search the data hyperbolas and assign picks based on a confidence level that they are in fact hyperbolas. Auto-target also tries to search for nearby hyperbolas and assign linearity to features. Close examination of the auto-target features selected indicates several potential issues. First, the algorithm seeks the highest amplitude feature, without regard for amplitude orientation. As noted in the last paragraph, void features should exhibit negative and then positive reflection coefficients. Close examination of the auto-target feature selection shows the variations between positive and negative amplitude waveforms. The second issue is the number of picks. While the auto-target approach is conservative, and designed not to miss features, there is a need for human interaction to identify appropriate target selection. Therefore, a simple auto-target approach to void location identification will not be appropriate.

Examination of interpretation in one area in detail ([Figure 15](#)) highlights some of the challenges associated with quantitative GPR interpretation when using multiple antennas. The area containing the hyperbolas (discussed in [Section 5.2](#)) shows good relationships between the features interpreted to be voids on both the 400 MHz and 900 MHz antennas. The resolution differences between the two become apparent when manually interpreted voids are examined.

For example, Feature "I" appears to be 3 separate features with the 900 MHz antenna, but only one feature with the 400 MHz antenna. Additionally hyperbolic shaped "noise" between features "A" and "B" can be interpreted as a subtle feature on the 400 MHz position adjustment was made to the data. This vertical shift in data was different on the data sets, in part to the wavelengths of the antennas. Another issue with multiple antenna comparisons is related to the inline location of features. Despite efforts to start each traverse at a consistent origin, variations in start location and potential measurement wheel slippage have effects over the limited distances being evaluated. The inline variation can be attributed to error of measurement and provides a bit of insight into position measurement repeatability. Given the differences present based upon antennas, focus for the remainder of the document will be on the 900 MHz antenna data since it provides the highest resolution, with adequate penetration.

All final processed GPR traverse data from Poamoho is presented in Appendix C for review. Interpretation of the GPR data indicates the presence of 43 potential targets as shown on Table 2 (below). To facilitate interpretation, features that were recognizably flat were referred to as "slabs" while all other features were referred to as targets. The location presented for targets represents the lateral center of the feature and the top. The width reference for targets is based upon examination of the wiggle-trace and amplitude data. The width for slabs is calculated based on inline distances. The thick and thin references on the table are related to apparent feature amplitude and shape, and are qualitative values not quantitative.

Table 2 Poamoho GPR Line 2 Interpreted Voids

Inline (feet)	Depth (ns)	Interpreted		Feature Type	Pick Confidence
		Width (in)	Thickness		
2.87	6.701	4		Target	1
9.25	12.748	6	Thin	Target	0.5
13.12	6.983	6-9		Target	1
16.83	2.811	6	Thin	Target	1
18.54	8.108	4		Target	0.5
20.54	2.764	15	Thin	Slab	1
21.79	2.811			Slab	1
23.37	3.889	9		Target	0.5
30.58	4.451	4	Thin	Target	1
34.66	9.748	4	Thin	Target	1
38.03	2.764	9		Slab	1
38.82	2.811			Slab	1
45.11	9.092	4	Thin	Target	0.2
46.53	2.811	9		Target	1
47.57	14.623	6		Target	0.2
50.03	2.811	14	Very Thin	Slab	1
51.20	2.998			Slab	1
54.86	2.764	6		Target	0.2
59.94	4.264	6	Thick	Target	1
64.44	4.686	4		Target	1

66.77	6.842	4		Target	1
73.19	2.764	12		Slab	1
74.23	2.811			Slab	1
75.31	9.936	2	Thin	Target	1
79.90	9.186	4	Thin	Target	1
84.81	4.17	4	Thin	Target	1
87.35	4.029	6		Target	1
92.18	5.014	4		Target	1
96.89	7.826	2		Target	1
100.56	11.811	13	Thin	Slab	1
101.68	11.764			Slab	1
104.89	6.326	6		Target	1
110.60	5.811	6-9	Thick	Target	0.8
115.76	4.967	6	Thin	Target	1
119.47	10.592	6		Target	0.5
122.22	7.592	2		Target	1
124.26	9.608	2		Target	1
126.43	7.639	3		Target	0.8
129.05	9.326	4	Thick	Target	1
131.34	11.717	8	Thick	Target	1
134.38	10.123	8	Thick	Slab	1
135.01	10.076			Slab	1
136.21	2.764	2		Target	1
136.84	2.764	3		Target	1
137.55	2.764	4		Target	1
140.50	4.686	6	Slope?	Target	1
147.92	6.748	8		Target	1
149.79	6.279	6		Target	1
152.71	3.748	4		Target	0.5

6.2.3. Poamoho Seismic Refraction

Seismic refraction data for this site is presented on [Figure 17](#). The refraction data was collected during reflection data acquisition and is constrained by the reflection acquisition parameters. Overall data quality is judged to be fair. Bedrock was not encountered with the refraction data. Near surface soil velocities were determined to be in the range of 600 to 1500 feet per second (FPS). The depth of penetration for the wavepath eikonal travelttime (WET) tomographic inversion was limited to 1.5 feet for most of the line due to the low velocities present. One limited area of low velocity is present between inline distances 55 and 60 feet.

The Delta-t-V tuning ray inversion identifies several locations of low velocity. The inversion approach is limited to the identification of the top of a low velocity feature, and depths to features below this point cannot be determined. Therefore, only feature tops are identified. An

alternate interpretation would be that most of the features interpreted as voids are simply velocity artifacts in the data. On [Figure 17](#), a number of low velocity features are identified as potential void features. The inline distances and depths are summarized on [Table 3](#), below.

Table 3 Poamoho Seismic Refraction Line 2 Interpreted Voids

Feature	Inline Distance (ft)		Width (ft)	Depth (ft)
	Start	End		
A	16.8	18.5	1.7	0.75
B	54.3	55.9	1.6	1.0
C	61.1	62.0	0.9	1.0
D	68.8	70.6	1.8	2.7
E	85.0	86.9	1.9	2.7
F	97.6	99.1	1.5	1.4
G	119.1	120.5	1.4	4.5
H	141.4	142.4	1.0	3.0
I	146.0	148.5	2.5	2.6

As observed on the table, no features are interpreted to be less than 1.0 feet below ground surface. This is believed to be a function of the refraction method and the 1-foot geophone spacing.

6.2.4. Poamoho Seismic Reflection

The common depth point (CDP) stack of the Poamoho seismic reflection data is presented on [Figure 18](#). The reflection data is 6-fold, suggesting there are 6 traces at each location that have been added together to make one CDP trace. Due to processing requirements, the CDP numbers shown on the figure are the same as base station numbers plus 1000. Therefore, inline distance of 10 is presented as CDP 1010. Observation of the stacked seismic section indicates undulating near surface reflectors. Posted over the section are the potential void features interpreted from the refraction data ([Table 3](#) above). Examination of the reflection section indicates variations in waveform are present at the locations of the refraction features. However, other waveform variations are also present, which could be interpreted to represent void features.

Two important features should be noted. The frequency of the data is such that one half cycle is 5 milliseconds (mS). This is a lower frequency than observed in the field records. When slight noise or imperfections in normal move out velocities are present, the addition of several traces has the effect of lowering the frequency of the data. Therefore, interpretation of the reflection data may be best served by examining the Poamoho common offset data contained in [Appendix D](#).

A more fundamental problem may be made when observing that most of the changes go all the way to the ground surface. Examination of the common offset data ([Appendix D](#)) suggests the data is not related to statics. Statics are surface based velocity anomalies that are inherent in CDP data when either the source or a receiver passes over the surface location contributing the velocity shift. Normally statics problems result in noisy, lower frequency data.

Due to the low frequency of the stacked data, and the near surface origin of reflection features that can be associated with the refraction features, the value of the reflection data for interpretation of small near surface features can be called into question. Therefore, no void feature interpretation is presented for the reflection data.

6.3. Waimanalo Research Station, Island of Oahu

6.3.1. Waimanalo EM

EM31 conductivities ranged from approximately 38 to 115 mS/m and 10 to 75 mS/m for the EM38 data. All conductivity measurements indicate high conductivity near the origin of the survey area, with decreasing conductivities toward higher station numbers.

Inphase response ranges from -15 to 20 ppt for both data sets. Abrupt changes in inphase response are present at an inline distance of 89 feet on the EM38 data set ([Figure 19](#)) which are absent on the EM31 ([Figure 20](#)) data. This response suggests a small, shallow metallic target or interference source at this location.

EMIGMA[®] modeling of EM data for this site is available digitally for review in detail, and summarized on [Figure 21](#). EM38 modeling suggests a low resistivity near surface layer, with increasing resistivities to a depth of 1 to 1.5-meters. The low resistivity layer is thicker toward the line origin, thinning along the line with increasing stations. No significant void features are present in this data set alone. The EM31 model supports the EM38 model extending the increasing resistivity to the depth of investigation. The combined EMIGMA[®] model presents the most interesting results. A modeled high resistivity layer is variable in both thickness and depth. This may be related to excavation activities associated with placement of the void features. Very high resistivities would be representative of subsurface voids, which in nature would have a near infinity resistivity. Therefore, the extreme resistivities should be considered as viable void features along this line.

The center line was imported into Surfer, a commercial software package that permits contouring and presentation of data. Surfer kriging algorithm was used to interpolate the modeled resistivity data to a 0.5 foot grid, which was contoured for detailed interpretation ([Figure 22](#)). High resistivity void features identified on the center line (line 2) in Waimanalo are summarized on [Table 4](#). The data suggests a significant lateral change in near surface resistivities at an inline distance of 32-feet, with an increased resistivity below 4-feet. Within the initial section of the line, nine potential void features are interpreted present. Lateral resolution of the model, as well as the contouring grid does not permit an estimate of small void sizes. At inline distances greater than 32-feet, only one shallow void target (feature "R") is interpreted present in the model data. However, a number of larger void targets are apparent. The large features all appear to be deeper than 5-feet.

Table 4 Waimanalo Line 2 Interpreted Resistivity Void Features

Feature	Inline (ft)	Depth (ft)	Interpretation
A	15.0	-2.4	Void rectangular
B	17.0	-2.5	Possible vertical
C	19.3	-2.9	Possible rectangular
D	23.0	-2.2	Void rectangular
E	24.9	-3.0	Void
F	27.0	-2.3	Void vertical
G	30.0	-2.9	Void
H	30.0	-3.1	Void
I	31.9	-0.1	Void vertical
J	34.5	-8.4	Possible void small and deep
K	52.9	-7.9	Void 3-foot diameter deep
L	57.9	-9.4	Void small deep
M	63.0	-5.7	Void
N	64.0	-6.8	Possible void
O	65.0	-5.7	Possible void 2-foot diameter
P	70.0	-5.8	Void
Q	75.9	-5.7	Possible void
R	77.0	-3.2	Possible void
S	81.0	-5.6	Possible 1-foot diameter void
T	86.0	-5.6	Possible void
U	87.1	-6.0	Possible void
V	124.0	-6.8	Void 1-foot diameter
W	127.5	-6.5	Void 2-foot diameter
X	130.4	-7.6	Void 3-foot diameter
Y	134.1	-7.7	Void 3-foot diameter
Z	133.8	-2.0	Void

6.3.2. Waimanalo GPR

In general, the GPR data for Waimanalo does not appear to have the resolution that was seen in Poamoho. The 270 MHz antenna data was collected and processed to produce a 125 nano-second (nS) record length. Examination of the data across a number of traverses suggests in the fatty clay soils of this site a 30 to 35 nS penetration is attainable with the soil moisture levels present at the time of the survey. Examination of data from other antennas suggests penetration is less with other antennas. The 400 MHz antenna data quality degrades below 25 nS, while the 900 MHz penetration is limited to approximately 20 nS. The high resolution 1.5 GHz antenna penetration is limited to approximately 10 nS. All final processed GPR traverse data from Waimanalo is presented in [Appendix E](#) for review.

Interpretation of the GPR data indicates the presence of 31 potential targets as shown on [Table 5](#) (below). To facilitate interpretation, features that were recognizably flat were referred to as "slabs" while all other features were referred to as targets. The location presented for targets represents the lateral center of the feature and the top. The width reference for targets is based upon examination of the wiggle-trace and amplitude data. The width for slabs is

calculated based on inline distances. The thick and thin references are related to apparent amplitude and waveform; and are qualitative values not quantitative.

Table 5 Waimanalo GPR Line 2 Interpreted Voids

Inline (feet)	Depth (ns)	Interpreted		Feature Type	Pick Confidence
		Width (in)	Thickness		
10.87	8.72	4		Target	1
17.12	2.95	3		Target	0.2
23.29	8.11	6		Target	1
24.91	5.25	6	Thick	Target	0.2
27.08	7.50	19		Slab	1
28.70	7.31			Slab	1
31.70	2.91	2		Target	1
38.91	8.72	6	Thick	Target	1
46.03	4.45	3	Thick	Target	0.2
52.24	2.91	2		Target	1
58.23	3.84	2		Target	0.2
61.65	3.84	4	Thick	Target	1
66.23	3.52	4		Target	0.2
70.15	3.89	4	Thin	Target	1
72.90	2.91	46		Slab	1
76.73	2.91			Slab	1
77.69	4.64	19	Dipping	Slab	1
79.27	4.17			Slab	1
82.27	5.30	6	Thick	Target	1
83.77	5.16	6		Target	1
88.23	5.06	4	Thin	Target	0.2
96.35	3.47	4		Target	1
102.68	5.58	6		Target	1
107.39	14.95	6		Target	0.2
109.89	5.44	38		Slab	1
113.05	3.89			Slab	1
114.93	4.27	4		Target	1
122.55	6.56	23		Slab	1
124.51	6.66			Slab	1
127.92	5.67	4		Target	1
133.38	3.75	2		Target	1
135.00	2.58	2		Target	1
136.80	4.22	2		Target	1
142.04	3.42	2		Target	1

6.3.3. Waimanalo Seismic Refraction

Seismic refraction data for this site is presented on [Figure 23](#). The refraction data was collected during reflection data acquisition and is constrained by the reflection acquisition parameters. Overall data quality is judged to be good. Bedrock was not encountered with the refraction data; however the 3,000 feet per second (FPS) response at 5-feet below ground surface under normal circumstances would be interpreted to represent weathered bedrock material. Near surface soil velocities were determined to be in the range of 500 to 1600 feet per second (FPS). The depth of penetration for the WET tomographic inversion was limited to approximately 5 feet for most of the line. One limited area of low velocity is present between inline distances 100 and 110 feet inline distance.

The Delta-t-V tuning ray inversion identifies several locations of low velocity, which would be expected for a void feature. The inversion approach is limited to the identification of the top of a low velocity feature, and depths to features below this point cannot be determined. Unlike Poamoho, the Delta-t-V data for this line does establish relatively consistent velocity fields for the subsurface. This suggests that most of the void features at the Waimanalo site are smaller than those of Poamoho. On [Figure 23](#), a number of low velocity features are identified as potential void features. The inline distances and depths are summarized on [Table 6](#), below.

Table 6 Waimanalo Seismic Refraction Line 2 Interpreted Voids

Feature	Inline Distance (ft)		Width (ft)	Depth (ft)
	Start	End		
A	19.3	20.7	1.3	-0.8
B	33.1	34.1	1.0	-1.0
C	39.9	41.5	1.6	-3.9
D	50.9	54.4	3.5	-5.6
E	54.8	55.9	1.1	-1.3
F	64.9	69.0	4.1	-2.6
G	72.1	72.4	0.4	-0.5
H	75.6	76.9	1.3	-0.8
I	81.8	82.8	1.0	-0.5
J	89.1	91.0	1.8	-1.2
K	99.0	99.2	0.2	-0.7
L	102.9	104.5	1.6	-0.7
M	111.8	114.9	3.2	-0.8
N	137.7	138.4	0.7	-0.6
O	150.1	152.9	2.8	-1.3
P	158.7	159.5	0.9	-0.9

An alternate interpretation would be that most of the features interpreted as voids below are simply velocity artifacts within the data. Using the Delta-t-V method, small areas of unusually high or low velocity can be created in the model based on very small data inconsistencies. In a homogeneous environment these features would be considered to be wrong. However, with careful attention to the data, in this particular application, the velocity variations are to be expected and are therefore appropriate within the model.

In general, more features were able to be interpreted within the Waimanalo refraction data than were apparent in the Poamoho refraction data. A more aggressive interpretation may interpret more, smaller features, but at this time, they are believed to represent noise in the data.

6.3.4. Waimanalo Seismic Reflection

The common depth point (CDP) stack of the Poamoho seismic reflection data is presented on [Figure 24](#). The reflection data is 6-fold, indicating there are 6 traces at each location that have been added together to make one CDP trace. Due to processing requirements, the CDP numbers shown on the figure are the same as station numbers plus 1000. Therefore, inline distance of 10 is presented as CDP 1010. Observation of the stacked seismic section indicates undulating near surface reflectors. Posted over the section are the potential void features interpreted from the refraction data ([Table 6](#) above). Examination of the reflection section indicates variations in waveform are present at the locations of the refraction features. However, other waveform variations are also present, which could be interpreted to represent void features.

Two important features should be noted. The frequency of the data is such that one half cycle is 5 milliseconds (mS). This is a lower frequency than observed in the field records. When slight noise or imperfections in normal move out velocities are present, the addition of several traces has the effect of lowering the frequency of the data.

A more fundamental problem may be made when observing that most of the changes go all the way to the ground surface. The “checkerboard” appearance between CDP 1095 and 1120 are similar to static problem noise. However, surface consistent statics were not able to resolve the issue on this particular line. Due to the low frequency data and apparent lack of resolution, no further interpretation of void features has been made from this reflection data.

6.4. Port of Kawaihae, Island of Hawaii

6.4.1. Kawaihae EM

EM31 conductivities ([Figure 25](#)) ranged from 420 to 530 mS/m and from 190 to 400 mS/m for the EM38 data ([Figure 26](#)). These are abnormally high conductivities, interpreted to be related to residual sodium and chloride ions in the dredge material which make up the soils of this site. Conductivities are generally consistent across the site, with slightly increasing conductivities in the EM31 horizontal dipole and EM38 vertical dipole data sets after between station 90 and the end of the lines. The depth of investigation of these two data sets suggests drier (lower conductivity) sandy material is present in this area.

At the Kawaihae site, magnetic susceptibility data was not present in the downloaded EM31 data set. Inphase response of the EM38 data ranges from 8 to 13 parts per thousand (ppt) of the total field strength for both data sets. No abrupt changes in inphase response are present in the data.

EMIGMA® modeling of EM data for this site (Figure 27) presented some challenges. The shallow EM38 data inversion indicates resistivities below 2.6 ohm-meters to a depth of 2 meters, the depth of investigation for this instrument. The EM31 data inversion indicates low resistivities continue to 5 meters and then increase to 1000 ohm-meters below this depth. Inversion modeling presents a very similar picture of the subsurface. In terms of geologic significance, these results are extremely unusual. Adjacent to the ocean, visual inspection of the site suggests conditions would result in a high resistivity near surface due to dry, well drained sandy material. The saltwater table is expected at or near 3-meters (10-feet), would be expected to result in conductive material at this depth. Therefore, the modeled high resistivity at depth is very unexpected, and warrants further assessment.

6.4.2. Kawaihae GPR

The 270 MHz antenna data was collected and processed to produce a 125 nano-second (nS) record length. Examination of the data across a number of traverses suggests in the sandy carbonate soils of this site a 50 nS penetration may have been attained. Examination of data from other antennas suggests penetration is less with other antennas. The 400 MHz antenna data quality degrades below 20 nS, while the 900 MHz penetration is limited to approximately 15 nS. The high resolution 1.5 GHz antenna penetration is limited to less than 10 nS. All final processed GPR traverse data from Kawaihae is presented in Appendix F for review.

Manual interpretation of the GPR data indicates the presence of 32 potential targets as shown on Table 7 (below). To facilitate interpretation, features that were recognizably flat were referred to as “slabs” while all other features were referred to as targets. The location presented for targets represents the lateral center of the feature and the top. The width reference for targets is based upon examination of the wiggle-trace and amplitude data. The width for slabs is calculated based on inline distances.

Table 7 Kawaihae GPR Line 2 Interpreted Voids

Inline (feet)	Depth (ns)	Interpreted Width (in)	Thickness	Feature Type	Pick Confidence
1.13	3.28	6		Target	1
2.75	6.89	6	Thick	Target	0.5
7.17	2.63	14		Slab	1
8.37	2.96			Slab	1
11.12	3.71	10	Dipping?	Target	1
18.41	3.33	4		Target	1
19.74	3.14	2		Target	1
25.37	5.07	30		Slab	1
27.91	5.11			Slab	1
38.74	3.05	2		Target	0.5
41.03	9.66	6		Target	1
42.53	3.28	23		Slab	1
44.45	3.24			Slab	1
45.90	15.61	4		Target	0.2
46.53	6.28	6		Target	1

50.69	11.11	4		Target	1
54.24	2.86	6	Thick	Target	0.2
55.69	2.91	2		Target	0.2
58.65	2.91	4		Target	0.2
63.61	10.13	6		Target	1
67.81	3.85	4		Target	1
75.35	3.66	2		Target	0.2
86.02	4.03	6		Target	1
91.10	15.71	6	Thick	Target	0.5
104.35	3.61	29		Slab	1
106.76	3.47			Slab	1
108.59	2.82	4		Target	1
113.22	4.41	23		Slab	1
115.18	4.32	6		Slab	1
115.72	11.96	12		Target	0.2
118.30	4.46	4		Target	1
128.21	4.22	6		Target	0.2
132.75	4.18	2		Target	1
140.25	4.55	6	Thick	Target	1
141.63	13.03	6		Target	1
143.79	3.80	2		Target	1
146.04	3.66	4		Target	0.2

Table 7 has to be used with extreme caution. Examination of all GPR data (Figure 28) indicates no traverse recorded 155-feet of data intended. The poorest data set (400 MHz) recorded only 122 feet of data, while the best data set (900 MHz) recorded 146.75 feet of data. While care was used in recording the data, the soft-sandy surface resulted in inline distance wheel slippage. This disparity was not observed by field personnel. Therefore, the interpreted presence of voids will not be easily re-established and the void widths are suspect.

6.4.3. Kawaihae Seismic Refraction

Seismic refraction data for this site is presented on Figure 29. The refraction data was collected during reflection data acquisition and is constrained by the reflection acquisition parameters. Overall data quality is judged to be fair. Neither bedrock nor watertable (anticipated velocity of 5,000 feet per second [FPS]) were encountered with the refraction data. Near surface soil velocities were determined to be in the range of 600 to 1400 feet per second (FPS). The depth of penetration for the WET tomographic inversion was limited to approximately 3.5 feet for most of the line due to the low velocities present.

The Delta-t-V tuning ray inversion identifies several locations of low velocity which would be expected for a void feature. The inversion approach is limited to the identification of the top of a low velocity feature and depths to features below this point cannot be determined. On Figure 29, a number of low velocity features are identified as potential void features. The inline

distances and depths are summarized on [Table 8](#) below. An alternate interpretation would be that most of the features interpreted as voids below are simply velocity artifacts within the data.

Table 8 Kawaihae Refraction Line 2 Interpreted Voids

Feature	Inline (ft)		Width (ft)	Depth (ft)
	Start	End		
A	-2.43	-0.53	1.90	-0.67
B	13.55	16.08	2.53	-2.80
C	24.02	24.47	0.45	-2.19
D	47.77	49.48	1.72	-1.75
E	53.27	53.72	0.45	-1.08
F	64.47	65.10	0.63	-0.84
G	67.54	67.99	0.45	-0.74
H	73.49	73.95	0.45	-1.83
I	95.16	95.97	0.81	-1.00

Surface observations of changed conditions with increased station number are reflected in the reduced number of low velocity features interpreted after inline distance 100. In general, fewer features were able to be interpreted within the Kawaihae refraction data than the other data sets collected.

6.4.4. Kawaihae Seismic Reflection

The common depth point (CDP) stack of the Kawaihae seismic reflection data is presented on [Figure 30](#). The reflection data is 6-fold, indicating there are 6 traces at each location that have been added together to make one CDP trace. Due to processing requirements, the CDP numbers shown on the figure are the same as station numbers plus 1000. Observation of the stacked seismic section indicates undulating near surface reflectors. Posted over the section are the potential void features interpreted from the refraction data ([Table 8](#) above). Examination of the reflection section indicates variations in waveform are present at the locations of the refraction features. However, other waveform variations are also present, which could be interpreted to represent void features.

Two important features should be noted. The frequency of the data is such that one half cycle is 5 milliseconds (mS). This is a lower frequency than observed in the field records. When slight noise or imperfections in normal move out velocities are present, the addition of several traces has the effect of lowering the frequency of the data.

7. GEOPHYSICAL DATA SUMMARY AND CONCLUSIONS

The investigation work scope included standard and/or routinely accepted practices of the geophysical industry, with adjustments made to accommodate the void features and research nature of the project. Dawood typically utilizes multiple geophysical investigation methods as a means to provide a series of checks and balances to produce subsurface models that reflect, as uniquely as possible, the subsurface conditions at the site. By nature, no subsurface survey is 100 percent accurate and Dawood cannot accept responsibility for inherent technique limitations, survey limitations or unforeseen site-specific conditions. The identified boundaries

separating materials of different physical properties may or may not coincide with boundaries separating materials of different lithologic, geologic or soil composition. This may result in the geophysical interpretation varying somewhat from the gross geologic, lithologic or soils setting of the site. With these constraints in mind, Dawood has drawn the following conclusions:

7.1. Poamoho Research Station, Island of Oahu

Raw EM data permitted the identification of a limited number of anomalous features in the data, but was unable to identify depth or diameter of these features. The EMIGMA[®] model does not identify the features that are observed in the raw EM data. The absence of these features is believed to be related to the highly resistive near surface layer identified by the model.

At Poamoho, the vertical velocity profile was found to be variable (Figure 8). The implication is that any depth estimates from the GPR data under the test conditions used will be variable at best.

Examination of the data across a number of traverses suggests in the lateritic soils of this site a 75 nS penetration is attainable, with the soil moisture levels at the time of the survey. This suggests a longer record window may be recorded in the future with the lower frequency antennas to assess deeper void features.

Interpretation of the GPR data indicates the presence of 43 potential voids, while seismic refraction data interpretation identified 9 potential voids. The disparity suggests the GPR interpretation may include some natural features, while the seismic refraction data overlooks some of the smaller features.

7.2. Waimanalo Research Station, Island of Oahu

Waimanalo was the only site where estimates of void targets were made using EM modeled resistivity values. Waimanalo also had the least conductive soils of the three sites assessed, and measured conductivities were within a “normal” range for the EM equipment.

Interpretation of the EM modeling identified 26 potential voids. GPR data indicates the presence of 31 potential voids, while seismic refraction data interpretation identified 16 potential voids.

7.3. Port of Kawaihae, Island of Hawaii

Kawaihae EM data was the highest measured conductivity, approaching the saturation limit for most EM equipment. The high conductivities provided some unusual model results. Adjacent to the ocean, the site gives an outward appearance of having a high resistivity near surface due to dry, well drained sandy material. A saltwater table is expected at or near 3-meters (10-feet). Therefore, the modeled high resistivity at this depth is very unexpected and warrants further assessment.

The high conductivity soils also reduced the depth of penetration with the GPR. The variability of the sandy soil surface provided additional and unique position measurement challenges for GPR data. Future work should assess the use of an artificial surface placed over the sand in order to reduce wheel slippage issues.

Interpretation of the GPR data indicates the presence of 32 potential voids, while seismic refraction data interpretation identified 9 potential voids. At this site, subsurface variability made "over-interpretation" of GPR data inevitable with more potential targets identified than are likely present. In part, some of the extraneous interpreted voids may be reef fragments, and the associated signal multiples, resulting in interpreted features of the proper polarity, but originating from improper targets.

7.4. Electromagnetic Methods

EMIGMA was chosen to perform EM modeling because it is one of the very few EM modeling programs available commercially. The use of this model is relatively straight forward and seemed to meet the survey needs and objectives. Models containing the EM31 data had a 7.532 meter (24.12 feet) model constructed, while the EM38 data alone were limited to 2.0 meters (6.5 feet). Models in EMIGMA are limited to 20 vertical layers. Therefore, the EM31 model vertical layer resolution is 0.3766 meters (1.2 feet), while the EM38 model vertical resolution is 0.1 meter (0.33 feet). Given the depths and sizes of the buried targets as a survey objective; the EM38 data and model alone should be sufficient to meet the survey depth objective of this project. However, limiting information to only the EM38 instrument alone could result in physical measurements and models being taken out of geologic context and therefore misconstrued.

In the lateritic soils of Poamoho, near surface resistive soils were present inhibiting effective modeling. Significant features were identified from the raw EM data that were absent in the modeled data.

In the carbonate soils of Kawaihae, EM values were extremely high and modeling provided no value. While well drained sandy soils would normally be resistive, the dredged origin of these soils suggests residual sodium chloride ions are likely contributing to the elevated conductivities measured present.

In the fatty clay soils of Waimanalo, an interpretation of voids was made from the modeled resistivities. The presence of small voids was identified. However, the lateral resolution of the model, as well as the contouring grid did not permit an estimate of small void sizes. Voids larger than 1-foot were size interpreted.

7.5. Ground Penetrating Radar Method

At Poamoho, the vertical velocity profile was found to be variable (Figure 8). The implication is that any depth estimates from the GPR data under the test conditions used will be variable at best.

Different GPR antenna's have different depths of penetration and resolution at any given site. In addition, features of interest can be masked when poor antennal contact with the ground occurs (Figure 12). In soft soil conditions such as Kawaihae, use of a survey wheel resulted in poor inline distance measurements (Figure 28).

GPR data provided the highest resolution data of the geophysical methods evaluated. However, the high resolution 1,500 MHz (1.5 GHz) antenna was limited in depth penetration to less than

1-foot at all sites. The 900 and 400 MHz antenna's experienced comparable penetration. Due to the depth of penetration, and the higher resolution, the 900 MHz antenna data became the focus of the interpretation for this report.

Manual interpretation of void-features is a necessity. However, even with the resolution, 900 MHz data presented interpretation challenges. Separation of voids from natural soil variations was a challenge. Nevertheless, the location of potential void features could be established. However, estimates of vertical void sizes were not made due to the disparity between GPR frequencies observed in the data.

7.6. Seismic Refraction Method

Seismic refraction provided unexpectedly useful results. Although the WET tomographic inversion was limited in depth of investigation due to slow velocities, the smoothing mitigated likely low velocity indicators of void features. However, the Delta-t-V method provided some remarkable low velocity features that were co-located with interpreted voids by other methods. The data indicates that the Delta-t-V method is subject to low velocity anomalies due to the approach used. Without insitu information, it is unclear how useful or valuable the Delta-t-V method may be.

First break picks on all lines was difficult due to the velocities of the soils. Normally, sound is a high frequency noise traveling at 1,100 feet per second (depending on temperature and humidity). The presence of noise often interfered with the interpretation of direct and first refracted arrival energy from the ground.

As observed on the tables, no features are interpreted to be less than 1.0 feet below ground surface. This is believed to be a function of the refraction method and the 1-foot geophone spacing. If shallower features are necessary, closer geophone spacing should be considered.

Vertical velocity variations of similar magnitude were observed at all sites. However, there was little velocity difference between the lateritic soils of Poamoho, the carbonate soils of Kawaihae, and the fatty clay soils of Waimanalo. Some basic velocity differences would be expected, with Poamoho expected to be the fastest and Kawaihae expected to be the slowest. This suggests the test may have been measuring excavation and construction consistency instead of seismic property differences between soil types. It is recommended that future testing collect data from an undisturbed area for comparison to the test area.

7.7. Seismic Reflection Method

Due to the low frequency of the stacked data, and the near surface origin of reflection features that can be associated with the refraction features, the value of the reflection data for interpretation of small near surface features can be called into question. Therefore, no void feature interpretation is presented for the reflection data.

At each site, the 6-fold CDP data resulted in lowered seismic frequencies relative to the field records. The origin of this is attributed to NMO velocity imperfections and near surface statics. However, a primary concern is the velocities measured. Refraction velocities were generally between 600 and 1,500 FPS. Therefore, two way travel times to shallow voids can be predicted as shown on the following table ([Table 9](#)).

Table 9 Anticipated Seismic Travel Times

(ft/sec)	(ft)	(mS)
600	3	0.010
700	3	0.009
800	3	0.008
900	3	0.007
1,000	3	0.006
1,100	3	0.005
1,200	3	0.005
1,300	3	0.005
1,400	3	0.004
1,500	3	0.004

This travel time prediction suggests that near surface voids will be present in the very near surface reflection data, and may not be identifiable. Using [Table 9](#) as a guide, seismic reflection is not recommended for features that are extremely small and near surface, unless a radical (by traditional standards) approach is undertaken. Future assessment should consider a further reduced sampling interval of 0.02 or 0.03125 mS, and a record length of 50 mS. Additionally, consideration should be made for the unusual use of transducers instead of geophones, with minimum frequencies of 500 hertz.

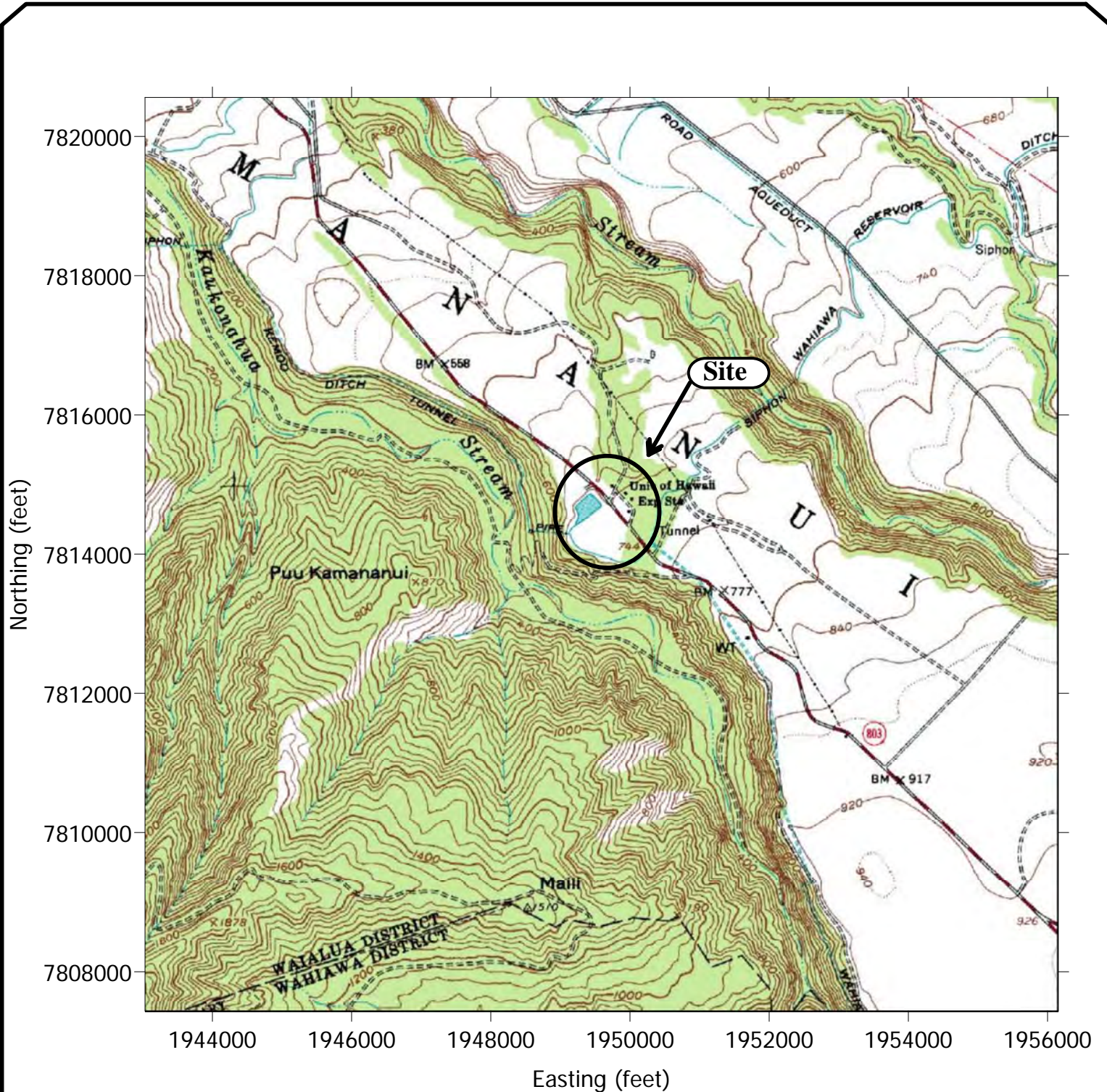
7.8. Caveats

Geophysical methods use remote physical measurements to identify, interpret, and categorize subsurface features. In many instances, there are a number of features that will provide the same physical measurement. Therefore, Dawood recommends that anomalies identified during geophysical investigations be verified using invasive methods (such as drilling or excavating). Furthermore, subsurface characteristics are variable.

8. REFERENCES

- Brueckl, E. 1987. The Interpretation of Traveltime Fields in Refraction Seismology. Geophysical Prospecting, volume 35, pp. 973-992.
- Gegrande, H. and Miller, H., 1985. Refraktionsseismik (in German). In: F. Bender (Editor), Angewandte Geowissenschaften II. Ferdinand Enke, Stuttgart; pp. 226-260. ISBN 3-432-91021-5.
- Hagerdoon, J.G., 1959. The Plus-Minus Method of Interpreting Seismic Refraction Sections. Geophysical Prospecting, volume 7, pp. 158-182.
- Jones, G.M. and Jovanovich, D.B. 1985. A ray inversion method for refraction analysis. Geophysics, volume 50, pp. 1701-1720.
- Ruehl, T., 1995. Determination of shallow refractor properties by 3D-CMP refraction seismic techniques. First Break, volume 13, pp. 69-77.
- Schuster, G.T. and Quintus-Bosz, A., 1993. Wavepath eikonal Traveltime Inversion Theory, Geophysics, Volume 58, PP. 1314-1323
- Watanabe, T. et al. 1999. Seismic traveltime tomography using Fresnel volume approach. SEG Houston 1999 Meeting, Expanded Abstracts.

Figures



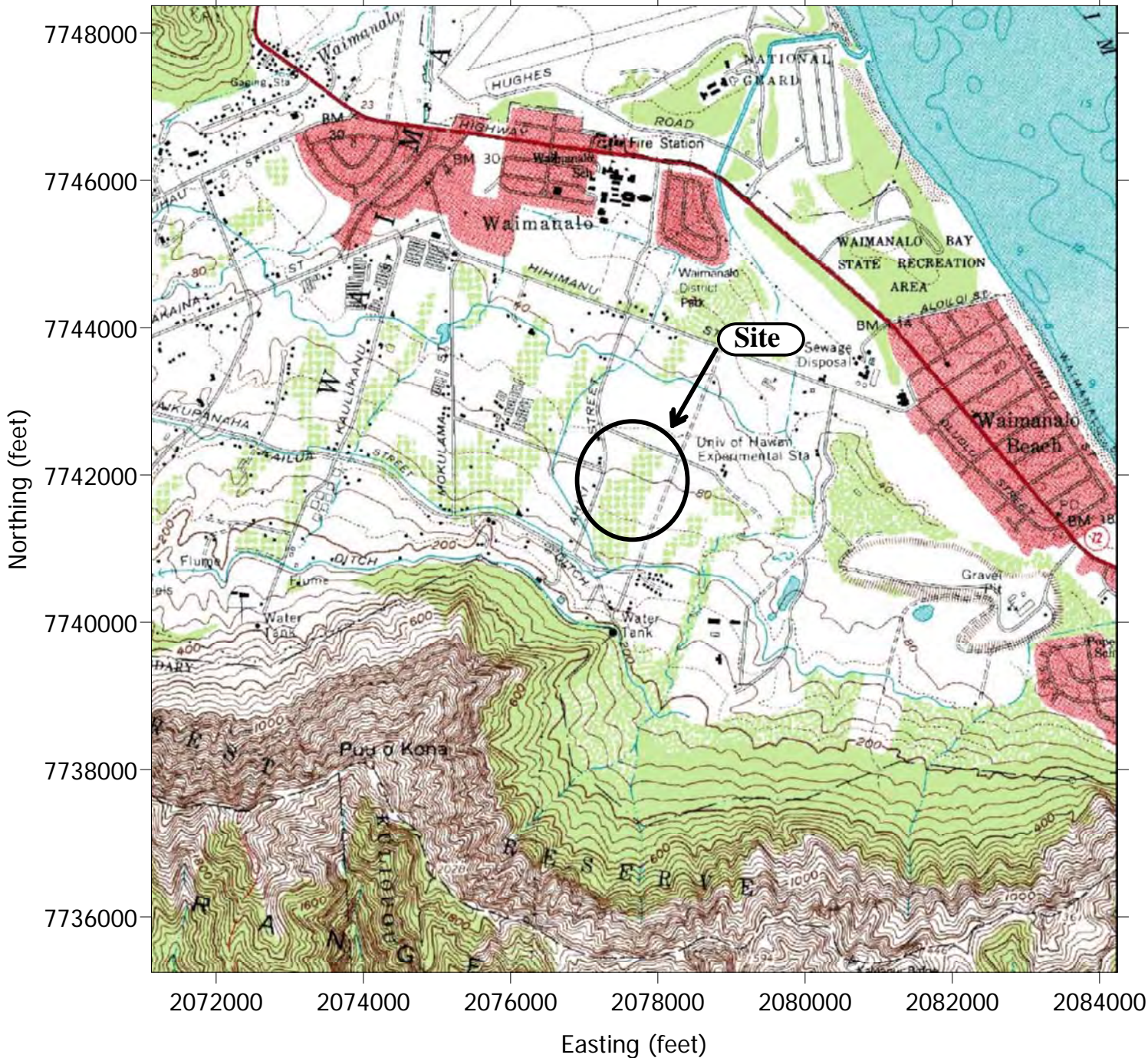
This map is from a library of scanned topographic maps that originate with published United States Geological Survey 1:24,000 scale quadrangle maps. Adjacent maps have been electronically spliced to facilitate presentation.

Site Location established using a global positioning system using North American Datum, 1983, Hawaii, Universal Transverse Mercator Projection Units are U.S. Survey Foot.



PROJECT: University of Hawaii, Manoa Poamoho, Hi	
REVISIONS	DATE

PROJECT NO.: 208044.01	 10105 ALLENTOWN BLVD. GRANTVILLE, PA. 17028 PHONE:(717)469-0937 FAX:(717)469-0938	SHEET NO.: 1
DRAWN BY: R.A.H.		
CHECKED BY: B.B.		
SCALE: AS SHOWN		
DATE: 7 July 2008	DRAWING TITLE: Poamoho Site Location Map	



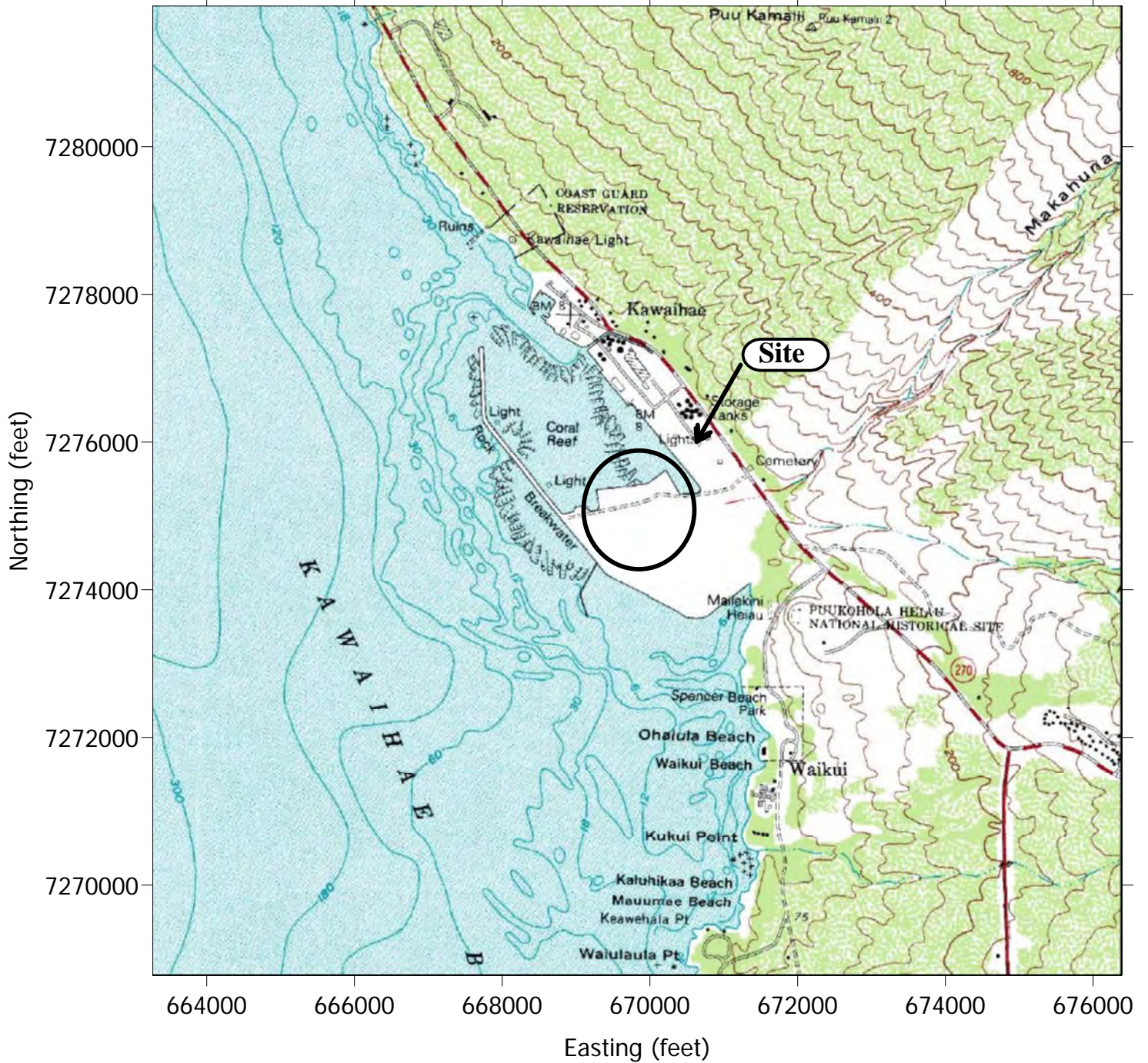
This map is from a library of scanned topographic maps that originate with published United States Geological Survey 1:24,000 scale quadrangle maps. Adjacent maps have been electronically spliced to facilitate presentation.

Site Location established using a global positioning system using North American Datum, 1983, Hawaii, Universal Transverse Mercator Projection Units are U.S. Survey Foot.



PROJECT: University of Hawaii, Manoa Waimanalo, HI	
REVISIONS	DATE

PROJECT NO.: 208044.01	 10105 ALLENTOWN BLVD. GRANTVILLE, PA. 17028 PHONE:(717)469-0937 FAX:(717)469-0938	SHEET NO.: 2
DRAWN BY: R.A.H.		
CHECKED BY: B.B.		
SCALE: AS SHOWN		
DATE: 07 July 2008	DRAWING TITLE: Waimanalo Site Location Map	



This map is from a library of scanned topographic maps that originate with published United States Geological Survey 1:24,000 scale quadrangle maps. Adjacent maps have been electronically spliced to facilitate presentation.

Site Location established using a global positioning system using North American Datum, 1983, Hawaii, Universal Transverse Mercator Projection Units are U.S. Survey Foot.



PROJECT: University of Hawaii, Manoa Kawaihae, HI	
REVISIONS	DATE

PROJECT NO.: 208044.01	 CONSULTING ENGINEERS 10105 ALLENTOWN BLVD. GRANTVILLE, PA. 17028 PHONE: (717)469-0937 FAX: (717)469-0938	SHEET NO.: 3
DRAWN BY: R.A.H.		
CHECKED BY: B.B.		
SCALE: AS SHOWN		
DATE: 07 July 2008	DRAWING TITLE: Kawaihae Site Location Map	



This air photograph is from NASA files.



PROJECT: University of Hawaii, Manoa Poamoho, Hi	
REVISIONS	DATE

PROJECT NO.: 208044.01	 CONSULTING ENGINEERS 10105 ALLENTOWN BLVD. GRANTVILLE, PA. 17028 PHONE:(717)469-0937 FAX:(717)469-0938
DRAWN BY: R.A.H.	
CHECKED BY: B.B.	
SCALE: AS SHOWN	
DATE: 7 July 2008	DRAWING TITLE: Poamoho Traverse Location Photo

SHEET NO.:
4



This air photograph is from NASA files.



PROJECT: University of Hawaii, Manoa Waimanalo, HI	
REVISIONS	DATE

PROJECT NO.: 208044.01	 CONSULTING ENGINEERS 10105 ALLENTOWN BLVD. GRANTVILLE, PA. 17028 PHONE:(717)469-0937 FAX:(717)469-0938
DRAWN BY: R.A.H.	
CHECKED BY: B.B.	
SCALE: AS SHOWN	
DATE: 07 July 2008	DRAWING TITLE: Waimanalo Traverse Location Photo

SHEET NO.:
5



This air photograph is from NASA files.

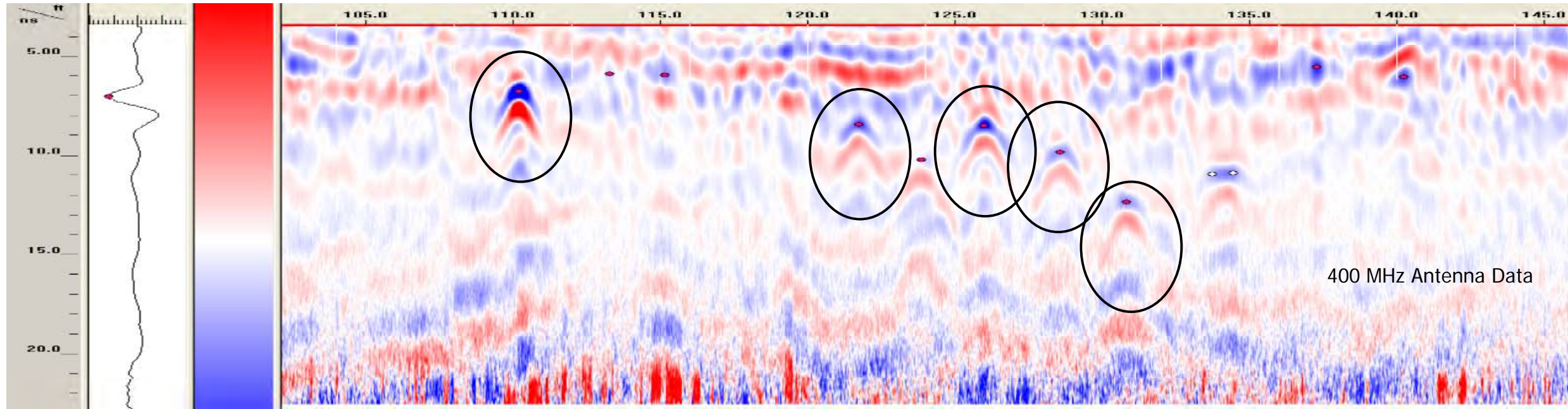


PROJECT: University of Hawaii, Manoa Kawaihae, Hi	
REVISIONS	DATE

PROJECT NO.: 208044.01	 CONSULTING ENGINEERS 10105 ALLENTOWN BLVD. GRANTVILLE, PA. 17028 PHONE:(717)469-0937 FAX:(717)469-0938
DRAWN BY: R.A.H.	
CHECKED BY: B.B.	
SCALE: AS SHOWN	
DATE: 07 July 2008	DRAWING TITLE: Kawaihae Traverse Location Photo

SHEET NO.:

6



PROJECT: University of Hawaii, Manoa	
Poamoho, HI	
REVISIONS	DATE

DAWOOD
 CONSULTING ENGINEERS
 10105 ALLEN TOWN ROAD, GRANVILLE, PA 17028
 PHONE: (717) 653-9331 FAX: (717) 653-9330

DRAWING TITLE: Target Hyperbola Example

PROJECT NO.:	208044.01
DRAWN BY:	R.A.H.
CHECKED BY:	B.B.
SCALE:	AS SHOWN
DATE:	5 Aug 2008

SHEET NO.: 7

Figure 8
Poamoho GPR Velocity Profile

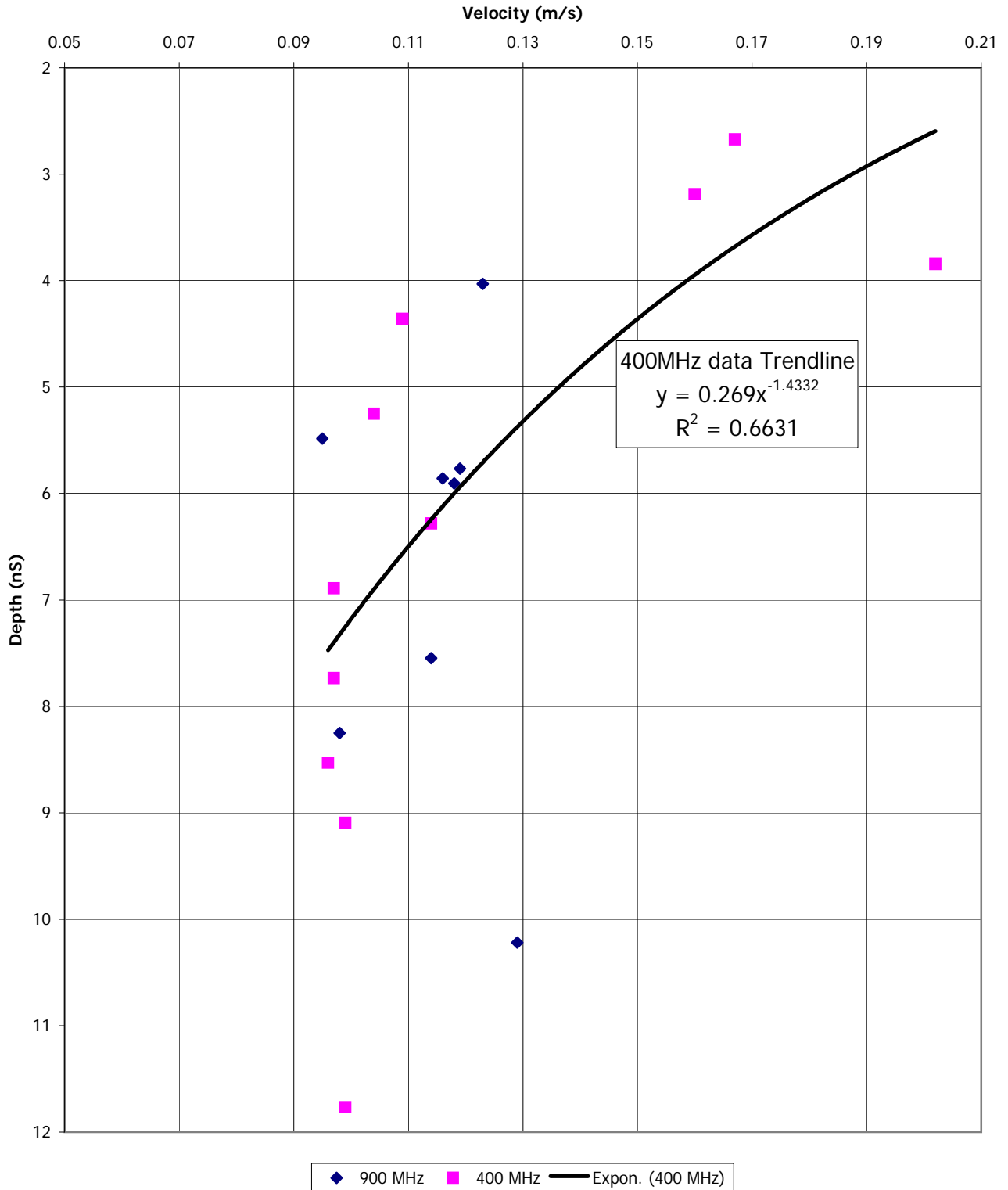
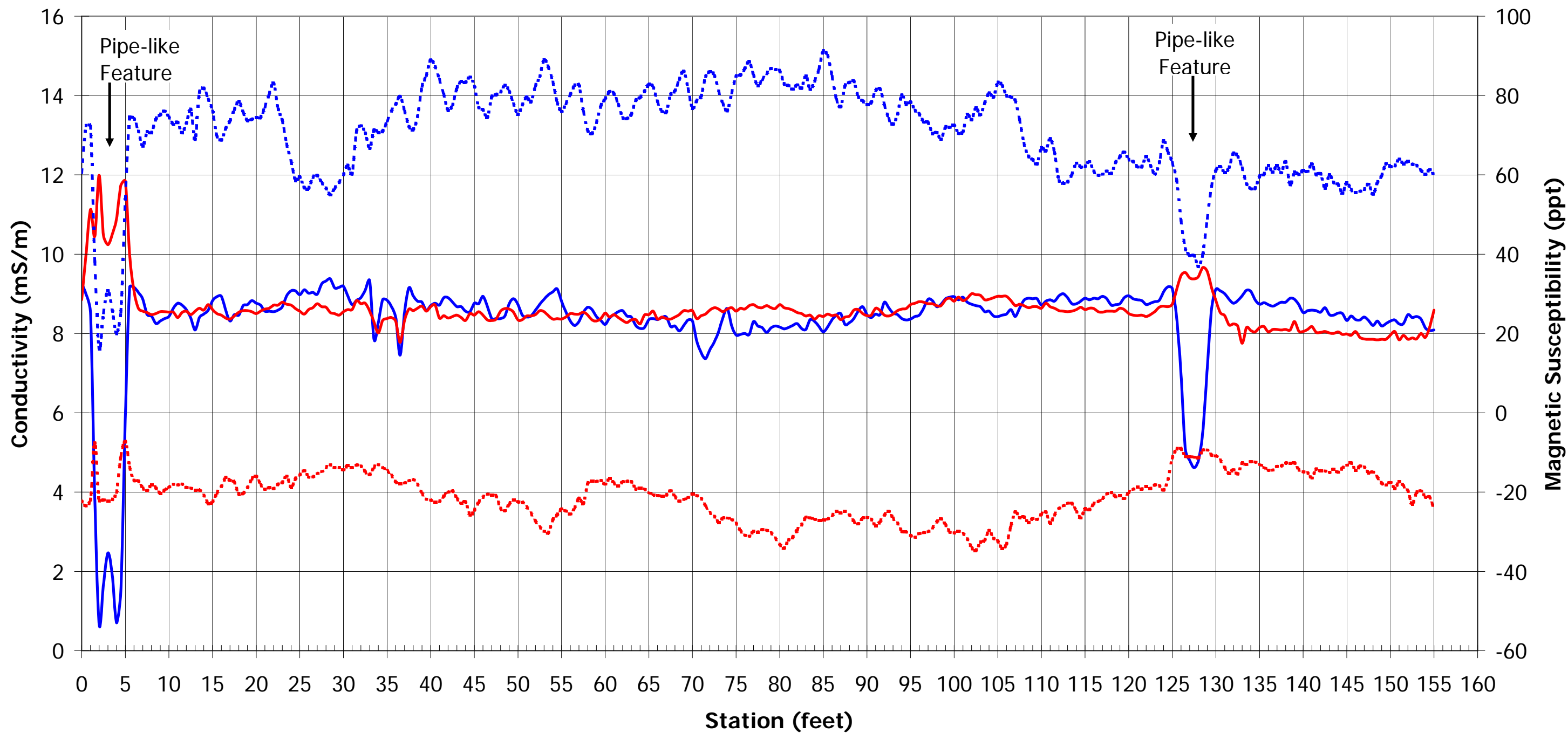
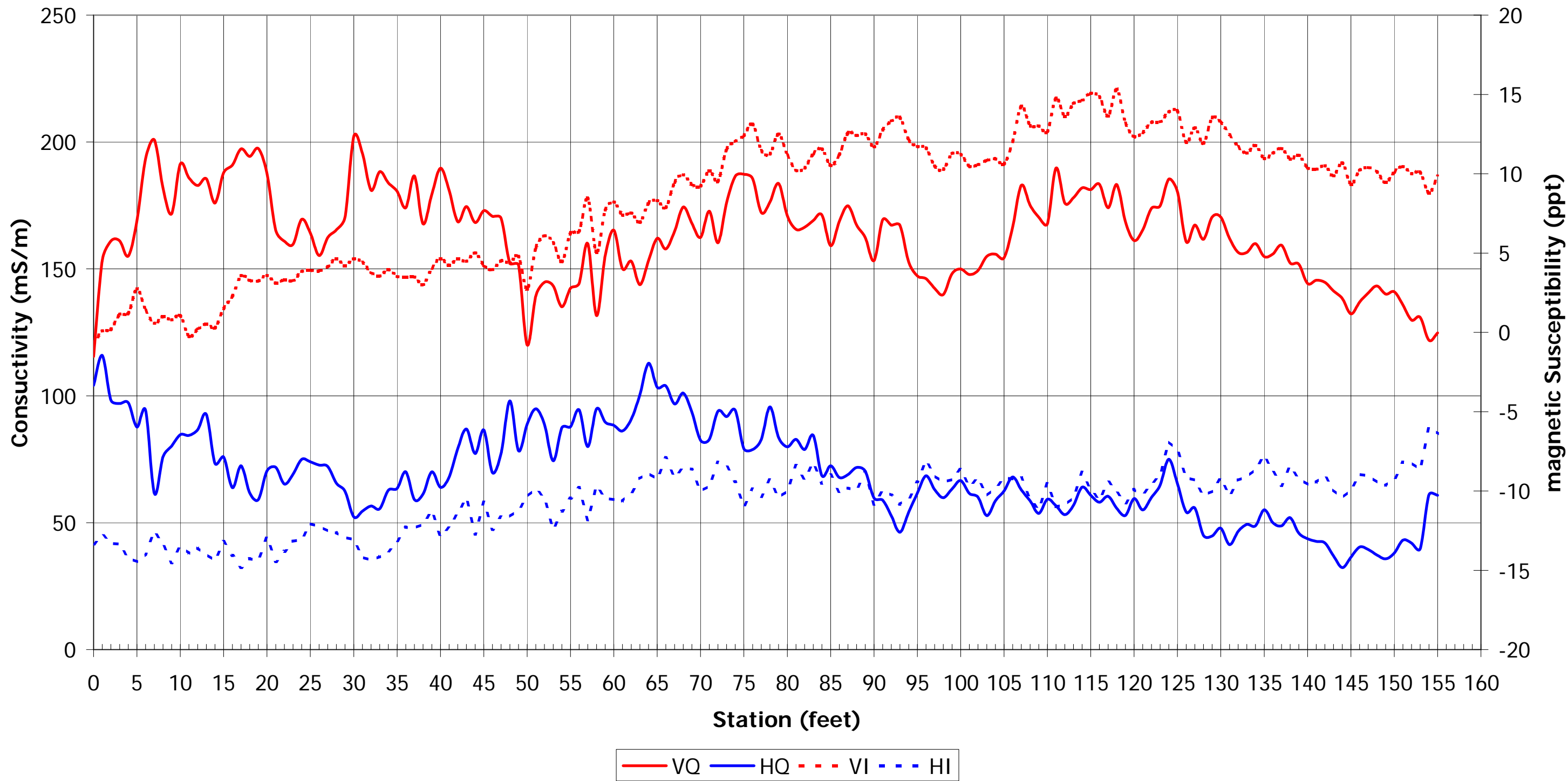


Figure 9
Poamoho EM38 Line 2 EM Data

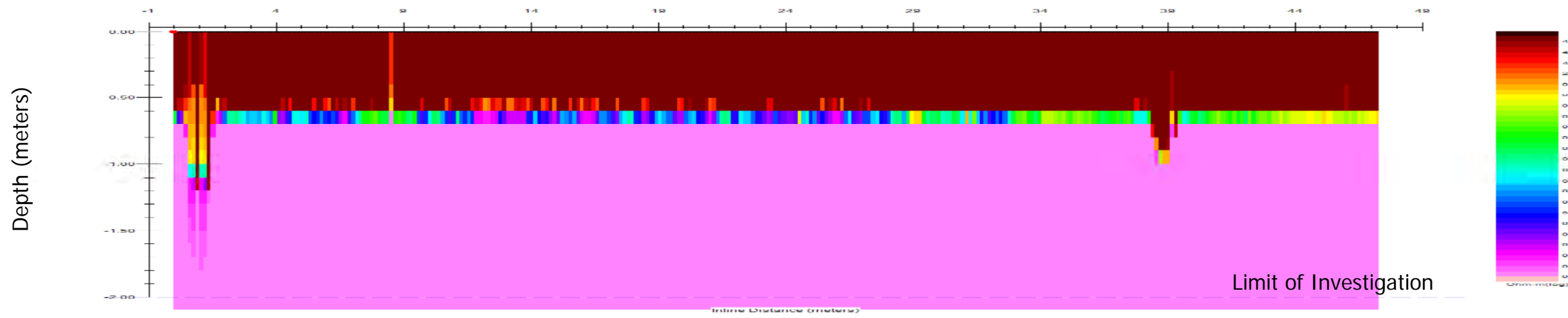


— QV — QH - - IV - - IH

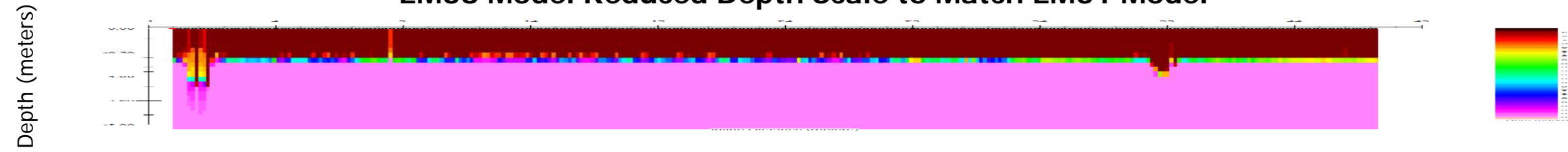
Figure 10
Poamoho EM31 Line 2 EM Data



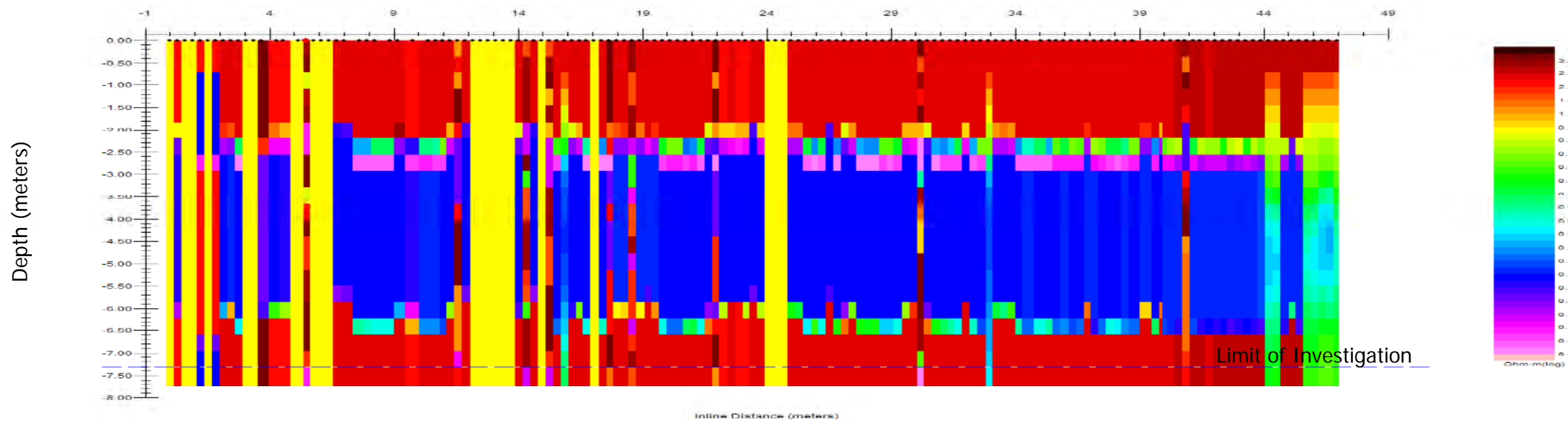
EM38 Model



EM38 Model Reduced Depth Scale to Match EM31 Model



EM31 Model



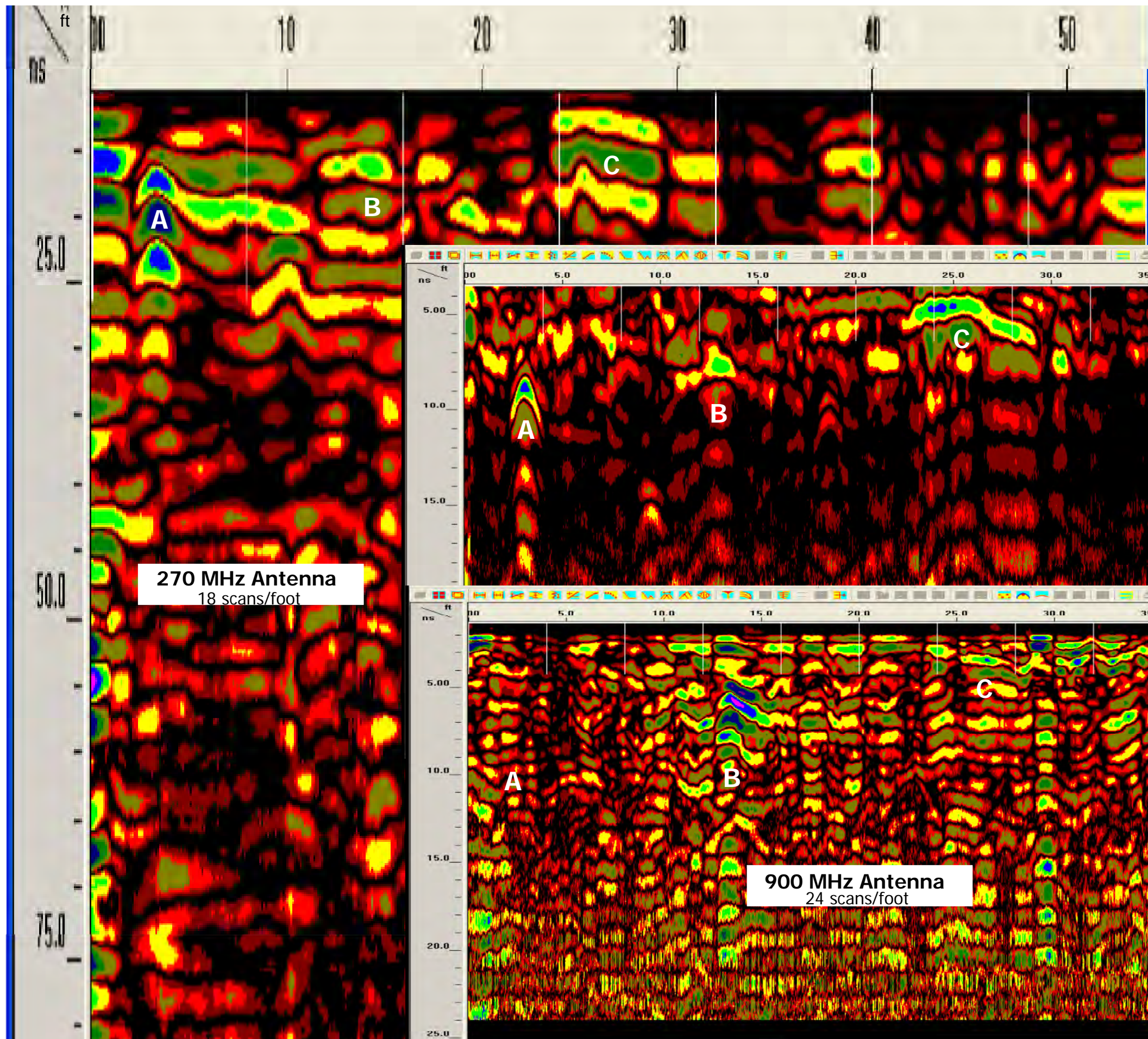
Note: Data Presented on this figure is modeled from the center (line2) data.

PROJECT:	University of Hawaii, Manoa
	Poamoho, HI
REVISIONS	DATE

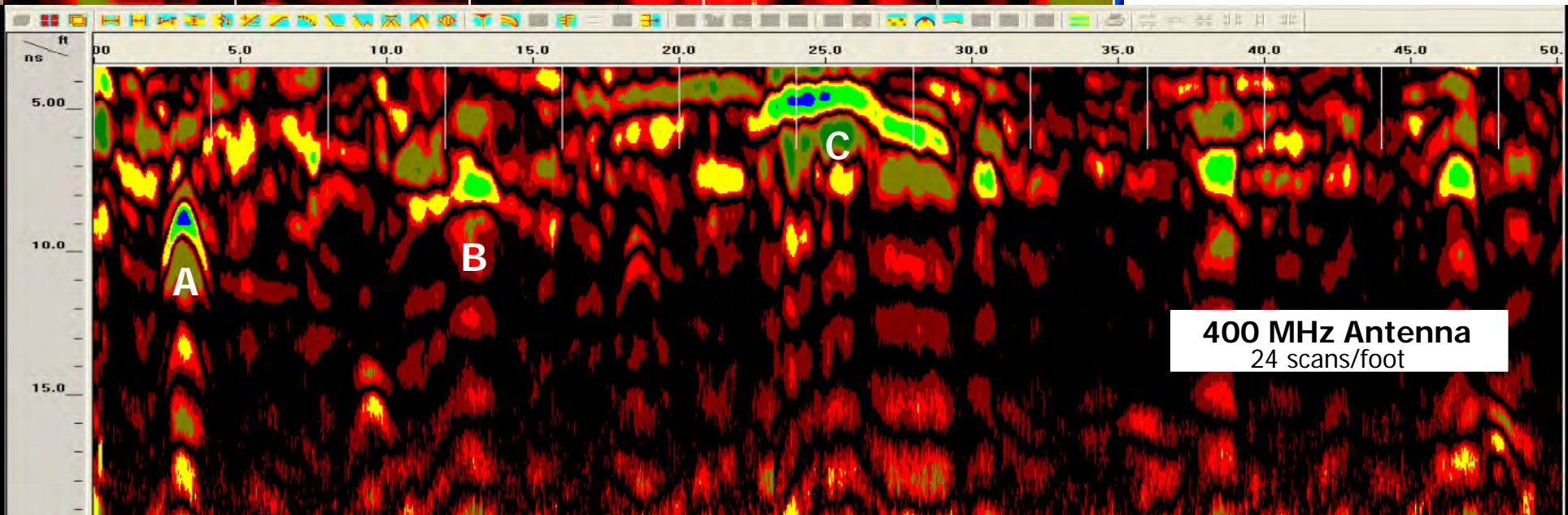
	CONSULTING ENGINEERS
	10105 ALLEN TOWN ROAD, GRANVILLE, PA 17028
PROJECT: (717) 653-7441 / (717) 653-9530	
DRAWING TITLE:	Poamoho Modeled Resistivities

PROJECT NO.:	208044.01
DRAWN BY:	R.A.H.
CHECKED BY:	B.B.
SCALE:	AS SHOWN
DATE:	5 Aug 2008

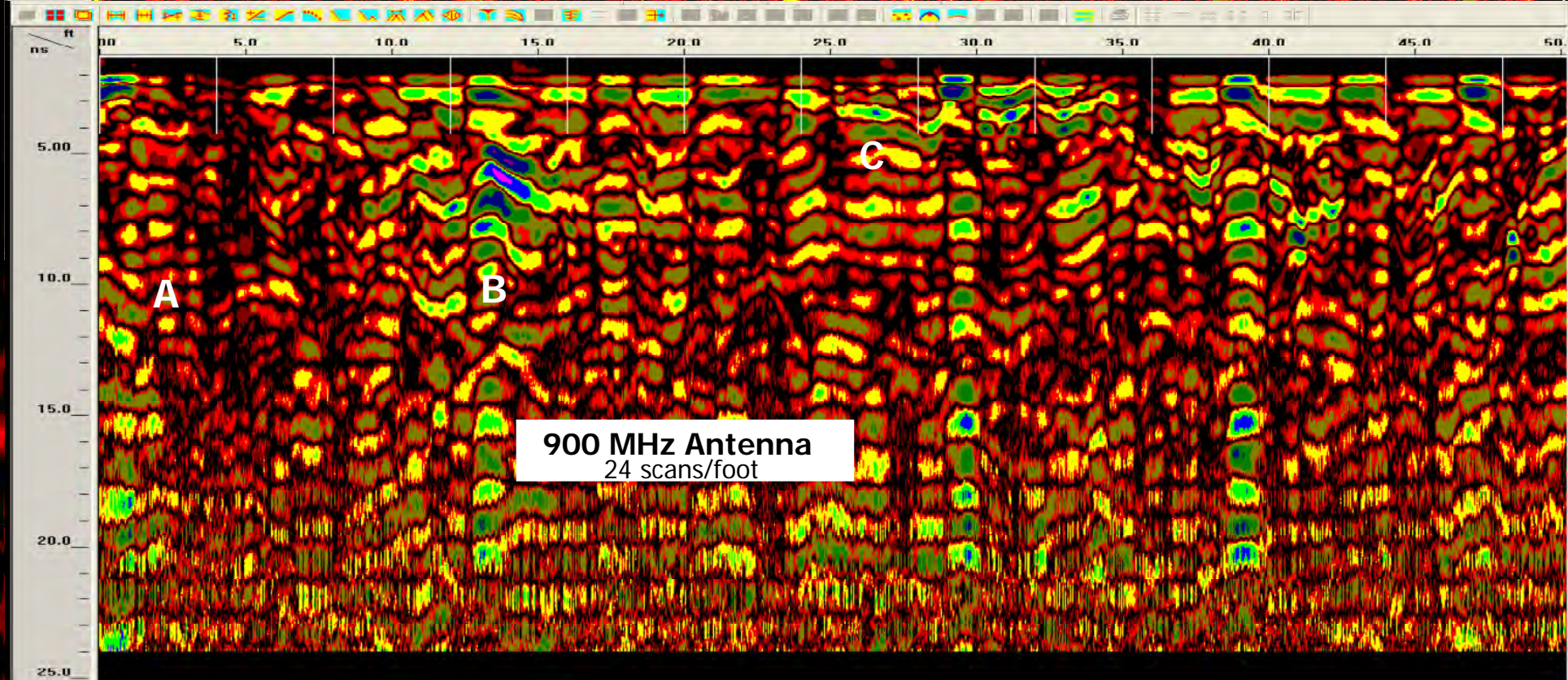
SHEET NO.: 11



270 MHz Antenna
18 scans/foot



400 MHz Antenna
24 scans/foot



900 MHz Antenna
24 scans/foot

PROJECT:	University of Hawaii, Manoa
	Poamoho, HI
REVISIONS	DATE

DAWOOD
CONSULTING ENGINEERS
10105 ALLENTOWN BLVD. GRANTVILLE, PA. 17028
PHONE: (717) 869-0637 FAX: (717) 869-0638

DRAWING TITLE:
Poamoho Antenna Comparison

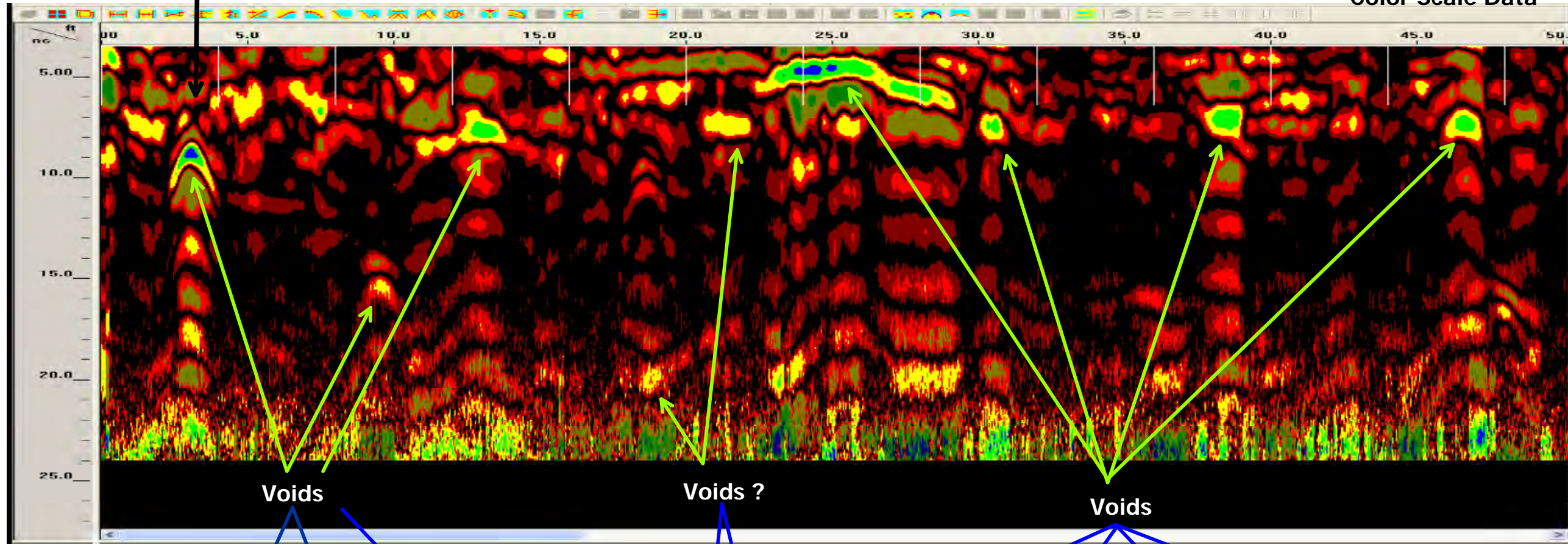
PROJECT NO.:	208044.01
DRAWN BY:	R.A.H.
CHECKED BY:	B.B.
SCALE:	AS SHOWN
DATE:	5 Aug 2008

SHEET NO.:

12

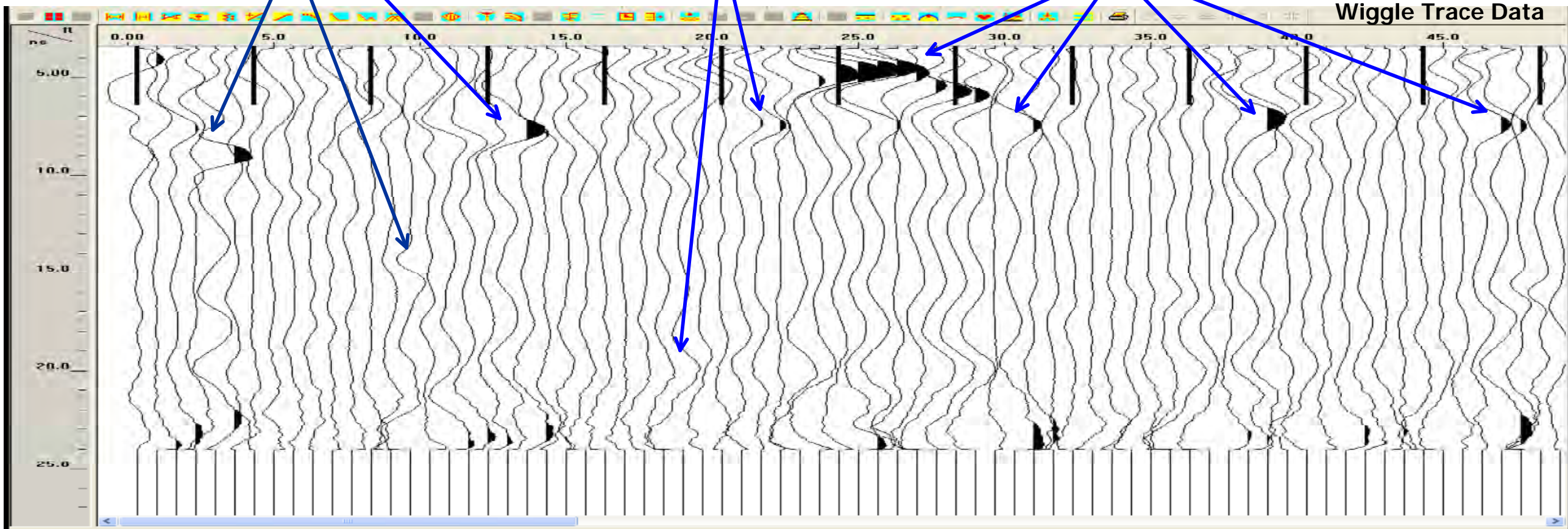
Classic Hyperbola

Color Scale Data



Note: this is from Poamoho Line 2 400 MHz antenna

Wiggle Trace Data



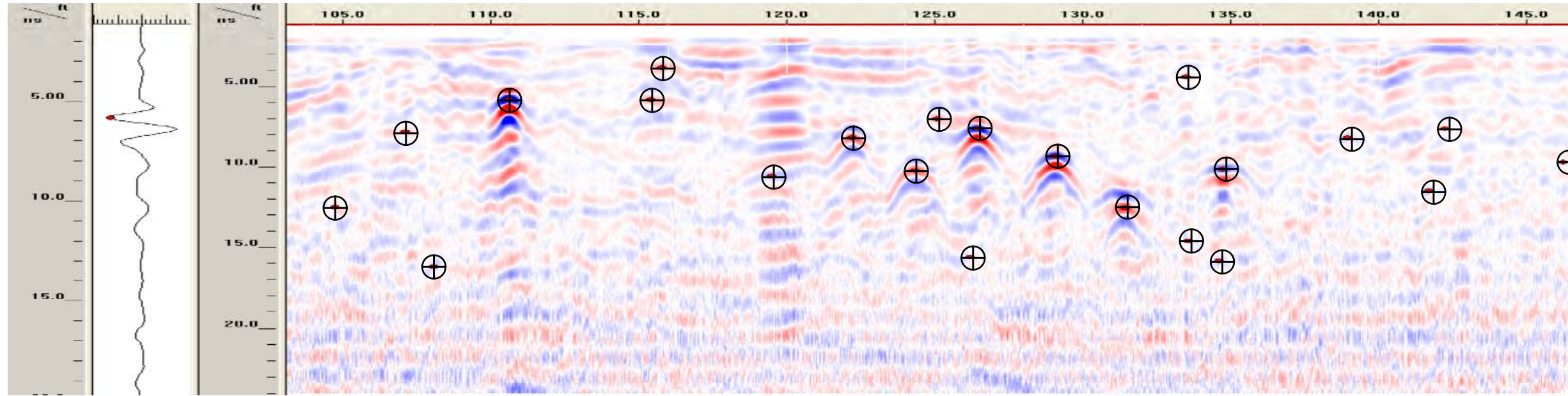
PROJECT:	University of Hawaii, Manoa	DATE
	Poamoho, HI	
REVISIONS		

DAWOOD	DRAWING TITLE:	Poamoho Void Examples
CONSULTING ENGINEERS		
10105 ALLENTOWN BLVD. GRANTVILLE, PA. 17028		
PHONE: (717) 869-0937 FAX: (717) 869-0938		

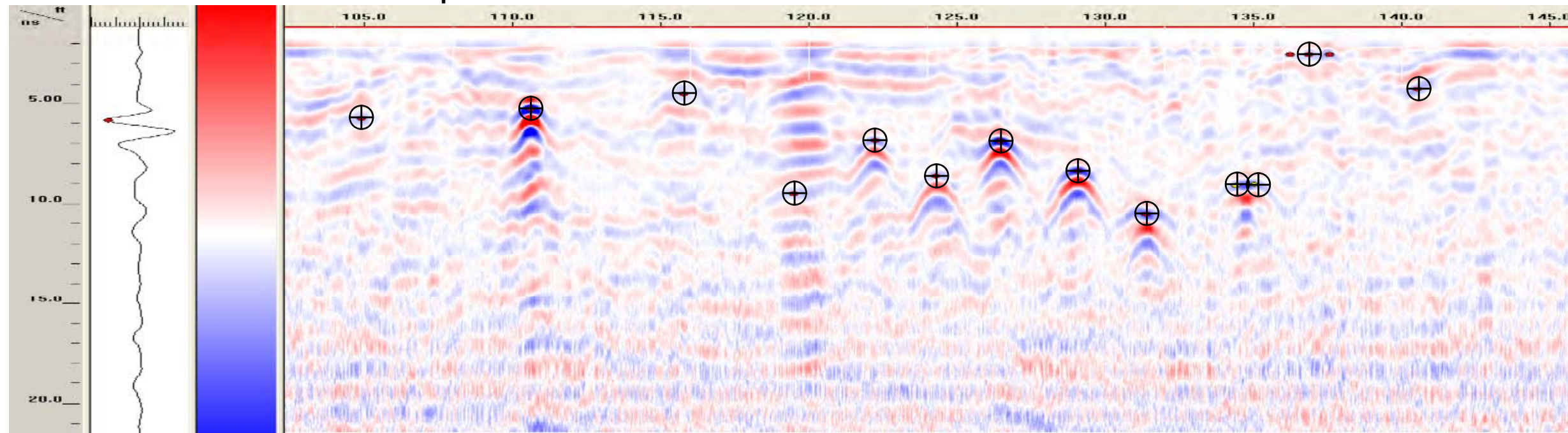
PROJECT NO.:	208044.01
DRAWN BY:	R.A.H.
CHECKED BY:	B.B.
SCALE:	AS SHOWN
DATE:	5 Aug 2008

SHEET NO.:
13

Automatic Feature Selection



Manual Interpretation



PROJECT:	University of Hawaii, Manoa
	Poamoho, HI
DATE:	
REVISIONS:	

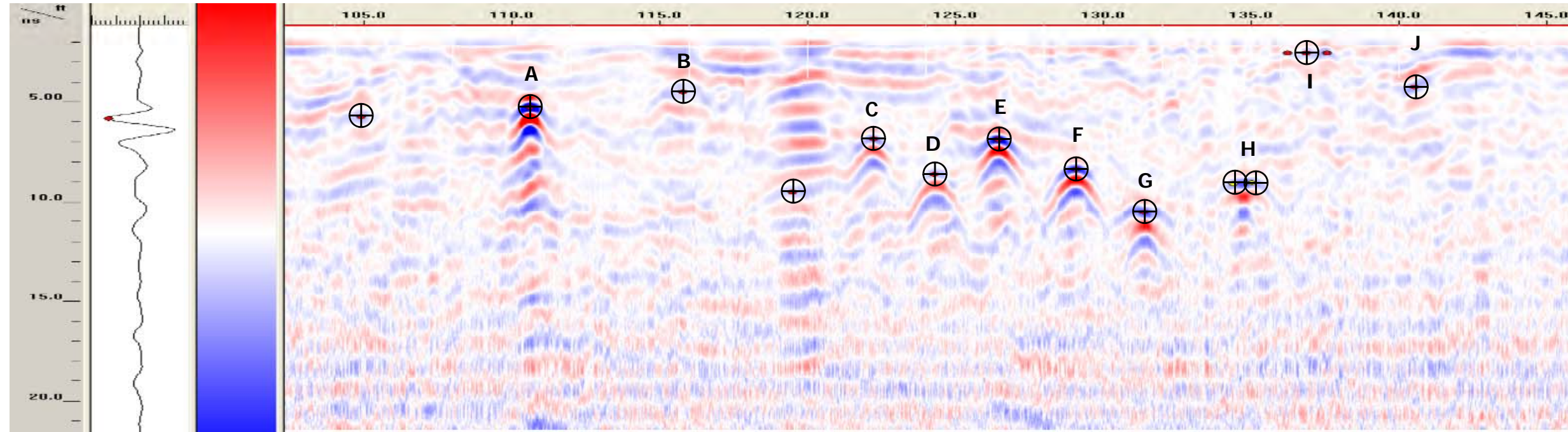
DAWOOD
CONSULTING ENGINEERS
10105 ALIEN TOWN SQUARE, GRANVILLE, OH 43028
PHONE: (614) 885-9321 FAX: (614) 885-9330
DRAWING TITLE:
GPR AutoPick Comparison

PROJECT NO.:	208044.01
DRAWN BY:	R.A.H.
CHECKED BY:	B.B.
SCALE:	AS SHOWN
DATE:	5 Aug 2008

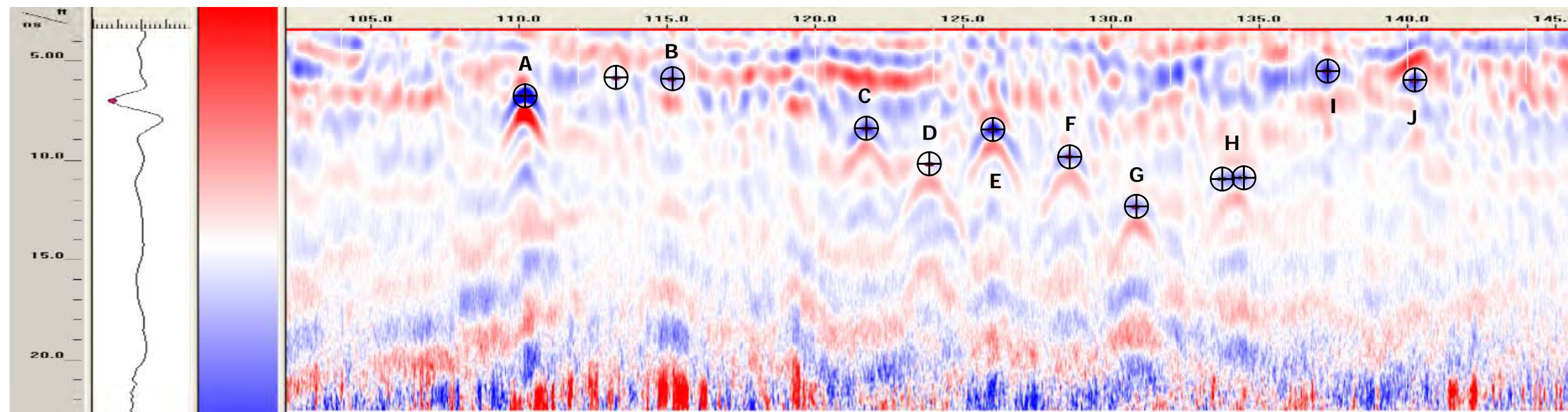
SHEET NO.:

14

900 MHz Antenna Data



400 MHz Antenna Data



PROJECT:	University of Hawaii, Manoa	
	Poamoho, HI	DATE
REVISIONS		

DAWOOD
 CONSULTING ENGINEERS
 10195 ALLEN TOWN ROAD, GRANVILLE, VA 22028
 PHONE: (703) 937-7444 FAX: (703) 937-9330

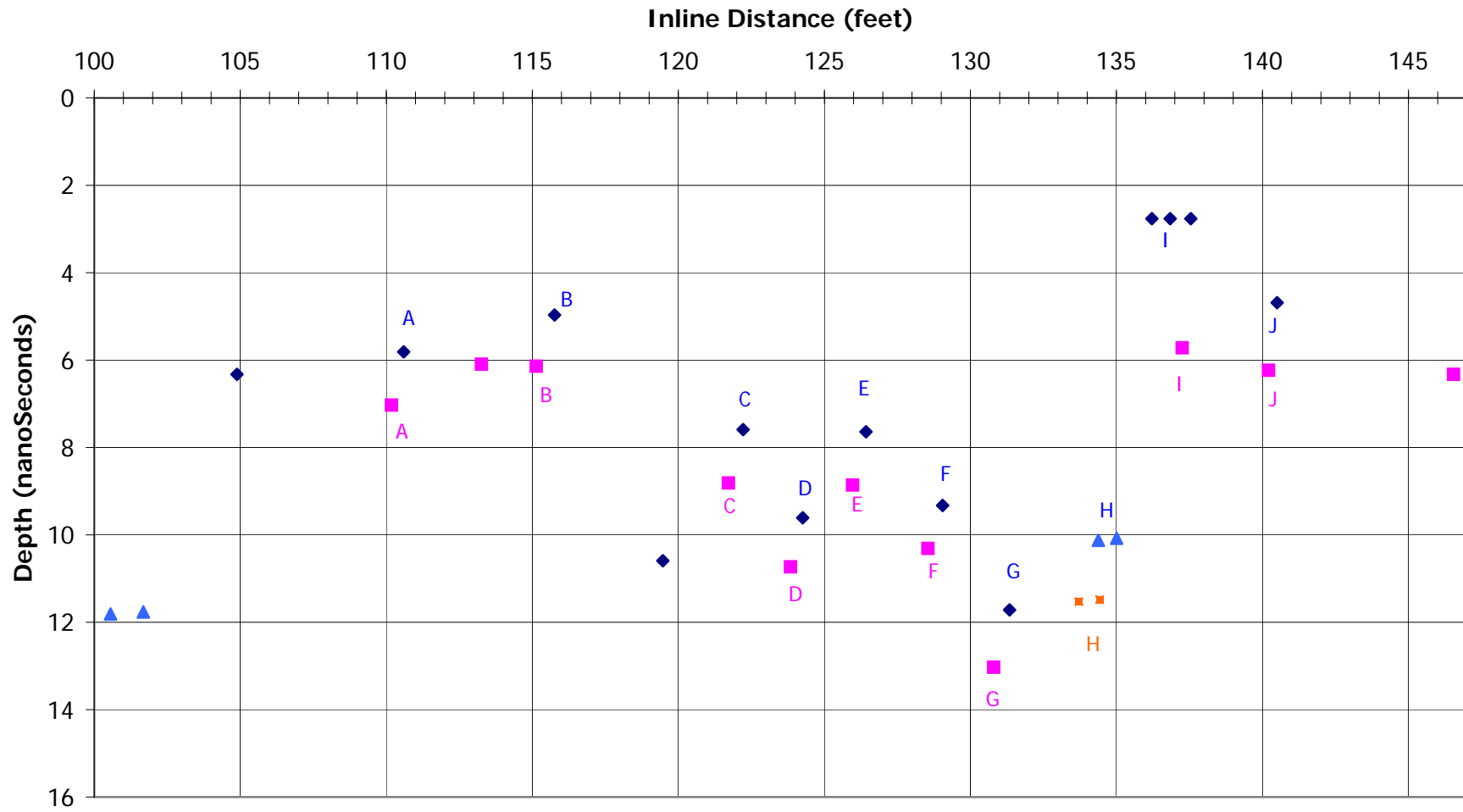
DRAWING TITLE:
Poamoho GPR Interpretation

PROJECT NO.:	208044.01
DRAWN BY:	R.A.H.
CHECKED BY:	B.B.
SCALE:	AS SHOWN
DATE:	5 Aug 2008

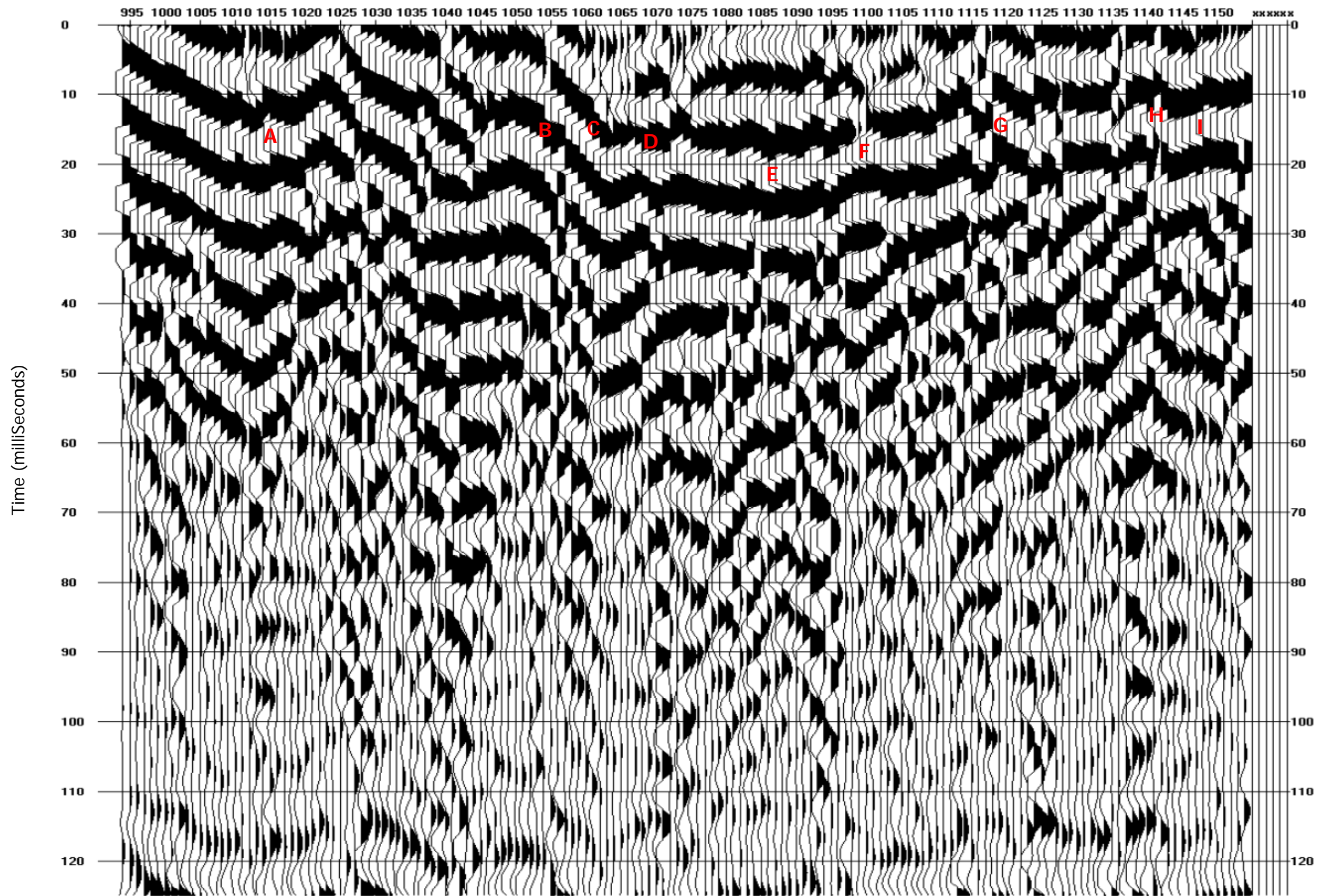
SHEET NO.:

15

Figure 16
Poamoho Target Comparison



◆ 900MHz Targets ■ 400MHz Targets ▲ 900MHz Slabs ■ 400 MHz Slabs



The X-scale is CDP number + 1000. The CDP number is inline distance

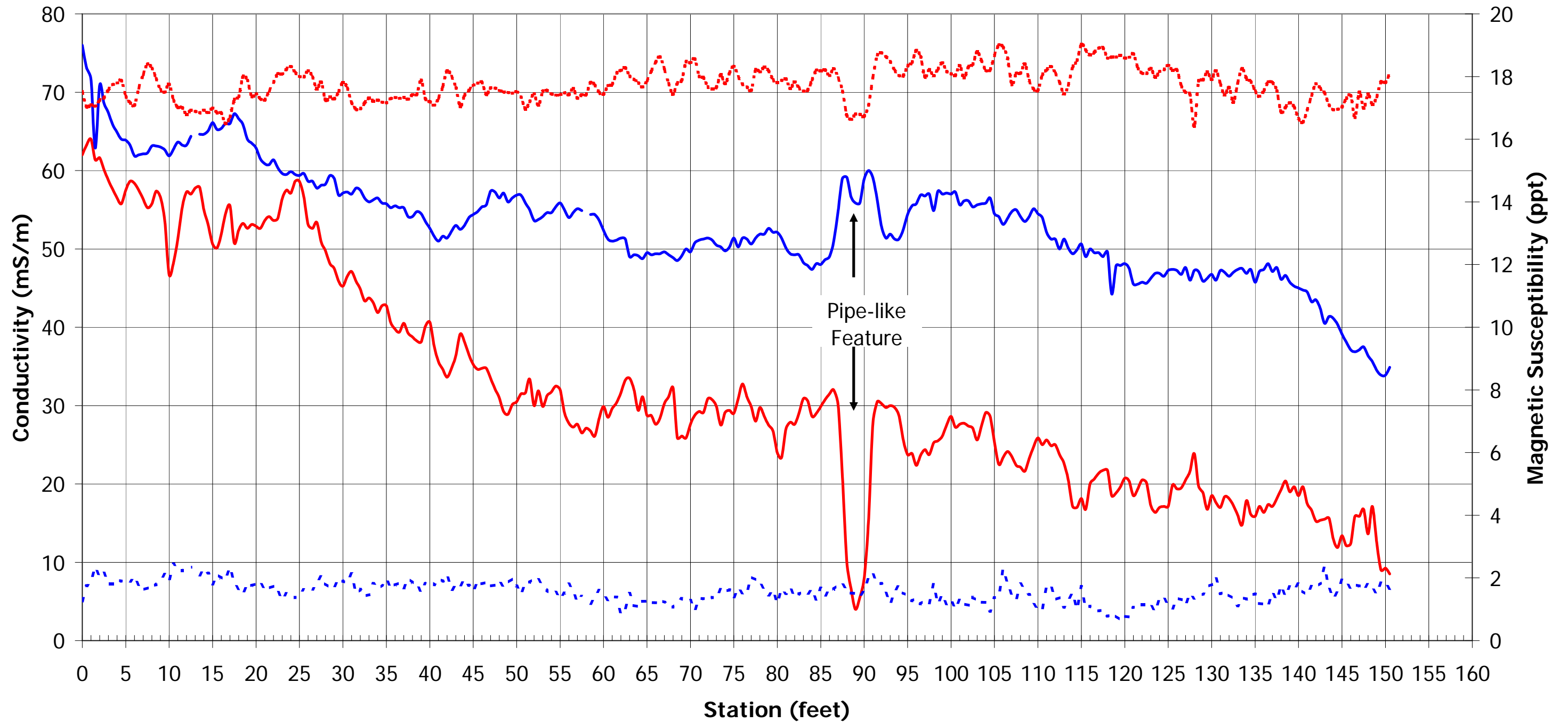
PROJECT: University of Hawaii, Manoa	
Poamoho, HI	
REVISIONS	DATE

 CONSULTING ENGINEERS 10105 ALLENTOWN BLVD. GRANTVILLE, PA. 17028 PHONE: (717) 869-0937 FAX: (717) 869-0938	DRAWING TITLE: Poamoho L2 Reflection CDP

PROJECT NO.:	208044.01
DRAWN BY:	R.A.H.
CHECKED BY:	B.B.
SCALE:	AS SHOWN
DATE:	5 Aug 2008

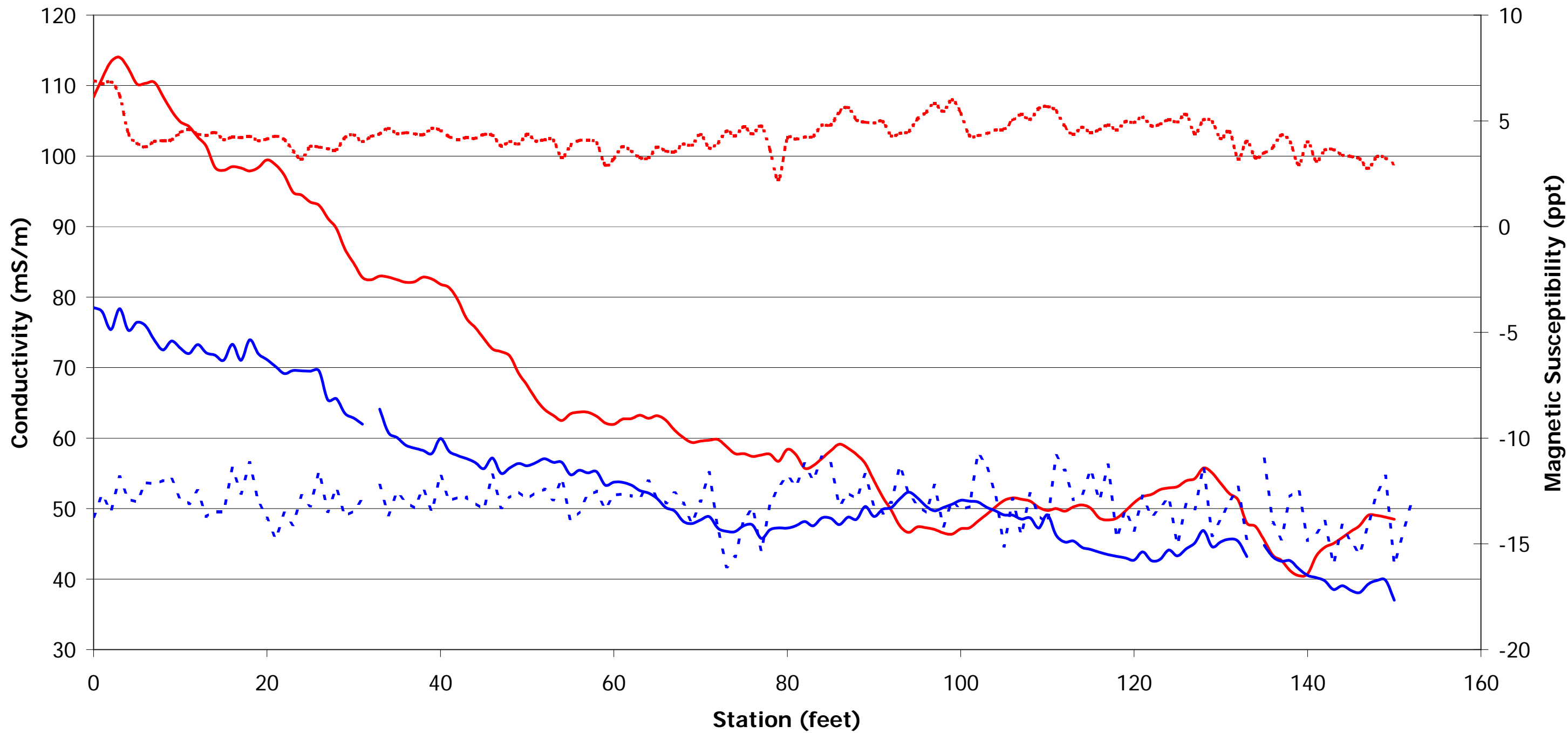
SHEET NO.:
18

Figure 19
Waimanalo EM38 Line 2 EM Data



— QV — QH - - - IV - - - IH

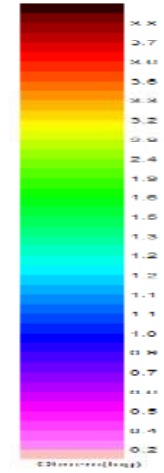
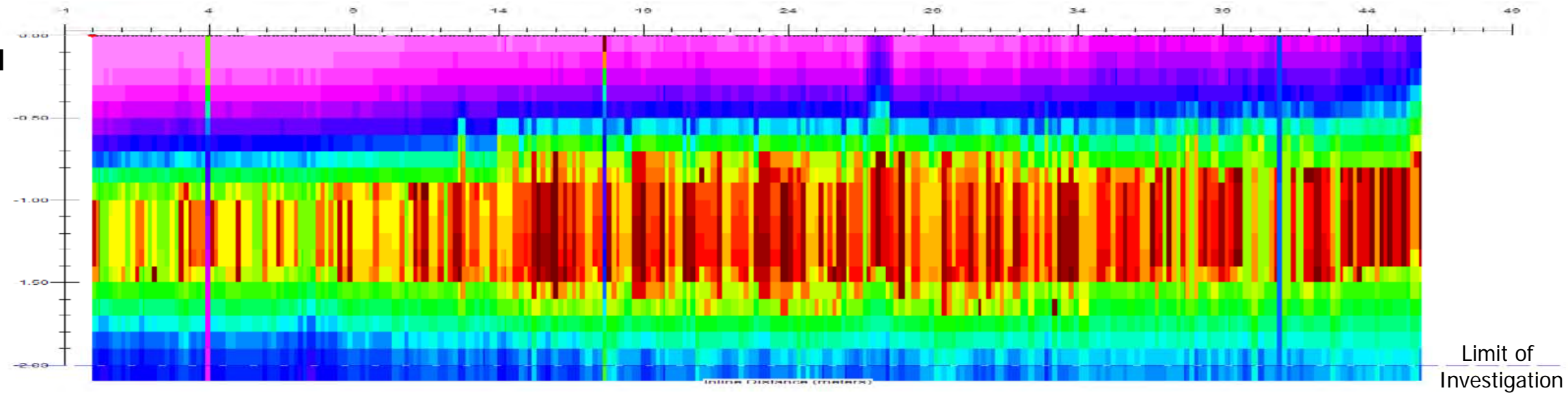
Figure 20
Waimanalo EM31 Line 2 EM Data



— QV — QH - - - IV - - - IH

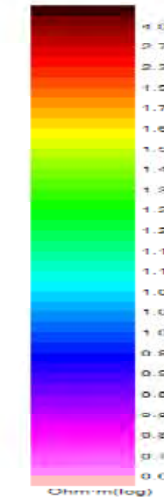
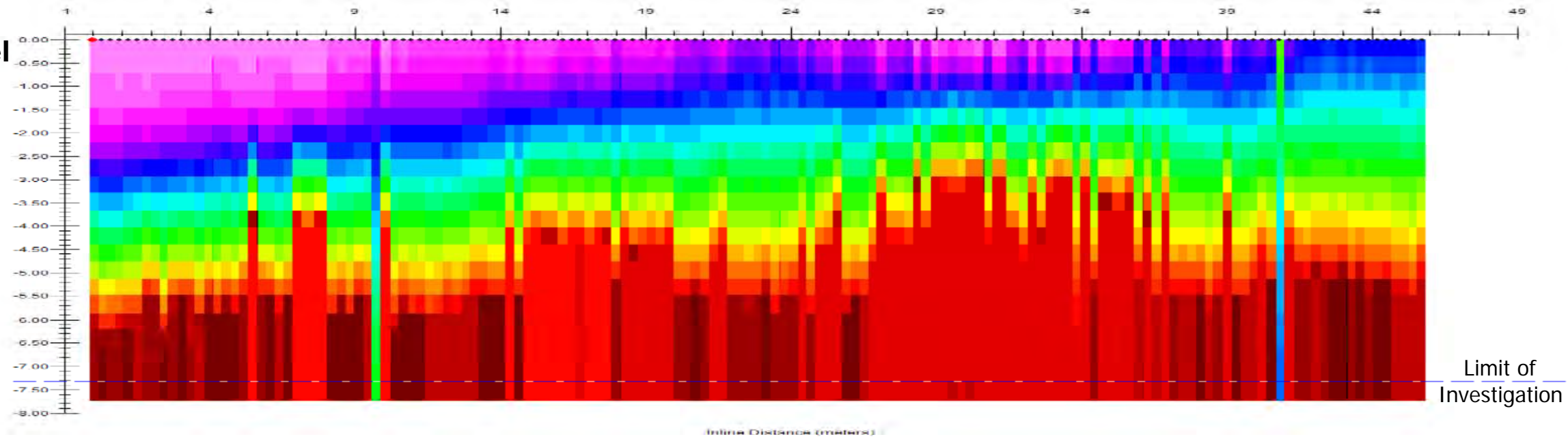
EM38 Model

Depth (meters)



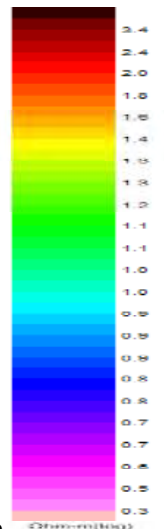
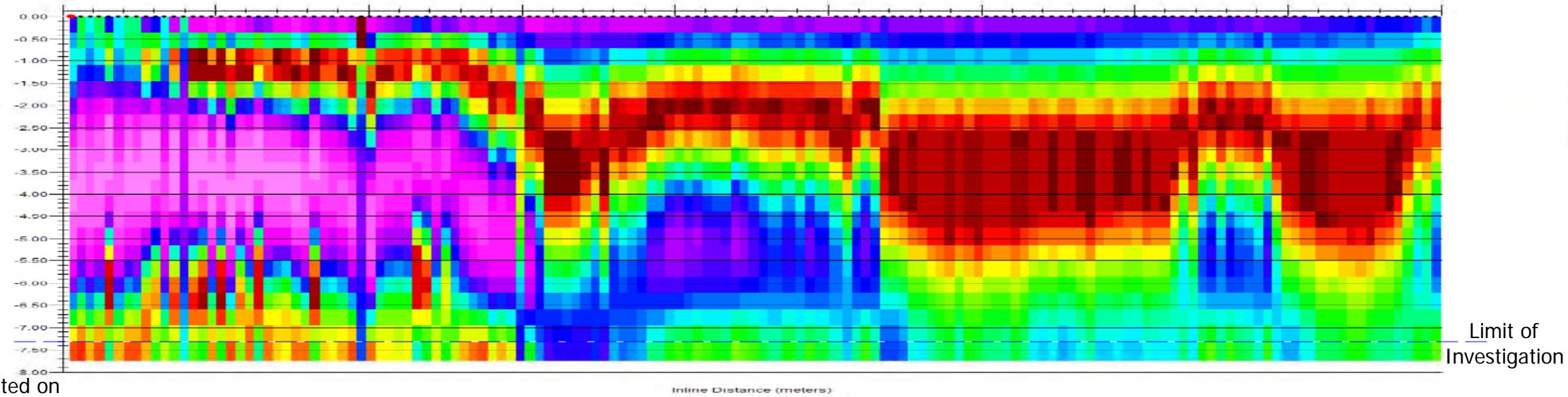
EM31 Model

Depth (meters)



Combined Model

Depth (meters)

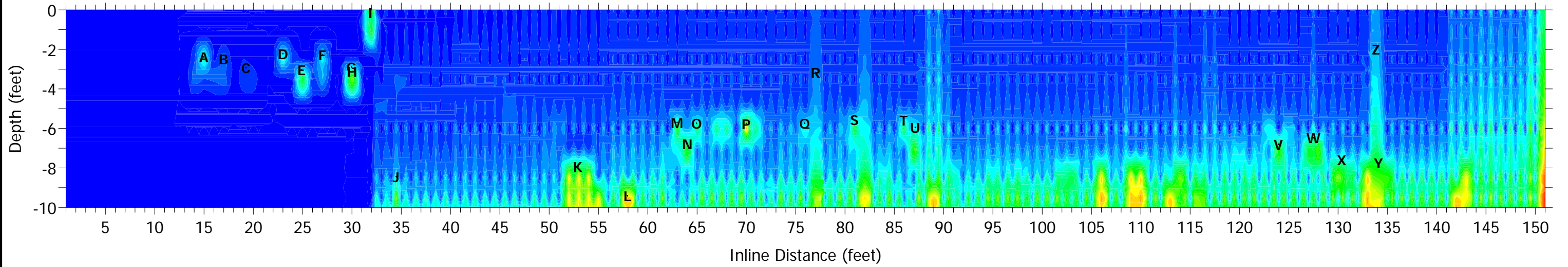


Note: Data Presented on this figure is modeled from the center (line2) data.

PROJECT:	University of Hawaii, Manoa Waimanalo, HI
DATE:	
REVISIONS:	

<p>DAWOOD CONSULTING ENGINEERS 10105 ALLEN TOWNSEND DR. GRANVILLE, OH 43028 PHONE: (614) 885-9321 FAX: (614) 885-9330</p>	DRAWING TITLE:	Waimanalo Modeled Resistivities
	PROJECT NO.:	208044.01
DRAWN BY:	R.A.H.	
CHECKED BY:	B.B.	
SCALE:	AS SHOWN	
DATE:	5 Aug 2008	
SHEET NO.:		

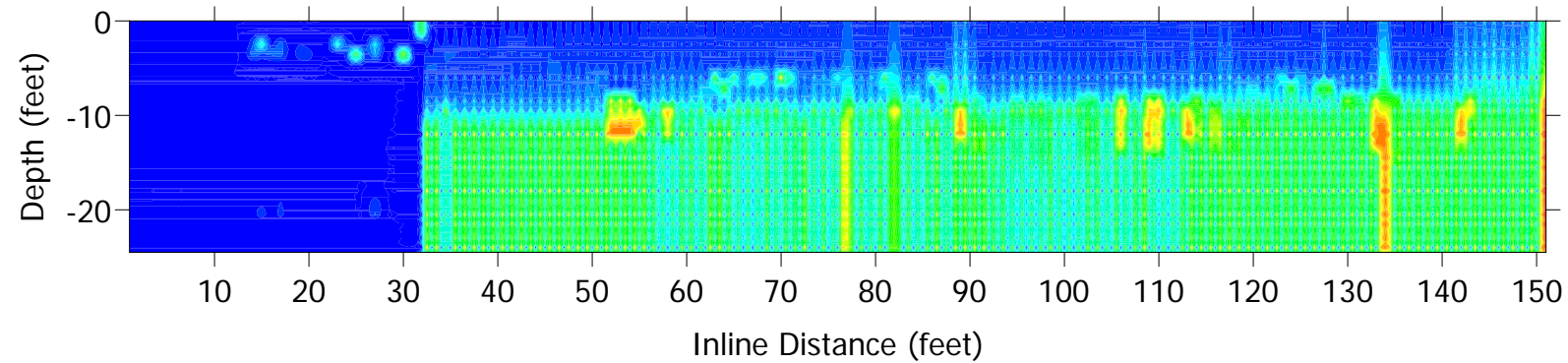
Exaggerated vertical scale



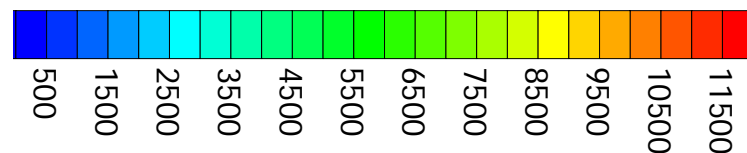
Legend

K Interpreted Void -
(see text for more information)

Entire Section, proportional scaling



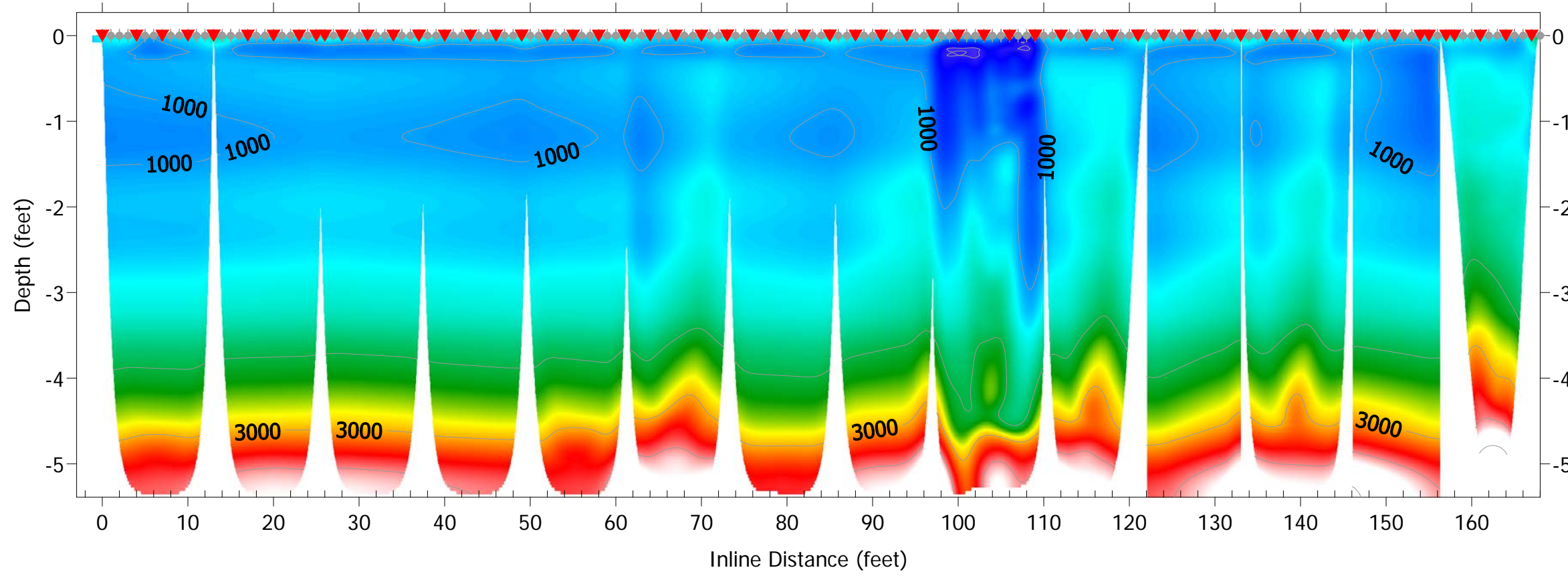
Model Resistivity (ohm-meters)



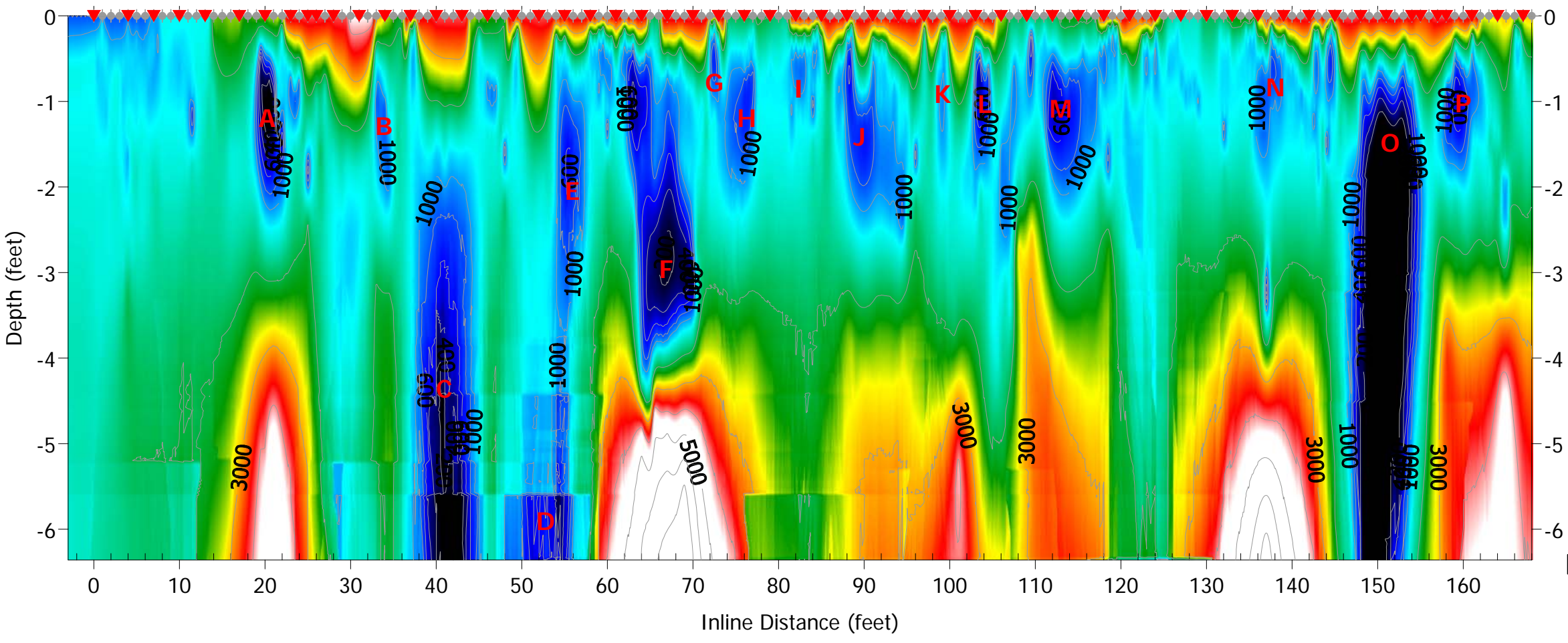
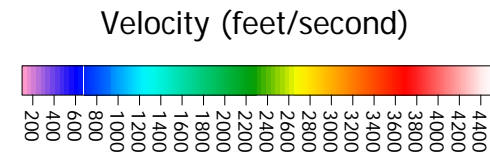
Data presented on this cross-section is from the center (line 2) of the survey area. The resistivity model has been gridded to a 0.5-foot by 0.5-foot grid using a kriging algorithm and contoured for presentation and interpretation.

PROJECT: University of Hawaii, Manoa Waimanalo, HI	DATE
	REVISIONS

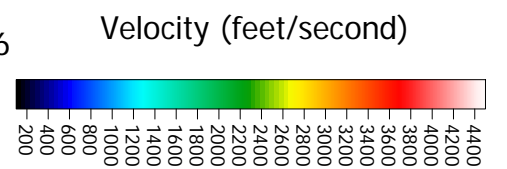
 <small>CONSULTING ENGINEERS 1015 ALLEN TOWN BLVD. GRANVILLE, OH 43028 PHONE: (614) 885-9321 FAX: (614) 885-9330</small>	DRAWING TITLE: Waimanalo Resistivity Interp.
	PROJECT NO.: 208044.01
DRAWN BY: R.A.H.	
CHECKED BY: B.B.	
SCALE: AS SHOWN	
DATE: 5 Aug 2008	
SHEET NO.:	



Full Waveform Eikonal Traveltime Tomography

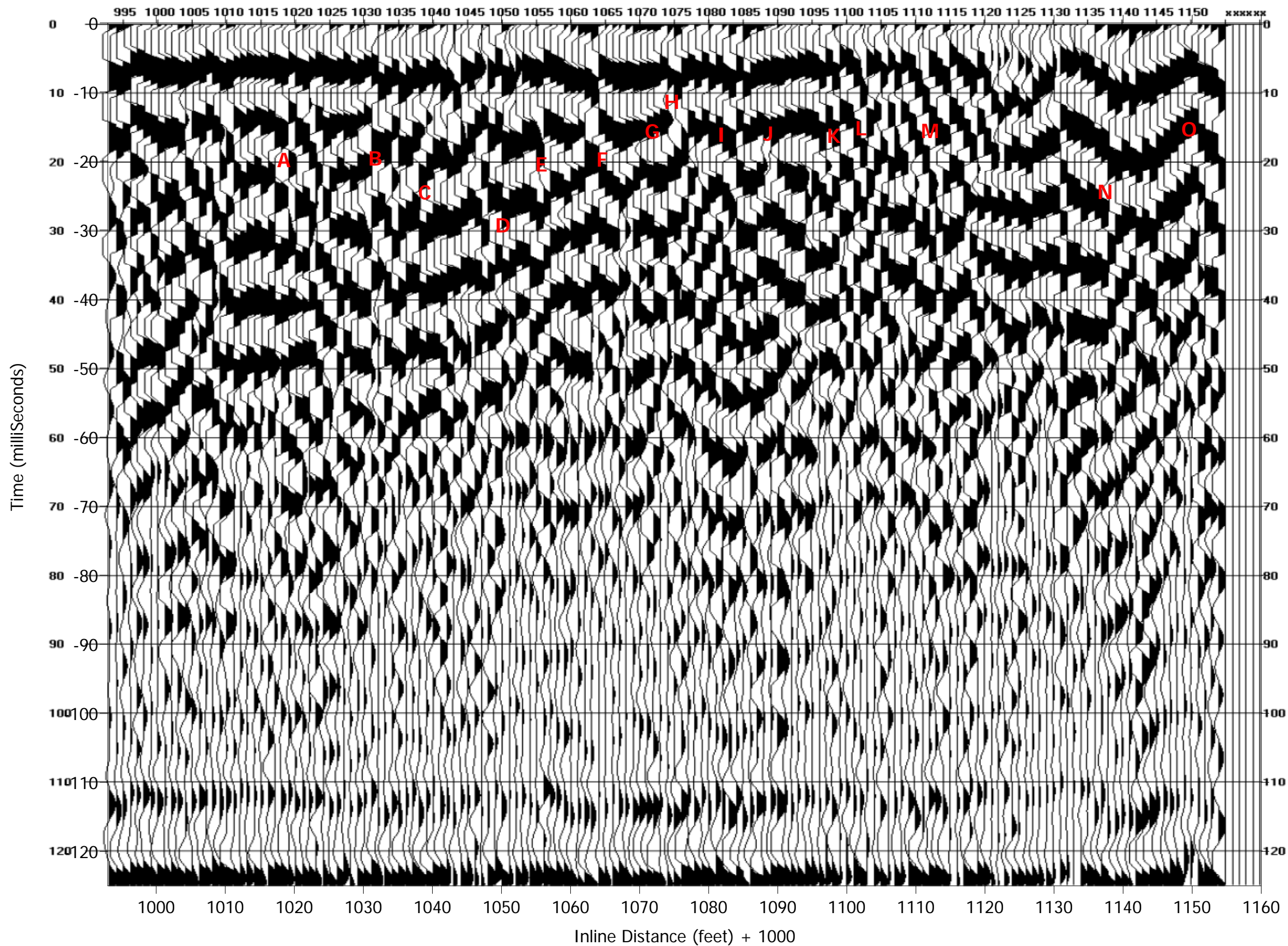


Delta-t-V pseudo 2D turning ray inversion



PROJECT:	University of Hawaii, Manoa
Waimanalo, HI	
REVISIONS	
DATE	

DRAWING TITLE:	Waimanalo Line 2 Refraction
PROJECT NO.:	208044.01
DRAWN BY:	R.A.H.
CHECKED BY:	B.B.
SCALE:	AS SHOWN
DATE:	5 Aug 2008
SHEET NO.:	23



The X-scale is CDP number + 1000. The CDP number is inline distance

PROJECT:	University of Hawaii, Manoa
	Waimanalo, HI
REVISIONS	DATE

DAWOOD	CONSULTING ENGINEERS
	10105 ALLENTOWN BLVD. GRANTVILLE, PA. 17028
	PHONE: (717) 869-0937 FAX: (717) 869-0938
DRAWING TITLE:	Waimanalo L2 Reflection CDP

PROJECT NO.:	208044.01
DRAWN BY:	R.A.H.
CHECKED BY:	B.B.
SCALE:	AS SHOWN
DATE:	5 Aug 2008

SHEET NO.:
20

Figure 25
Kawaihae EM38 Line 2 EM Data

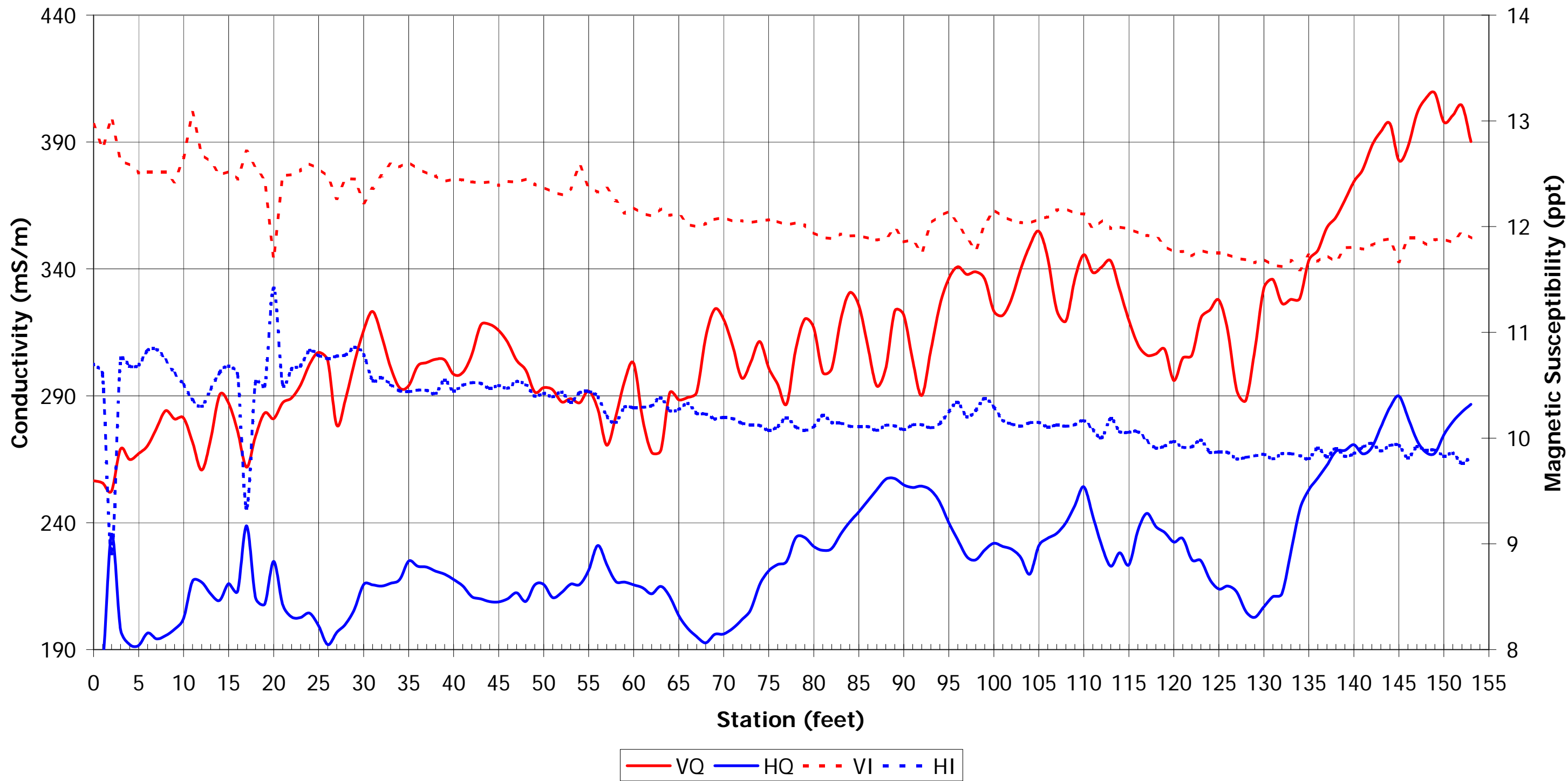
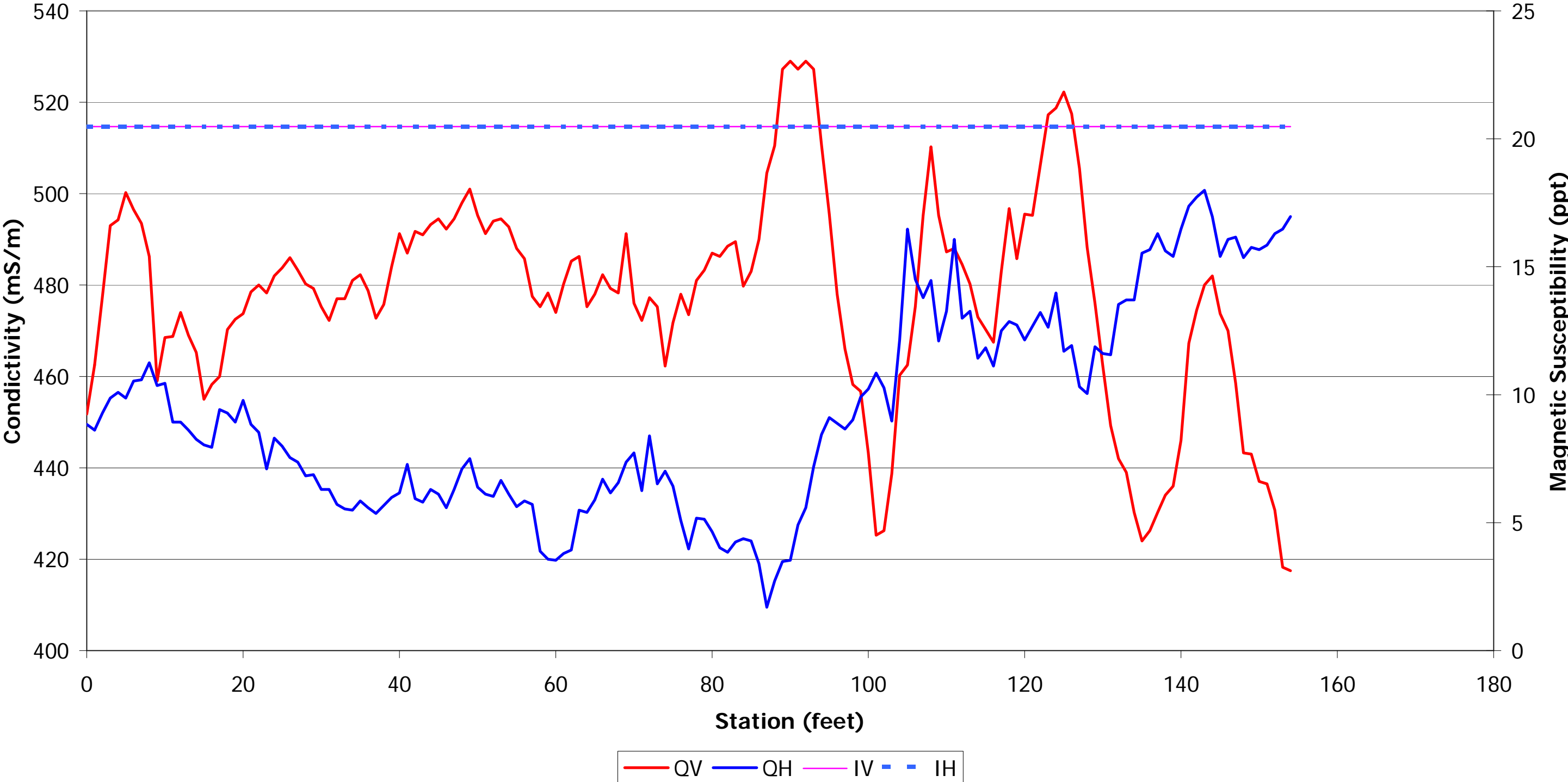
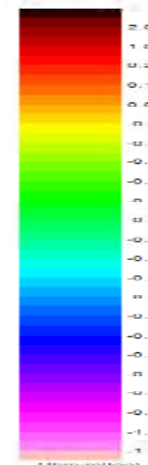
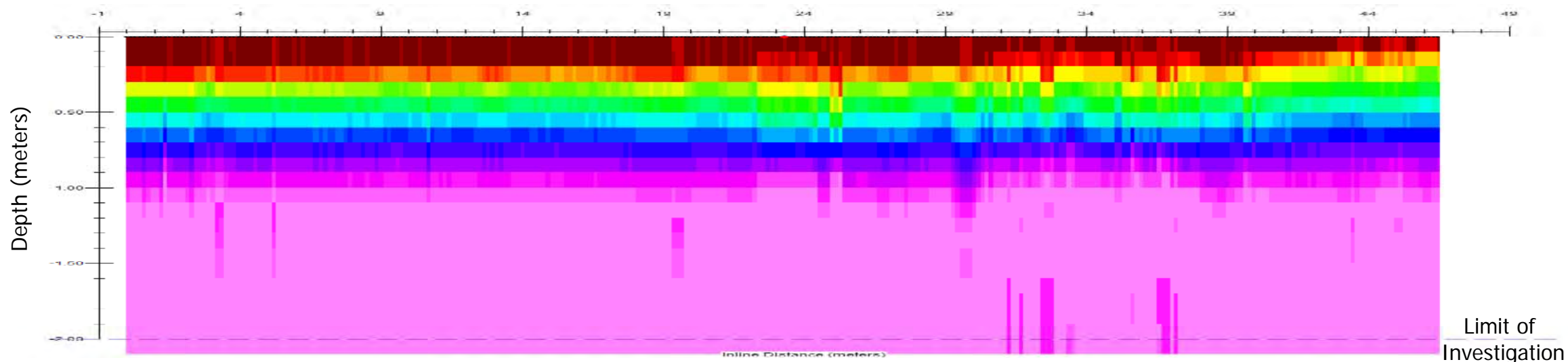


Figure 26
Kawaihae EM31 Line 2 EM Data

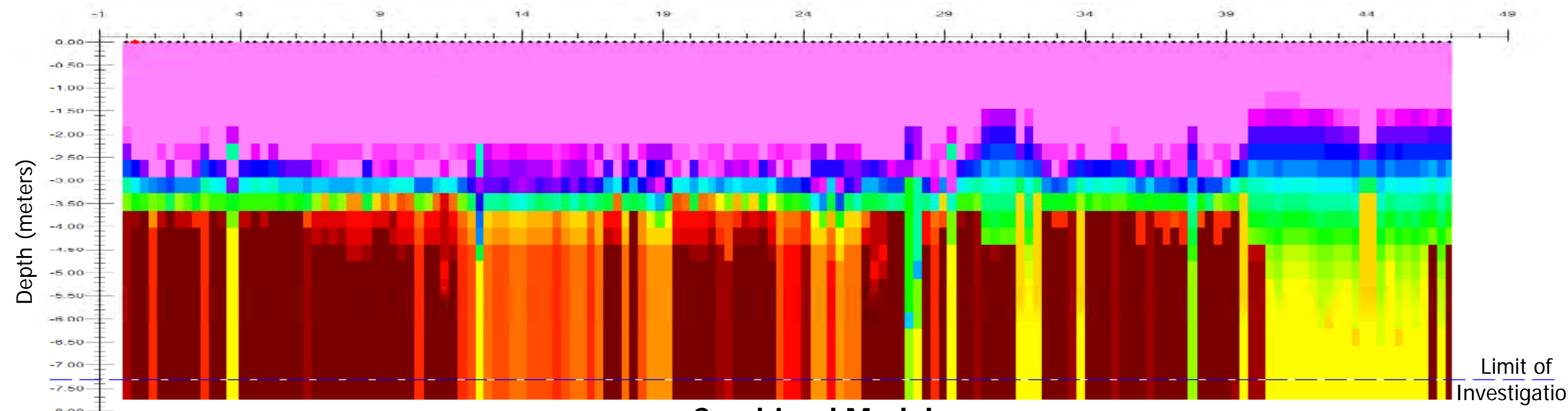


EM38 Model

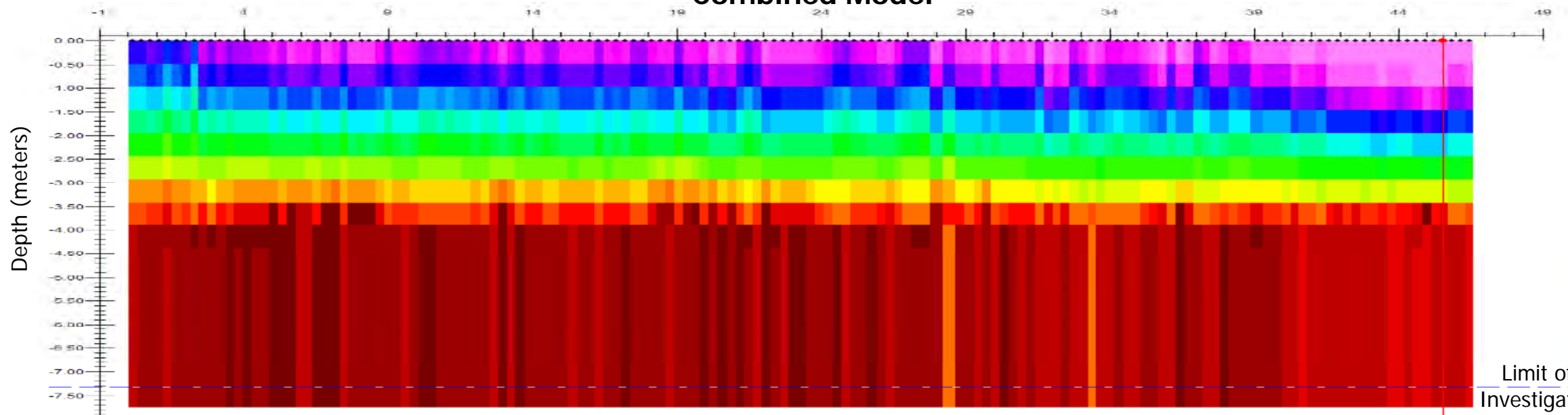


Note: Data Presented on this figure is modeled from the center (line2) data.

EM31 Model



Combined Model

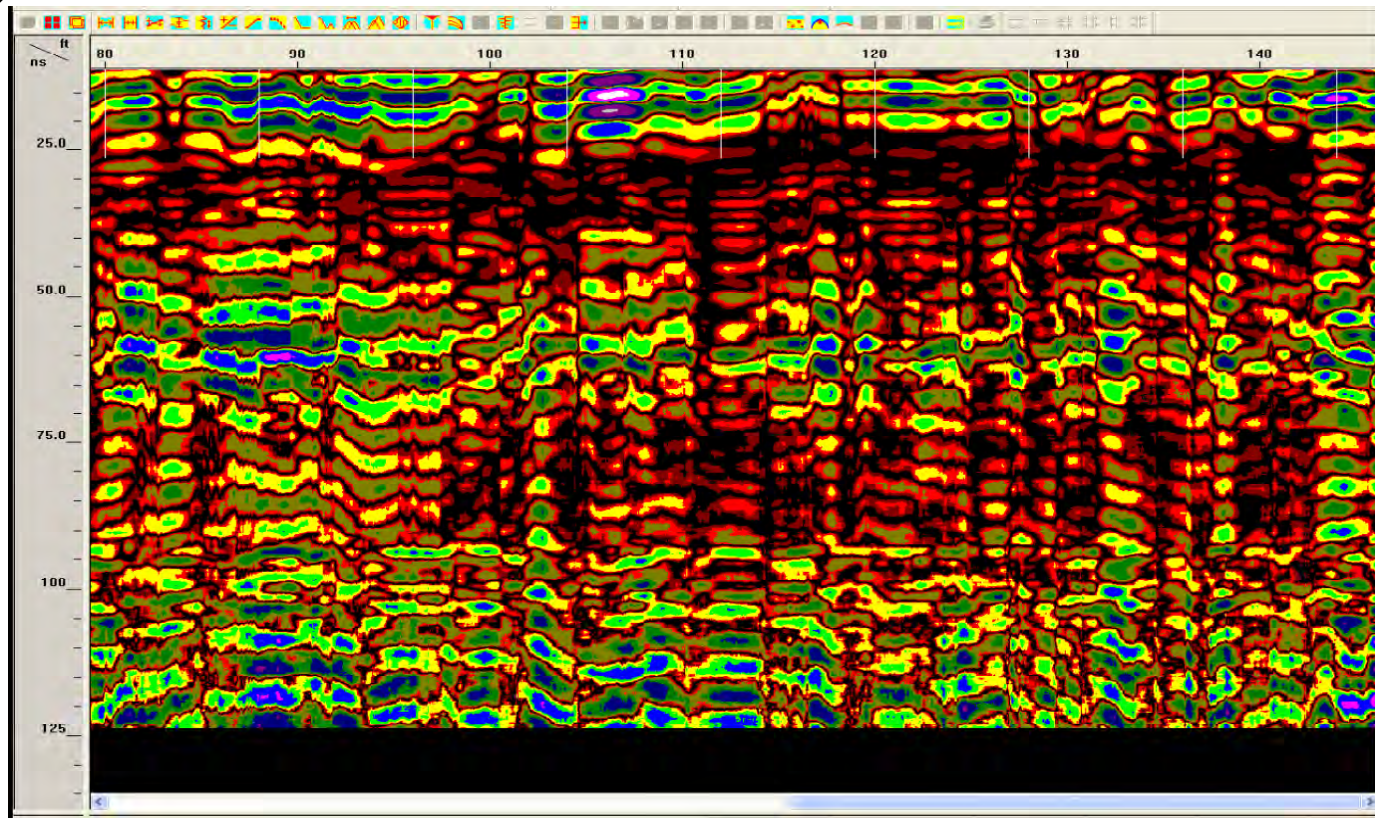


Inline Distance (feet)

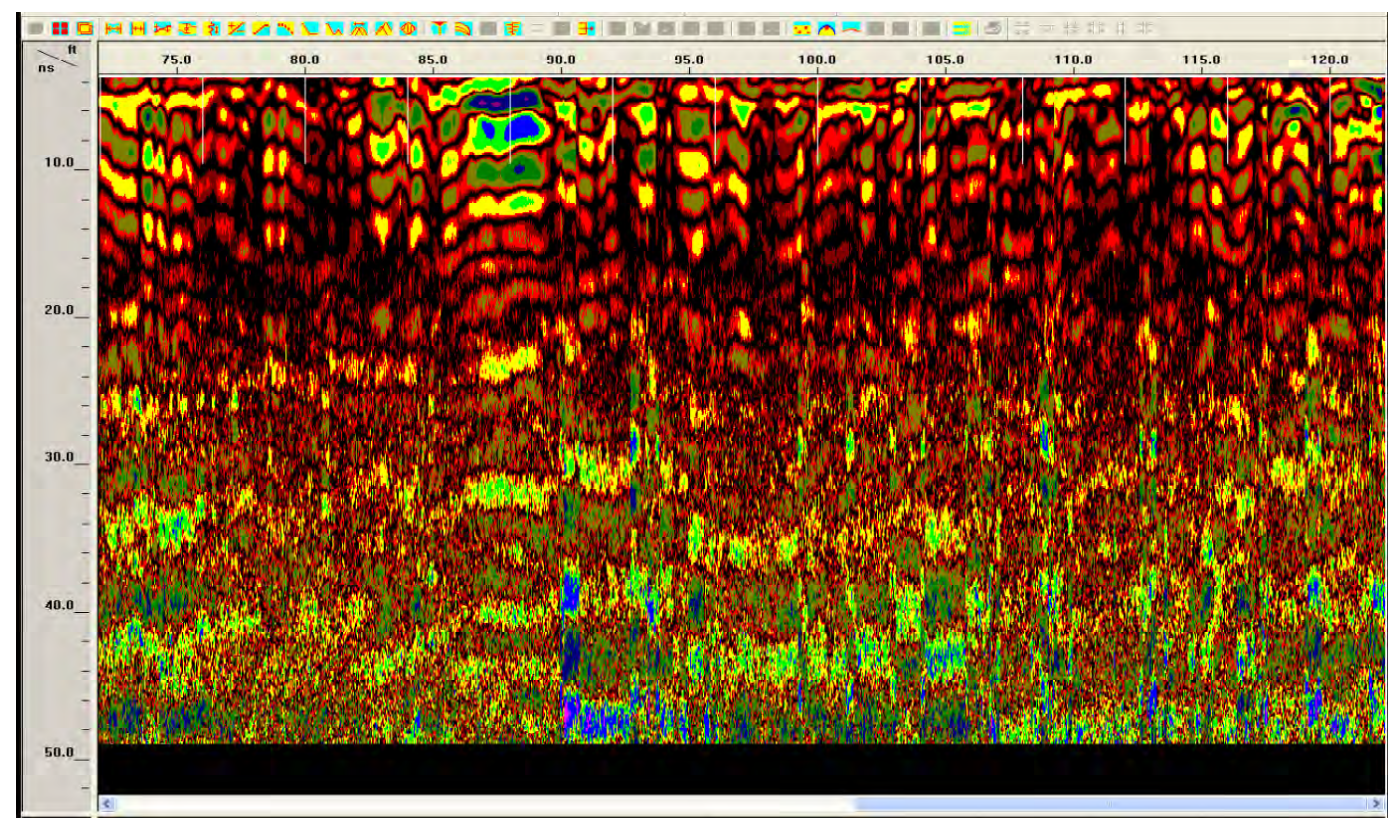
PROJECT:	University of Hawaii, Manoa Kawaihae, HI	DATE:	
REVISIONS:			

DAWOOD	CONSULTING ENGINEERS 1015 ALIEN HOLLOW LANE, SUITE 100, KAILUA, HI 96734 PHONE: (808) 261-0000 FAX: (808) 261-0000
DRAWING TITLE:	Kawaihae Modeled Resistivities

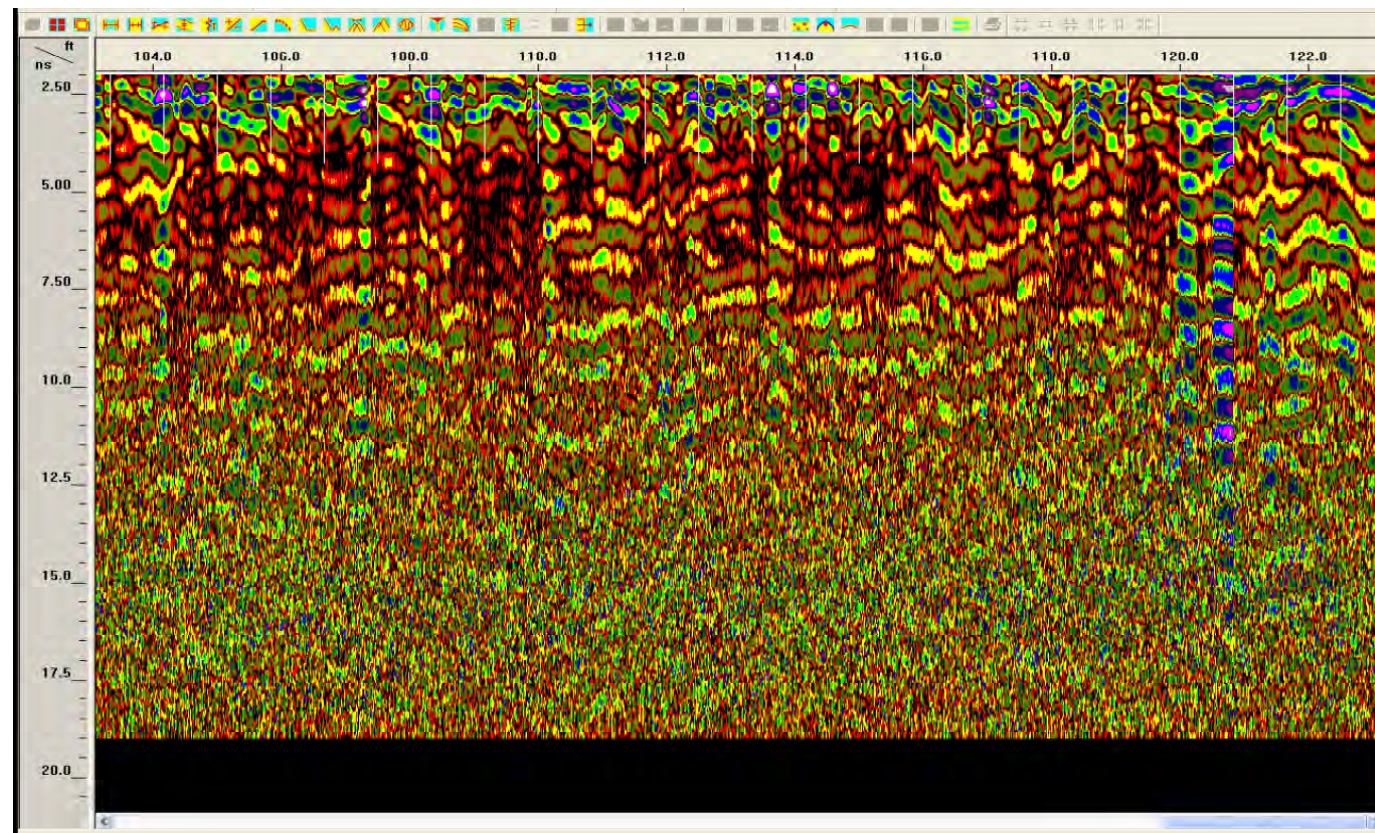
PROJECT NO.:	208044.01
DRAWN BY:	R.A.H.
CHECKED BY:	B.B.
SCALE:	AS SHOWN
DATE:	5 Aug 2008
SHEET NO.:	



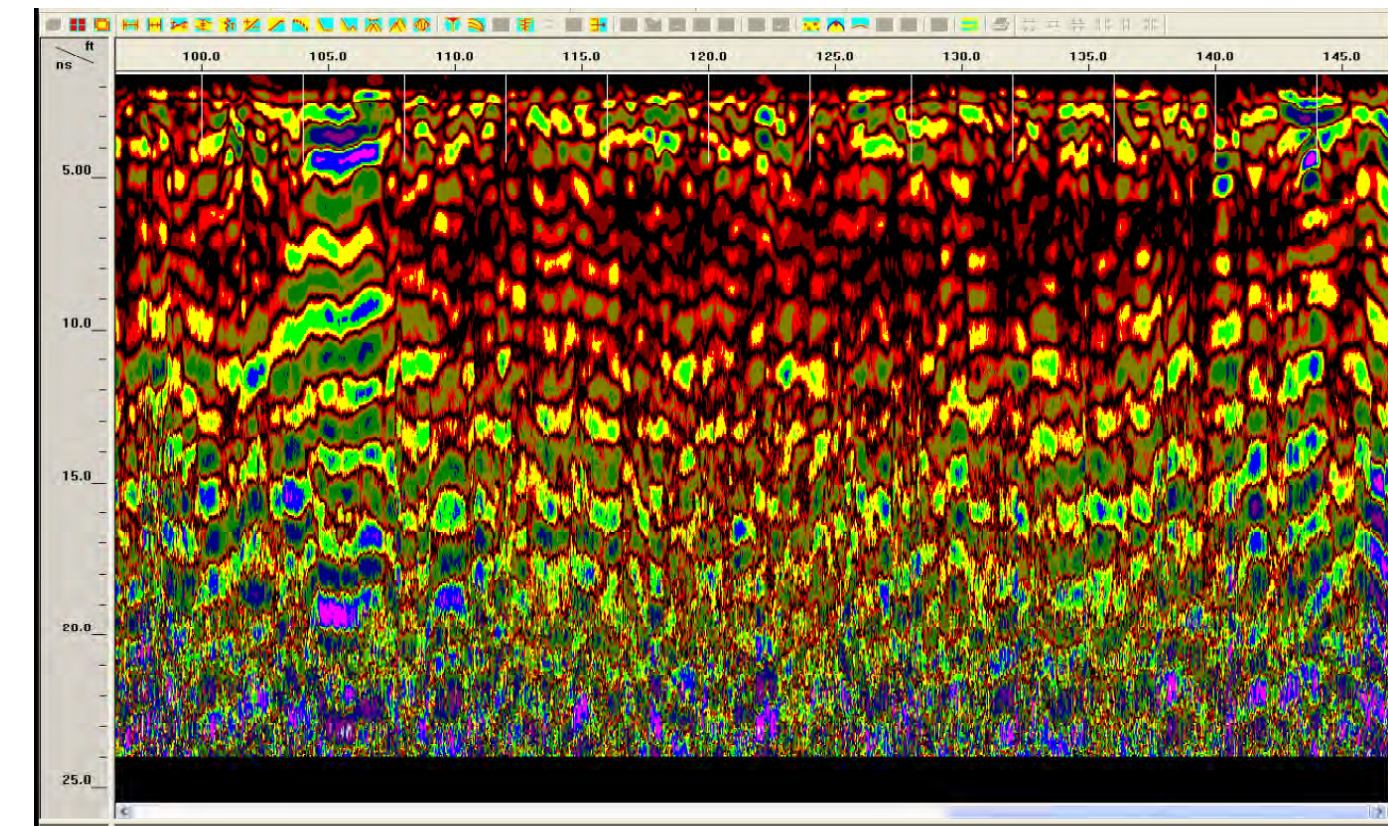
270 MHz
146.0 feet



400 MHz
122.08 feet



1.5 GHz
123.17 feet



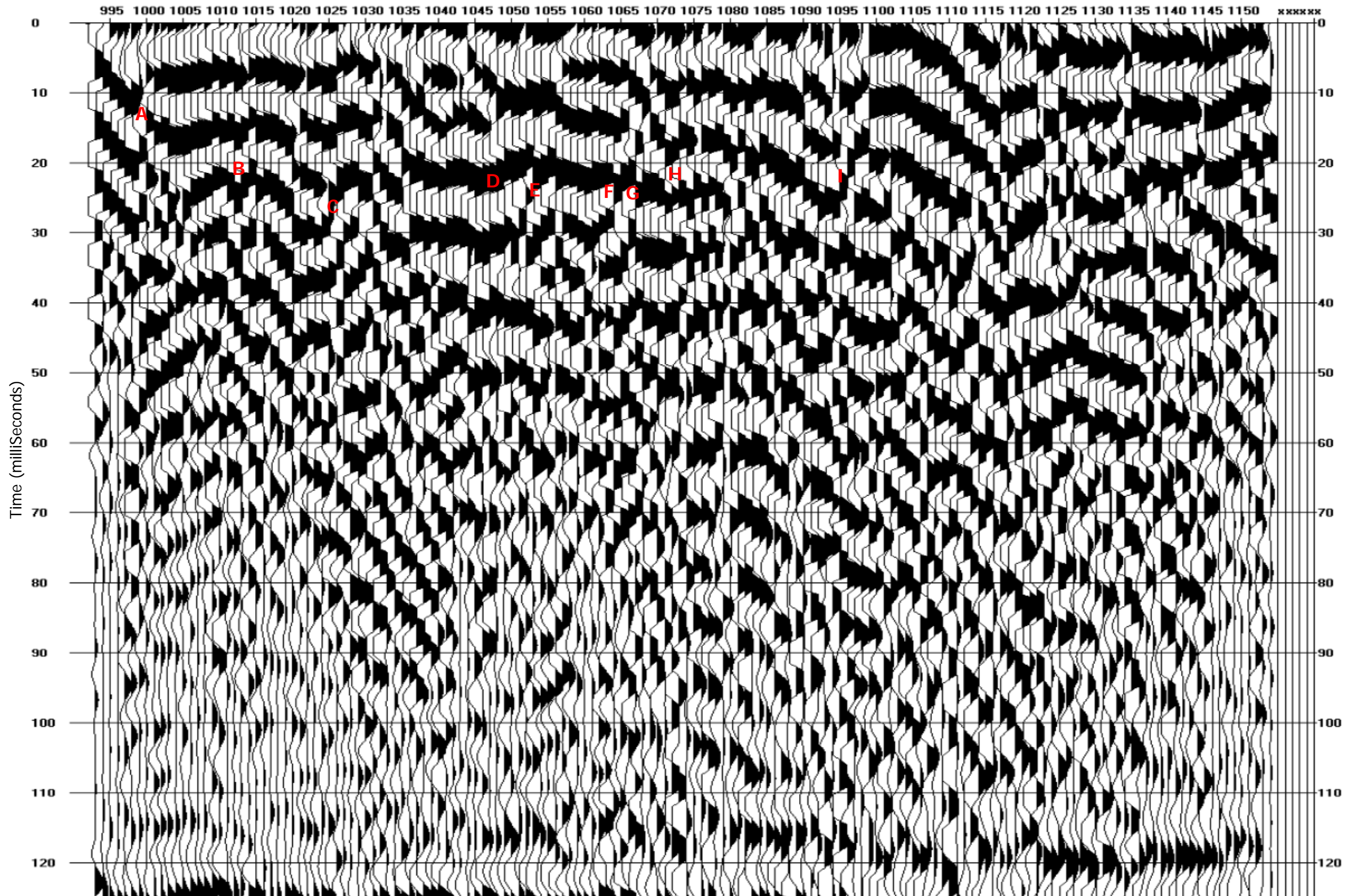
900 MHz
146.75 feet

PROJECT:	
University of Hawaii, Manoa	
Kawaojoe, HI	
REVISIONS	DATE

	CONSULTING ENGINEERS
	10105 ALLENTOWN BLVD. GRANTVILLE, PA. 17028
PHONE: (717) 869-0937 FAX: (717) 869-0938	
DRAWING TITLE:	Kawaihae GPR Line Lengths

PROJECT NO.:	208044.01
DRAWN BY:	R.A.H.
CHECKED BY:	B.B.
SCALE:	AS SHOWN
DATE:	5 Aug 2008

SHEET NO.:
28



The X-scale is CDP number + 1000. The CDP number is inline distance

PROJECT: University of Hawaii, Manoa Kawaihae, HI	
REVISIONS	DATE

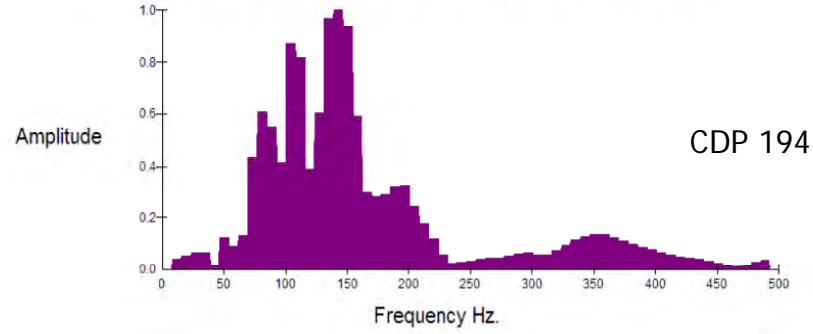
 CONSULTING ENGINEERS 10105 ALLENTOWN BLVD. GRANTVILLE, PA. 17028 PHONE: (717) 869-0937 FAX: (717) 869-0938	DRAWING TITLE: Kawaihae L2 Reflection CDP

PROJECT NO.:	208044.01
DRAWN BY:	R.A.H.
CHECKED BY:	B.B.
SCALE:	AS SHOWN
DATE:	5 Aug 2008

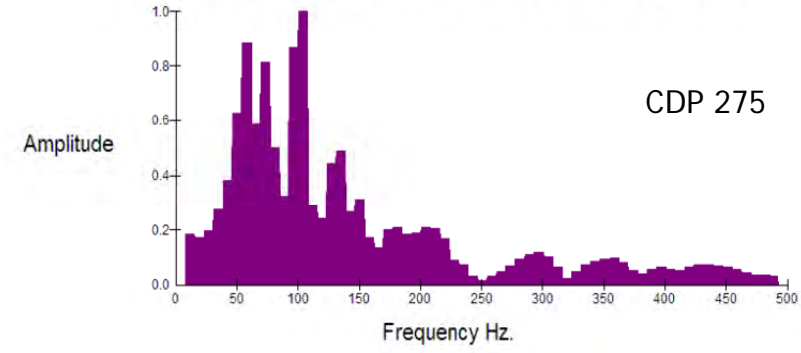
SHEET NO.:
30

Appendix A – Spectral Analysis for Seismic Reflection Data

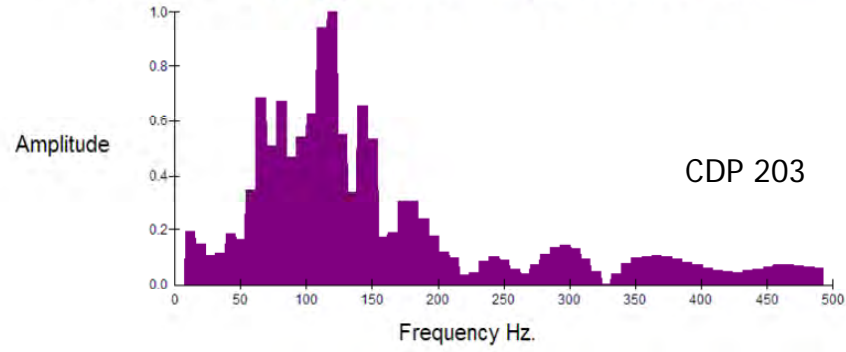
Spectrum of Trace(s)- 1-3 - C:\Ref1W2\WAI2ACDP.DAT



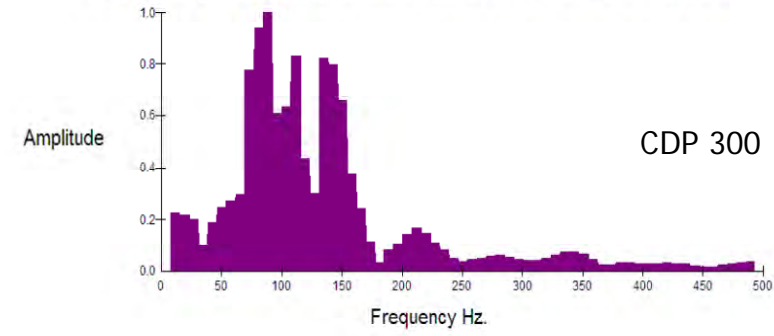
Spectrum of Trace(s)- 1-8 - C:\Ref1W2\WAI2ACDP.DAT



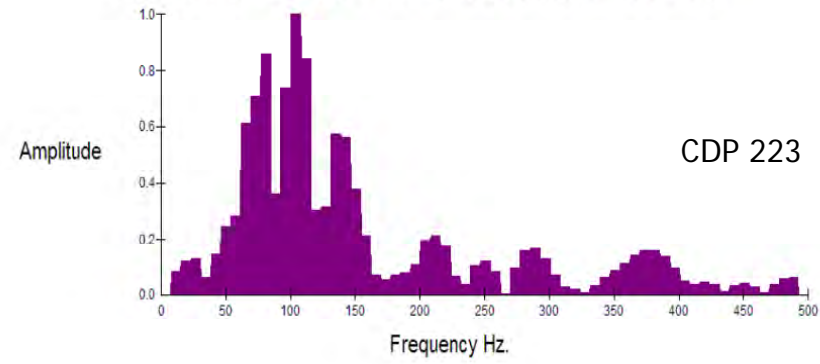
Spectrum of Trace(s)- 1-5 - C:\Ref1W2\WAI2ACDP.DAT



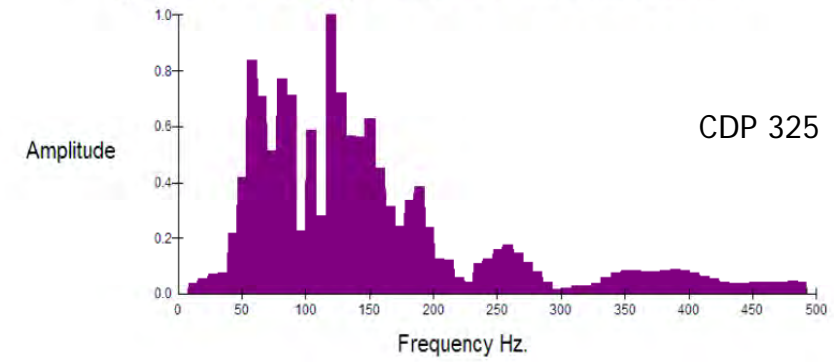
Spectrum of Trace(s)-5,8, 1-10 - C:\Ref1W2\WAI2ACDP.DAT



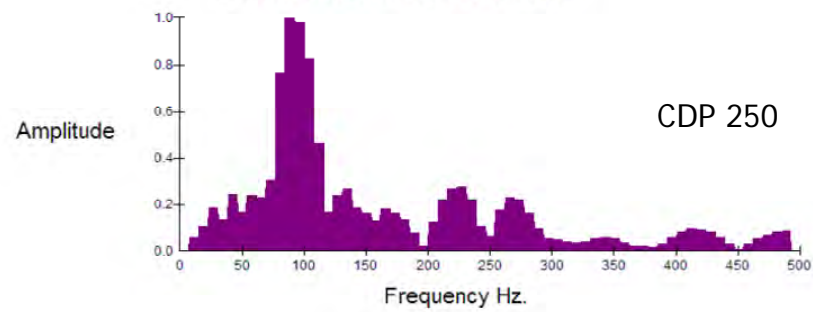
Spectrum of Trace(s)- 1-12 - C:\Ref1W2\WAI2ACDP.DAT



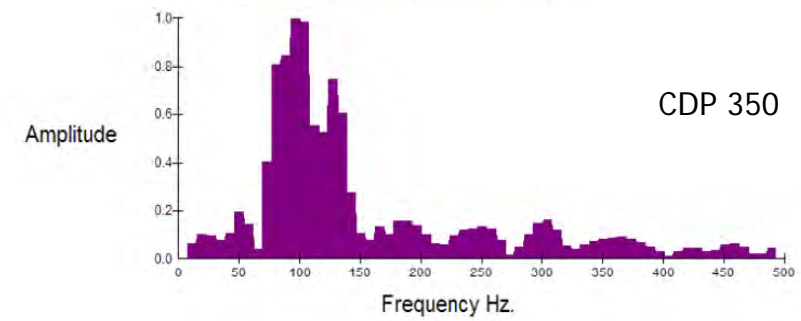
Spectrum of Trace(s)- 1-9 - C:\Ref1W2\WAI2ACDP.DAT



Spectrum of Trace(s)- 1-11 - C:\Ref1W2\WAI2ACDP.DAT



Spectrum of Trace(s)- 1-12 - C:\Ref1W2\WAI2ACDP.DAT



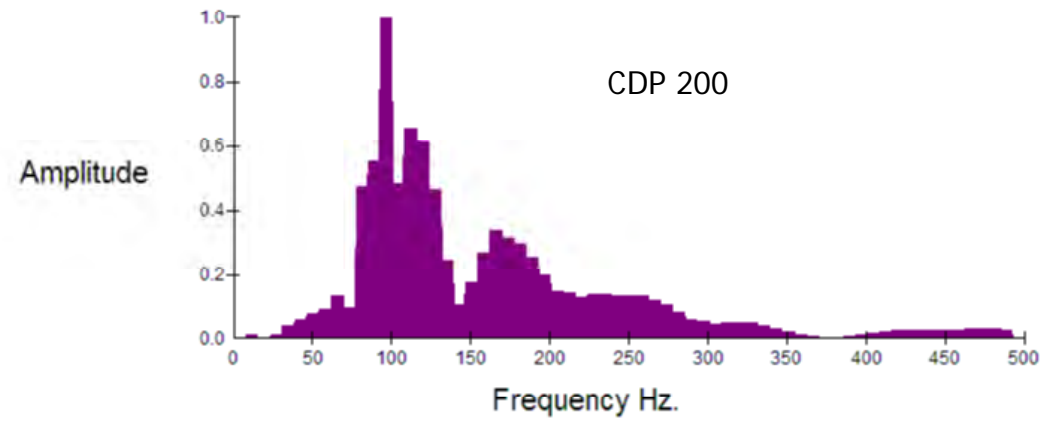
PROJECT:	University of Hawaii, Manoa	
	Waimanalo, HI	
REVISIONS		DATE

DRAWING TITLE:	Waimanalo L2 Seismic Frequencies	
	DAWOOD	
	CONSULTING ENGINEERS	
	10105 ALLENTOWN BLVD. GRANTVILLE, PA. 17028	
	PHONE: (717) 485-9537 FAX: (717) 485-0938	

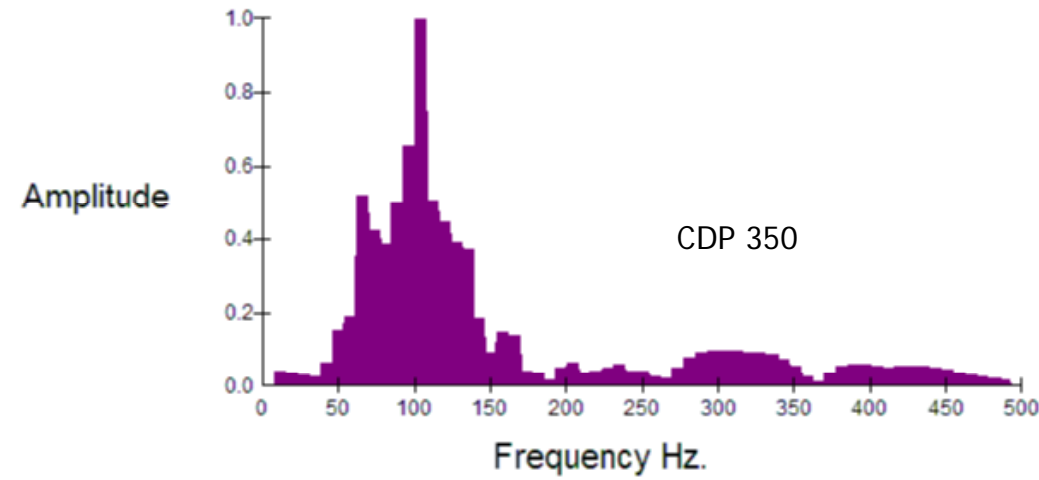
PROJECT NO.:	208044.01
DRAWN BY:	R.A.H.
CHECKED BY:	B.B.
SCALE:	AS SHOWN
DATE:	5 Aug 2008

SHEET NO.:

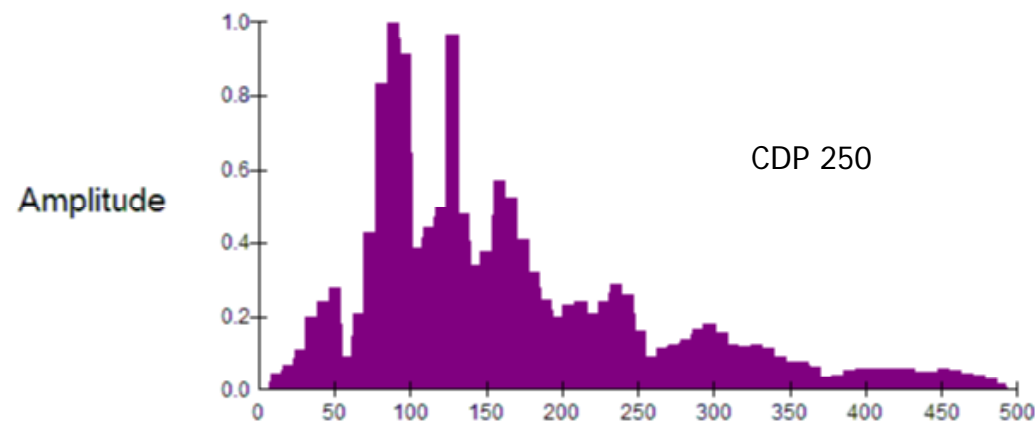
Spectrum of Trace(s)- 1-7 -
C:\RefIP2\POA2ACDP.DAT



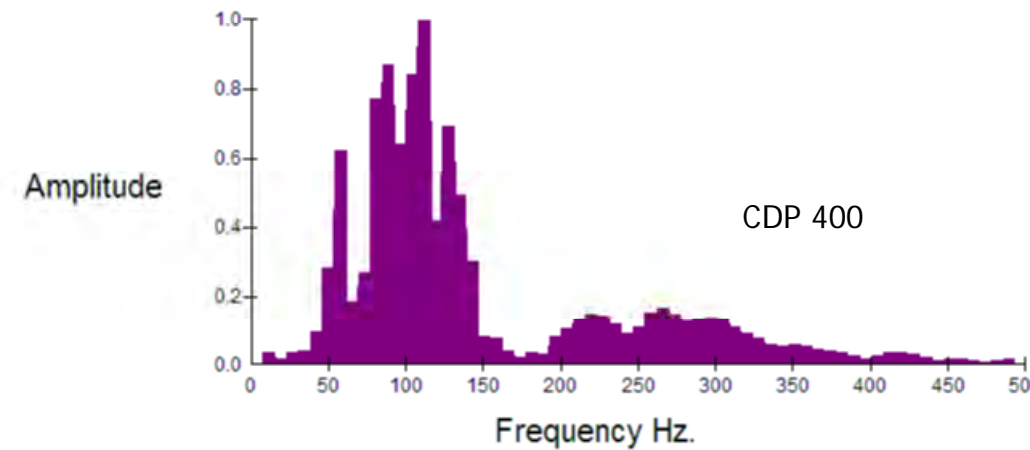
Spectrum of Trace(s)- 1-8 -
C:\RefIP2\POA2ACDP.DAT



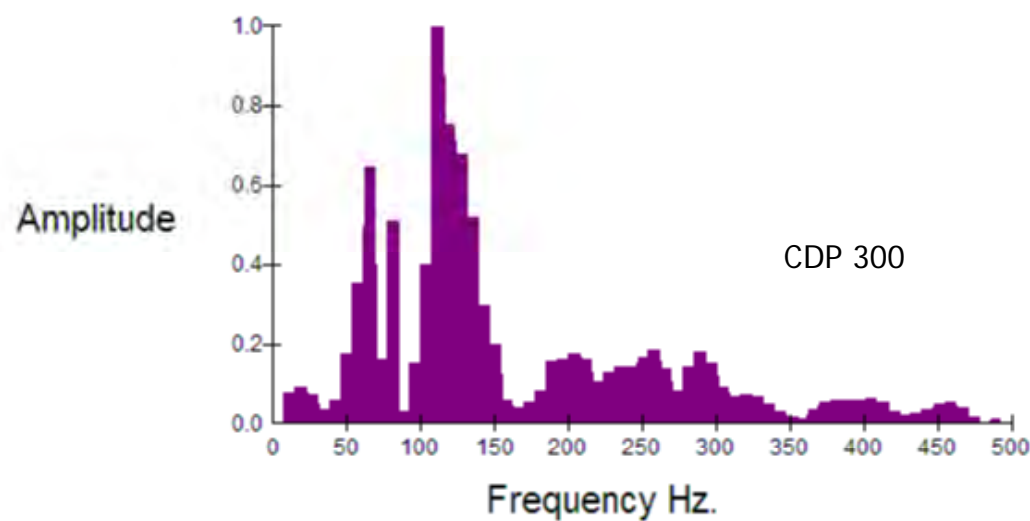
Spectrum of Trace(s)- 1-8 -
C:\RefIP2\POA2ACDP.DAT



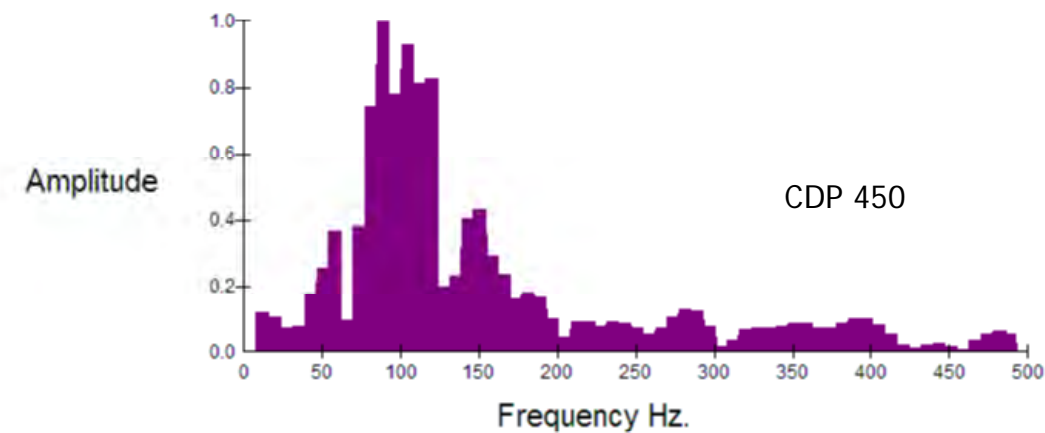
Spectrum of Trace(s)- 1-9 -
C:\RefIP2\POA2ACDP.DAT



Spectrum of Trace(s)- 1-9 -
C:\RefIP2\POA2ACDP.DAT



Spectrum of Trace(s)- 1-8 -
C:\RefIP2\POA2ACDP.DAT



PROJECT:	University of Hawaii, Manoa	
	Poamoho, HI	DATE
REVISIONS		

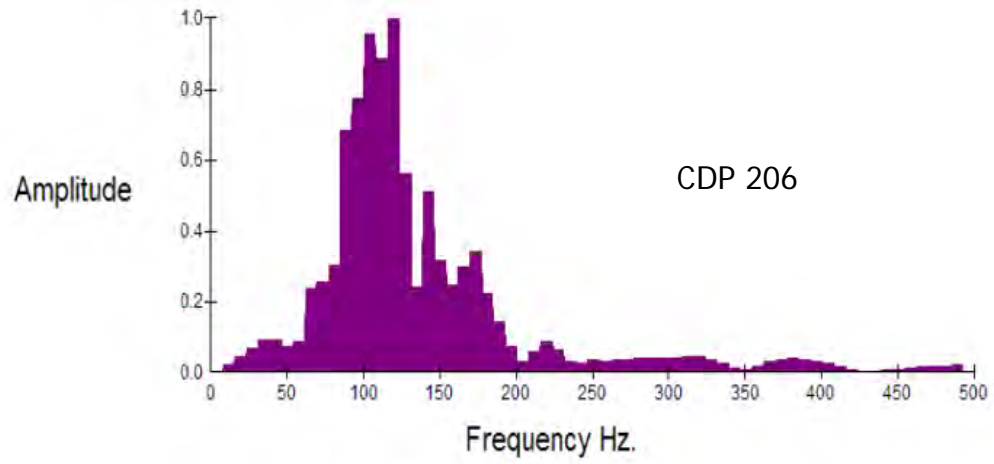
DAWOOD
CONSULTING ENGINEERS
10105 ALLENTOWN BLVD. GRANTVILLE, PA. 17028
PHONE: (717) 869-0937 FAX: (717) 869-0938

DRAWING TITLE:
Poamoho L2 Seismic Frequencies

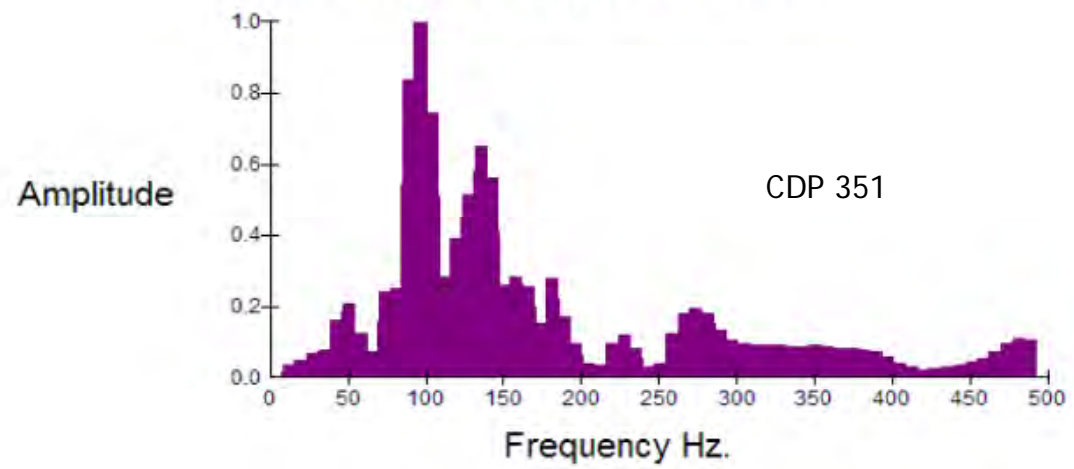
PROJECT NO.:	208044.01
DRAWN BY:	R.A.H.
CHECKED BY:	B.B.
SCALE:	AS SHOWN
DATE:	5 Aug 2008

SHEET NO.:

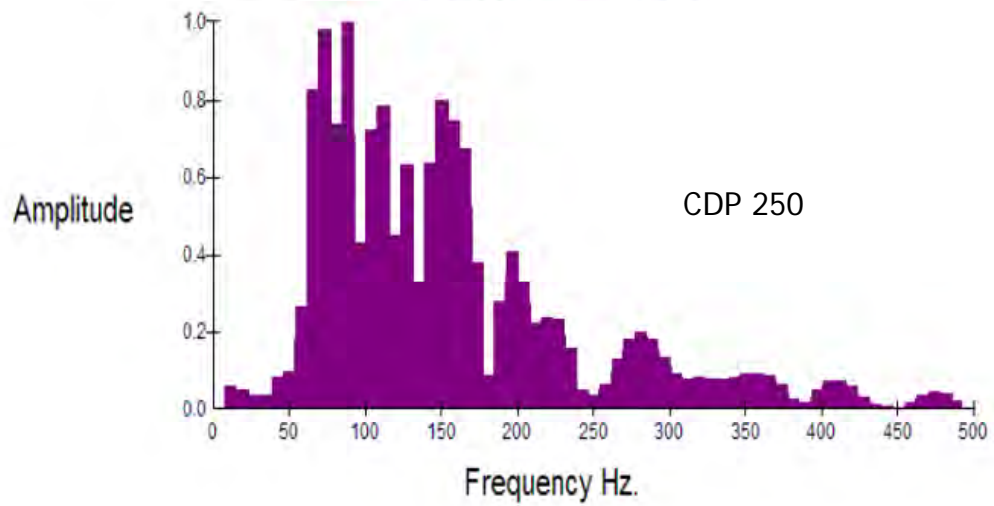
Spectrum of Trace(s)- 1-6 -
C:\RefIK0\KAW0ACDP.DAT



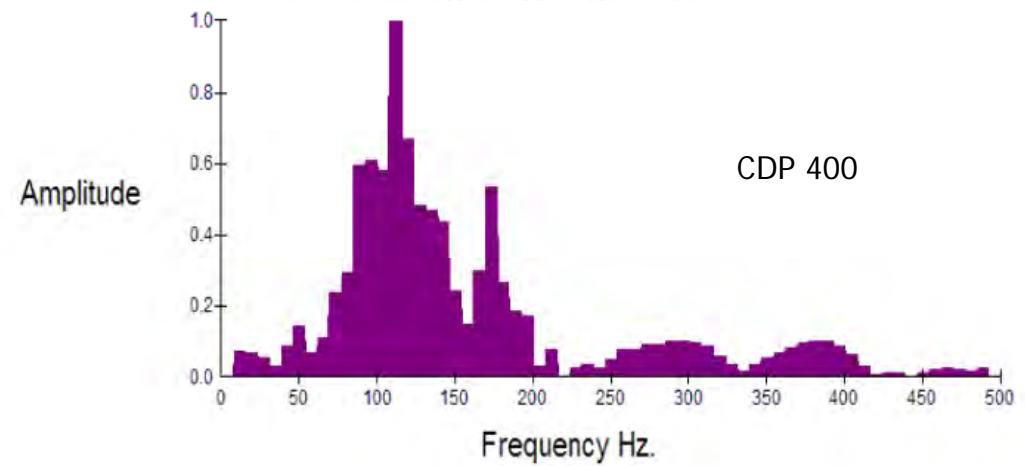
Spectrum of Trace(s)- 1-11 -
C:\RefIK0\KAW0ACDP.DAT



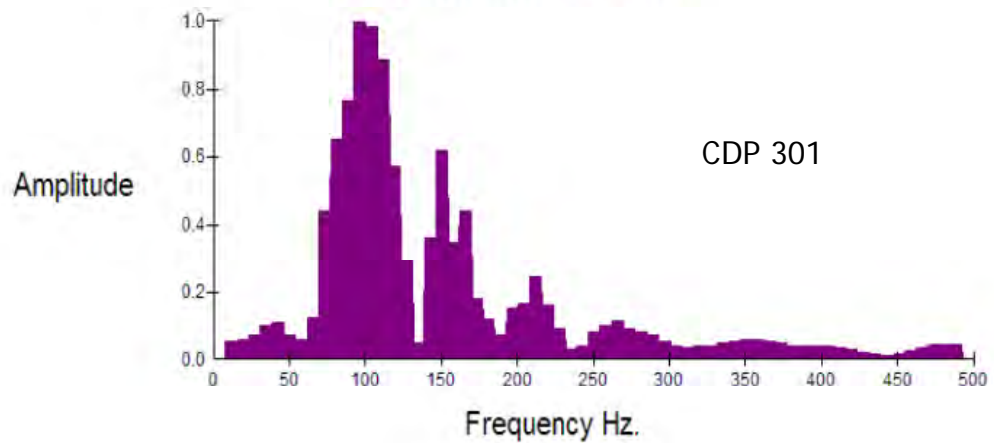
Spectrum of Trace(s)- 1-11 -
C:\RefIK0\KAW0ACDP.DAT



Spectrum of Trace(s)- 1-8 -
C:\RefIK0\KAW0ACDP.DAT



Spectrum of Trace(s)- 1-8 -
C:\RefIK0\KAW0ACDP.DAT



PROJECT: University of Hawaii, Manoa Kawaihae, HI	REVISIONS	DATE

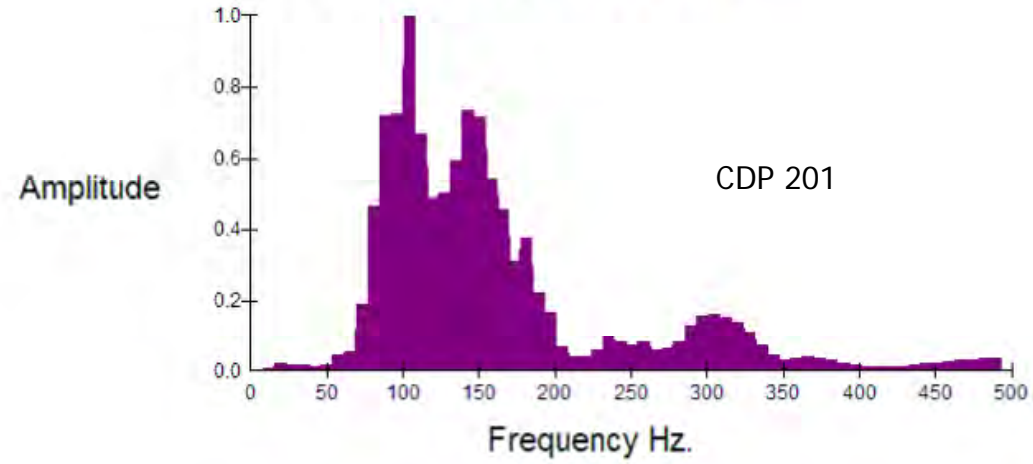
DAWOOD
CONSULTING ENGINEERS
1015 ALI LANE, SUITE 200, KAWAIIHAE, HI 96726
PHONE: (808) 933-7441 FAX: (808) 933-0530

DRAWING TITLE:
Kawaihae L0 Seismic Frequencies

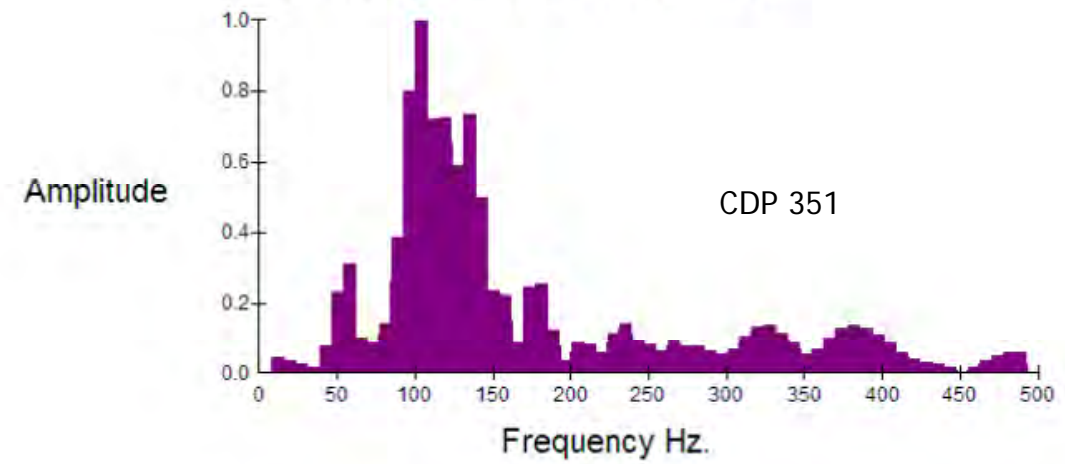
PROJECT NO.:	208044.01
DRAWN BY:	R.A.H.
CHECKED BY:	B.B.
SCALE:	AS SHOWN
DATE:	5 Aug 2008

SHEET NO.:

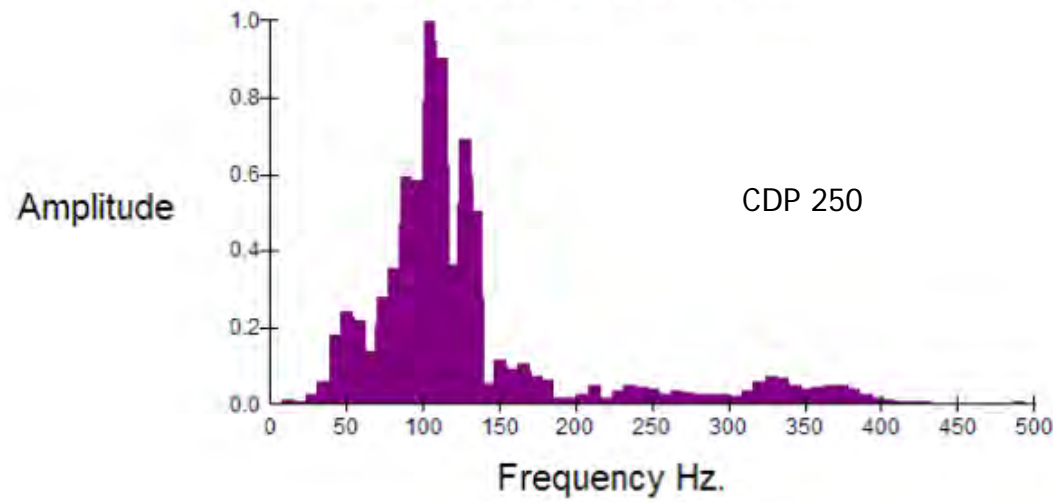
Spectrum of Trace(s)- 1-4 -
C:\RefIK2\KAW2ACDP.DAT



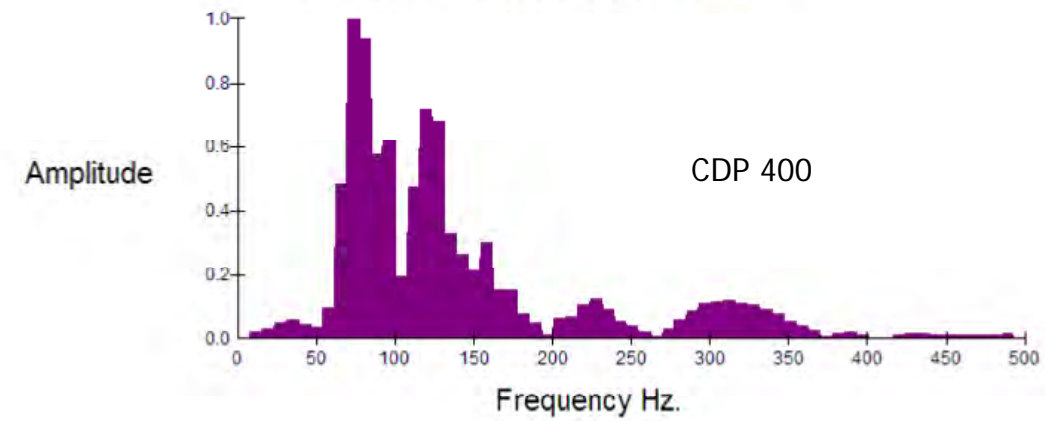
Spectrum of Trace(s)- 1-12 -
C:\RefIK2\KAW2ACDP.DAT



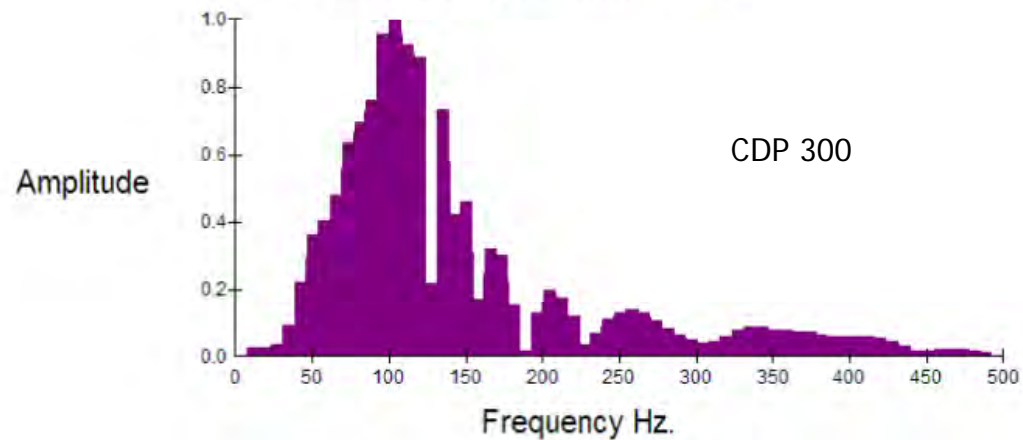
Spectrum of Trace(s)- 1-11 -
C:\RefIK2\KAW2ACDP.DAT



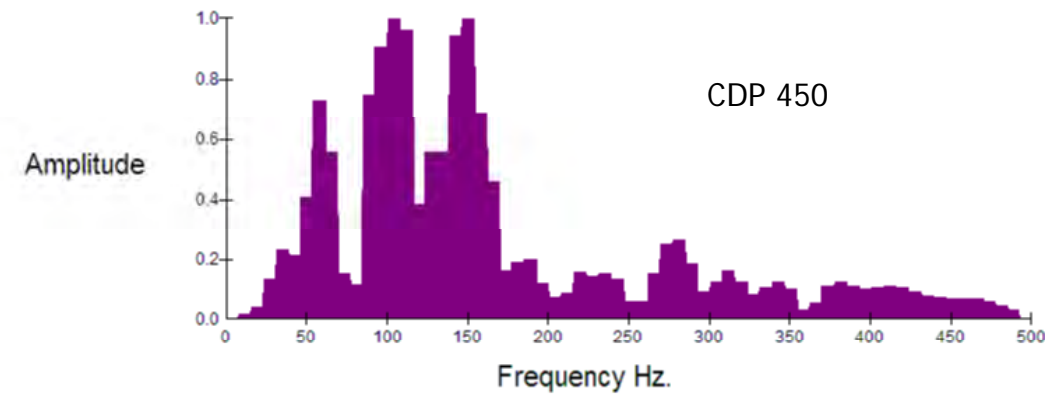
Spectrum of Trace(s)- 1-7 -
C:\RefIK2\KAW2ACDP.DAT



Spectrum of Trace(s)- 1-7 -
C:\RefIK2\KAW2ACDP.DAT



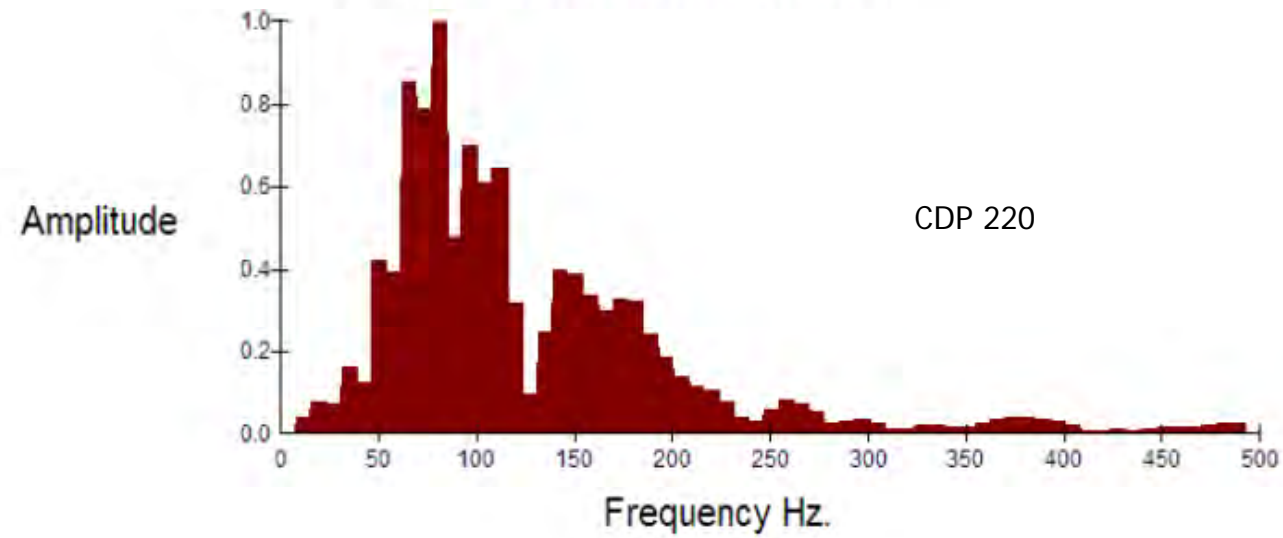
Spectrum of Trace(s)- 1-12 -
C:\RefIK2\KAW2ACDP.DAT



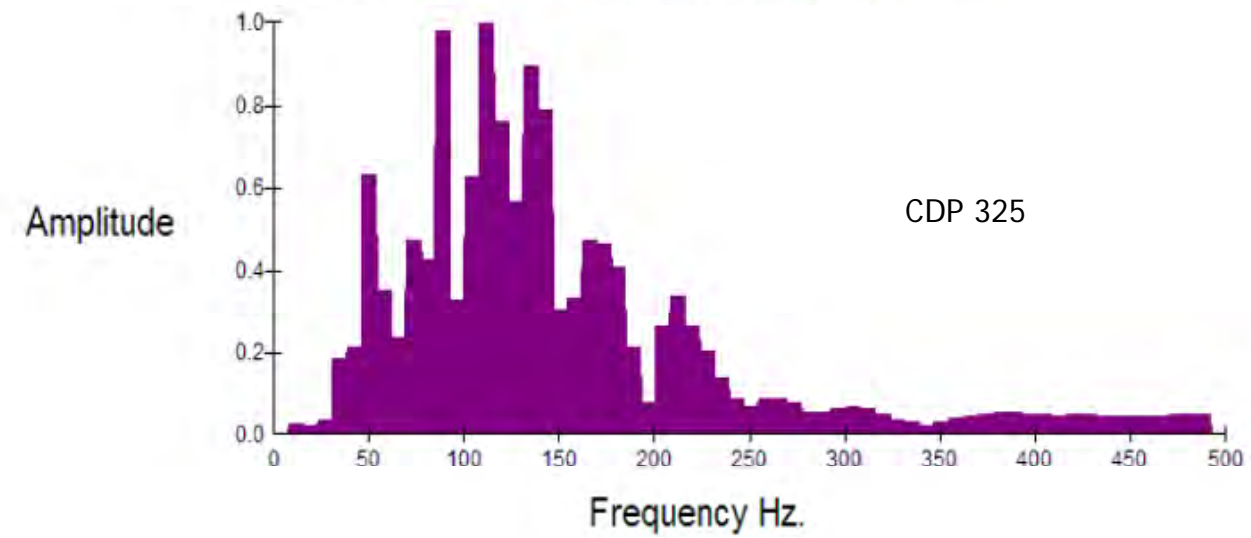
PROJECT: University of Hawaii, Manoa Kawaihae, HI	DATE
	REVISIONS

 CONSULTING ENGINEERS 1015 ALI LANE, SUITE 200, KAWAIIHAE, HI 96728 PHONE: (808) 933-7343 FAX: (808) 933-9330	DRAWING TITLE: Kawaihae L2 Seismic Frequencies
	PROJECT NO.: 208044.01 DRAWN BY: R.A.H. CHECKED BY: B.B. SCALE: AS SHOWN DATE: 5 Aug 2008 SHEET NO.:

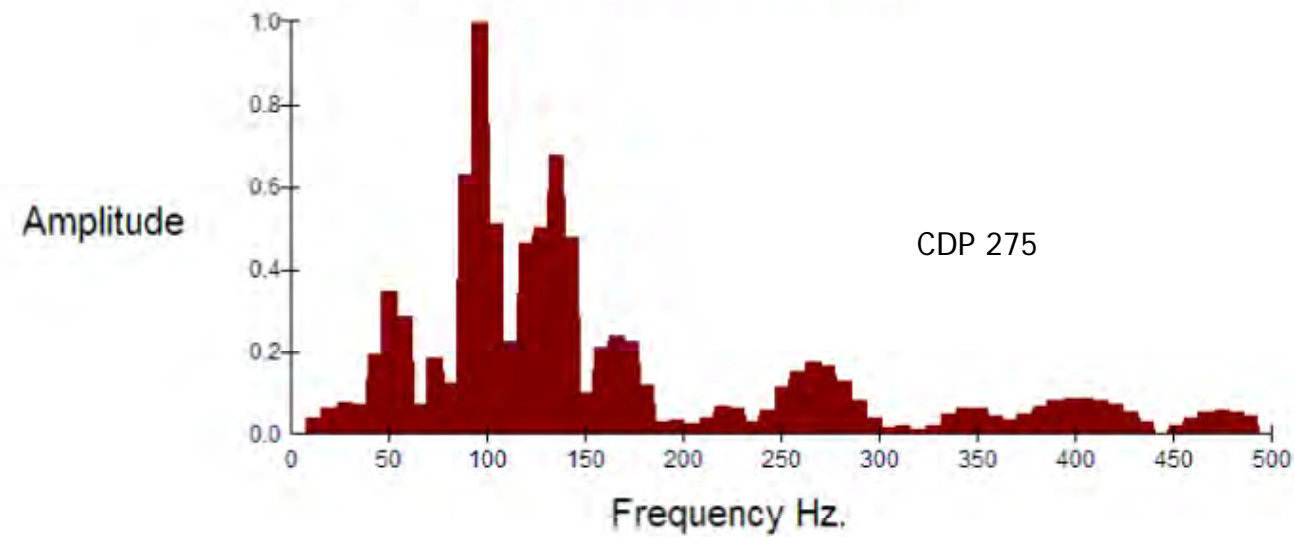
Spectrum of Trace(s)- 1-12 -
C:\Ref\W4\WAI4ACDP.DAT



Spectrum of Trace(s)- 1-8 -
C:\Ref\W4\WAI4ACDP.DAT



Spectrum of Trace(s)- 1-8 -
C:\Ref\W4\WAI4ACDP.DAT



PROJECT:	University of Hawaii, Manoa	
	Waimanalo, HI	DATE
REVISIONS		

 CONSULTING ENGINEERS 10105 ALLENTOWN BLVD. GRANTVILLE, PA. 17028 PHONE: (717) 485-0937 FAX: (717) 485-0938	DRAWING TITLE:
	Waimanalo L4 Seismic Frequencies

PROJECT NO.:	208044.01
DRAWN BY:	R.A.H.
CHECKED BY:	B.B.
SCALE:	AS SHOWN
DATE:	5 Aug 2008

SHEET NO.:

Appendix B – Normal Move Out (NMO) Panels for Seismic Reflection Data

Velocities:
(feet/second)

500

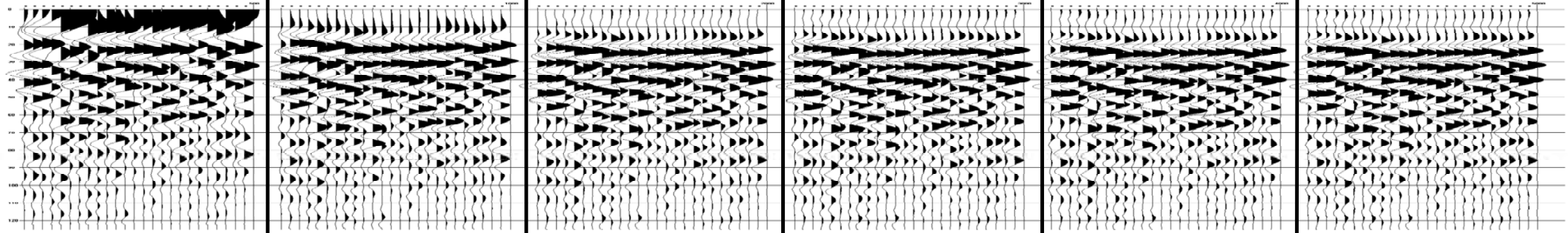
1000

2000

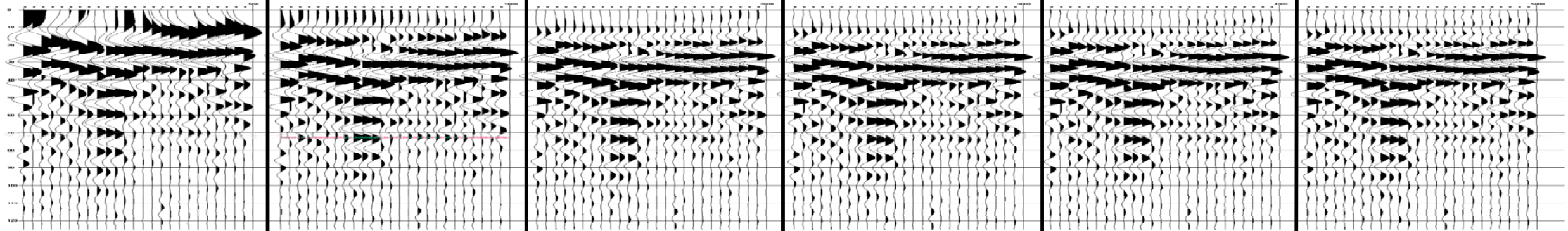
3000

4000

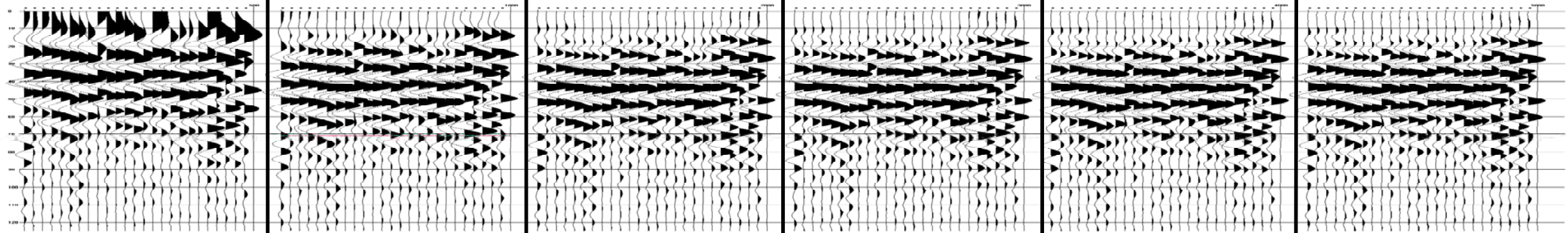
5000



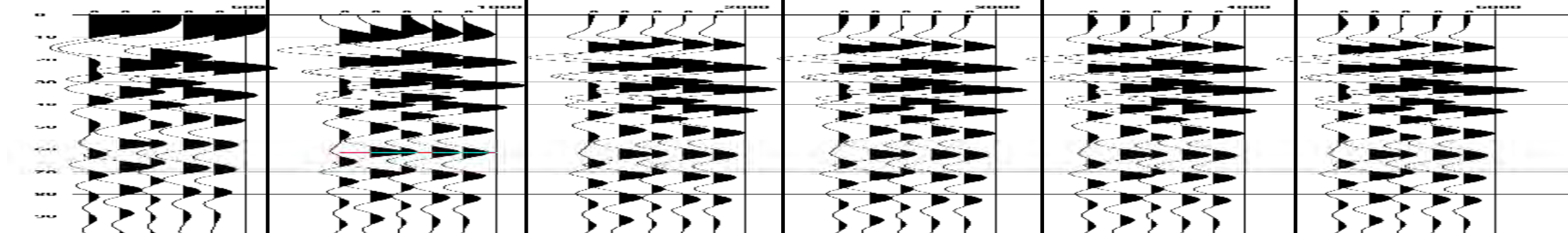
CDP 1100



CDP 1050



CDP 1100



CDP 1150

PROJECT:
University of Hawaii, Manoa
Waimanalo HI

REVISIONS	DATE

CONSULTING ENGINEERS
10105 ALLENTOWN BLVD. GRANTVILLE, PA. 17028
PHONE: (717) 469-0937 FAX: (717) 469-0938

DRAWING TITLE:
Waimanalo L2 NMO Panels

PROJECT NO.:	208044.01
DRAWN BY:	R.A.H.
CHECKED BY:	B.B.
SCALE:	AS SHOWN
DATE:	5 Aug 2008
SHEET NO.:	

Velocities:
(feet/second)

500

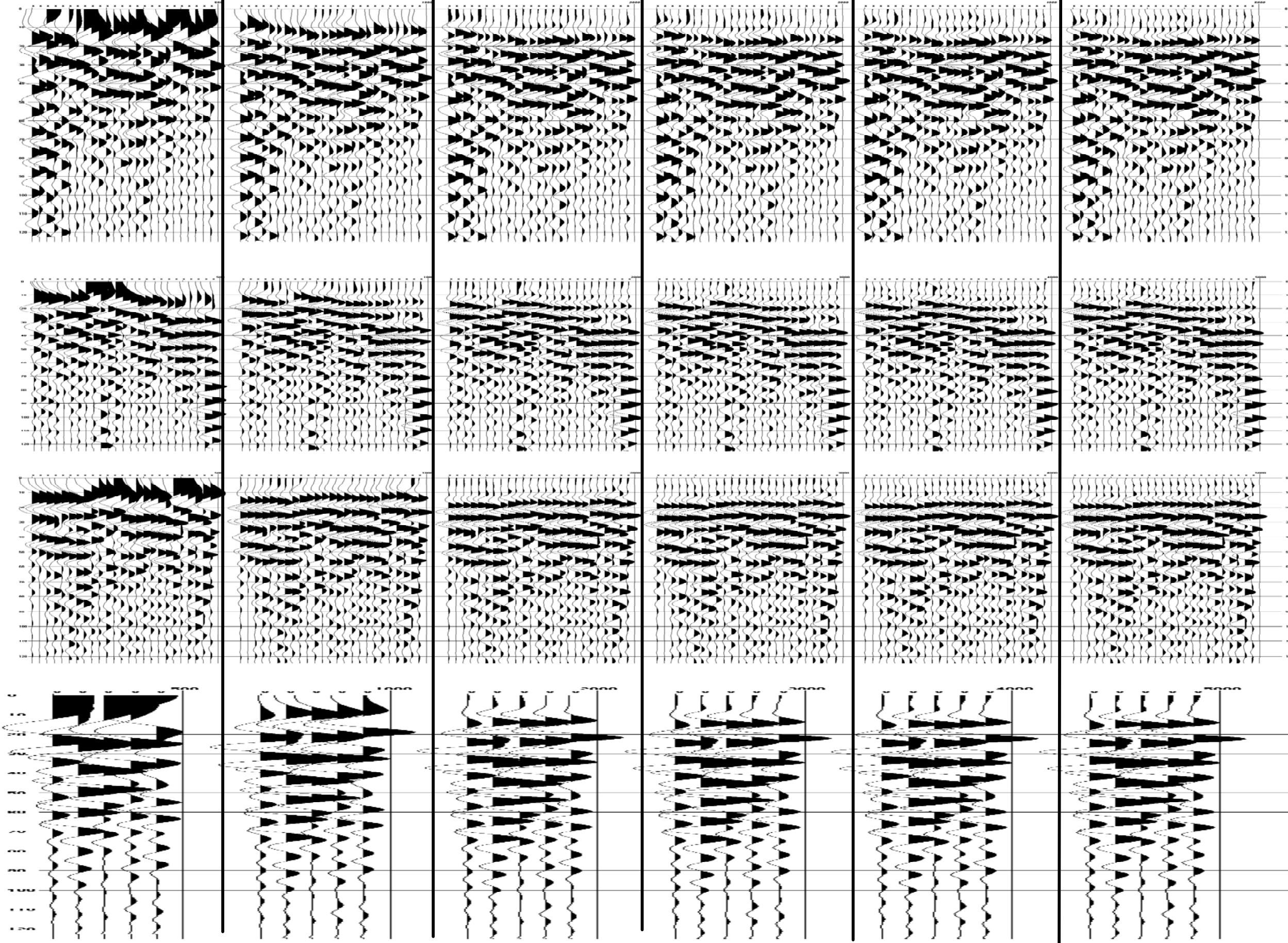
1000

2000

3000

4000

5000



CDP 1100

CDP 1050

CDP 1100

CDP 1150

PROJECT:
University of Hawaii, Manoa
Poamoho, HI

REVISIONS	DATE

CONSULTING ENGINEERS
10105 ALLENTOWN BLVD. GRANTVILLE, PA. 17028
PHONE: (717) 469-0937 FAX: (717) 469-0938

DRAWING TITLE:
Poamoho L2 NMO Velocity Panels

PROJECT NO.:	208044.01
DRAWN BY:	R.A.H.
CHECKED BY:	B.B.
SCALE:	AS SHOWN
DATE:	5 MAY 2008
SHEET NO.:	

Velocities:
(feet/second)

500

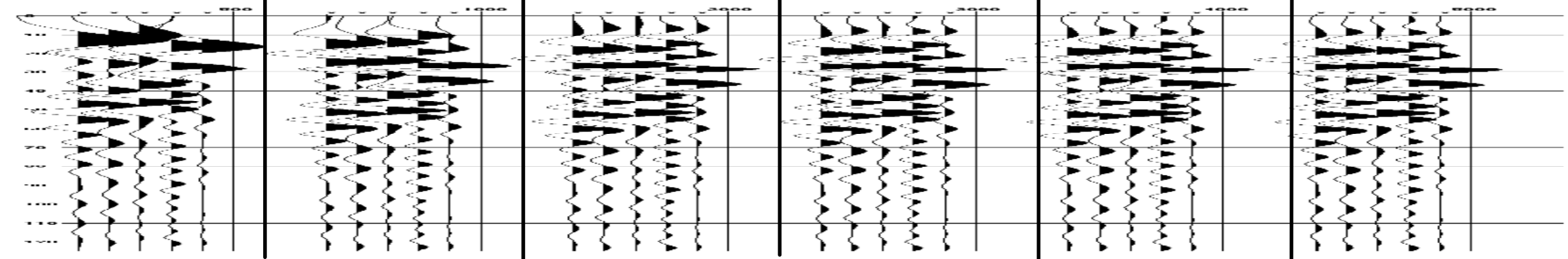
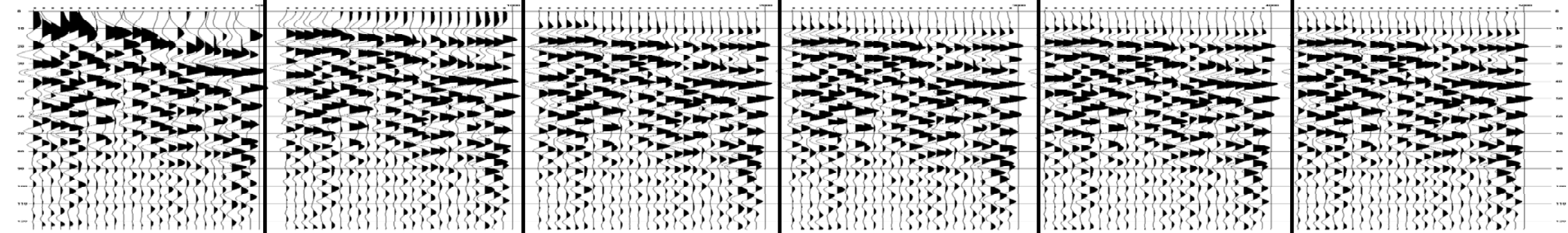
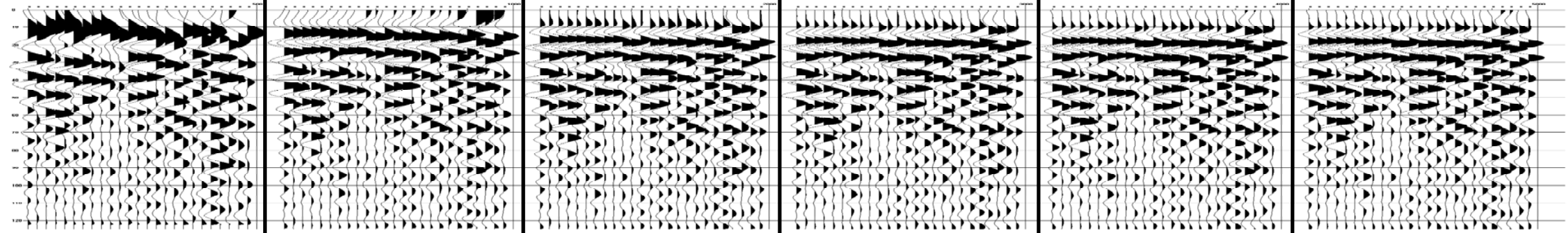
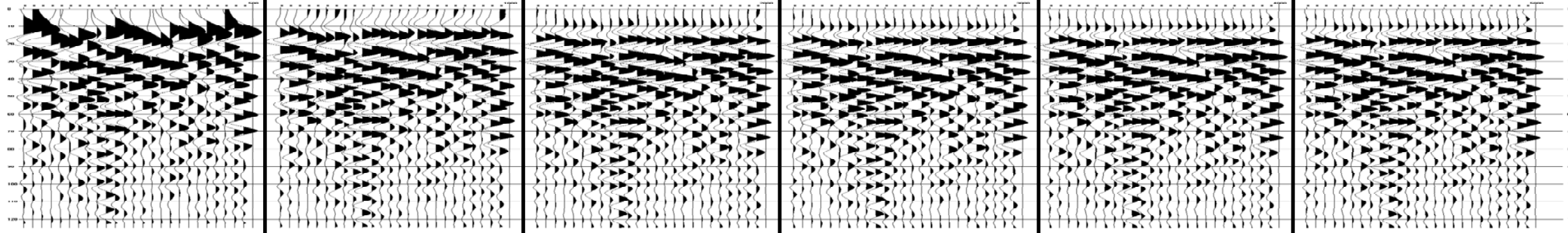
1000

2000

3000

4000

5000



PROJECT:
University of Hawaii, Manoa
Kawaihae, HI

REVISIONS	DATE

CONSULTING ENGINEERS
10105 ALLENTOWN BLVD. GRANTVILLE, PA. 17028
PHONE: (717) 469-0937 FAX: (717) 469-0938

DRAWING TITLE:
Kawaihae L2 NMO Velocity Panels

PROJECT NO.:	208044.01
DRAWN BY:	R.A.H.
CHECKED BY:	B.B.
SCALE:	AS SHOWN
DATE:	5 Aug 2008
SHEET NO.:	

Velocities:
(feet/second)

500

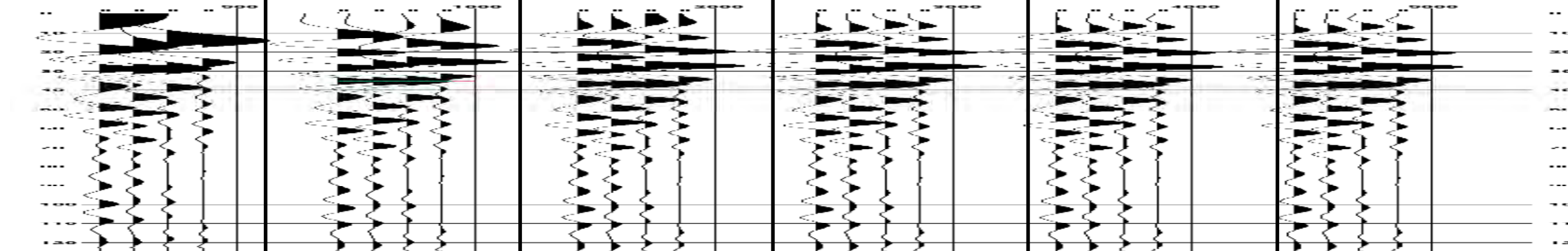
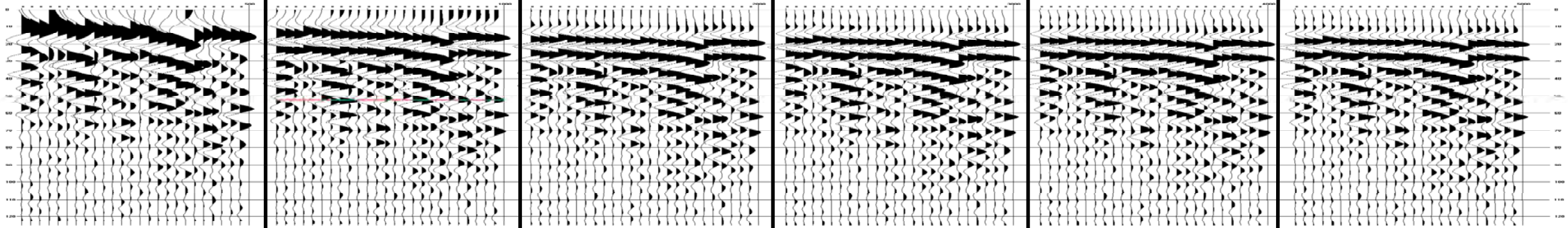
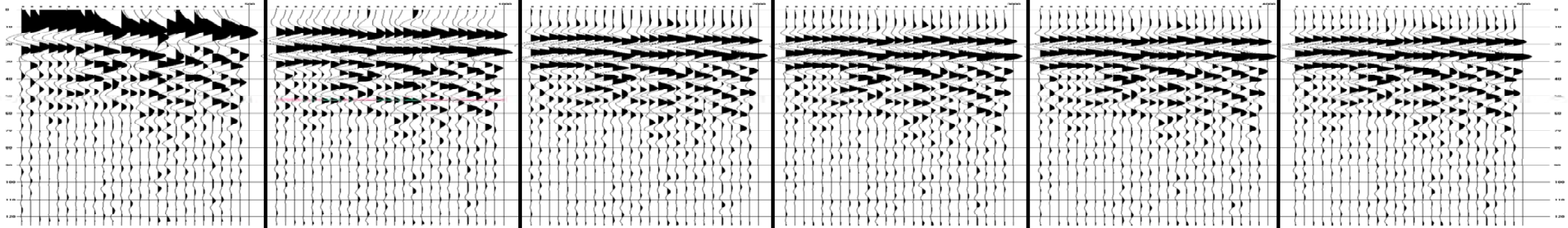
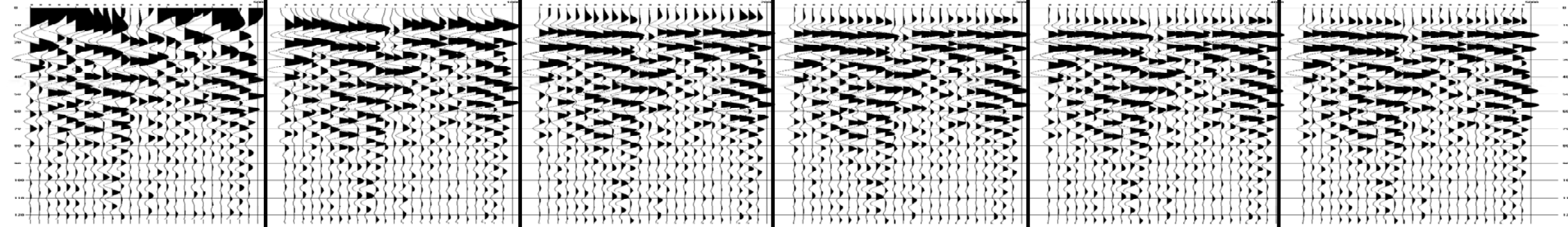
1000

2000

3000

4000

5000



PROJECT:
University of Hawaii, Manoa
Poamoho, HI

REVISIONS	DATE

CONSULTING ENGINEERS
10105 ALLENTOWN BLVD. GRANVILLE, PA. 17028
PHONE: (717) 469-0937 FAX: (717) 469-0938

DRAWING TITLE:
Kawaihae LO NMO Velocity Panels

PROJECT NO.:	208044.01
DRAWN BY:	R.A.H.
CHECKED BY:	B.B.
SCALE:	AS SHOWN
DATE:	5 MAY 2008
SHEET NO.:	

Velocities:
(feet/second)

500

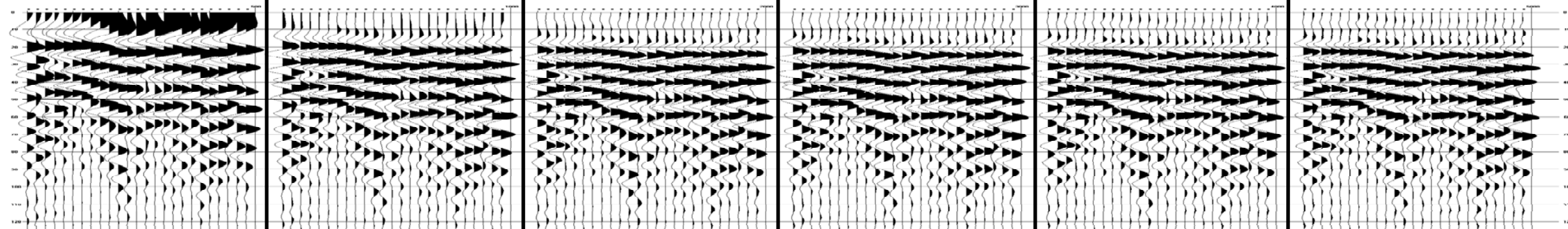
1000

2000

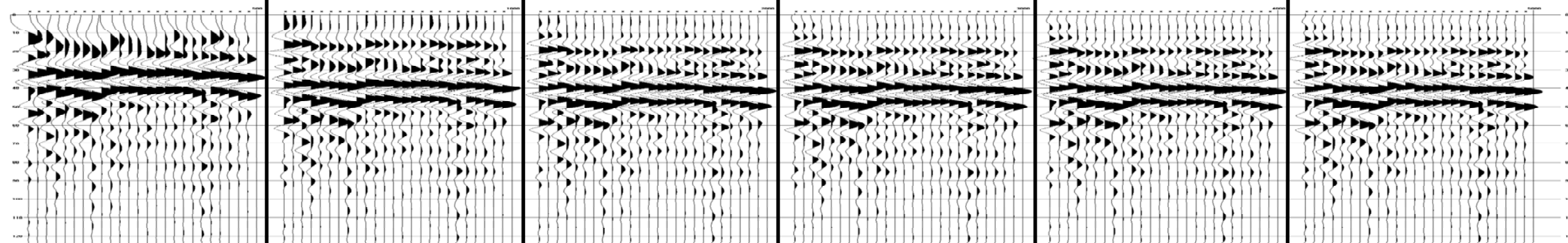
3000

4000

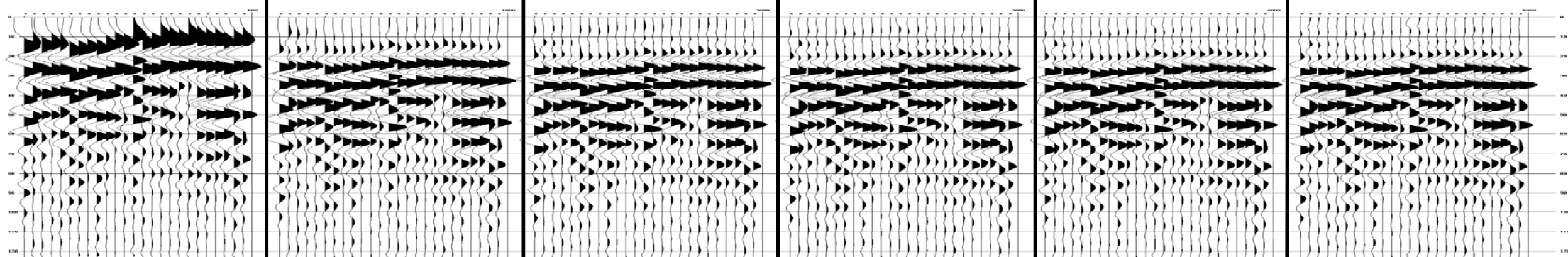
5000



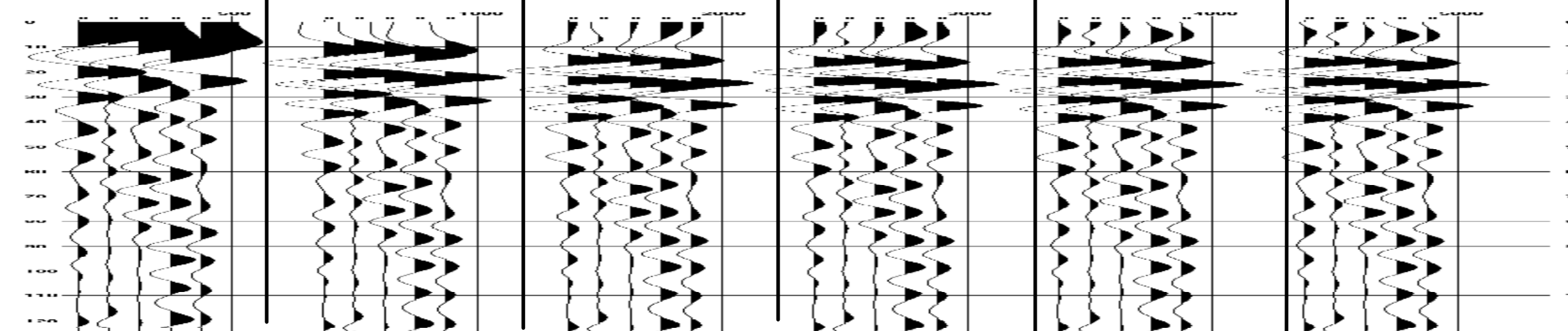
CDP 1100



CDP 1050



CDP 1100



CDP 1150

PROJECT:
University of Hawaii, Manoa
Waimanalo HI

REVISIONS	DATE

CONSULTING ENGINEERS
10105 ALLENTOWN BLVD. GRANTVILLE, PA. 17028
PHONE: (717) 469-0937 FAX: (717) 469-0938

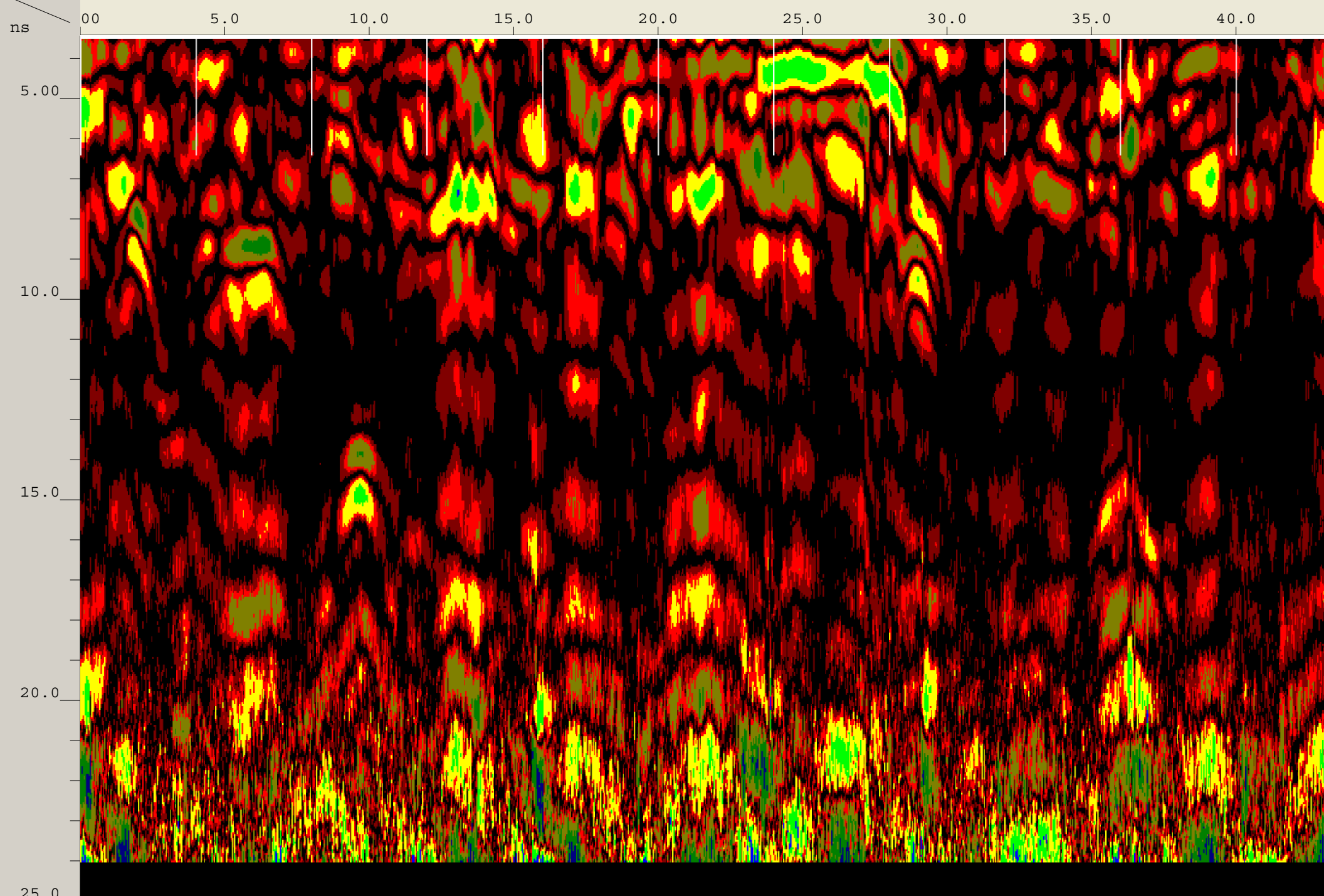
DRAWING TITLE:
Waimanalo L4 NMO Panels

PROJECT NO.: 208044.01
DRAWN BY: R.A.H.
CHECKED BY: B.B.
SCALE: AS SHOWN
DATE: 5 Aug 2008
SHEET NO.:

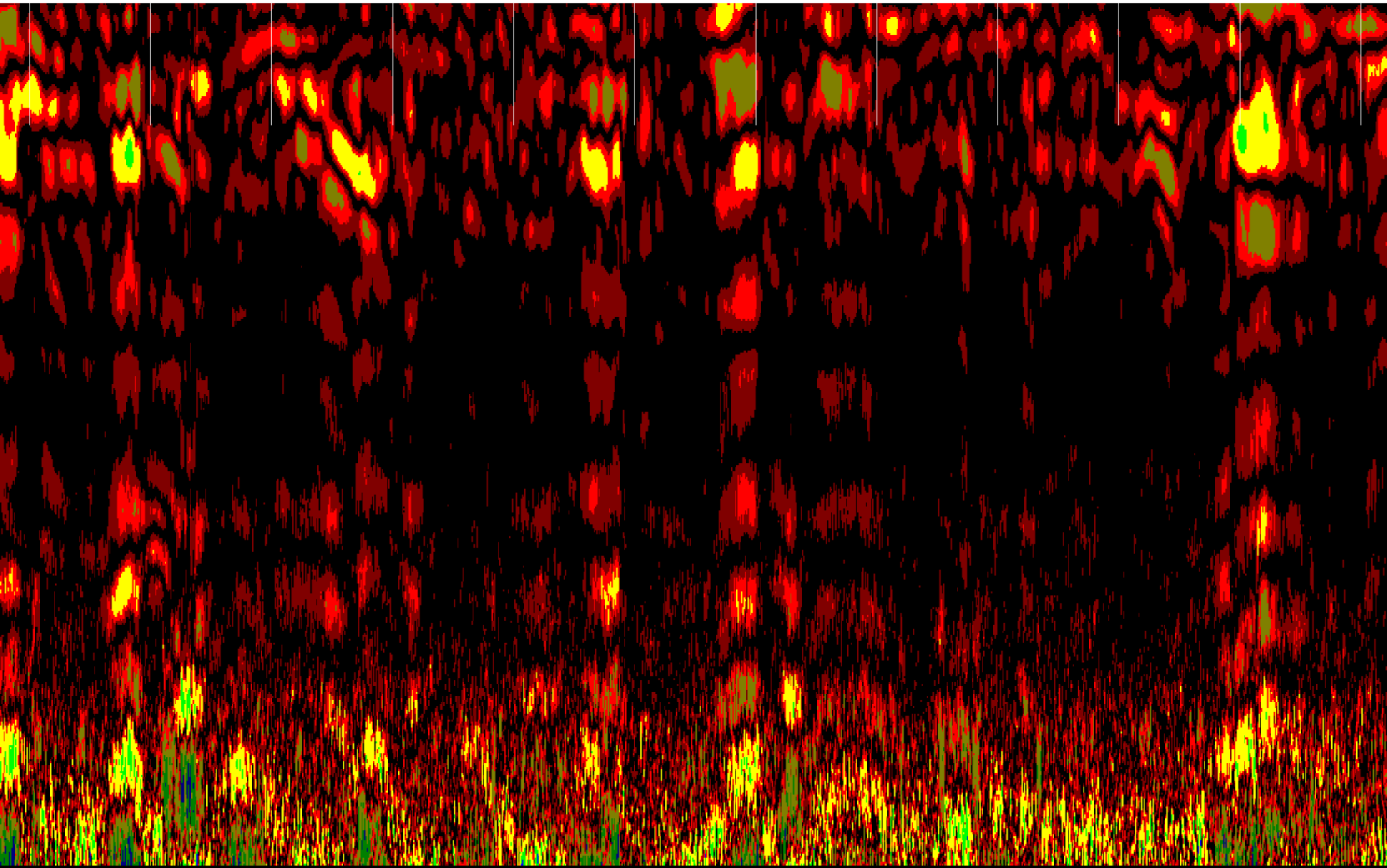
Appendix C – Poamoho GPR Traverse Data

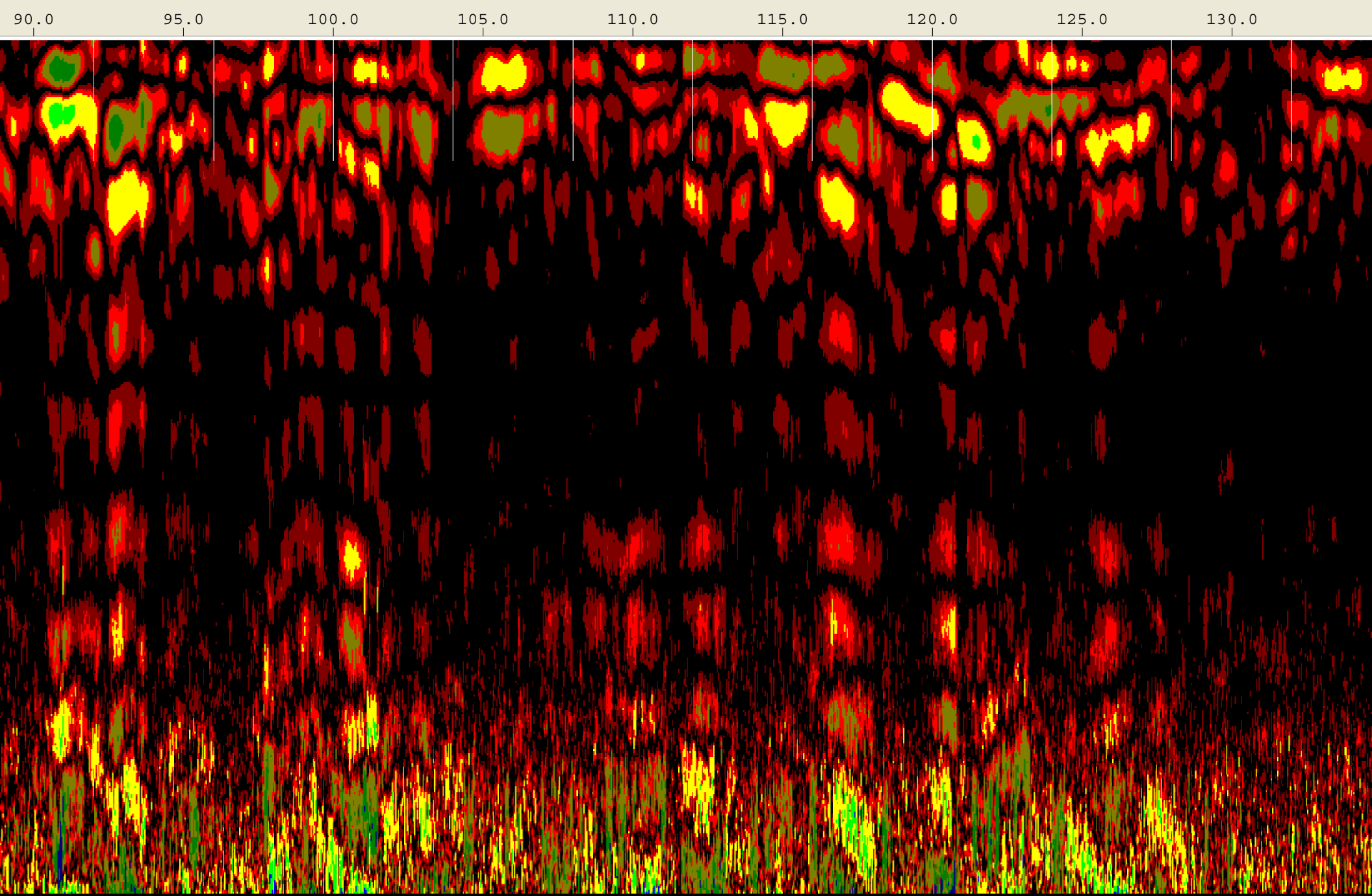
Created Jun, 17 2008, 12:14:00 Modified Jun, 17 2008, 12:15:42
Channel(s) 1 Samples/Scan 512 Bits/Sample 16
Scans/Second 100 Scans/Meter 78.7402 Meters/Mark 1.2192
Diel Constant 39.3258

CHANNEL 1 400MHz
Position 3.42 nS Range 24 nS
Position Correction 1.04 nS
Vert IIR LP N =1 F =800 MHz
Vert IIR HP N =1 F =100 MHz
Range Gain (dB) 8.0 8.0 38.0
Position Correction 3.42 nS
Horz Boxcar Bkgr N=1023

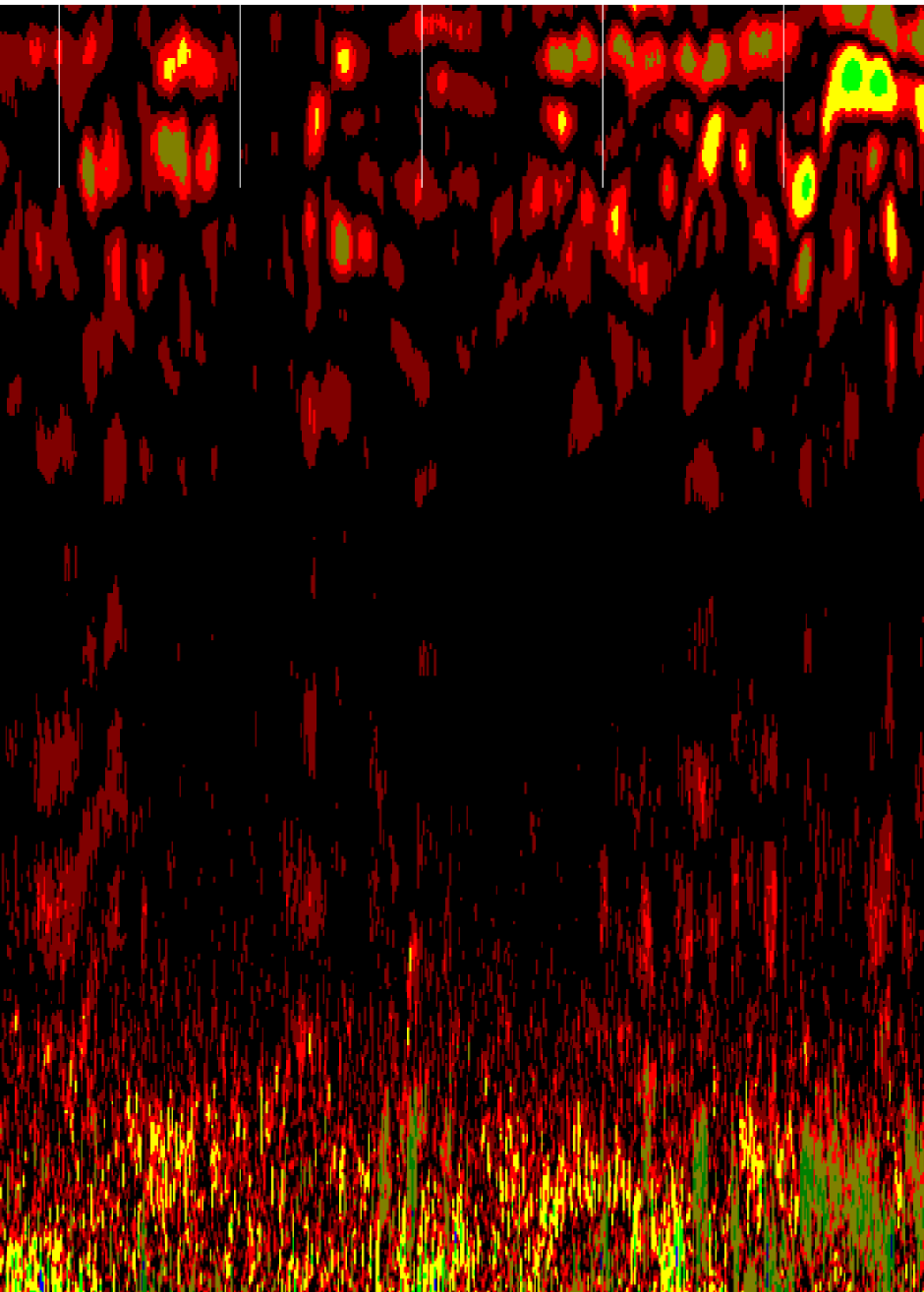


45.0 50.0 55.0 60.0 65.0 70.0 75.0 80.0 85.0



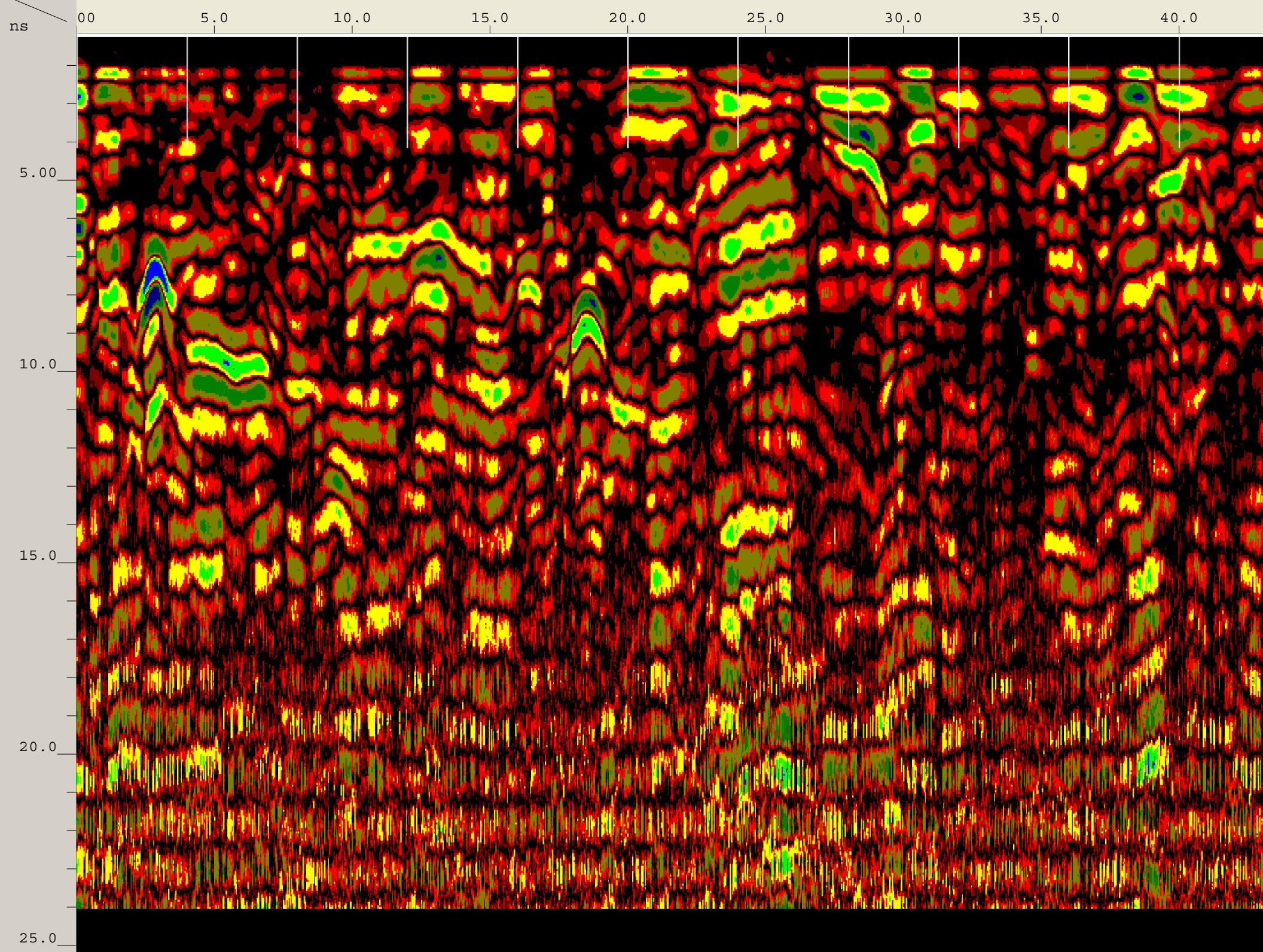


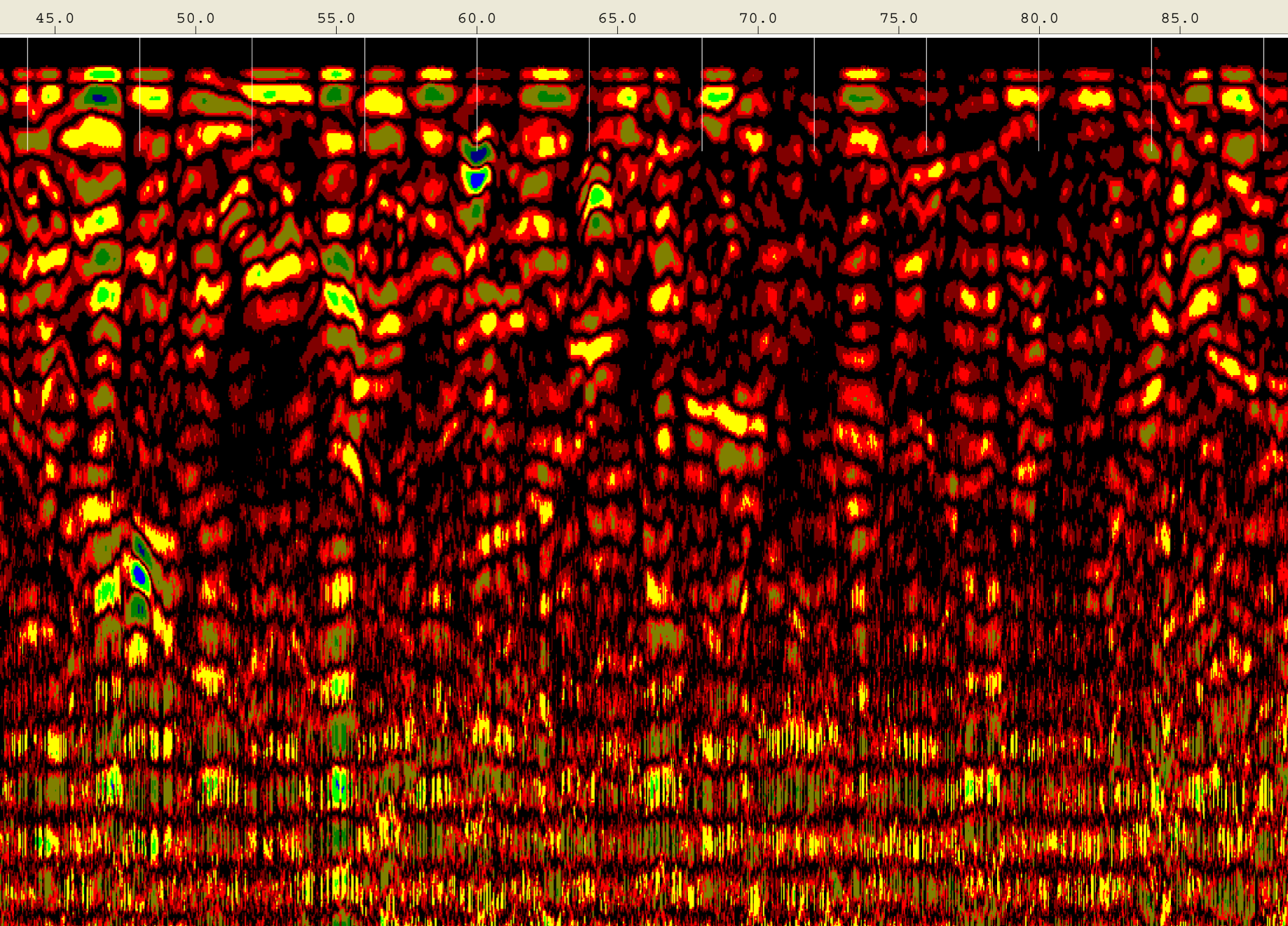
135.0 140.0 145.0 150.0 155.0

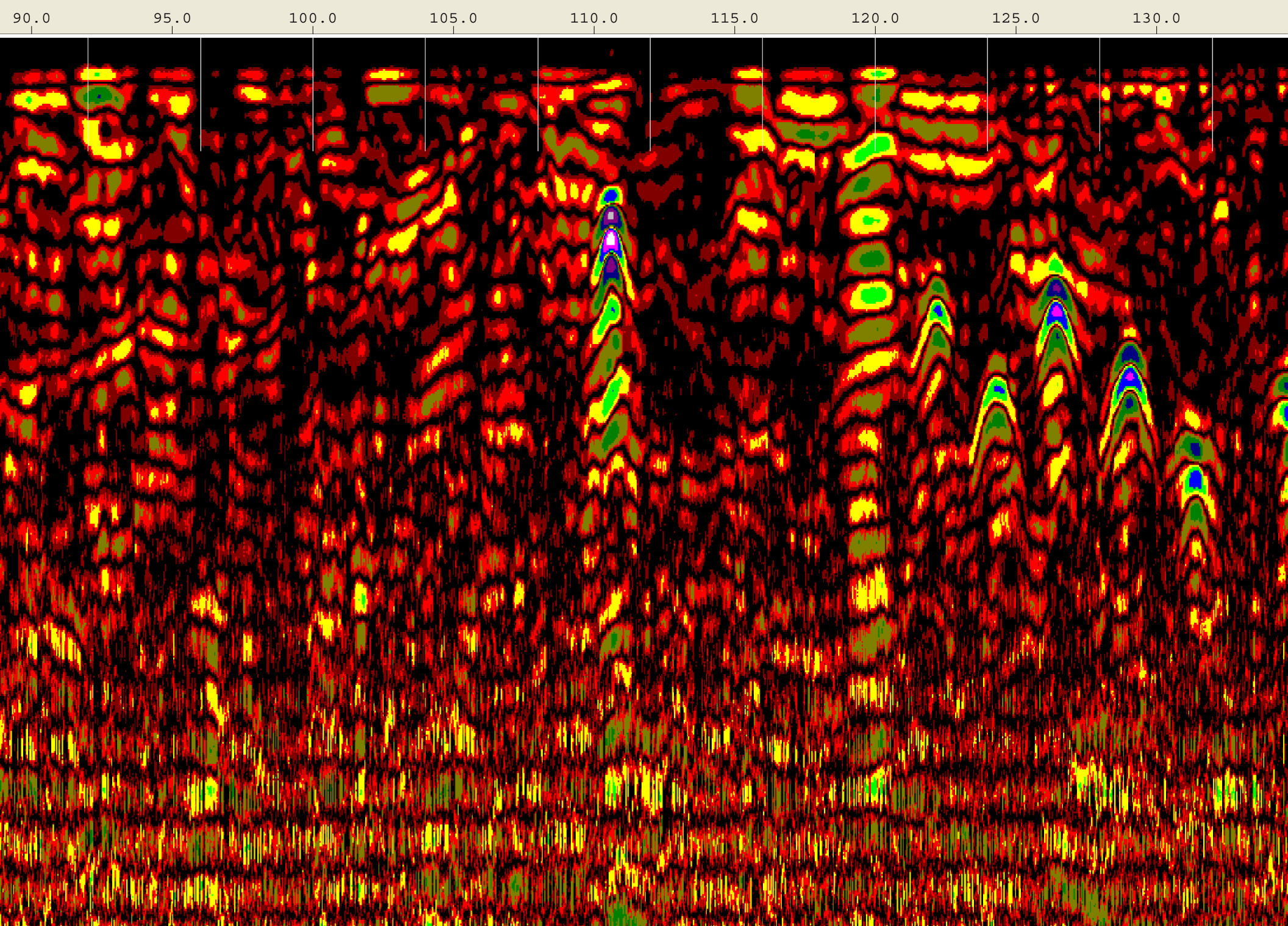


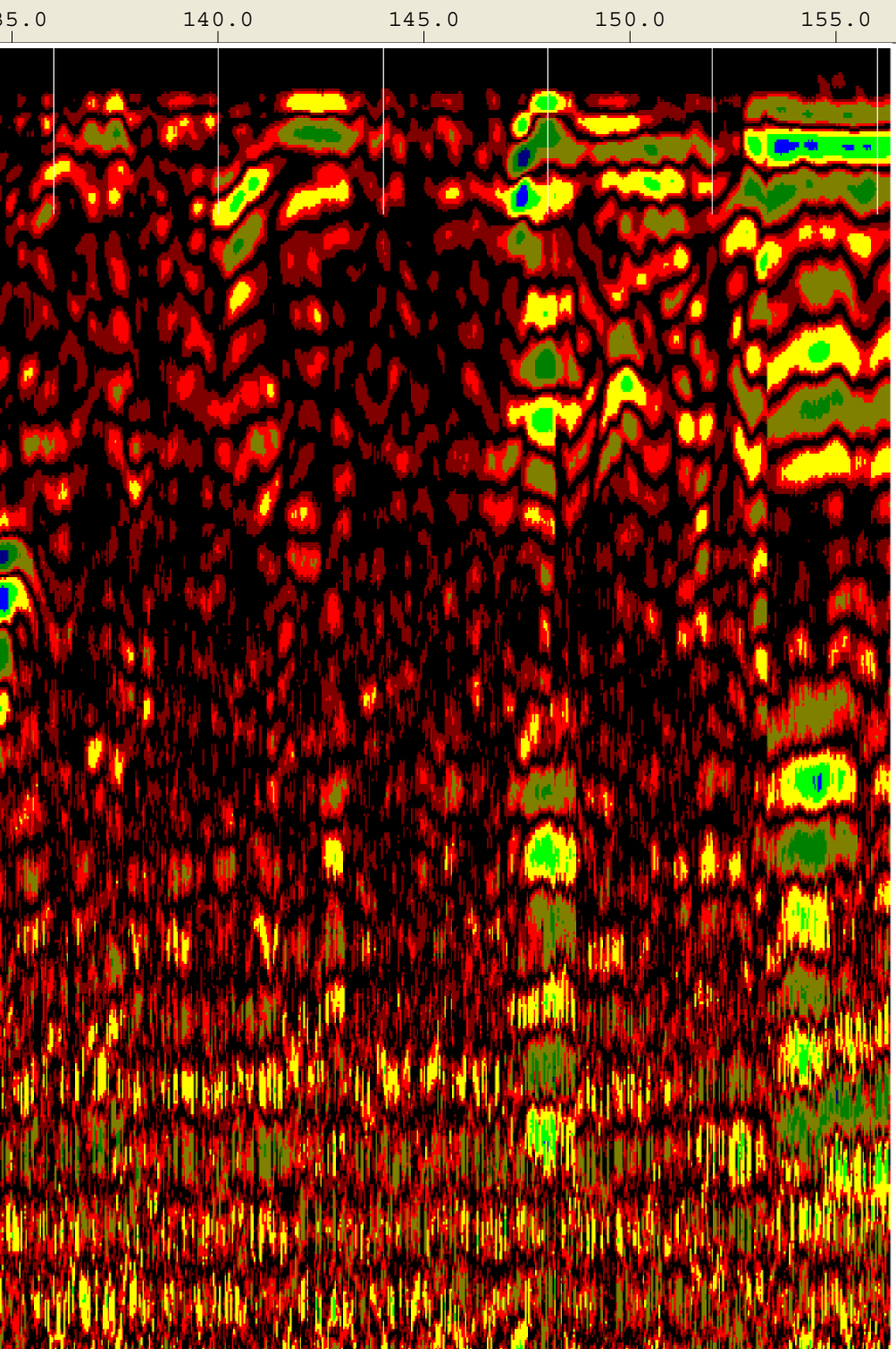
Created Jun, 17 2008, 12:26:56 Modified Jun, 17 2008, 12:33:10
Channel(s) 1 Samples/Scan 512 Bits/Sample 16
Scans/Second 100 Scans/Meter 78.7402 Meters/Mark 1.2192
Diel Constant 7.4816

CHANNEL 1 900MHz
Position 1.17 nS Range 24 nS
Range Gain (dB) 5.0 34.0 43.0
Position Correction 1.04 nS
Vert IIR LP N =1 F =2500 MHz
Vert IIR HP N =1 F =225 MHz
Position Correction 1.17 nS
Horz Boxcar Bkgr N=1023



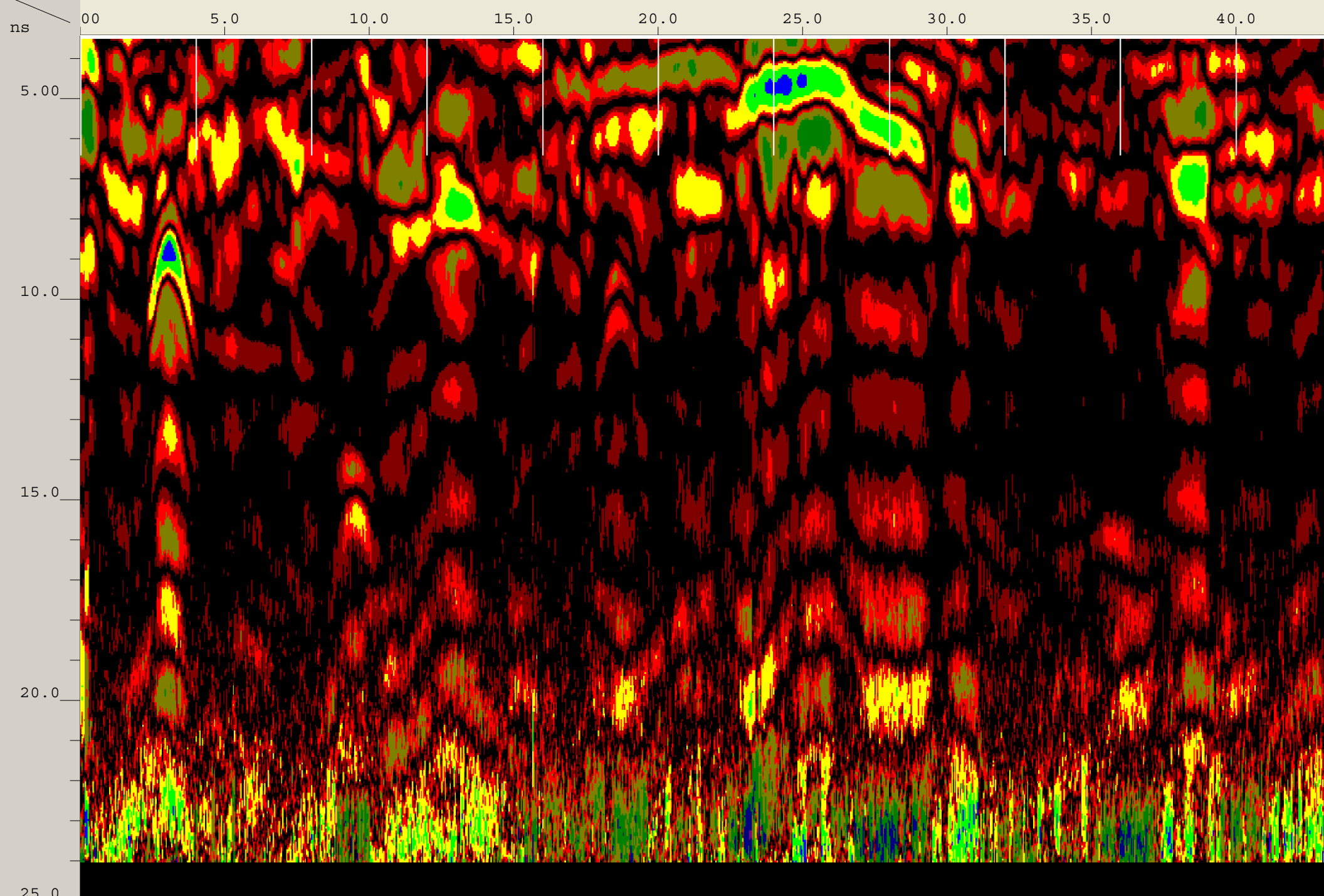




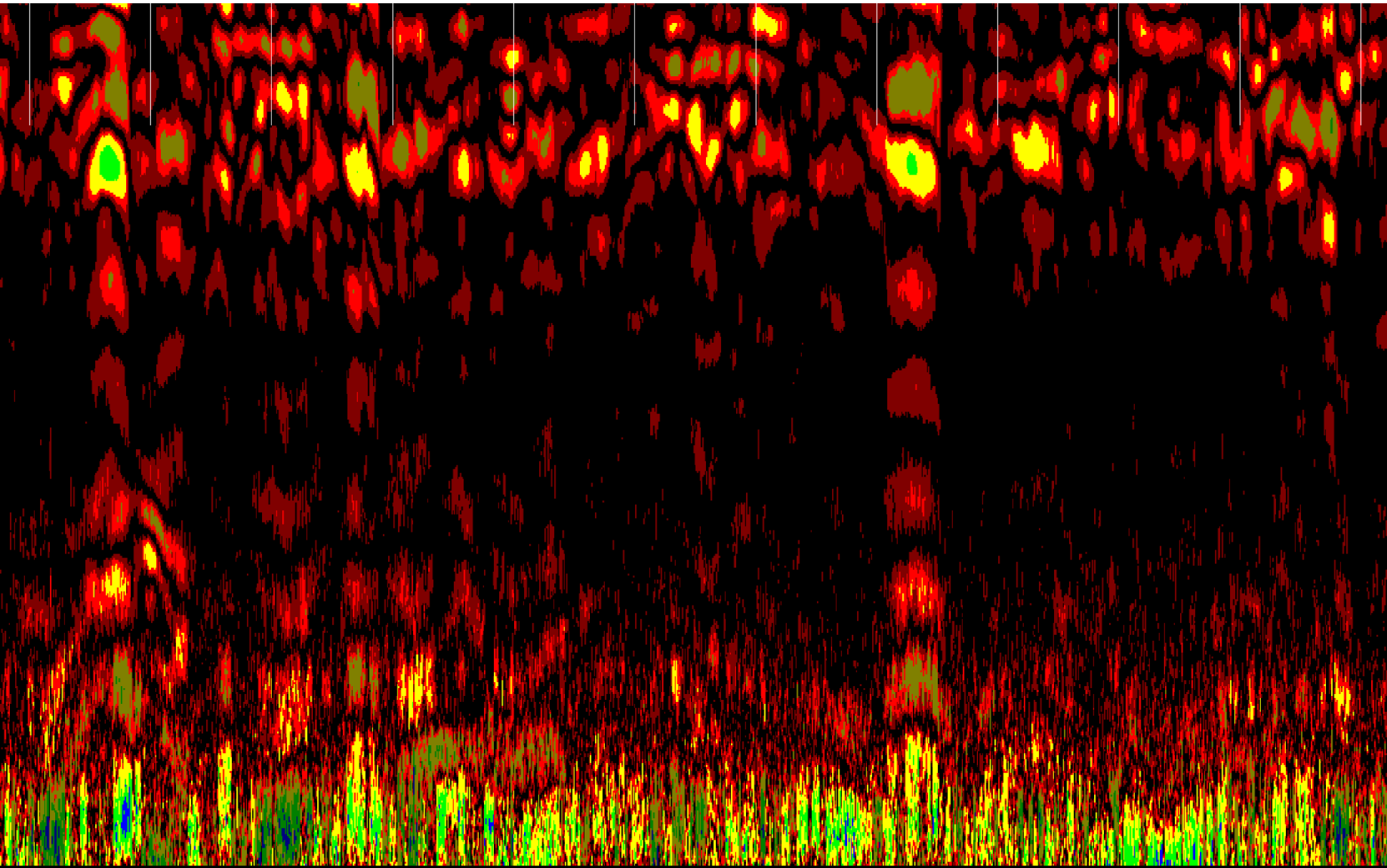


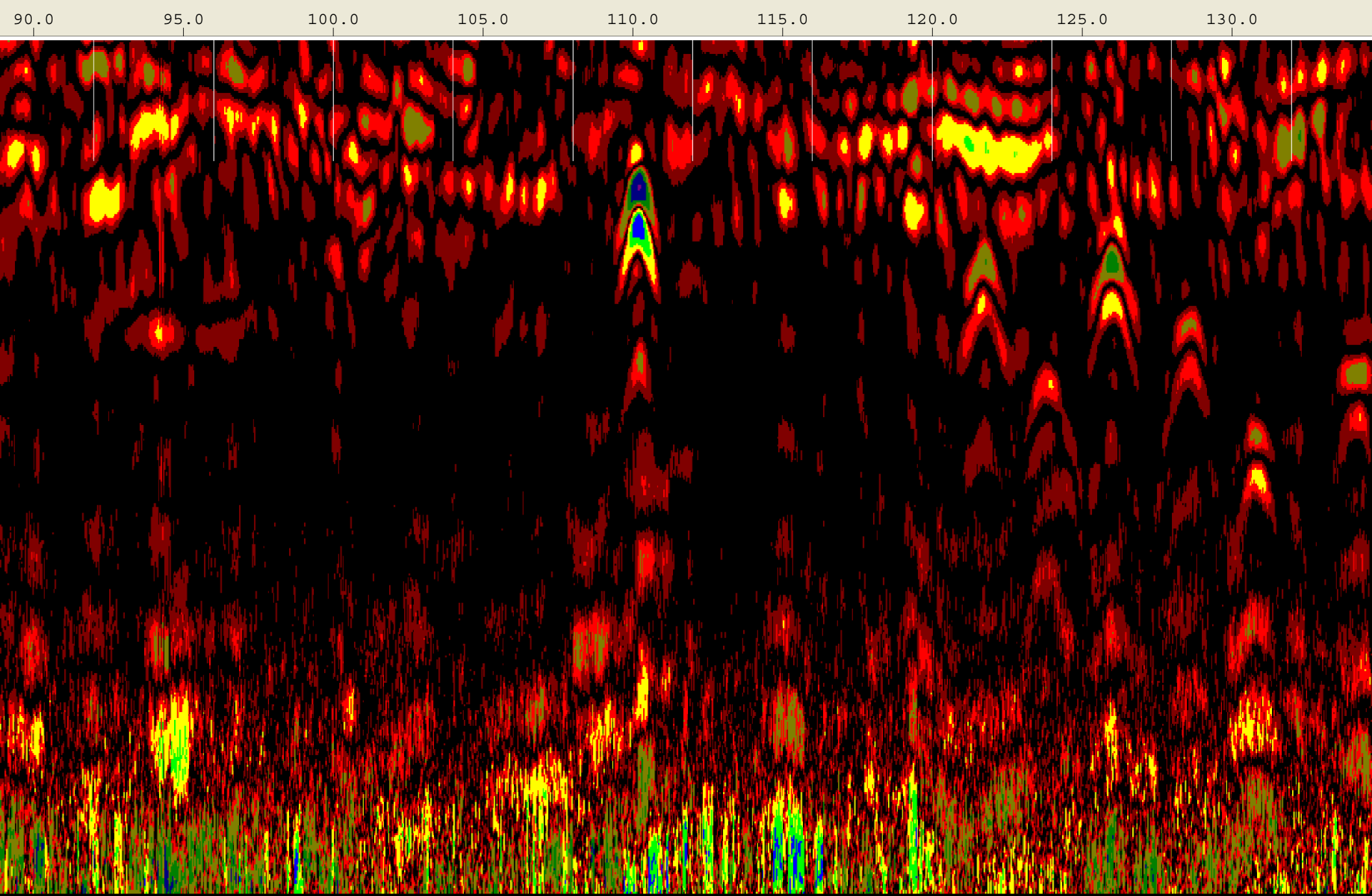
Created Jun, 17 2008, 11:44:50 Modified Jun, 17 2008, 11:56:32
Channel(s) 1 Samples/Scan 512 Bits/Sample 16
Scans/Second 100 Scans/Meter 78.7402 Meters/Mark 1.2192
Diel Constant 15.637

CHANNEL 1 400MHz
Position 3.42 nS Range 24 nS
Position Correction 1.04 nS
Vert IIR LP N =1 F =800 MHz
Vert IIR HP N =1 F =100 MHz
Range Gain (dB) 8.0 8.0 38.0
Position Correction 3.42 nS
Horz Boxcar Bkgr N=1023

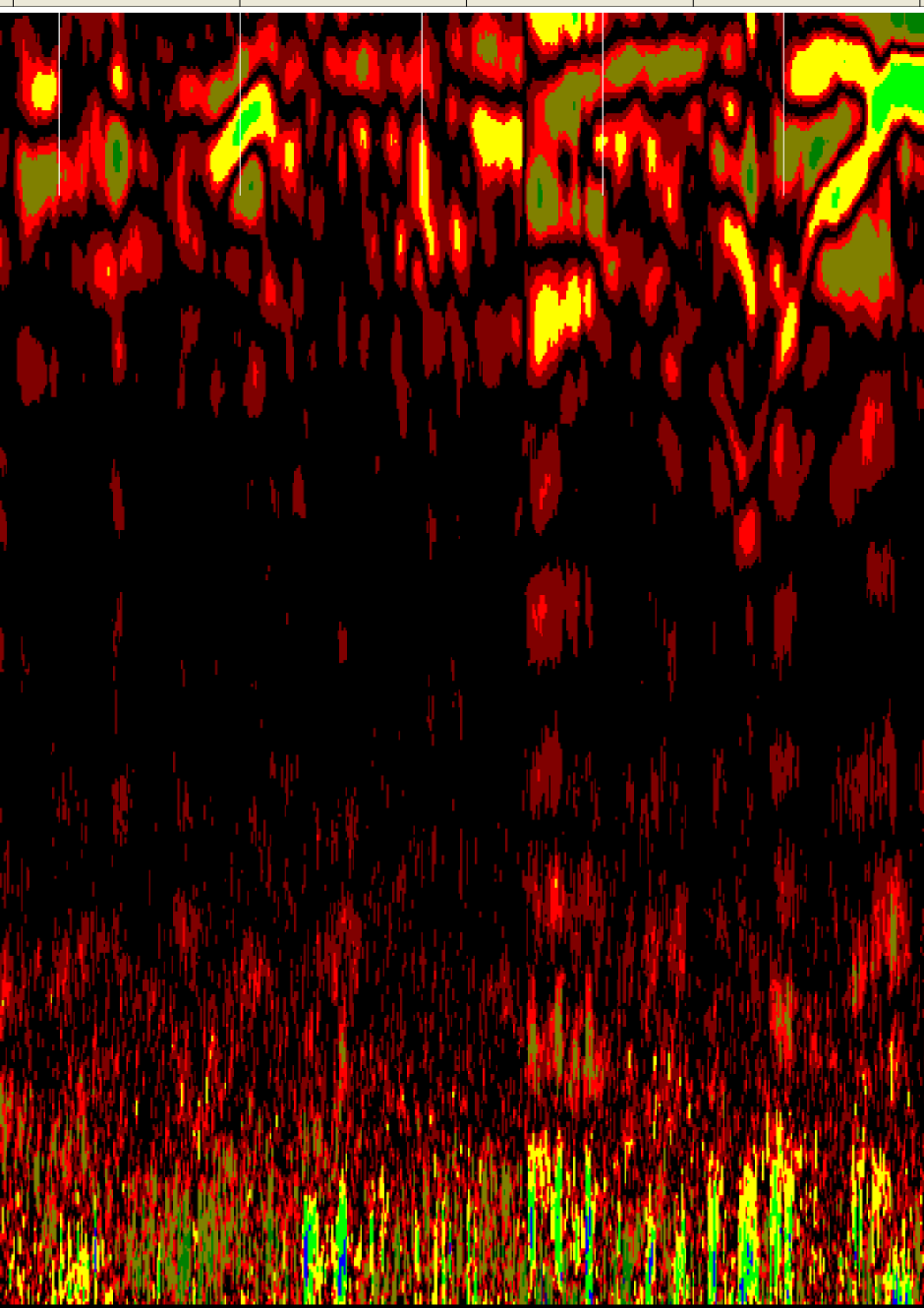


45.0 50.0 55.0 60.0 65.0 70.0 75.0 80.0 85.0



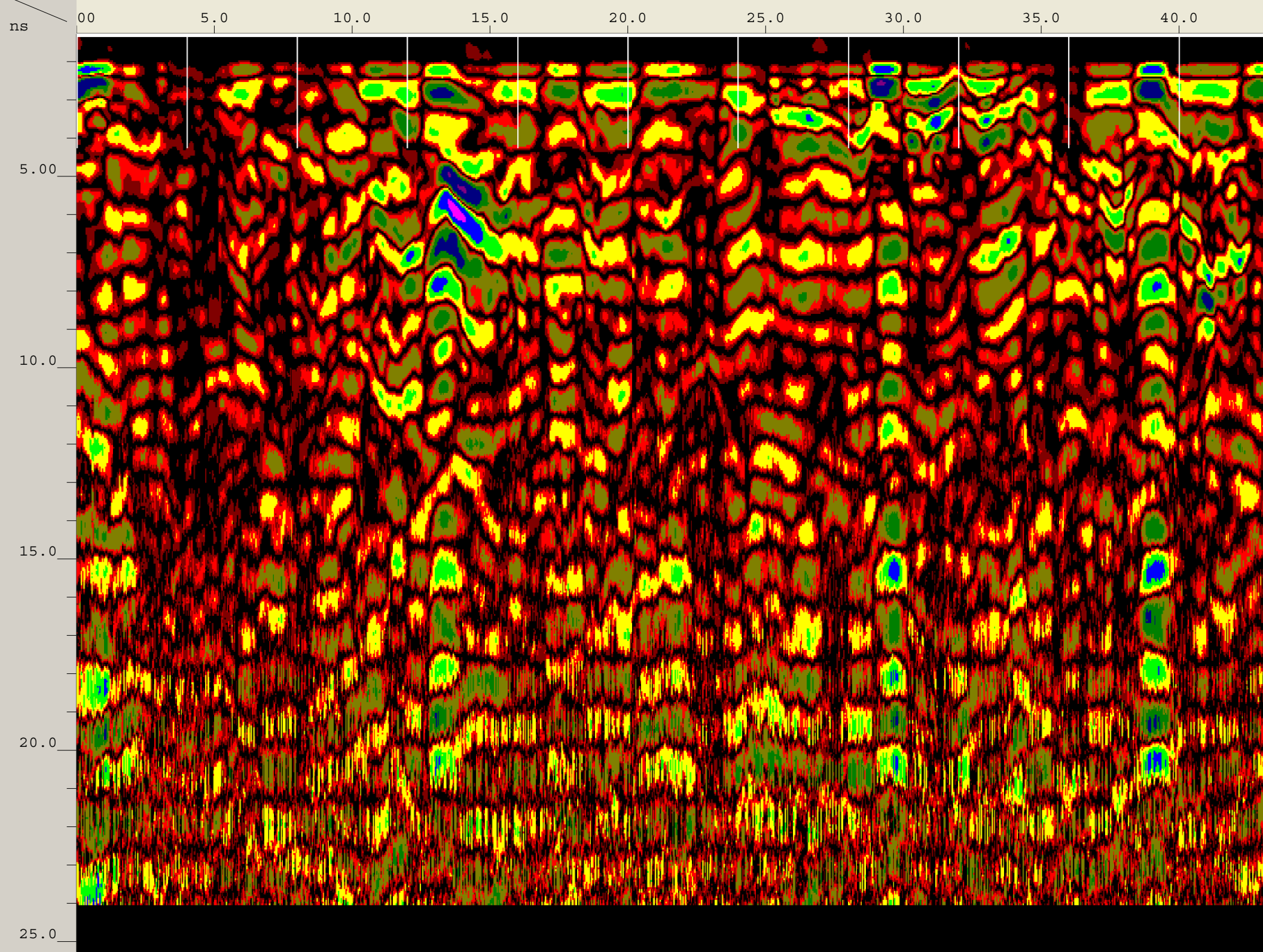


135.0 140.0 145.0 150.0 155.0

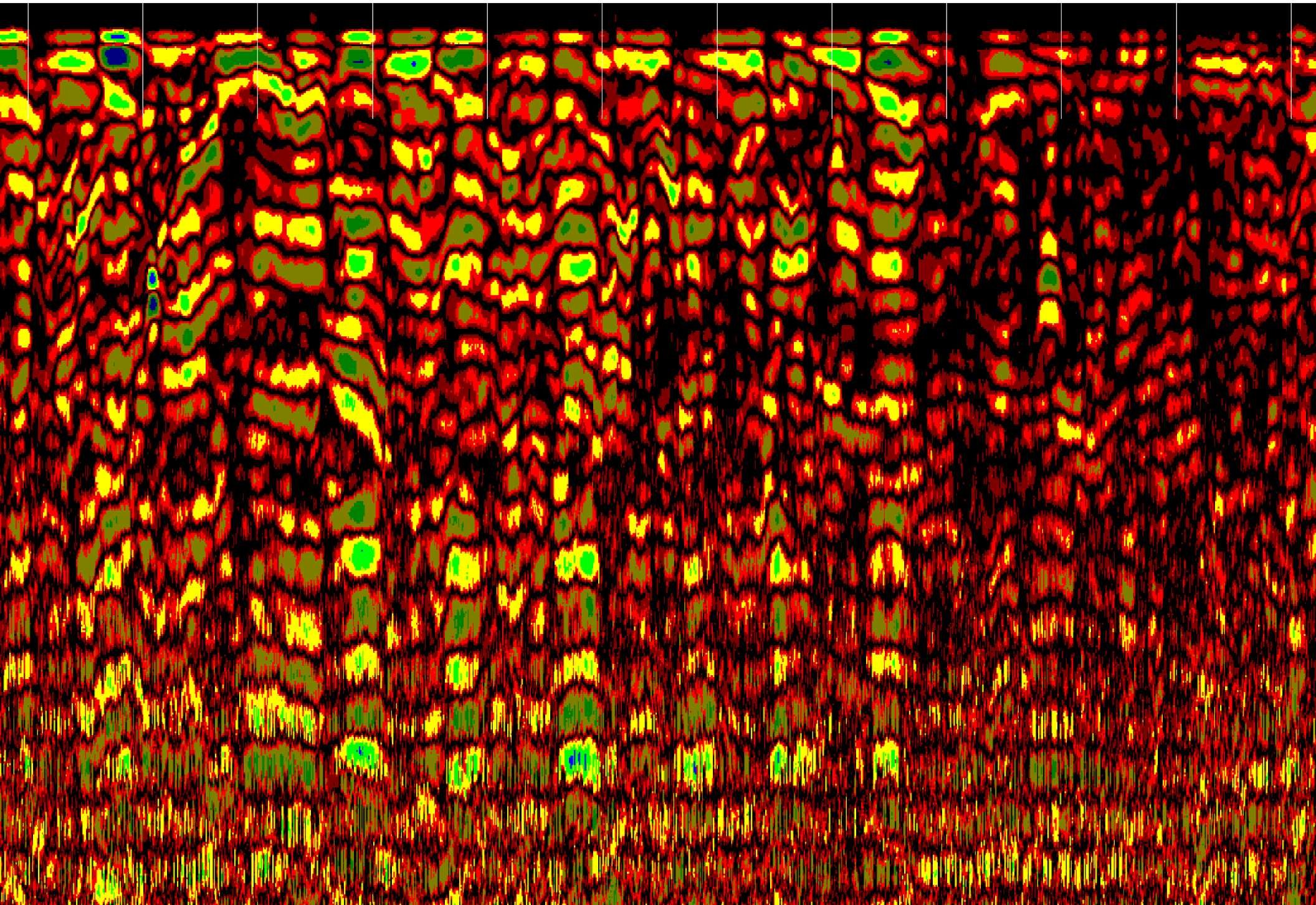


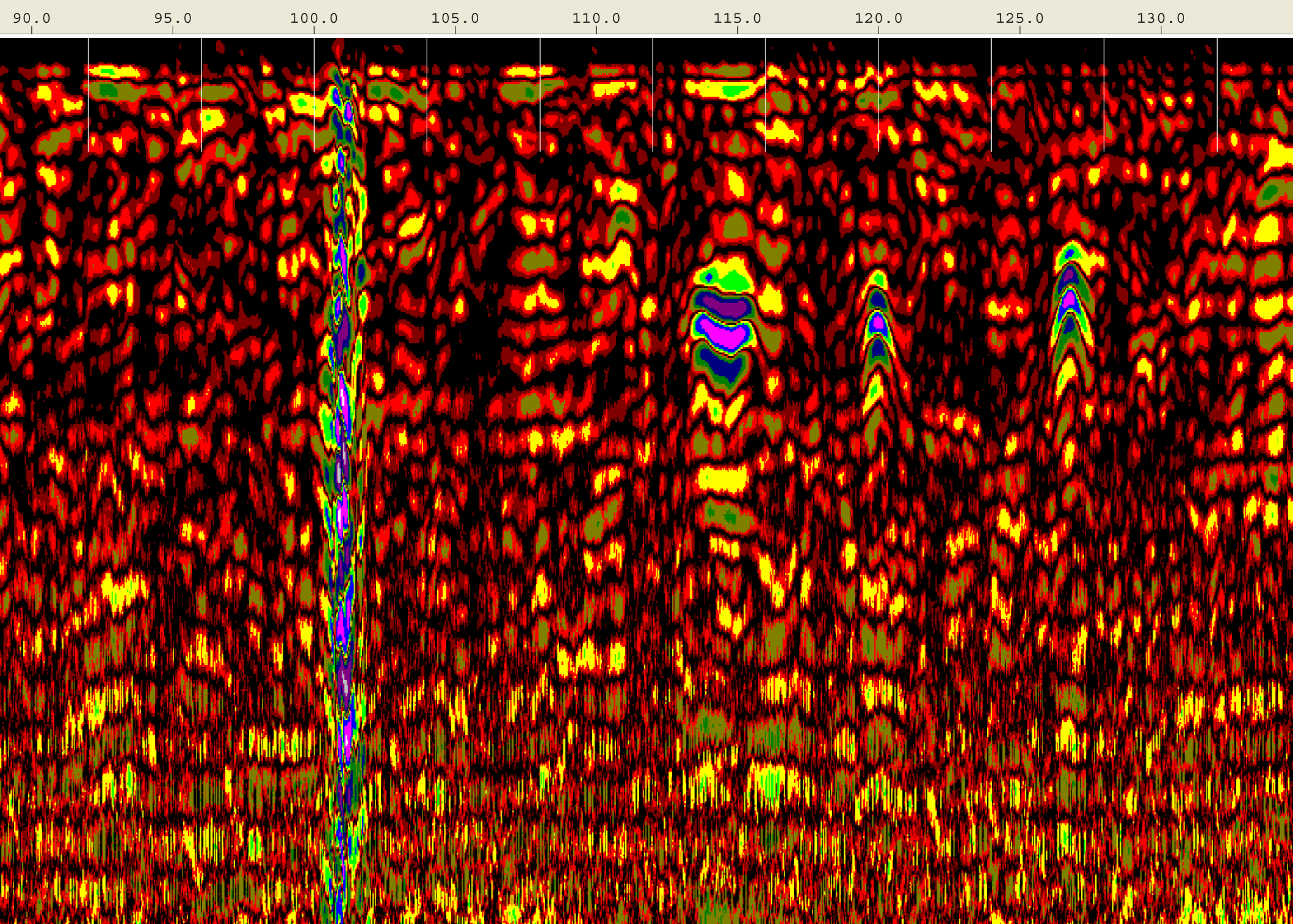
Created Jun, 17 2008, 12:37:24 Modified Jun, 17 2008, 12:39:46
Channel(s) 1 Samples/Scan 512 Bits/Sample 16
Scans/Second 100 Scans/Meter 78.7402 Meters/Mark 1.2192
Diel Constant 10.0038

CHANNEL 1 900MHz
Position 1.27 nS Range 24 nS
Range Gain (dB) 5.0 34.0 43.0
Position Correction 1.04 nS
Vert IIR LP N =1 F =2500 MHz
Vert IIR HP N =1 F =225 MHz
Position Correction 1.27 nS
Horz Boxcar Bkgr N=1023

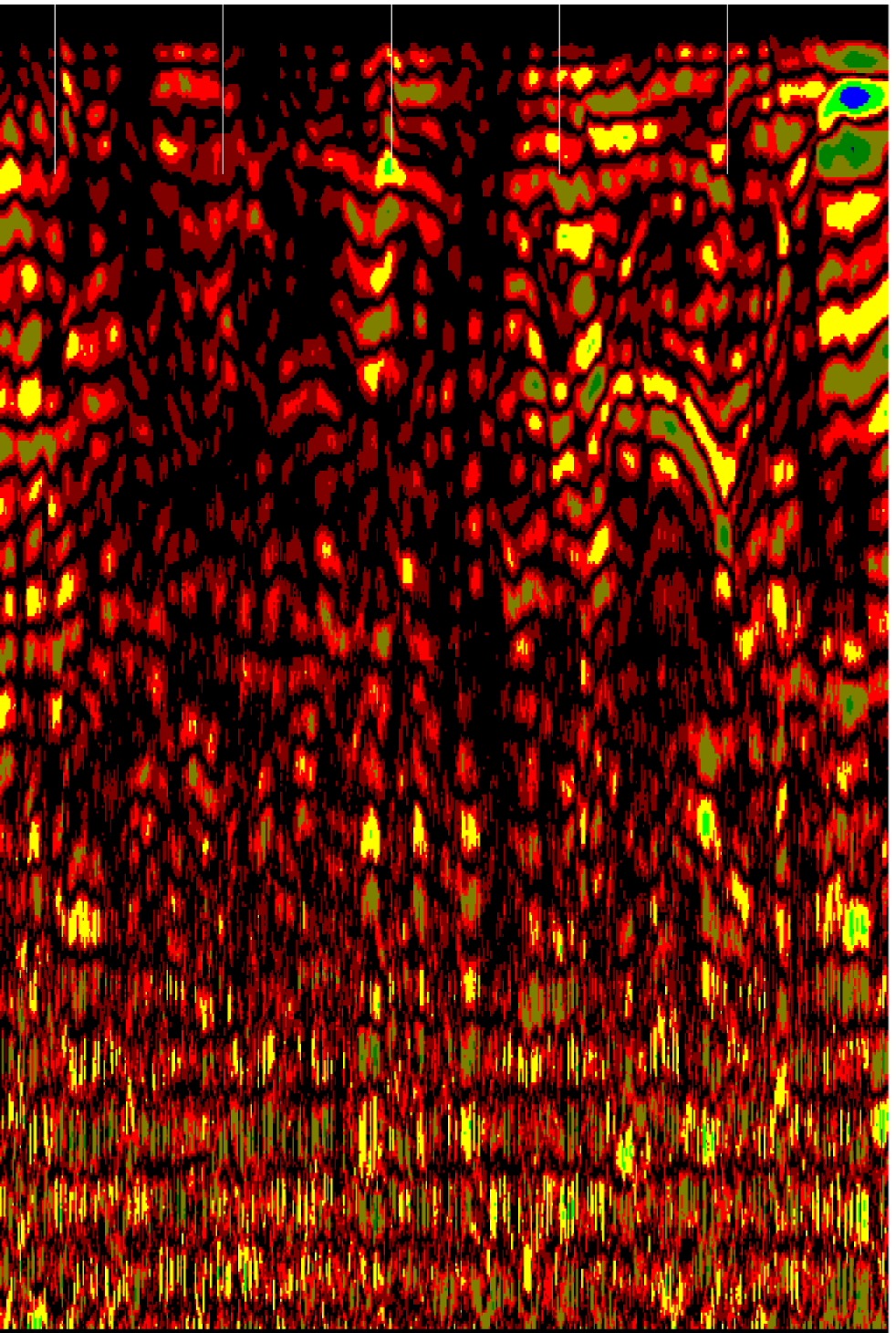


45.0 50.0 55.0 60.0 65.0 70.0 75.0 80.0 85.0



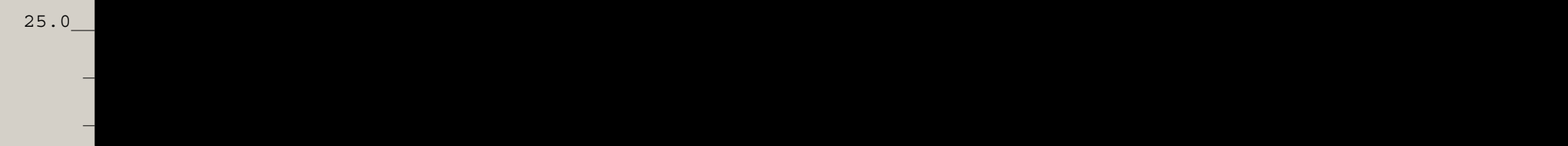
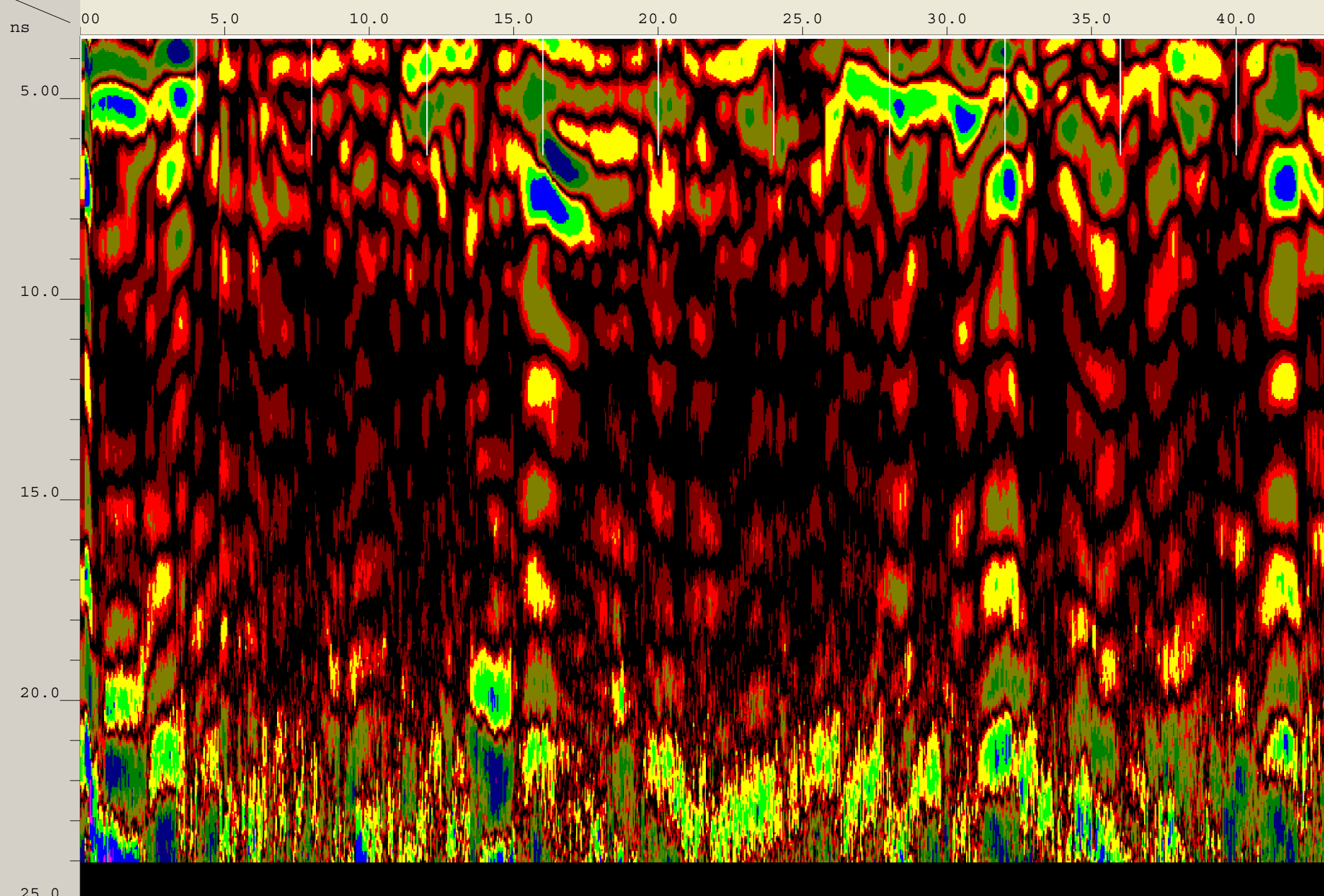


135.0 140.0 145.0 150.0 155.0

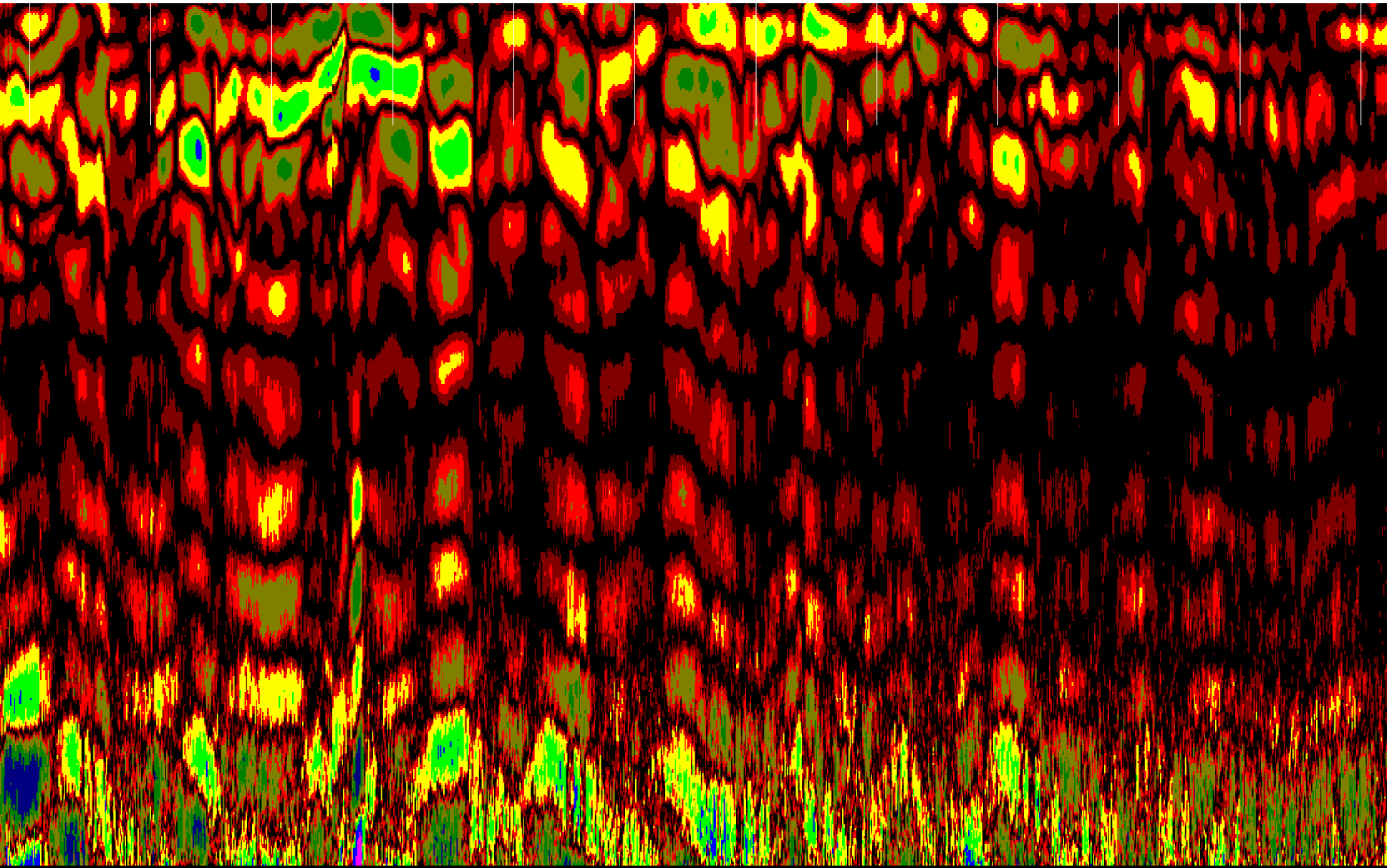


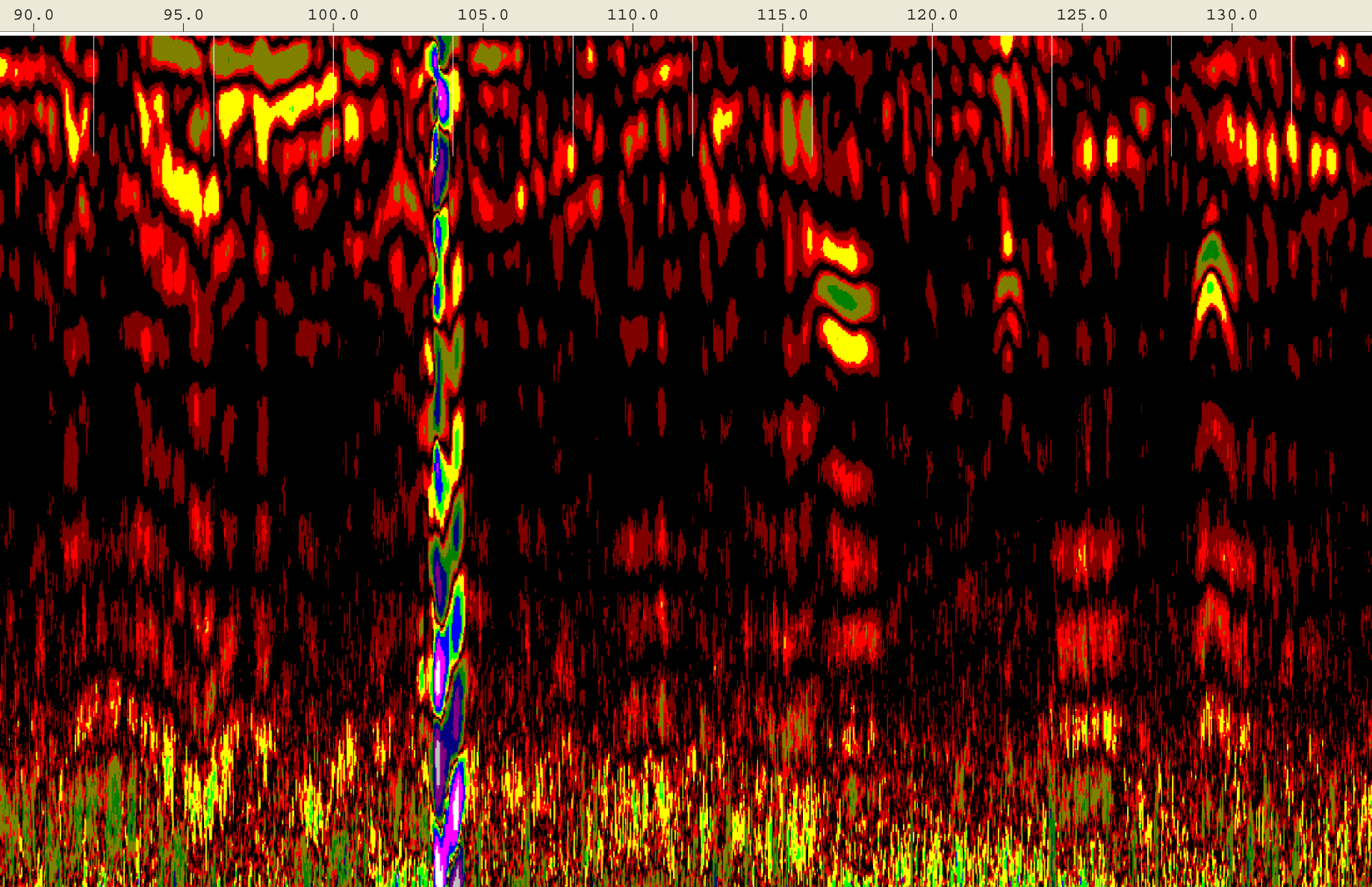
Created Jun, 17 2008, 12:09:50 Modified Jun, 17 2008, 12:13:56
Channel(s) 1 Samples/Scan 512 Bits/Sample 16
Scans/Second 100 Scans/Meter 78.7402 Meters/Mark 1.2192
Diel Constant 19.2341

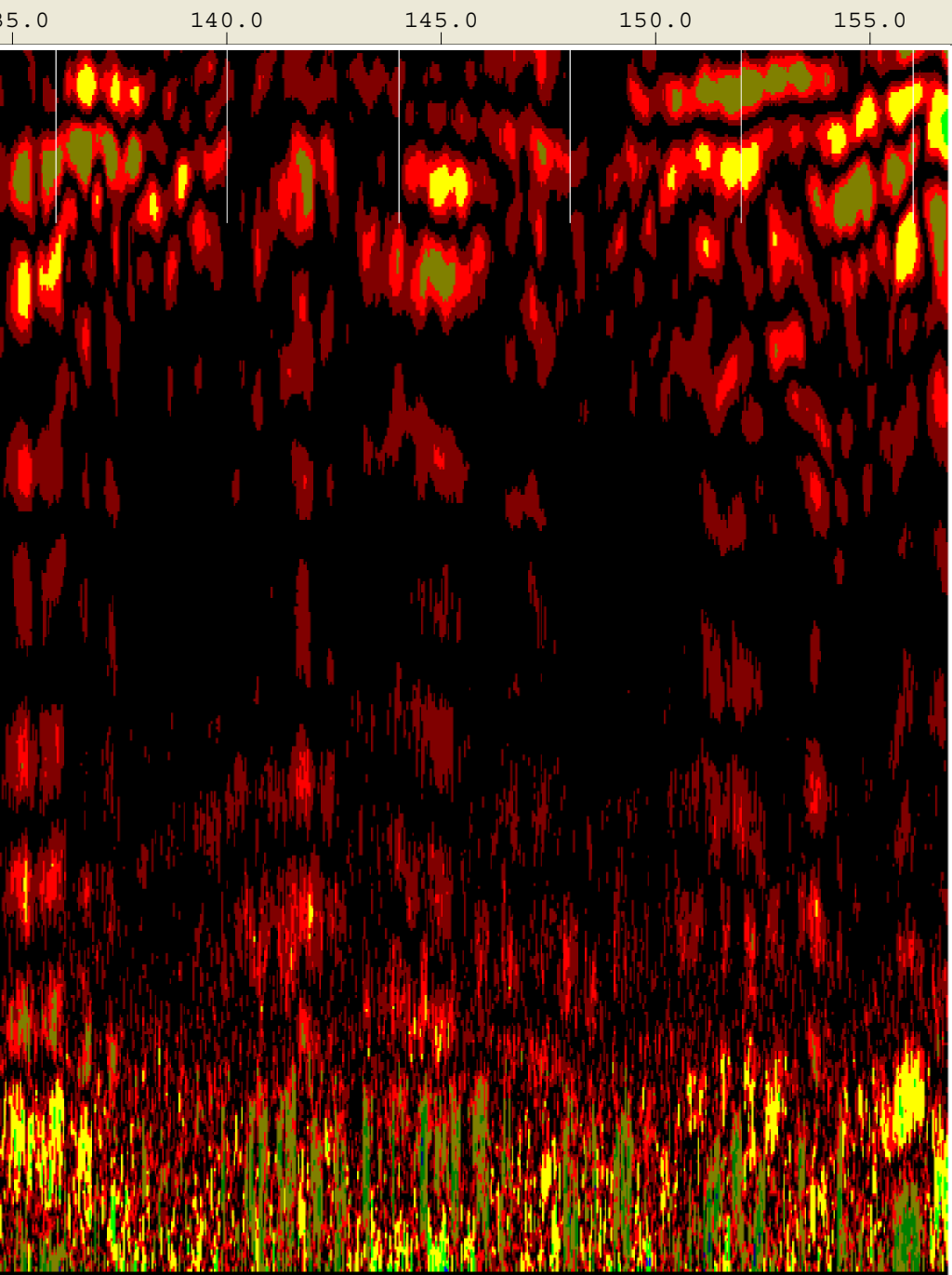
CHANNEL 1 400MHz
Position 3.42 nS Range 24 nS
Position Correction 1.04 nS
Vert IIR LP N =1 F =800 MHz
Vert IIR HP N =1 F =100 MHz
Range Gain (dB) 8.0 8.0 38.0
Position Correction 3.42 nS
Horz Boxcar Bkgr N=1023



45.0 50.0 55.0 60.0 65.0 70.0 75.0 80.0 85.0

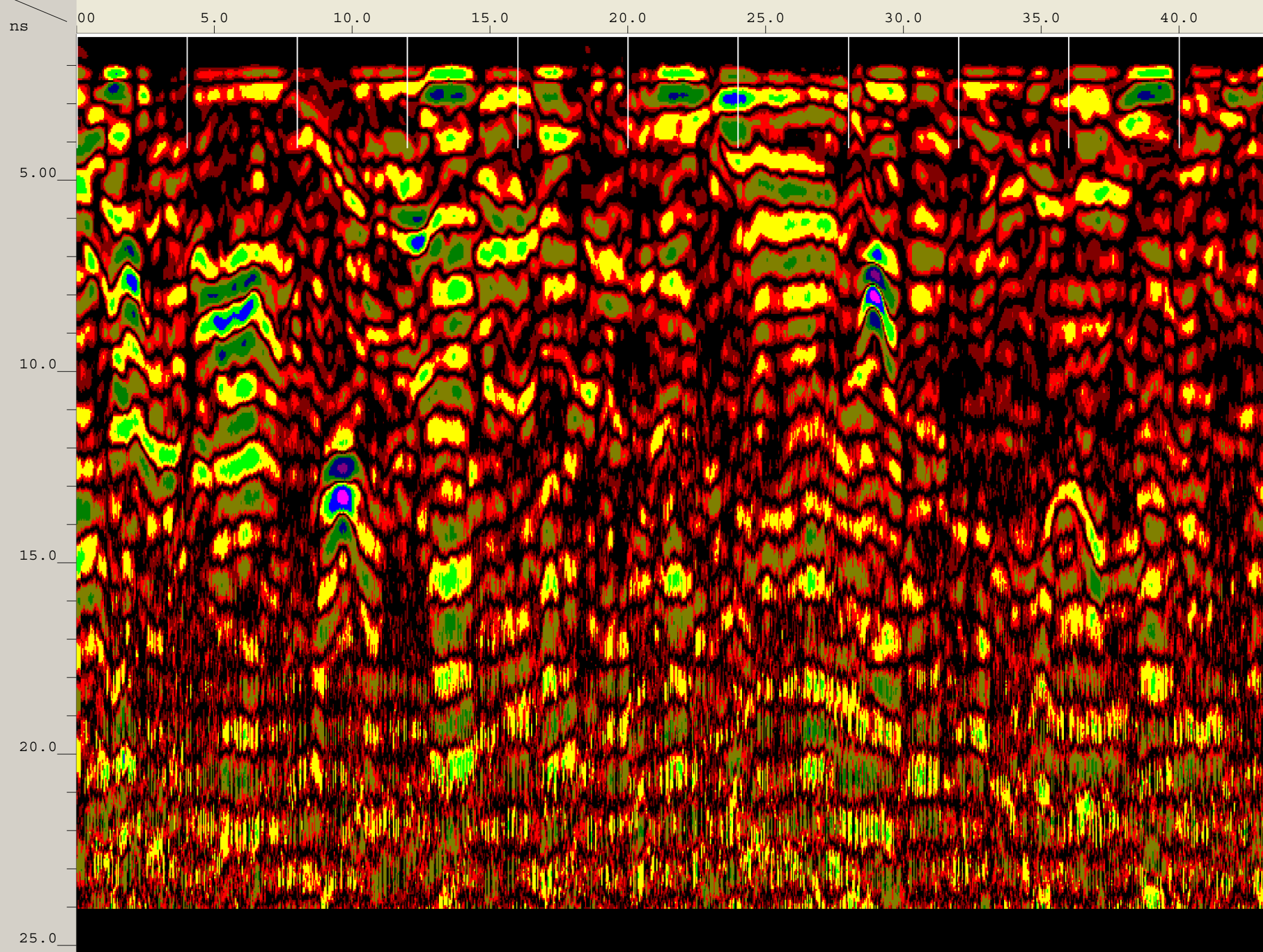


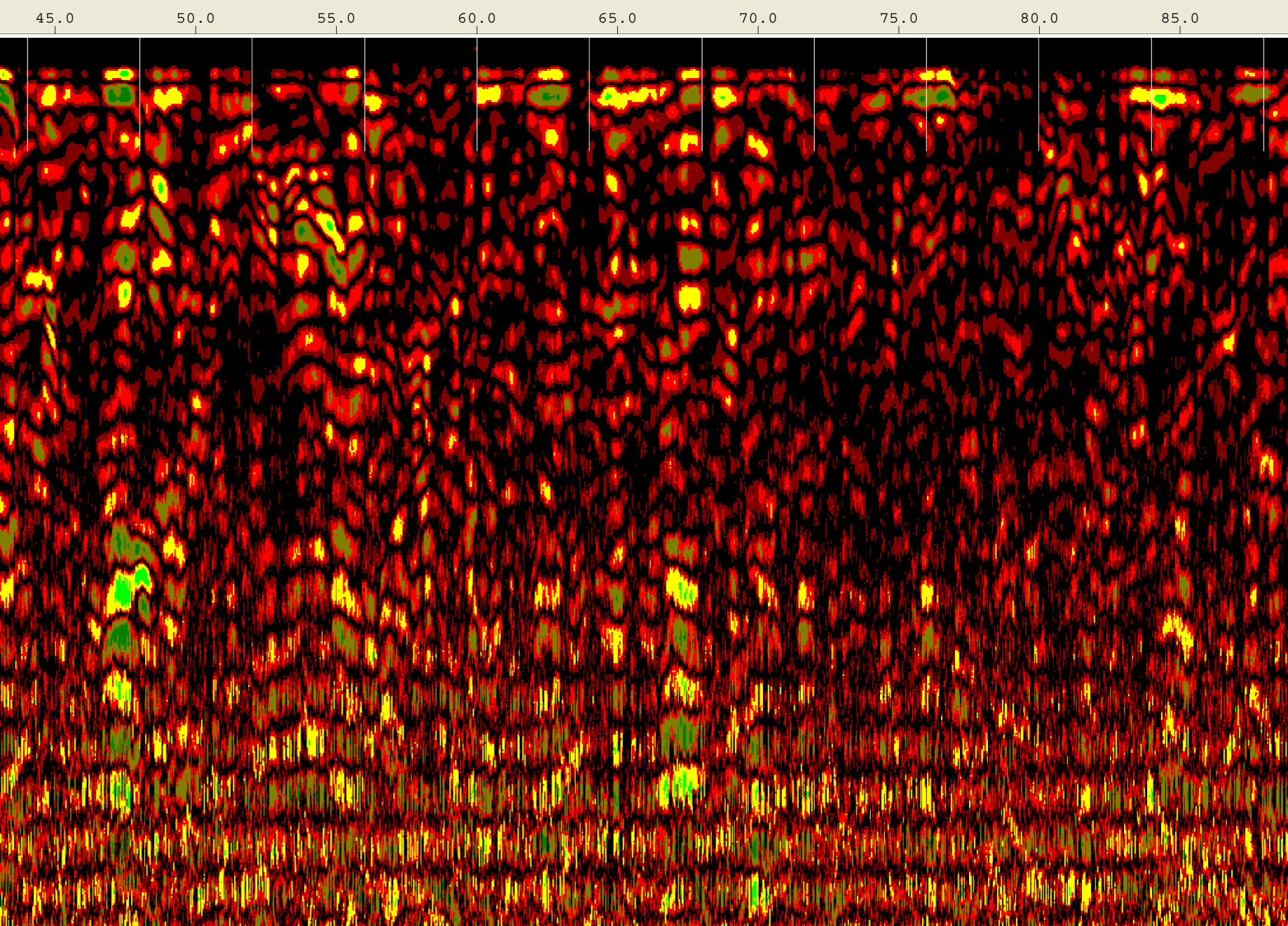


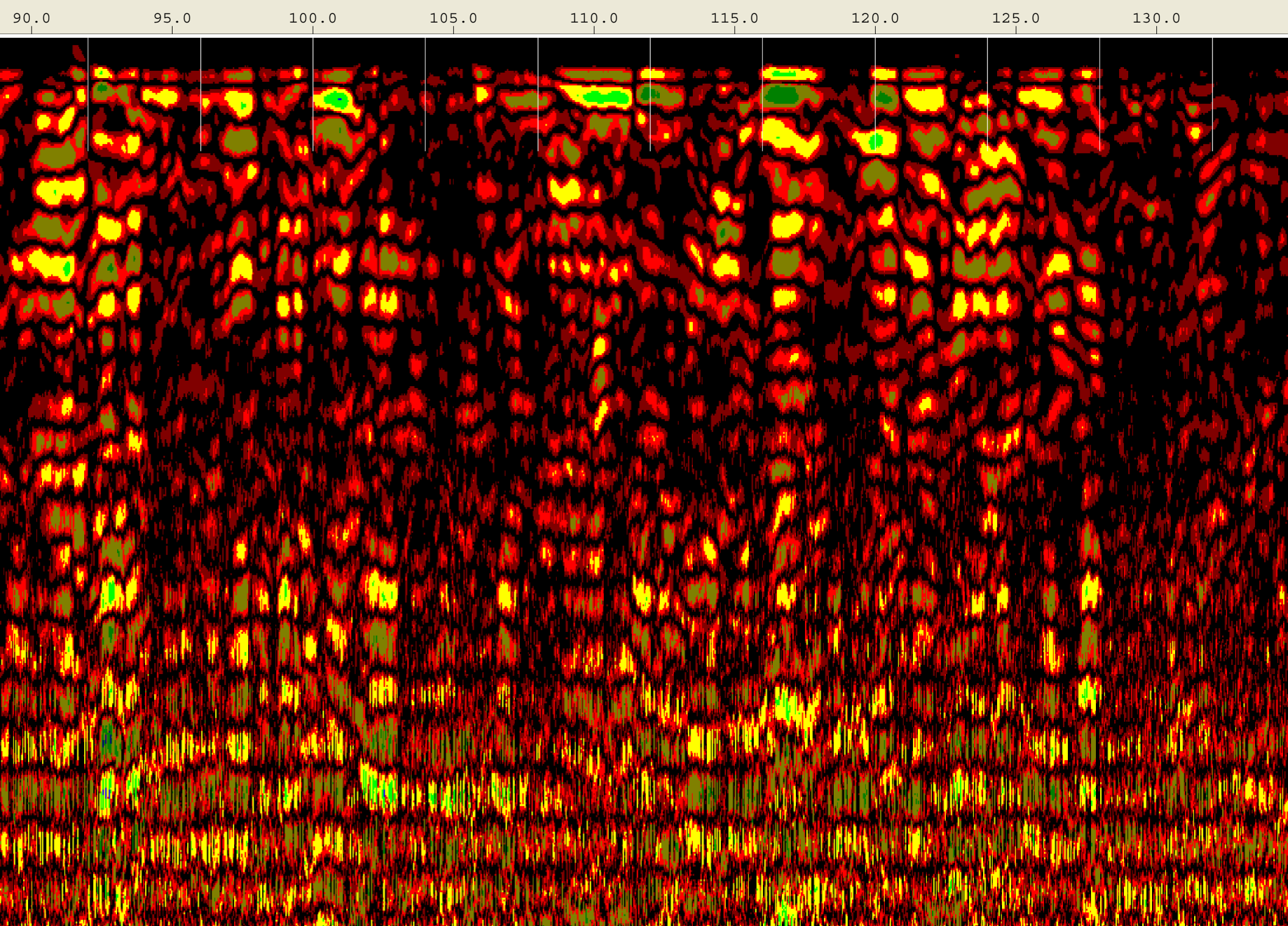


Created Jun, 17 2008, 12:33:16 Modified Jun, 17 2008, 12:37:18
Channel(s) 1 Samples/Scan 512 Bits/Sample 16
Scans/Second 100 Scans/Meter 78.7402 Meters/Mark 1.2192
Diel Constant 10.7852

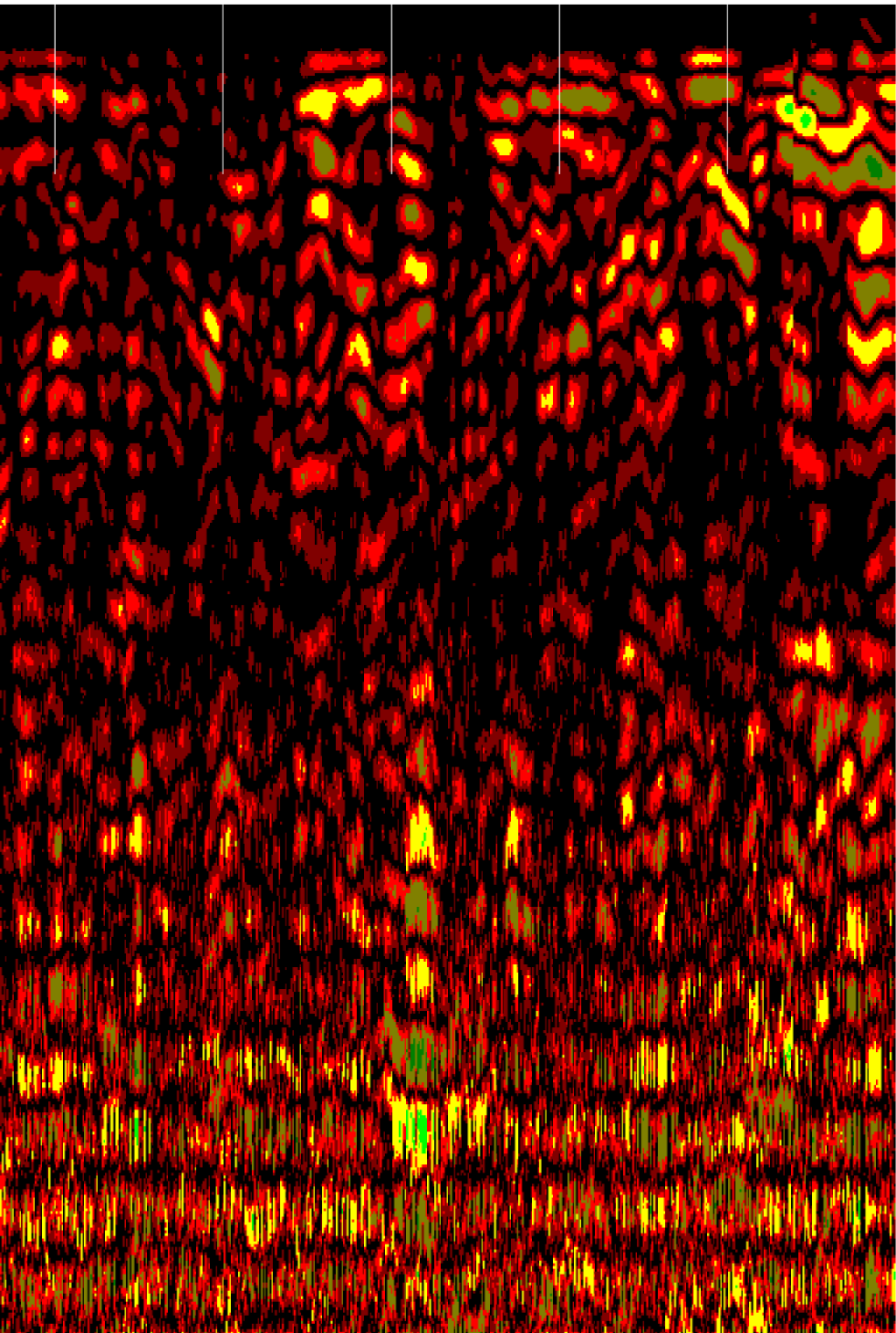
CHANNEL 1 900MHz
Position 1.17 nS Range 24 nS
Range Gain (dB) 5.0 34.0 43.0
Position Correction 1.04 nS
Vert IIR LP N =1 F =2500 MHz
Vert IIR HP N =1 F =225 MHz
Position Correction 1.17 nS
Horz Boxcar Bkgr N=1023



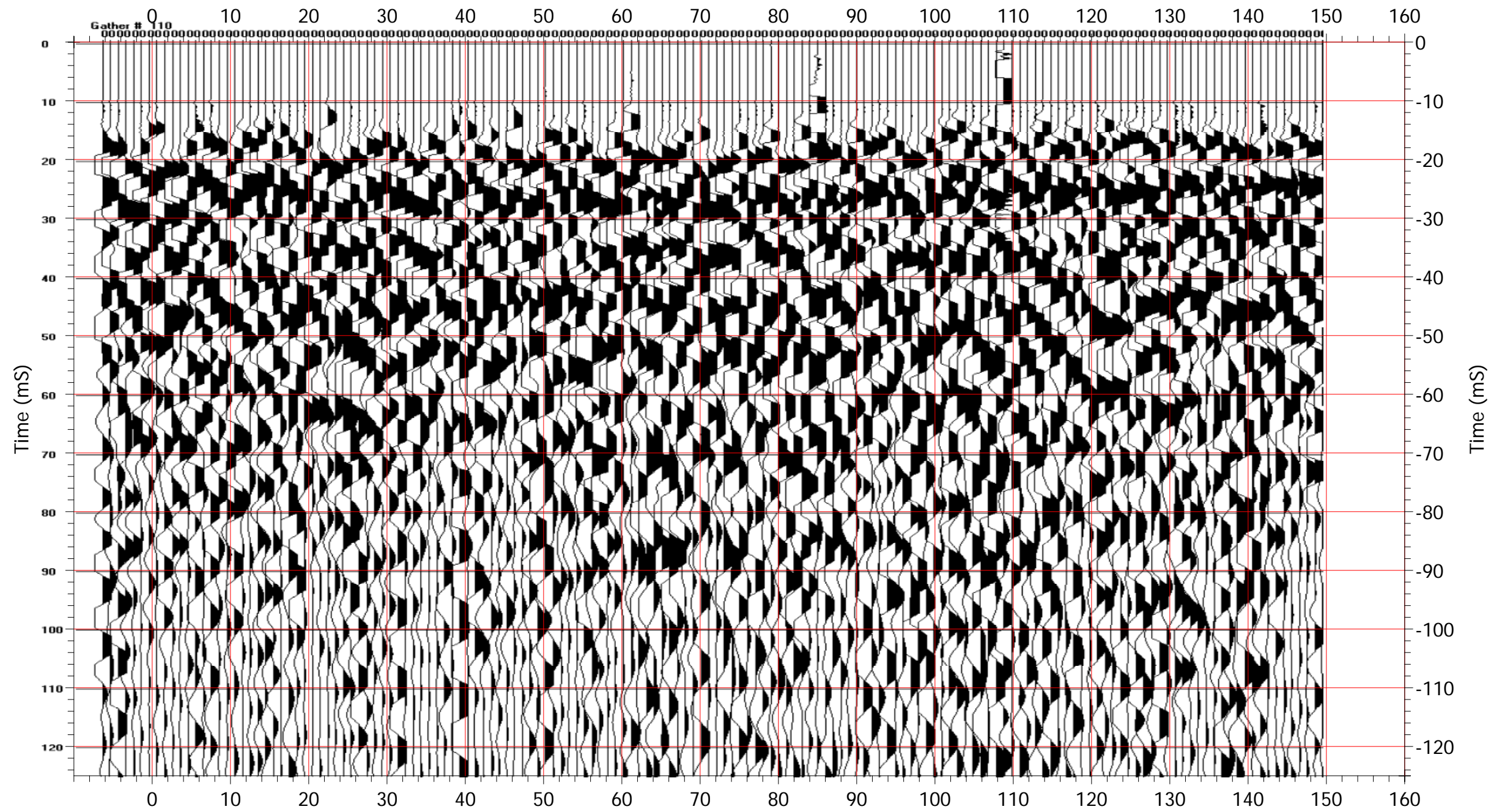




135.0 140.0 145.0 150.0 155.0



Appendix D – Poamoho Common Offset Data



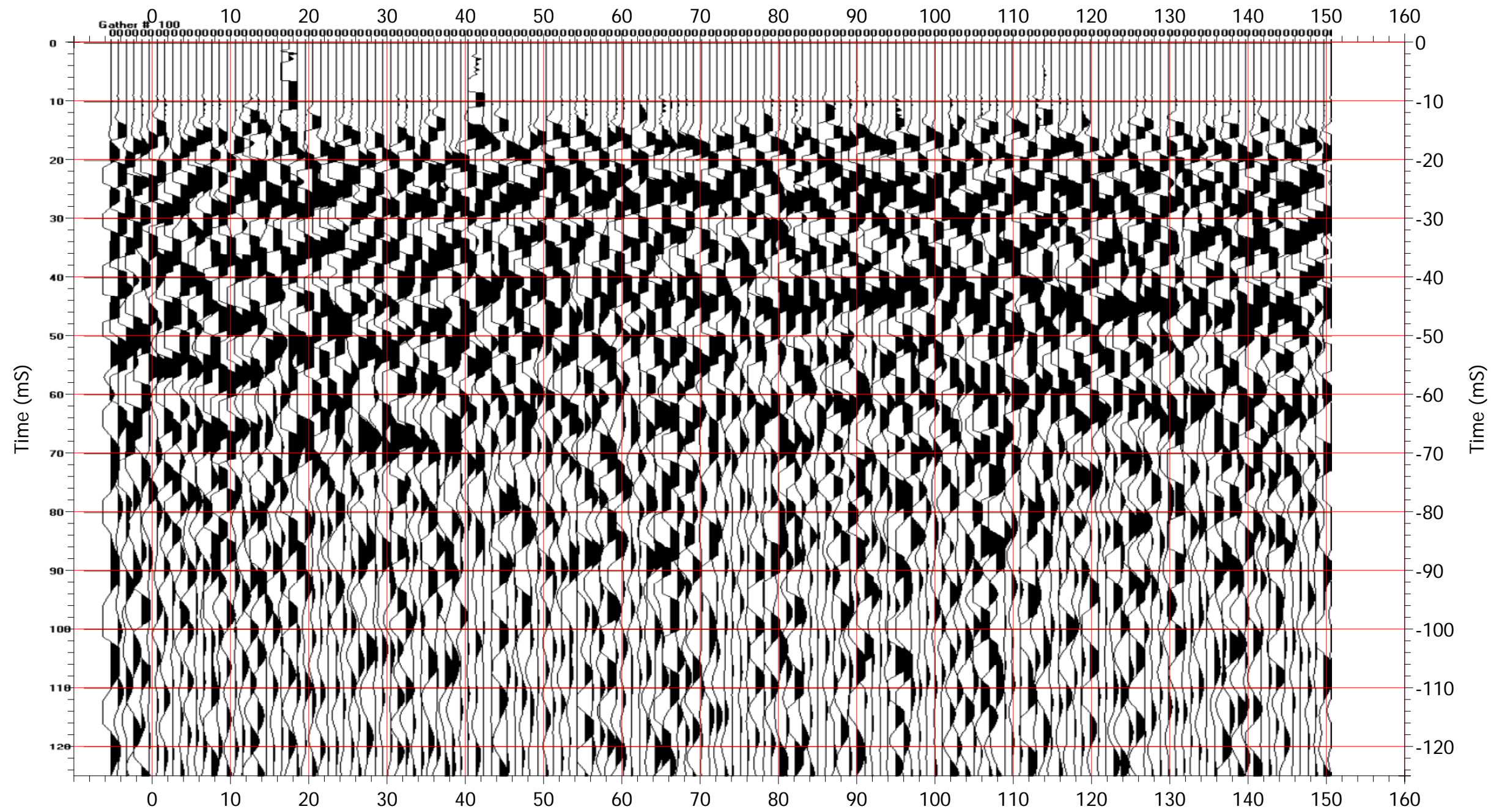
PROJECT: University of Hawaii, Manoa Poamoho, HI	
REVISIONS	DATE

 CONSULTING ENGINEERS 10105 ALLENTOWN BLVD. GRANTVILLE, PA. 17028 PHONE: (717) 869-0937 FAX: (717) 869-0938	DRAWING TITLE: Poamoho Common Offset Sta. 11

PROJECT NO.:	208044.01
DRAWN BY:	R.A.H.
CHECKED BY:	B.B.
SCALE:	AS SHOWN
DATE:	5 Aug 2008

SHEET NO.:

1



PROJECT: University of Hawaii, Manoa	
Poamoho, HI	
REVISIONS	DATE

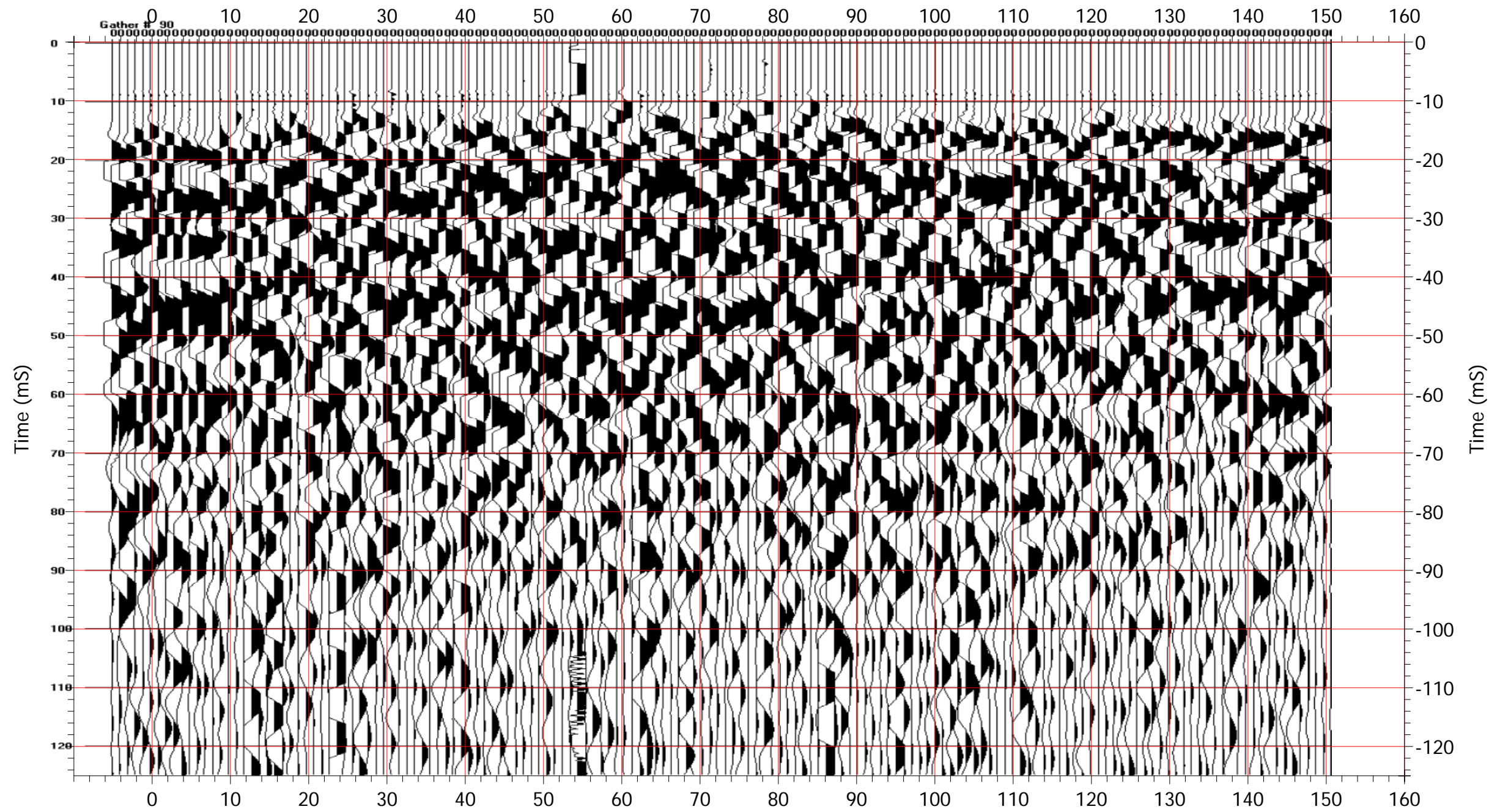
DAWOOD
CONSULTING ENGINEERS
10105 ALLENTOWN BLVD. GRANTVILLE, PA. 17028
PHONE: (717) 869-0937 FAX: (717) 869-0938

DRAWING TITLE:
Poamoho Common Offset Sta. 10

PROJECT NO.:	208044.01
DRAWN BY:	R.A.H.
CHECKED BY:	B.B.
SCALE:	AS SHOWN
DATE:	5 Aug 2008

SHEET NO.:

1



PROJECT: University of Hawaii, Manoa	
Poamoho, HI	
REVISIONS	DATE

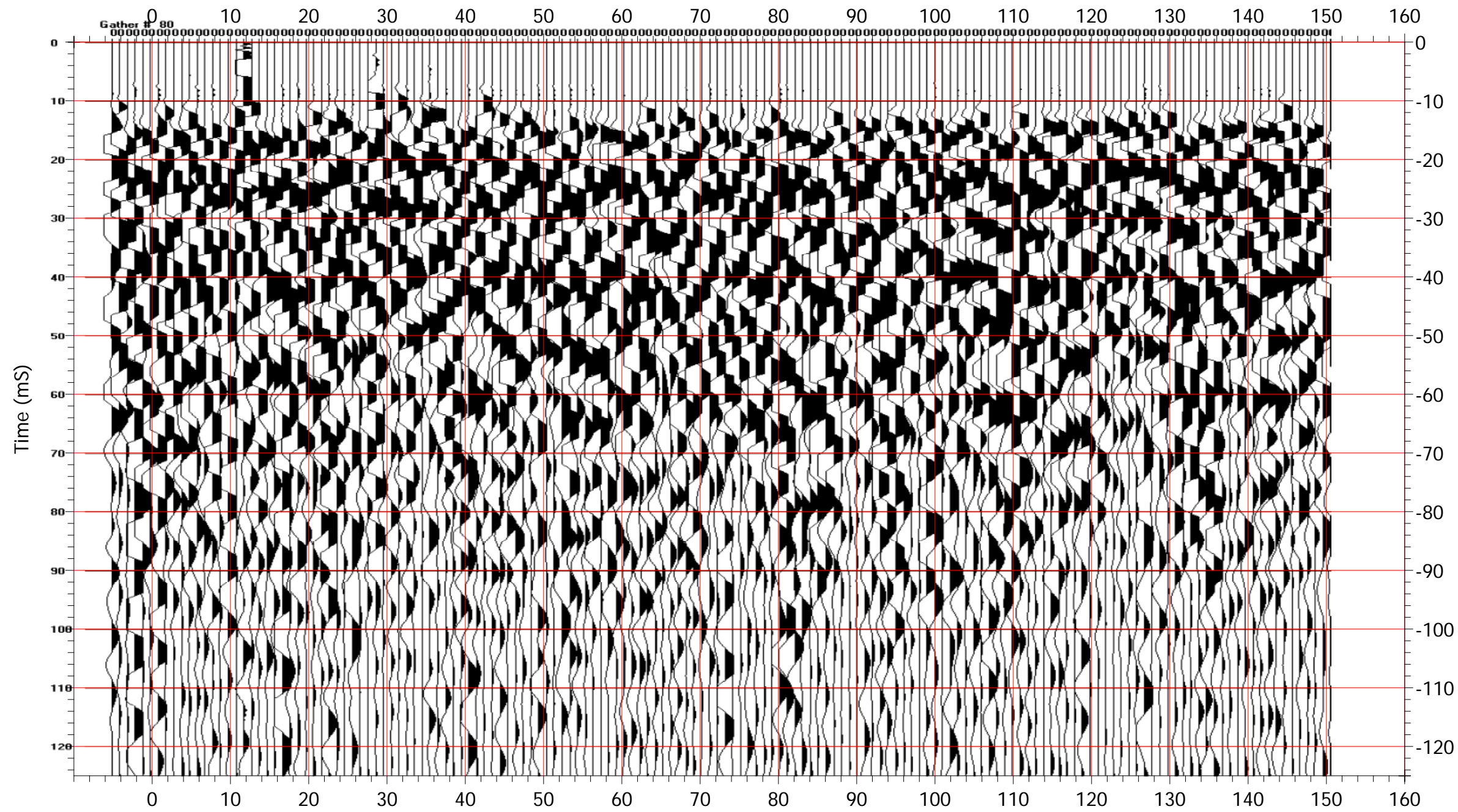
DAWOOD
 CONSULTING ENGINEERS
 10105 ALLENTOWN BLVD. GRANTVILLE, PA. 17028
 PHONE: (717) 869-0937 FAX: (717) 869-0938

DRAWING TITLE:
Poamoho Common Offset Sta. 09

PROJECT NO.:	208044.01
DRAWN BY:	R.A.H.
CHECKED BY:	B.B.
SCALE:	AS SHOWN
DATE:	5 Aug 2008

SHEET NO.:

1



PROJECT: University of Hawaii, Manoa	
Poamoho, HI	
REVISIONS	DATE

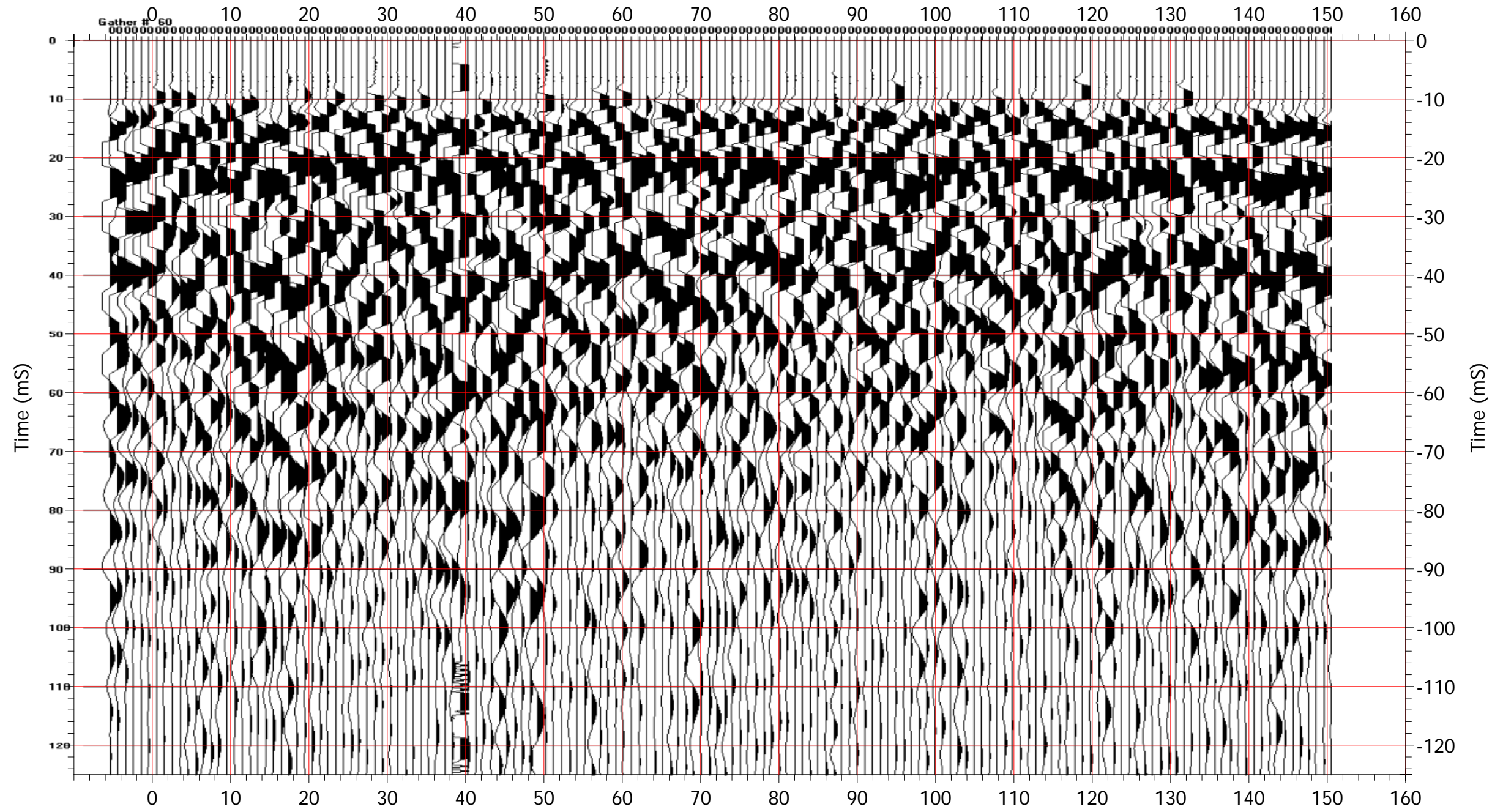
DAWOOD
CONSULTING ENGINEERS
10105 ALLENTOWN BLVD. GRANTVILLE, PA. 17028
PHONE: (717) 869-0937 FAX: (717) 869-0938

DRAWING TITLE:
Poamoho Common Offset Sta. 08

PROJECT NO.:	208044.01
DRAWN BY:	R.A.H.
CHECKED BY:	B.B.
SCALE:	AS SHOWN
DATE:	5 Aug 2008

SHEET NO.:

1



PROJECT: University of Hawaii, Manoa Poamoho, HI	
REVISIONS	DATE

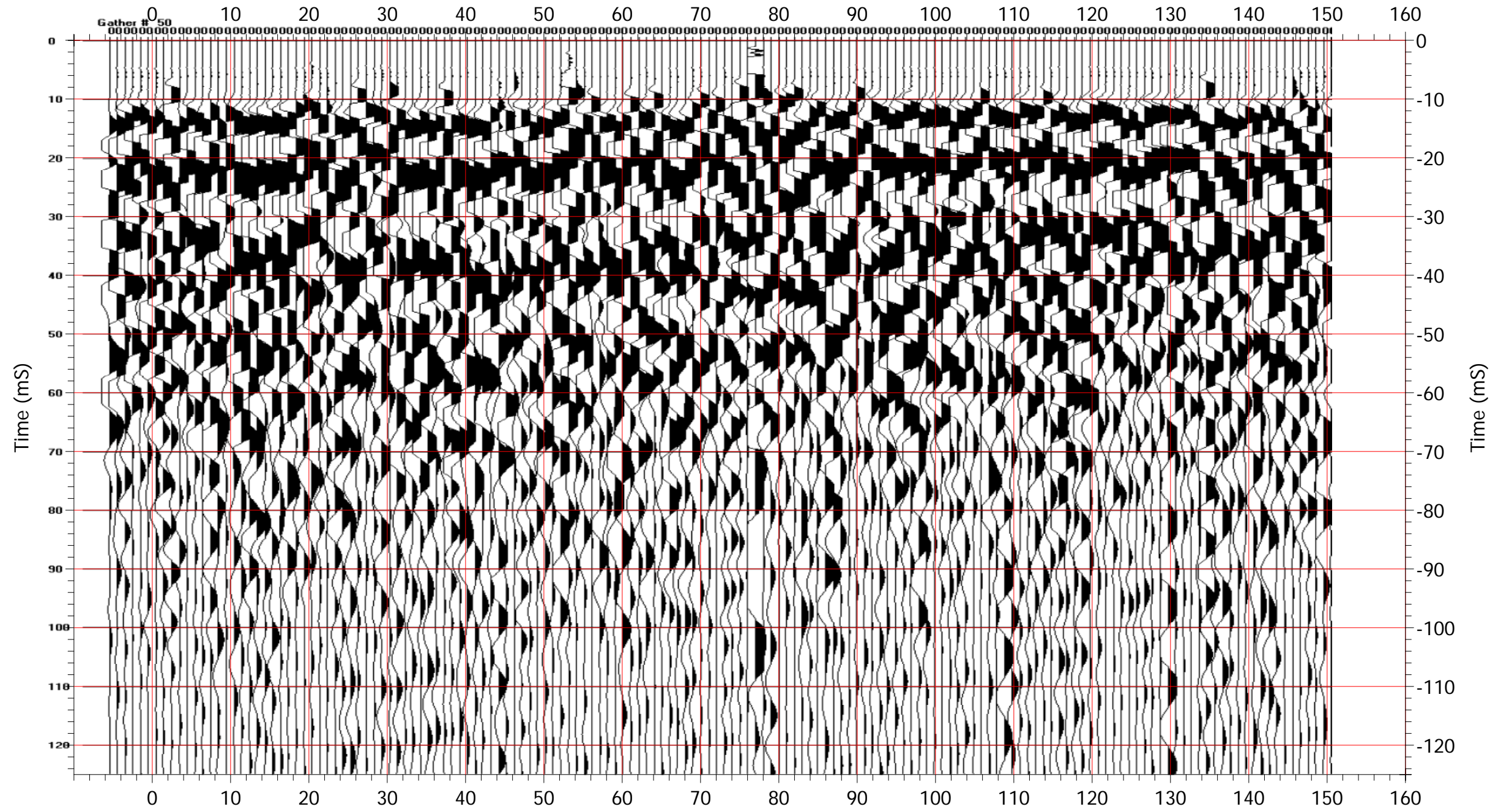
DAWOOD
CONSULTING ENGINEERS
10105 ALLENTOWN BLVD. GRANTVILLE, PA. 17028
PHONE: (717) 869-0937 FAX: (717) 869-0938

DRAWING TITLE:
Poamoho Common Offset Sta. 06

PROJECT NO.:	208044.01
DRAWN BY:	R.A.H.
CHECKED BY:	B.B.
SCALE:	AS SHOWN
DATE:	5 Aug 2008

SHEET NO.:

1



PROJECT: University of Hawaii, Manoa Poamoho, HI	
REVISIONS	DATE

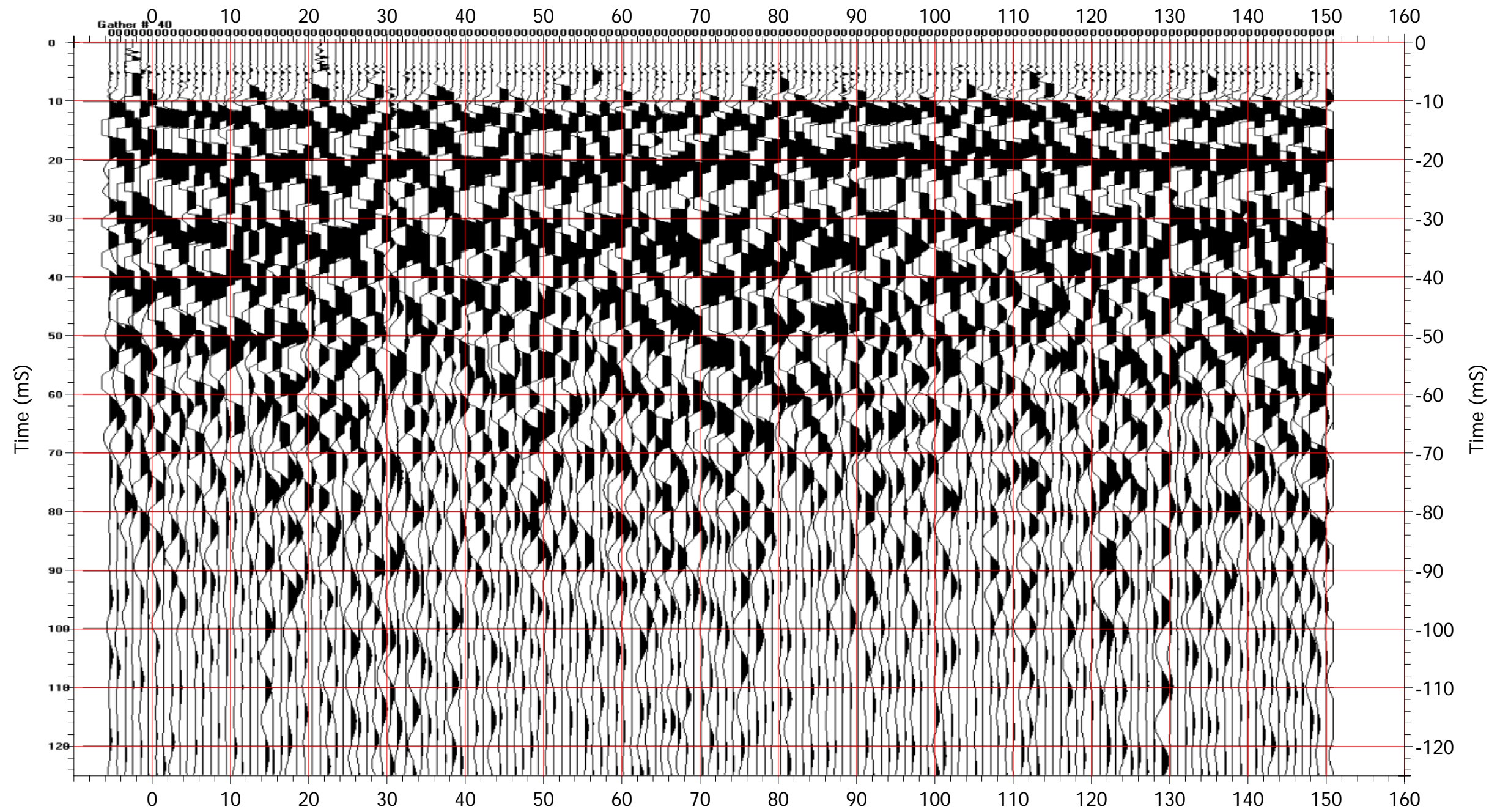
DAWOOD
CONSULTING ENGINEERS
10105 ALLENTOWN BLVD. GRANTVILLE, PA. 17028
PHONE: (717) 869-0937 FAX: (717) 869-0938

DRAWING TITLE:
Poamoho Common Offset Sta. 05

PROJECT NO.:	208044.01
DRAWN BY:	R.A.H.
CHECKED BY:	B.B.
SCALE:	AS SHOWN
DATE:	5 Aug 2008

SHEET NO.:

1



PROJECT: University of Hawaii, Manoa Poamoho, HI	
REVISIONS	DATE

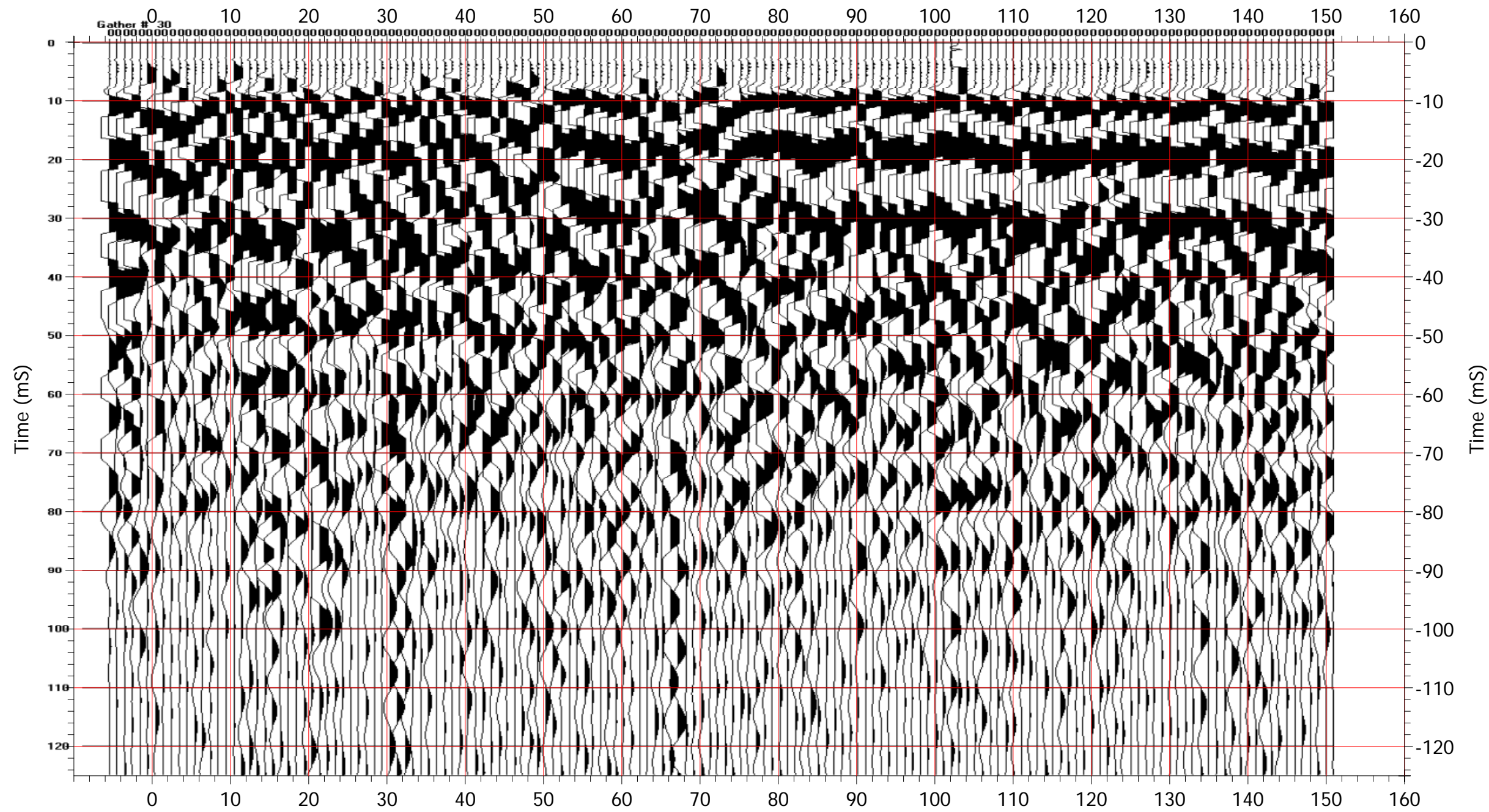
DAWOOD
CONSULTING ENGINEERS
10105 ALLENTOWN BLVD. GRANTVILLE, PA. 17028
PHONE: (717) 869-0937 FAX: (717) 869-0938

DRAWING TITLE:
Poamoho Common Offset Sta. 04

PROJECT NO.:	208044.01
DRAWN BY:	R.A.H.
CHECKED BY:	B.B.
SCALE:	AS SHOWN
DATE:	5 Aug 2008

SHEET NO.:

1



PROJECT: University of Hawaii, Manoa	
Poamoho, HI	
REVISIONS	DATE

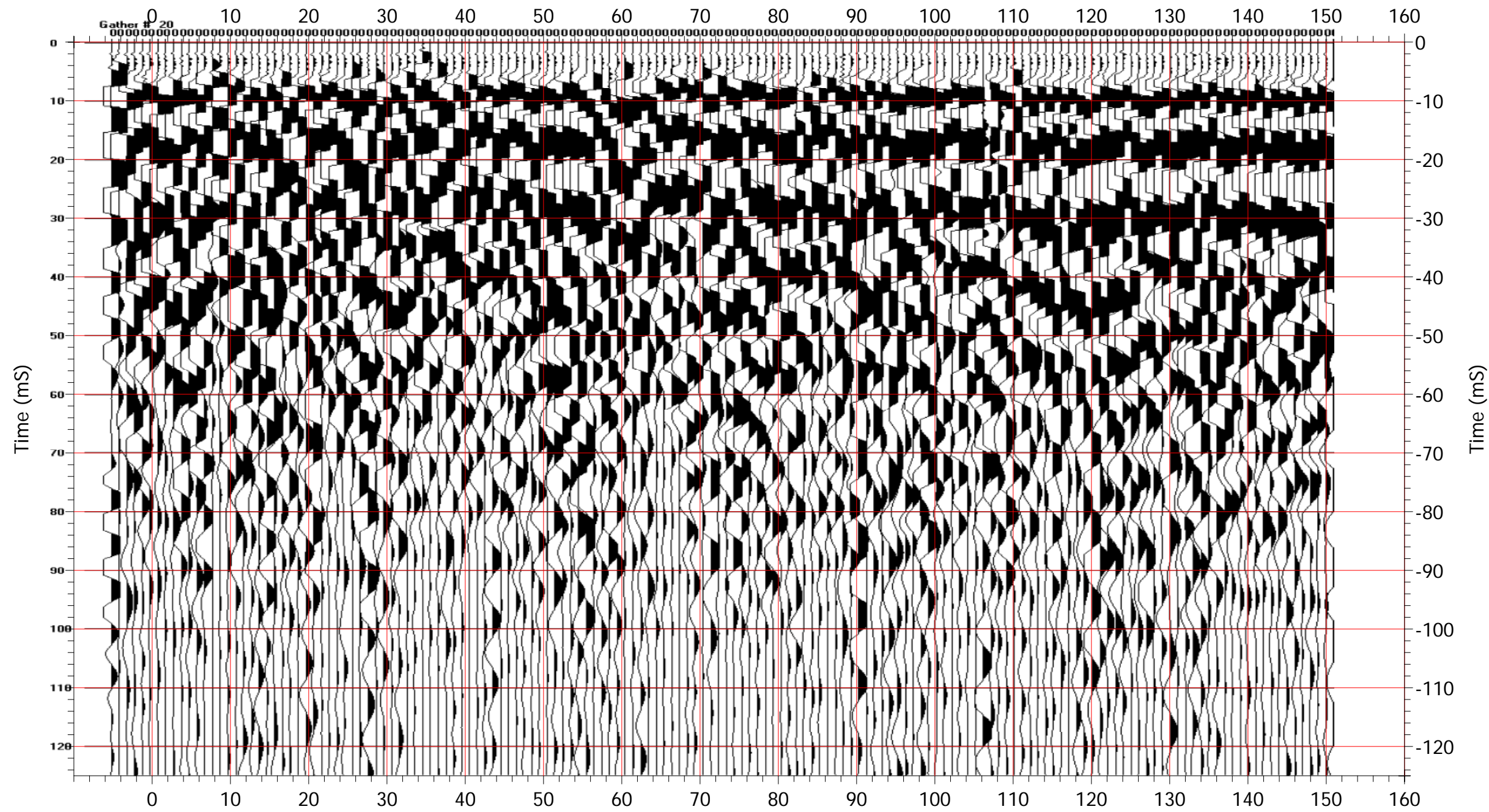
DAWOOD
CONSULTING ENGINEERS
10105 ALLENTOWN BLVD. GRANTVILLE, PA. 17028
PHONE: (717) 869-0937 FAX: (717) 869-0938

DRAWING TITLE:
Poamoho Common Offset Sta. 03

PROJECT NO.:	208044.01
DRAWN BY:	R.A.H.
CHECKED BY:	B.B.
SCALE:	AS SHOWN
DATE:	5 Aug 2008

SHEET NO.:

1



PROJECT: University of Hawaii, Manoa Poamoho, HI	
REVISIONS	DATE

DAWOOD
CONSULTING ENGINEERS
10105 ALLENTOWN BLVD. GRANTVILLE, PA. 17028
PHONE: (717) 869-0937 FAX: (717) 869-0938

DRAWING TITLE:
Poamoho Common Offset Sta. 02

PROJECT NO.:	208044.01
DRAWN BY:	R.A.H.
CHECKED BY:	B.B.
SCALE:	AS SHOWN
DATE:	5 Aug 2008

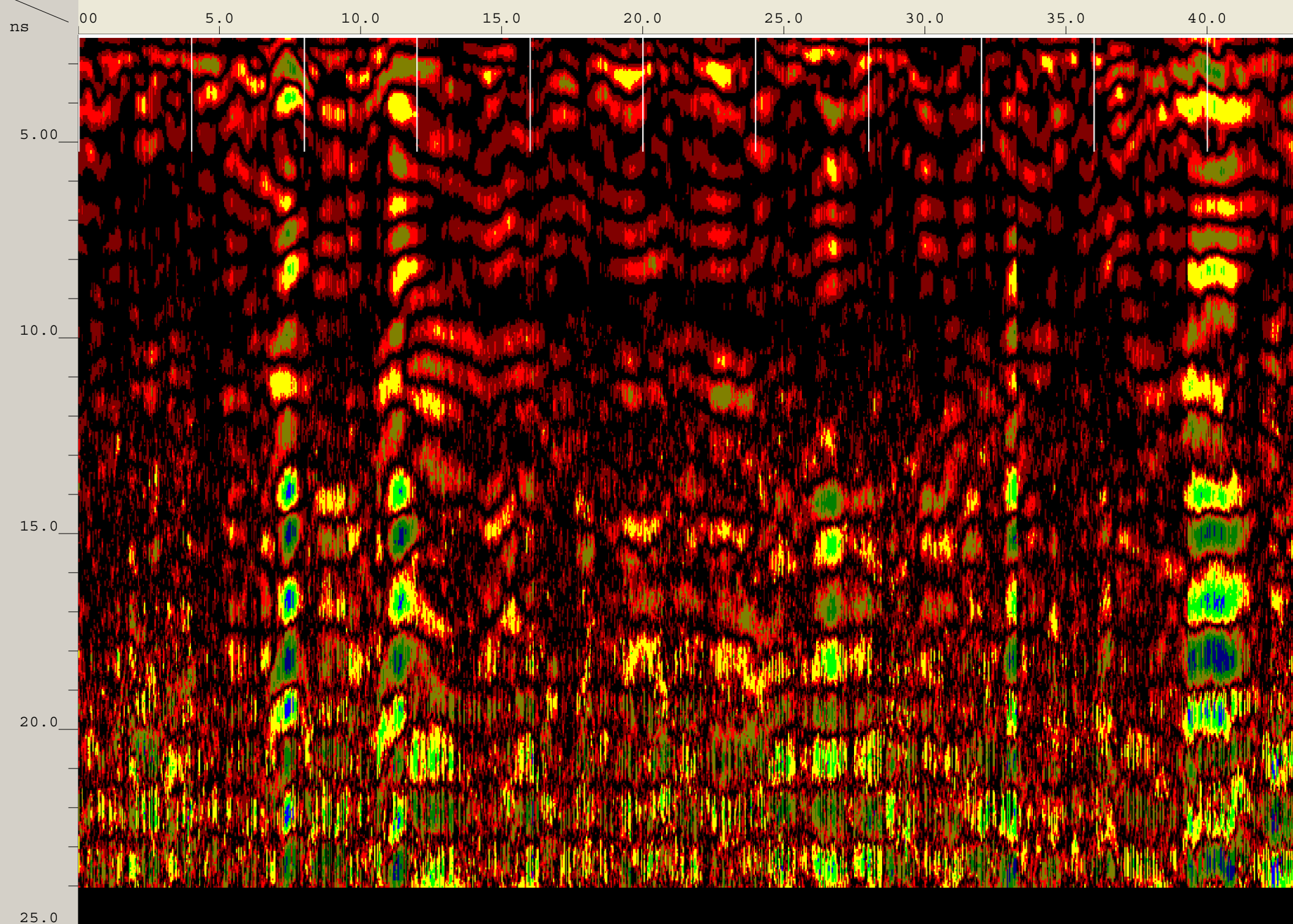
SHEET NO.:

1

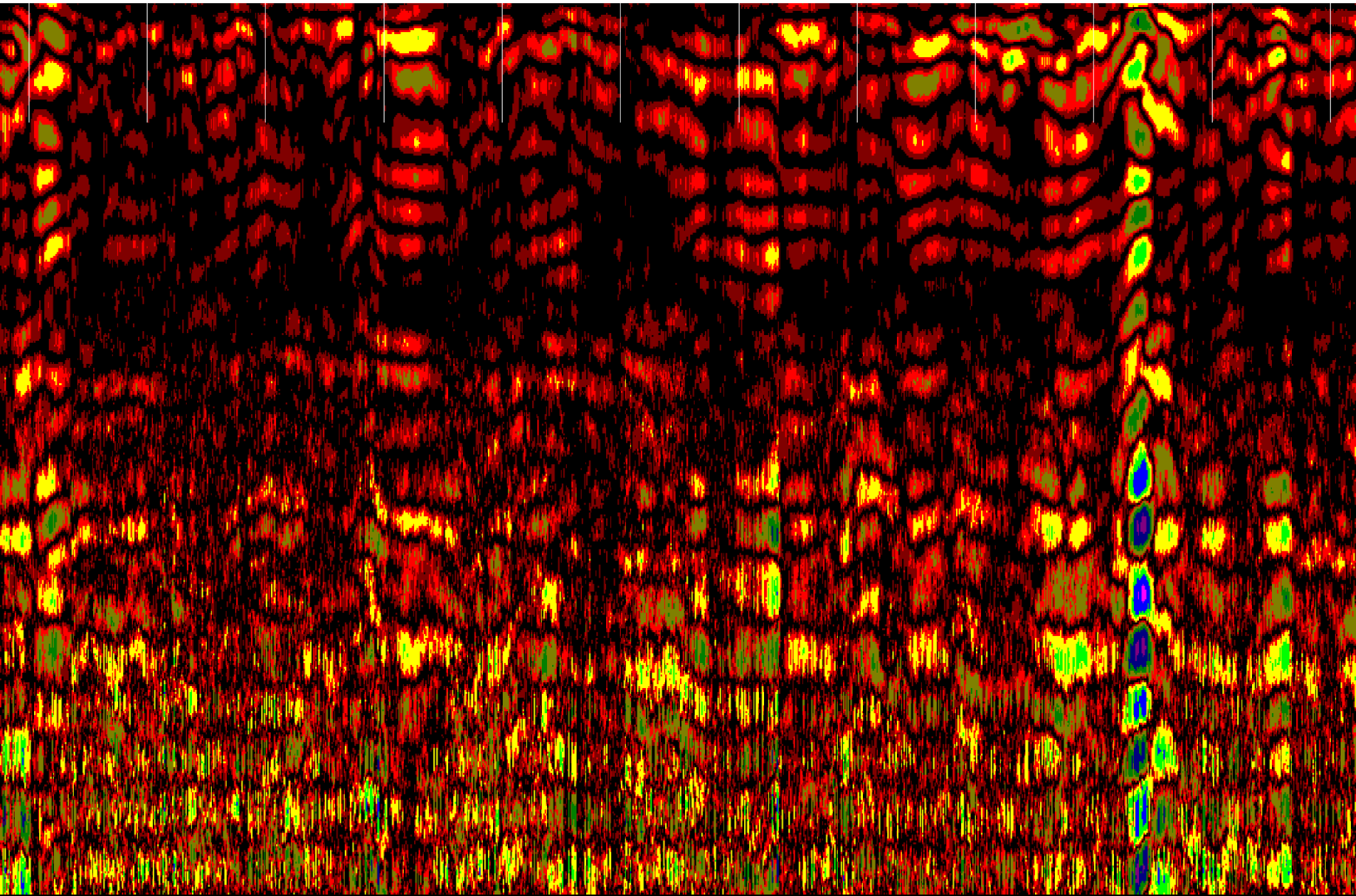
Appendix E – Waimanalo GPR Traverse Data

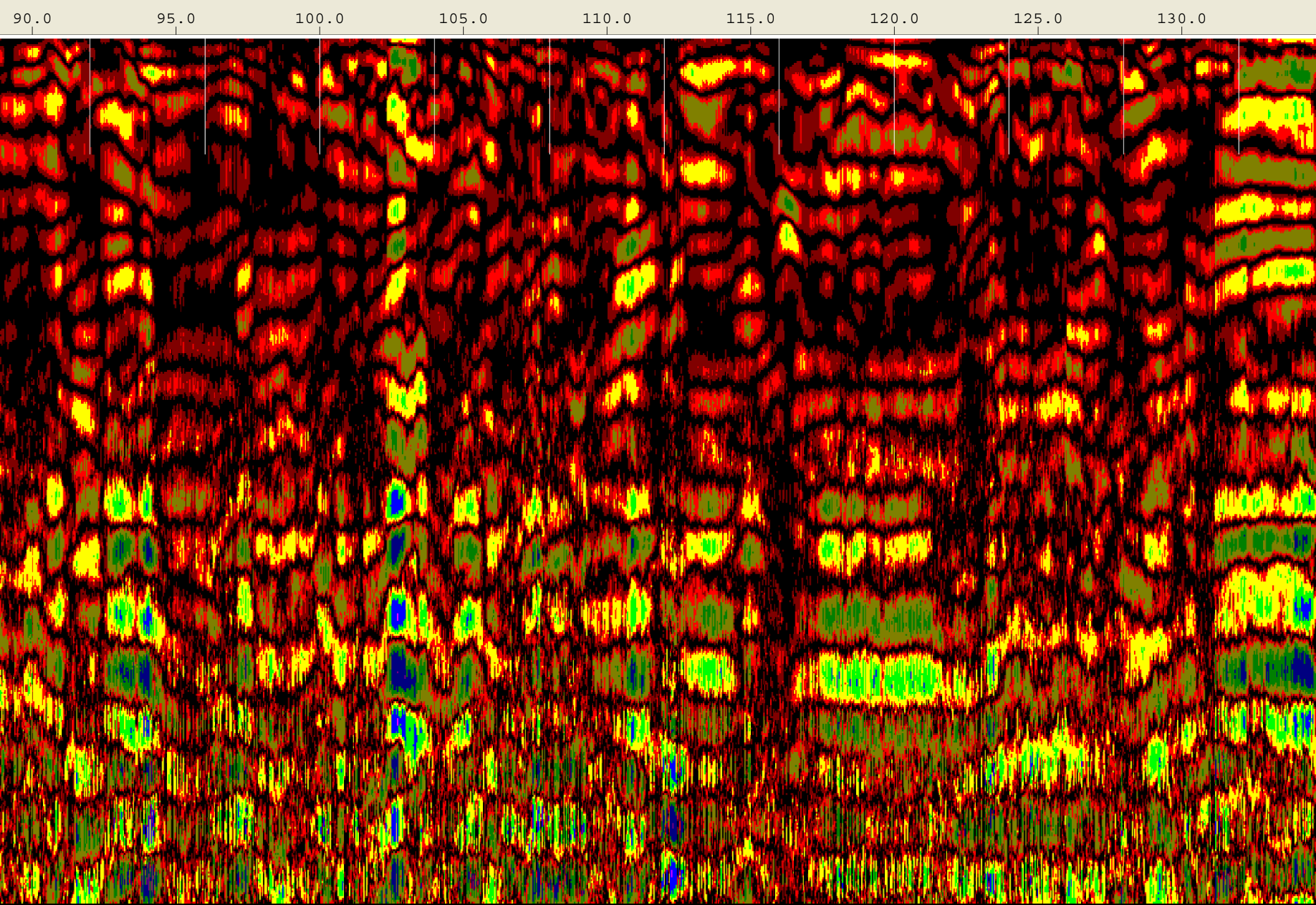
Created Jun, 19 2008, 12:24:14 Modified Jun, 19 2008, 12:27:30
Channel(s) 1 Samples/Scan 512 Bits/Sample 16
Scans/Second 100 Scans/Meter 78.7402 Meters/Mark 1.2192
Diel Constant 8.13067

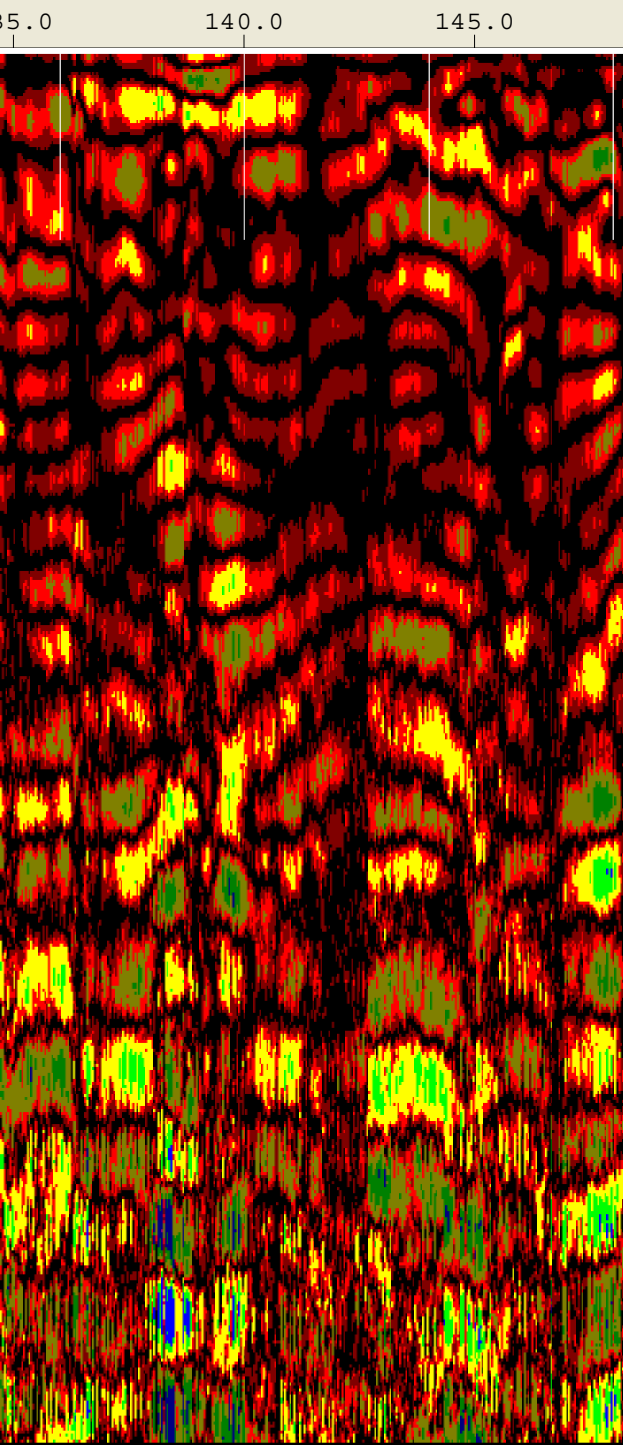
CHANNEL 1 900MHz
Position 2.25 nS Range 24 nS
Position Correction 1.04 nS
Vert IIR LP N =1 F =2500 MHz
Vert IIR HP N =1 F =225 MHz
Range Gain (dB) 2.0 34.0 42.0
Position Correction 2.25 nS
Horz Boxcar Bkgr N=1023
Auto Gain N=1
G=0 TC=0



45.0 50.0 55.0 60.0 65.0 70.0 75.0 80.0 85.0

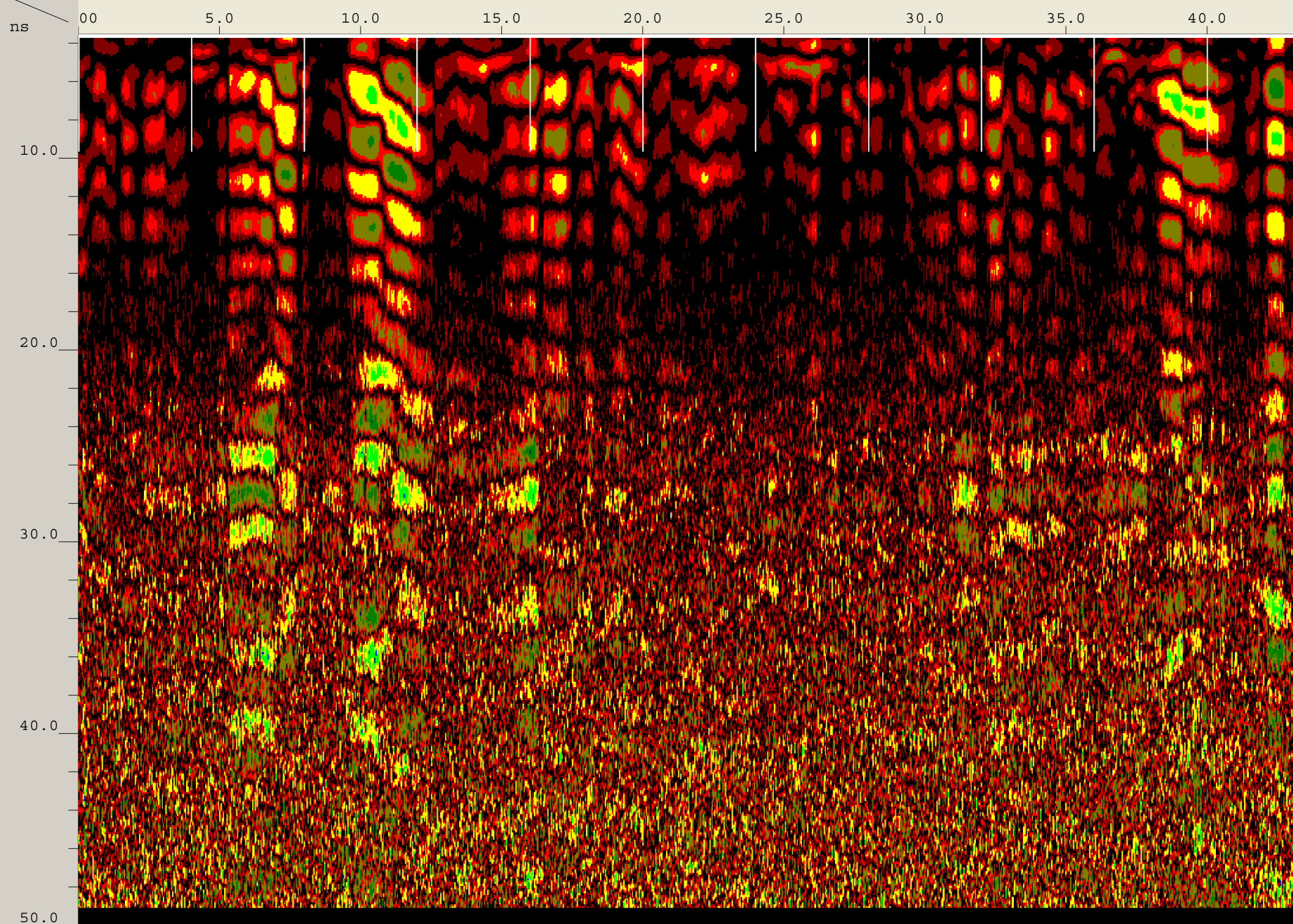




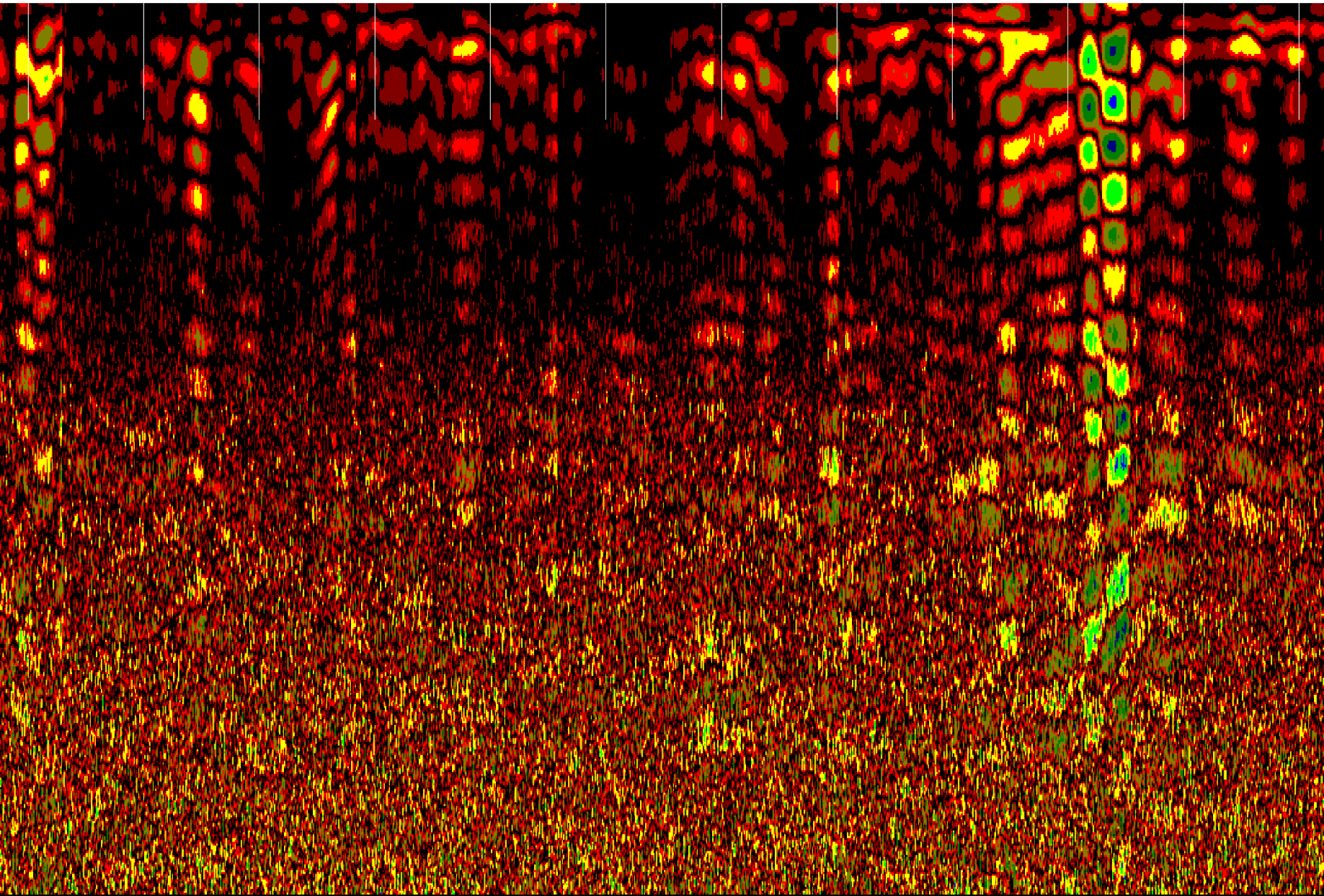


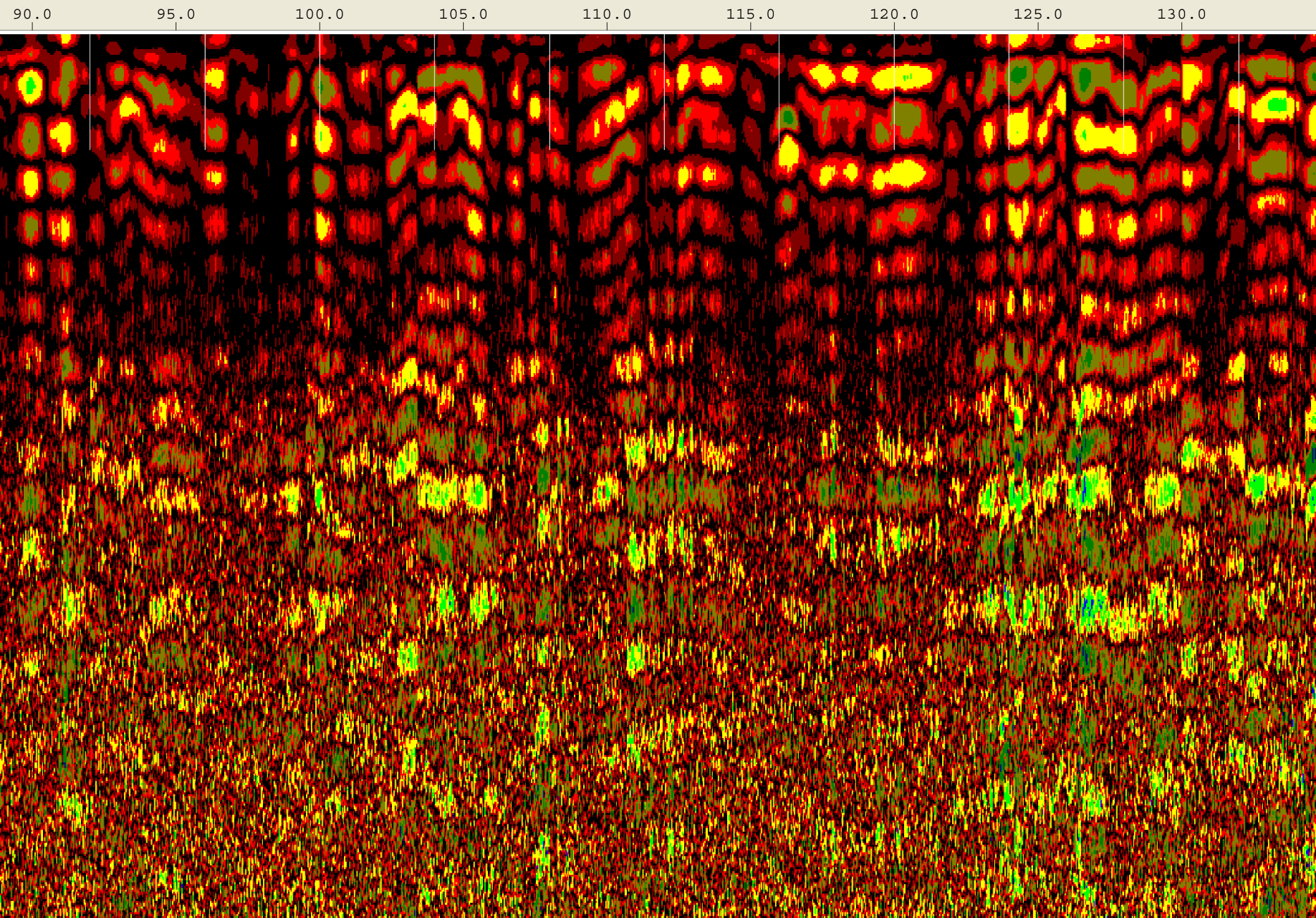
Created Jun, 19 2008, 12:06:20 Modified Jun, 19 2008, 12:09:50
Channel(s) 1 Samples/Scan 512 Bits/Sample 16
Scans/Second 100 Scans/Meter 78.7402 Meters/Mark 1.2192
Diel Constant 9.5931

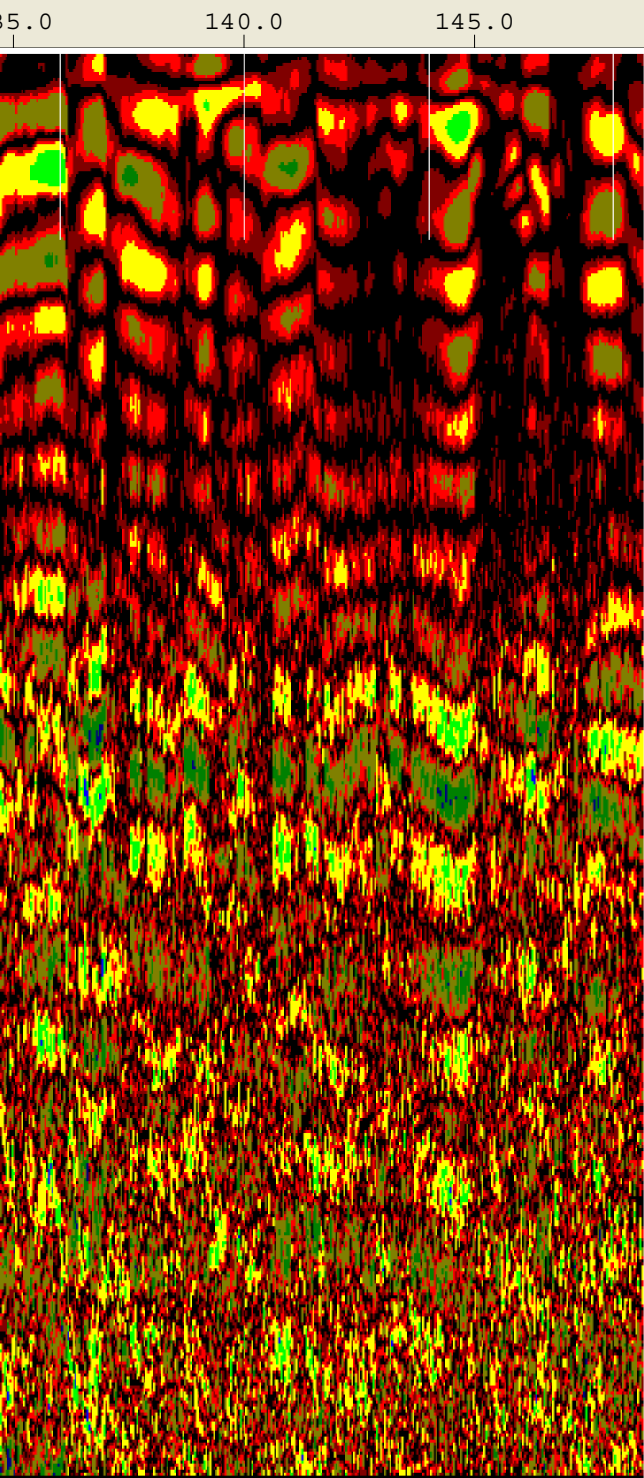
CHANNEL 1 400MHz
Position 3.54 nS Range 49 nS
Range Gain (dB) -1.0 31.0 38.0
Position Correction 1.04 nS
Vert IIR LP N =1 F =800 MHz
Vert IIR HP N =1 F =100 MHz
Position Correction 3.54 nS
Horz Boxcar Bkgr N=1023



45.0 50.0 55.0 60.0 65.0 70.0 75.0 80.0 85.0

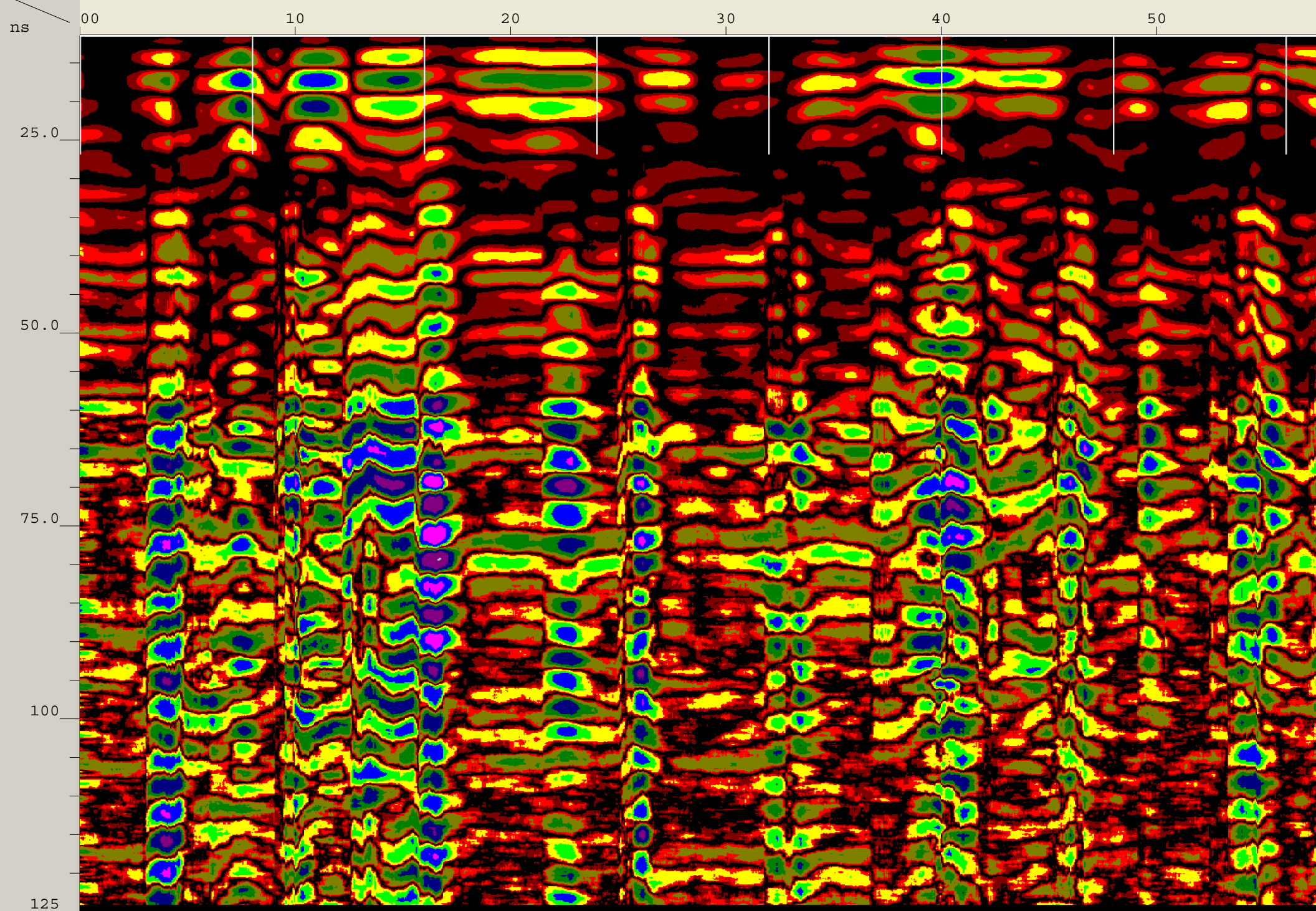




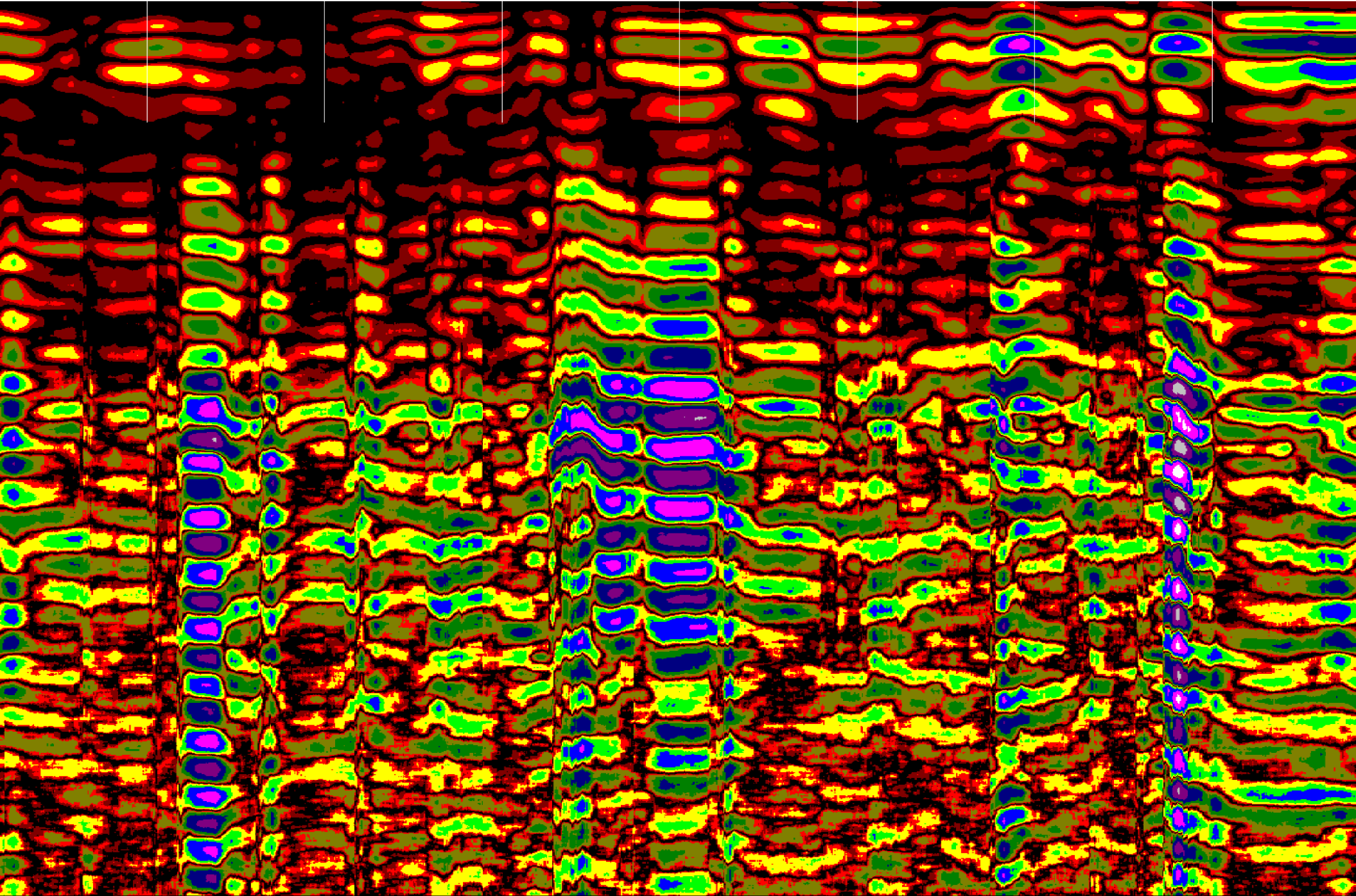


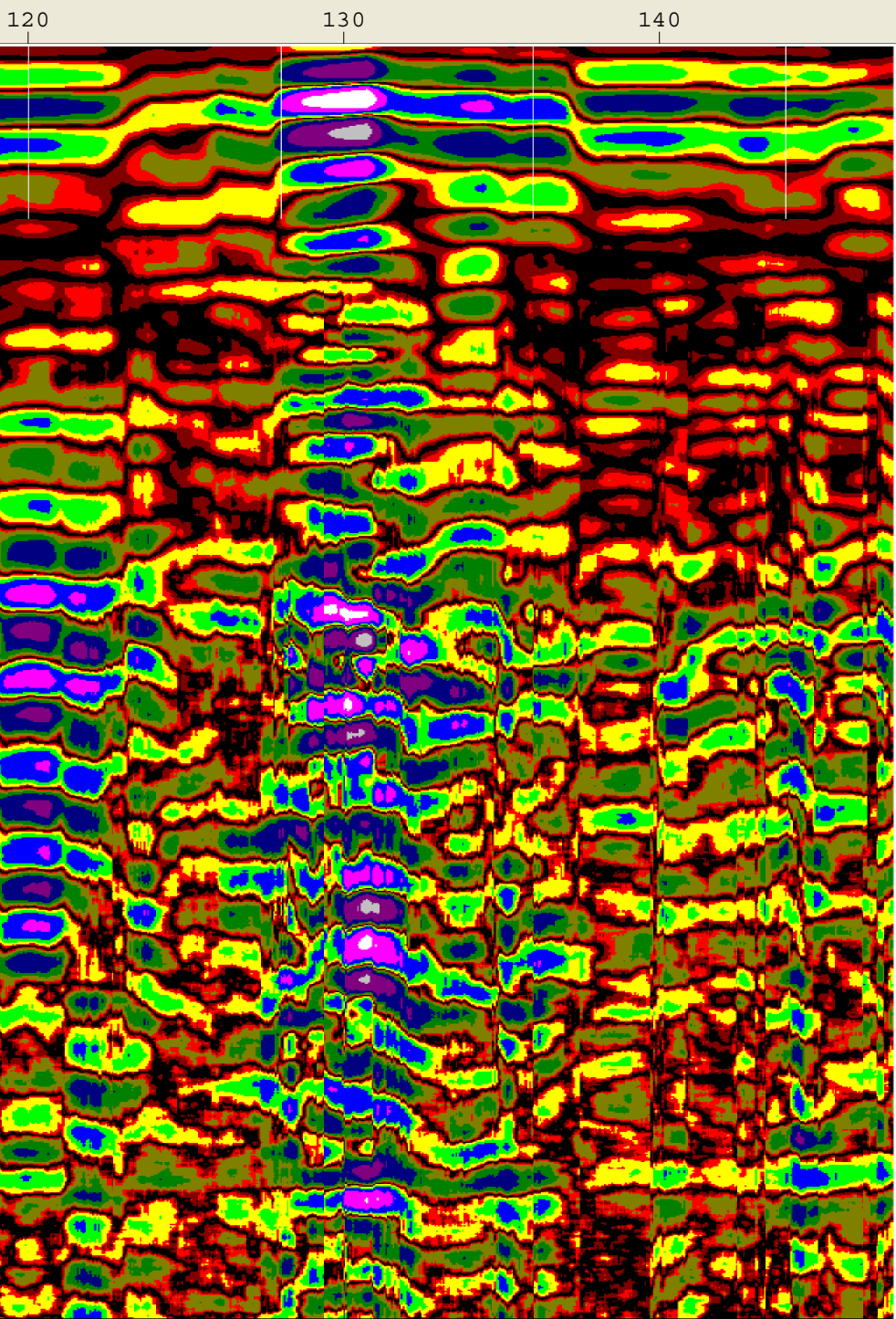
Created Jun, 19 2008, 11:25:36 Modified Jun, 19 2008, 11:30:46
Channel(s) 1 Samples/Scan 1024 Bits/Sample 16
Scans/Second 64 Scans/Meter 59.0551 Meters/Mark 2.4384
Diel Constant 6

CHANNEL 1 270MHz
Position 11.38 nS Range 124 nS
Vert IIR LP N =1 F =700 MHz
Vert IIR HP N =1 F =75 MHz
Horz IIR Stack TC =11
Position Correction -4.725 nS
Range Gain (dB) -18.0 50.0 54.0
Position Correction 11.38 nS
Horz Boxcar Bkgr N=1023
Range Gain (L) 1.0 3.7 1.0
1.0 1.0 1.0
1.0



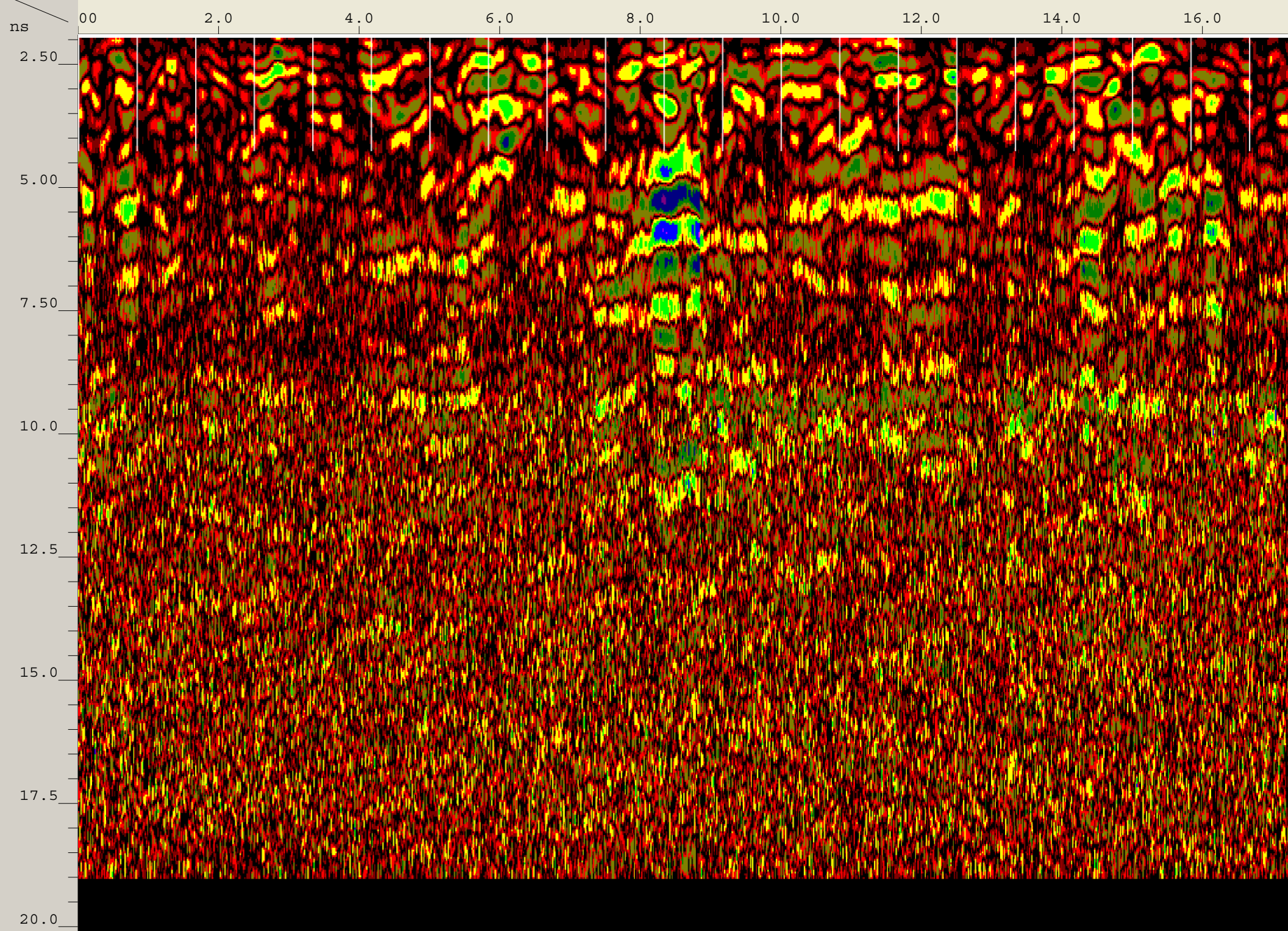
60 70 80 90 100 110



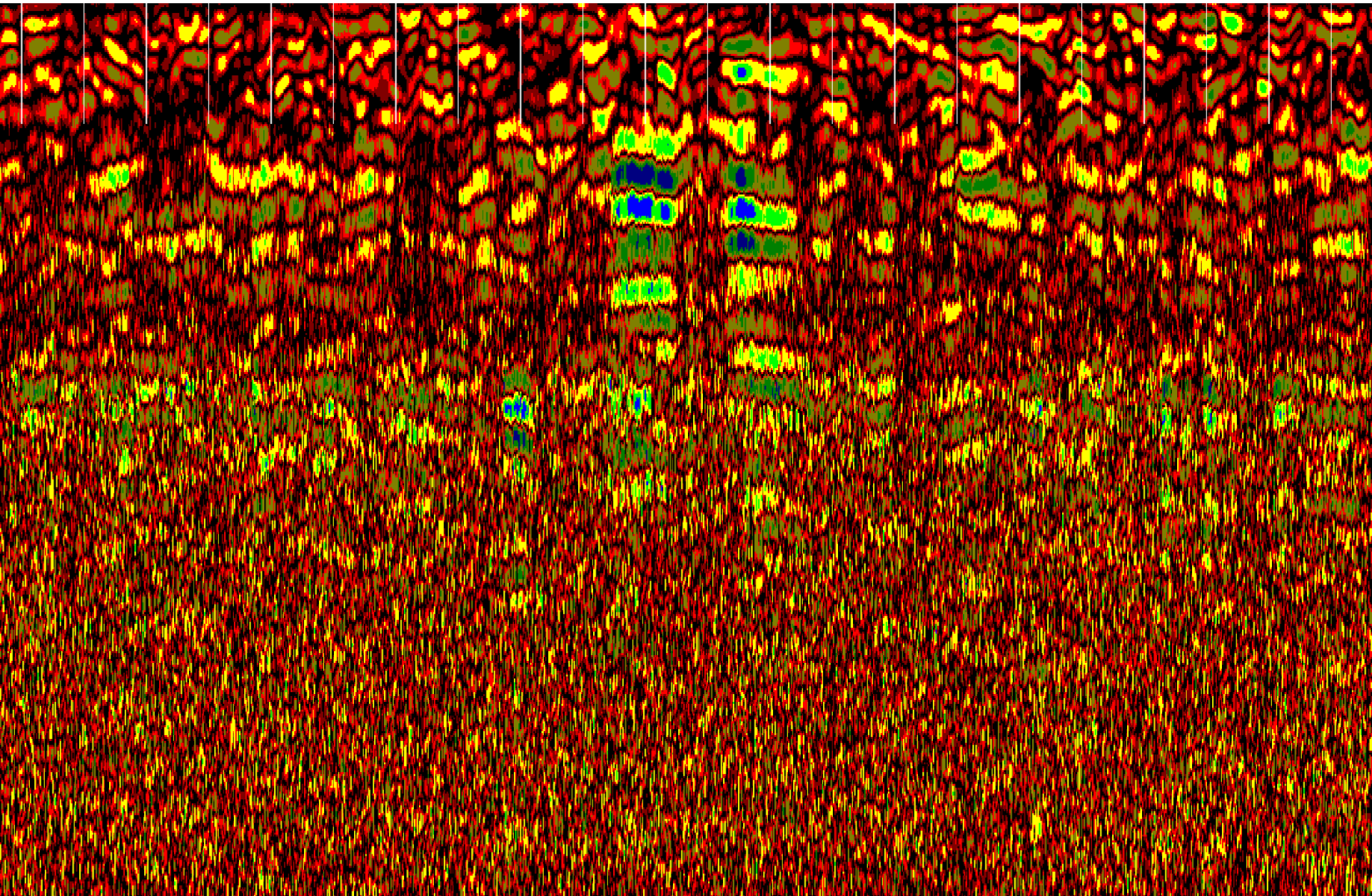


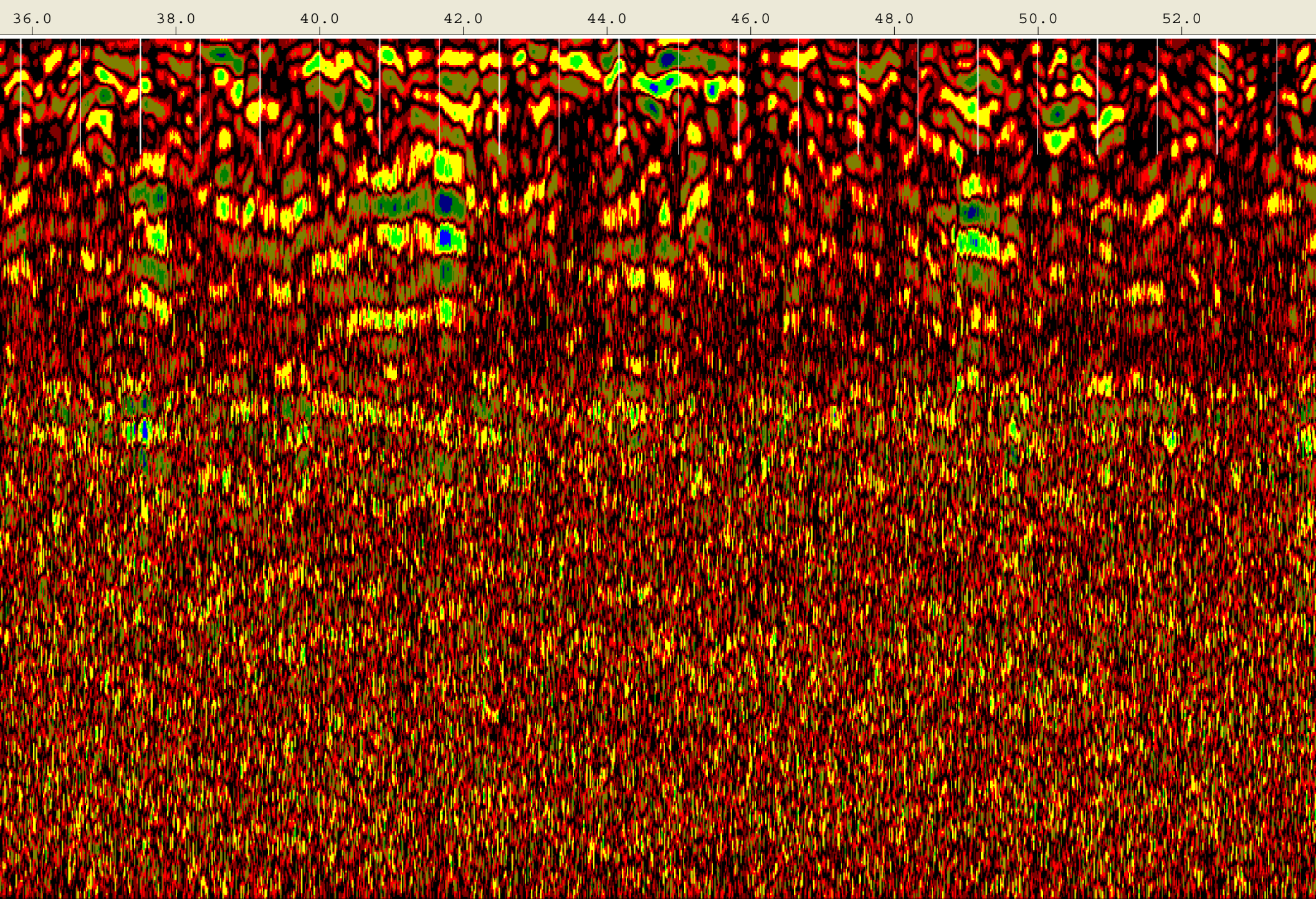
Created Jun, 19 2008, 13:23:50 Modified Jun, 19 2008, 13:28:10
Channel(s) 1 Samples/Scan 512 Bits/Sample 16
Scans/Second 100 Scans/Meter 196.85 Meters/Mark 0.254
Diel Constant 4.95451

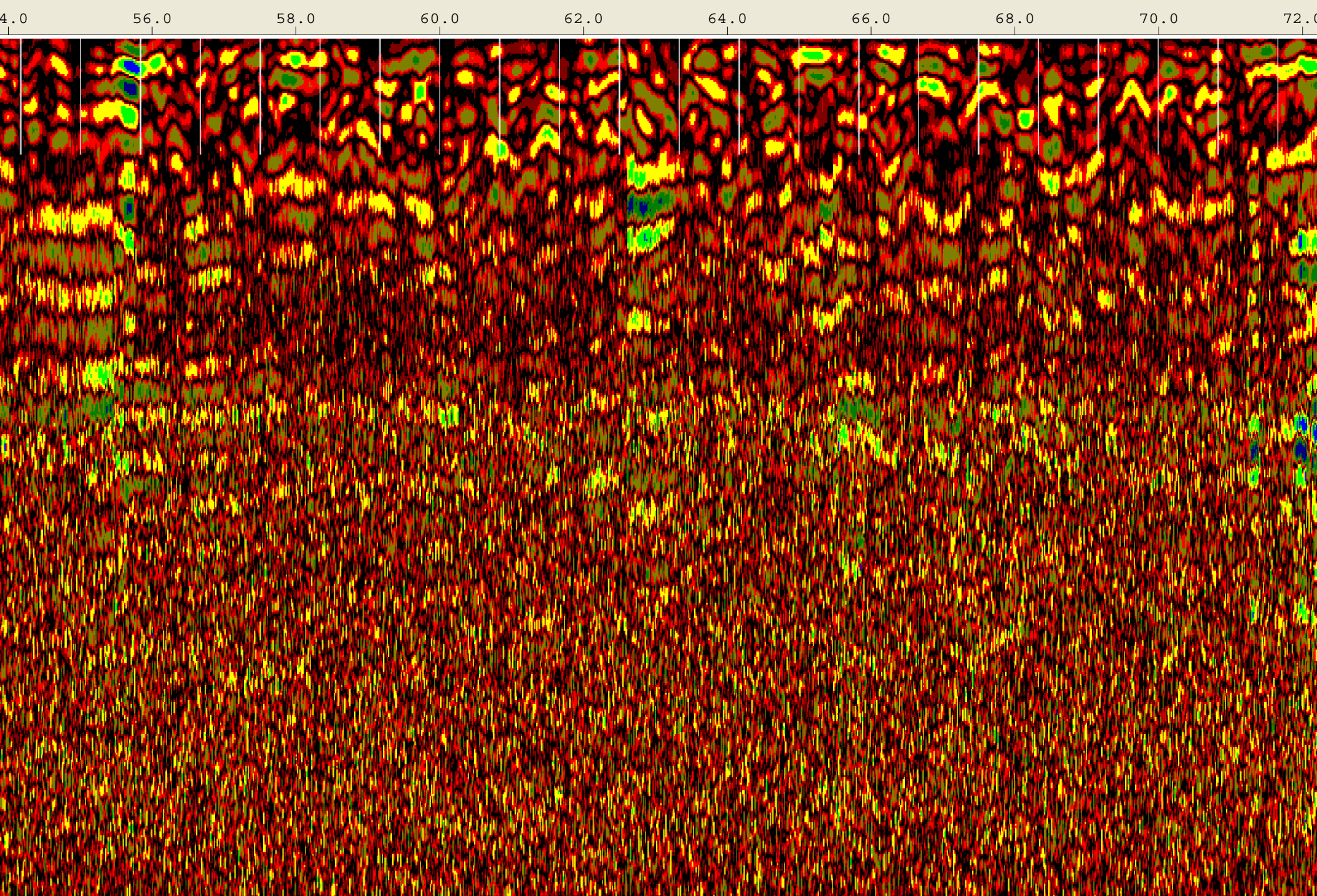
CHANNEL 1 1.5/1.6GHZ
Position 1.89 nS Range 19 nS
Range Gain (dB) -14.0 10.0 31.0
31.0 31.0
Position Correction 6.9 nS
Vert IIR HP N =1 F =10 MHz
Vert Boxcar LP F =1930 MHz
Vert Boxcar HP F =295 MHz
Position Correction 1.89 nS
Horz Boxcar Bkgr N=1023
Range Gain (L) 1.8 6.1 1.8
1.6 1.8 1.9
1.0



18.0 20.0 22.0 24.0 26.0 28.0 30.0 32.0 34.0







74.0

76.0

78.0

80.0

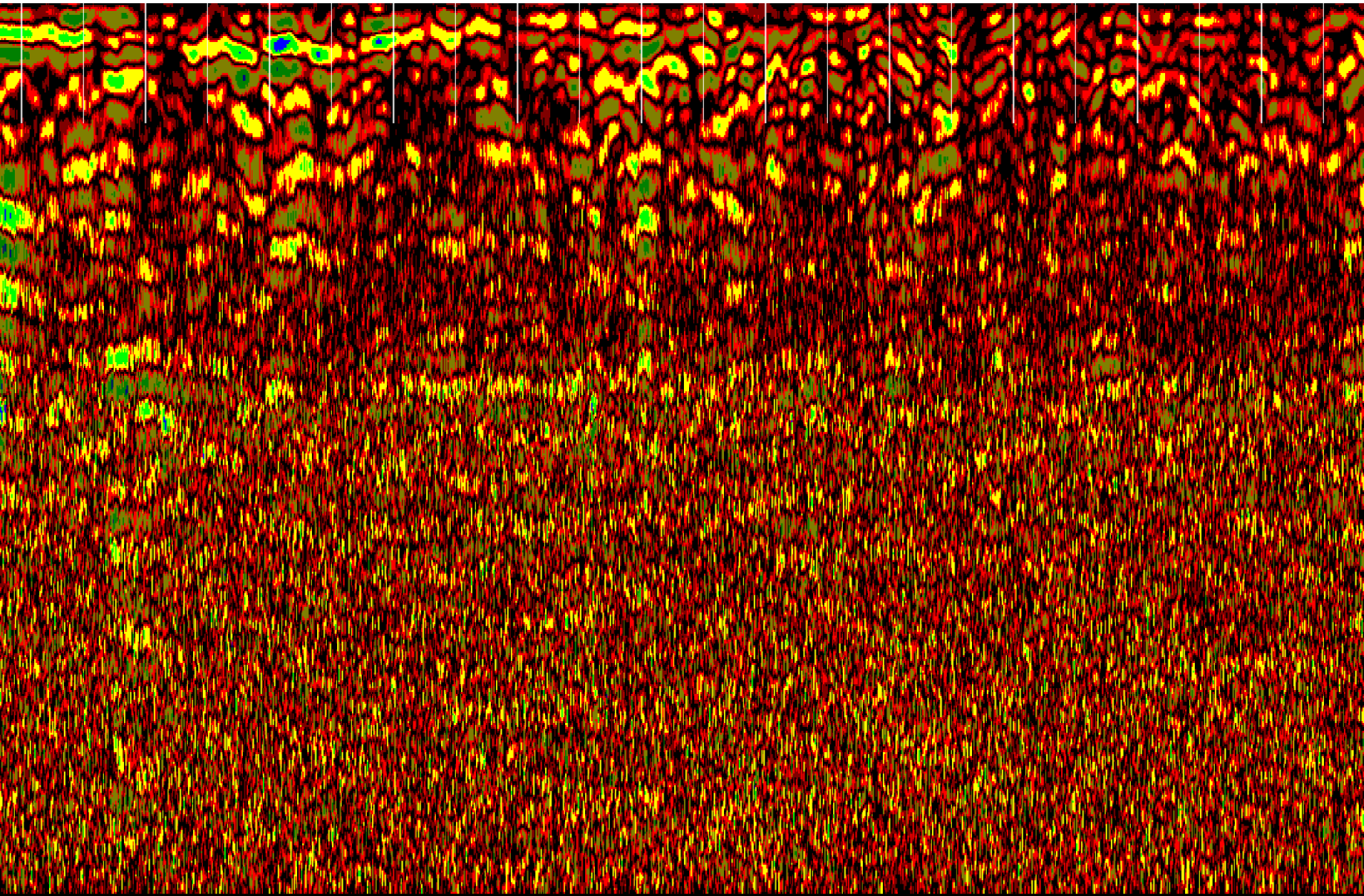
82.0

84.0

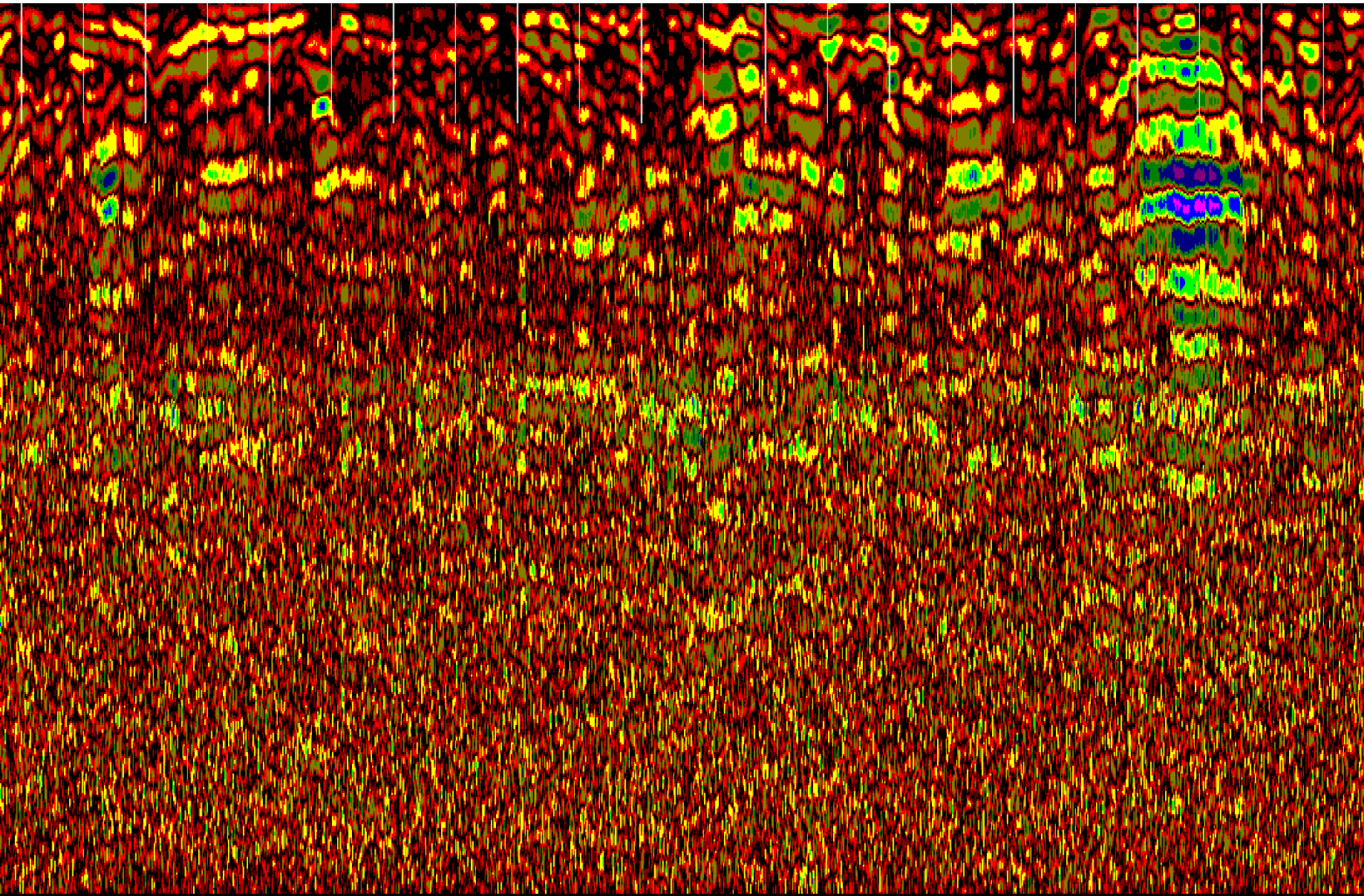
86.0

88.0

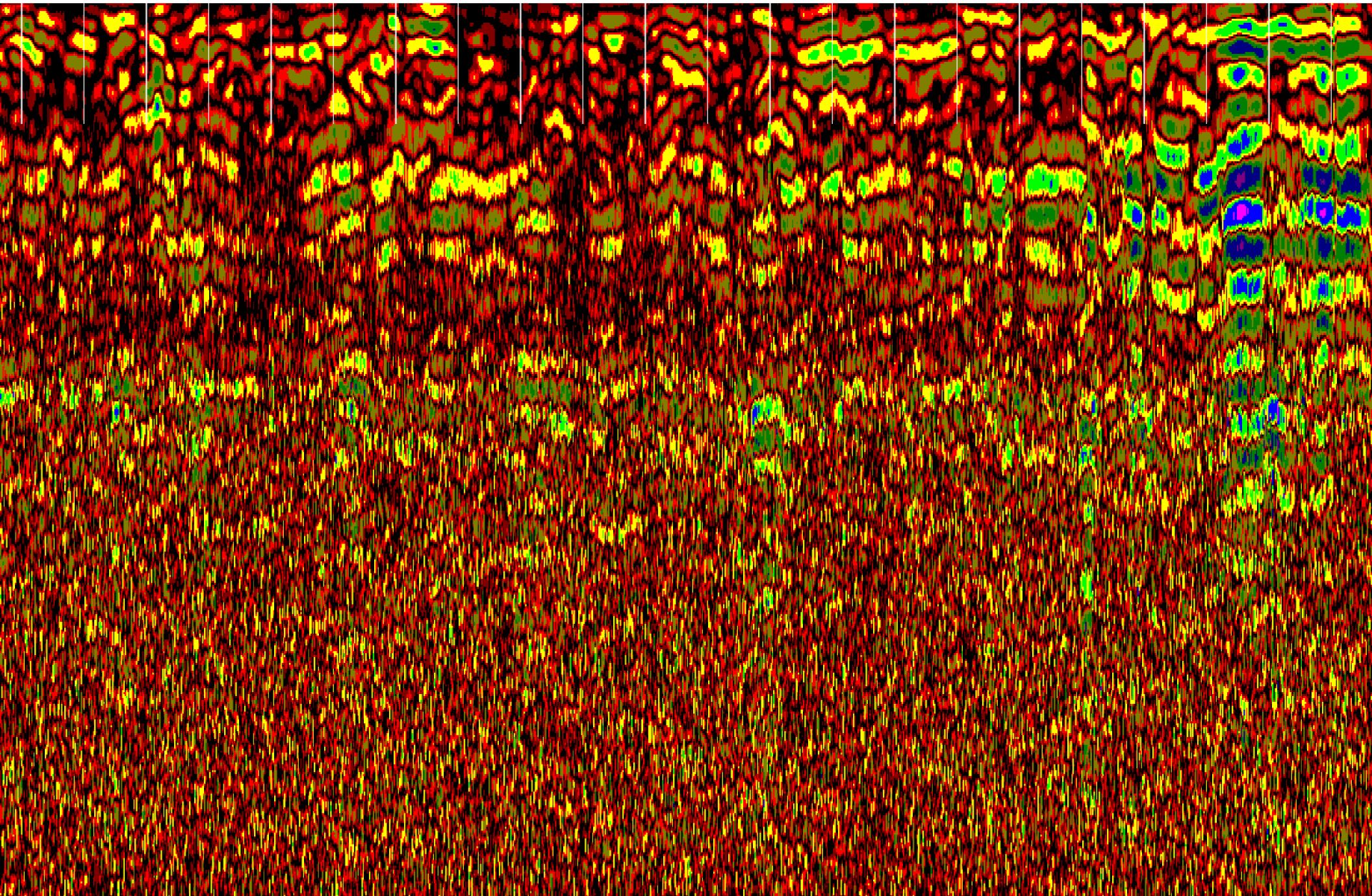
90.0



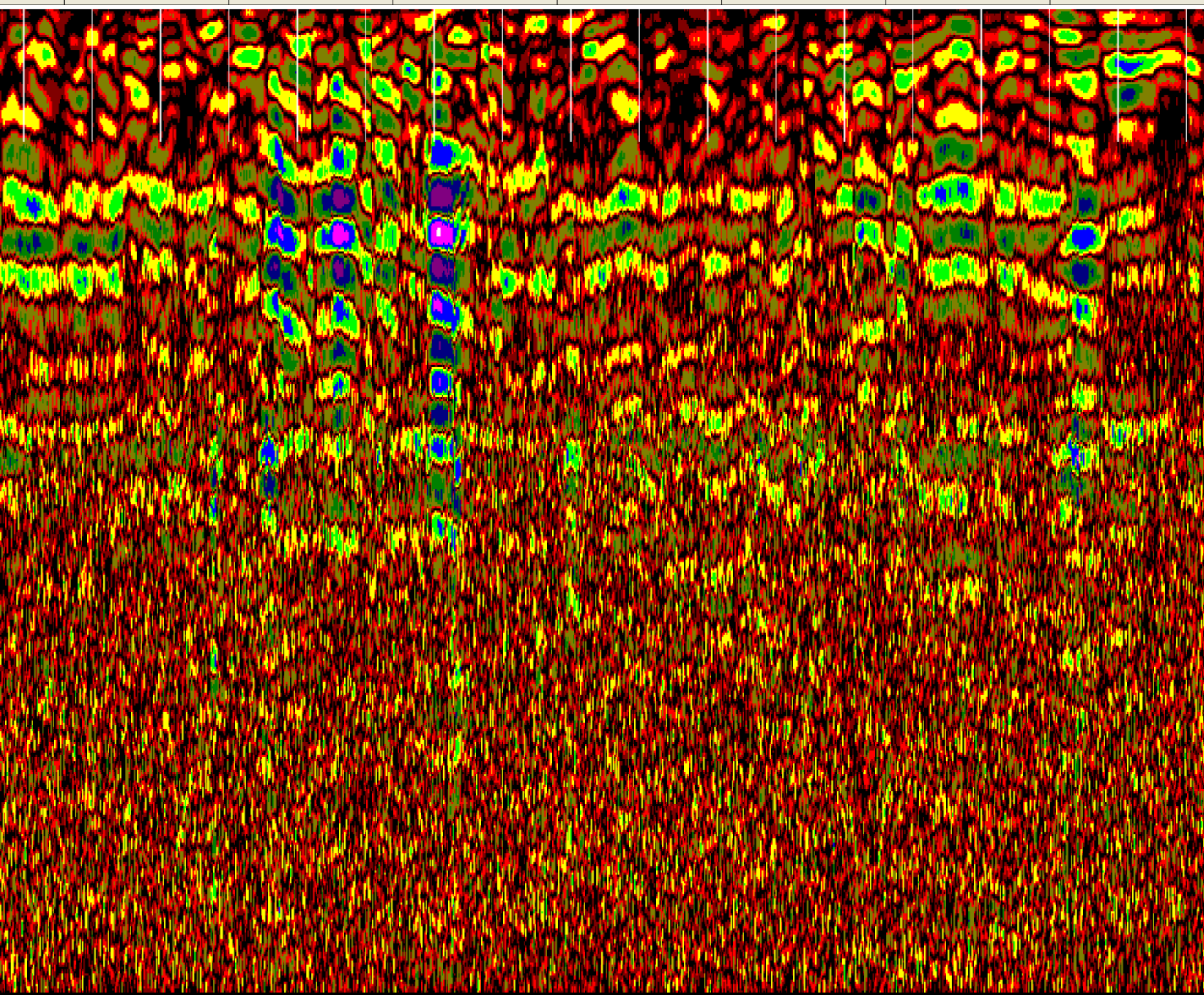
92.0 94.0 96.0 98.0 100.0 102.0 104.0 106.0 108.0



110.0 112.0 114.0 116.0 118.0 120.0 122.0 124.0 126.0

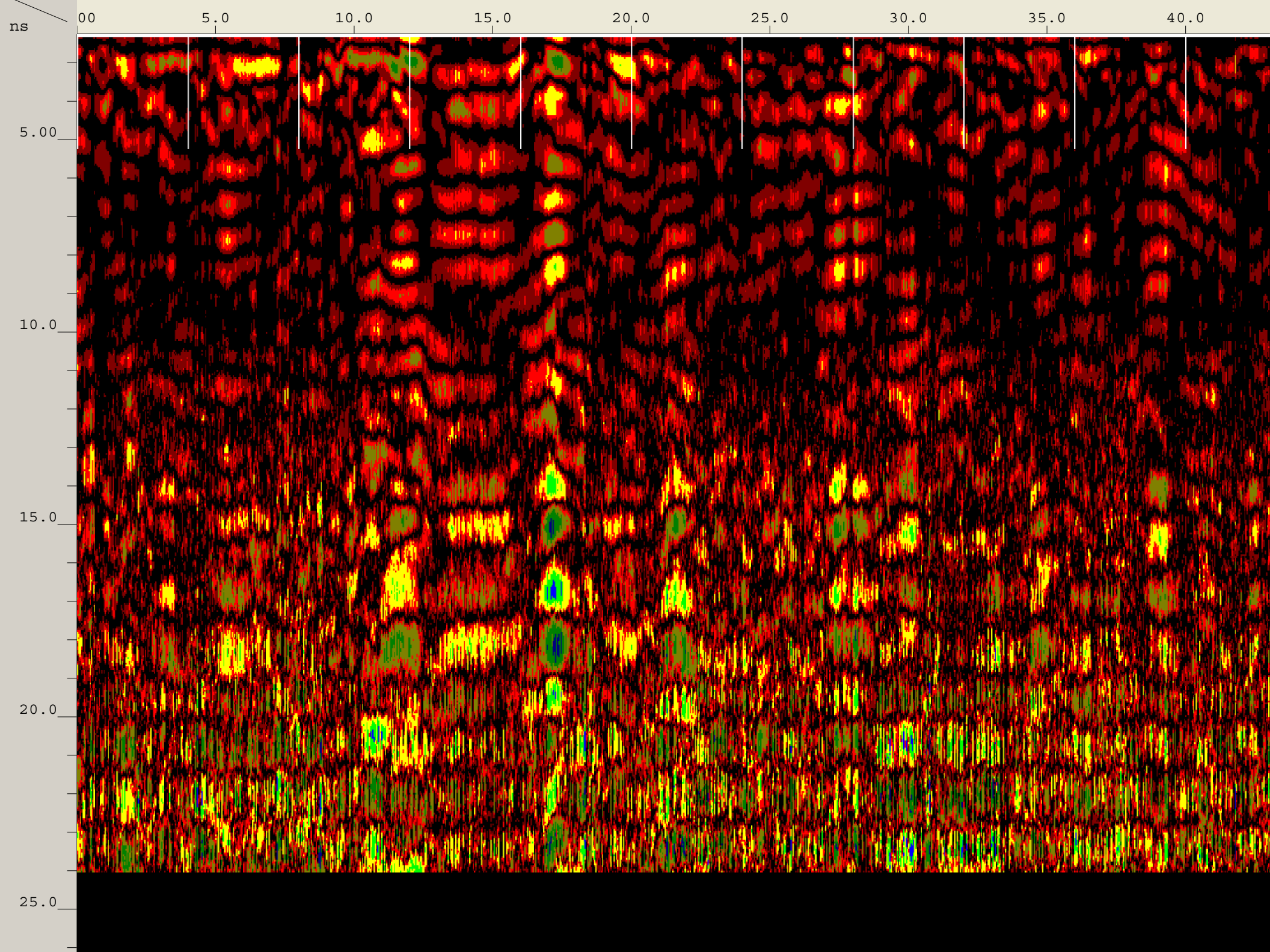


128.0 130.0 132.0 134.0 136.0 138.0 140.0

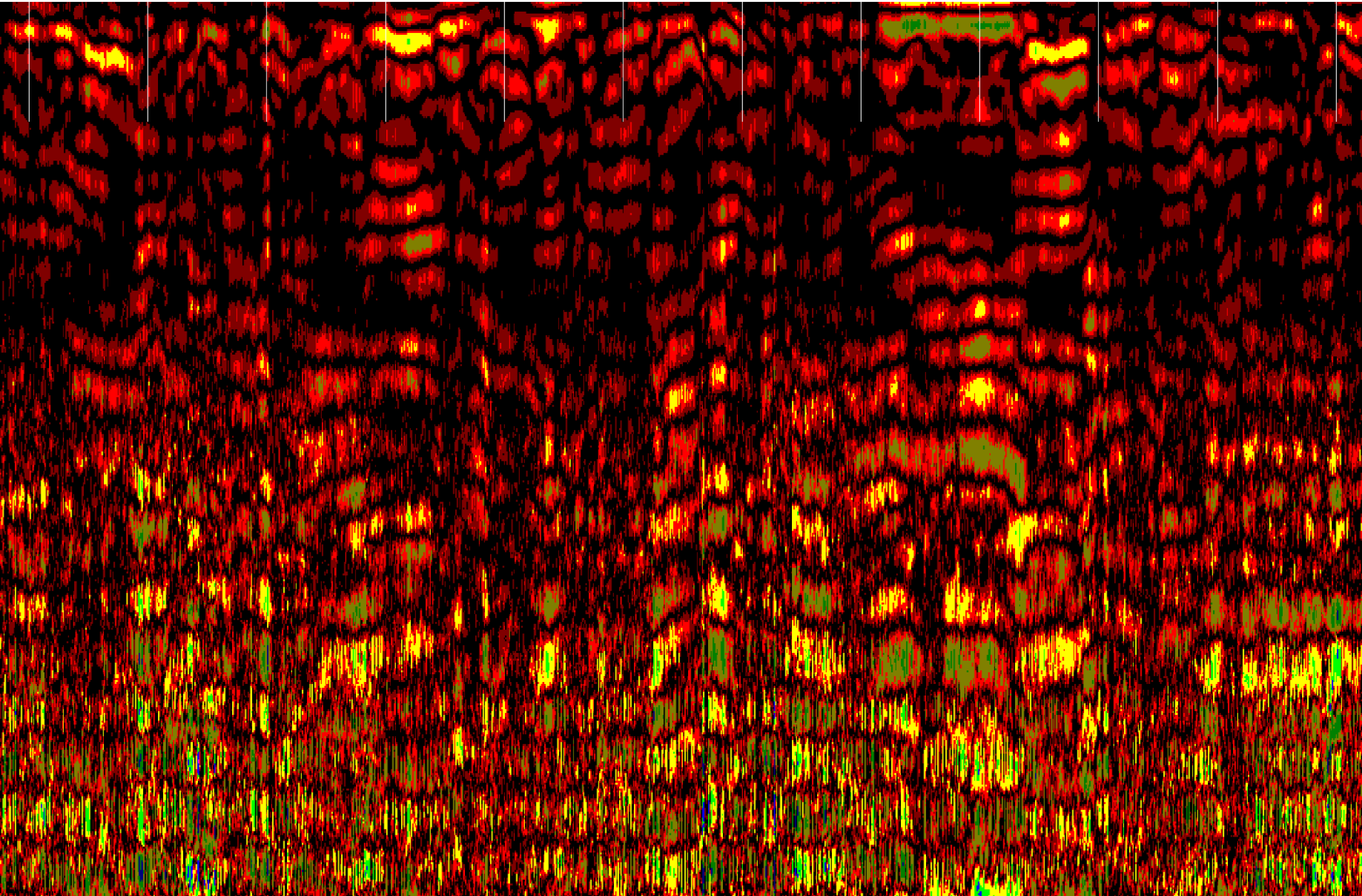


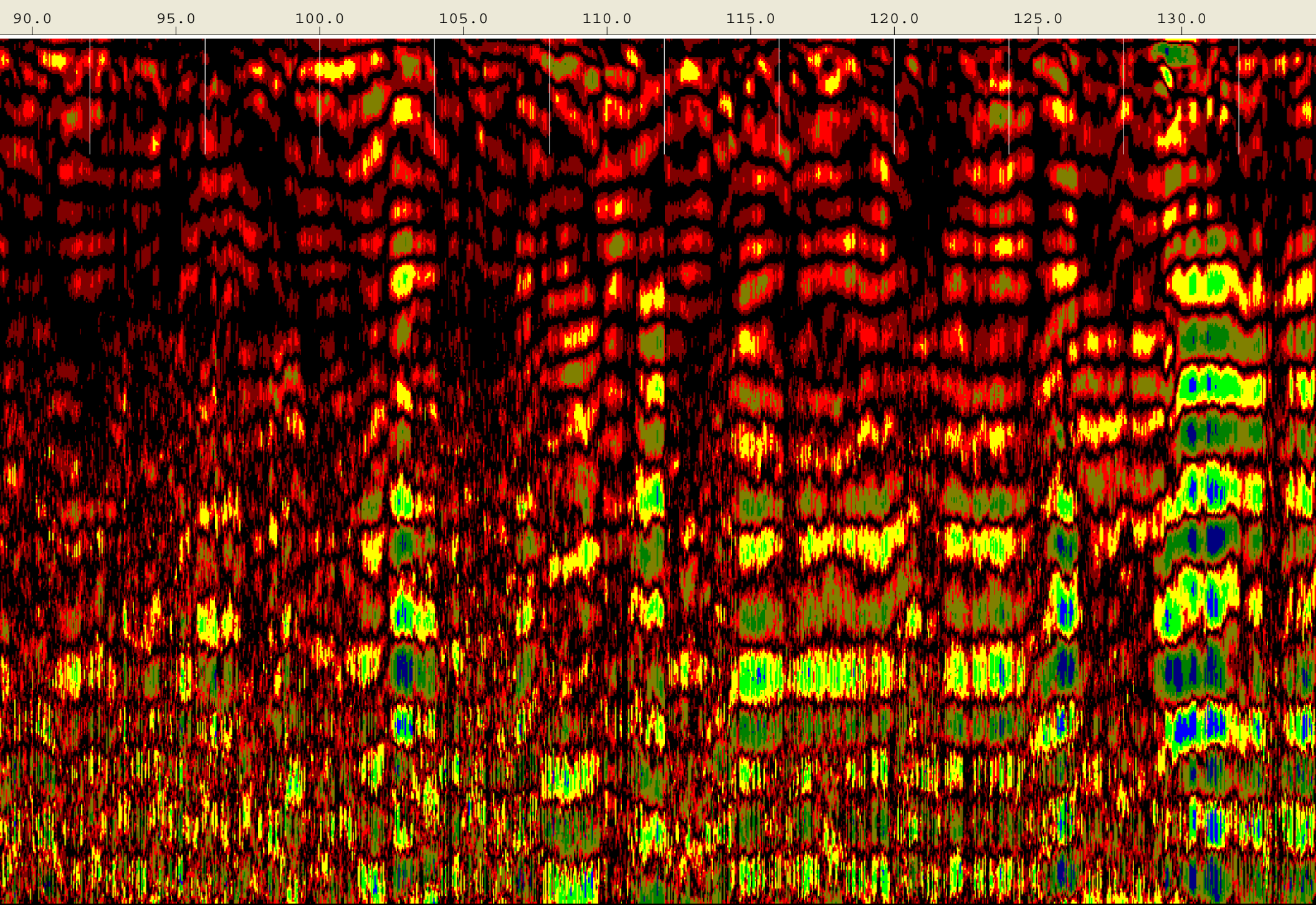
Created Jun, 19 2008, 12:21:04 Modified Jun, 19 2008, 12:24:10
Channel(s) 1 Samples/Scan 512 Bits/Sample 16
Scans/Second 100 Scans/Meter 78.7402 Meters/Mark 1.2192
Diel Constant 11.1605

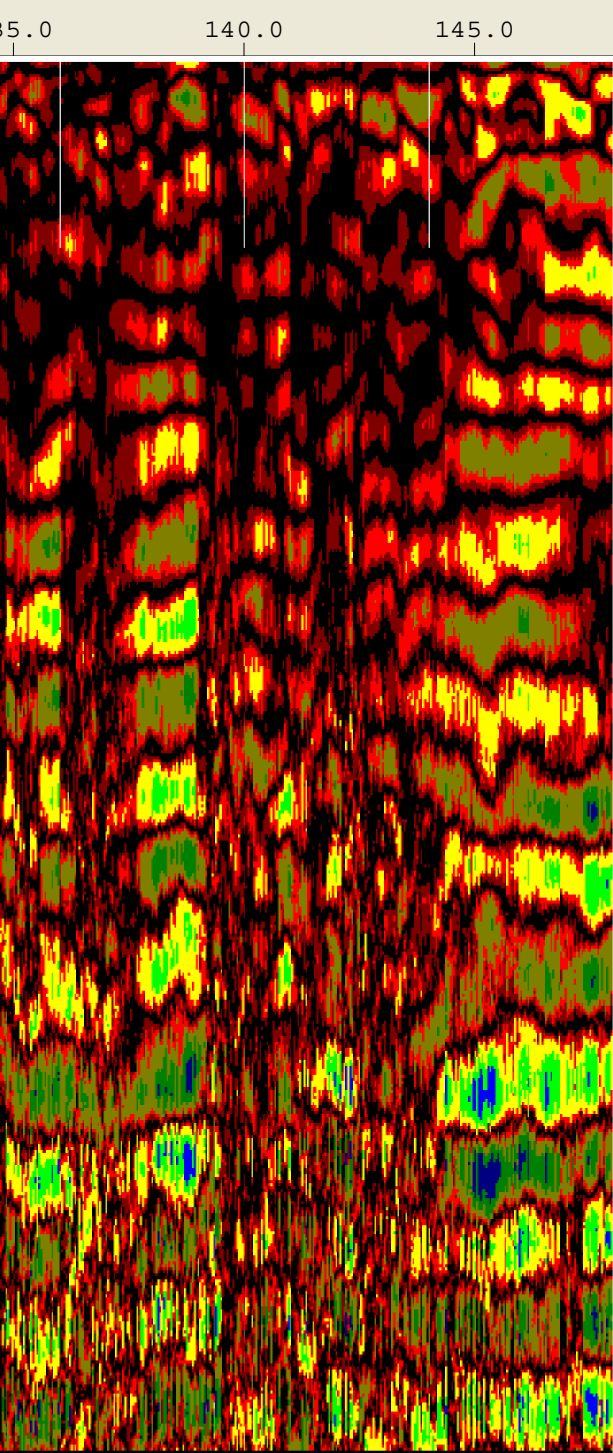
CHANNEL 1 900MHz
Position 2.25 nS Range 24 nS
Position Correction 1.04 nS
Vert IIR LP N =1 F =2500 MHz
Vert IIR HP N =1 F =225 MHz
Range Gain (dB) 2.0 34.0 42.0
Position Correction 2.25 nS
Horz Boxcar Bkgr N=1023
Auto Gain N=1
G=0 TC=0



45.0 50.0 55.0 60.0 65.0 70.0 75.0 80.0 85.0

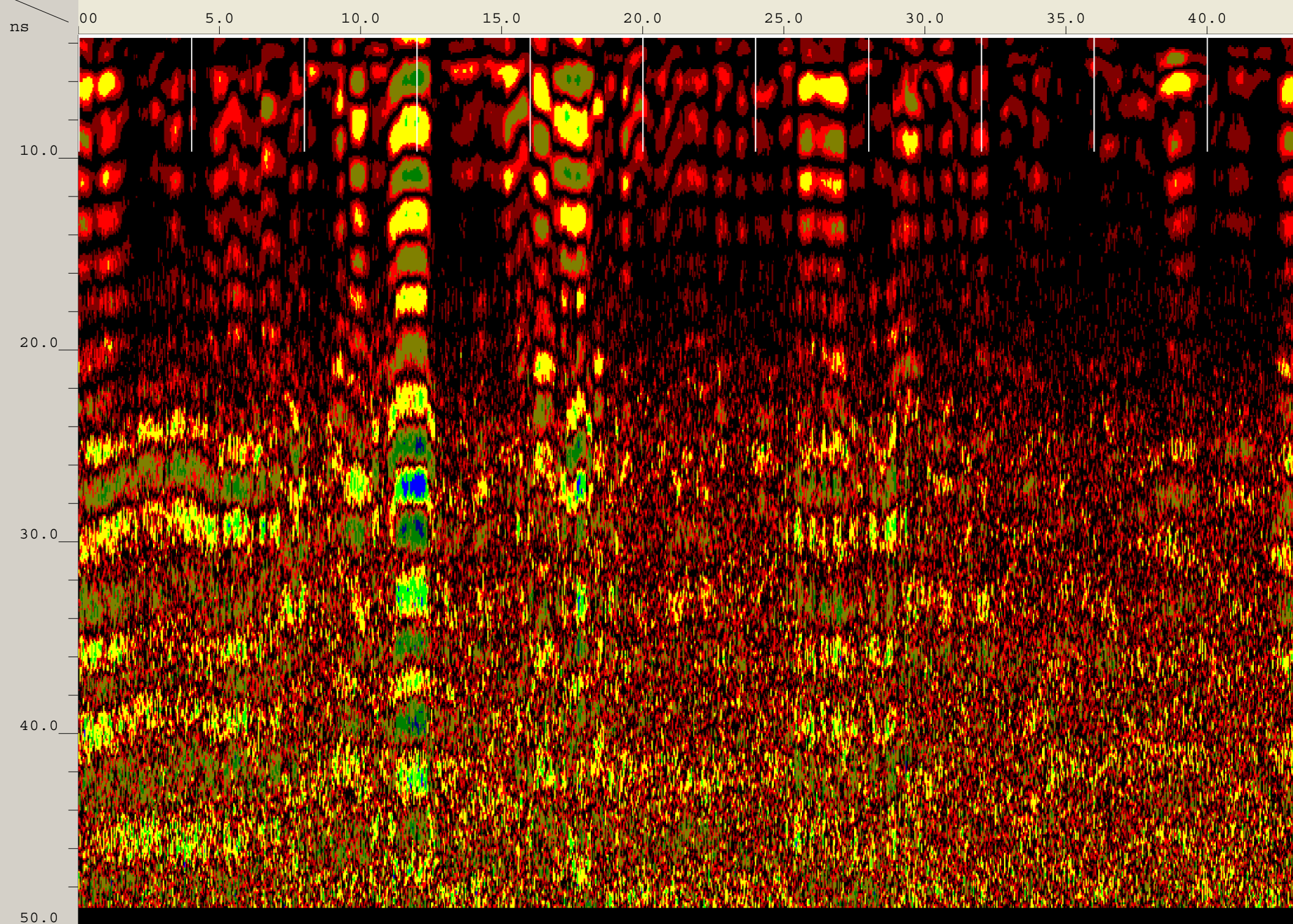


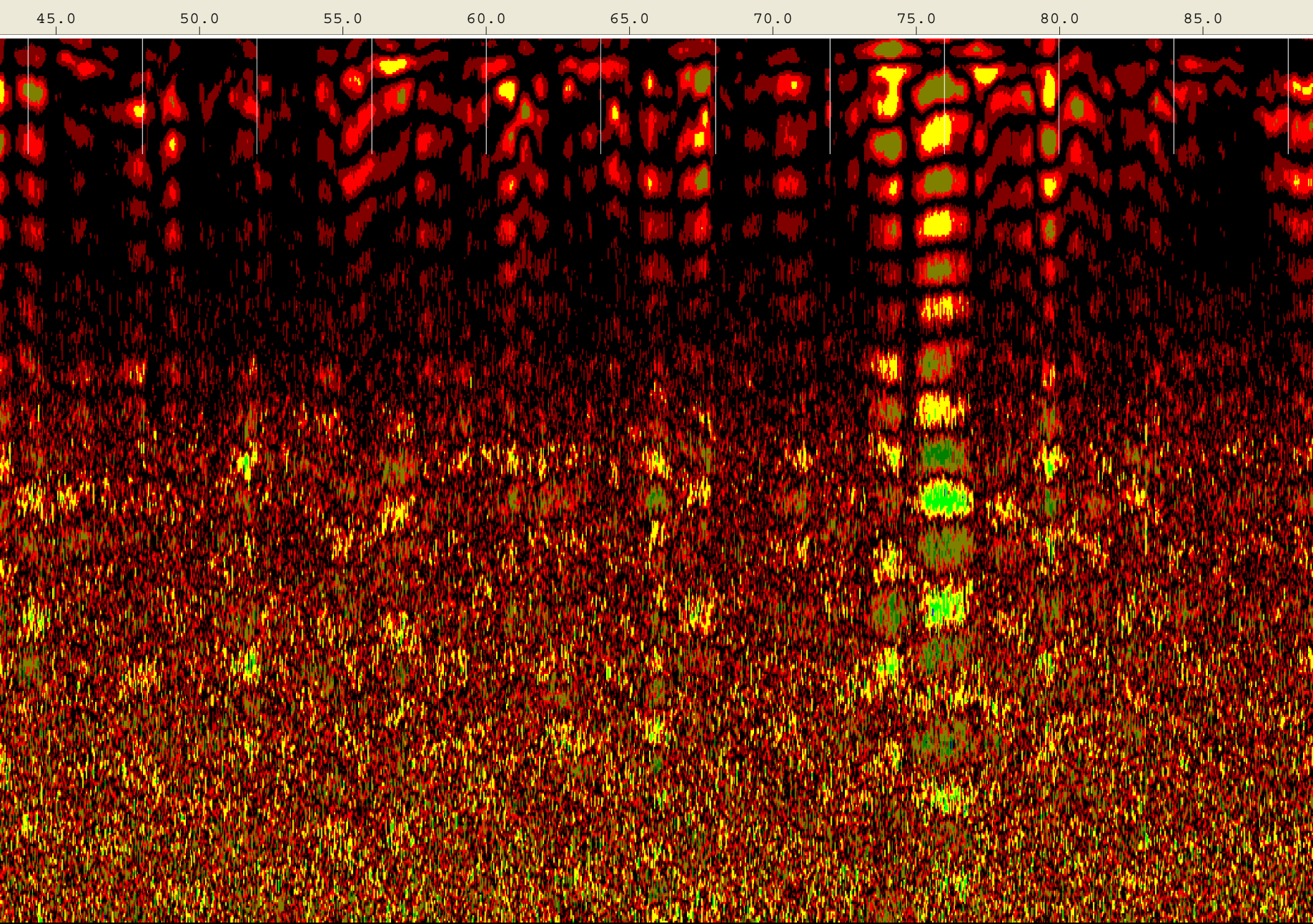


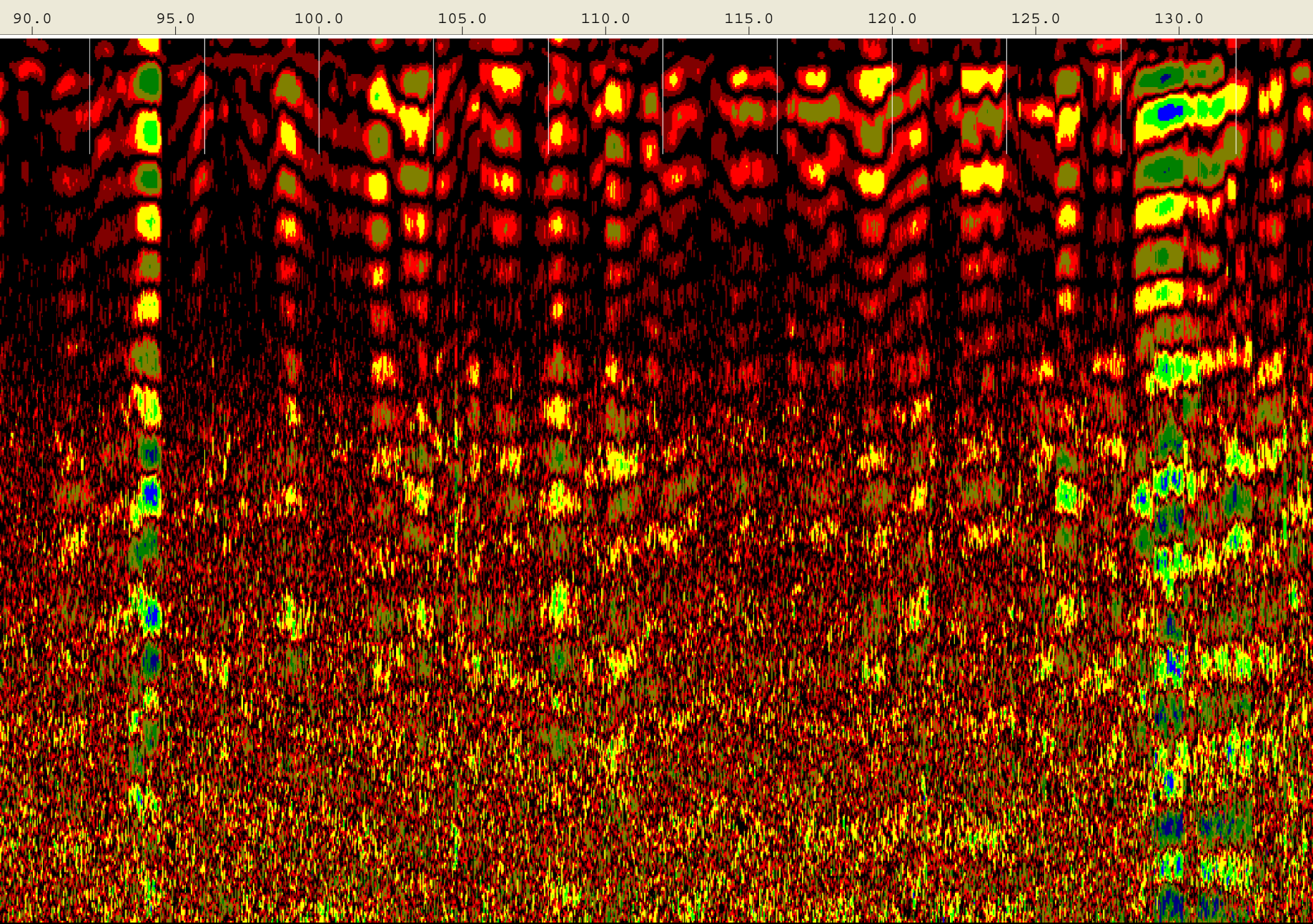


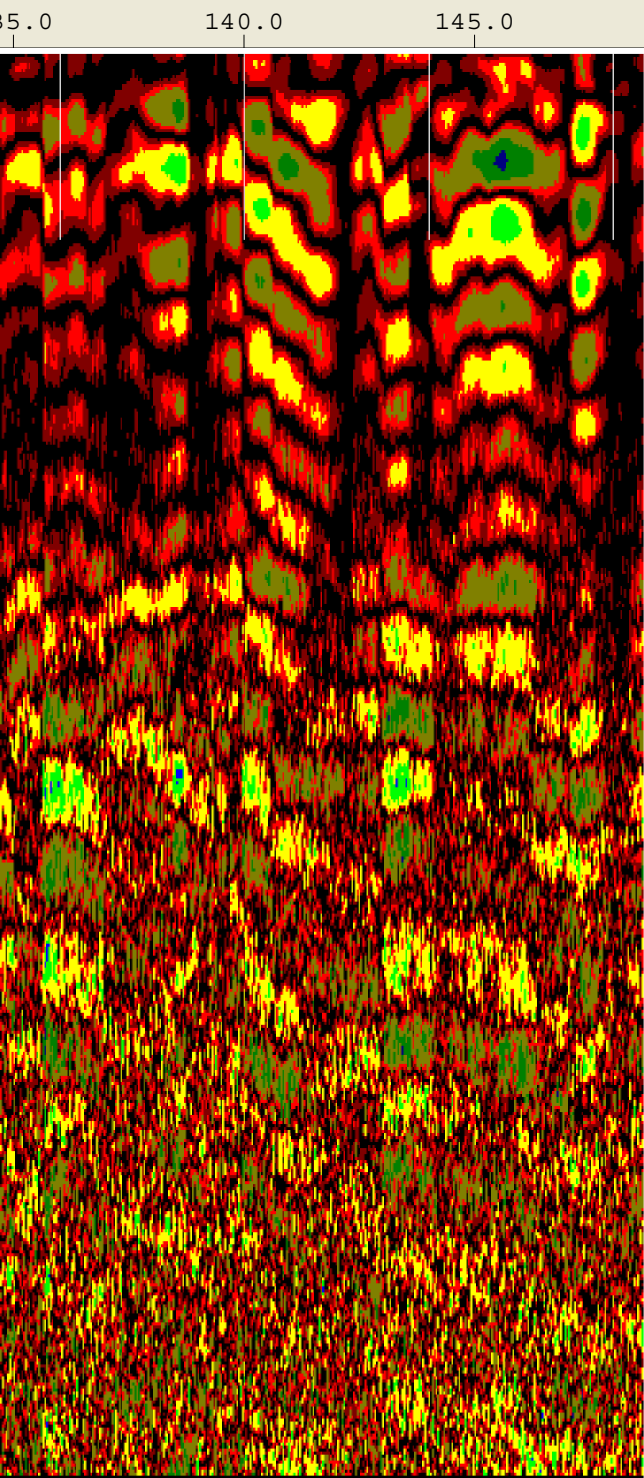
Created Jun, 19 2008, 12:01:44 Modified Jun, 19 2008, 12:06:14
Channel(s) 1 Samples/Scan 512 Bits/Sample 16
Scans/Second 100 Scans/Meter 78.7402 Meters/Mark 1.2192
Diel Constant 4.173

CHANNEL 1 400MHz
Position 3.54 nS Range 49 nS
Range Gain (dB) -1.0 31.0 38.0
Position Correction 1.04 nS
Vert IIR LP N =1 F =800 MHz
Vert IIR HP N =1 F =100 MHz
Position Correction 3.54 nS
Horz Boxcar Bkgr N=1023



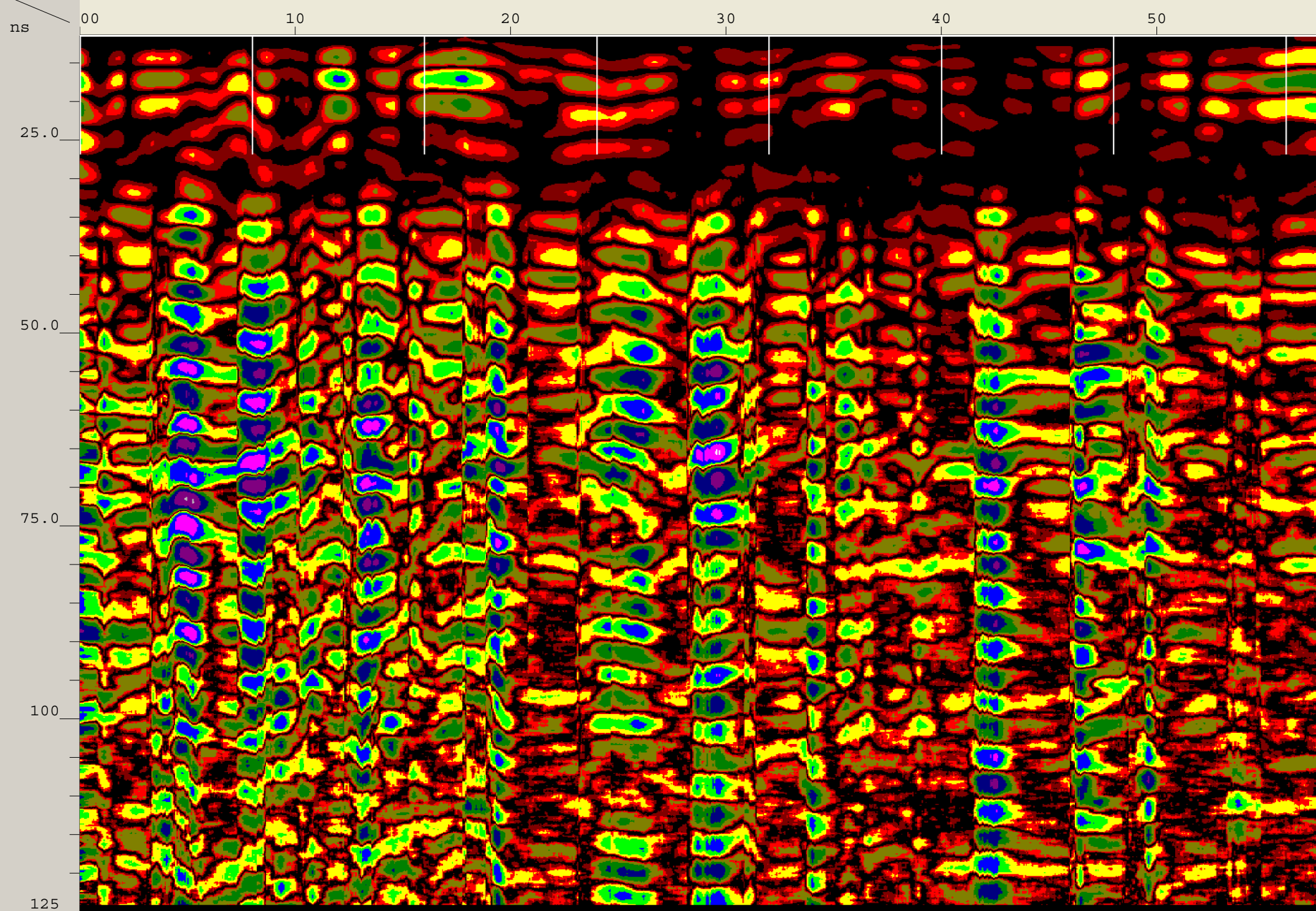




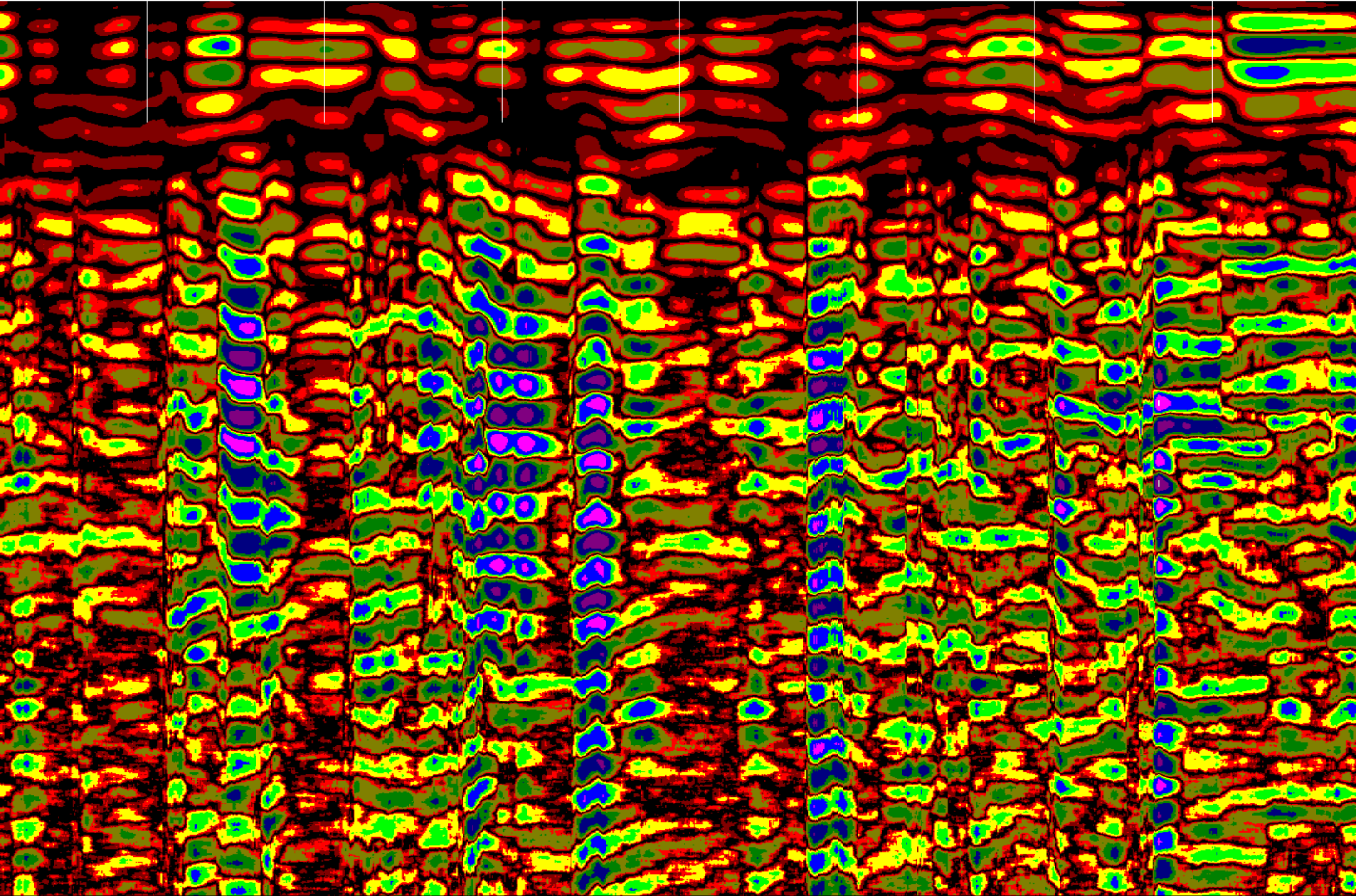


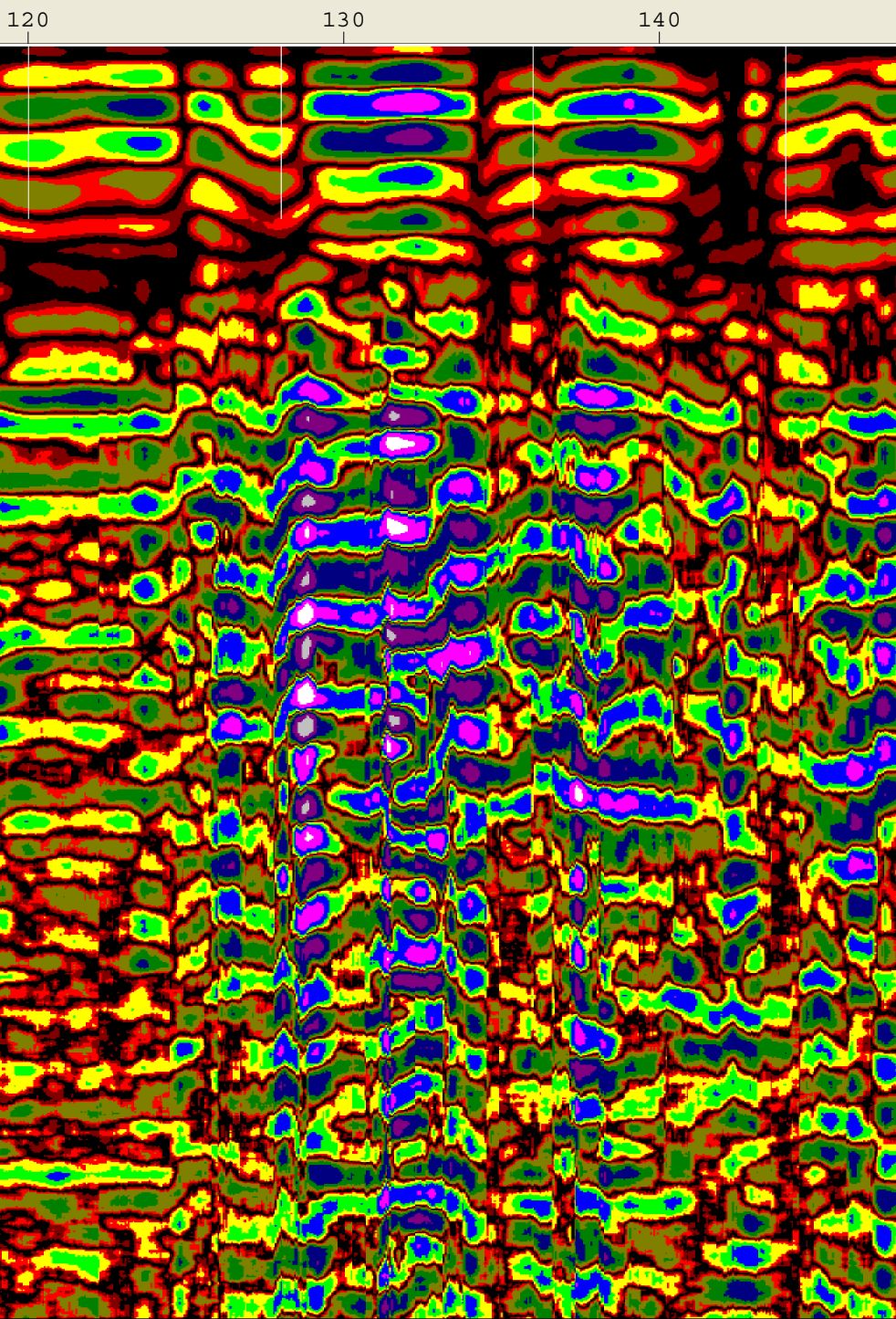
Created Jun, 19 2008, 11:30:52 Modified Jun, 19 2008, 11:35:08
Channel(s) 1 Samples/Scan 1024 Bits/Sample 16
Scans/Second 64 Scans/Meter 59.0551 Meters/Mark 2.4384
Diel Constant 6

CHANNEL 1 270MHz
Position 11.38 nS Range 124 nS
Vert IIR LP N =1 F =700 MHz
Vert IIR HP N =1 F =75 MHz
Horz IIR Stack TC =11
Position Correction -4.725 nS
Range Gain (dB) -18.0 50.0 54.0
Position Correction 11.38 nS
Horz Boxcar Bkgr N=1023
Range Gain (L) 1.0 4.4 1.0
1.0 1.0 1.0



60 70 80 90 100 110





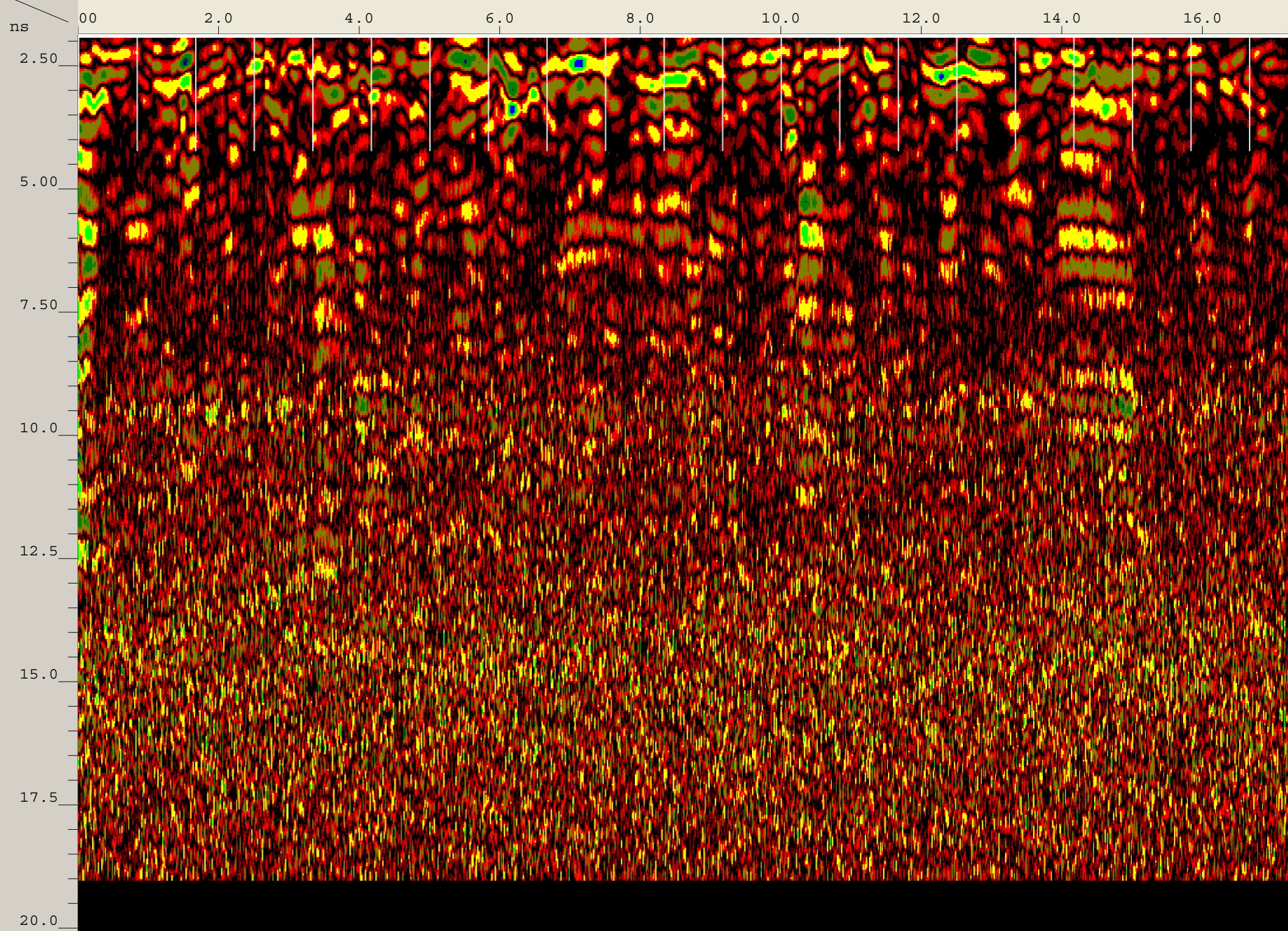
120

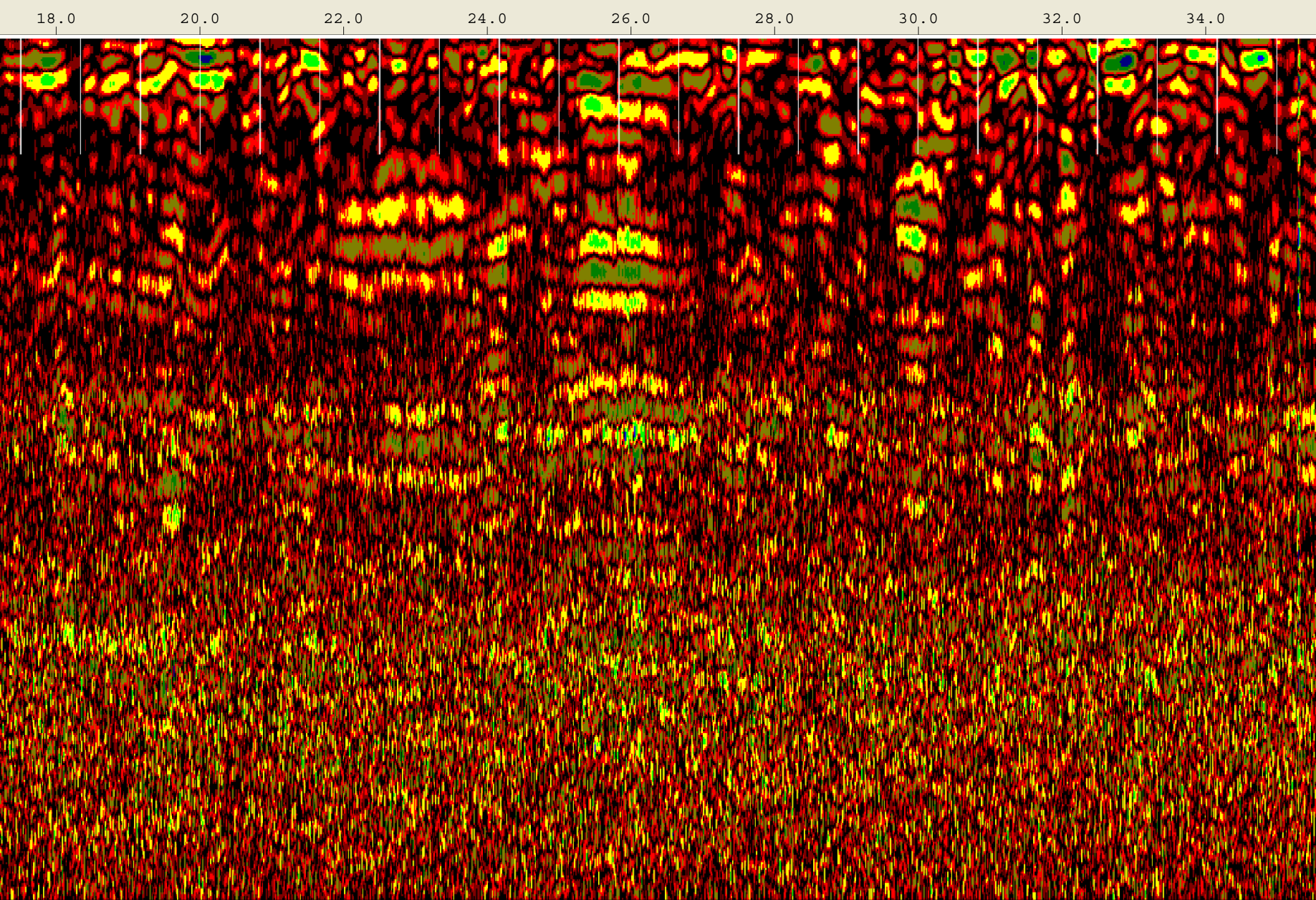
130

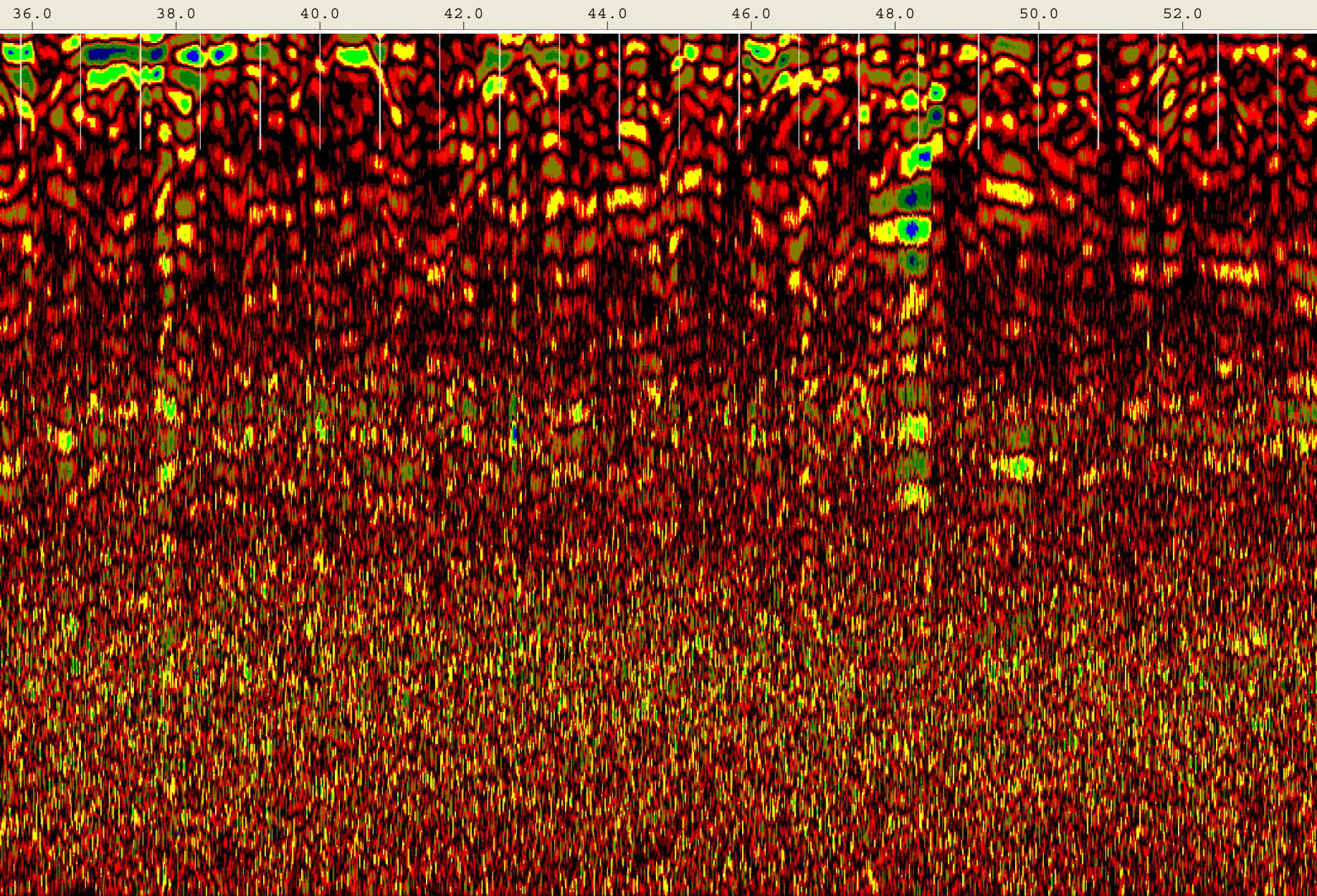
140

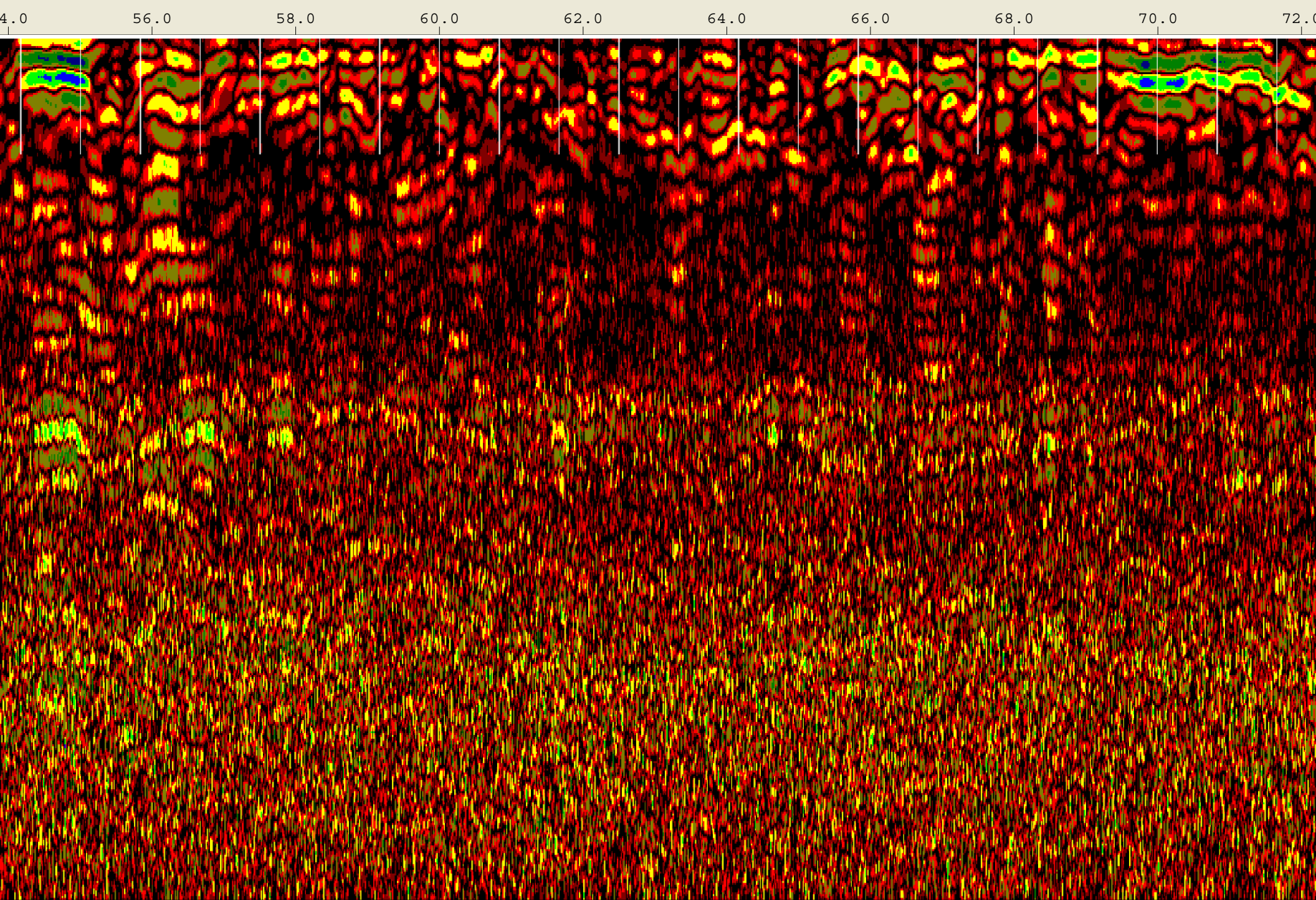
Created Jun, 19 2008, 13:10:52 Modified Jun, 19 2008, 13:15:40
Channel(s) 1 Samples/Scan 512 Bits/Sample 16
Scans/Second 100 Scans/Meter 196.85 Meters/Mark 0.254
Diel Constant 14.9009

CHANNEL 1 1.5/1.6GHz
Position 1.86 nS Range 19 nS
Range Gain (dB) -14.0 10.0 31.0
31.0 31.0
Position Correction 6.9 nS
Vert IIR HP N =1 F =10 MHz
Vert Boxcar LP F =1930 MHz
Vert Boxcar HP F =295 MHz
Position Correction 1.86 nS
Horz Boxcar Bkgr N=1023
Range Gain (L) 2.3 3.4 1.4
1.1 2.1 1.8
1.0









74.0

76.0

78.0

80.0

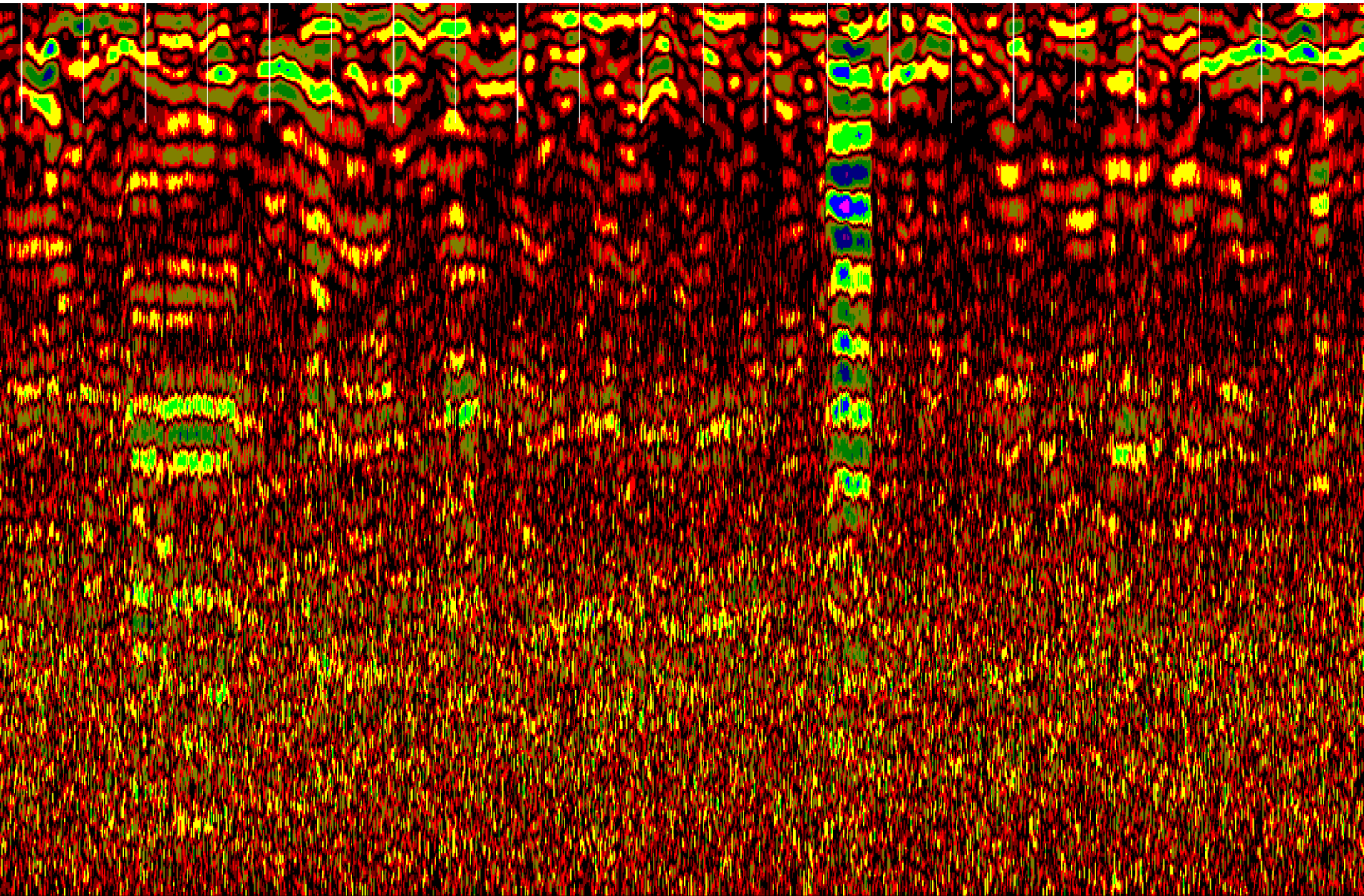
82.0

84.0

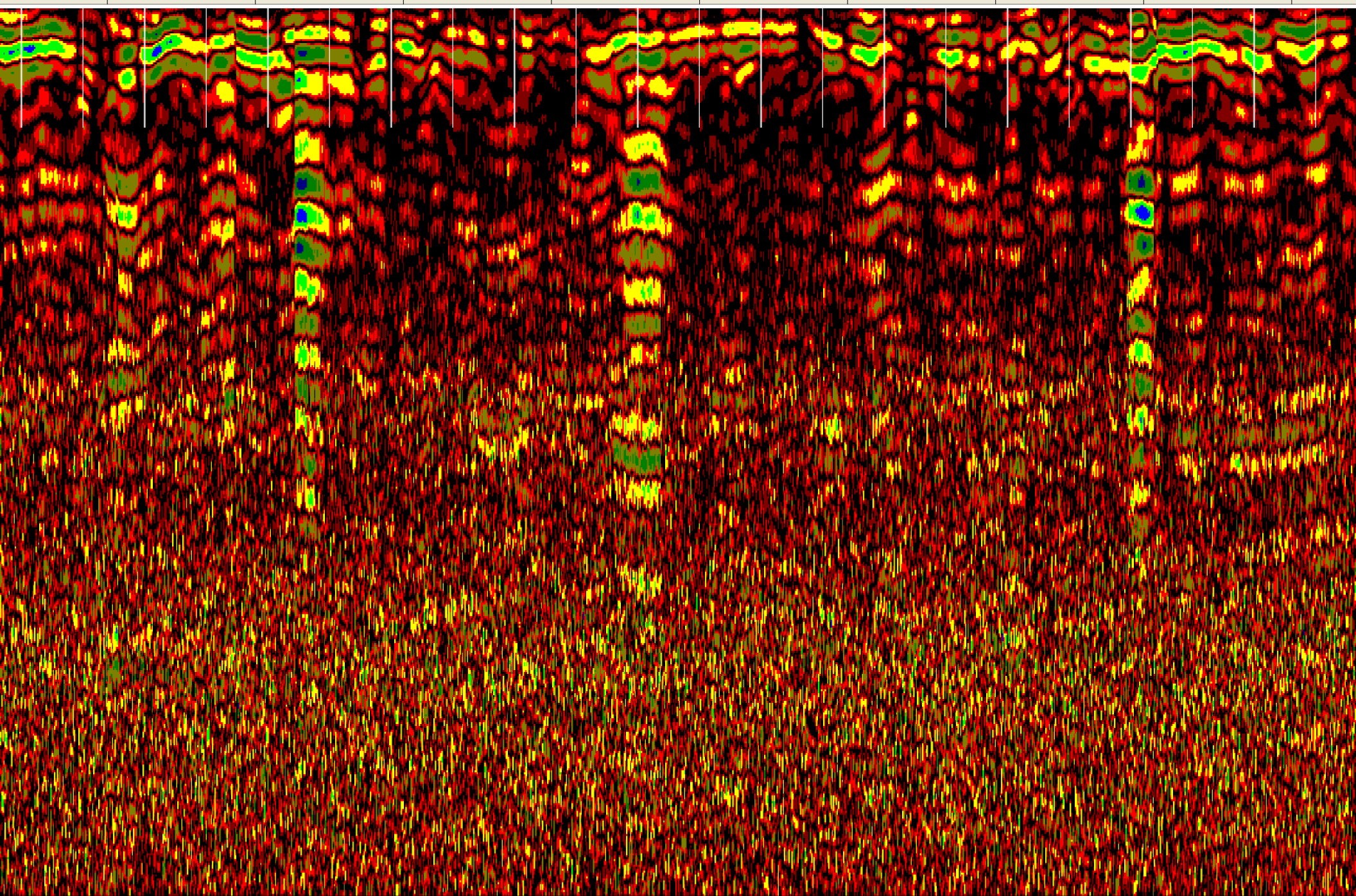
86.0

88.0

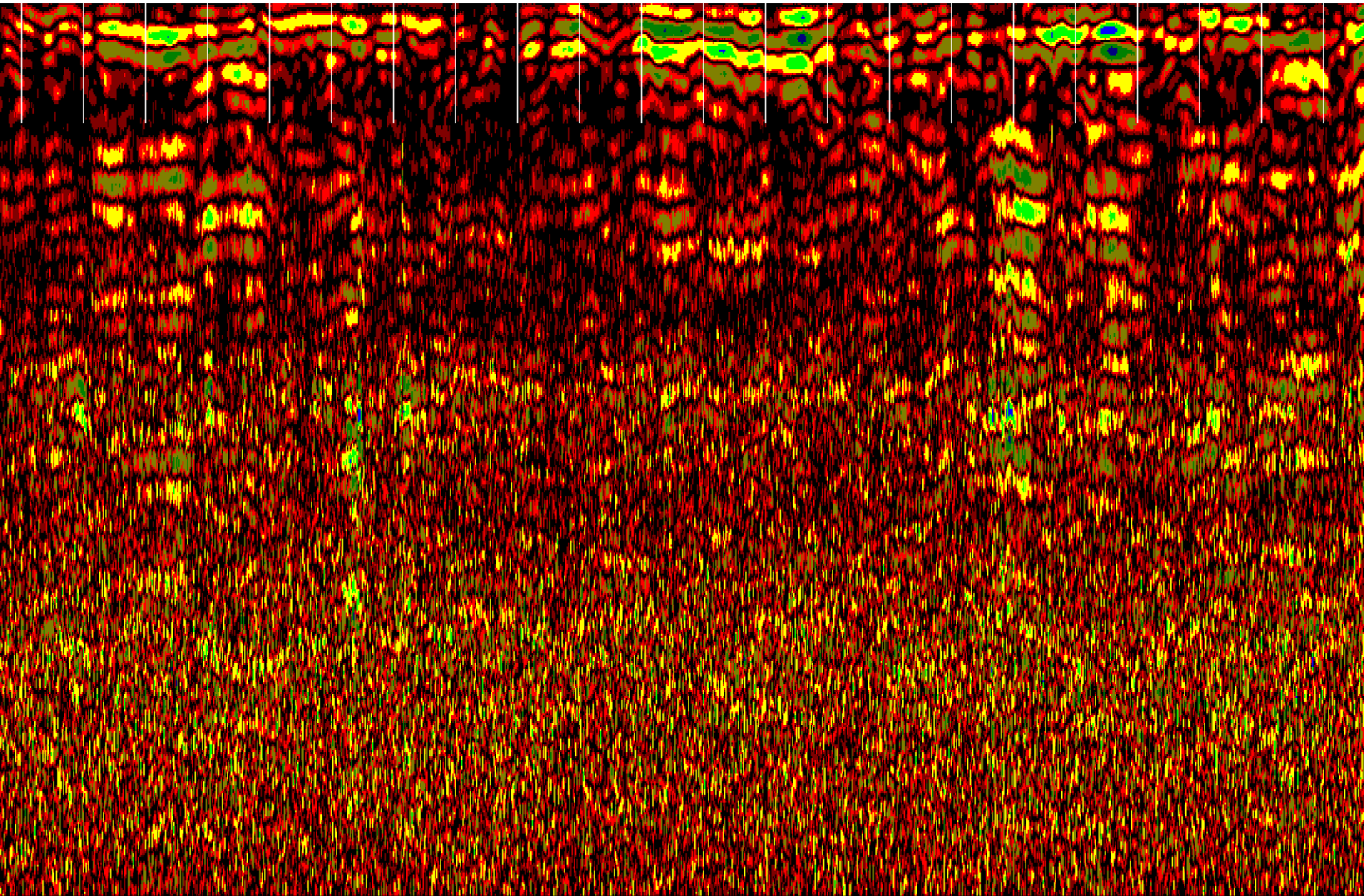
90.0

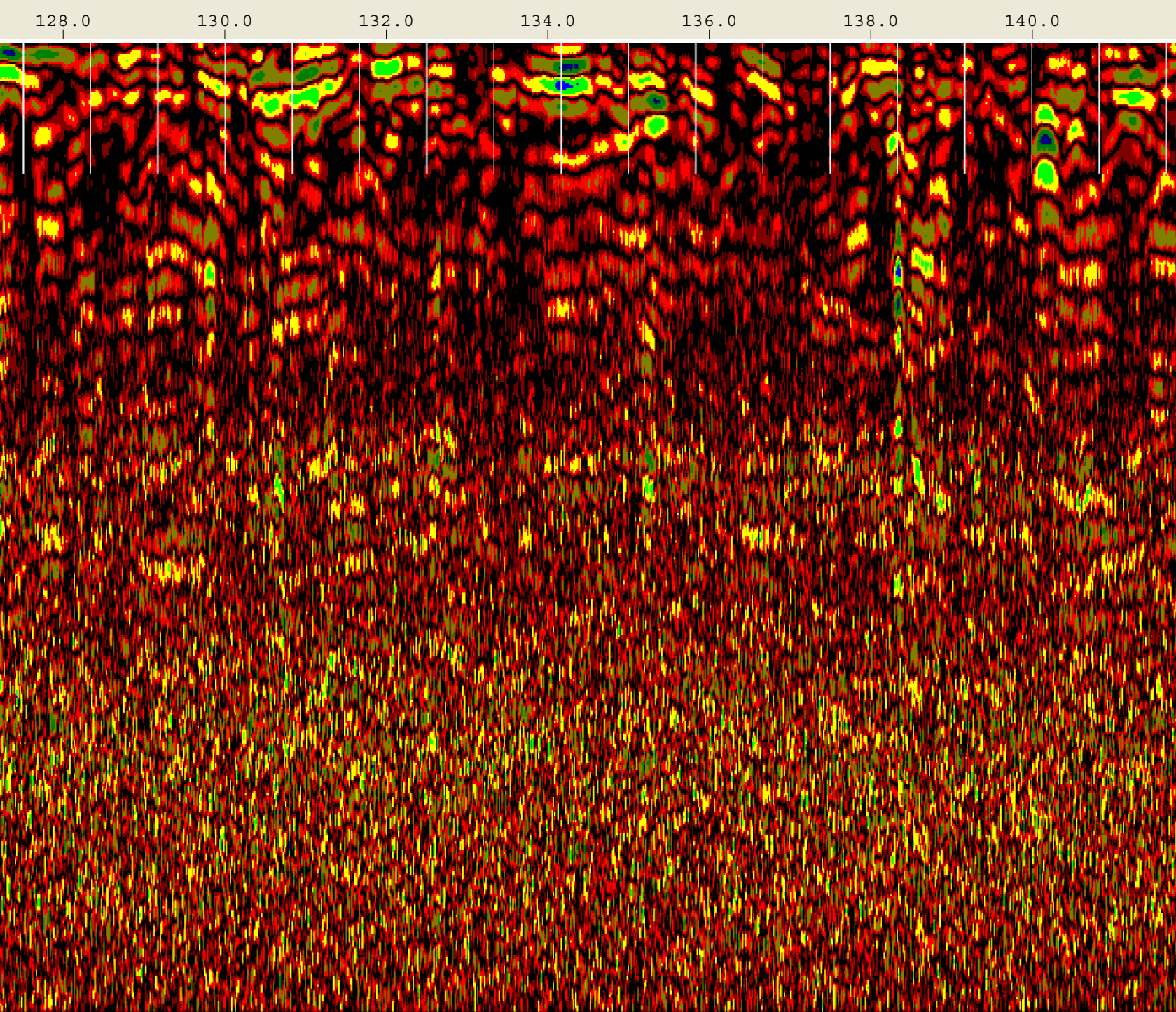


92.0 94.0 96.0 98.0 100.0 102.0 104.0 106.0 108.0



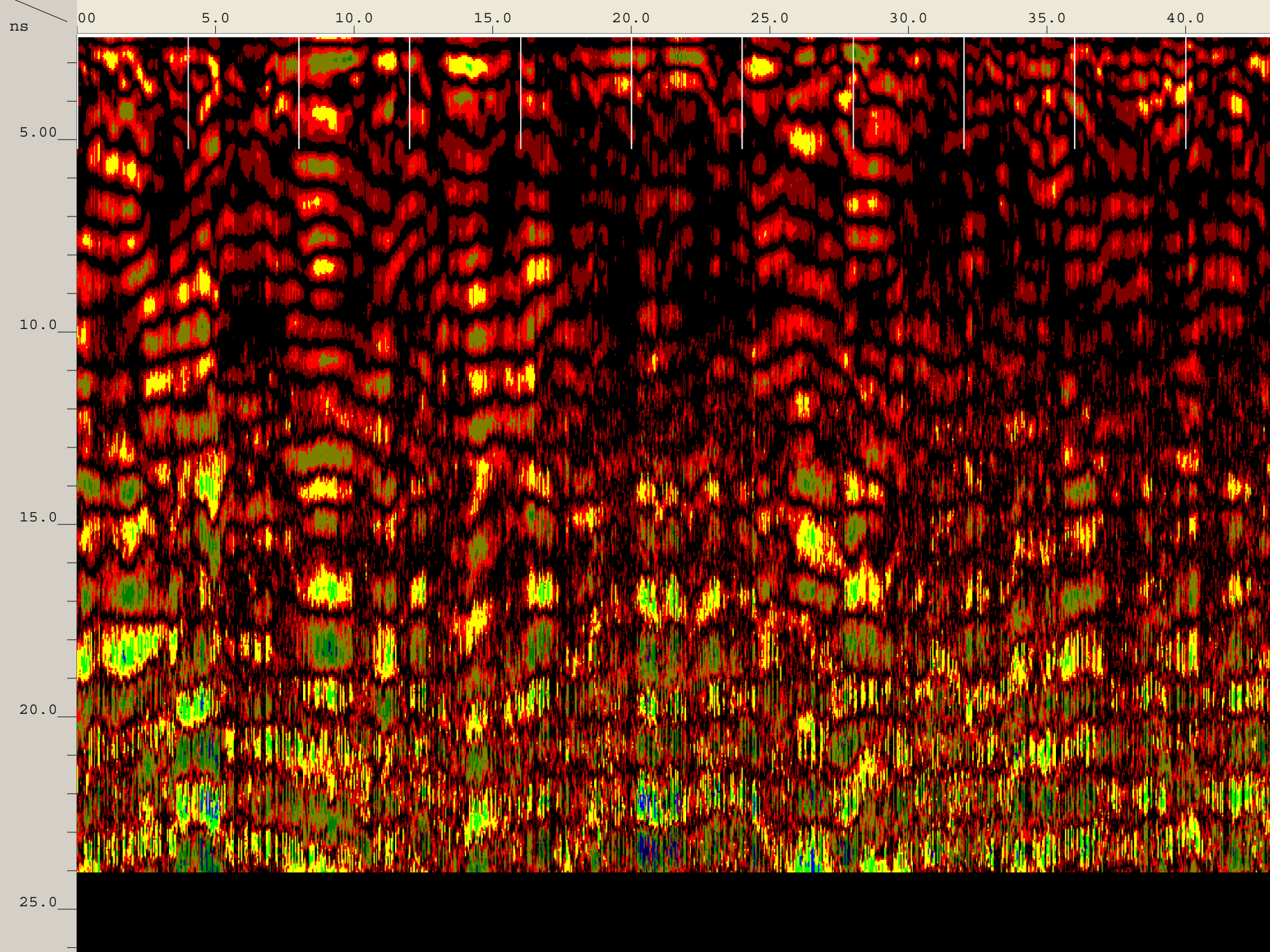
110.0 112.0 114.0 116.0 118.0 120.0 122.0 124.0 126.0



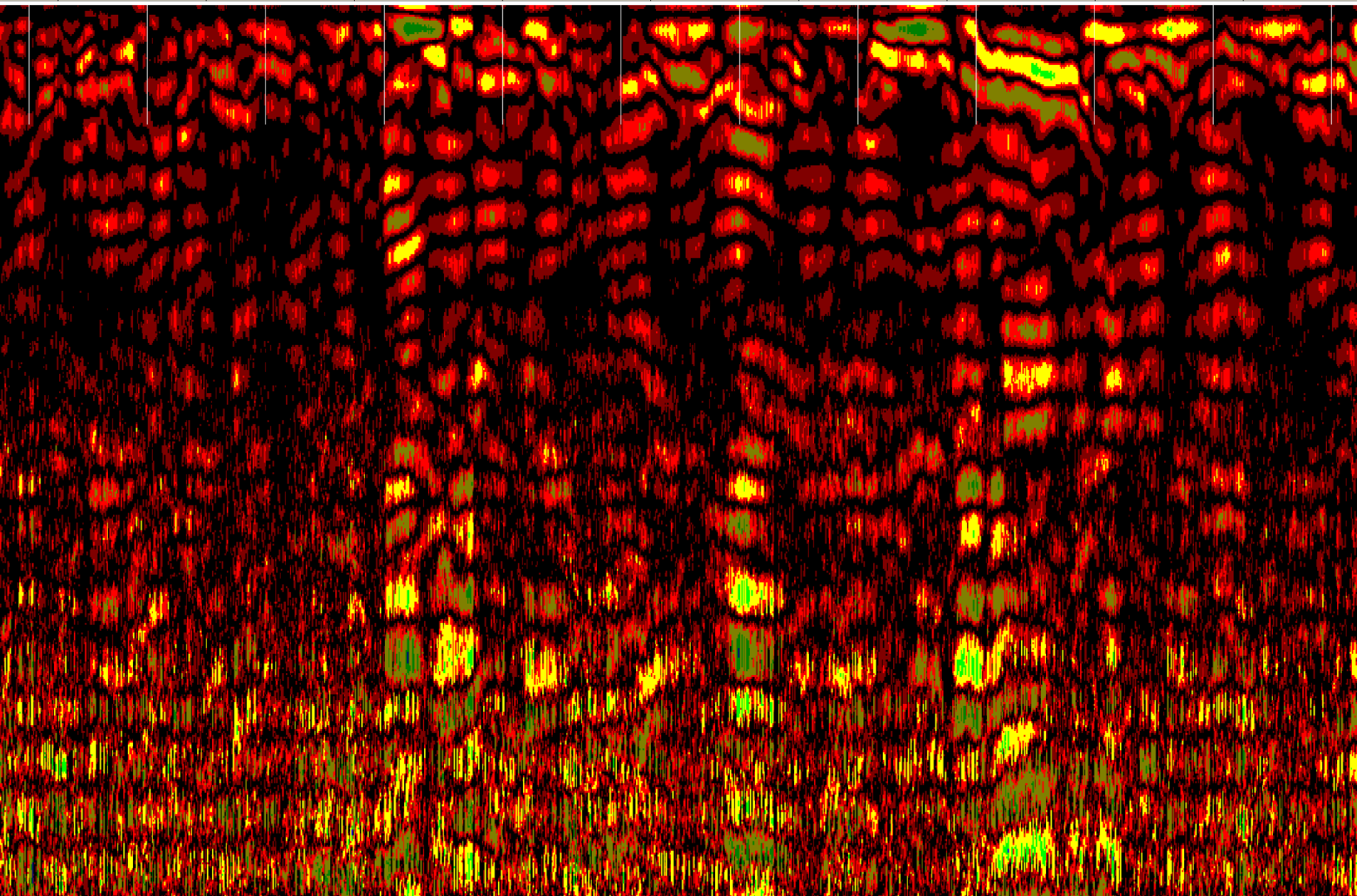


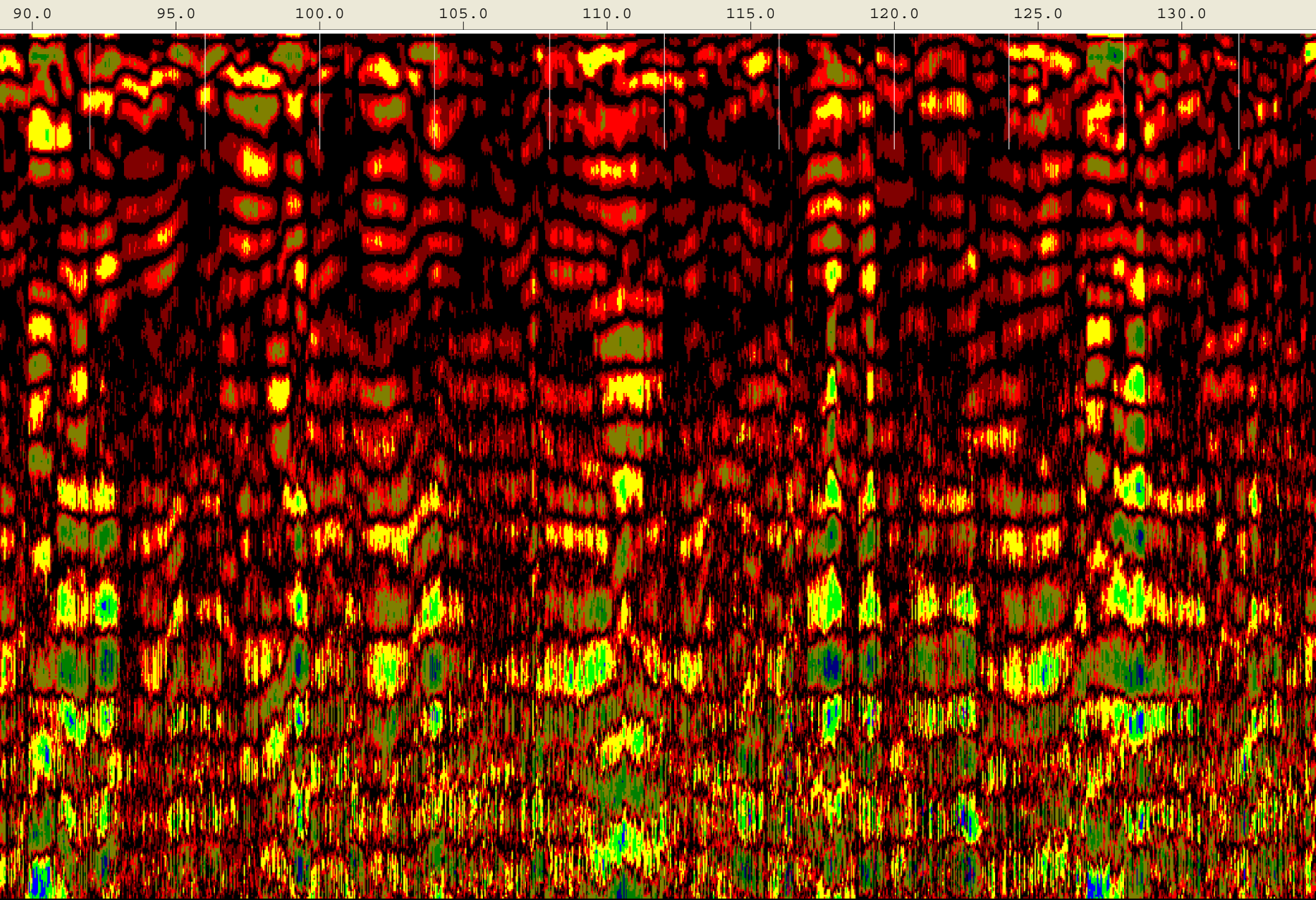
Created Jun, 19 2008, 12:16:58 Modified Jun, 19 2008, 12:21:00
Channel(s) 1 Samples/Scan 512 Bits/Sample 16
Scans/Second 100 Scans/Meter 78.7402 Meters/Mark 1.2192
Diel Constant 7.5818

CHANNEL 1 900MHz
Position 2.25 nS Range 24 nS
Position Correction 1.04 nS
Vert IIR LP N =1 F =2500 MHz
Vert IIR HP N =1 F =225 MHz
Range Gain (dB) 2.0 34.0 42.0
Position Correction 2.25 nS
Horz Boxcar Bkgr N=1023
Auto Gain N=1
G=0 TC=0

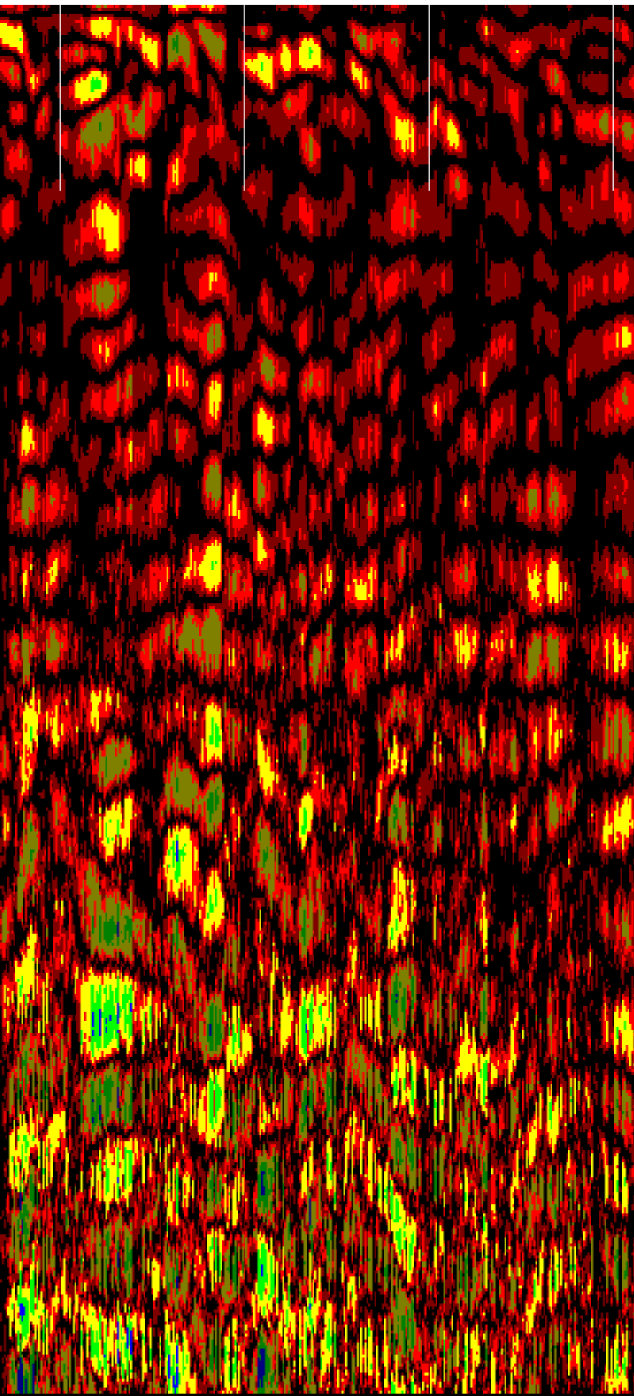


45.0 50.0 55.0 60.0 65.0 70.0 75.0 80.0 85.0



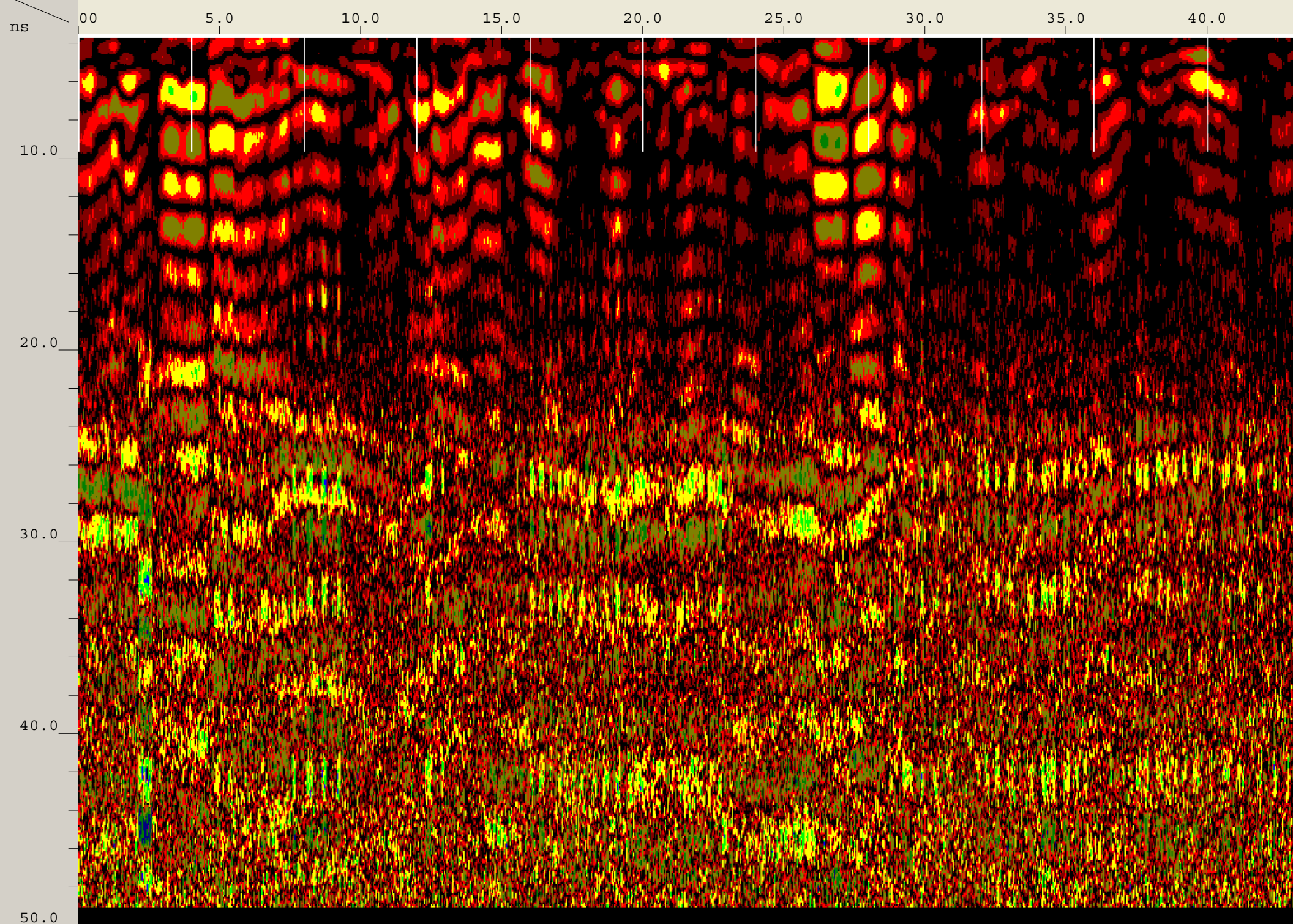


135.0 140.0 145.0

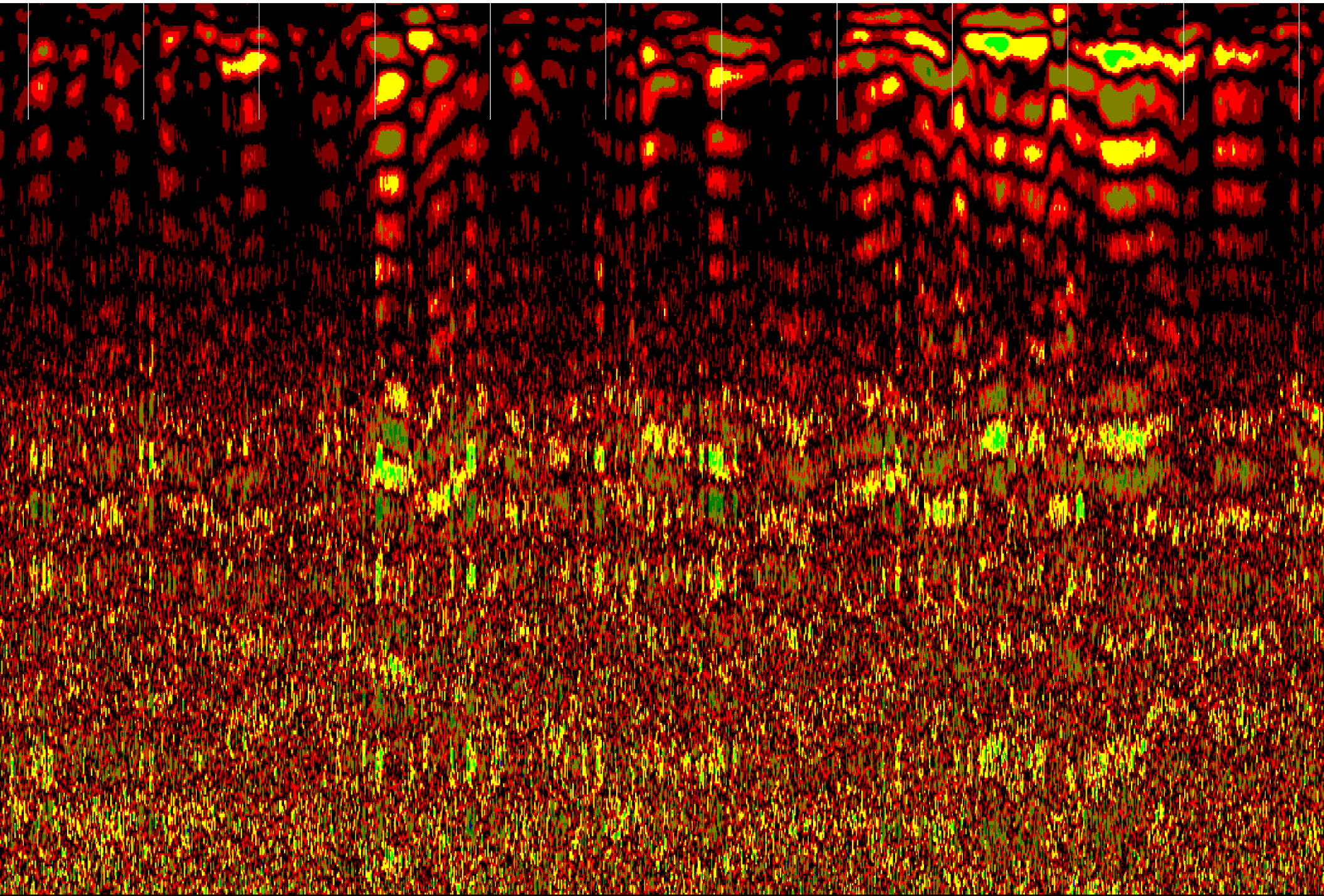


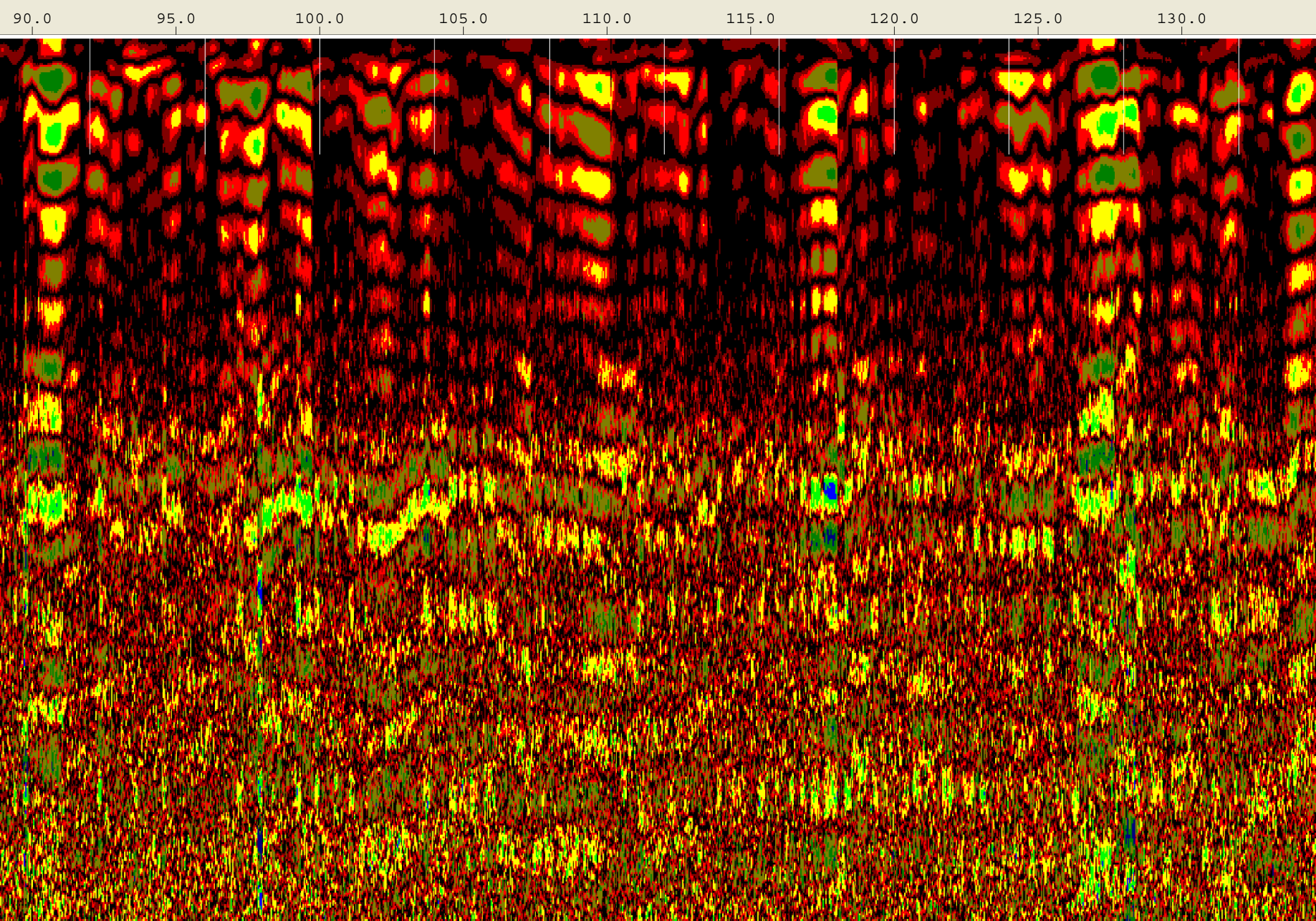
Created Jun, 19 2008, 11:57:58 Modified Jun, 19 2008, 12:01:38
Channel(s) 1 Samples/Scan 512 Bits/Sample 16
Scans/Second 100 Scans/Meter 78.7402 Meters/Mark 1.2192
Diel Constant 7.50463

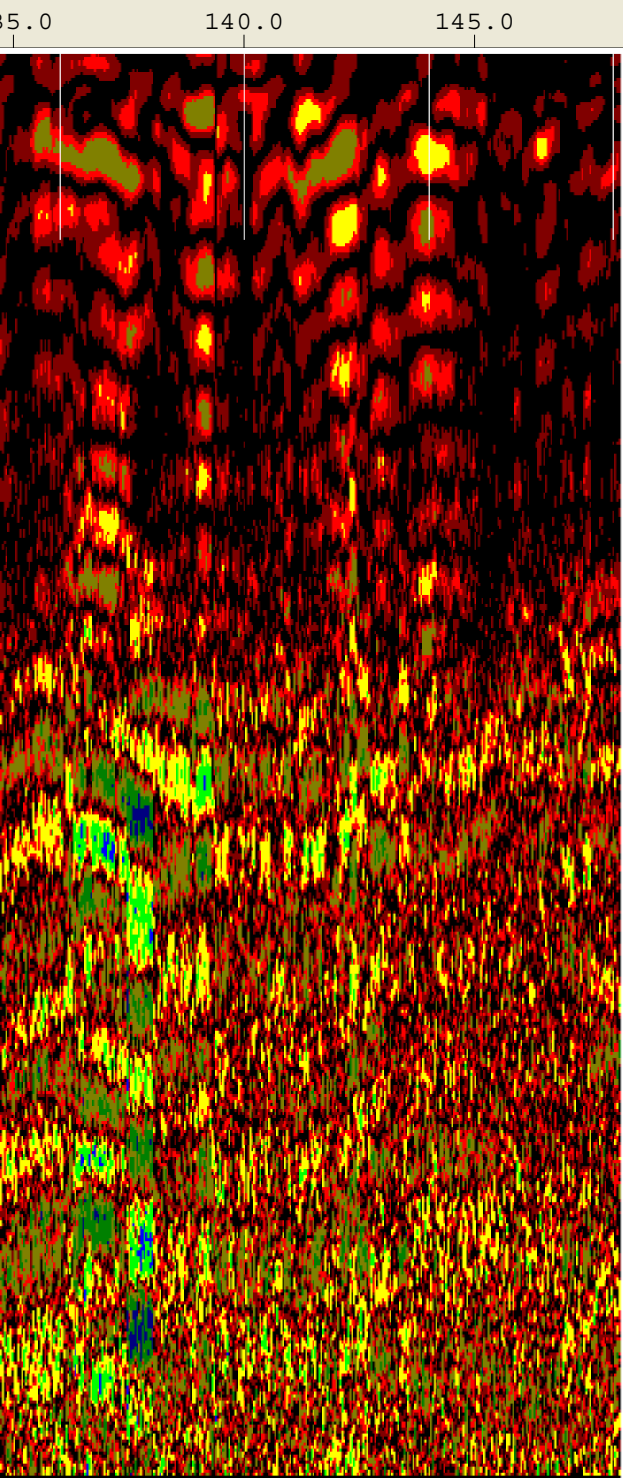
CHANNEL 1 400MHz
Position 3.54 nS Range 49 nS
Range Gain (dB) -1.0 31.0 38.0
Position Correction 1.04 nS
Vert IIR LP N =1 F =800 MHz
Vert IIR HP N =1 F =100 MHz
Position Correction 3.54 nS
Horz Boxcar Bkgr N=1023



45.0 50.0 55.0 60.0 65.0 70.0 75.0 80.0 85.0

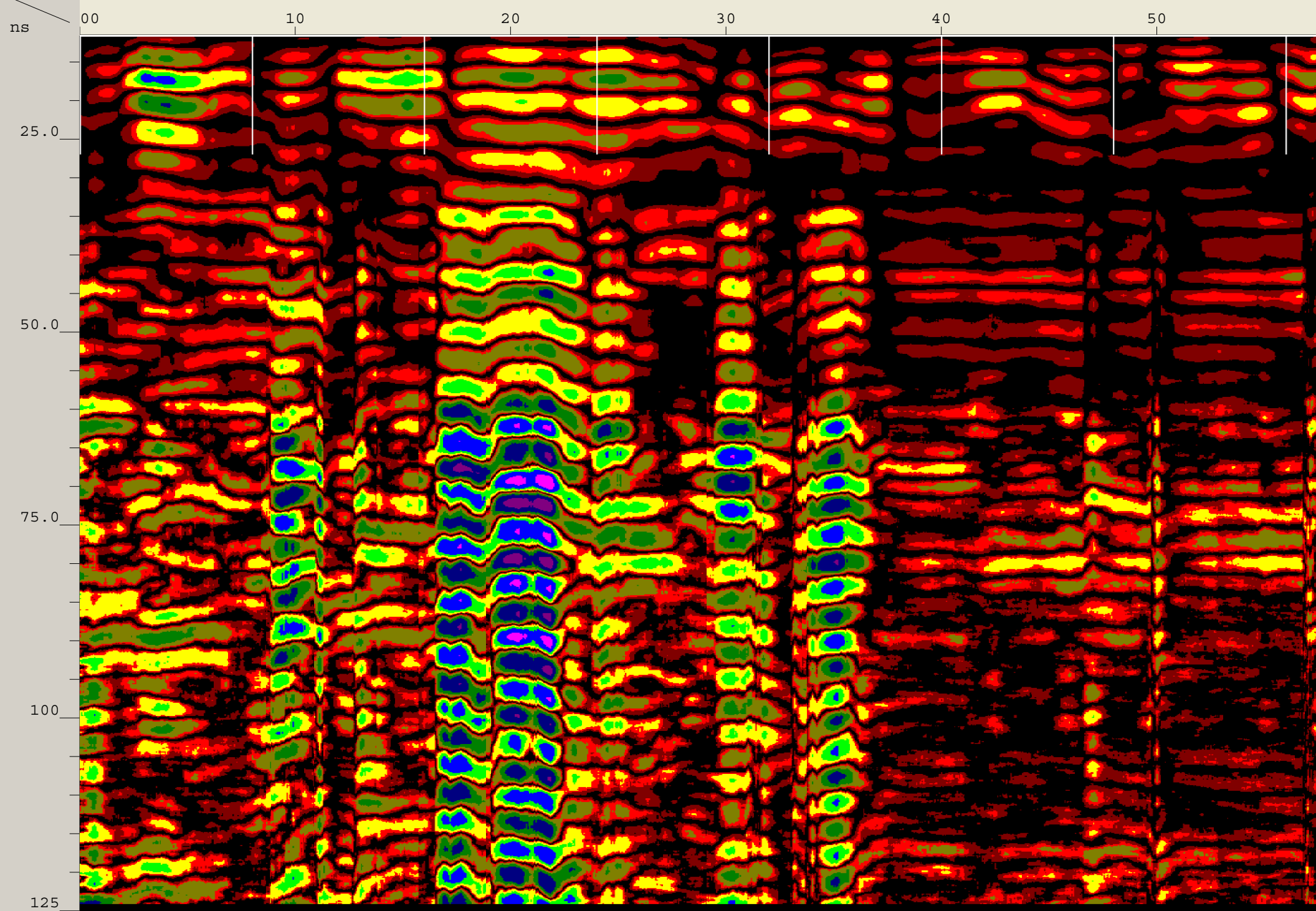




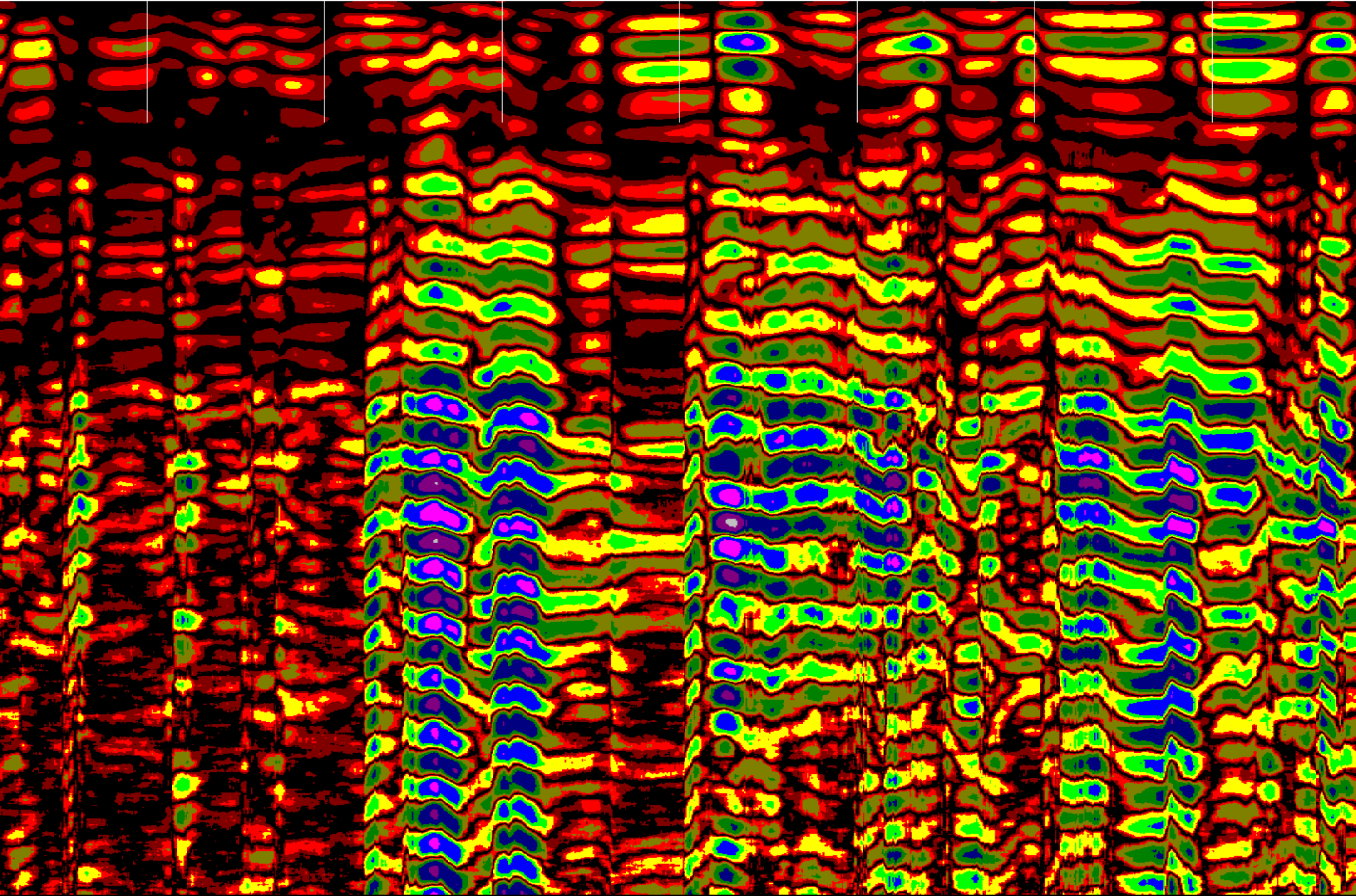


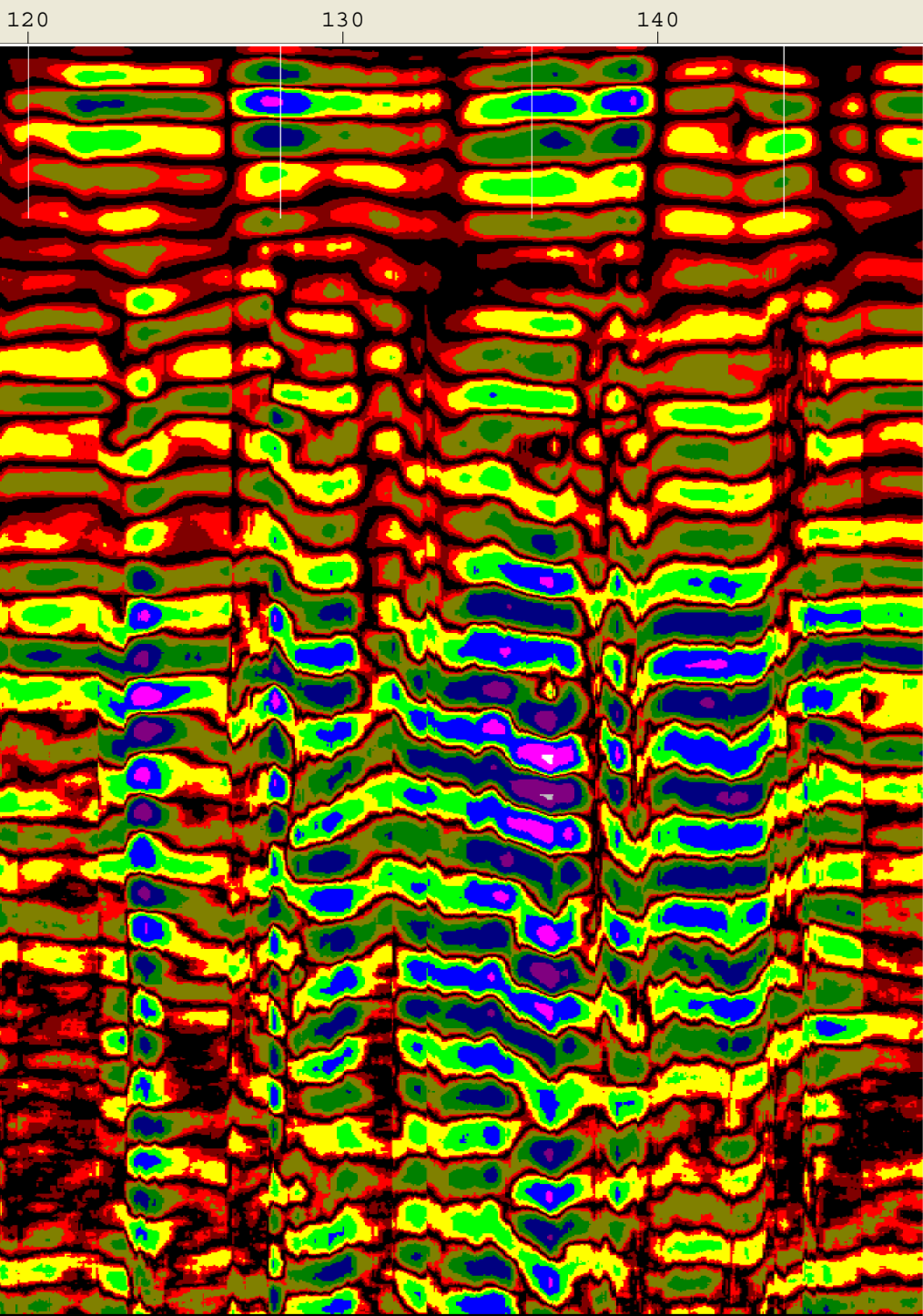
Created Jun, 19 2008, 11:35:14 Modified Jun, 19 2008, 11:39:00
Channel(s) 1 Samples/Scan 1024 Bits/Sample 16
Scans/Second 64 Scans/Meter 59.0551 Meters/Mark 2.4384
Diel Constant 6

CHANNEL 1 270MHz
Position 11.5 nS Range 124 nS
Vert IIR LP N =1 F =700 MHz
Vert IIR HP N =1 F =75 MHz
Horz IIR Stack TC =11
Position Correction -4.725 nS
Range Gain (dB) -18.0 50.0 54.0
Position Correction 11.5 nS
Horz Boxcar Bkgr N=1023
Range Gain (L) 1.2 3.3 0.5
0.6 0.6 0.5
1.0



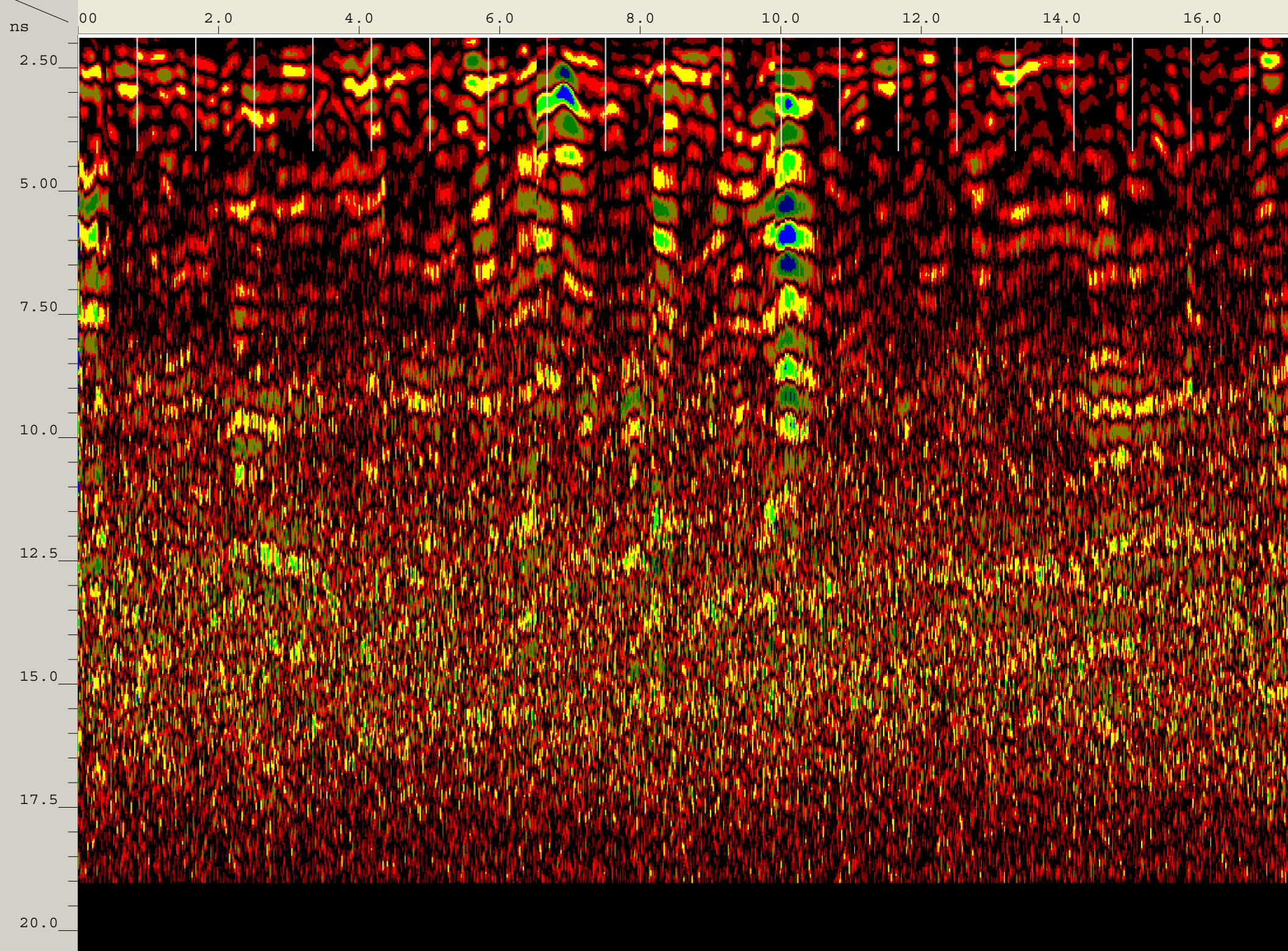
60 70 80 90 100 110

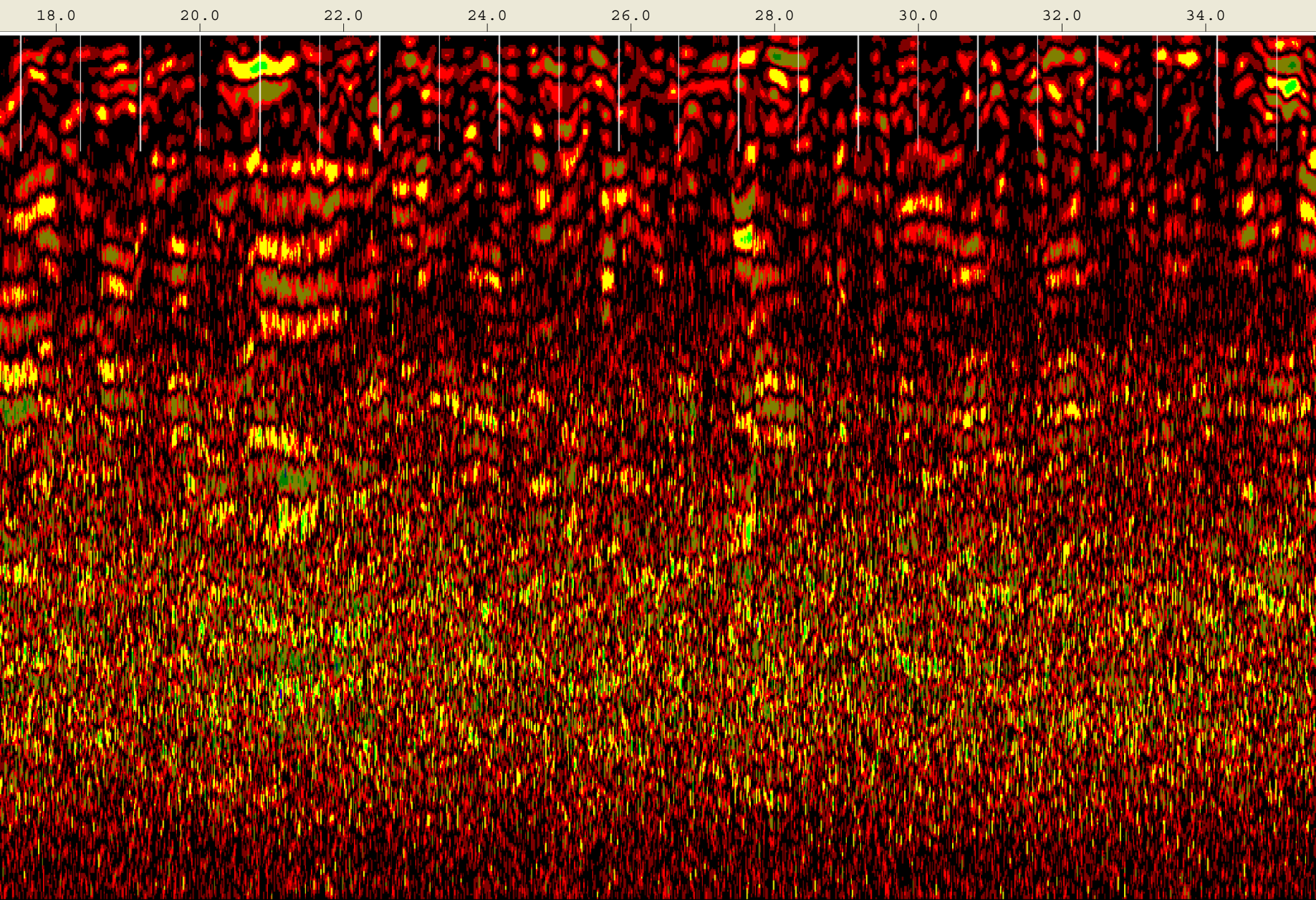


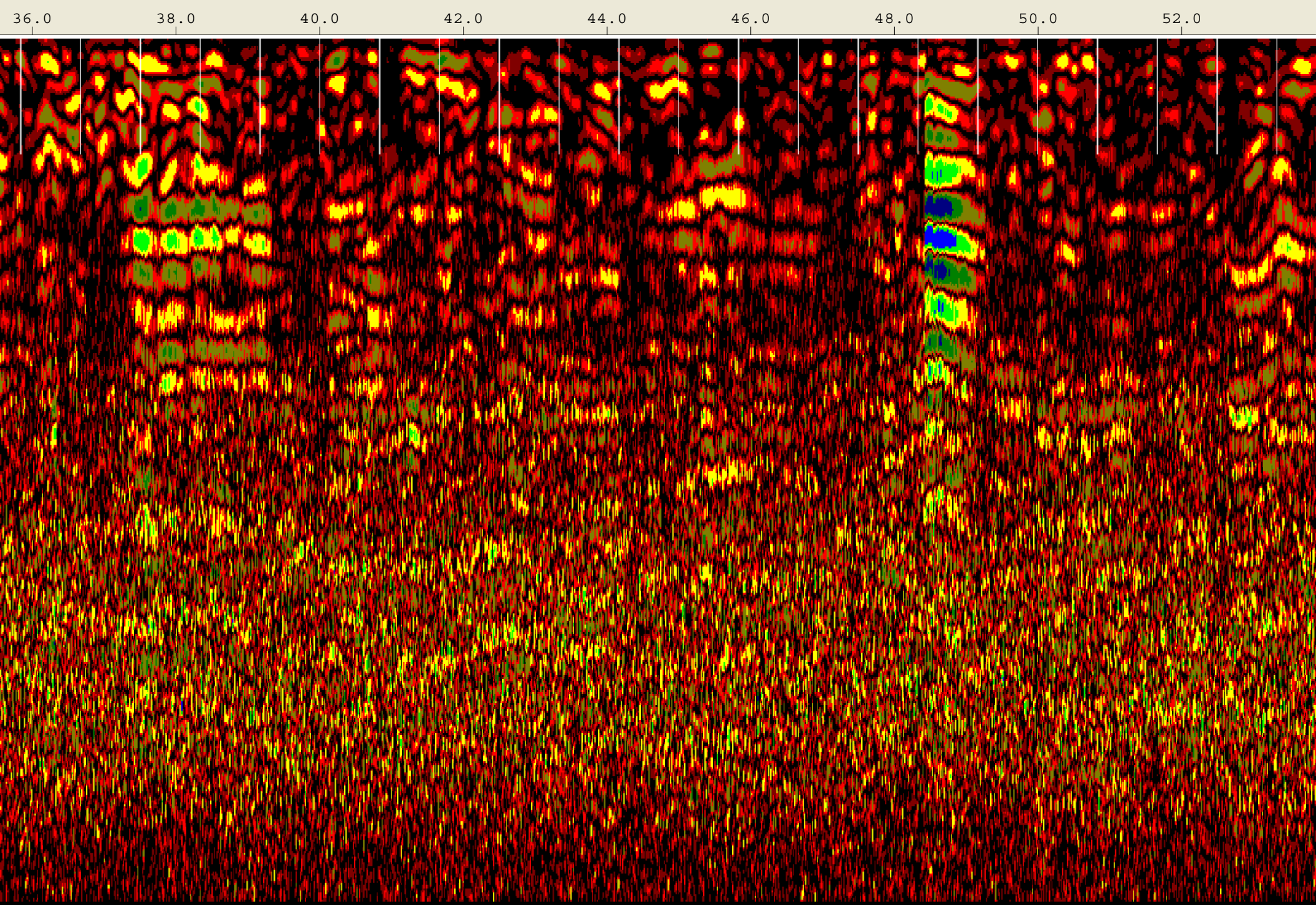


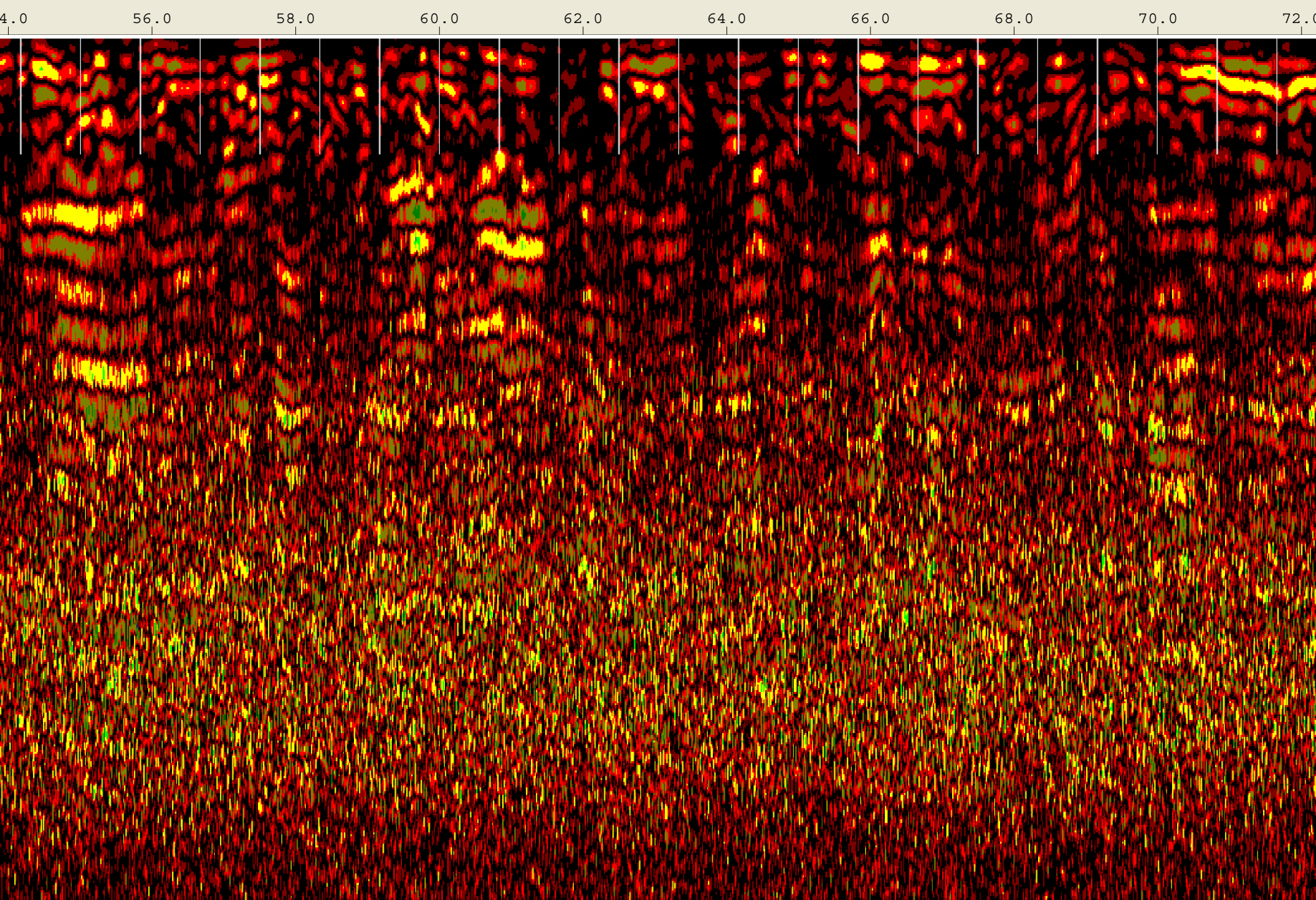
Created Jun, 19 2008, 13:28:22 Modified Jun, 19 2008, 13:33:36
Channel(s) 1 Samples/Scan 512 Bits/Sample 16
Scans/Second 100 Scans/Meter 196.85 Meters/Mark 0.254
Diel Constant 15.7472

CHANNEL 1 1.5/1.6GHz
Position 1.82 nS Range 19 nS
Range Gain (dB) -14.0 10.0 31.0
31.0 31.0
Position Correction 6.9 nS
Vert IIR HP N =1 F =10 MHz
Vert Boxcar LP F =1930 MHz
Vert Boxcar HP F =295 MHz
Position Correction 1.82 nS
Horz Boxcar Bkgr N=1023
Range Gain (L) 1.0 3.7 1.8
1.0 1.8 2.1
1.0 1.0









74.0

76.0

78.0

80.0

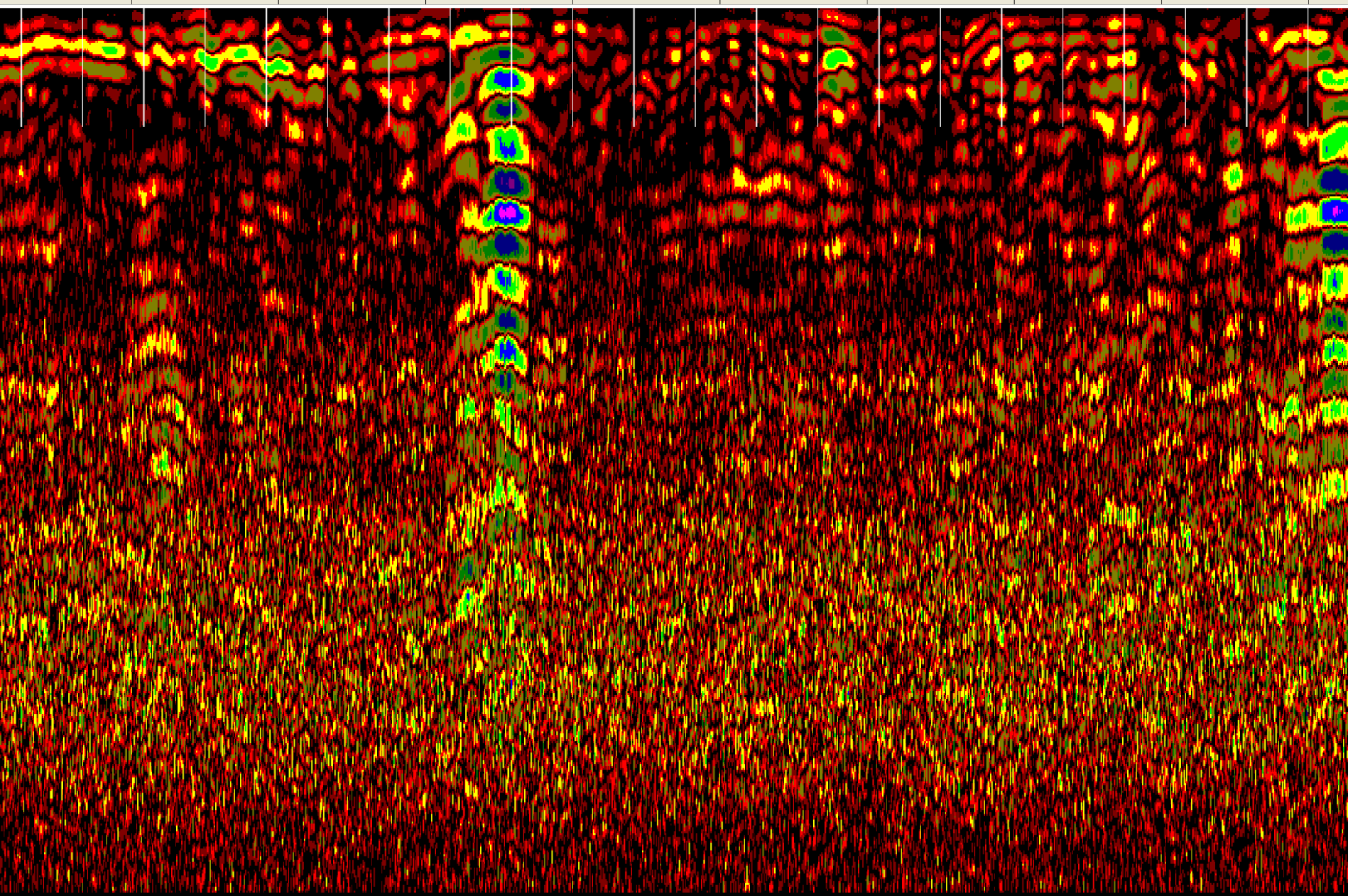
82.0

84.0

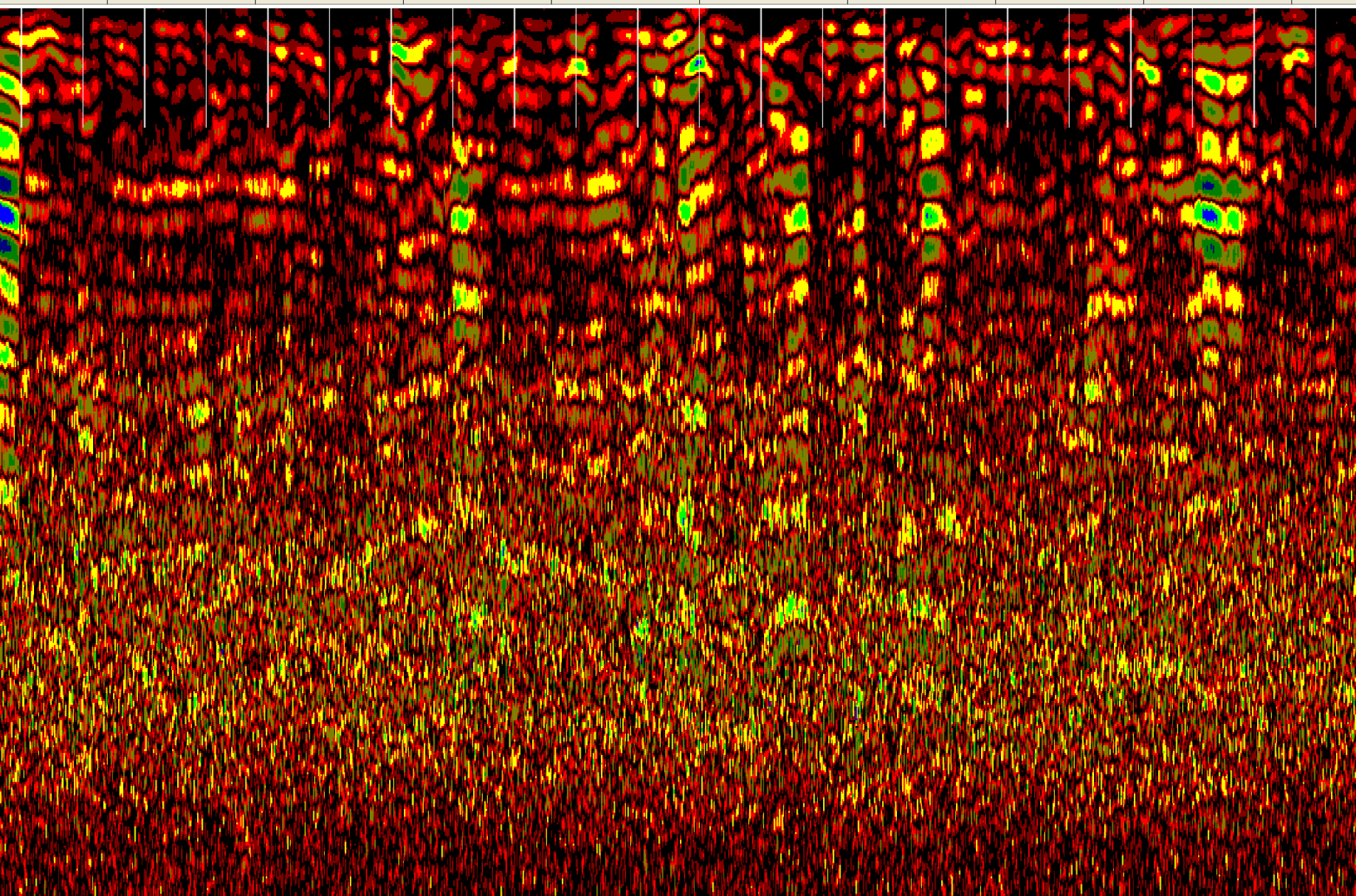
86.0

88.0

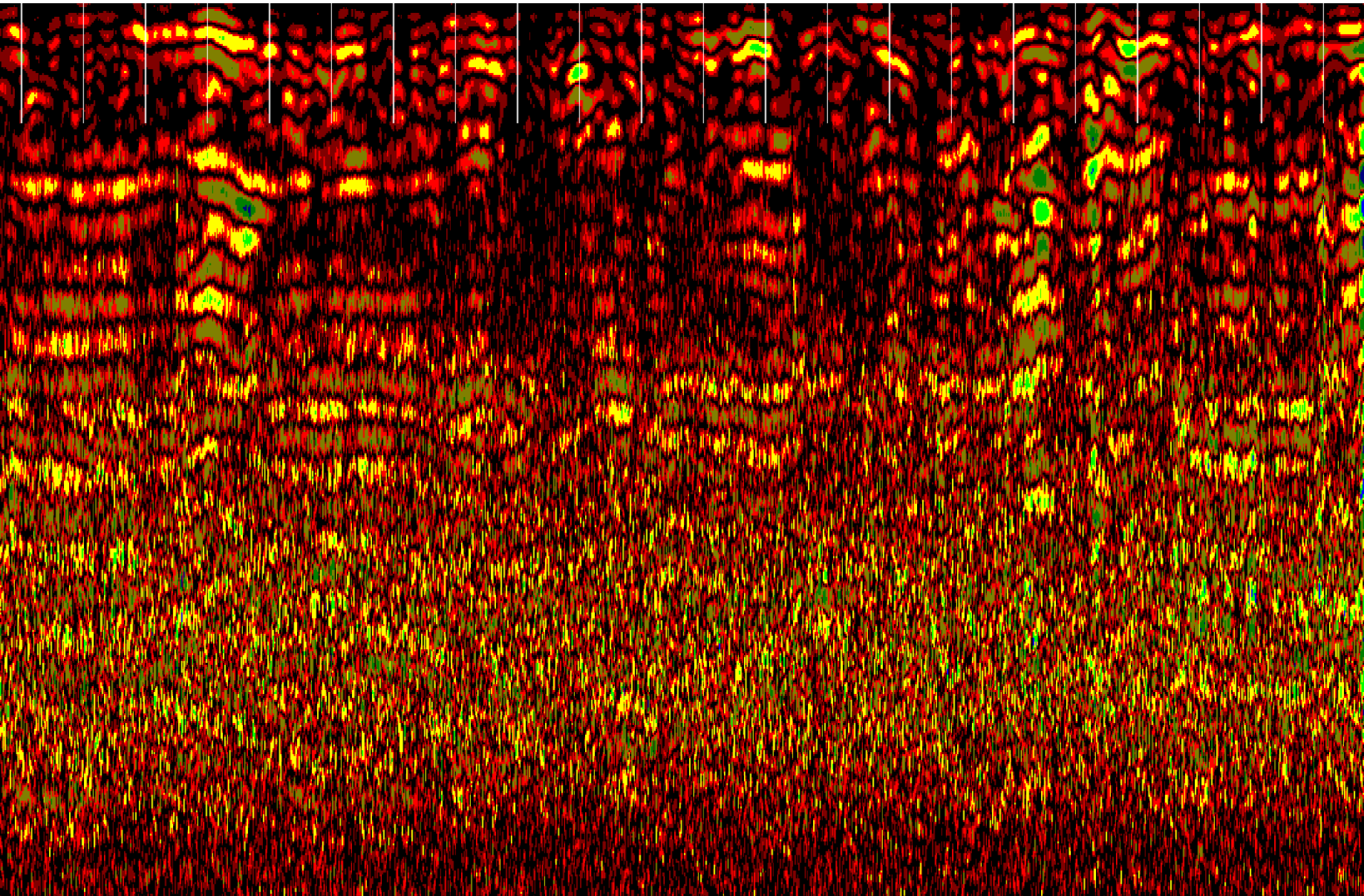
90.0

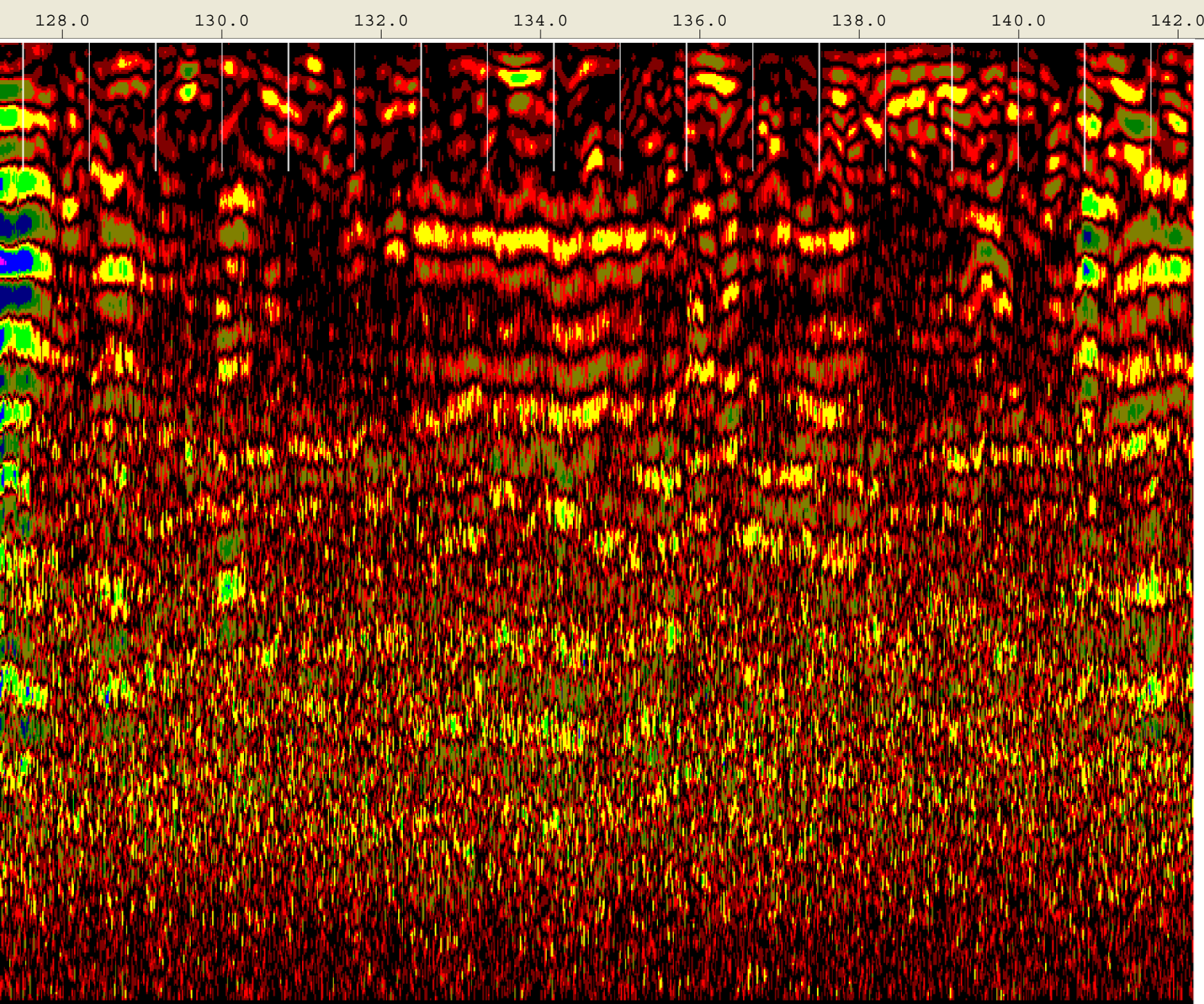


92.0 94.0 96.0 98.0 100.0 102.0 104.0 106.0 108.0



110.0 112.0 114.0 116.0 118.0 120.0 122.0 124.0 126.0

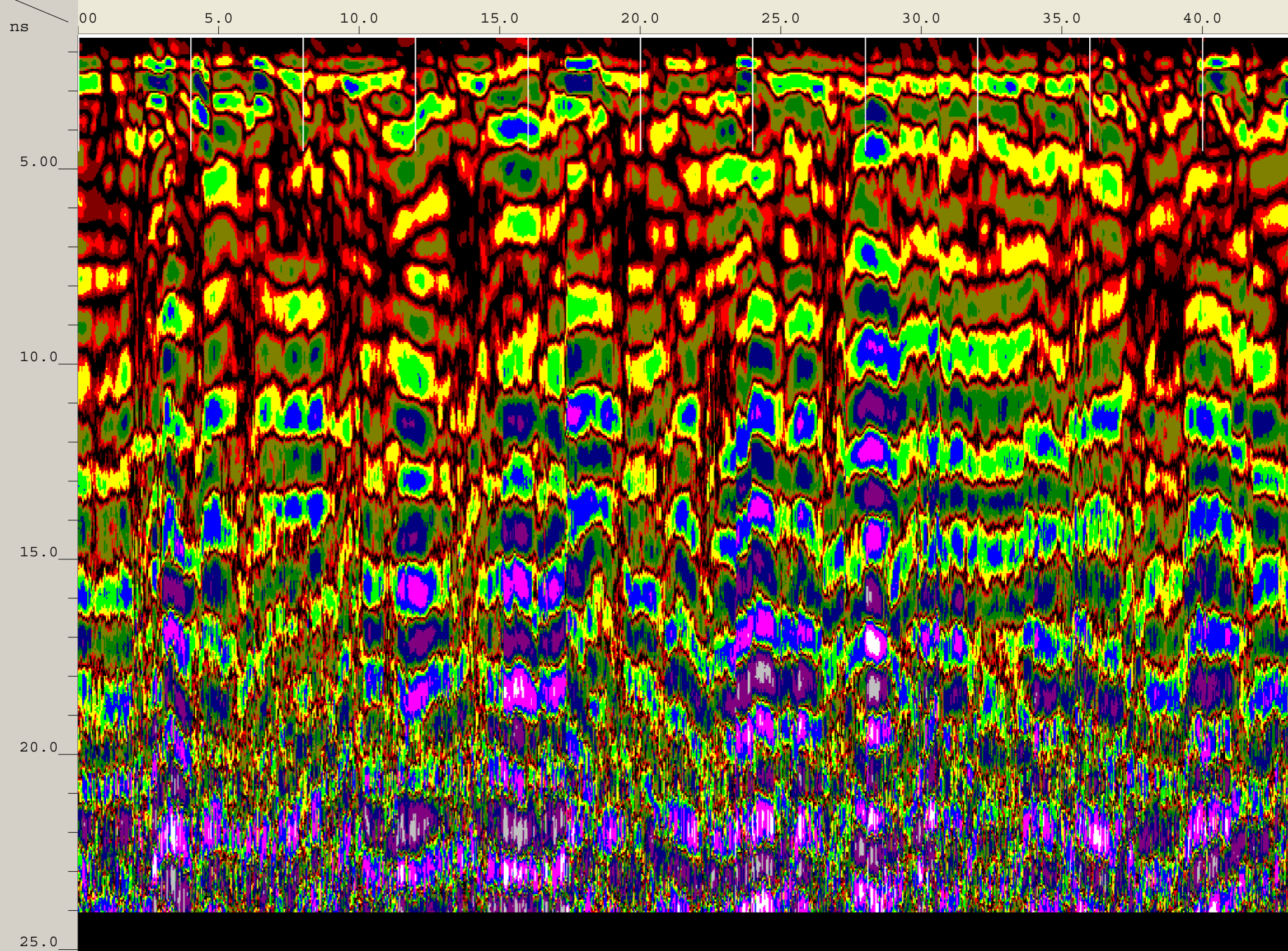




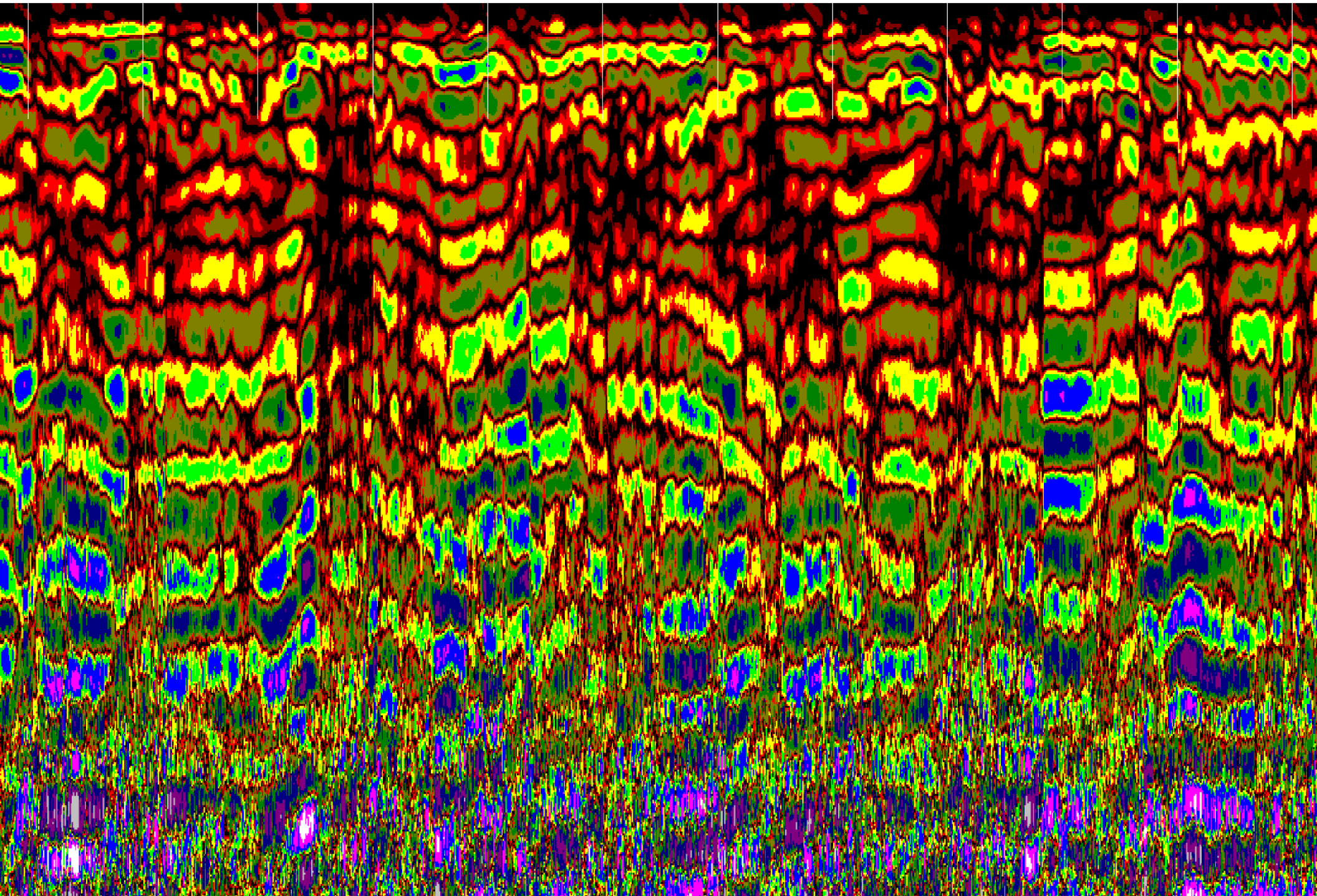
Appendix F – Kawaihae GPR Traverse Data

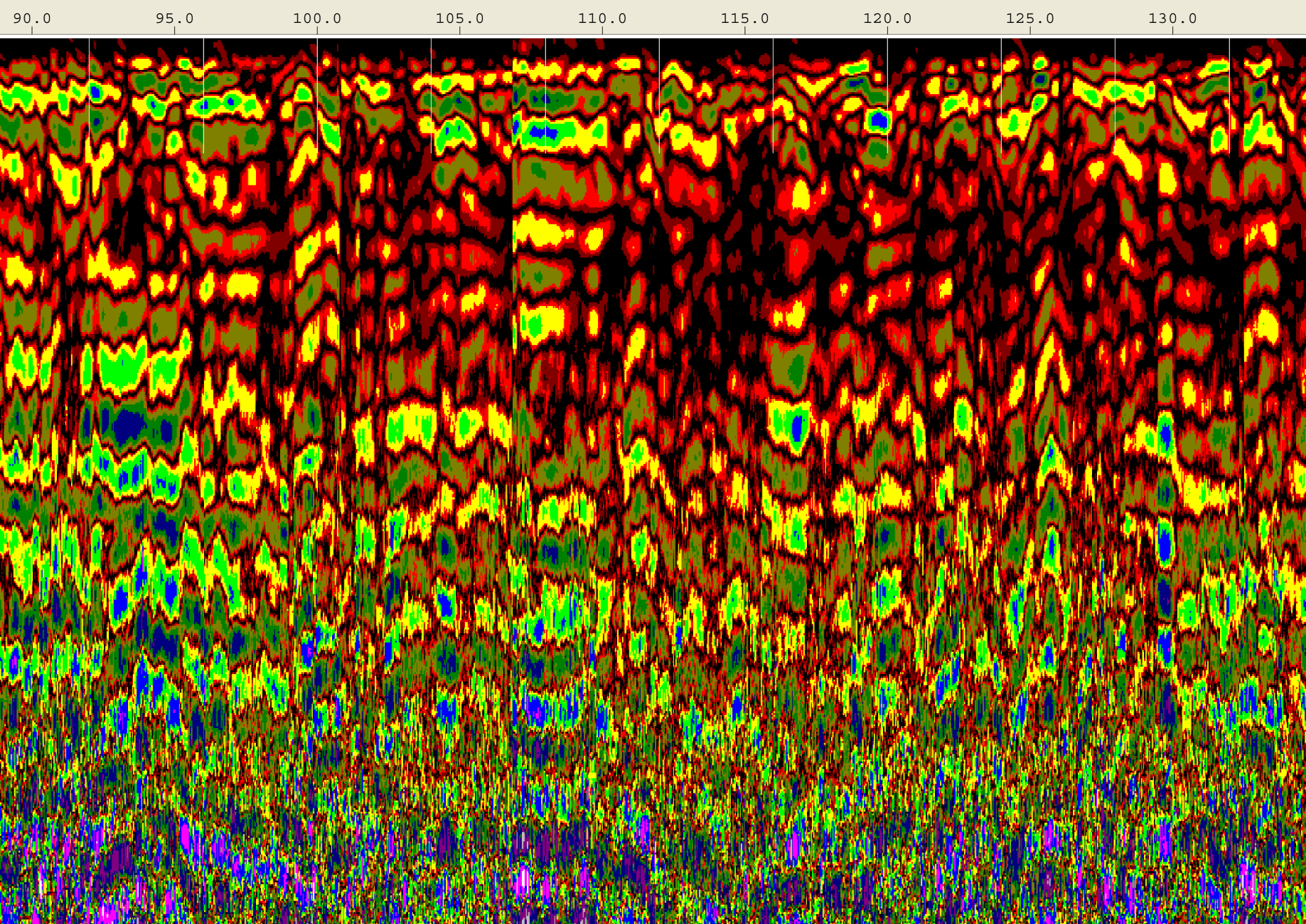
Created Jun, 22 2008, 12:15:38 Modified Jun, 22 2008, 12:17:16
Channel(s) 1 Samples/Scan 512 Bits/Sample 16
Scans/Second 100 Scans/Meter 78.7402 Meters/Mark 1.2192
Diel Constant 6.59332

CHANNEL 1 900MHz
Position 1.55 nS Range 24 nS
Position Correction 1.04 nS
Vert IIR LP N =1 F =2500 MHz
Vert IIR HP N =1 F =225 MHz
Range Gain (dB) 4.0 38.0 56.0
Position Correction 1.55 nS
Horz Boxcar Bkgr N=1023

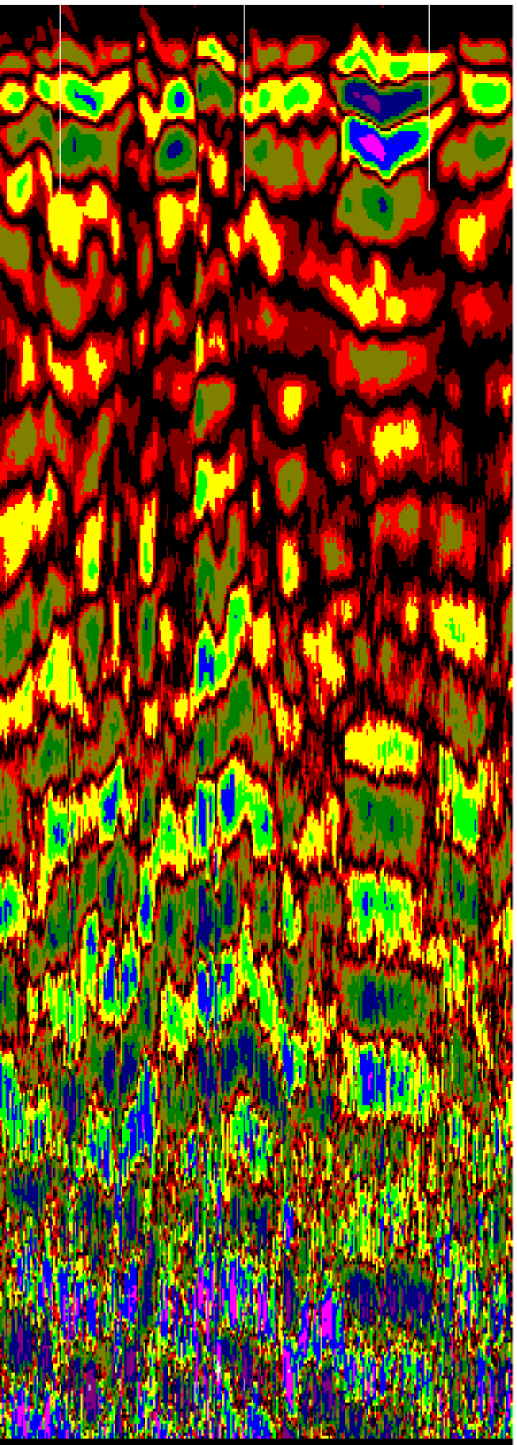


45.0 50.0 55.0 60.0 65.0 70.0 75.0 80.0 85.0



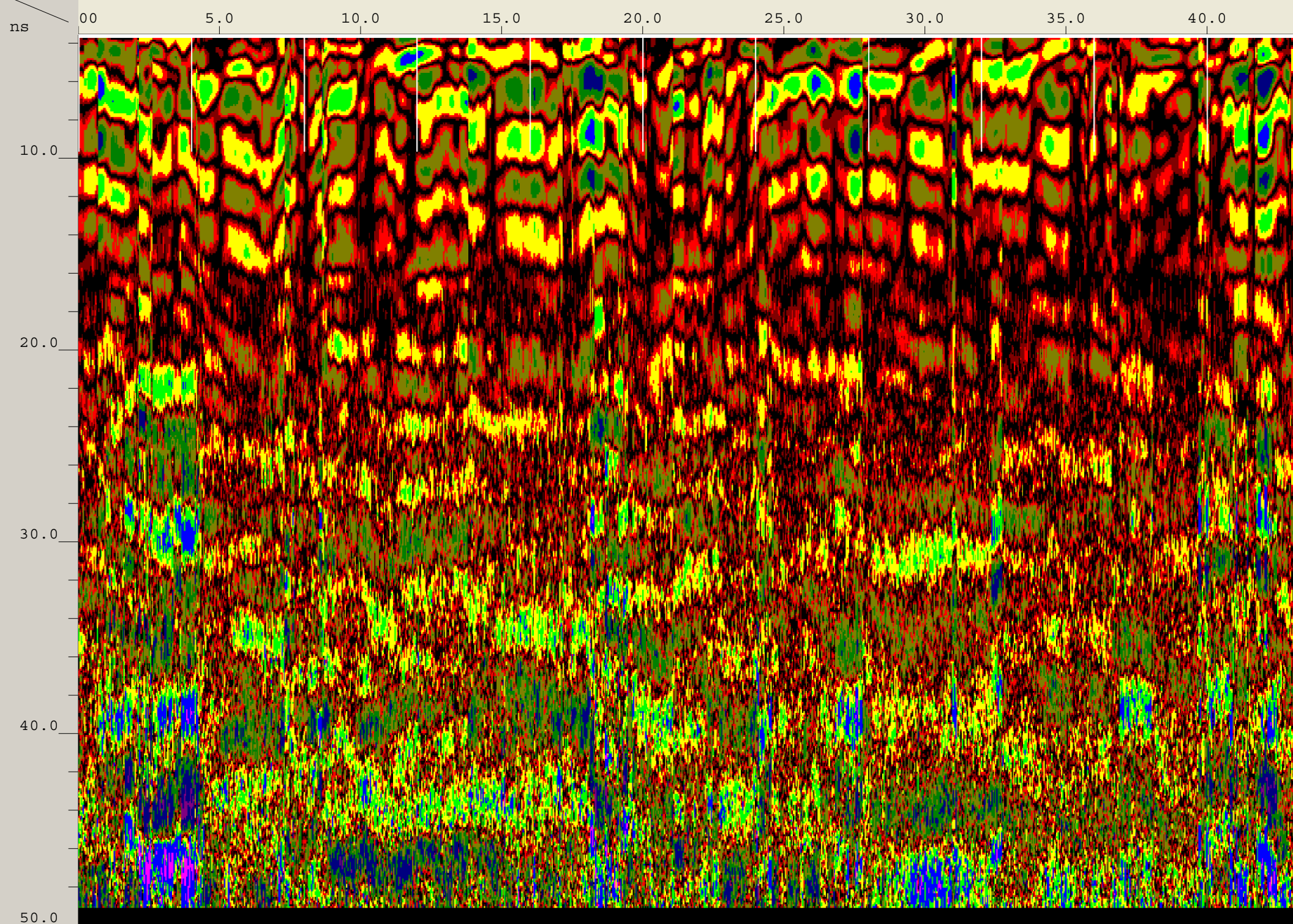


135.0 140.0 145.0

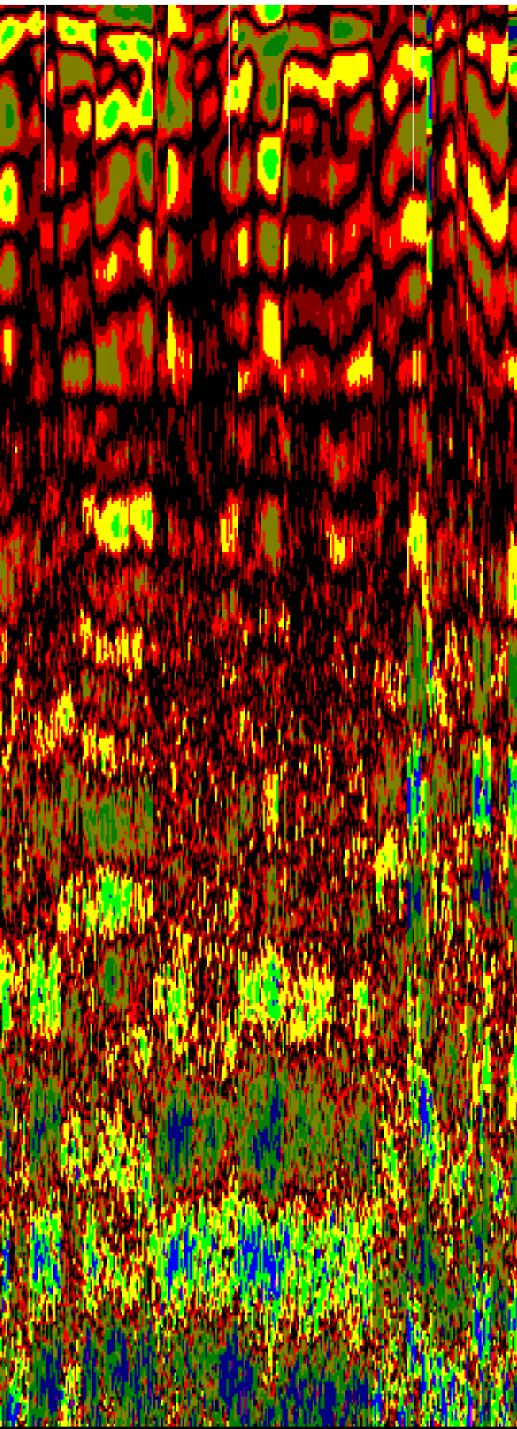


Created Jun, 22 2008, 11:30:08 Modified Jun, 22 2008, 11:38:00
Channel(s) 1 Samples/Scan 512 Bits/Sample 16
Scans/Second 100 Scans/Meter 78.7402 Meters/Mark 1.2192
Diel Constant 80

CHANNEL 1 400MHz
Position 3.54 nS Range 49 nS
Position Correction 1.04 nS
Vert IIR LP N =1 F =800 MHz
Vert IIR HP N =1 F =100 MHz
Range Gain (dB) 0.0 32.0 43.0
Position Correction 3.54 nS
Horz Boxcar Bkgr N=1023

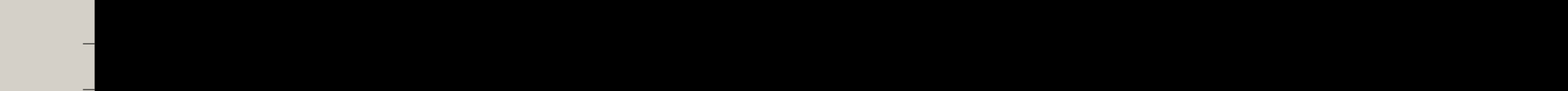
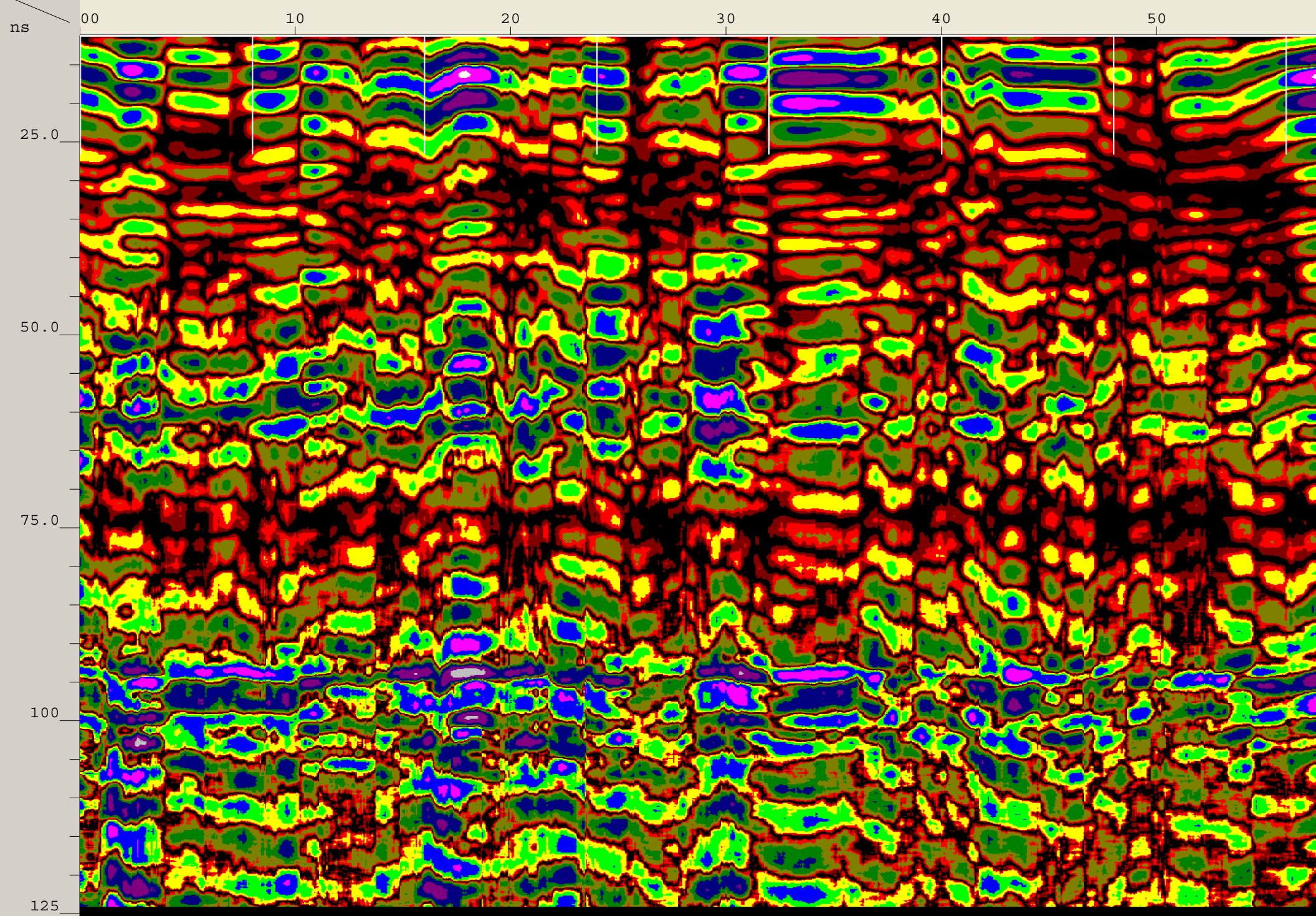


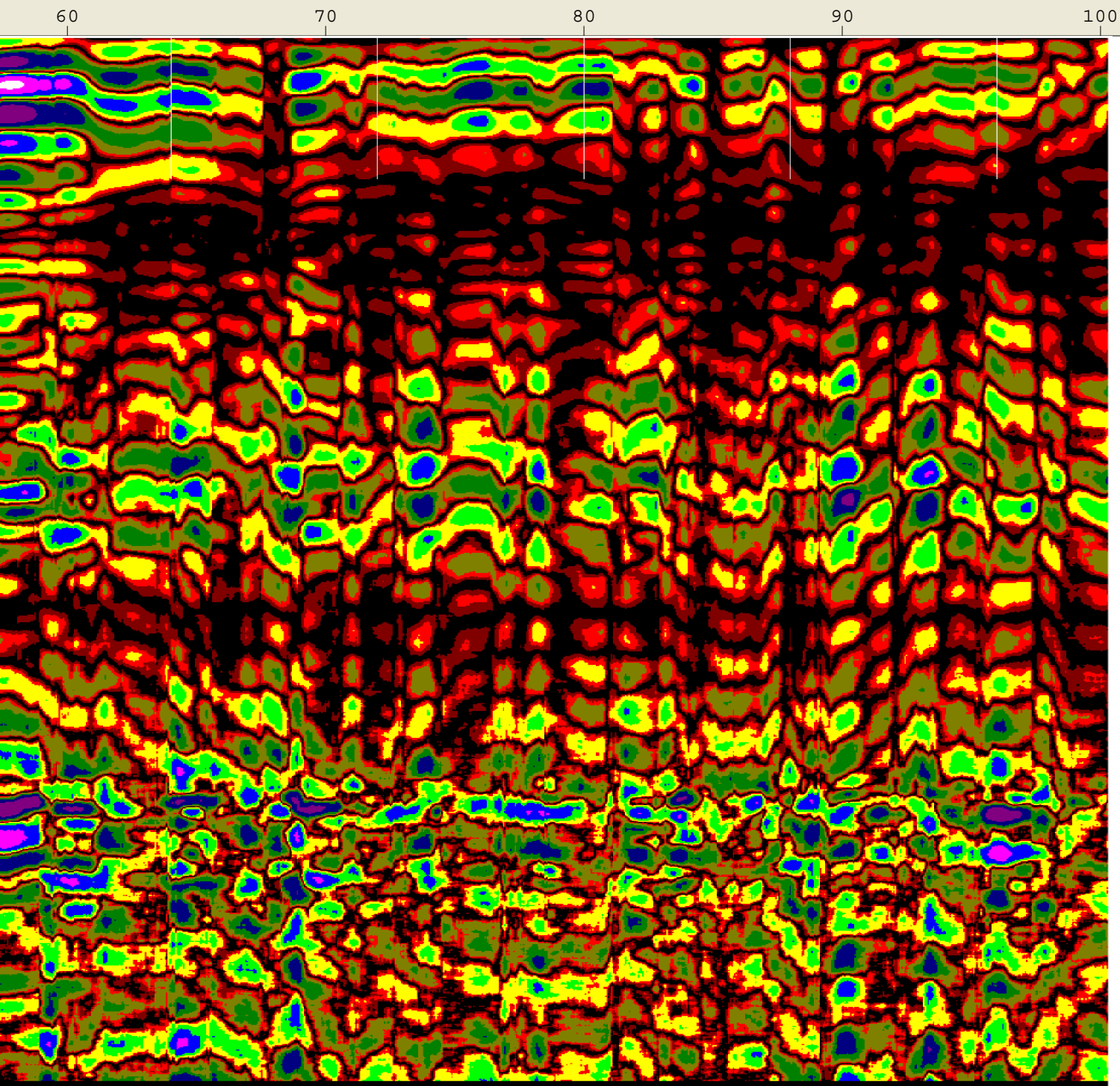
45.0 50.0



Created Jun, 22 2008, 11:01:00 Modified Jun, 22 2008, 11:05:24
Channel(s) 1 Samples/Scan 1024 Bits/Sample 16
Scans/Second 64 Scans/Meter 59.0551 Meters/Mark 2.4384
Diel Constant 6

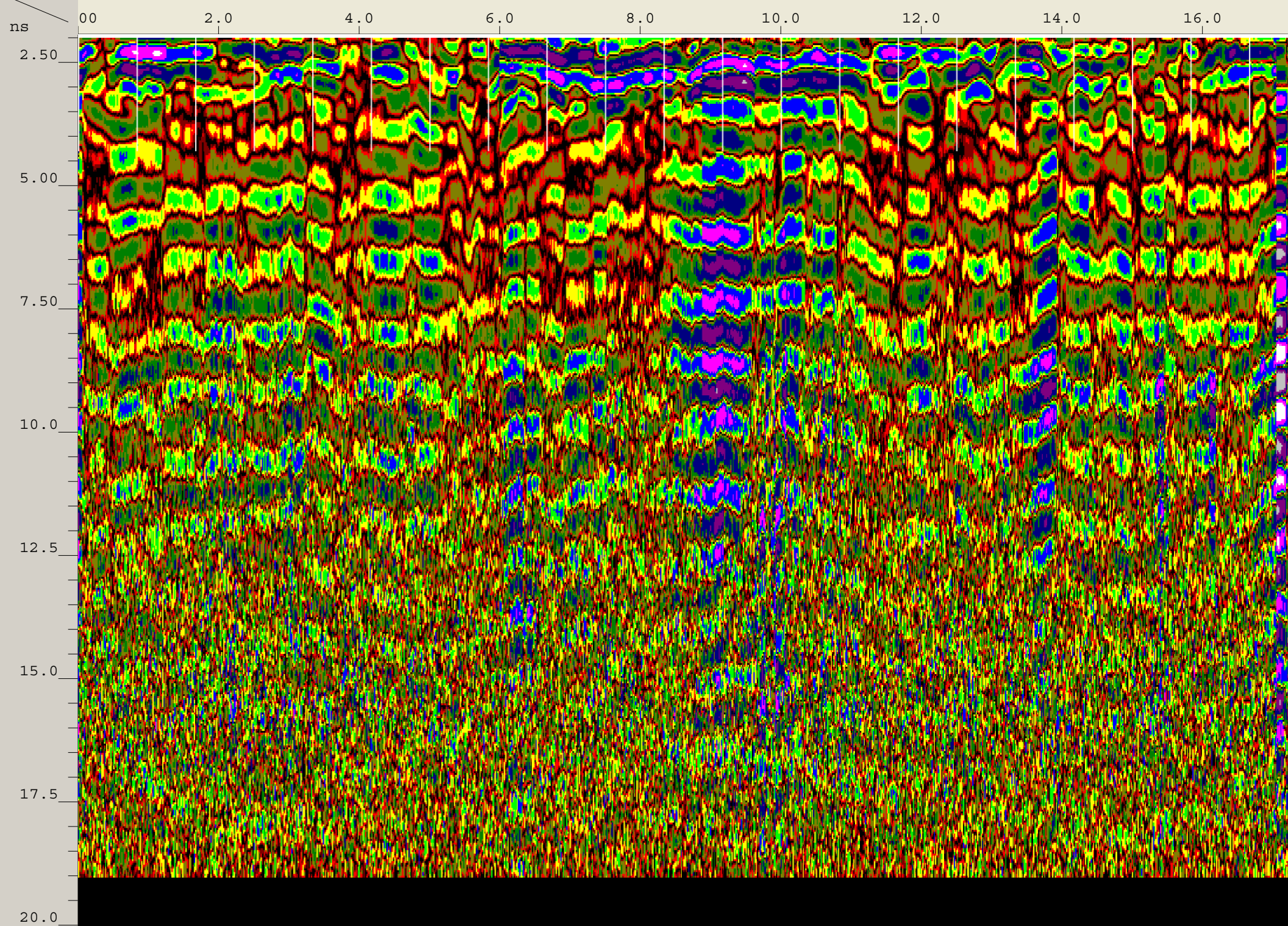
CHANNEL 1 270MHz
Position 11.14 nS Range 124 nS
Range Gain (dB) -19.0 34.0 56.0
Position Correction -4.35 nS
Vert IIR LP N =1 F =700 MHz
Vert IIR HP N =1 F =75 MHz
Horz IIR Stack TC =11
Position Correction 11.14 nS
Horz Boxcar Bkgr N=1023
Range Gain (L) 2.6 10.0 9.7
1.0 3.9 1.3
1.0



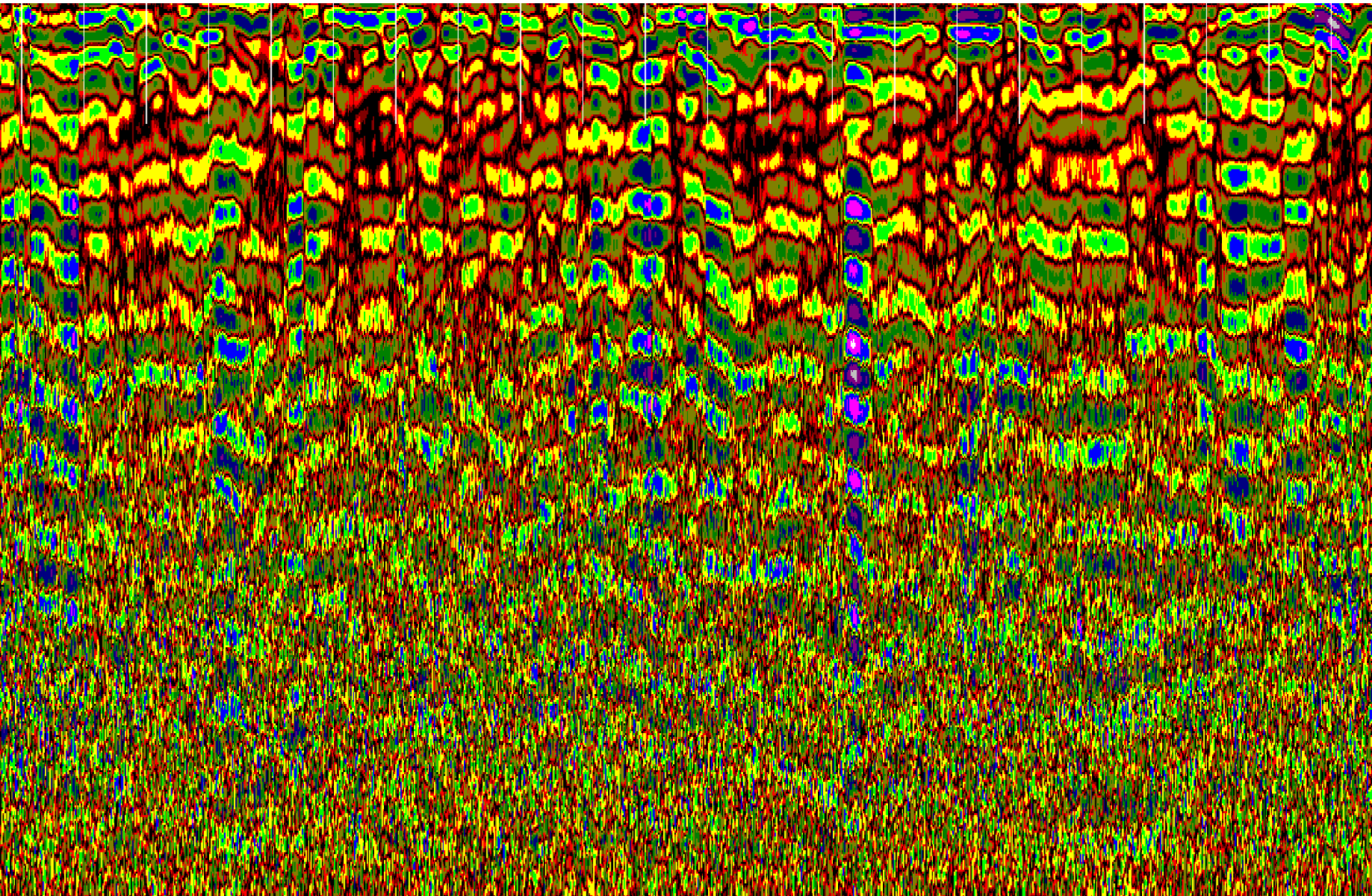


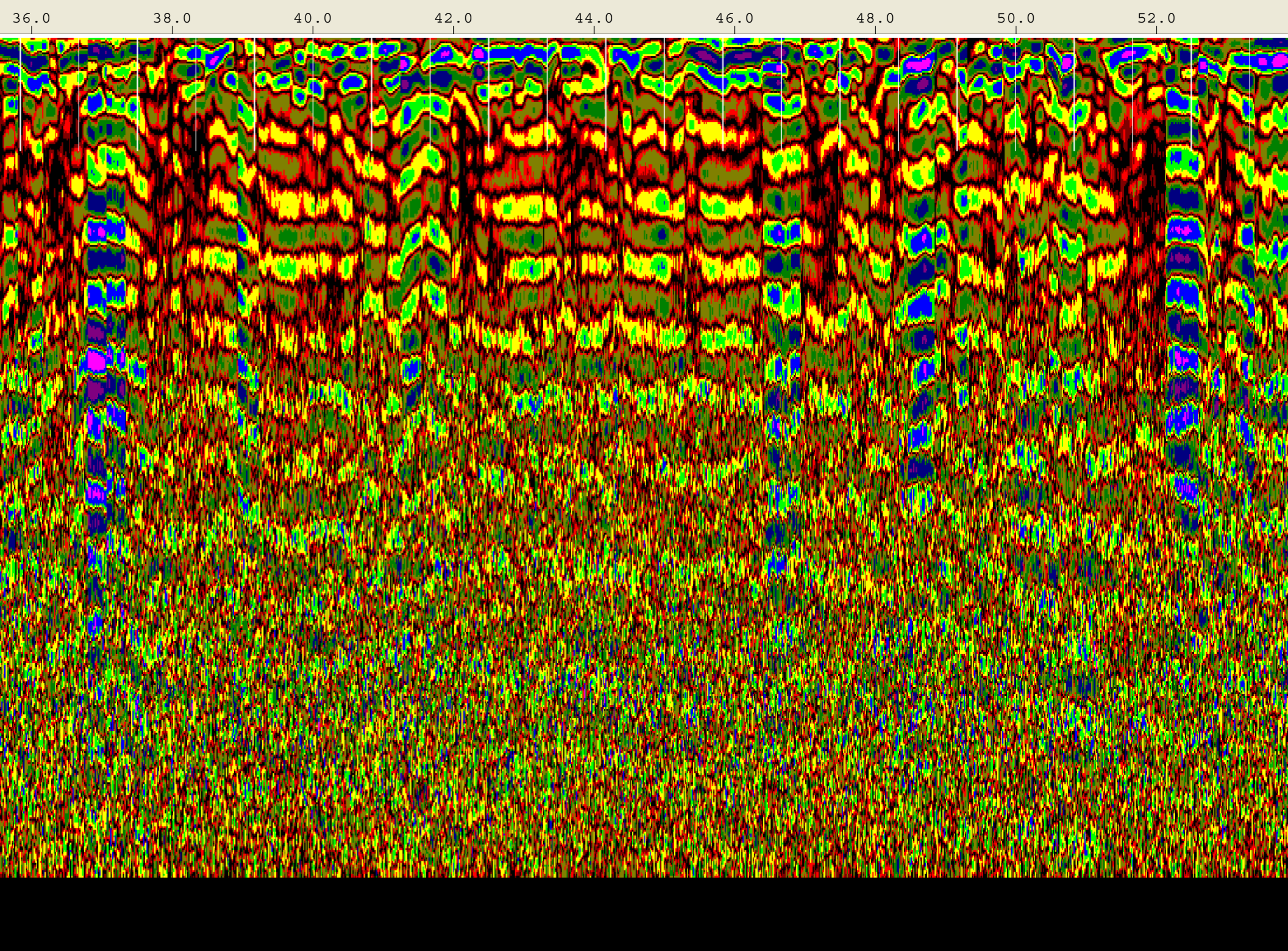
Created Jun, 22 2008, 12:39:56 Modified Jun, 22 2008, 12:46:16
Channel(s) 1 Samples/Scan 512 Bits/Sample 16
Scans/Second 100 Scans/Meter 196.85 Meters/Mark 0.254
Diel Constant 19.8777

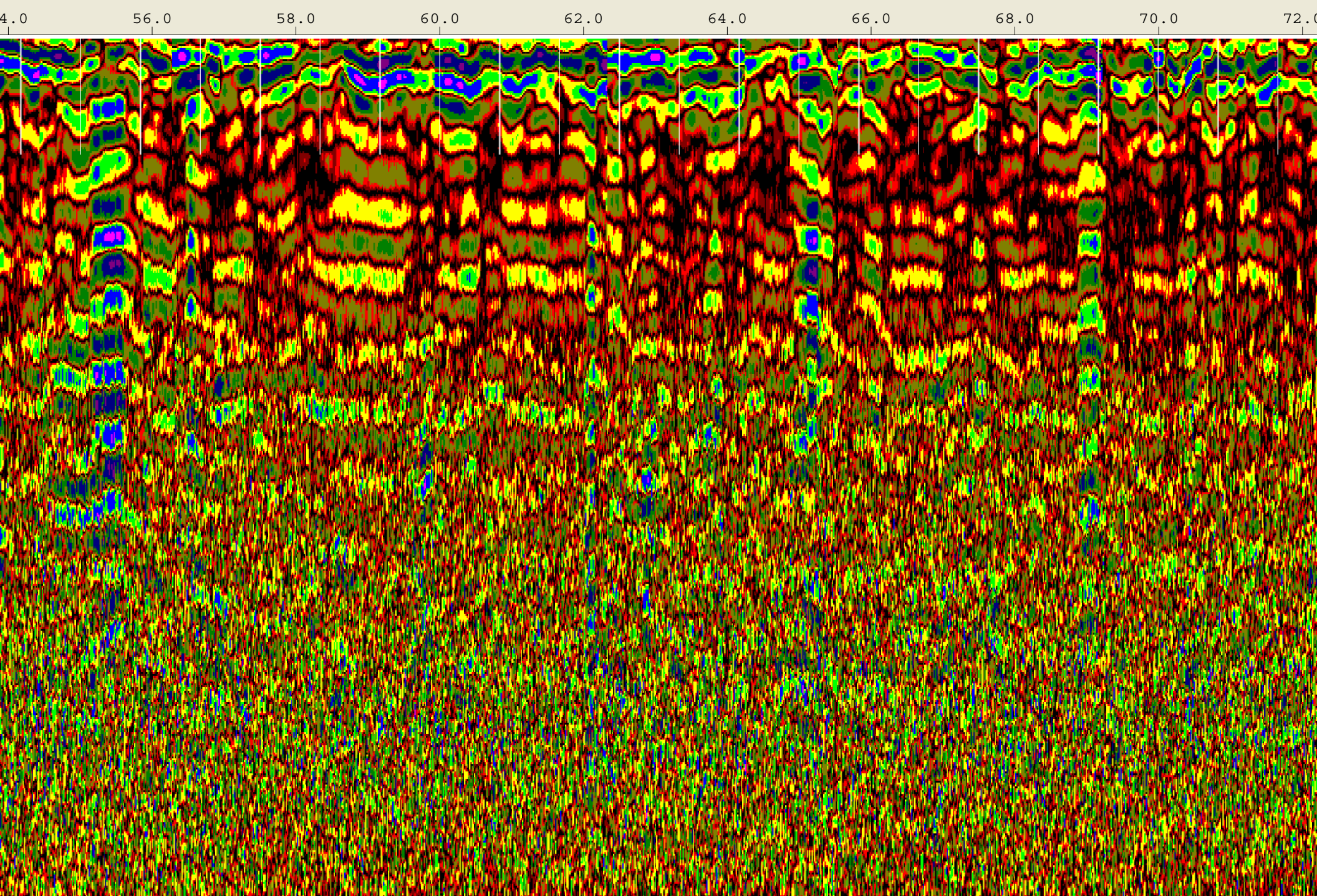
CHANNEL 1 1.5/1.6GHz
Position 1.93 nS Range 19 nS
Range Gain (dB) -2.0 5.0 30.0
30.0 30.0
Position Correction 6.775 nS
Vert IIR HP N =1 F =10 MHz
Vert Boxcar LP F =1930 MHz
Vert Boxcar HP F =295 MHz
Position Correction 1.93 nS
Horz Boxcar Bkgr N=1023
Range Gain (L) 1.9 5.7 3.5
2.1 3.4 4.8
3.8 1.0



18.0 20.0 22.0 24.0 26.0 28.0 30.0 32.0 34.0







74.0

76.0

78.0

80.0

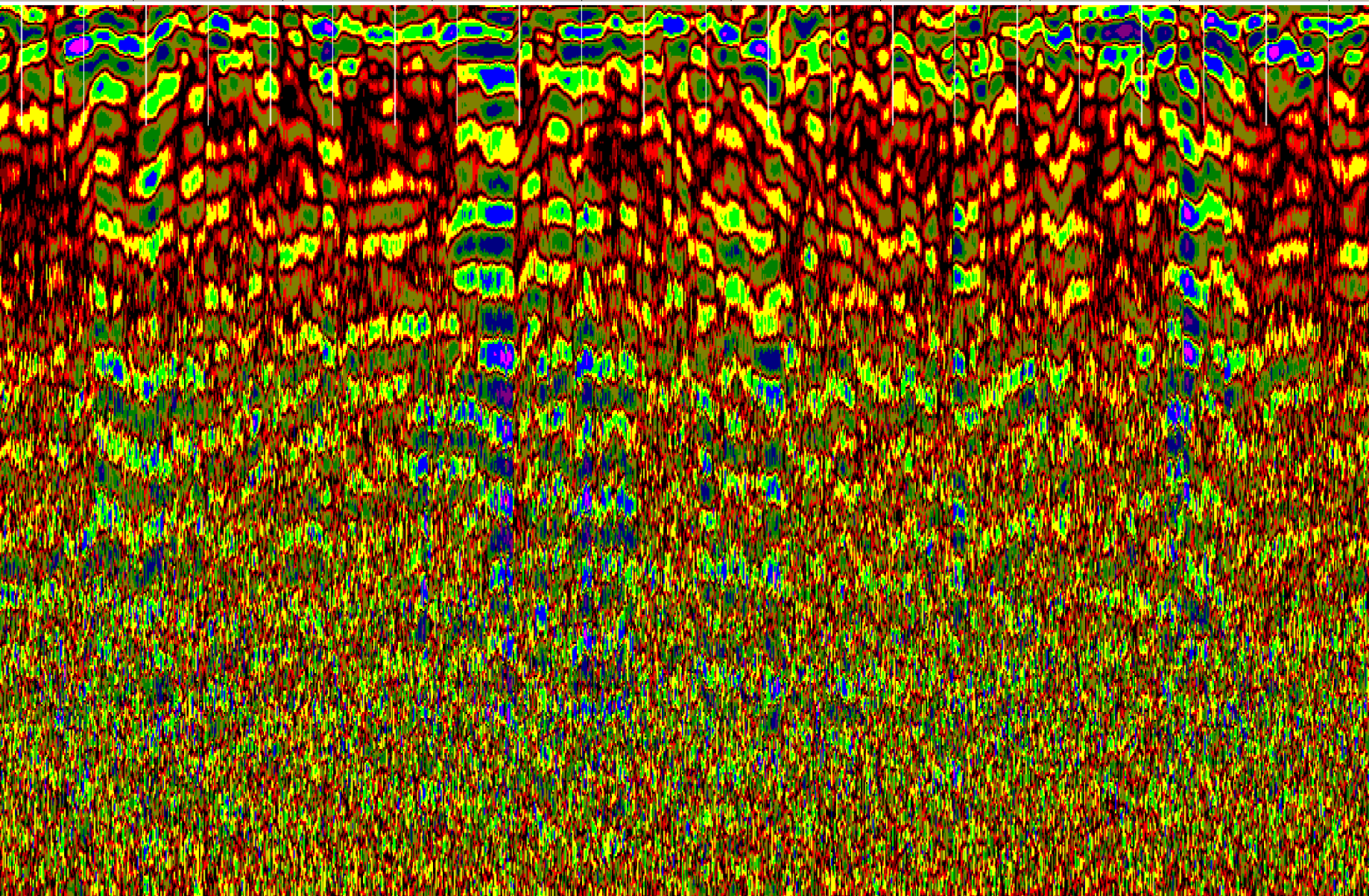
82.0

84.0

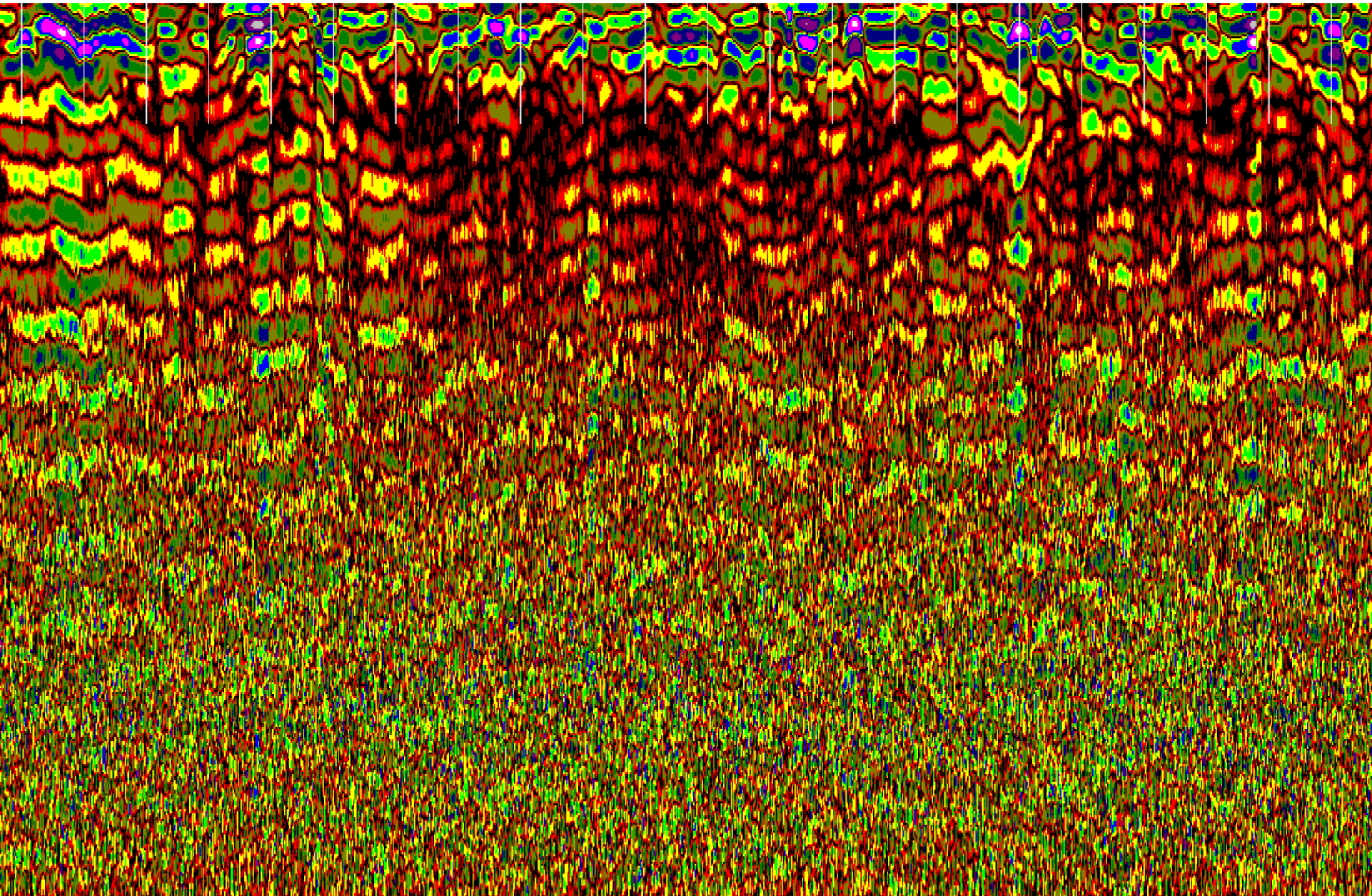
86.0

88.0

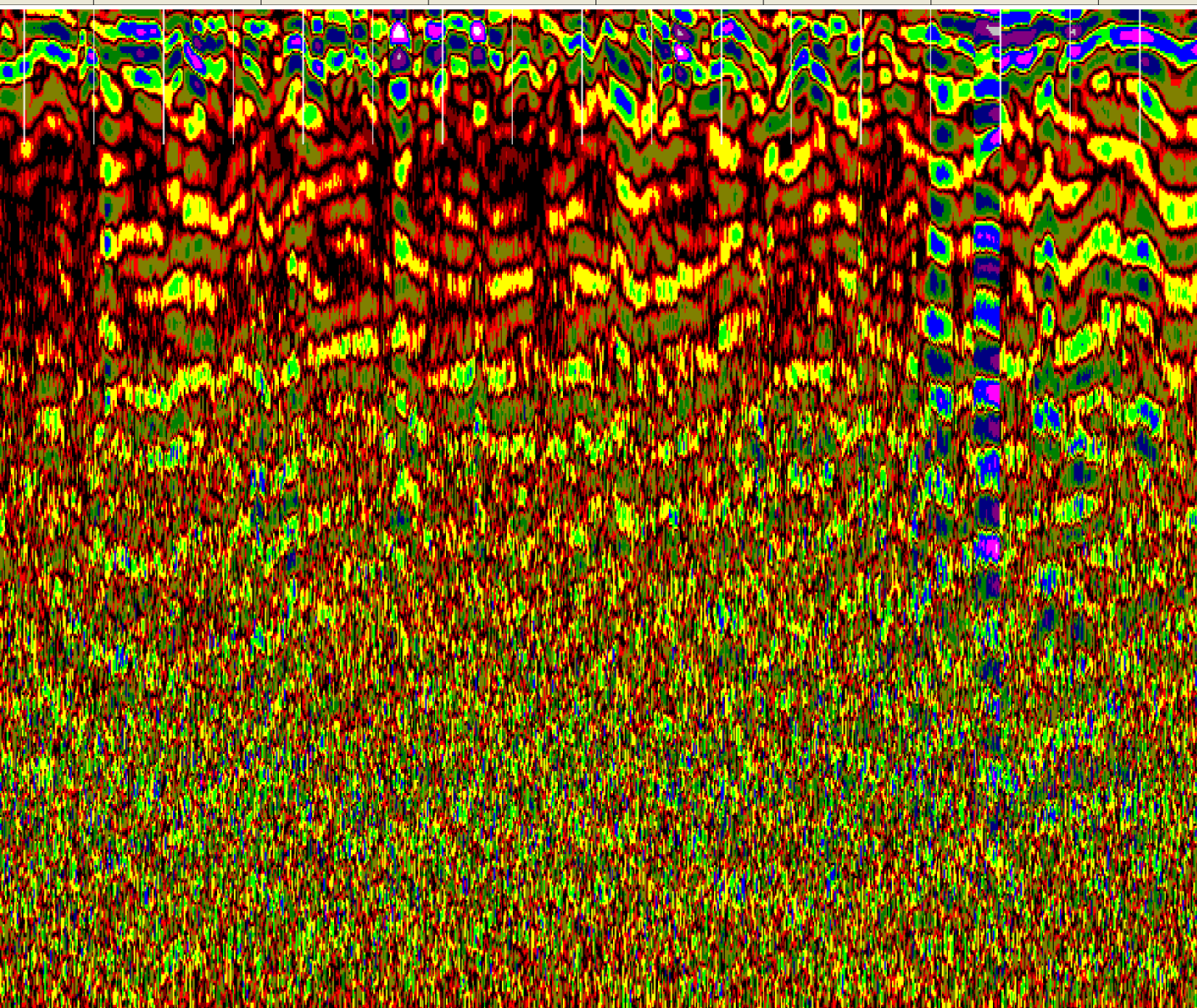
90.0



92.0 94.0 96.0 98.0 100.0 102.0 104.0 106.0 108.0

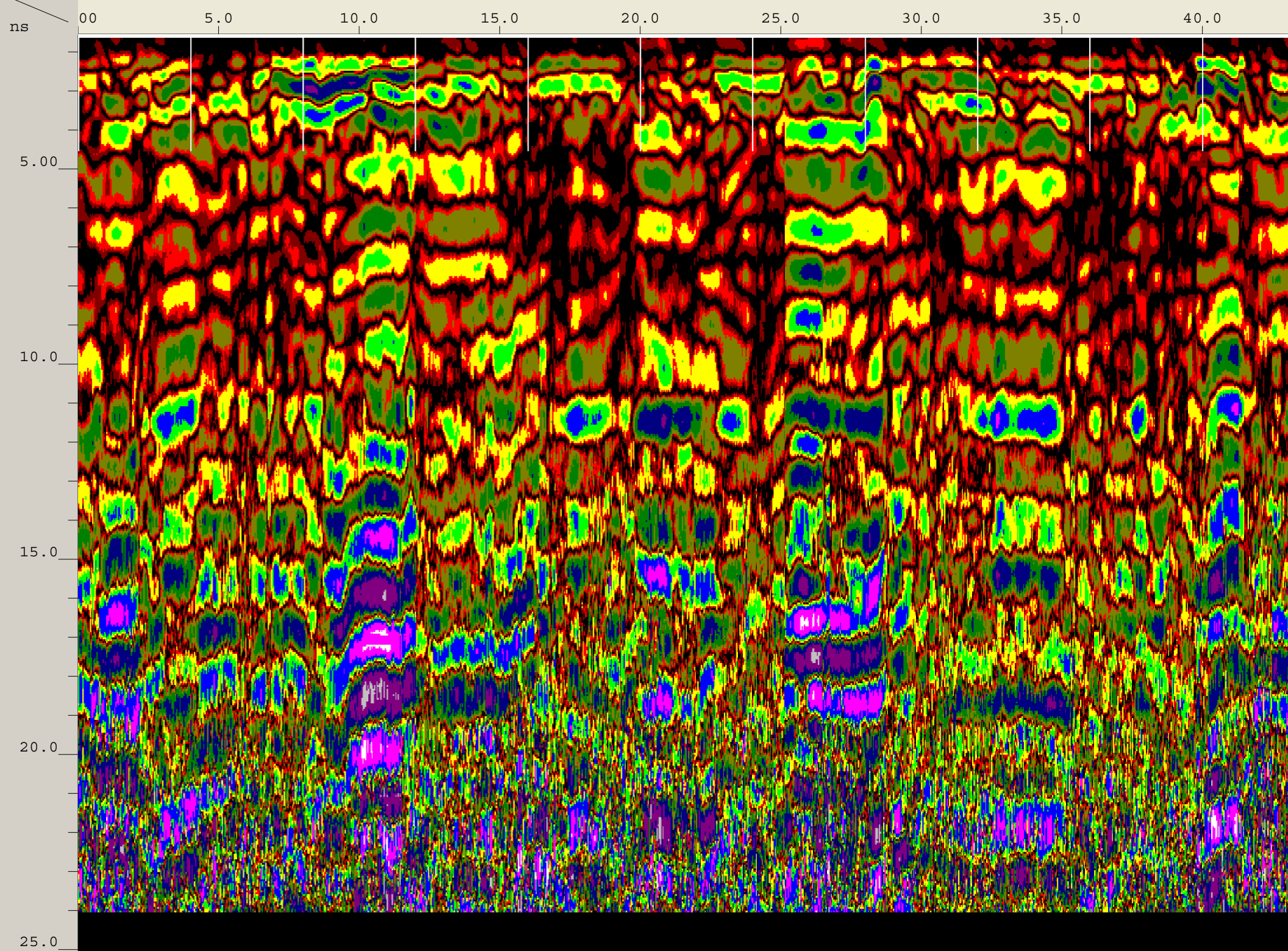


110.0 112.0 114.0 116.0 118.0 120.0 122.0

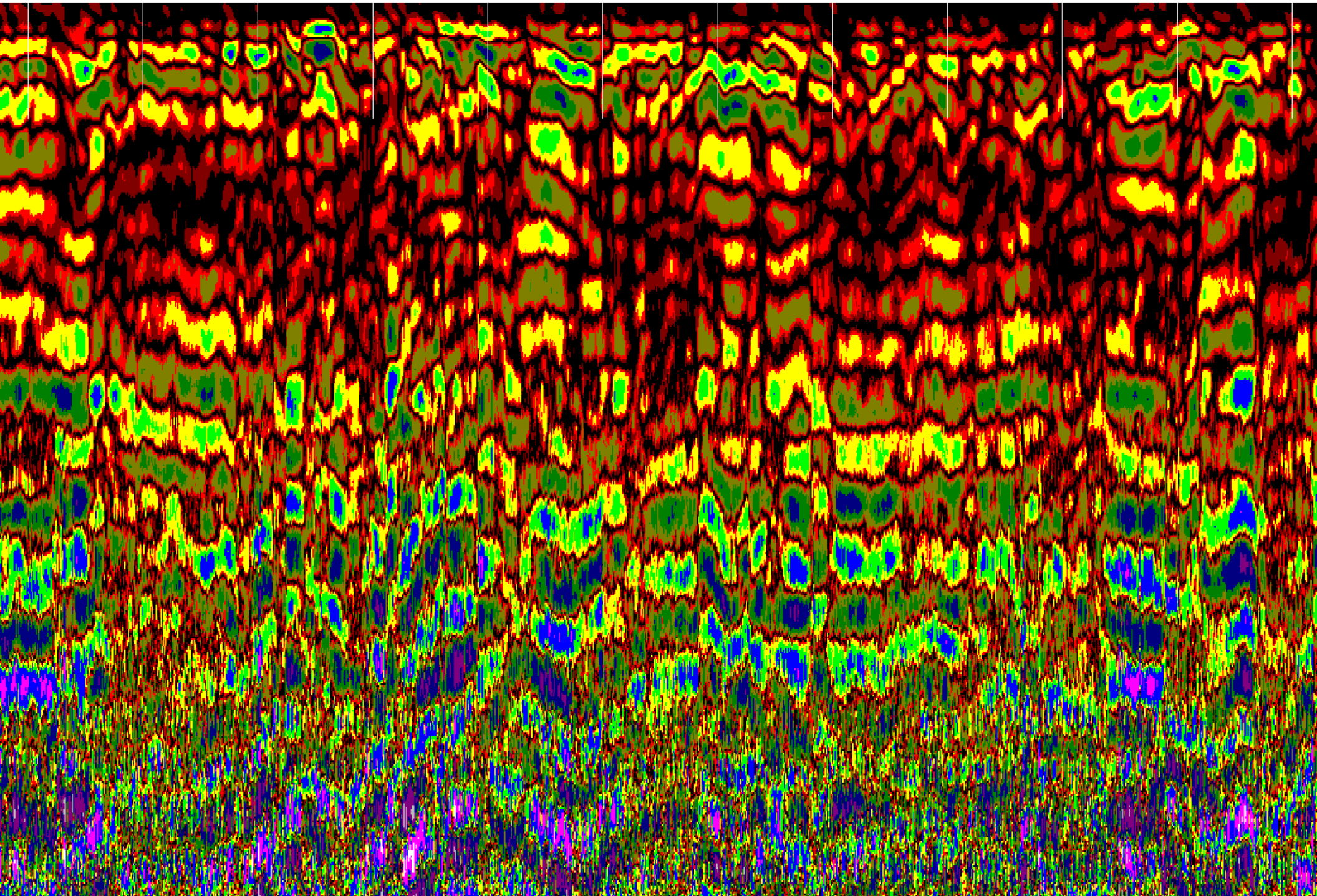


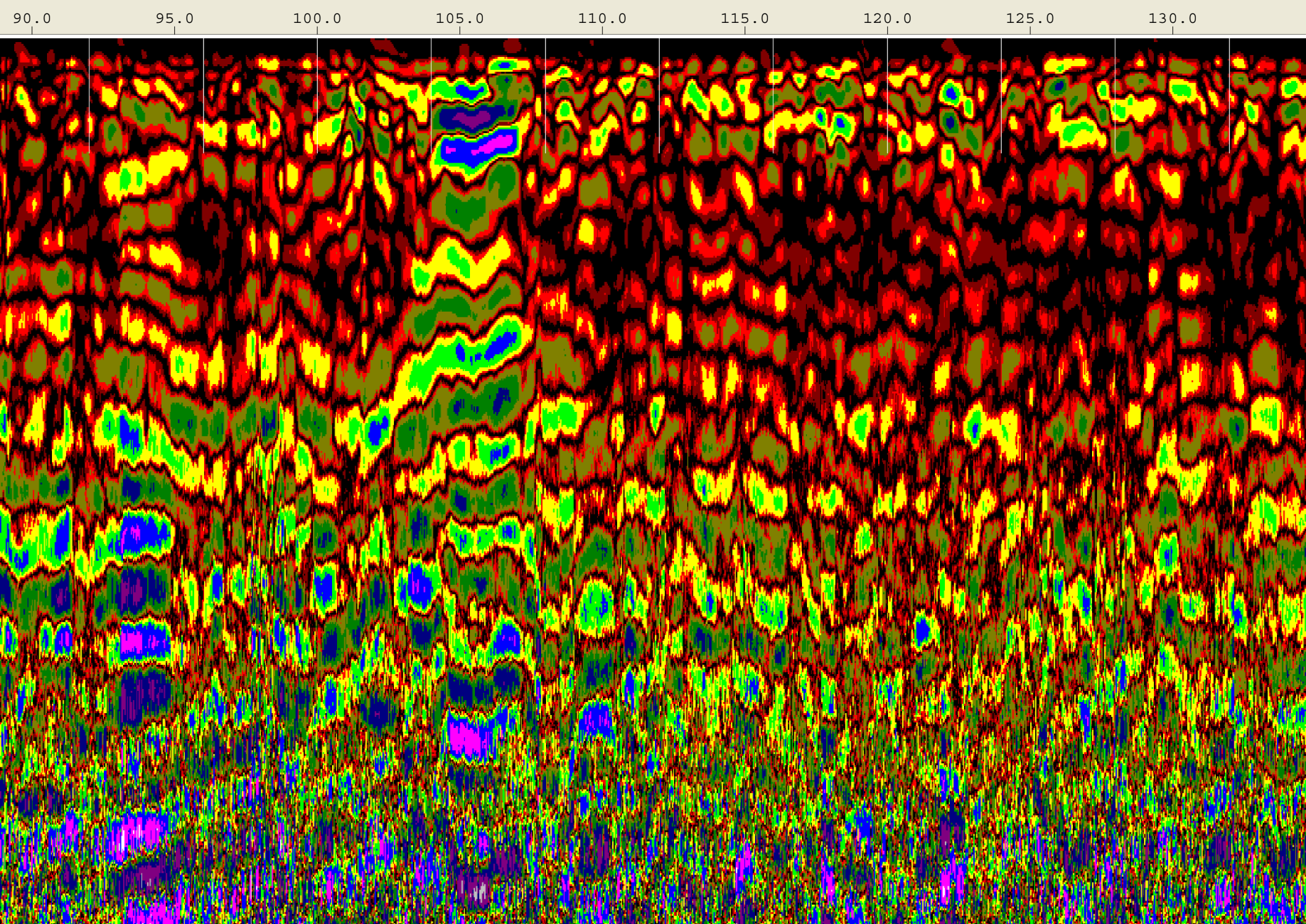
Created Jun, 22 2008, 12:10:08 Modified Jun, 22 2008, 12:15:32
Channel(s) 1 Samples/Scan 512 Bits/Sample 16
Scans/Second 100 Scans/Meter 78.7402 Meters/Mark 1.2192
Diel Constant 14.4397

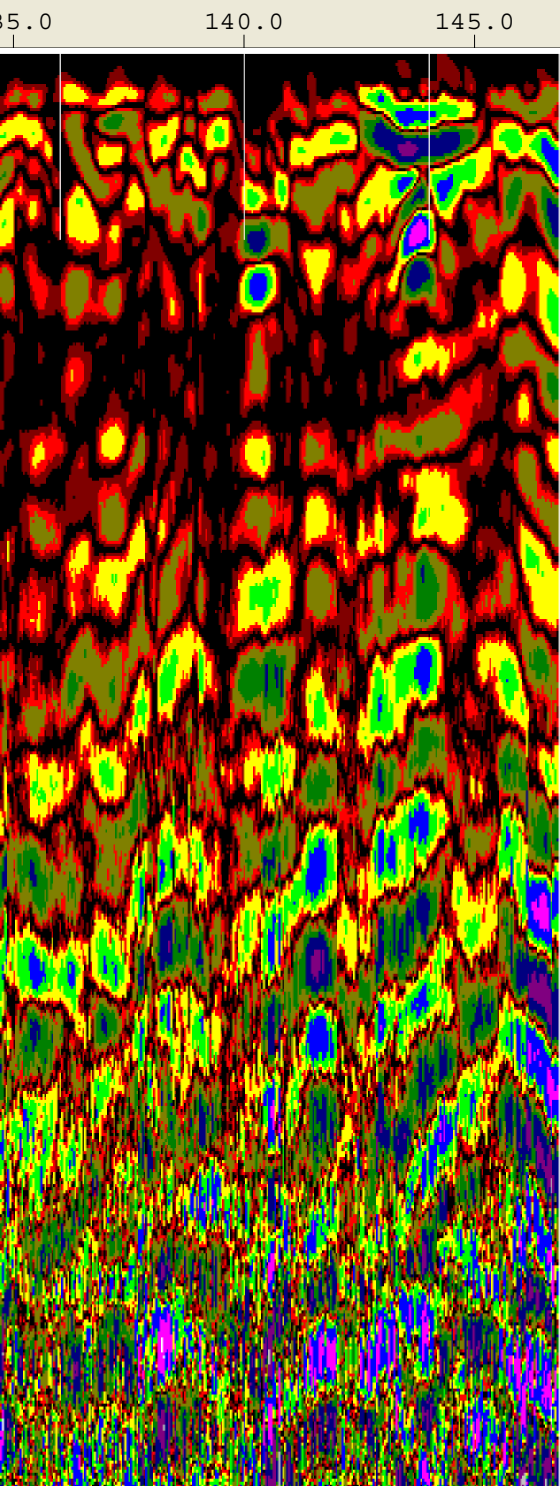
CHANNEL 1 900MHz
Position 1.55 nS Range 24 nS
Position Correction 1.04 nS
Vert IIR LP N =1 F =2500 MHz
Vert IIR HP N =1 F =225 MHz
Range Gain (dB) 4.0 38.0 56.0
Position Correction 1.55 nS
Horz Boxcar Bkgr N=1023



45.0 50.0 55.0 60.0 65.0 70.0 75.0 80.0 85.0

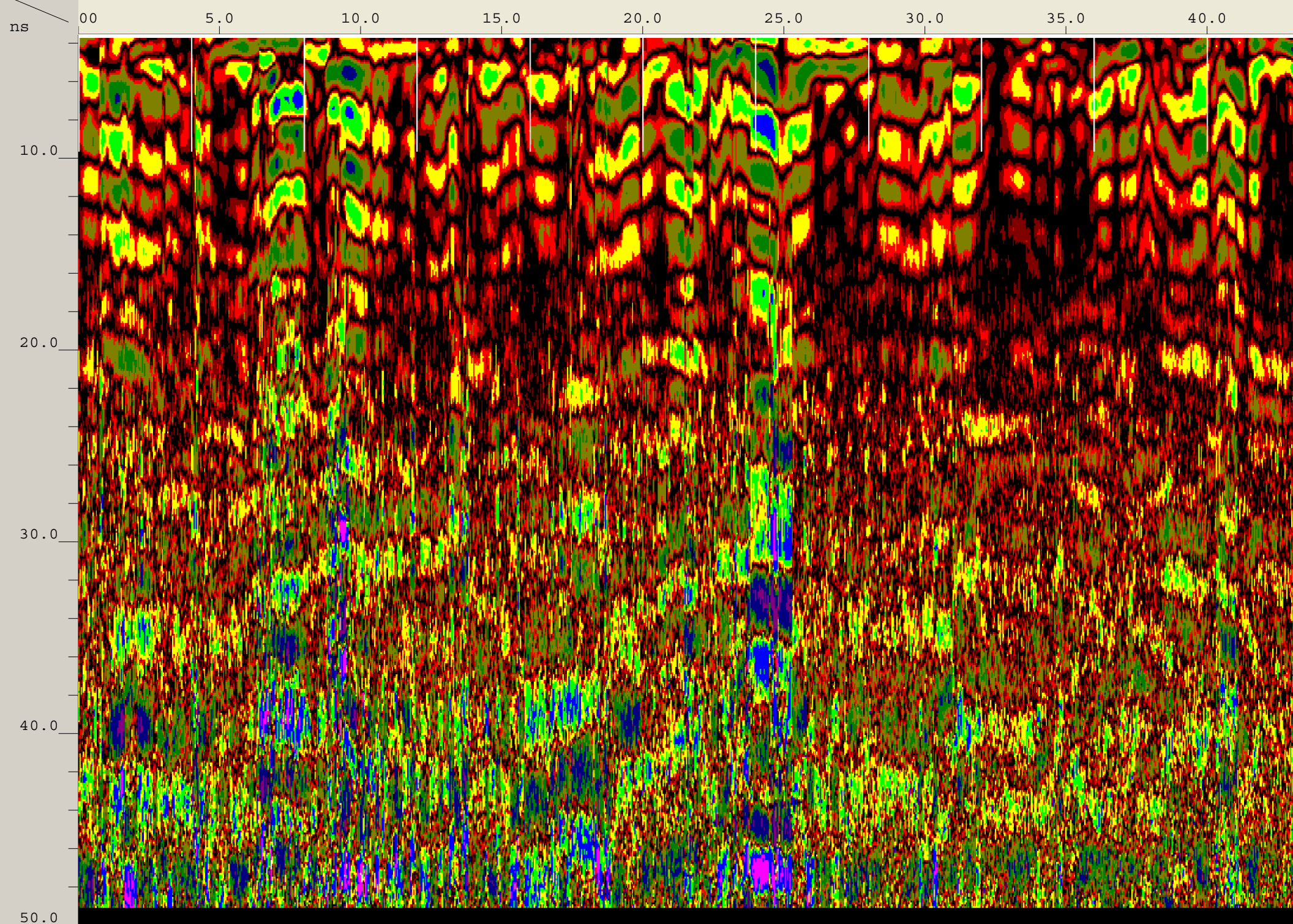




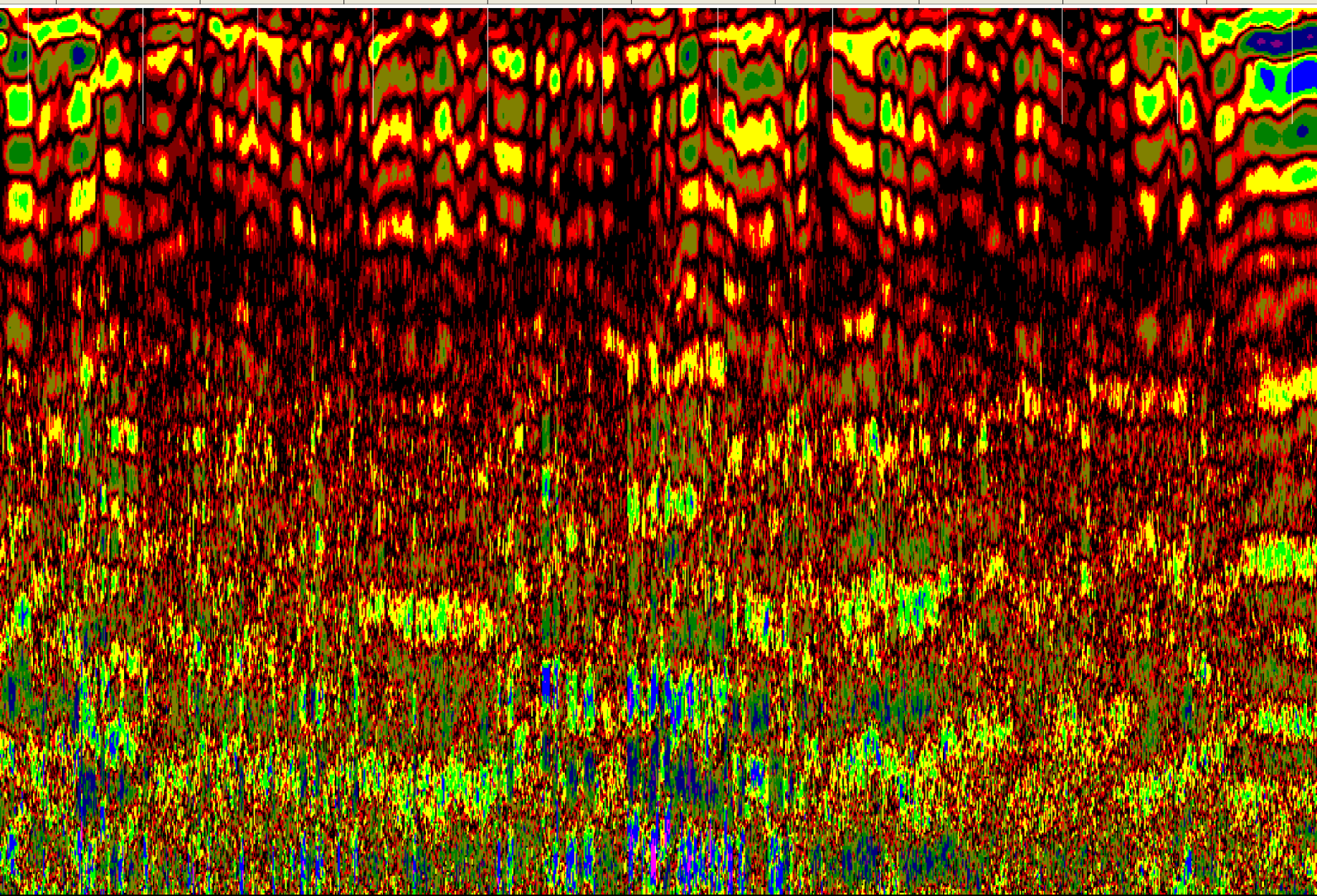


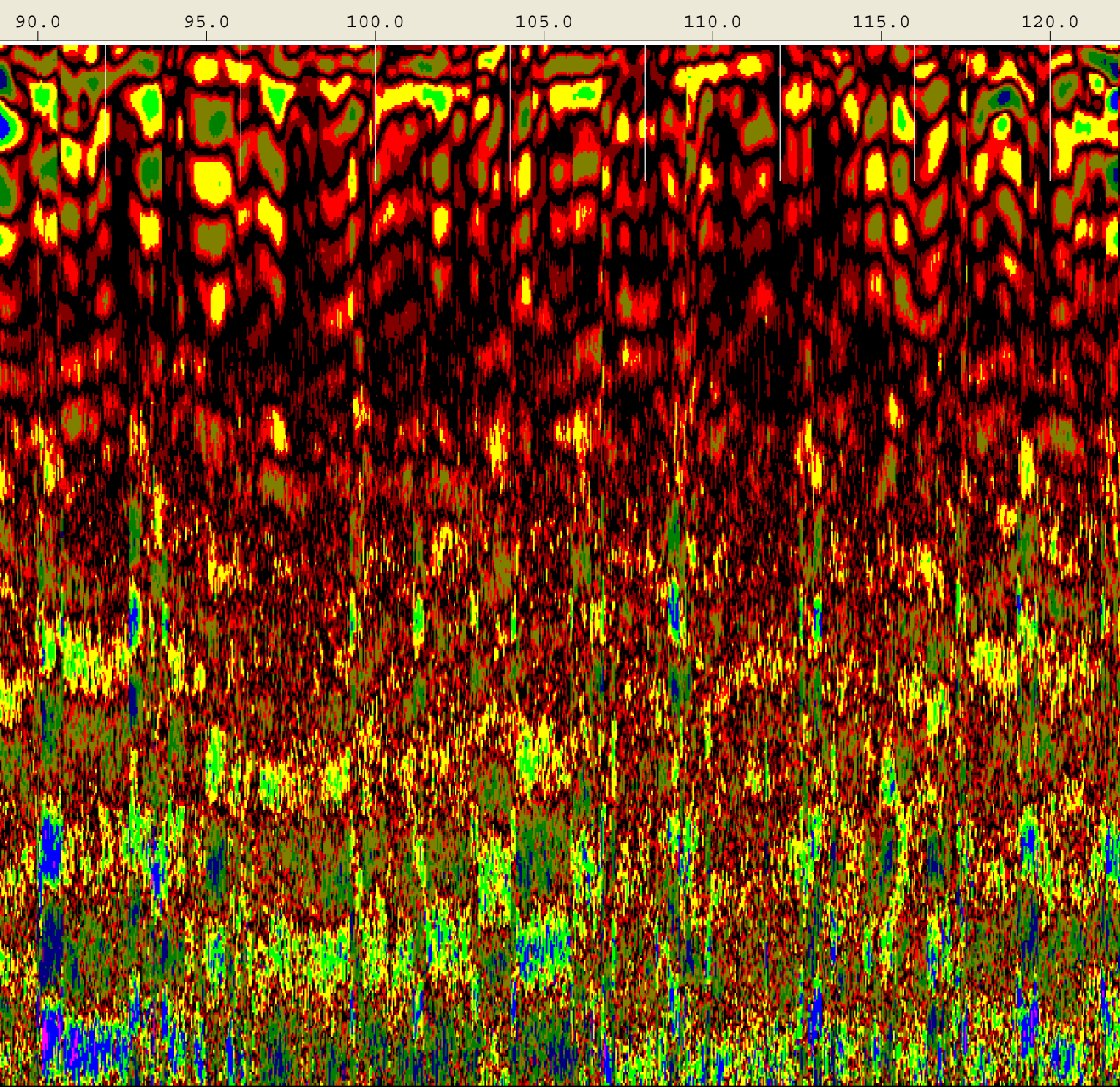
Created Jun, 22 2008, 11:22:34 Modified Jun, 22 2008, 11:29:14
Channel(s) 1 Samples/Scan 512 Bits/Sample 16
Scans/Second 100 Scans/Meter 78.7402 Meters/Mark 1.2192
Diel Constant 80

CHANNEL 1 400MHz
Position 3.54 nS Range 49 nS
Position Correction 1.04 nS
Vert IIR LP N =1 F =800 MHz
Vert IIR HP N =1 F =100 MHz
Range Gain (dB) 0.0 32.0 43.0
Position Correction 3.54 nS
Horz Boxcar Bkgr N=1023



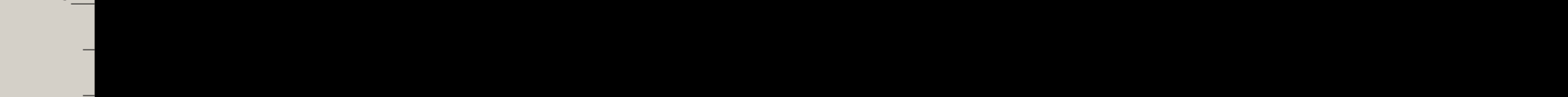
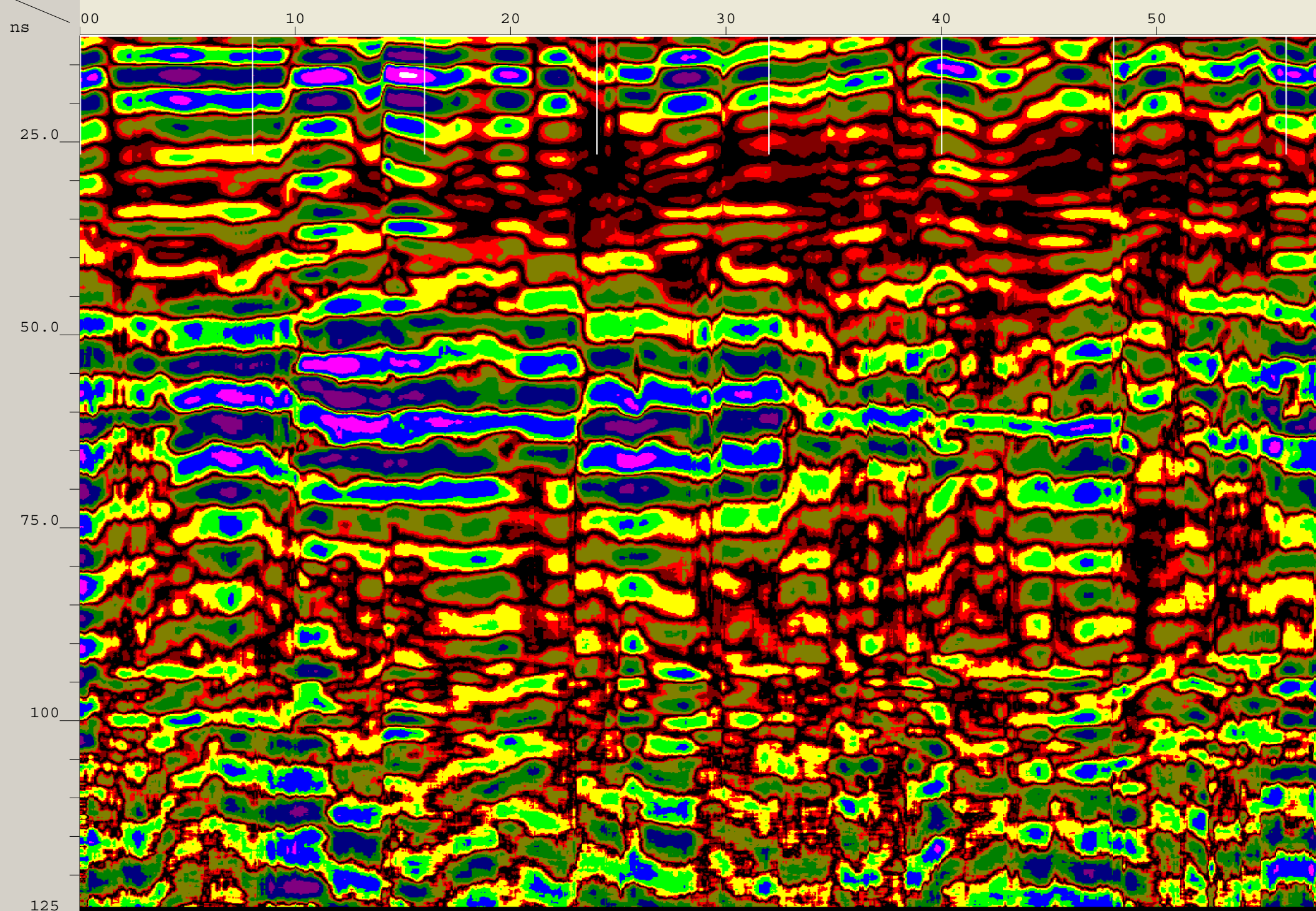
45.0 50.0 55.0 60.0 65.0 70.0 75.0 80.0 85.0





Created Jun, 22 2008, 10:50:48 Modified Jun, 22 2008, 10:58:56
Channel(s) 1 Samples/Scan 1024 Bits/Sample 16
Scans/Second 64 Scans/Meter 59.0551 Meters/Mark 2.4384
Diel Constant 6

CHANNEL 1 270MHz
Position 11.14 nS Range 124 nS
Vert IIR LP N =1 F =700 MHz
Vert IIR HP N =1 F =75 MHz
Horz IIR Stack TC =11
Position Correction -4.35 nS
Range Gain (dB) -19.0 34.0 56.0
Position Correction 11.14 nS
Horz Boxcar Bkgr N=1023
Range Gain (L) 3.7 9.5 8.8
2.0 1.4 1.7
1.0



60

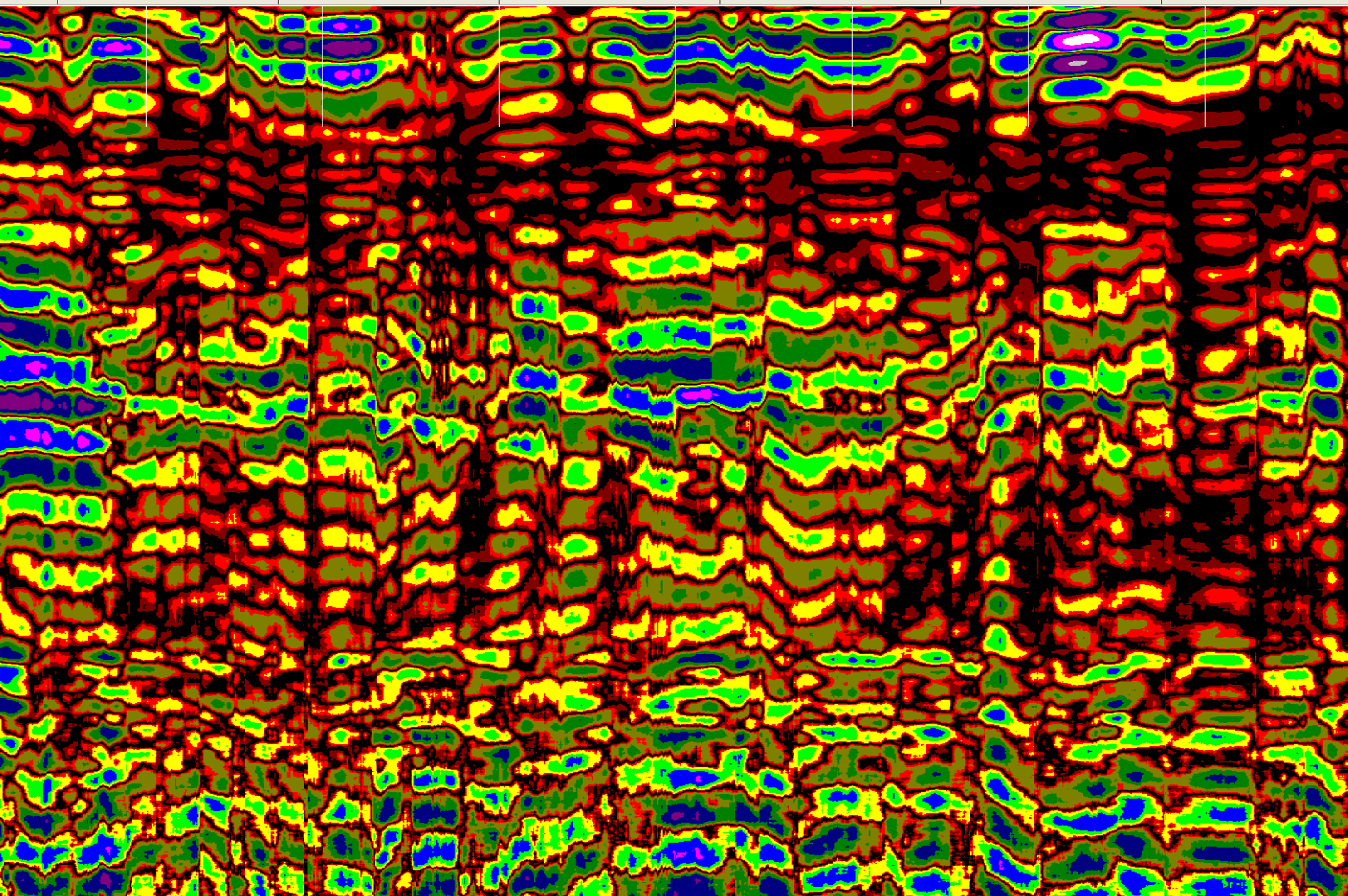
70

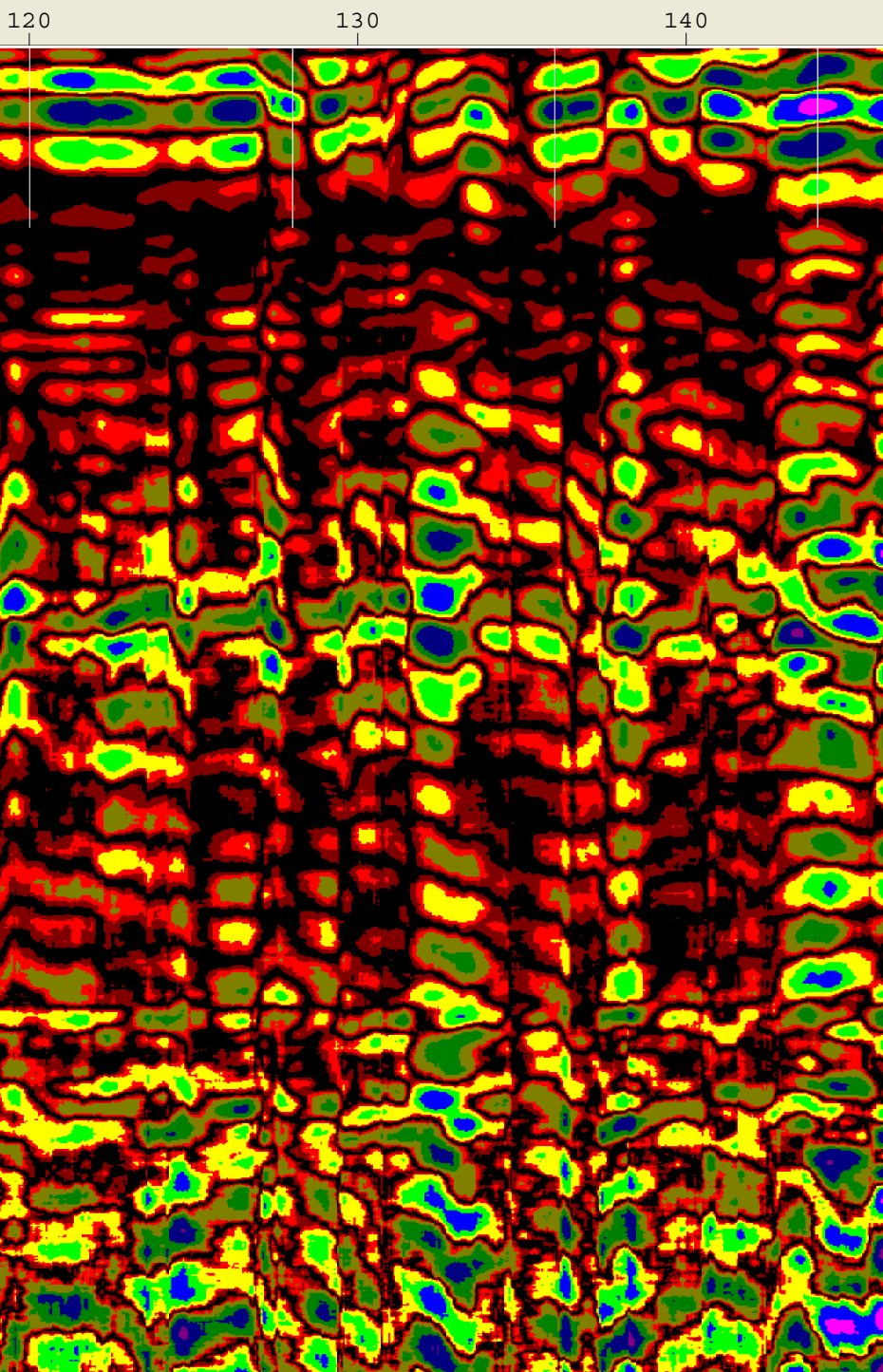
80

90

100

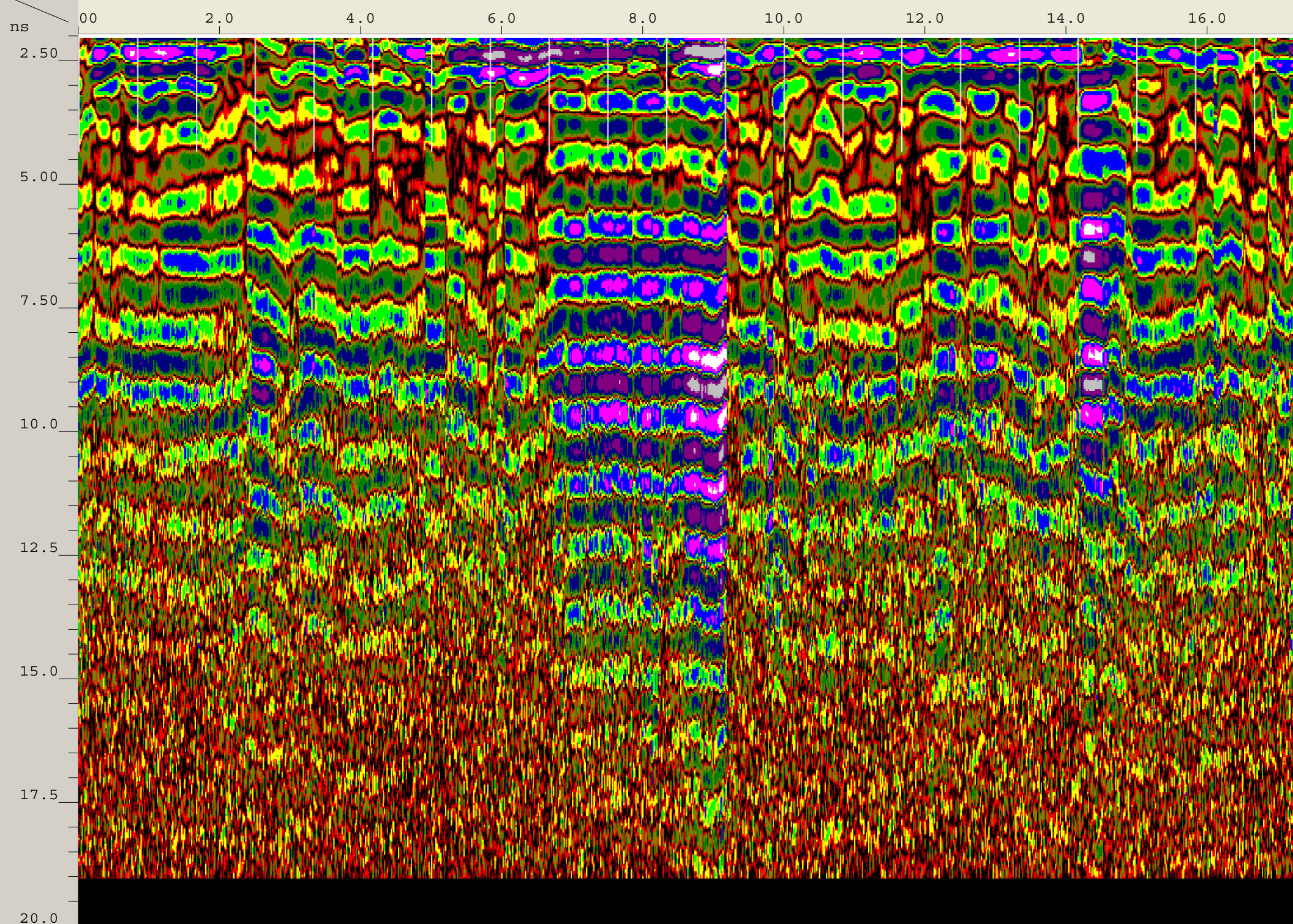
110



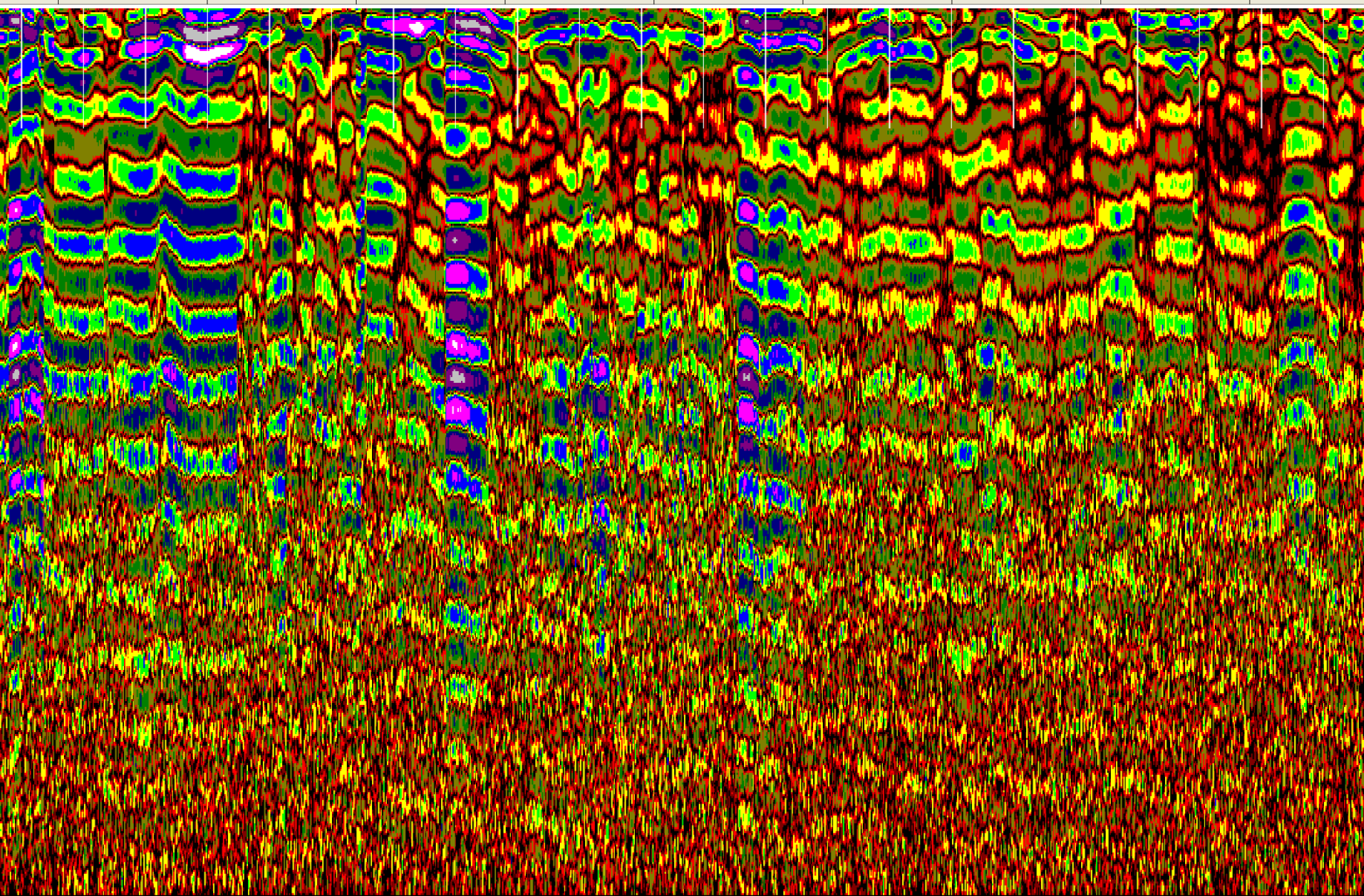


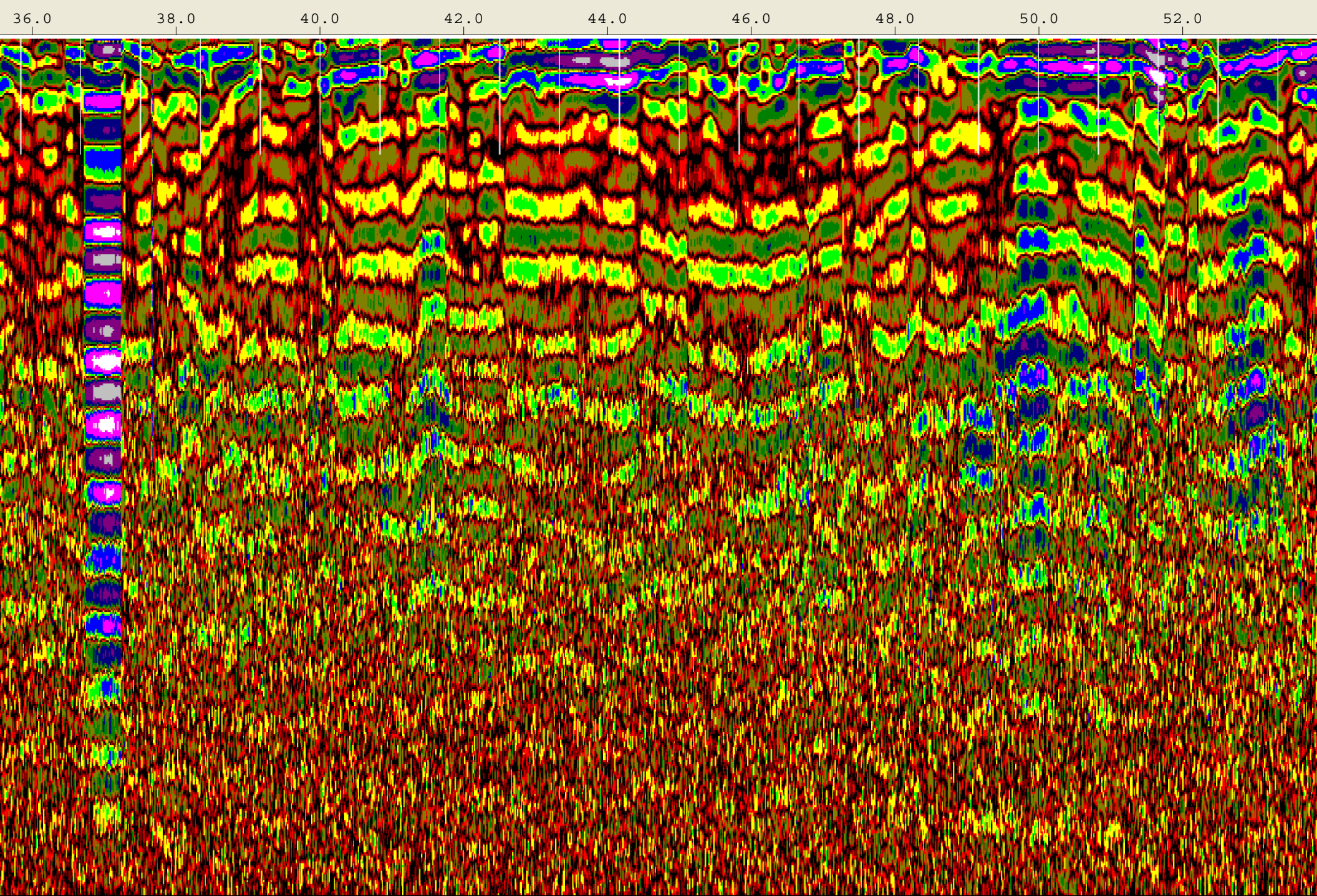
Created Jun, 22 2008, 12:33:14 Modified Jun, 22 2008, 12:39:46
Channel(s) 1 Samples/Scan 512 Bits/Sample 16
Scans/Second 100 Scans/Meter 196.85 Meters/Mark 0.254
Diel Constant 9.18105

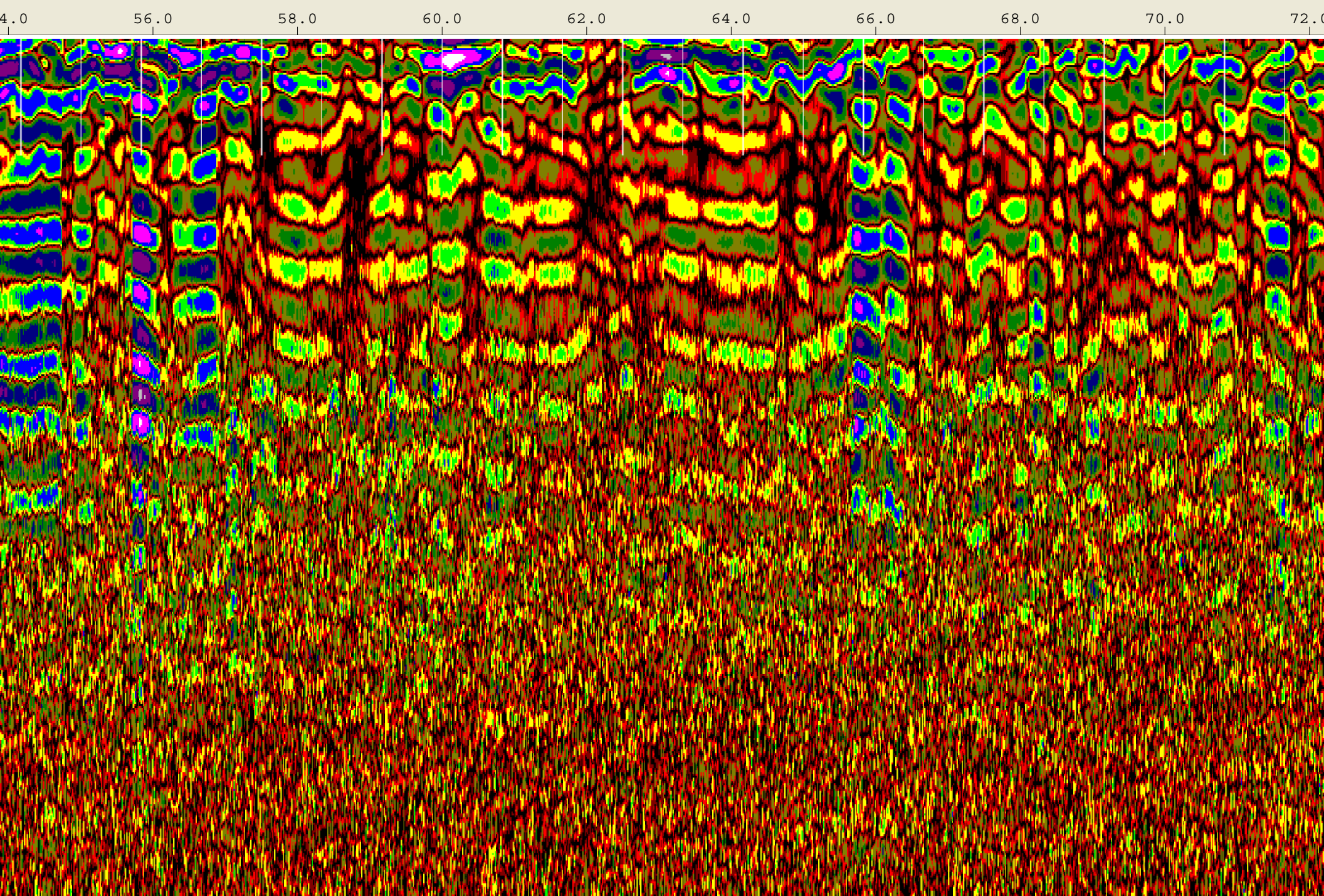
CHANNEL 1 1.5/1.6GHz
Position 1.97 nS Range 19 nS
Range Gain (dB) -2.0 5.0 30.0
30.0 30.0
Position Correction 6.775 nS
Vert IIR HP N =1 F =10 MHz
Vert Boxcar LP F =1930 MHz
Vert Boxcar HP F =295 MHz
Position Correction 1.97 nS
Horz Boxcar Bkgr N=1023
Range Gain (L) 2.7 6.1 3.5
2.0 2.7 2.2
2.2 1.0



18.0 20.0 22.0 24.0 26.0 28.0 30.0 32.0 34.0







74.0

76.0

78.0

80.0

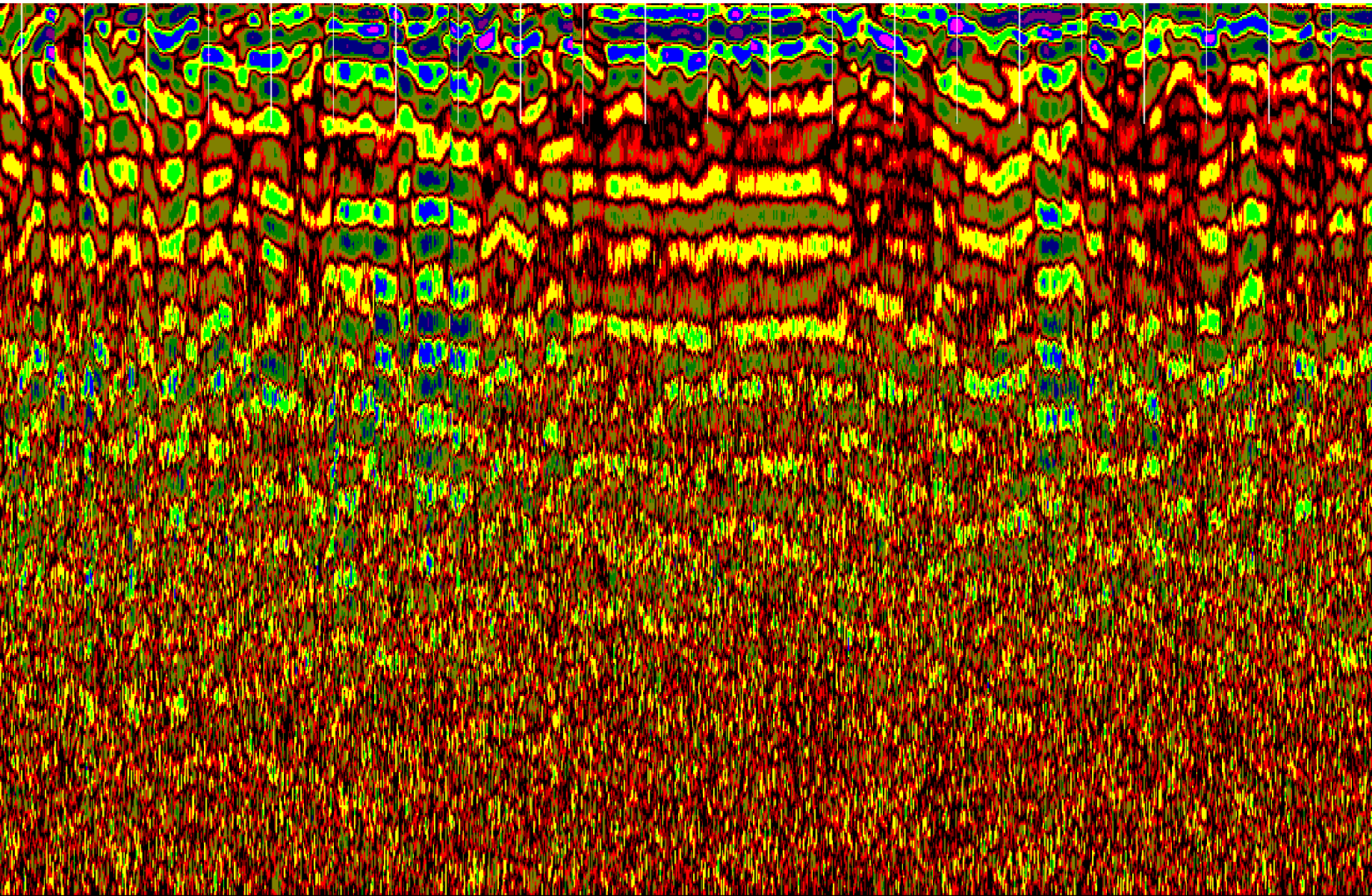
82.0

84.0

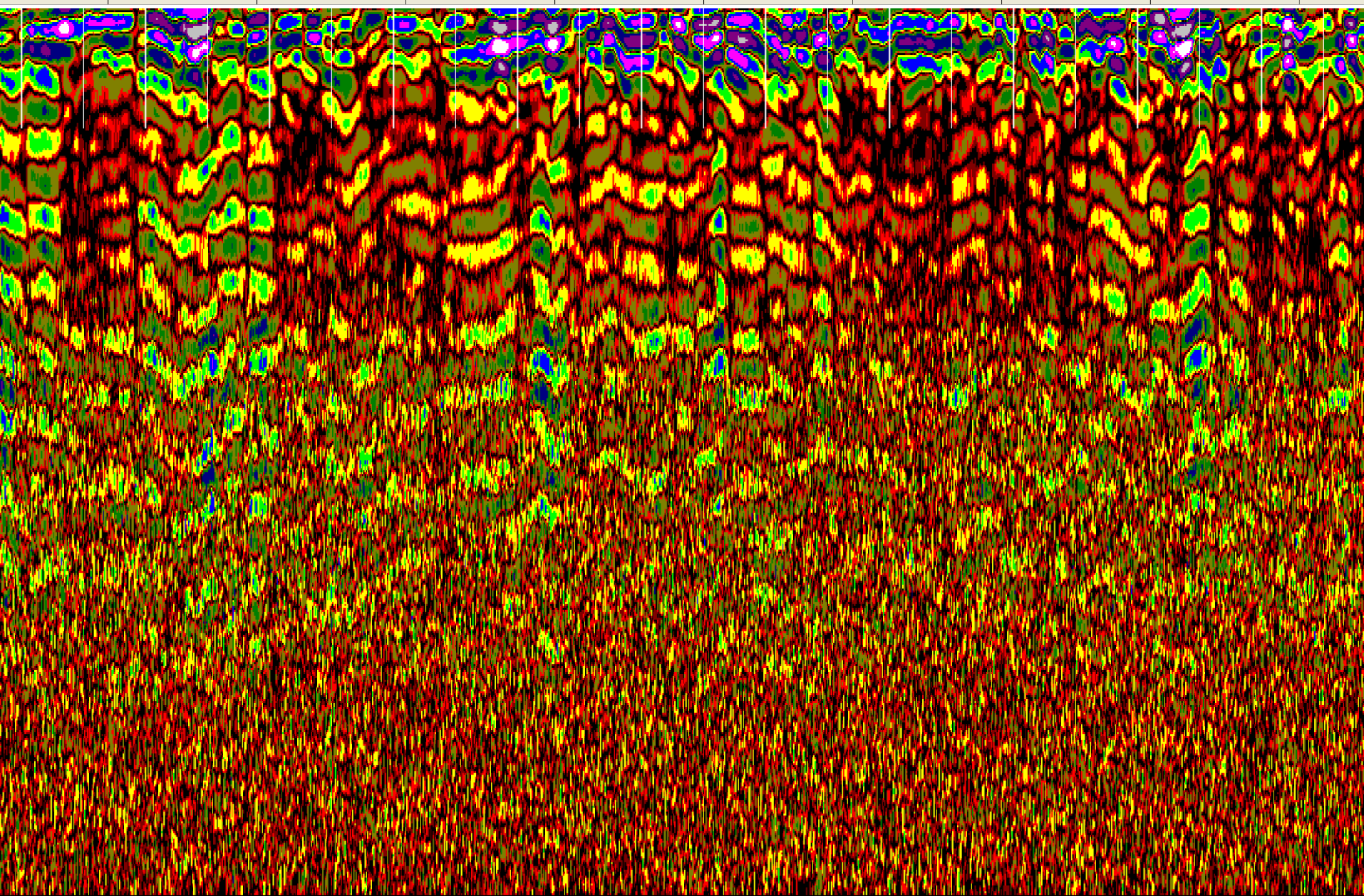
86.0

88.0

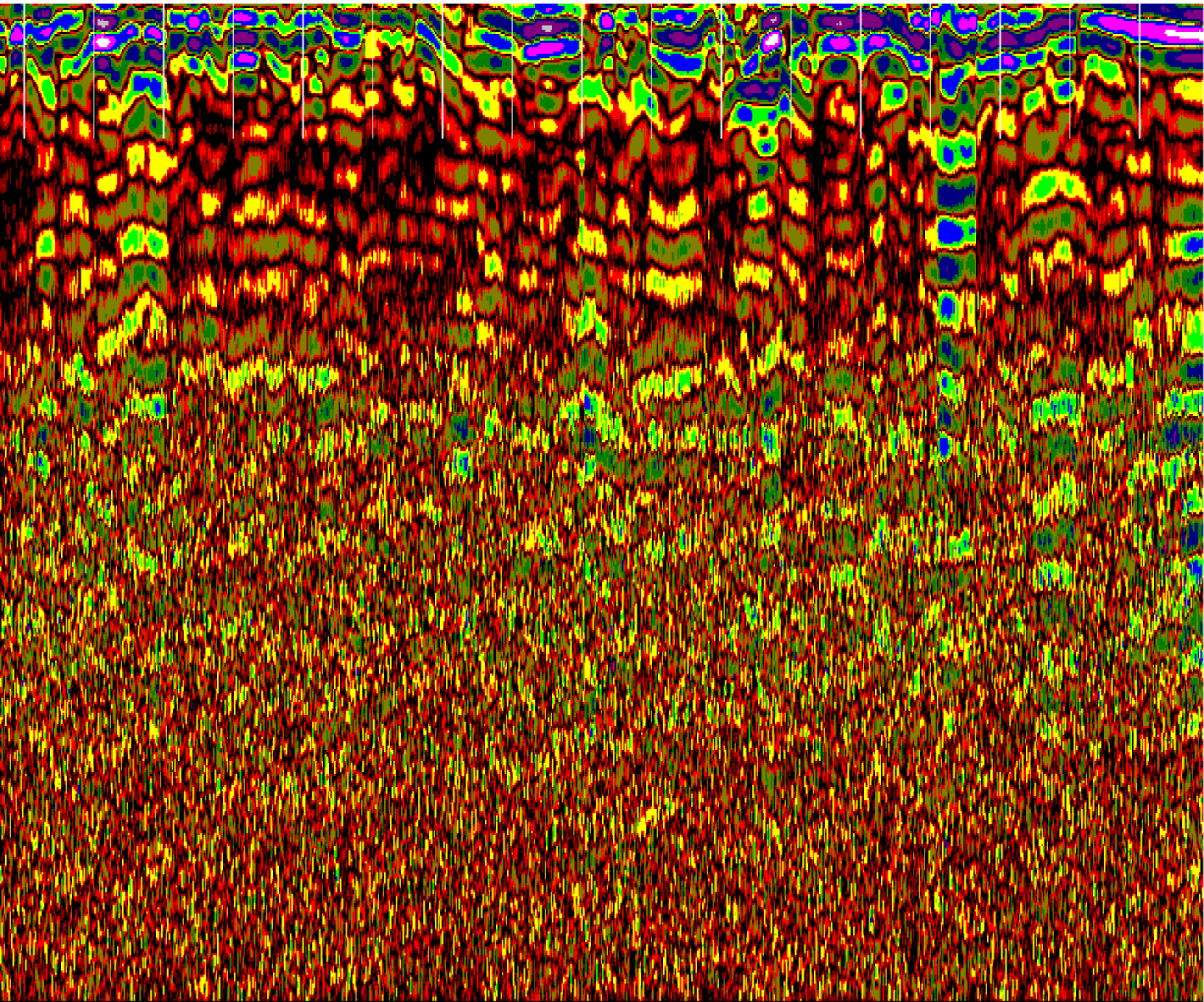
90.0



92.0 94.0 96.0 98.0 100.0 102.0 104.0 106.0 108.0

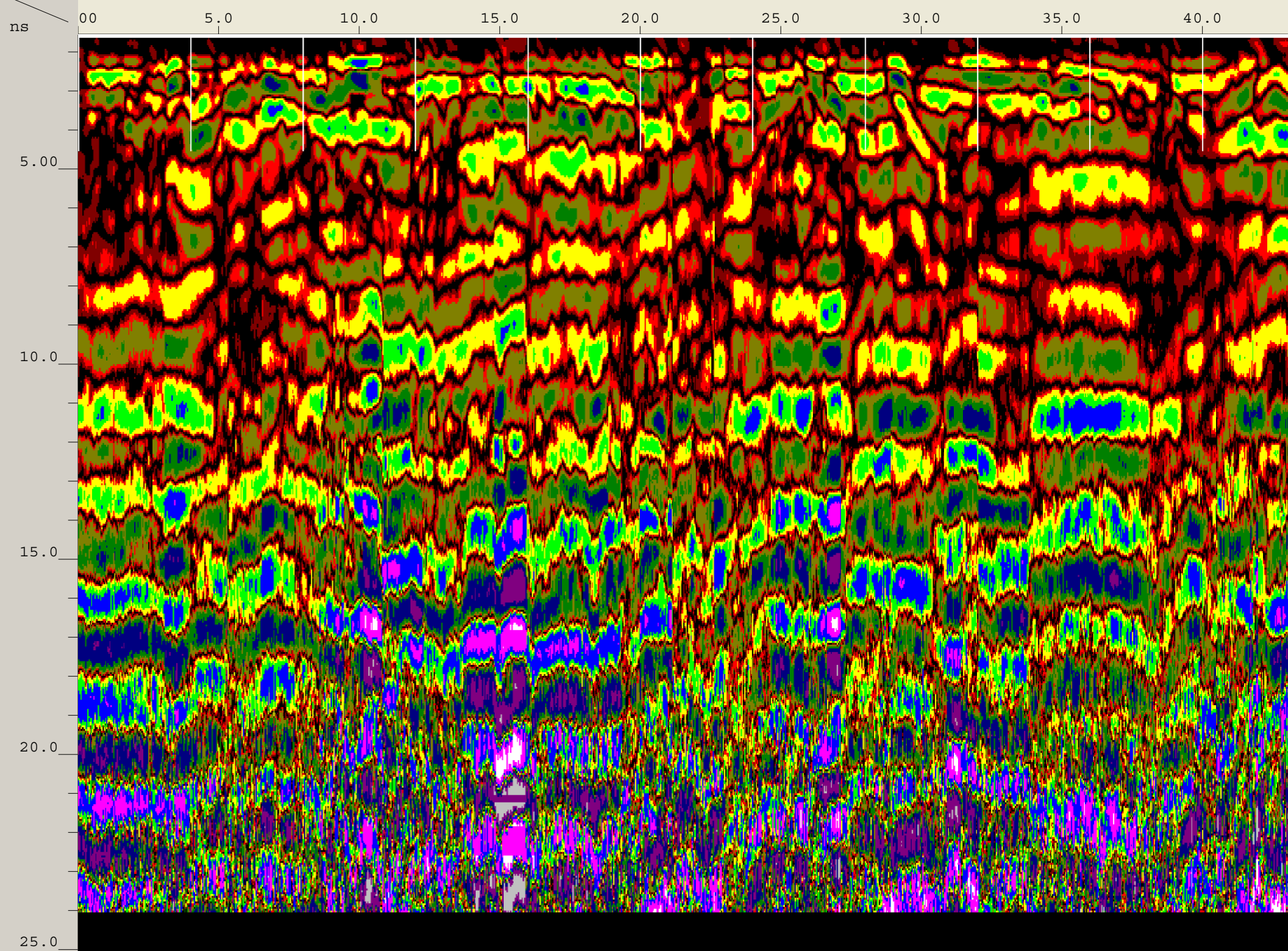


110.0 112.0 114.0 116.0 118.0 120.0 122.0

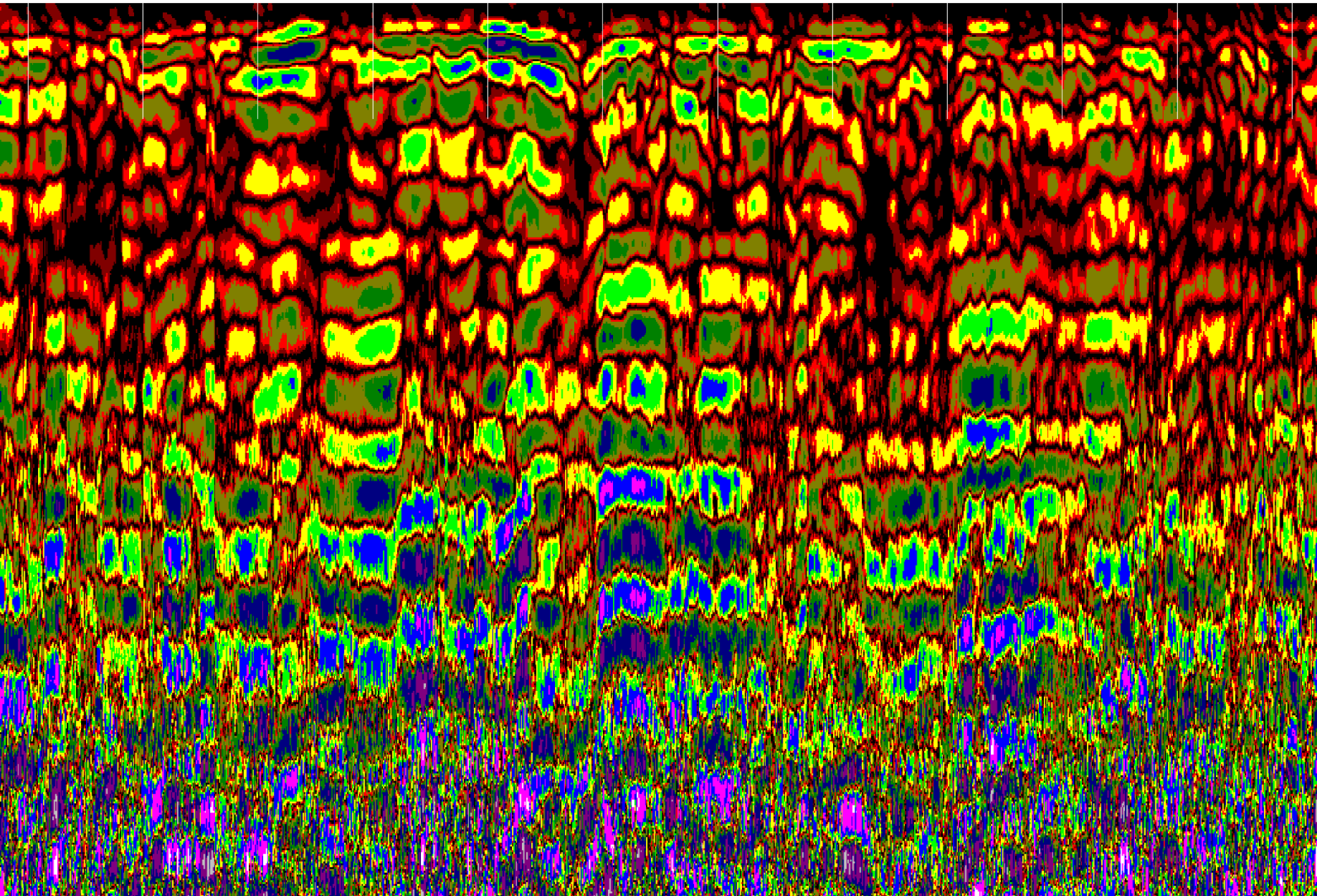


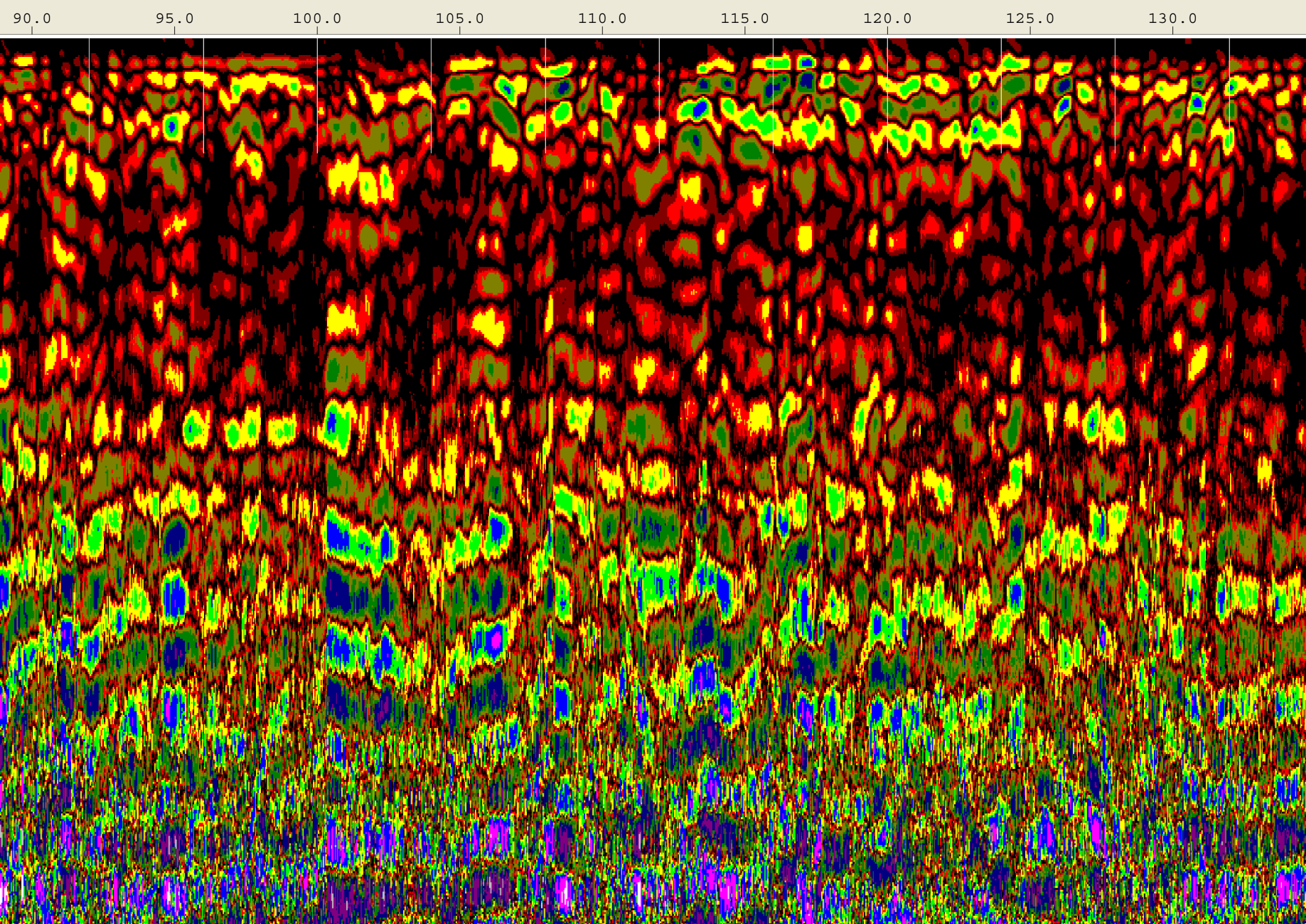
Created Jun, 22 2008, 12:06:06 Modified Jun, 22 2008, 12:10:02
Channel(s) 1 Samples/Scan 512 Bits/Sample 16
Scans/Second 100 Scans/Meter 78.7402 Meters/Mark 1.2192
Diel Constant 80

CHANNEL 1 900MHz
Position 1.55 nS Range 24 nS
Position Correction 1.04 nS
Vert IIR LP N =1 F =2500 MHz
Vert IIR HP N =1 F =225 MHz
Range Gain (dB) 4.0 38.0 56.0
Position Correction 1.55 nS
Horz Boxcar Bkgr N=1023

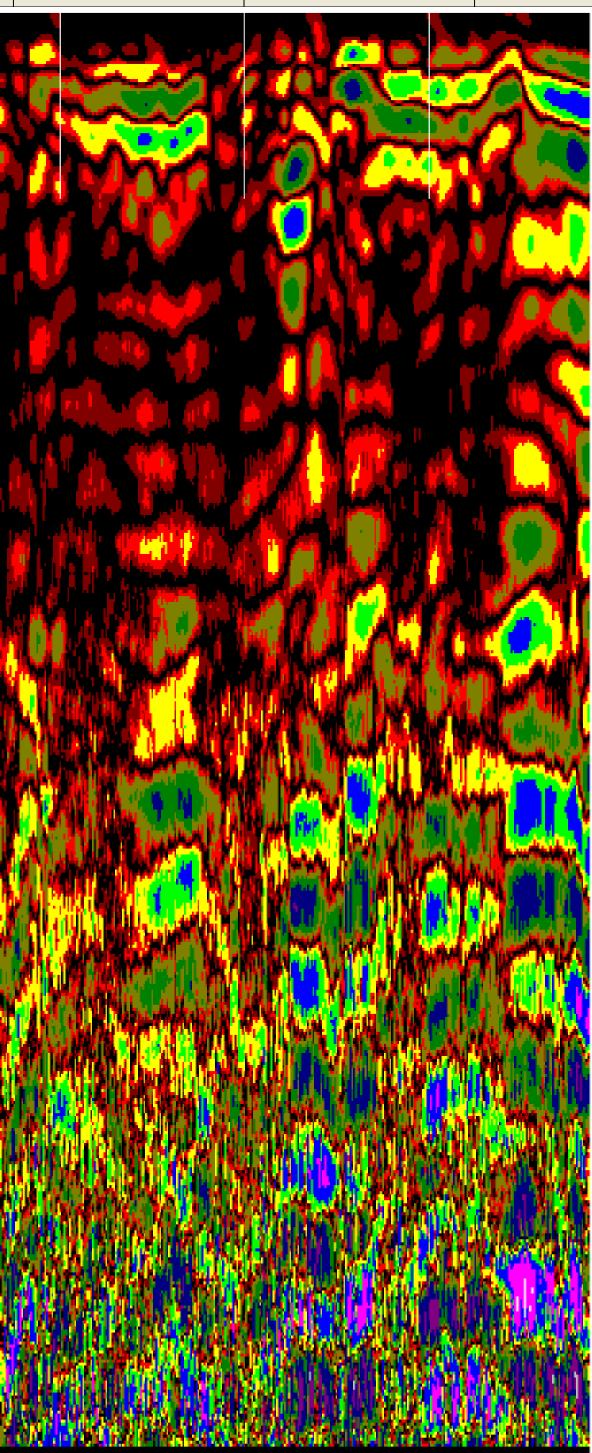


45.0 50.0 55.0 60.0 65.0 70.0 75.0 80.0 85.0



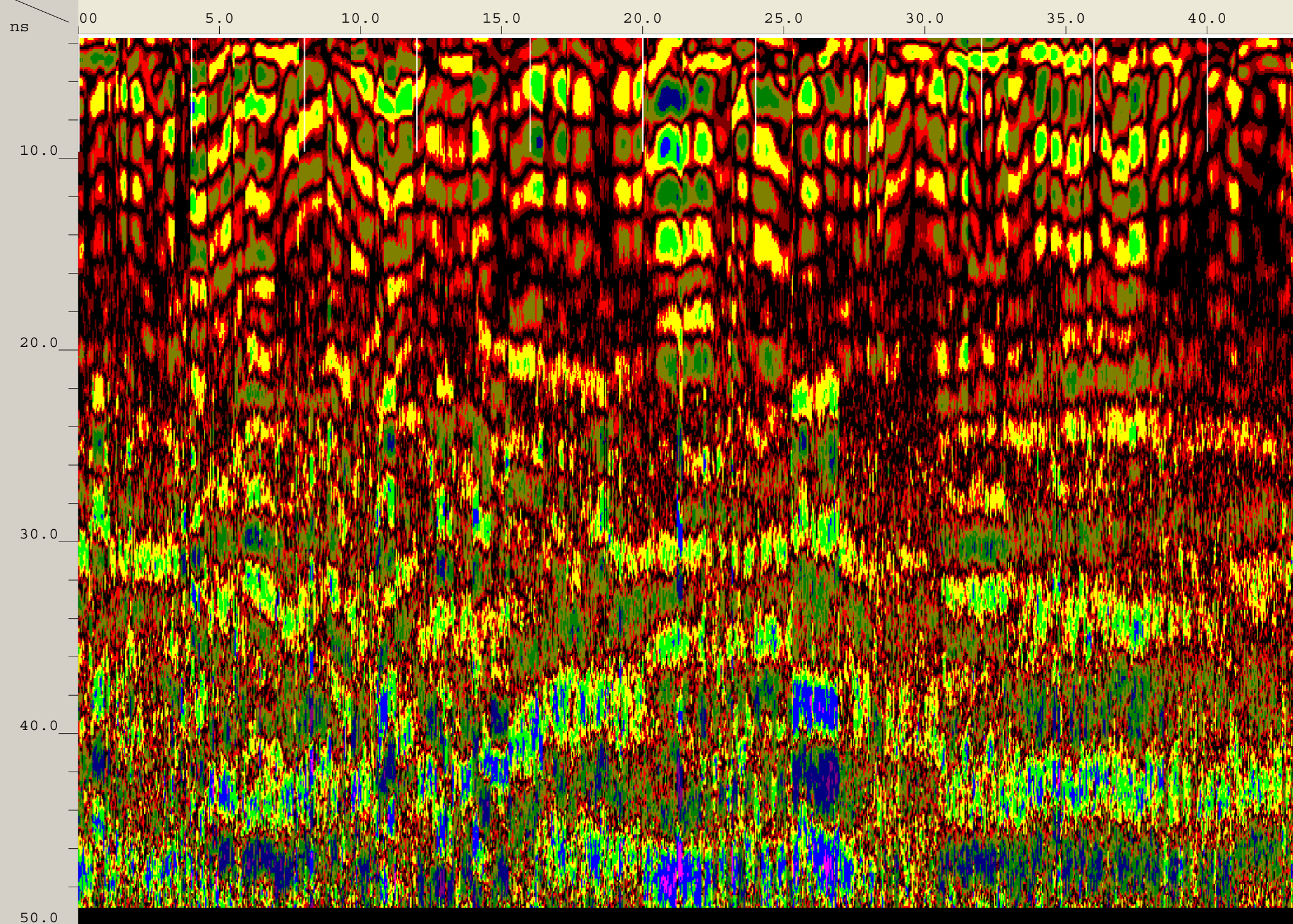


135.0 140.0 145.0

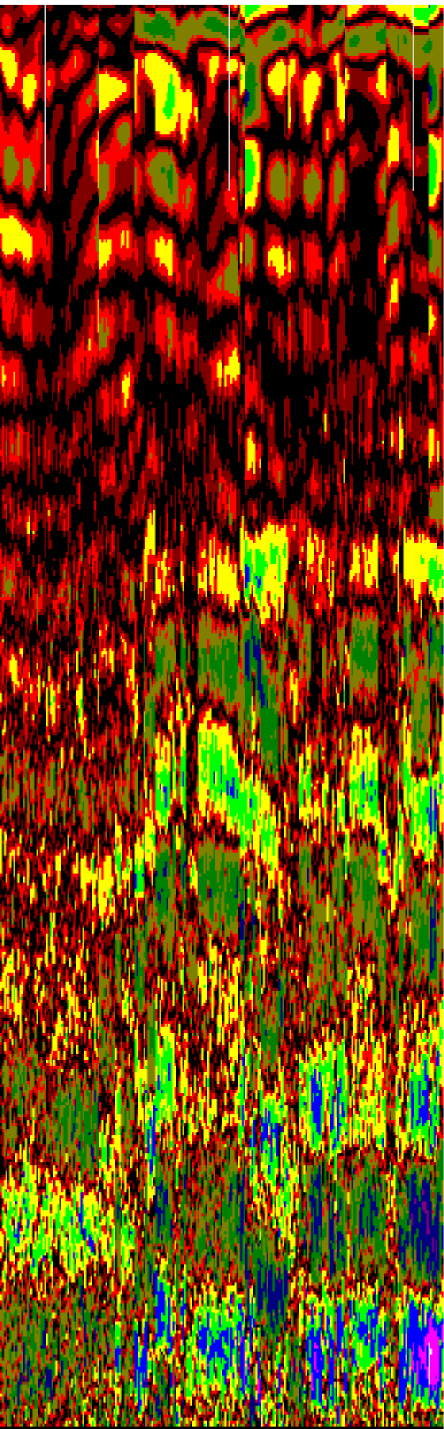


Created Jun, 22 2008, 11:18:06 Modified Jun, 22 2008, 11:22:32
Channel(s) 1 Samples/Scan 512 Bits/Sample 16
Scans/Second 100 Scans/Meter 78.7402 Meters/Mark 1.2192
Diel Constant 80

CHANNEL 1 400MHz
Position 3.54 nS Range 49 nS
Position Correction 1.04 nS
Vert IIR LP N =1 F =800 MHz
Vert IIR HP N =1 F =100 MHz
Range Gain (dB) 0.0 32.0 43.0
Position Correction 3.54 nS
Horz Boxcar Bkgr N=1023

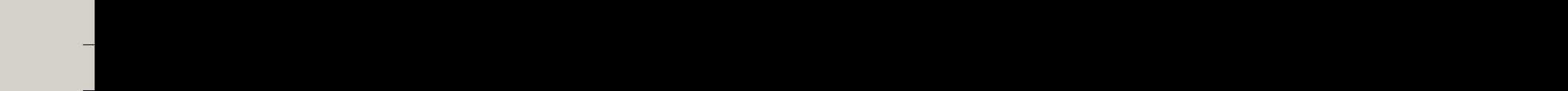
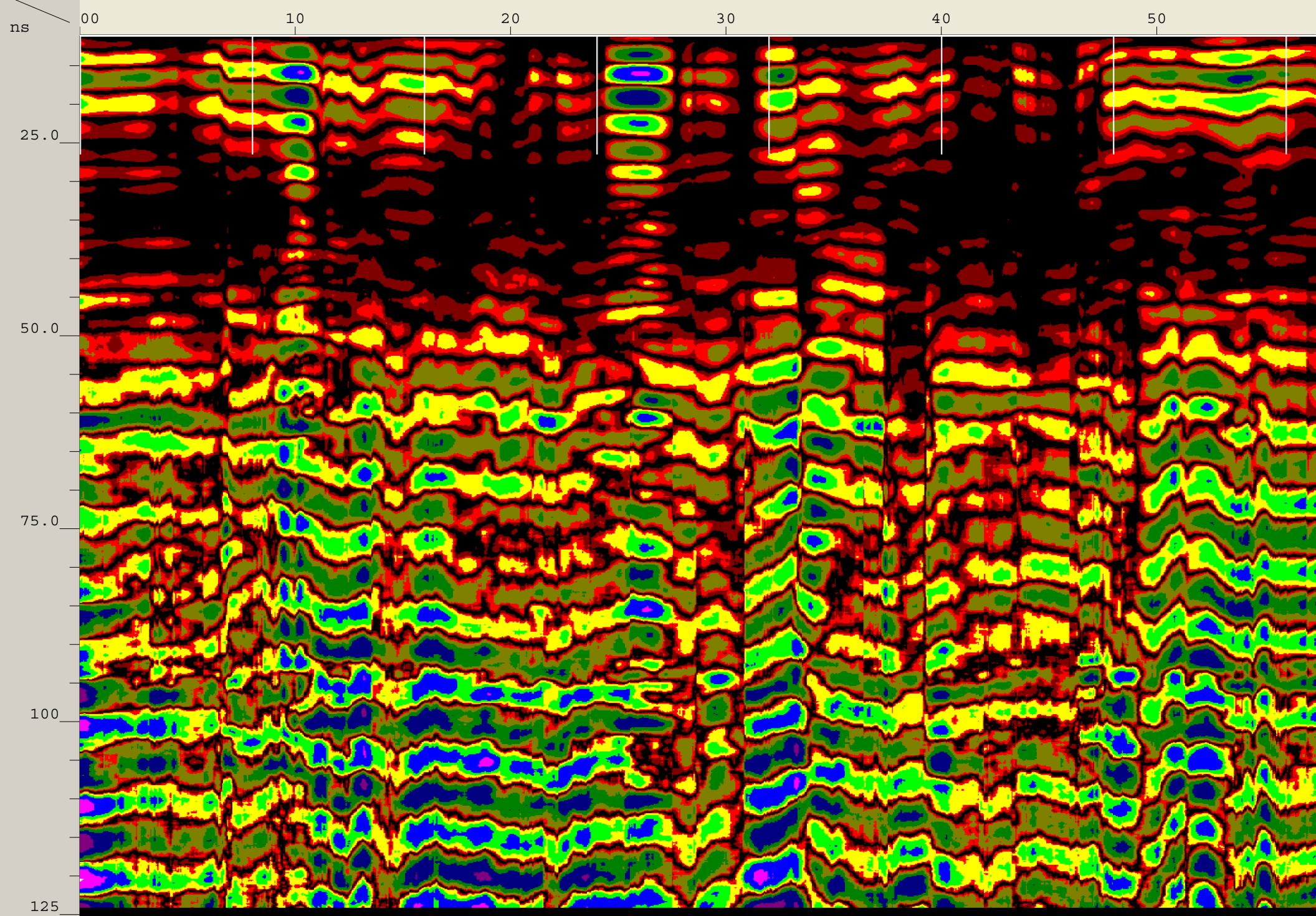


45.0 50.0

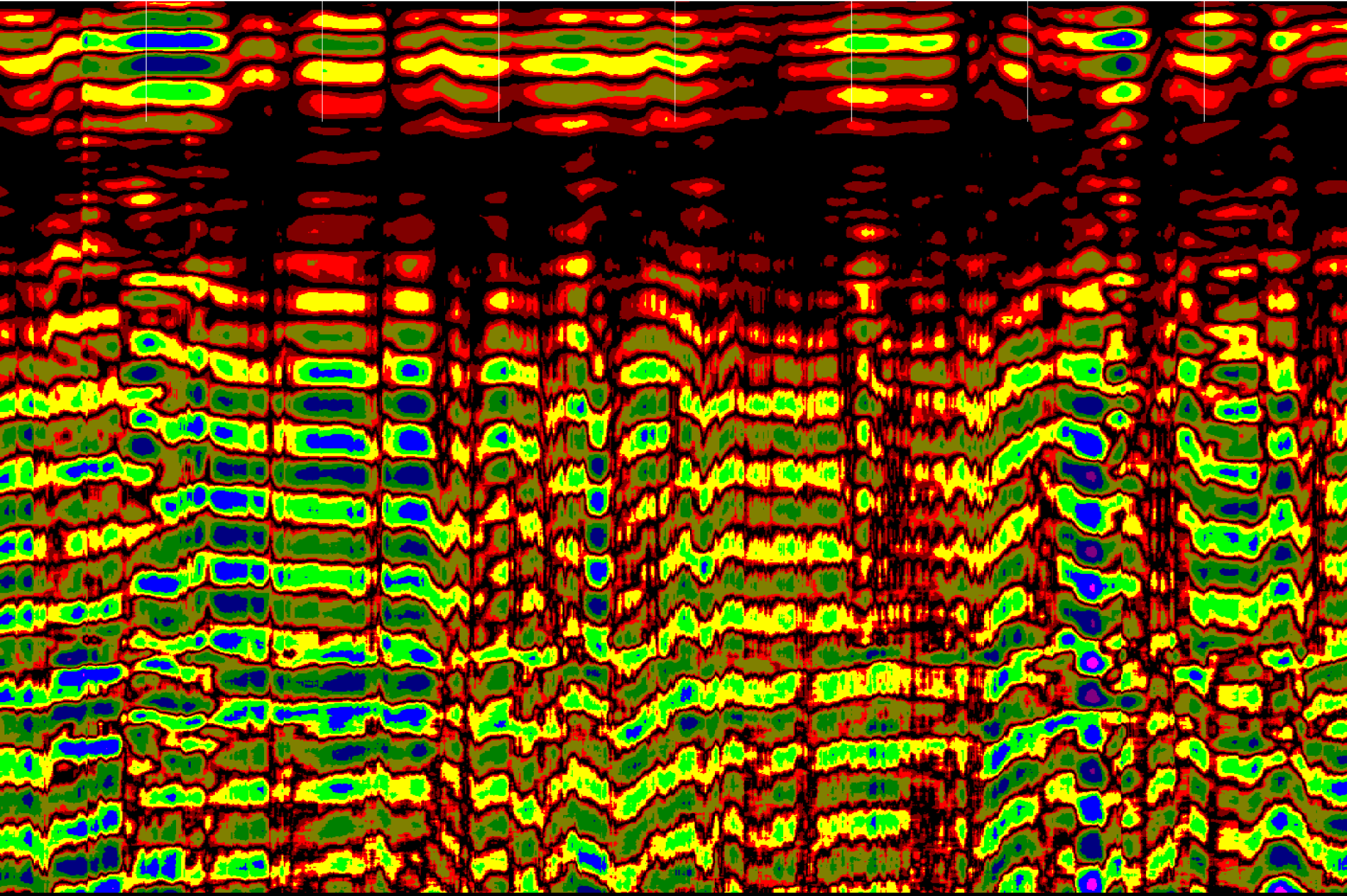


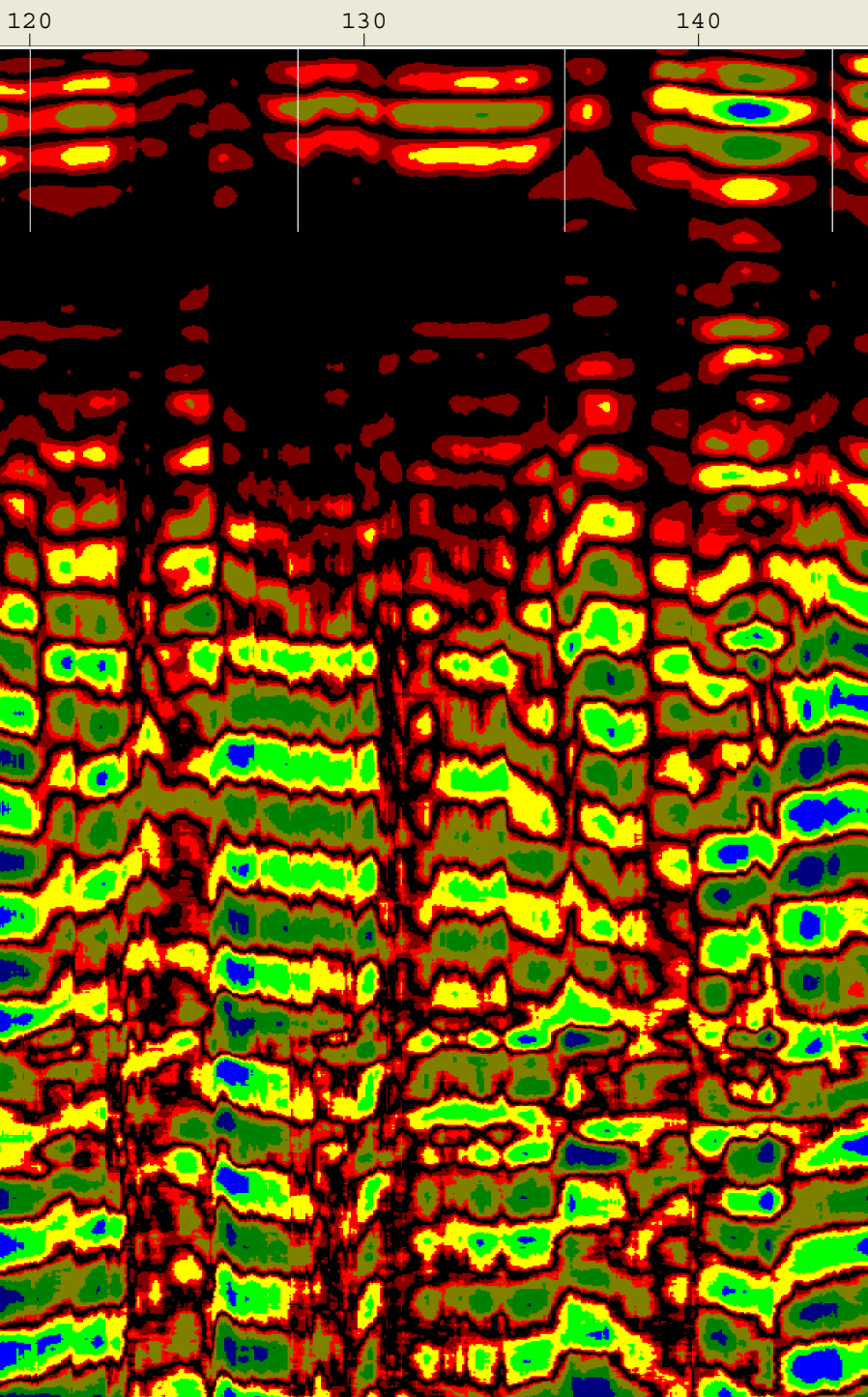
Created Jun, 22 2008, 10:45:14 Modified Jun, 22 2008, 10:50:42
Channel(s) 1 Samples/Scan 1024 Bits/Sample 16
Scans/Second 64 Scans/Meter 59.0551 Meters/Mark 2.4384
Diel Constant 6

CHANNEL 1 270MHz
Position 11.02 nS Range 124 nS
Vert IIR LP N =1 F =700 MHz
Vert IIR HP N =1 F =75 MHz
Horz IIR Stack TC =11
Position Correction -4.35 nS
Range Gain (dB) -19.0 34.0 56.0
Position Correction 11.02 nS
Horz Boxcar Bkgr N=1023
Range Gain (L) 1.0 4.9 4.9
2.9 2.0 1.0
1.0



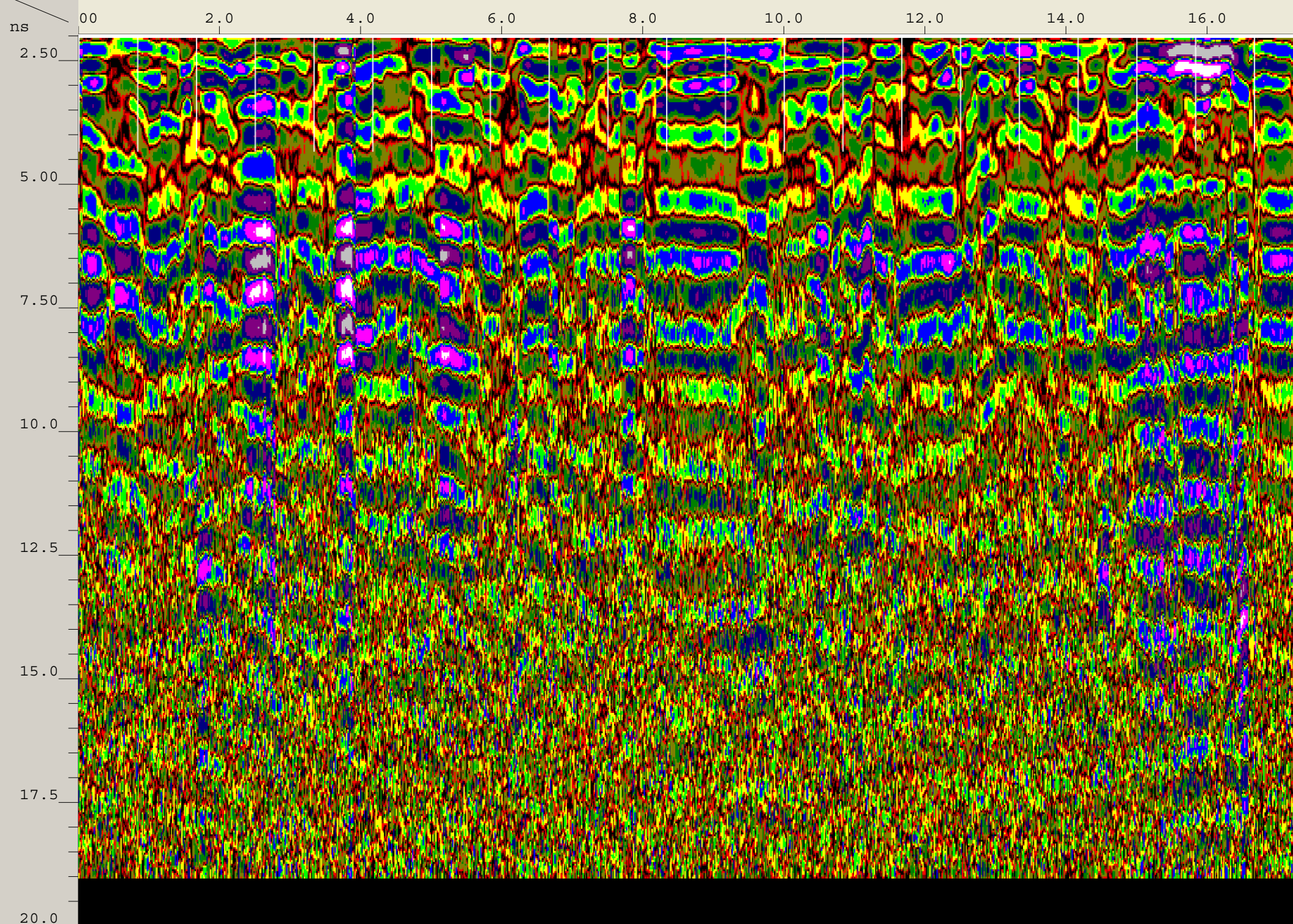
60 70 80 90 100 110



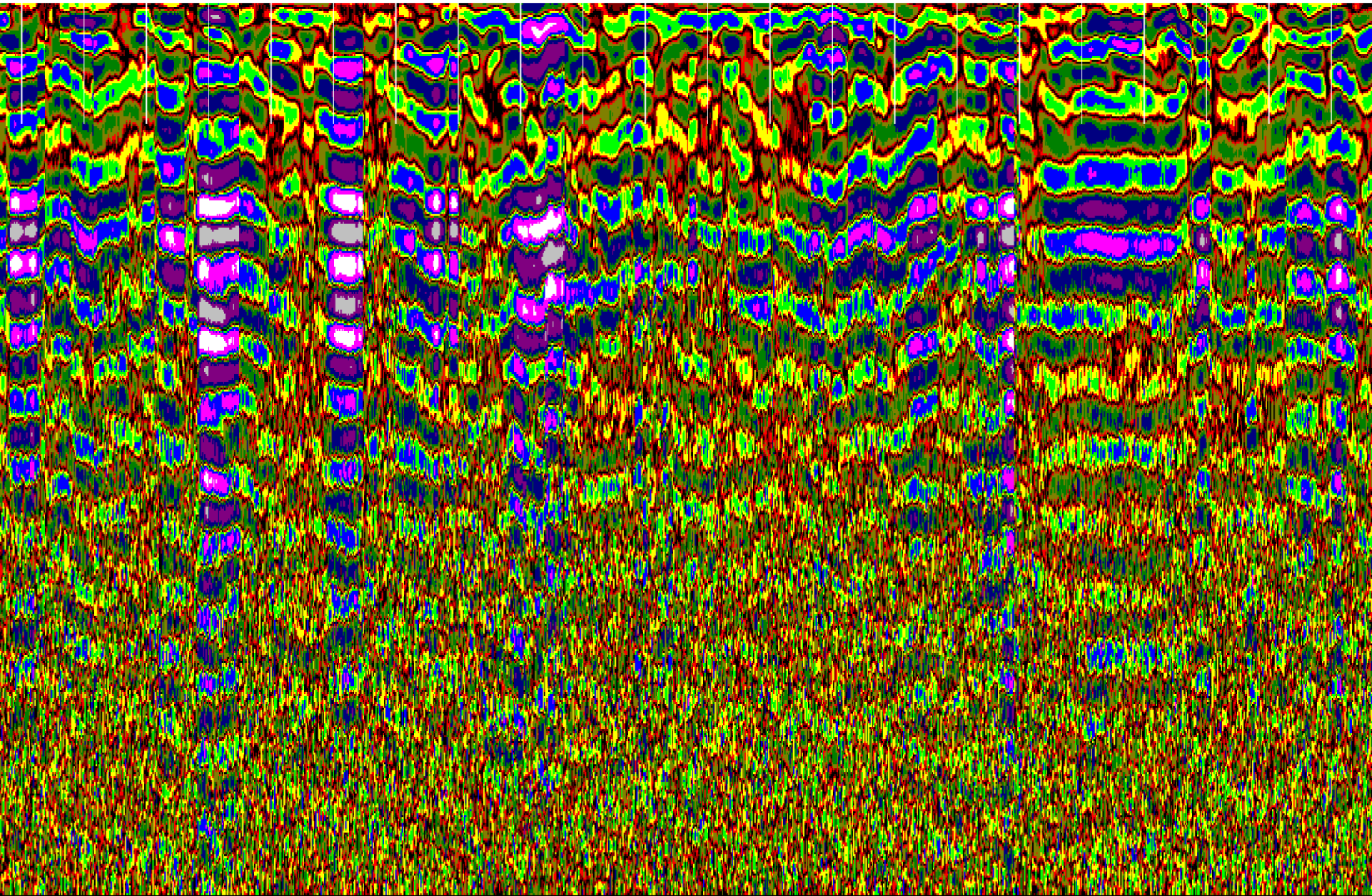


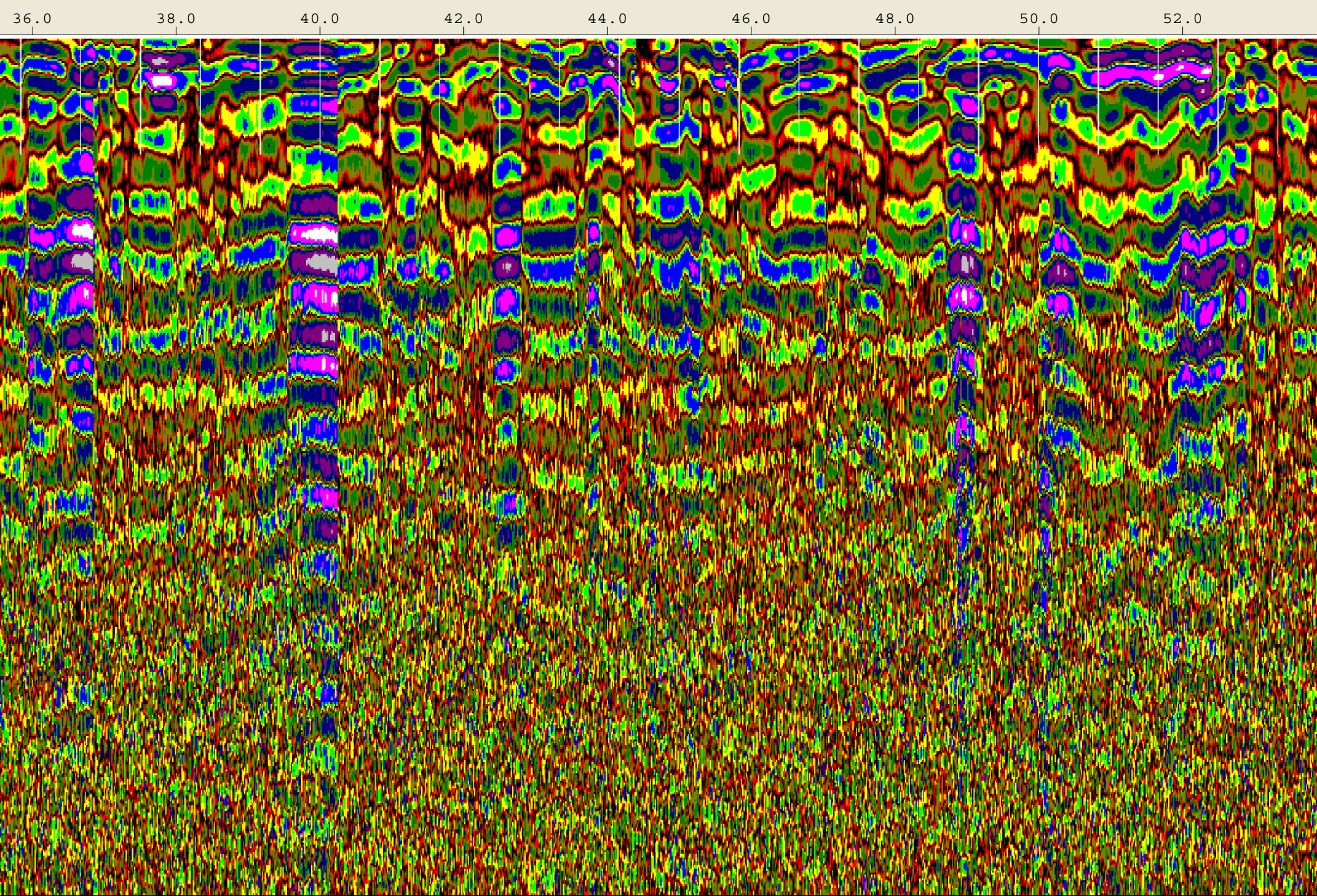
Created Jun, 22 2008, 12:46:24 Modified Jun, 22 2008, 12:51:04
Channel(s) 1 Samples/Scan 512 Bits/Sample 16
Scans/Second 100 Scans/Meter 196.85 Meters/Mark 0.254
Diel Constant 12.3316

CHANNEL 1 1.5/1.6GHz
Position 1.97 nS Range 19 nS
Range Gain (dB) -2.0 5.0 30.0
30.0 30.0
Position Correction 6.775 nS
Vert IIR HP N =1 F =10 MHz
Vert Boxcar LP F =1930 MHz
Vert Boxcar HP F =295 MHz
Position Correction 1.97 nS
Horz Boxcar Bkgr N=1023
Range Gain (L) 1.4 8.2 8.8
1.8 2.9 4.0
4.2 4.2 4.2

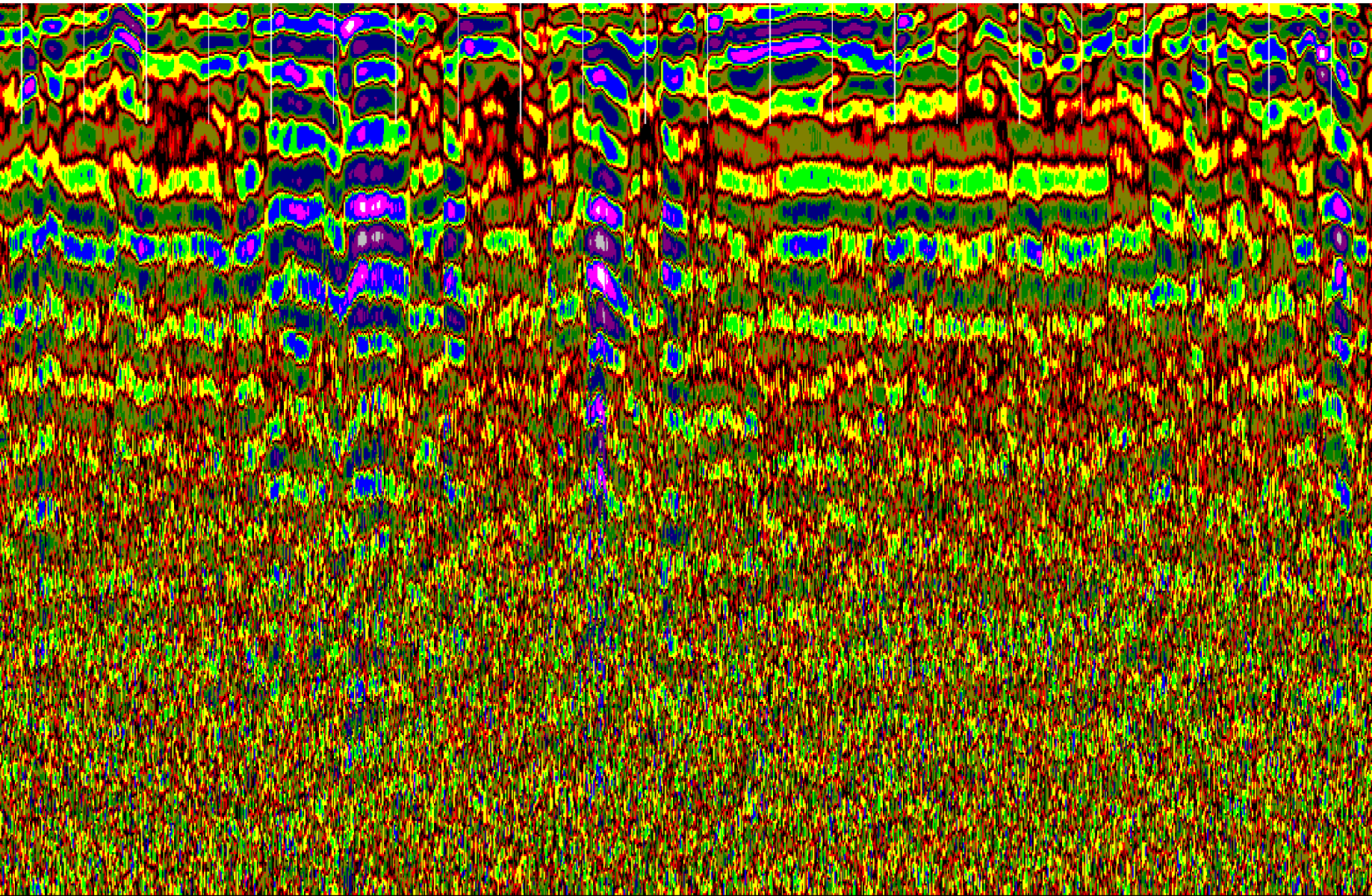


18.0 20.0 22.0 24.0 26.0 28.0 30.0 32.0 34.0





4.0 56.0 58.0 60.0 62.0 64.0 66.0 68.0 70.0 72.0



74.0

76.0

78.0

80.0

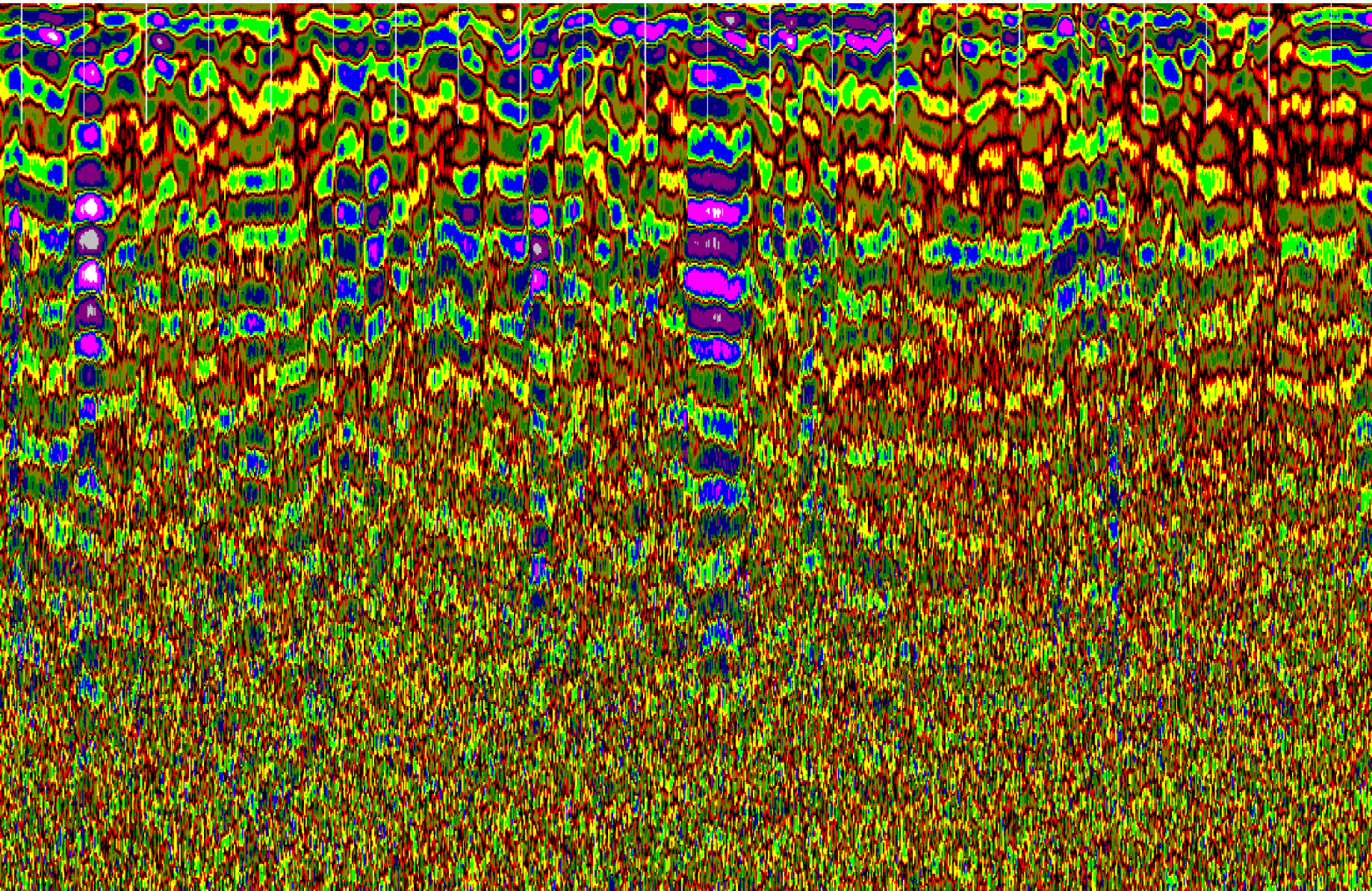
82.0

84.0

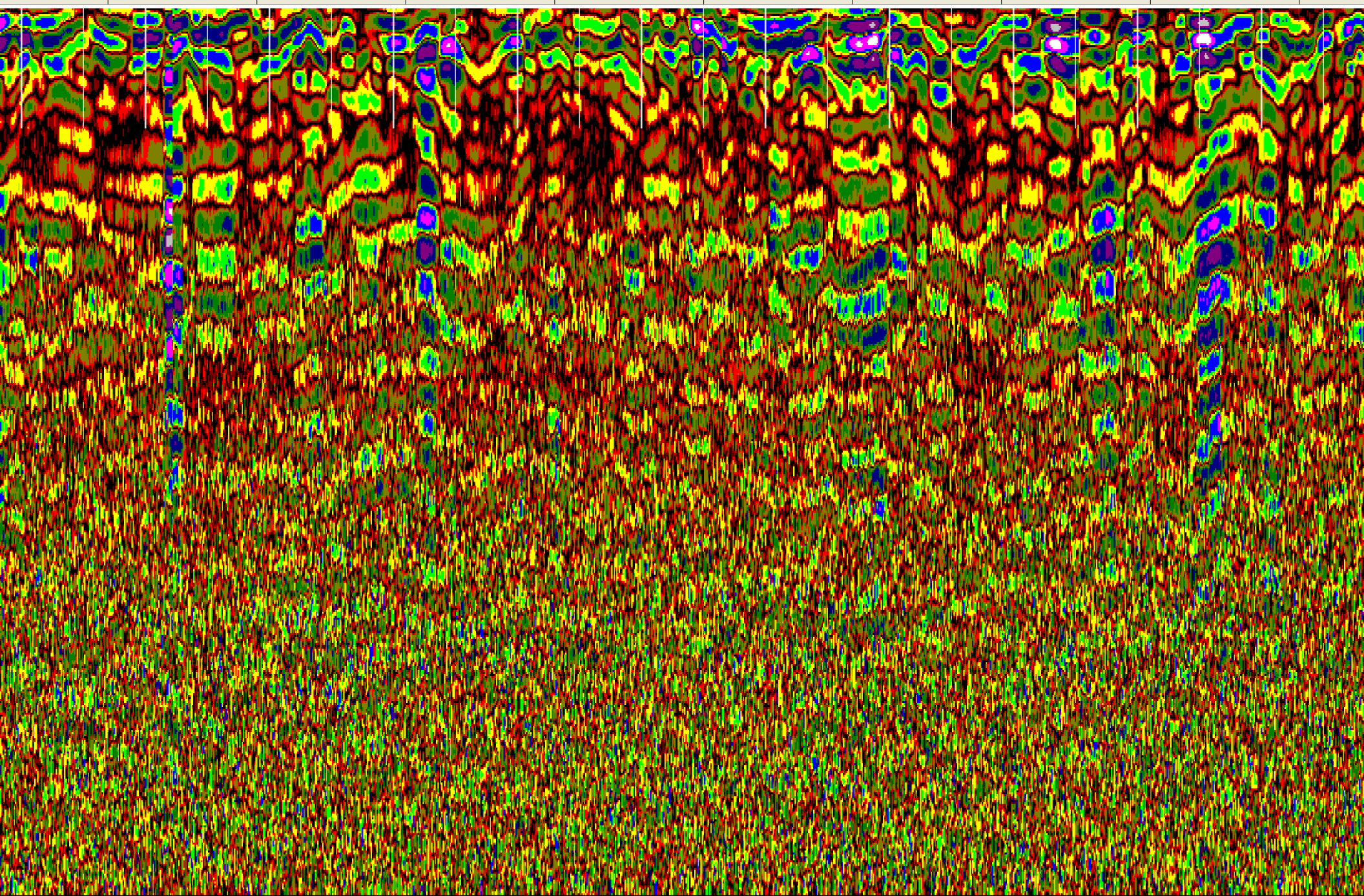
86.0

88.0

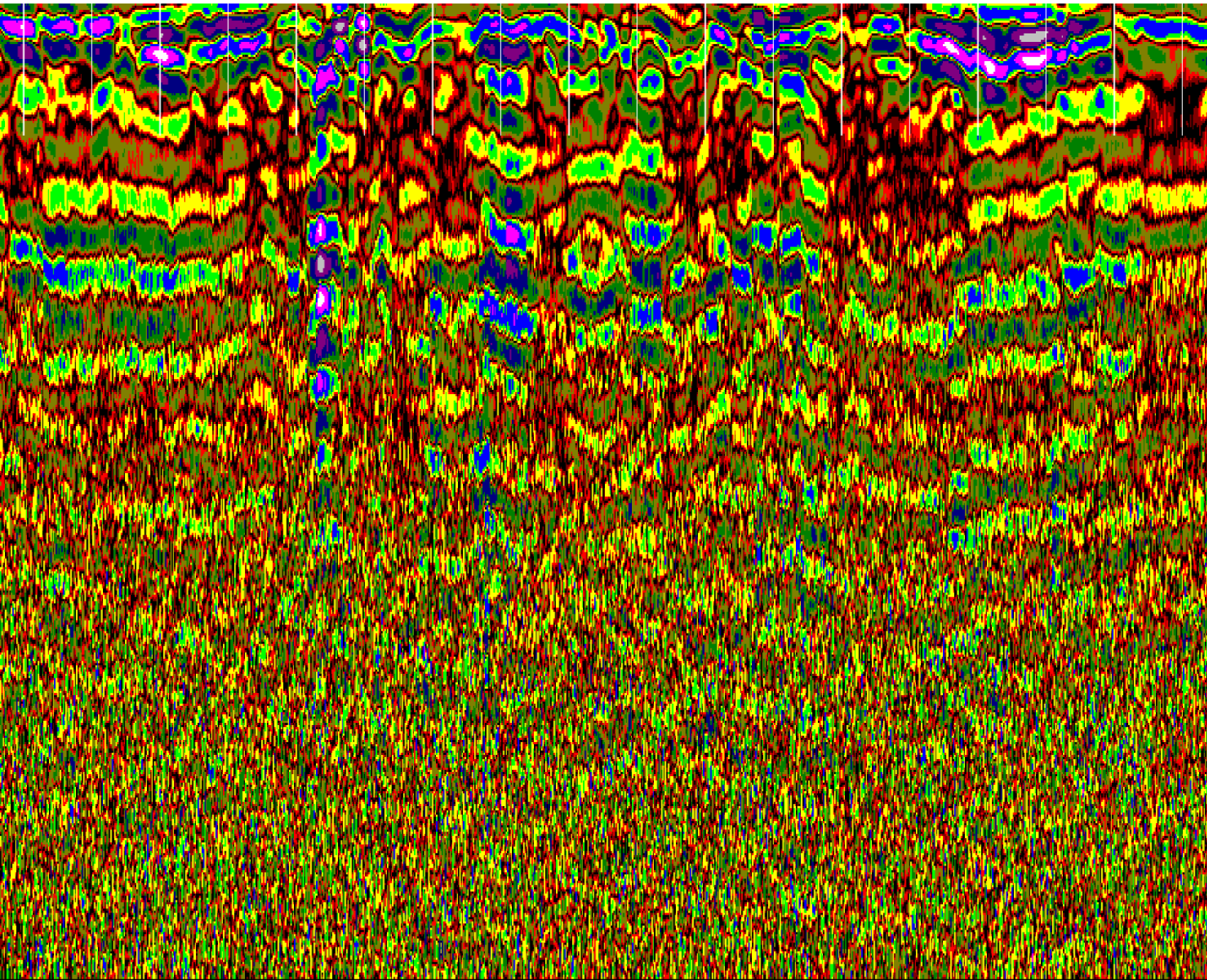
90.0



92.0 94.0 96.0 98.0 100.0 102.0 104.0 106.0 108.0



110.0 112.0 114.0 116.0 118.0 120.0 122.0

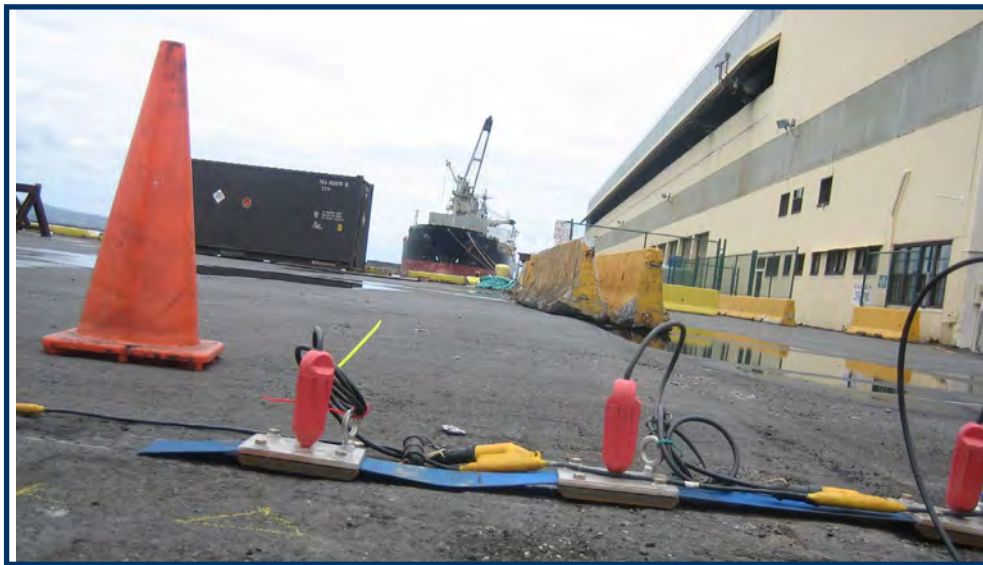


Consultant Report, Dawood (2008): Port of Hilo Geophysical Investigation

UNIVERSITY OF HAWAII
at Manoa

**PORT OF HILO GEOPHYSICAL
INVESTIGATION REPORT**

AUGUST 1, 2008



DAWOOD
PEOPLE ENGINEERING INNOVATION



10105 Allentown Boulevard, Grantville, Pennsylvania 17028
Phone: (717) 469-0937 Fax: (717) 469-0938
Dawood Project No. **208044.01**

UNIVERSITY OF HAWAII
at Manoa

PORT OF HILO GEOPHYSICAL
INVESTIGATION REPORT

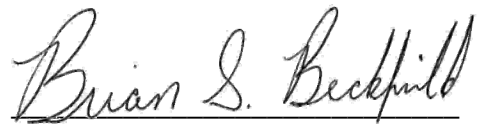
AUGUST 1, 2008

Report Prepared by:



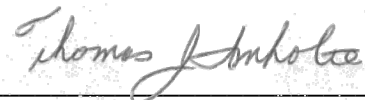
Rick A. Hoover, PG
Director, Geophysical Services

Report Reviewed by:



Brian Beckfield, PG
Geophysical Manager

Approved for Distribution



Thomas J. Imholte, PE
Manager Geotechnical Services



DAWOOD

PEOPLE ENGINEERING INNOVATION

10105 Allentown Boulevard, Grantville, Pennsylvania 17028

Phone: (717) 469-0937 Fax: (717) 469-0938

Dawood Project No. 208044.01



UNIVERSITY
of HAWAII
MANOA

TABLE OF CONTENTS

1. Introduction	1
2. Site Description	1
3. Introduction to the Nondestructive Geophysical Methods Employed	1
3.1. Ground Penetrating Radar	1
3.1.1. GPR Principles	2
3.1.2. GPR Limitations	3
3.2. Seismic Refraction	3
3.2.1. Seismic Refraction Limitations.....	4
4. Geophysical Data Collection	5
4.1. GPR Site Specific Data Collection Parameters	5
4.2. Refraction Data Collection Method.....	6
5. Geophysical Data Processing	6
5.1. GPR Processing	6
5.2. Refraction Data Processing	7
6. Geophysical Data Presentation	7
6.1. GPR.....	7
6.2. Seismic Refraction	8
6.3. Geophysical Data Integration.....	9
7. Geophysical Data Summary and Conclusions	10
8. References	12

Figures

Figure 1 – Location Map	Following Text
Figure 2 – Survey Area	Following Text
Figure 3 – GPR Traverse Locations	Following Text
Figure 4 – Refraction Locations	Following Text
Figure 5 – GPR Processing	Following Text
Figure 6 – GPR Traverse 75 Interpretation	Following Text
Figure 7 – GPR Traverse 120 Interpretation	Following Text
Figure 8 – Refraction Crossing Line	Following Text
Figure 9 – Refraction Line 38	Following Text
Figure 10 – Refraction Low Velocity Areas	Following Text
Figure 11 – Cross Line Comparison	Following Text

Tables:

Table 1 – Typical Compressional Velocities for Common Material	4
--	---

1. INTRODUCTION

The ground surface at the Port of Hilo has been subject to settlement over the years. Two separate origins for the settlement have been presented by others. One idea is the concept of subsurface soil erosion caused by soil erosion through volcanic lava tubes in the area. The other is differential settlement due to the increased cargo loads passing through the port. The differential settlement poses a hazard to personnel and cargo as equipment is subject to tipping during movement.

Non-destructive geophysical testing was identified as a means to assess subsurface conditions at the port. The work was performed as an application of subsurface void testing which was being undertaken at three other field sites in the region. Three different geophysical methods were identified for void testing including electromagnetic (EM), seismic and ground penetrating radar (GPR). The design approach utilized included reasonably common geophysical tools, with acquisition parameters adjusted to meet the survey objective.

Due presence of cargo containers, and equipment movement at the Port, EM was not utilized at this facility. Additionally, seismic acquisition parameters described below may not have been optimal for this survey due to site noise. The combination of access, equipment and personnel provided an opportunity to collect reasonable geophysical data to establish a basis for future, and more detailed assessments.

2. SITE DESCRIPTION

Hilo is located on eastern side of the island of Hawaii. Port of Hilo is located on the eastern part of town ([Figure 1](#)), just north of the Hilo Airport. Hilo is located east of the two active volcanoes, which dominate the landscape of the island, and the underlying bedrock material on the island is from volcanic lava flows.

Soils at the port of Hilo are carbonate sands and gravels with a relatively shallow water table. The site is potentially underlain by volcanic tubes can be present from historic volcanic activity. The volcanic tubes can provide soil migration pathways for subsurface soil erosion and the formation of sinkholes. The saltwater-table at this site is approximately 10-feet below ground surface.

3. INTRODUCTION TO THE NONDESTRUCTIVE GEOPHYSICAL METHODS EMPLOYED

3.1. Ground Penetrating Radar

Ground-penetrating radar (GPR) is useful in locating and identifying features buried below grade level with a high degree of resolution. Common applications include the use of GPR to determine or verify the location and sizes of underground storage tanks (USTs), map utilities, delineate buried wastes, evaluate sinkhole/collapse features, detect archaeological features, and perform structural assessments.

3.1.1. GPR Principles

GPR systems produce cross-sectional images of subsurface features by transmitting discrete radar pulses into the subsurface and recording the echoes or reflections from interfaces between materials with differing dielectric properties. In principle, GPR is entirely analogous to a medical sonogram or ultrasound, except that GPR uses electromagnetic (radar) energy rather than acoustic (sound) energy and is therefore sensitive to electrical properties (as opposed to ultrasound which is sensitive to densities).

Cross-sectional images of subsurface objects and layers are generated by rapidly and repeatedly transmitting radar pulses into the subsurface as the GPR transmitter and receiver are moved along a survey traverse. For each pulse, the antenna receiver records the reflections from subsurface dielectric contrasts. Data is a measurement of reflected energy amplitude vs. travel time. Successive reflections are plotted side-by-side on the record and produce a cross-sectional image of the dielectric variations in the subsurface.

Reflection amplitudes are dependent on the magnitude of the dielectric contrast at depth. Since the electrical properties of most soils and metal tanks or pipes are dramatically different, these targets produce dramatic and characteristic reflections, which can be easily recognized on a radar record. Concrete, fiberglass, and plastic pipes, as well as tanks and other structures also produce recognizable, but more subtle reflections since they have electrical properties that more closely match many soils. Terra cotta pipes are often difficult to recognize since the electrical properties of terra cotta (clay) are very close to many clay-rich soils. Reflections are also obtained from naturally occurring electrical interfaces such as soil/bedrock, soil/air, bedrock/air, dry soil/saturated soils (i.e. the groundwater table), and other subsurface contacts.

The dielectric permeativity and electrical conductivity (frequently dictated by moisture content) of the soils and the frequency of the radar energy effectively control the depth of penetration by the radar systems. For a given radar frequency, a coherent pulse will travel more deeply into less conductive materials. In highly conductive materials (such as damp clays), the pulse is dissipated at very shallow depths (sometimes measured in inches). Using a transmission antenna with a lower frequency can increase penetration, but this causes a loss of resolution. Frequencies commonly employed fall within the 80 to 900 MHz range. In general, the use of GPR is limited to depths of 15 feet or less (although in very dry sand or bedrock, penetration depths up to 100 feet have been obtained).

Resolution of GPR systems is dependent on the frequency of the antenna employed. Very high frequency antennas (900 MHz or greater) can resolve features one-quarter inch or less in diameter (i.e. reinforcing rods), but penetrate to depths of only one or two feet. The most commonly used antennae (designed for optimum transmission at frequencies of 120 to 500 MHz) can resolve linear features with dimensions as small as one or two inches, at penetration depths up to 10 feet (i.e. utility lines, etc.).

Since they produce cross-sectional images GPR records are usually interpreted visually, often in real time. In the absence of a feature with known depth on the record, an absolute depth scale is unavailable, and only relative depth information can be obtained. However, if a feature with a known depth can be scanned, its position on the record establishes an empirical absolute depth scale.

Since the GPR antenna is towed at a sometimes-uneven speed, placing fiducial marks on the record at known locations or spacing along the profile achieves positioning along the record.

Unlike other electrical, EM, and magnetic techniques, GPR can provide relative (and sometimes absolute) data on the depth to various features. Most other techniques can delineate anomalies through contouring of measurements collected on a grid, or recognition of audible alarms or needle deflections, but cannot readily provide target depths. Because of the rapid pulse rate, GPR is probably the most continuous profiling technique. It is also one of the quickest (although not easiest) to perform. The antenna may be towed by hand at walking speed, or towed behind a vehicle at greater speeds for more extensive surveys. These capabilities make GPR particularly suited to reconnaissance-level stratigraphic or water table profiling, and scanning for unknown or suspected underground structures.

3.1.2. GPR Limitations

The greatest limitation of GPR is the loss of penetration in electrically conductive materials such as damp clays. This can be insidious, since an absolute depth scale is rarely available. In any GPR survey, an attempt should be made to locate and profile a nearby object or feature within known depth to ensure that sufficient penetration is being achieved. A single known utility or an auger-hole may be sufficient to calibrate the GPR penetration in many cases.

Since there is a trade-off between penetration depth and resolution, it may be difficult (or impossible) to choose an antenna with the correct frequency to attain the necessary penetration while maintaining the necessary resolution. An incorrect frequency selection will result in missing the desired feature.

Ringing, or antenna multiples from a single reflector are usually seen on the commonly raw, unprocessed GPR profiles. Although an experienced interpreter can usually recognize them, they can be misleading to the beginner.

The GPR antennae commonly used for shallow scanning are shielded to look only downward. However, unshielded antennae are occasionally used. Unshielded antennae are susceptible to spurious reflections from overhead or nearby structures, such as power lines, buildings, cars, etc. All antennas used on this site were shielded.

3.2. Seismic Refraction

The seismic refraction method uses a linear spread of 24 energy sensors (geophones) with one energy source locations off each end of the spread, and at a number of locations along the spread. Energy imparted into the subsurface reflects and refracts at soil and bedrock interfaces in the subsurface. As reflected and refracted energy is returned to the surface, geophones (receivers) change the energy (ground motion) into electrical signals for the seismograph. The seismograph measures the time, from energy transmission to energy reception at the geophone, which is a known distance from the source. Given the travel time and the distance, a velocity of the subsurface materials can be computed. Information on the lithology and density of subsurface materials can be gained by measuring the subsurface velocities. A series

of sequential spreads and energy locations can be used to create a profile of the subsurface velocities across the investigation area.

Most igneous and metamorphic rocks have little or no porosity, and velocities depend mainly on the elastic properties of the minerals making up the rock material itself. This is also the case with massive limestone, dolomites and evaporates. Sandstone, shale and certain kinds of soft limestone has more complex microstructures with pore spaces between grains which may contain fluids or softer types of material such as clay. For such rock or soil, velocity is very dependant on porosity and the material filling the pores.

Table 1 Typical Compressional Velocities for Common Materials

Material	Typical Minimum (feet/second)	Typical Maximum (feet/second)
Unconsolidated Soils	500	2,500
Consolidated, Clayey Soils	2,000	4,500
Saturated Soil	4,800	5,200
Shale Bedrock	6,000	12,000
Sandstone Bedrock	9,000	14,000
Limestone Bedrock	12,000	18,000
Crystalline Bedrock	15,000	19,000
Basalts	16,500	20,000
Gneiss	12,000	24,000
Marble	13,000	23,000

In general, igneous rocks have seismic velocities which show a narrower range of variation than sedimentary or metamorphic rocks. Sedimentary rock velocities will also be dependent upon their age and depths of burial. Metamorphic rock velocities depend upon the composition of their host rock and the degree of metamorphic activity at the location of the survey.

3.2.1. Seismic Refraction Limitations

The presence of vibration sources near the seismic survey can provide unwanted noise, which can degrade the quality of the data and at times obscure the intended seismic source energy. Seismic refraction method has difficulty identifying the presence of a subsurface velocity inversion, where subsurface conditions change from a fast velocity material to a slow velocity material. When the low velocity material can be identified, depths to refractors below the low velocity material are suspect. Seismic refraction tomography represents the best method to address this issue, but seismic data in these settings are subject to cautious interpretation.

4. GEOPHYSICAL DATA COLLECTION

At the Port of Hilo, the locations of traverses were based upon site features and observed. Due to the dynamic nature of the port, data collection was established as access and egress was available. Interviews were conducted with site personnel to identify historic problem areas, and areas that have been subject to reconstruction activities to minimize settlement problems. Based on these interviews, and access available, several areas were established for assessment. Data was collected in three, overlapping areas, with three specific histories and survey objectives. The first area is in the barge off-load area (Figure 2), where repairs have been made, but subsidence is still present near the repairs. The second area encompasses Pier 2 Warehouse, where no settlement has been described in front of the warehouse, but settlement is apparent to the south. The third area is in front of the Pier 1 Warehouse, where settlement has occurred and repairs were limited. The third area is adjacent to the first area, separated by jersey barriers to control access and demark areas of differing port activities.

4.1. GPR Site Specific Data Collection Parameters

Dawood used a Model SIR-3000 GPR unit manufactured by Geophysical Survey Systems, Inc., of New Hampshire. A single antenna with a central frequency of 400 megahertz (MHz) was used. Data at the Port of Hilo was collected in time mode. The wheel encoder was non-functional at the time of data collection. Significant profiles were recorded in two directions so offsets from the start and end of the line could be better estimated.

A dielectric constant of 6.0 was used for all sites to estimate depths to features identified in the GPR record during field activities. This constant was developed based on general soil information, and may be incorrect for site-specific applications. No subsurface utilities with known depth were used to calibrate the measurements.

A crude grid was established using the southwest corner of Pier 1 as an origin. A number of generally shorter GPR traverses were collected in the barge off-loading area (Figure 3), with longer lines extending to the storage area to the south and east. Two longer lines in particular, were replicated with the seismic refraction survey discussed below. The first longer line to be replicated, Line 38, was collected starting near where the barges tie onto the pier, oriented to the south. Line 38 was located 38-feet in front of the Pier 2 Warehouse, and was parallel to the front of this structure. The second line replicated with seismic started on the southern edge of the northern-most door on the Pier 2 Warehouse. This second regional line, the "Crossing Line" crossed the barge unloading area and proceeded in front of the Pier 1 Warehouse.

All data was digitally recorded, with each traverse represented by a separate data file. Data file numbers, line locations, and survey traverse direction were recorded in a field log-book as the data was collected. Data acquisition parameters such as filename, antenna, samples/trace, scans/second, range-gain, vertical infinite impulse response (IIR) filters and horizontal trace stacking are stored in the header of each traverse. Each traverse was reviewed at the conclusion of data collection for preliminary evaluation and data quality assurance. Data acquisition parameters were adjusted as necessary based upon this review. Data was downloaded to a personal computer daily for back-up.

4.2. Refraction Data Collection Method

Seismic refraction data was collected north to south along GPR Line 38, and east to west along the GPR Crossing Line (Figure 4). The seismic refraction survey data was collected with 24 geophones mounted on a land streamer with 1.5-foot geophone spacing. This geophone spacing represented the largest geophone spacing that could be performed at the time of the refraction survey, given the take-out cables present for the shallow void assessment project.

A 20-lb sledge-hammer was used for the compressional seismic survey. Nine source locations were used along each spread. Sources were located 6.0-feet off the end of the spread near geophone 1 (Station -4), 0.75-feet off the end of the spread near geophone 1 (Station -0.5), between geophones 4 and 5 (Station 4.5), between geophones 8 and 9 (Station 8.5), between geophones 12 and 13 (Station 12.5), between geophones 16 and 17 (Station 16.5), between geophones 20 and 21 (Station 20.5), and 0.75-feet from Geophone 24 (Station 24.5), and 6 foot from geophone 24 (Station 28.5). Source locations within the spread were offset laterally 0.75 feet (9-inches). Line 38 consisted of 9 separate spreads, while Crossing Line consisted of 14 spreads.

The data was digitally recorded for analysis and reduction. The data quality was monitored as it was recorded to ensure adequate information and resolution was available for interpretation. The seismograph used was a Geode seismograph manufactured by Geometrics of San Jose CA. This 24-bit resolution instrument works well in noisy areas permitting deeper investigation with better resolution. The instruments 14 kHz bandwidth yields the highest resolution, which is necessary for detailed surveys such as this. All activities performed by the field crew in collecting the data were recorded in digital activity logs for each seismic spread location. These activity logs provide a means to assess and evaluate any data that may be suspect subsequent to the conclusion of field activities.

5. GEOPHYSICAL DATA PROCESSING

5.1. GPR Processing

A copy was made of each radar record, and renamed to reflect the line and antenna being used. RADAN™ software written by Geophysical Survey Systems was used to process and interpret the renamed GPR data. An example of the effects of GPR processing can be observed on Figure 5. Position adjustment was made to the data. This time shift of the data places the first positive peak of the direct wave from a ground coupled, bistatic antenna to time zero. This permits the data to be examined so that the ground surface can be considered to be at time zero. Next, a finite impulse response (FIR) horizontal high pass filter, was applied to the data to remove background noise. Background noise shows up as horizontal, low frequency bands in the data (caused most commonly by antenna ringing) to be removed from the data. This step can remove indications of flat-lying water table reflections. A filter length of 1023 scans was used. The final step removed excess data traces from the beginning and ends of the data files. For data presentation four adjacent traces were stacked to shorten the apparent length of the line.

The depth of penetration was variable in the data. However, GPR processing improved the apparent depth of penetration of the GPR data to approximately 35 nano-seconds (nS). Prior to

processing, the apparent depth of penetration was approximately 20 nS. Because the survey objective is geologic in nature, no processing was performed to quantify reflectors in the subsurface. No velocity analysis was performed.

5.2. Refraction Data Processing

Rayfract[®] written by Intelligent Resources Incorporated of Vancouver B.C was used to analyze the refraction data. Rayfract[®] permits the interpreter to pick first-energy breaks in the seismic data and be mapped to refractors manually or semi-automatically, based upon apparent (instantaneous) common mid point velocities. Seismic energy travel time is processed on a per-refractor basis according to three different interpretation methods, Common-Midpoint time refraction (Gegrande and Miller, 1985, Ruehl, 1995), Plus-Minus (Hagerdoon, 1959), and Wavefront (Brueckl, 1987, Jones and Jovanovich, 1985). Additionally, a Delta-t-v method (Gegrande and Miller, 1985) was used as a comparative method to assess model stability and consistency. The Delta-t-v method permits pseudo-2D tuning ray inversion which delivers a continuous one-dimensional depth verses velocity profile for all profile stations. This approach permits the identification of systematic velocity increases (such as top-of-rock or basement) and strong velocity anomalies such as low velocity fault zones, faults, or high velocity dykes. As a final processing step, the Delta-t-v results are subjected to WET (Wavepath Eikonal Traveltime) tomographic processing (Schuster, 1993, Watanabe, 1999).

During data analysis, Dawood examined data recorded by each of the 24-geophones for each source recorded. Dawood identified the onset of seismic energy and evaluated noise content. As necessary, data was gained or filtered to highlight energy associated with the seismic source, and de-emphasize site noise. Data for this site was subject to WET tomographic processing based on a smoothed velocity field across the entire section. This approach was chosen to minimize lateral variations and establish most efficiently the vertical velocity profile of the area surveyed. During data modeling, the 1D and 2D velocities were examined in detail. Dawood also examined the relationship between the modeled first break energy and interpreted first break energy picks.

In general at this site, the Delta-t-v analysis did not provide a significant advantage over the smooth WET inversion of the refraction data, and is not presented below. Similar results were found from both processing methods. While velocity anomalies are expected to be present, the velocity fields are adequately slow to change to be facilitated using standard tomographic analysis; therefore the Delta-t-v analytical data is not presented below. The refraction data was not adequately deep penetrating to identify significant strong lateral velocity anomalies such as faults or intrusions that may be present in the bedrock of the site.

6. GEOPHYSICAL DATA PRESENTATION

6.1. GPR

GRP Line 75, located 75 feet from the waterfront, is oriented east to west (Figure 3). Nearest the Jersey barrier soil stratigraphy is discontinuous, with few continuous reflectors above the water table (Figure 6). This area is reportedly subject to settlement. Closer to the barge ramp, more continuous reflectors are present. The lateral continuity of these reflectors is interpreted to represent engineered fill associated with reconstruction in this area. Along the extreme

western edge of the line, the discontinuous high amplitude reflectors near the surface are characteristic of reinforced concrete. The high amplitude features appear as characteristic hyperbolas on the expanded GPR record which is only presented in digital form. The concrete is not obvious at the surface as the entire area is asphalt covered.

GPR Line 120 starts started on the southern edge of the northern-most door on the Pier 2 Warehouse, and ends 120-feet from the waterfront (Figure 3). GPR Line 120 has discontinuous high reflections characteristic of reinforced concrete near the Pier 2 Warehouse entrance (Figure 7). Immediately to the west of the buried concrete high amplitude response continues, however the discontinuous hummocky nature of the reflectors suggests pieces of broken concrete rather than an organized constructed structure. Onsite personnel suggest there is an old pier in this area. Therefore, some of the variability may be related to edge effects associated with the old pier structure. Further to the east, more parallel, flat lying reflectors are present which have been interpreted as engineered fill. In the lower section, deep (near 20 nS) large diameter high amplitude reflectors are present, and interpreted to represent buried structures. The high amplitude (purple) reflectors dipping to the east could represent bedrock, suggesting the buried structures have the potential to be lava tubes. However the absence of high reflector features immediately to the east discounts this interpretation somewhat. Further to the east in the lower section, two utilities are interpreted present based on the hyperbolic shape and high amplitude of the features. Between the utilities, an area of historic subsidence is present. The large number of parallel, continuous reflectors in this area suggests this feature has been subject to a number of remedial solutions in the past. To the east of the utility, and close to the Jersey barrier, the discontinuous near surface is present again, suggesting fill, and subsidence issues will be present.

Intact, buried concrete is only interpreted present near the barge, and in the front of Pier 2 Warehouse. With the exception of the concrete, the lateral continuity of interpreted engineered fill is present at all locations described by onsite personnel to have been reconstructed. Hummocky, discontinuous reflectors were prevalent in all areas described as having settlement issues. Bedrock may be an interpretation from GPR data, however this interpretation requires verification before it can be extended into other areas of this port facility.

6.2. Seismic Refraction

Overall data quality is judged to be good. The Crossing Line started 6-feet from the southern edge of the northern-most door on the Pier 2 Warehouse, and is oriented to the east, toward the northern corner of the Quonset™ hut located to the southeast of the Pier 1 Warehouse (Figure 4). The depth profile for this line (depth verses inline distance) is presented as Figure 8. Velocities less than 6,000 feet per second (fps) are interpreted to represent unconsolidated material. Commonly the water table is expressed as a relatively flat refractor, with a velocity of approximately 5,000 fps. However, the water table (less than 10-feet below ground surface) is not a dominant feature at this site, and is not expressly exhibited. Velocities between 6,000 and 8,000 fps are interpreted to represent weathered bedrock material. Competent bedrock velocities are interpreted to be present in material exhibiting velocities in excess of 8,000 fps. Competent bedrock depth is variable across the area surveyed. Variability in the overall depth of the profile presented is related to the refractor wavepaths based upon the interpreted first break picks. Areas presented with a shallow profile are due to poor signal

to noise ratio within the data, or the dominance of nearby high velocity refractors dominating the energy wavepaths.

Three abnormally low velocity zones are present on the Crossing Line indicated by the letters "A", "B", and "C". Feature "A", located at inline distance between 130 and 135 feet is extremely narrow, and deep. Feature "B", located between 315 and 365 feet inline is a shallow, low velocity zone interpreted to represent under consolidated material. Nearby feature "C", located between 425 and 465 feet inline is very similar to Feature "B". The locations of these features is shown on [Figure 10](#).

Line 38 starts near the edge of Pier 2 and trends to the southwest running parallel to and thirty-eight feet in front of the Pier 2 Warehouse ([Figure 4](#)). Velocities and depths of investigation are similar to those encountered on the Crossing Line. A wide low velocity area is present crossing most of the area in front of the Warehouse building. The most extreme low velocity area, extending from 100 to 140 feet is toward the southern warehouse door. This low velocity is identified as Feature "D" on [Figure 9](#) and shown on the [Figure 10](#) map. Data velocities and data quality obscure the northern limit of this feature, which may extend to inline distance of approximately 77 feet. South of the Pier 2 Warehouse, no significant low velocity zones are present. The topographically low area of concern near the stormwater drop does not contain abnormal velocity variations. In the area of the stormwater drop, shallow weathered bedrock is indicated. Competent bedrock material remains approximately 10 feet below ground surface.

6.3. Geophysical Data Integration

A comparison of the crossing line geophysical data is presented on [Figure 11](#). Anomalous features "A", "B", and "C" are all present in both data sets, however, the level of detail differs between the two data sets.

The GPR data is limited in two fashions. Due to equipment malfunction, the GPR data was collected with a horizontal time scale, with 100 scans per second instead of the more normal distance scale with a number of scans per foot. Lacking a target with known depth, the GPR vertical scale is also presented in time, which is a common presentation method. In either case, the high resolution of the GPR permits a detailed assessment of soil stratigraphy in the subsurface across the traverse. The narrow width of Feature "A", with soil stratigraphy dipping to both the east and west suggests this feature may be a fracture with nearly vertical dip. Feature "B" is also narrower on the GPR than on the seismic data. The GPR data indicates more internal geometric variation than can be observed on the seismic data. At Feature "C" the most significant feature on the GPR is the "sag" present in the shallow portion of the section. Close examination of the GPR data indicates soil stratigraphy dipping to the east and west, but these features are not clear and obvious.

The seismic refraction data was recorded with an unusually close geophone spacing, which permitted an unusually detailed lateral assessment of the area. This is at the expense of depth of investigation, which may be useful given the higher velocity material that is present at the very bottom of the section. Seismic velocities have some useful engineering relationships that can provide value. In general, lower velocity material generally represents "softer" materials, which at this site will be the material subject to settlement issues.

7. GEOPHYSICAL DATA SUMMARY AND CONCLUSIONS

The investigation work scope included standard and/or routinely accepted practices of the geophysical industry. Dawood typically utilizes multiple geophysical investigation methods as a means to provide a series of checks and balances to produce subsurface models that reflect, as uniquely as possible, the subsurface conditions at the site. By nature, no subsurface survey is 100 percent accurate and Dawood cannot accept responsibility for inherent technique limitations, survey limitations or unforeseen site-specific conditions. The identified boundaries separating materials of different physical properties may or may not coincide with boundaries separating materials of different lithologic, geologic or soil composition. This may result in the geophysical interpretation varying somewhat from the gross geologic, lithologic or soils setting of the site. With these constraints in mind, Dawood has drawn the following conclusions:

1. Both GPR and seismic refraction methods provided useful information about the site features related to settlement issues. The methods provided complementary geophysical methods to assess the subsurface at this site.
2. Site conditions, which include the movement of cargo and the presence of a shallow saltwater-table, did not significantly limit the geophysical data for the site.
3. Top of bedrock, where interpreted present is variable in depth. Highly variable conditions were found to be present in the unconsolidated materials.
4. GPR data, collected in this instance in time mode, provided insight into soil stratigraphy at the site. Future GPR data collection in this area should be performed in distance mode.
5. GPR data was effectively processed to enhance the apparent depth of penetration. The presence of saltwater and salt vadose zone did not significantly limit the depth of penetration of the GPR.
6. Future GPR data should be processed using a long FIR horizontal high pass filter to remove flat lying reflectors and enhance depth penetration for detailed examination of the subsurface. When utility hyperbolas are present in the GPR data, velocities should be used to estimate depths to features of interest.
7. The GPR provided a rapid data collection method that was able to discriminate between those areas where reconstruction has occurred and numerous flat lying reflectors were present, and areas subject to settlement issues, where discontinuous hummocky reflector pattern was observed.
8. Seismic refraction data was collected with a short (1.5-foot) geophone spacing due to access timing, and available equipment. Future refraction data should be collected with a 5-foot geophone spacing to improve the rate of field crew productivity and depth of penetration of the refraction data.
9. Seismic refraction data result in data with depth scales both vertically and horizontally, which help to plan future work activities. This contrasts with GPR, which traditionally

has a vertical time scale, or at best an estimated depth time scale. Future geophysical work in this area should consider the future application of the data and determine the value and virtue of vertical depth scales before data collection.

10. Seismic refraction data identified unconsolidated material, weathered bedrock, and intermittently competent bedrock. These subsurface layers are variable across the site.
11. Seismic refraction data identified a number of low velocity areas of limited extent. These low velocity areas were generally present in areas where site personnel indicated settlement concerns.
12. Apparent settlement south of the Pier 2 Warehouse, near the stormwater drop, was not accompanied by a low velocity feature. Therefore, based upon the seismic data, this area would not be expected to be subject to significant settlement.
13. Future data collection should be organized in a systematic fashion with parallel traverses collected in a fashion that permits mapping of important site features. Given site activities observed, future surveys should be closely coordinated with port activities to minimize the impact on port work.

Geophysical methods use remote physical measurements to identify, interpret, and categorize subsurface features. In many instances, there are a number of features that will provide the same physical measurement. Therefore, Dawood recommends that anomalies identified during geophysical investigations be verified using invasive methods (such as drilling or excavating) prior to the initiation of remedial design activities.

8. REFERENCES

Brueckl, E. 1987. The Interpretation of Traveltime Fields in Refraction Seismology. Geophysical Prospecting, volume 35, pp. 973-992.

Gegrande, H. and Miller, H., 1985. Refraktionsseismik (in German). In: F. Bender (Editor), Angewandte Geowissenschaften II. Ferdinand Enke, Stuttgart; pp. 226-260. ISBN 3-432-91021-5.

Hagerdoon, J.G., 1959. The Plus-Minus Method of Interpreting Seismic Refraction Sections. Geophysical Prospecting, volume 7, pp. 158-182.

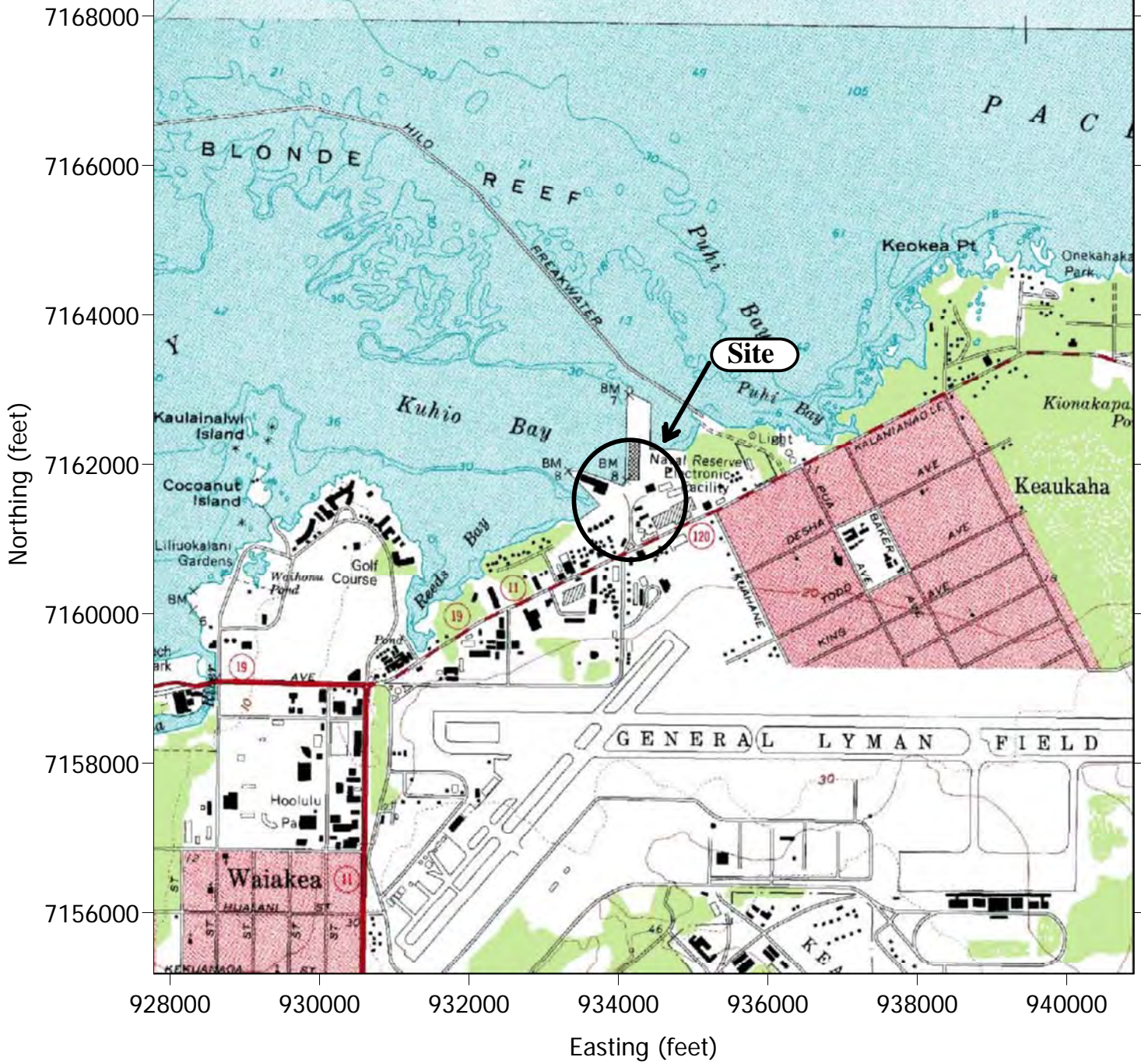
Jones, G.M. and Jovanovich, D.B. 1985. A ray inversion method for refraction analysis. Geophysics, volume 50, pp. 1701-1720.

Ruehl, T., 1995. Determination of shallow refractor properties by 3D-CMP refraction seismic techniques. First Break, volume 13, pp. 69-77.

Schuster, G.T. and Quintus-Bosz, A., 1993. Wavepath eikonal Traveltime Inversion Theory, Geophysics, Volume 58, PP. 1314-1323

Watanabe, T. et al. 1999. Seismic traveltime tomography using Fresnel volume approach. SEG Houston 1999 Meeting, Expanded Abstracts.

Figures



This map is from a library of scanned topographic maps that originate with published United States Geological Survey 1:24,000 scale quadrangle maps. Adjacent maps have been electronically spliced to facilitate presentation.

Site Location established using a global positioning system using North American Datum, 1983, Hawaii, Universal Transverse Mercator Projection Units are U.S. Survey Foot.



PROJECT: University of Hawaii, Manoa Hilo, HI	
REVISIONS	DATE

PROJECT NO.: 208044.01	 10105 ALLENTOWN BLVD. GRANTVILLE, PA. 17028 PHONE:(717)469-0937 FAX:(717)469-0938	SHEET NO.: 1
DRAWN BY: R.A.H.		
CHECKED BY: B.B.		
SCALE: AS SHOWN		
DATE: 07 July 2008	DRAWING TITLE: Hilo Site Location Map	



This air photograph is from Digital Globe and is a QuickBird satellite image from 6 May 2005



Site Photograph is projected system using Universal Transverse Mercator projection and the World Geodetic Datum, 1983. Units have been converted to feet.

PROJECT: University of Hawaii, Manoa Hilo, Hi	
REVISIONS	DATE

PROJECT NO.: 208044.01	 CONSULTING ENGINEERS 10105 ALLENTOWN BLVD. GRANTVILLE, PA. 17028 PHONE:(717)469-0937 FAX:(717)469-0938	SHEET NO.: 2
DRAWN BY: R.A.H.		
CHECKED BY: B.B.		
SCALE: AS SHOWN		
DATE: 07 July 2008	DRAWING TITLE: Survey Area	



This air photograph is from Digital Globe and is a QuickBird satellite image from 6 May 2005



Site Photograph is projected system using Universal Transverse Mercator projection and the World Geodetic Datum, 1983. Units have been converted to feet.

PROJECT: University of Hawaii, Manoa Hilo, HI	
REVISIONS	DATE

PROJECT NO.: 208044.01	 CONSULTING ENGINEERS 10105 ALLENTOWN BLVD. GRANTVILLE, PA. 17028 PHONE:(717)469-0937 FAX:(717)469-0938	SHEET NO.: 3
DRAWN BY: R.A.H.		
CHECKED BY: B.B.		
SCALE: AS SHOWN		
DATE: 07 July 2008	DRAWING TITLE: GPR Traverse Locations	



This air photograph is from Digital Globe and is a QuickBird satellite image from 6 May 2005

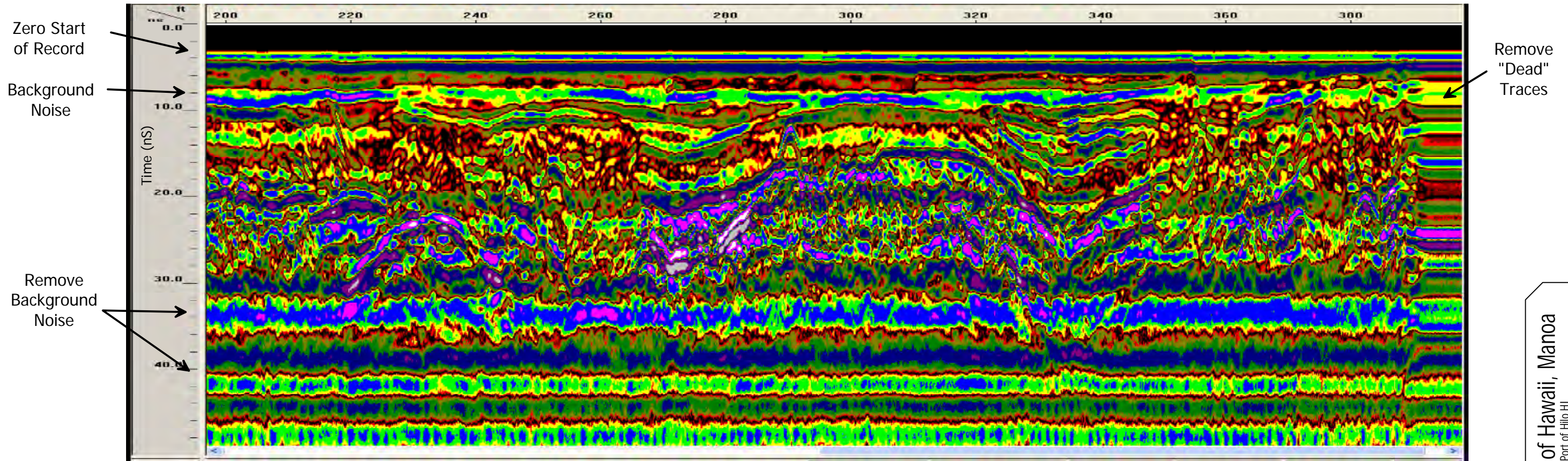


Site Photograph is projected system using Universal Transverse Mercator projection and the World Geodetic Datum, 1983. Units have been converted to feet.

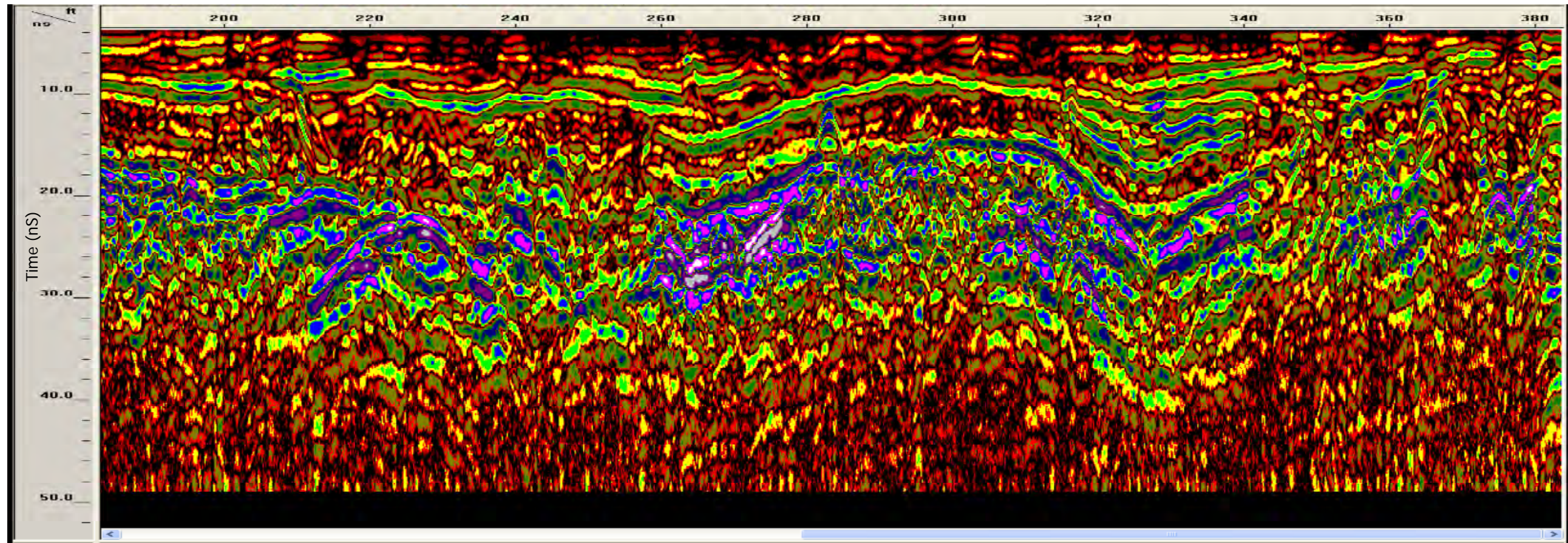
PROJECT: University of Hawaii, Manoa Hilo, Hi	
REVISIONS	DATE

PROJECT NO.: 208044.01	 CONSULTING ENGINEERS 10105 ALLENTOWN BLVD. GRANTVILLE, PA. 17028 PHONE:(717)469-0937 FAX:(717)469-0938	SHEET NO.: 4
DRAWN BY: R.A.H.		
CHECKED BY: B.B.		
SCALE: AS SHOWN		
DATE: 07 July 2008	DRAWING TITLE: Seismic Refraction Locations	

UNPROCESSED GPR RECORD



PROCESSED GPR RECORD



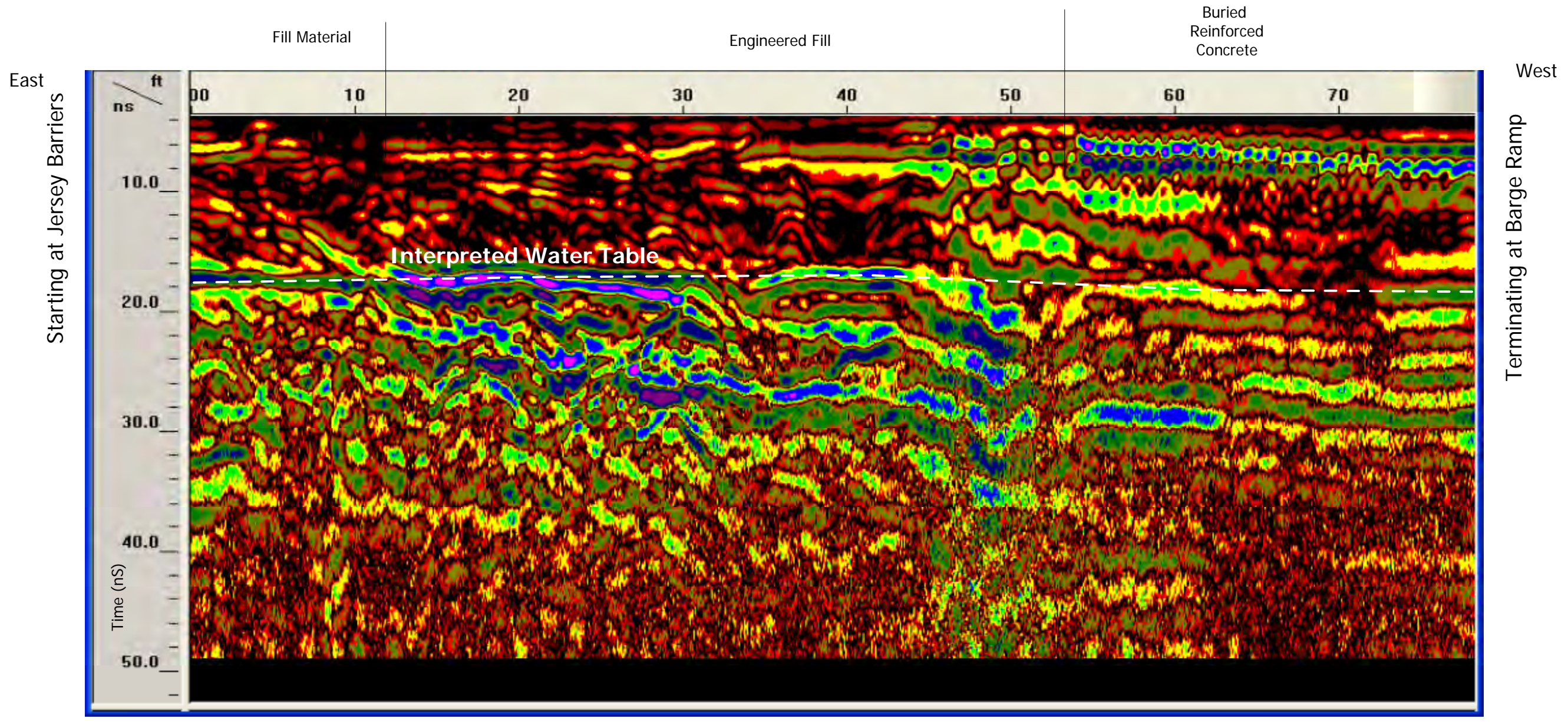
PROJECT: University of Hawaii, Manoa	
Port of Hilo HI	
REVISIONS	DATE

DAWOOD
 CONSULTING ENGINEERS
 10105 ALLENTOWN BLVD. GRANTVILLE, PA. 17028
 PHONE: (717) 869-0937 FAX: (717) 869-0938

DRAWING TITLE: GPR Processing

PROJECT NO.:	208044.01
DRAWN BY:	R.A.H.
CHECKED BY:	B.B.
SCALE:	AS SHOWN
DATE:	29 July 2008

SHEET NO.: **5**



PROJECT:	University of Hawaii, Manoa
	Port of Hilo HI
REVISIONS	DATE

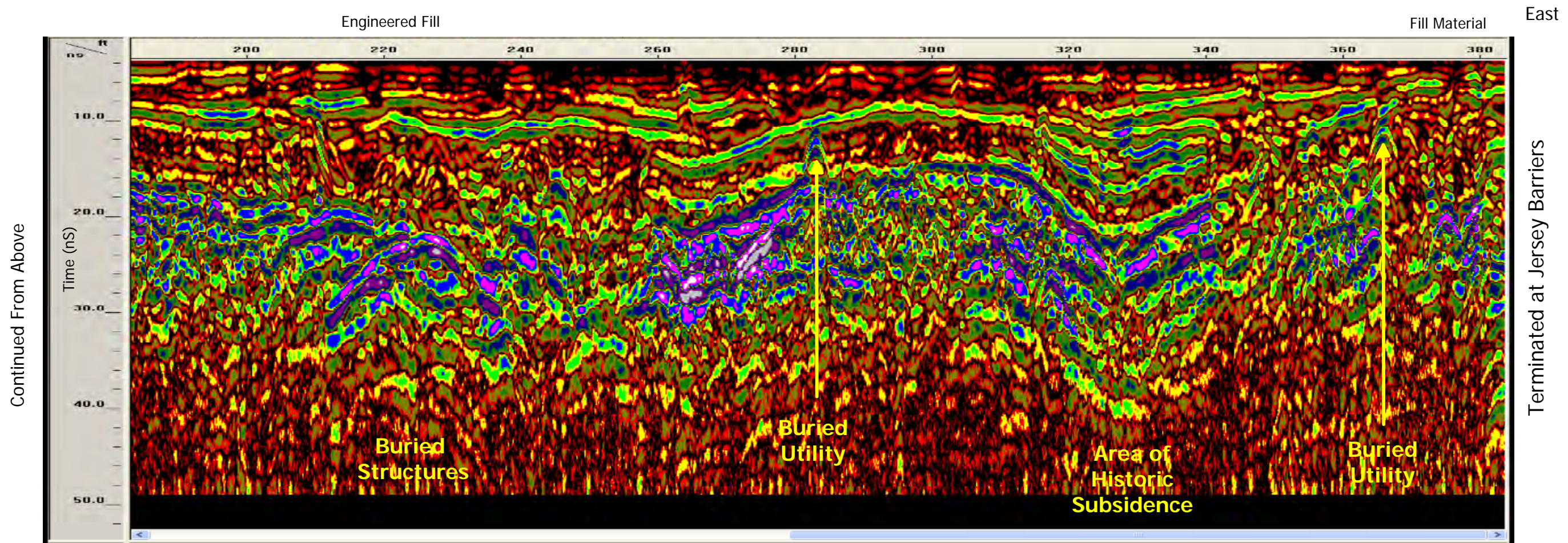
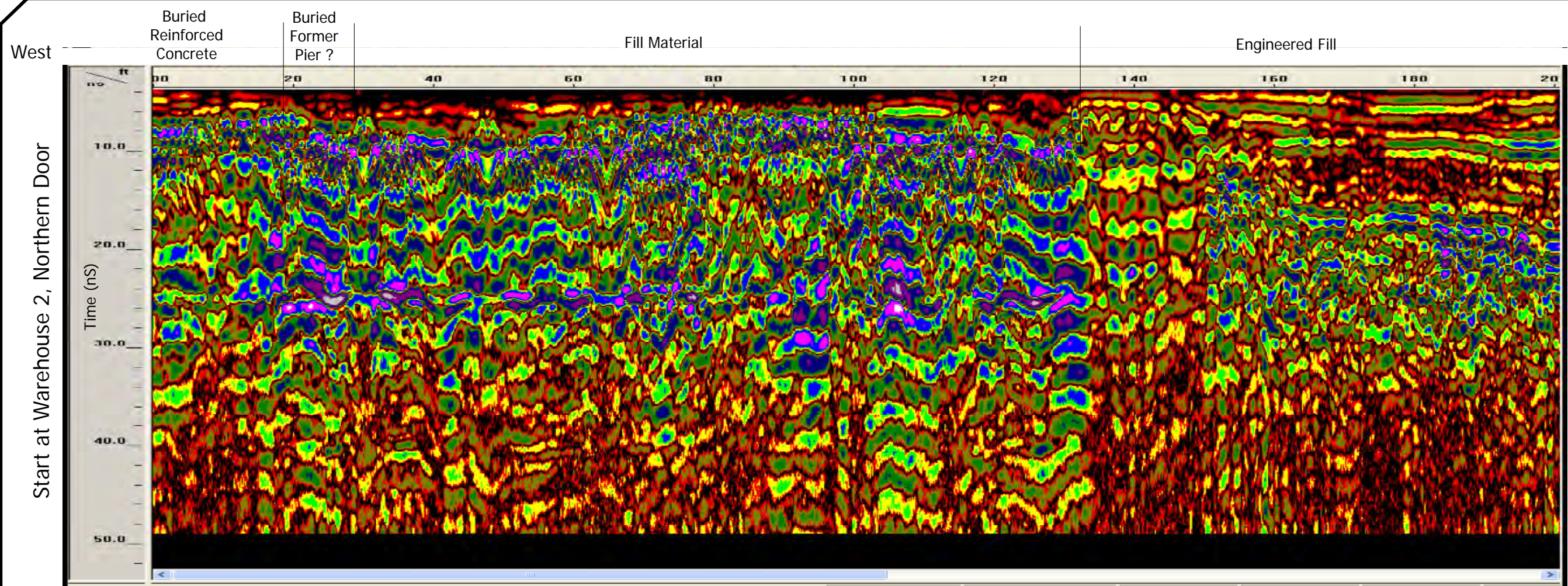
DAWOOD
CONSULTING ENGINEERS
10105 ALLENTOWN BLVD. GRANTVILLE, PA. 17028
PHONE: (717) 869-0937 FAX: (717) 869-0938

DRAWING TITLE:
GPR Traverse 75 Interpretation

PROJECT NO.:	208044.01
DRAWN BY:	R.A.H.
CHECKED BY:	B.B.
SCALE:	AS SHOWN
DATE:	29 July 2008

SHEET NO.:

6

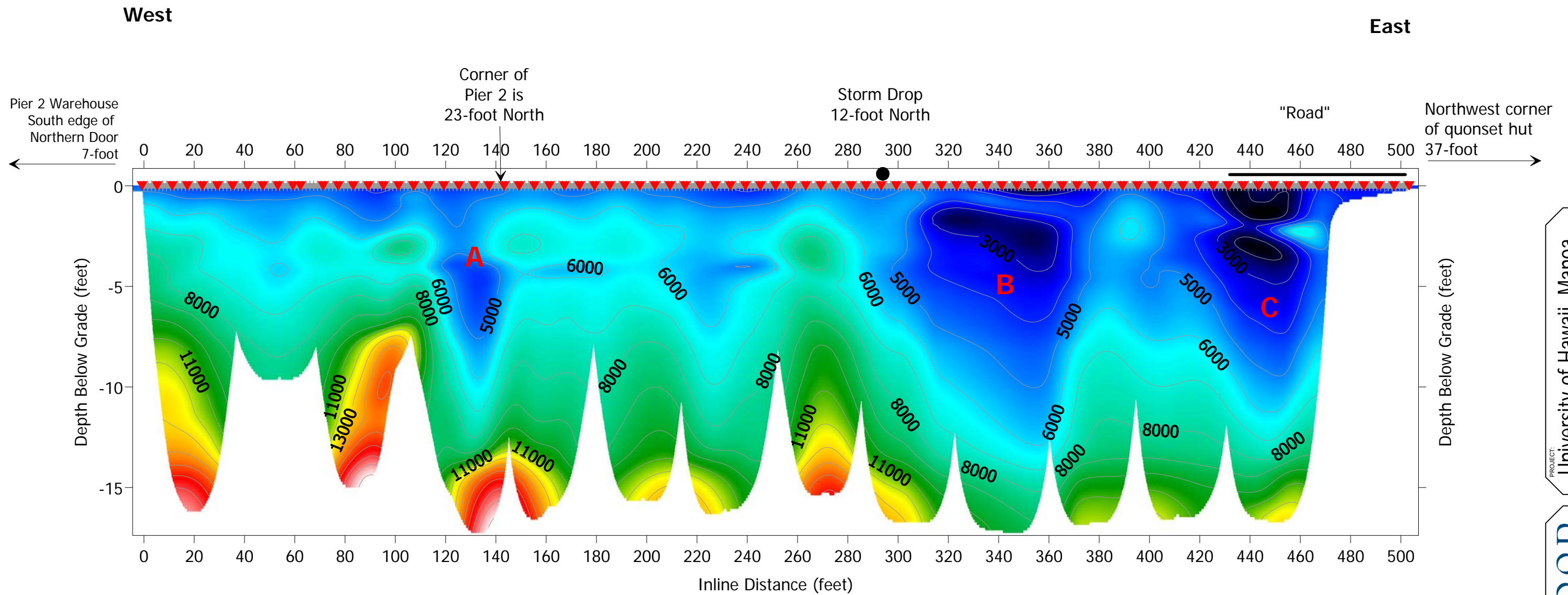


PROJECT:	University of Hawaii, Manoa	
	Port of Hilo HI	
REVISIONS		DATE

DAWOOD
 CONSULTING ENGINEERS
 10105 ALLENTOWN BLVD. GRANTVILLE, PA. 17028
 PHONE: (717) 869-0937 FAX: (717) 869-0938

DRAWING TITLE:
GPR Traverse 120 Interpretation

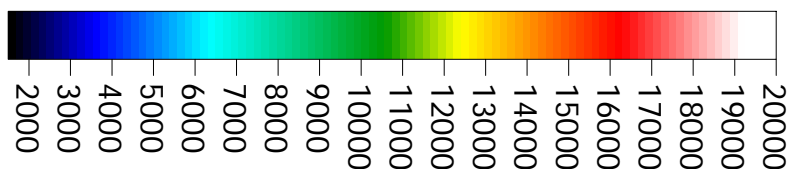
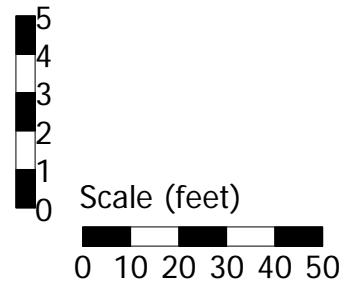
PROJECT NO.:	208044.01
DRAWN BY:	R.A.H.
CHECKED BY:	B.B.
SCALE:	AS SHOWN
DATE:	29 July 2008



LEGEND

▼ Source Location

★ Geophone Location

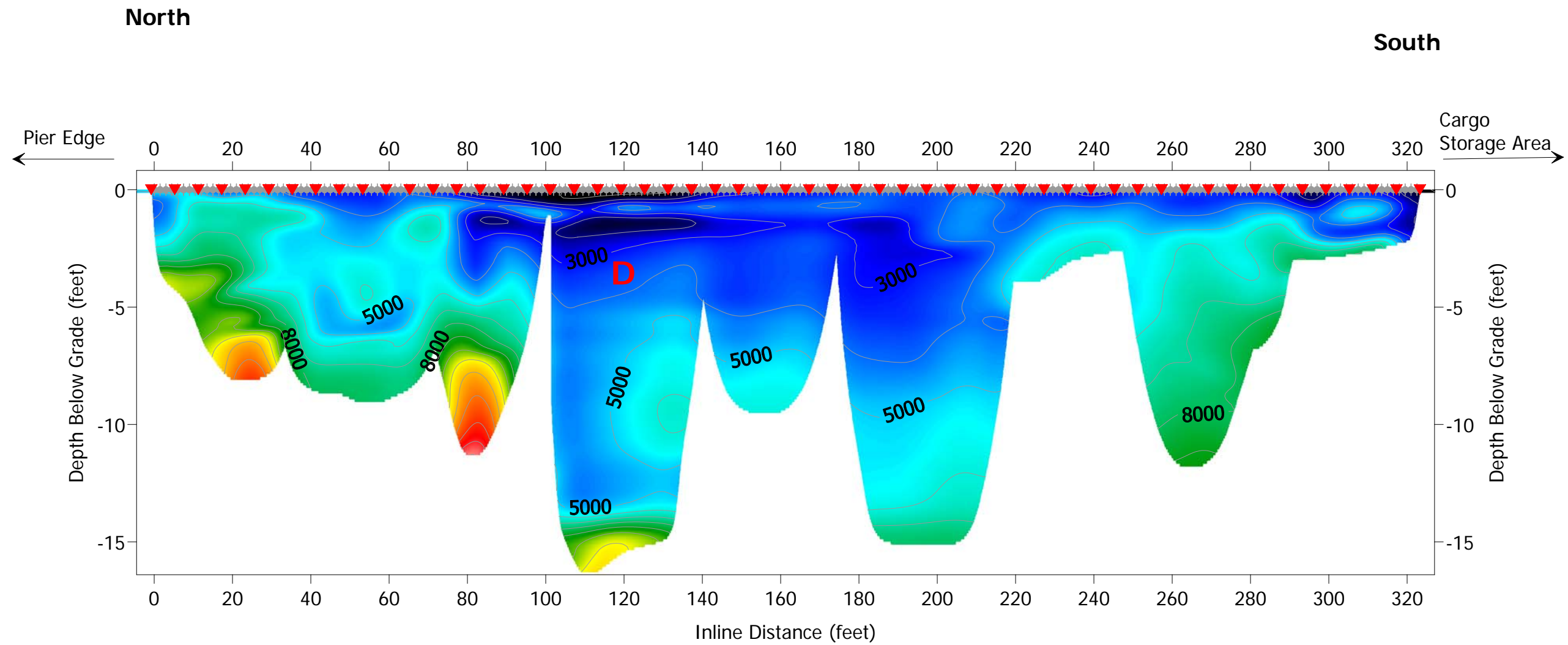


PROJECT: University of Hawaii, Manoa	
Part of Hilo Hawaii	
REVISIONS	DATE

DAWOOD
CONSULTING ENGINEERS
10105 ALLENTOWN BLVD. GRANTVILLE, PA. 17028
PHONE: (717) 469-0937 FAX: (717) 469-0938

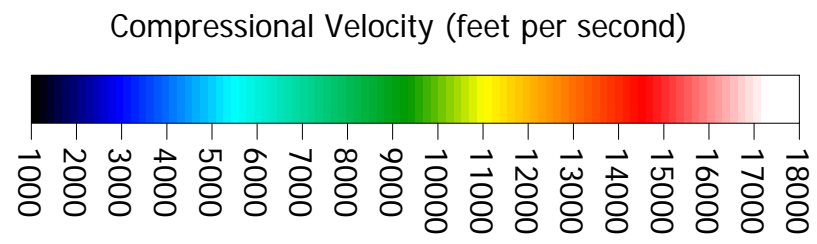
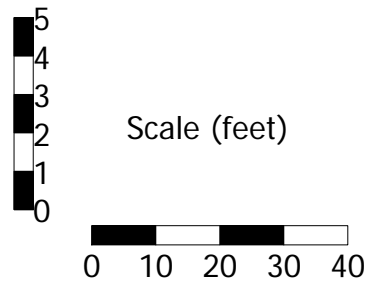
DRAWING TITLE: Seismic Refraction Crossing Line

PROJECT NO.:	208044.01
DRAWN BY:	R.A.H.
CHECKED BY:	B.B.
SCALE:	AS SHOWN
DATE:	July 22, 2008
SHEET NO.:	8



LEGEND

- ▼ Source Location
- + Geophone Location



PROJECT: University of Hawaii, Manoa	
Part of Hilo Hawaii	
REVISIONS	DATE

DAWOOD
 CONSULTING ENGINEERS
 10105 ALLENTOWN BLVD. GRANTVILLE, PA. 17028
 PHONE: (717) 465-0937 FAX: (717) 465-0938

DRAWING TITLE: Seismic Refraction Line 38

PROJECT NO.:	208044.01
DRAWN BY:	R.A.H.
CHECKED BY:	B.B.
SCALE:	AS SHOWN
DATE:	July 22, 2008
SHEET NO.:	9



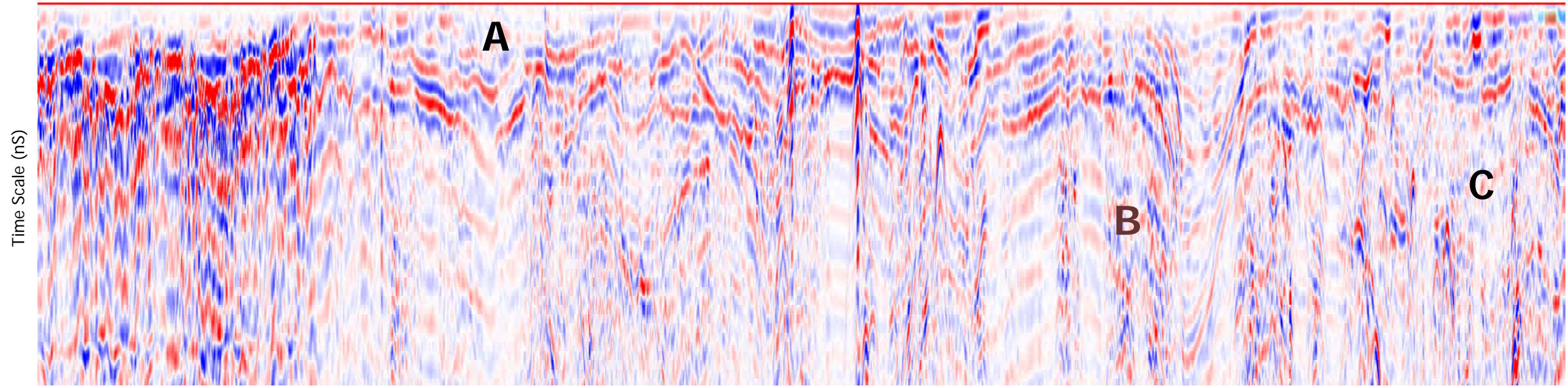
This air photograph is from Digital Globe and is a QuickBird satellite image from 6 May 2005



Site Photograph is projected system using Universal Transverse Mercator projection and the World Geodetic Datum, 1983. Units have been converted to feet.

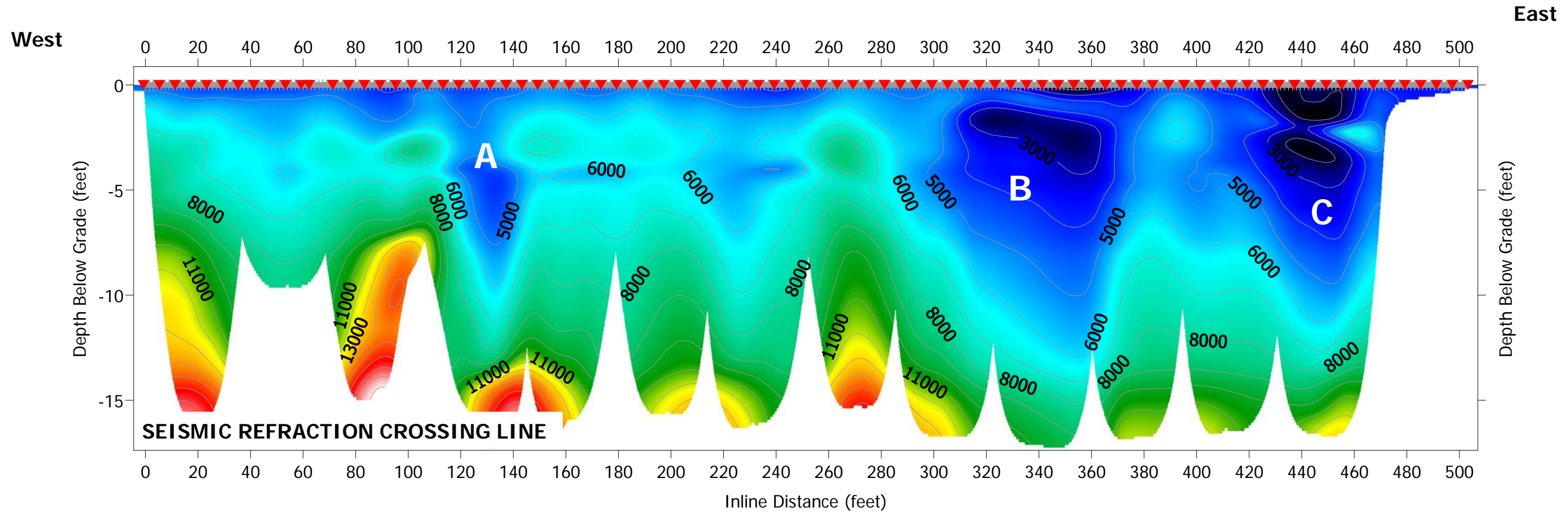
PROJECT: University of Hawaii, Manoa Hilo, Hi	
REVISIONS	DATE

PROJECT NO.: 208044.01	 CONSULTING ENGINEERS 10105 ALLENTOWN BLVD. GRANTVILLE, PA. 17028 PHONE:(717)469-0937 FAX:(717)469-0938	SHEET NO.: 10
DRAWN BY: R.A.H.		
CHECKED BY: B.B.		
SCALE: AS SHOWN		
DATE: 07 July 2008	DRAWING TITLE: Refraction Concern Areas	



GPR CROSSING LINE

GPR data collected in time mode - Horizontal scale will be slightly variable.



SEISMIC REFRACTION CROSSING LINE

PROJECT:	University of Hawaii, Manoa
DATE:	
REVISIONS:	

DRAWING TITLE:	Cross Line Comparison
PROJECT NO.:	208044.01
DRAWN BY:	R.A.H.
CHECKED BY:	B.B.
SCALE:	AS SHOWN
DATE:	July 22, 2008
SHEET NO.:	11

DAWOOD
 CONSULTING ENGINEERS
 10105 ALLENTOWN BLVD. GRANTVILLE, PA. 17028
 PHONE: (717) 869-0937 FAX: (717) 869-0938